DOCTOR OF PHILOSOPHY

Finite element studies of the modified KdV equation.

Geyikli, Turabi

Award date:
1994

Awarding institution:
Bangor University

Link to publication

Finite Element Studies of the Modified KdV Equation

Thesis submitted to the University of Wales in support of an application for the degree of Philosophiæ Doctor

Turabi Geyikli

supervised by

Dr. L.R.T. Gardner

1980 MATHEMATICS SUBJECT CLASSIFICATION: 35Q20, 65D07, 65N30, 65N35, 76B25.

KEY WORDS: Finite Element methods, Collocation, Splines, Solitons, Solitary waves, Method of lines, Korteweg-de Vries Equations.

T. GEYIKLI,
School of Mathematics,
University College of North Wales,
Bangor,
Gwynedd LL57 1UT.
U.K.

July 1994

Acknowledgements

I would like to thank my supervisor, Dr. L. R. T. Gardner, for suggesting the topic of research and his help, enthusiastic interest, and encouragement throughout the period of this work and guidance during the preparation of this thesis. I am also deeply grateful to Dr. G. A. Gardner for her continual helpful advice, discussion and valuable time.

Many thanks to friends and to various members at the School of Mathematics for their support, I have greatly enjoyed working with them during the my studies.

It is my pleasure to acknowledge the support and encouragement of my beloved wife and my son, in all stages of the preparation of this thesis.

I am also grateful to the University of İnönü, Republic of Türkiye, for providing me with a maintenance grant.

Summary

The main aim of this study is the construction of new efficient and accurate numerical algorithms based on the B-spline finite element method, for solution of the Korteweg-de Vries (KdV) and Modified Korteweg-de Vries ($MKdV$) equations.

In the following chapters; the theoretical background to the KdV and $MKdV$ equations is discussed, and existing numerical methods are described. Numerical solutions to the KdV and $MKdV$ equations are obtained using the Galerkin and modified Petrov-Galerkin method with quadratic B-spline finite elements over which the non-linear term is locally linearised. The numerical algorithms have been validated by studying the motion, interaction and development of solitons. We have demonstrated that these algorithms can faithfully represent the amplitude of a single soliton over many time steps and the interaction of two solitons. A new numerical solution for the $MKdV^-$ equation is obtained using a "lumped" Galerkin method with quadratic B-spline finite elements. The motion, interaction and generation of solitary waves are studied using the method.

An unconditionally stable numerical algorithm is implemented for the solution of the $MKdV$ equation using a collocation method with quartic B-spline finite elements. The algorithm is validated through a single soliton simulation. In further numerical experiments forced boundary conditions $u = U_0$ are applied at the end $x = 0$ and the generated states of solitary waves are studied. The solitary wave states generated by applying a positive impulse followed immediately by an equal negative impulse is dependent on the period of forcing. The solitary waves generated by these various forcing functions possess many of the attributes of free solitons.

Contents

Chapter 1

Introduction

Many scientists have used differential equations to model many physical problems. Scott Russell [62] studied the KdV solitary wave in 1844. The words 'solitary wave' were coined by Scott Russell himself, mainly because this type of wave motion stands apart from the other type of oscillatory wave motion. After him, the solitary wave of translation was briefly mentioned by various mathematicians including Stokes [73] and Boussinesq [10]. Korteweg and de Vries [44] derived their now famous equation for the propagation of waves in one direction on the surface of a shallow canal. A generalisation of the KdV equation has the form [20, 51, 53]:

$$U_t + \epsilon U^p U_x + \mu U_{xxx} = 0$$

where p, ϵ and μ are given parameters. When p=1 we have the Korteweg-de Vries (KdV) equation. The most simple generalisation comes with p=2, which is the Modified Korteweg-de Vries ($MKdV$) equation. This equation has been used to model accoustic waves in certain anharmonic lattices [85] and Alfén waves in a collisionless plasma [66, 43]. Gardner and Morikawa derived the KdV equation to describe long wave propagation perpendicular to a uniform magnetic field in cold lossless (collisionless) plasmas [86]. Many other researchers have also derived the KdV equation. Zabusky [85, 87] and Kruskal [45] showed that the KdV equation governs longitudinal waves propagating in a one dimensional lattice of equal masses coupled by non-linear springs the Fermi Pasta Ulam problem. Some physicists applied the KdV equation in the plasma physics. e.g. Berezin and Karpman [9] and by Washimi and Taniuti [83] in their study of ion acoustic waves in a cold plasma. Wijngaaden [79] found that it described pressure waves in a liquid gas bubble mixture. The theoretical aspects of the solution of the KdV equation have attracted attention. In particular, the problem of existence and uniqueness of solution for certain classes of initial conditions have been studied many authers including Lax [48], Sjoberg [70] and Gardner [21]. These authors have examined the existence of solitary wave or soliton solutions.

The KdV equation was solved numerically first by Zabusky and Kruskal [88] using a finite difference method. They discovered the properties of the interaction of two solitary waves, and they defined the concept of a soliton as a localised (solitary) wave that propagates at a uniform speed and preserves its shape and speed when it interacts with a second solitary wave but does suffer a phase shift. Also Greig and Morris [39] proposed a Hopscotch finite difference method and compared it with the original Zabusky and Kruskal [88] leap frog scheme and found that it gave better results [39].

The other methods; the application of spectral, pseudospectral and Fourier transform or series expansion methods to the KdV equation have been studied by Schamel [65], Abe and Inoue [1], Gazdag [37] , Canosa and Gazdag [12]. Fornberg and Whitham [20] have discussed the numerical solution of the KdV equation, using a pseudospectral method. Also, they have studied the higher order generalised KdV equation. Wahlbin [82] has used the finite element method, and suggested a dissipative Galerkin method in which the same trial and test functions are used. The basis functions are smoothed splines constructed from piecewise polynomials of order three or higher, and the elements are of equal length h. Alexander and Morris [4] used cubic splines and a range of dissipation coefficients from zero to one. Sanz-Serna and Christie [64] proposed a modified Petrov-Galerkin method with piecewise linear trial and cubic spline test functions. Schoombie [72] has used Petrov-Galerkin methods, which were either dissipative or nondissipative in form and contain the Sanz-Serna and Christie method as a special case.

The Korteweg-de Vries and modified Korteweg-de Vries equations are important nonlinear partial differential equations, which arise in the study of many different physical systems for which analytic solutions have only been found for a very restricted set of initial conditions.

Thus numerical methods are necessary to effect solutions for a wide range of initial conditions. In this thesis attempts are made to produce numerical methods based on the B-spline finite element method which are superior to those already being used.

In chapter 2, a short review of the KdV and $MKdV$ equation is given. The origin of the analytical solution is discussed. Soliton solutions of the KdV and $MKdV$ equations, which are nondispersive propagation solutions are mentioned together with the conservation laws. In chapter 3, we give a short review of the numerical solution method for the KdV and $MKdV$ equations, and also we give a short review of spline functions and B-spline finite elements.

In chapter 4, we show a new B-spline finite element algorithm using the Galerkin method with trial and test functions quadratic B-spline. Also, a modified Petrov-Galerkin algorithm set up for the KdV equation. The element matrices are determined algebraically using REDUCE [40]. Assembling the element matrices together and using a Crank-Nicolson difference scheme for the time derivative leads to a 5-banded system of nonlinear algebraic equations which is solved by a penta-diagonal algorithm. The method is tested by calculating how the L_2 error norm varies during the motion of a single and double soliton and comparing this with the error obtained by earlier authors for similar experiments. The first three conservation laws are also computed for the simulations.

In chapter 5, we set up a new numerical solution to the modified Korteweg-de Vries equation obtained using a 'lumped' Galerkin method with quadratic B-spline finite elements. The element matrices are determined algebraically using REDUCE [40]. Assembling the element matrices together and using a Crank-Nicolson difference scheme for the time derivative leads to a 5-banded system of nonlinear algebraic equations which is solved by a penta-diagonal algorithm. The method is tested by calculating how the L_2 - and L_∞ error norms vary during the motion of a single and double soliton and comparing this with the error obtained by earlier authors for similar experiments. The first three conservation laws are computed for simulations using a single soliton, a double soliton, Gaussian initial condition and also a tanh initial condition.

In chapter 6, we set up a new numerical solution for the Modified Korteweg-de Vries minus equation using a 'lumped' Galerkin method with quadratic B-spline finite elements. The element matrices are determined algebraically using REDUCE [40]. Assembling the element matrices together and using a Crank-Nicolson difference scheme for the time derivative leads to a 5-banded system of nonlinear algebraic equations which is solved by a penta-diagonal algiruthm. The method is tested by calculating how the L_2 - and L_∞ - error norms varies during the motion of a single soliton and a double soliton simulation. The first three conservation laws are computed for simulations using a single soliton, a double soliton, a kink pair, interaction of a soliton with a kink, interaction of a soliton with a kink pair, the generation of kink and solitons from a tanh initial conditions and non symmetric tanh initial conditions.

In chapter 7, we set up an unconditionally stable numerical algorithm for the $MKdV$ equation based on collocation with quartic spline interpolation polynomials over finite elements. Using a Crank-Nicolson difference scheme for the time derivative leads to a 5-banded system of nonlinear algebraic equations which is solved by a penta-diagonal algorithm. The algorithm is validated through a single soliton simulation. The first four conservation laws are computed for simulations using a single soliton. In further numerial experiments forced boundary conditions $u = U_0$ are applied at the end $x = 0$ and the generated states of solitary waves are studied. The solitary waves generated by these various forcing functions posses many of the attributes of free solitons.

Chapter 2

A short review of solutions of the Korteweg-de Vries and Modified Korteweg-de Vries equations

2.1 Physical Review

In this present chapter, we will study the KdV and $MKdV$ equations. At the present time many scientists are interested in nonlinear wave motion, which can be observed in many branches of applied mathematics, physics, and engineering.

At present one of the most important nonlinear wave equations is the Korteweg-de Vries equation (KdV) and also the modified Korteweg-de Vries equation ($MKdV$). The KdV equation was originally derived in 1895 by Korteweg and de Vries [44] to describe the behaviour of one dimensional shallow water waves with small but finite amplitude. In many problems, investigations have shown that the effect of nonlinear terms in the partial differential equations can act such as to counterbalance the effect of dispersion, and the balance of dispersion and nonlinearity in the equation resuls in a stable solitary wave solution called a soliton. A soliton has the following remarkable properties.

i-) In a collision with another soliton it preserves its original shape and speed, although a phase shift may exist after the collision.

ii-) A general initial profile after a long time breaks up into a train of solitons together with a disturbance which disperses with time.

Comments about the solitary wave were first made by John Scott Russell [62], who it is reported, saw a heap of water, caused from the prow of a stopped barge, continue upon its course along the channel without a change in its shape and diminution in its speed. Further investigations to verify this phenomenon were made by Airy [7], Stokes [73], Boussinesq [10] and Rayleigh [59] in the following 60 years after Russell. All those notions of solitary waves raised by authors were confirmed by Korteweg and de-Vries's study [44].

Recently the KdV equation has been derived by Vliegenthart [80] for shallow water waves. The KdV equation for long waves in shallow water may be written as

$$\eta_t + \sqrt{gh_0}[1 + \frac{3}{2}(\eta/h_0)]\eta_x + \frac{1}{6}\sqrt{gh_0}h_0^2\eta_{xxx} = 0 \tag{2.1}$$

where x denotes the coordinate along the horizontal bottom, t the time, $\eta(x,t)$ the local wave-height above the undisturbed depth h_0, and g the acceleration of gravity and the subcripts x and t denote differentiation.

The non-dimensional parameters ϵ and μ are defined by

$$\epsilon = \frac{a}{h_0}, \qquad \mu = \frac{1}{6}(\frac{h_0}{\lambda_0})^2$$

where a and λ_0 denote the dominant amplitude and wavelength. We introduce the dimensionless variables

$$\bar{\xi} = x/\lambda_0, \quad \bar{t} = t\sqrt{gh_0}/\lambda_0, \quad \bar{\eta} = \frac{3}{2}\eta(\epsilon h_0).$$

Subsititution of these new variables into equation(2.1) and omitting the bars gives the equation

$$\eta_t + \eta_\xi + \epsilon\eta\eta_\xi + \mu\eta_{\xi\xi\xi} = 0. \tag{2.2}$$

Let us define $\eta = u$ and the new independent variable x, as $x = \xi - t$, then equation (2.2) is transformed into the Korteweg-de Vries (KdV) equation

$$U_t + \epsilon UU_x + \mu U_{xxx} = 0 \tag{2.3}$$

A generalized Korteweg-de Vries equation is given by,[51, 53, 20]

$$U_t + \epsilon U^p U_x + \mu U_{xxx} = 0, \qquad \text{p=1,2,}\cdots \tag{2.4}$$

The most important case after p=1, is p=2, when the resulting equation has the form

$$U_t + \epsilon U^2 U_x + \mu U_{xxx} = 0, \tag{2.5}$$

and is known as the modified Korteweg-de Vries ($MKdV$) equation. Moreover, the sign of the nonlinear term may be changed to obtain the non-trivial alternative equation:

$$U_t - \epsilon U^2 U_x + \mu U_{xxx} = 0, \tag{2.6}$$

The soliton solutions of the $MKdV^-$ equation are distinct from those of the $MKdV^+$ equation and cannot be derived from them, also $MKdV^-$ equation's solitons moves to the left on the axes, but $MKdV^+$ equation's solitons moves to the right.

Note that changing the sign of the nonlinear term in the KdV equation itself yields nothing new since the resulting equation is reduced to (2.3) by changing the sign of U [51].

A most interesting feature is that KdV equation can be solved analytically in some circumstances. The travelling wave solution of the KdV equation is found, by using the following transformations.

$$U(x,t) = U(X), \qquad X = x - ct \tag{2.7}$$

where c represents the constant velocity of wave travelling in the positive direction of the x-axis. Substitution of (2.7) into (2.4) leads to the ordinary differential equation

$$-cU' + \epsilon U^p U' + \mu U''' = 0, \tag{2.8}$$

where a prime denotes differentiation with respect to x. It can be solved by known solution techniques as

$$U^p(x,t) = \frac{c(p+1)(p+2)}{2\epsilon}\mathrm{sech}^2[\frac{p}{2}\sqrt{\frac{c}{\mu}}(x - ct - x_0)] \tag{2.9}$$

For p=1 we have the solution

$$U(x,t) = \frac{3c}{\epsilon}\mathrm{sech}^2[\frac{1}{2}\sqrt{\frac{c}{\mu}}(x - ct - x_0)] \tag{2.10}$$

Equation (2.10) describes a soliton with amplitude $\frac{3c}{\epsilon}$ which is proportional to its velocity. A larger soliton moves faster than a smaller one. The soliton's width is proportional to $\sqrt{\frac{\mu}{c}}$ and the constant x_0 plays the role of a phase shift. If the coefficient of the nonlinear term in equation (2.4) has a negative sign and p is odd then the solution is negative, that is:

$$U^p(x,t) = -\frac{c(p+1)(p+2)}{2\epsilon}\mathrm{sech}^2[\frac{p}{2}\sqrt{\frac{c}{\mu}}(x - ct - x_0)] \tag{2.11}$$

if p is even, the solution is a not a solitary wave. When $p = 2$, in equation (2.4), the equation is known as the modified KdV equation. When $p = 3$, in equation (2.4), the equation is a strongly nonlinear KdV equation;

$$U_t + \epsilon U^3 U_x + \mu U_{xxx} = 0, \tag{2.12}$$

Chen [14] has used Galerkin's method to obtain its analytic solution.

Another way of getting a single soliton solution of the KdV equation is to use the linear Bargman method [47], based on the assumption that there exists a potential for the Schrodinger equation

$$(k^2 - u)y + y'' = 0, \tag{2.13}$$

where k^2 is an eigenvalue parameter which remains constant as t varies and u satisfies the KdV equation. An interesting property of the KdV- equation is the interaction of solitons. It has been shown that taller waves have faster speeds than smaller ones.

2.1.1 Interaction of two solitons

Consider two solitons initially placed on the real line with the taller one to the left of the shorter one. When time increases the greater speed of the taller soliton means that it eventually catches up with the shorter one and they undergo a nonlinear interaction according to the KdV equation. They emerge from the interaction completely preserved in shape and speed, as if no interaction has taken place. This was first observed experimentally by Russel [62] and numerically by Zabusky and Kruskal [88]. Zabusky [85] showed the exact interaction of two solitons numerically and Lax [48] gave the analytic proof of the soliton properties. Lamb [47], Dodd [18], Wadati [81] and Whitham [84] have drived an analytic solution for the KdV equation, they used $\epsilon = 6.0, \mu = 1.0$, when the initial condition for the two soliton solution is given by

$$U(x,t) = 2(\ln(F))_{xx} \tag{2.14}$$

where

$$
\begin{aligned}
&F = 1 + \exp(\eta_1) + \exp(\eta_2) + \beta \exp(\eta_1 + \eta_2) \\
&\beta = [\tfrac{\alpha_1 - \alpha_2}{\alpha_1 + \alpha_2}]^2 \\
&\eta_i = \alpha_i x - \alpha_i^3 t + d_i, \qquad \text{i=1,2}
\end{aligned}
\tag{2.15}
$$

Similarly the exact solution of the $MKdV$ equation with $\epsilon = 6.0, \mu = 1.0$ for the two soliton case has been found by Taha and Ablowitz [75] as

$$
U(x,t) = i(\ln(f^*/f))_{xx} \tag{2.16}
$$

where $*$ denotes a complex conjugate, and

$$
\begin{aligned}
&f = 1 + i\exp(\eta_1) + i\exp(\eta_2) - \beta \exp(\eta_1 + \eta_2) \\
&\beta = [\tfrac{\alpha_1 - \alpha_2}{\alpha_1 + \alpha_2}]^2 \\
&\eta_i = \alpha_i x - \alpha_i^3 t + d_i, \qquad \text{i=1,2.}
\end{aligned}
\tag{2.17}
$$

For the case of N-solitons, an analytic proof that they are unchanged after interaction has been given by using the inverse scattering method [51]. This method generates the well known N-soliton solutions possessing the property that amplitudes and velocities, as well as the shapes, are preserved.

More generally, arbitrary initial conditions used with the KdV equation will evolve into a number of solitons moving off to the right and an oscillatory dispersing state moving off to the left. Because of the dependence of the soliton speed on its amplitude, the solitons will sort themselves out, eventually ending up as a parade of solitons moving to the right with monotonically increasing amplitudes from left to the right. Those solutions involving only solitons, and showing no oscilatory behaviour, are called pure soliton solutions or N-soliton solutions [52]. A new applications of the KdV-equation, given by Gardner and Morikawa [34], was discovered in the study of collision-free hydromagnetic waves. The existence and uniqueness of solitary wave solutions for certain types of initial condition have been dealt with by Sjoberg [70], Lax [48] and Gardner [21].

2.2 Conservation laws for the KdV and $MKdV$ equations

Partial differential equations possess an infinite number of conservation laws. An important state in the development of the general method of solution for the KdV equation is that solutions obey an infinite number of independent conservation laws. Definition[2, pages 21–22]: For the partial differential equation

$$u(x,t,u(x,t)) = 0, \tag{2.18}$$

where $x \in R, t \in R$ (real numbers) are temporal and spatial variables and $u(x,t) \in R$ the dependent variable, a conservation law is an equation of the form

$$\frac{\partial}{\partial t}T_i + \frac{\partial}{\partial x}X_i = 0 \tag{2.19}$$

which is satisfied for all solutions of the equations. Where $T_i(x,t)$ the conserved density, and $X_i(x,t)$, the associated flux, which are, in general, functions of x, t, u and the partial derivatives of u; $\frac{\partial}{\partial t}$ denotes the partial derivative with respect to t; and $\frac{\partial}{\partial x}$ the partial derivative with respect to x.

If additionally, u tends to zero as $|x| \to \infty$ sufficiently rapidly,

$$\frac{\partial}{\partial t}\int_{-\infty}^{\infty} T_i(x,y) = 0. \tag{2.20}$$

Therefore

$$\int_{-\infty}^{\infty} T_i(x,y) = b, \tag{2.21}$$

where b, a constant, is the conserved density.

For the KdV equation, the first three conservation laws are:

$$\begin{aligned}
&\underbrace{u_t}_{T_i}+\underbrace{(\epsilon\frac{u^2}{2}+\mu u_{xx})_x}_{X_i}=0\\
&\underbrace{(\frac{u^2}{2})_t}_{T_i}+\underbrace{[\epsilon\frac{u^3}{3}+\mu(uu_{xx}-\frac{u^2}{2}x)]_x}_{X_i}=0\\
&\underbrace{(\frac{u^3}{3}-\frac{\mu}{\epsilon}u_x^2)_t}_{T_i}+\underbrace{[\epsilon\frac{u^4}{4}+\mu(u^2u_{xx}+\frac{2}{\epsilon}u_tu_x)+\frac{\mu^2}{\epsilon}u_{xx}]_x}_{X_i}=0.
\end{aligned} \tag{2.22}$$

The first of these is just the KdV-equation itself and corresponds to conservation of momentum. Multiplying equation (2.3) by u and integrating leads to the second conservation law, which is known as the conservation of energy. The third was discovered by Whitham [84]. The fourth and fifth conservation laws were found by Kruskal and Zabuska [89]. Finally Miura and his collaborators[52] developed an ingenious method of generating a whole sequence of conservation laws. The first four conserved quantities can be written as:

$$\begin{aligned}
I_1 &= \textstyle\int_{-\infty}^{\infty} u dx\\
I_2 &= \textstyle\int_{-\infty}^{\infty} u^2 dx\\
I_3 &= \textstyle\int_{-\infty}^{\infty}[u^3-\frac{3}{\epsilon}\mu u_x^2]dx\\
I_4 &= \textstyle\int_{-\infty}^{\infty}[u^4-\frac{12}{\epsilon}\mu u u_x^2+\frac{36}{5\epsilon^2}\mu^2u_{xx}^2]dx.
\end{aligned} \tag{2.23}$$

For the modified Korteweg-de Vries equation (2,5) there are also many polynomial conservation laws. Miura [52], Miura, Gardner and Kruskal [54] have found the first four conservative quantities, which can be written as:

$$\begin{aligned}
I_1 &= \textstyle\int_{-\infty}^{\infty} u dx\\
I_2 &= \textstyle\int_{-\infty}^{\infty} u^2 dx\\
I_3 &= \textstyle\int_{-\infty}^{\infty}[u^4-\frac{6}{\epsilon}\mu u_x^2]dx\\
I_4 &= \textstyle\int_{-\infty}^{\infty}[u^6-\frac{30}{\epsilon}\mu u^2u_x^2+\frac{18}{\epsilon^2}\mu^2u_{xx}^2]dx.
\end{aligned} \tag{2.24}$$

For $p>2$ there are only three conservation laws. Zabusky [85]-[86], Miura

[52] and Fornberg-Whitham [20] have found the first three conservative quantities, which can be written as:

$$
\begin{aligned}
I_1 &= \textstyle\int_{-\infty}^{\infty} u\,dx \\
I_2 &= \textstyle\int_{-\infty}^{\infty} u^2\,dx \\
I_3 &= \textstyle\int_{-\infty}^{\infty} (u^{p+2} - \frac{(p+1)(p+2)}{2\epsilon}\mu u_x^2)\,dx
\end{aligned}
\tag{2.25}
$$

Chapter 3

A short review of Numerical Methods for solving the KdV and Modified KdV equations

3.1 Numerical Methods for solving the KdV and $MKdV$ Equations

In this chapter we shall study numerical methods for the solution of partial differential equations. Improvements in numerical techniques, together with the rapid advance in computer technology allow many of the partial differential equations arising from Engineering and Scientific applications to be solved. We shall focus our attention on making a survey of the numerical methods used for solving the Korteweg-de Vries equation

$$U_t + \epsilon U U_x + \mu U_{xxx} = 0 \tag{3.1}$$

and the modified Korteweg-de Vries equation

$$U_t + \epsilon U^2 U_x + \mu U_{xxx} = 0 \tag{3.2}$$

where; ϵ and μ are positive parameters, U_t first derivative of U with respect to time, U_x and U_{xxx} are the first and third derivatives of U with respect to space. The focus will be given to make a brief survey of numerical methods. Numerical solutions will be examined under 4 headings,

i-) Finite difference methods,

ii-) Finite Fourier transform or pseudospectral methods,

iii-) Fourier expansion methods, and

iv-) Finite element methods.

In the finite difference approximation of a differential equation, the derivatives in the equations are replaced by difference quotients which involve the values of the solution at discrete mesh points of the domain. First, Zabusky and Kruskal [88] have used an explicit difference element method to solve the KdV equation. Their study is interesting due to the discovery of properties of the solitary waves, such as, interaction of two solitary waves and also they saw that a bigger soliton travels faster than smaller one, after time evolves, the large soliton overtakes the smaller soliton. In their method, both time and space steps are kept small to provide a reasonable and accurate result. Goda [38] and the Hopscotch method [39] solve the KdV equation using implicit finite difference schemes, which were suggested to provide consistent and accurate solutions. Chu, [15] used a finite difference method to study the generation of solitary wave solutions of the KdV equation, by the boundary forcing; and they applied a trapezoidal boundary forcing. Also Camassa and Wu [11] re-studied the different forms of the boundary forcing for solving KdV equation. Taha and Ablowitz [74] studied a local difference scheme, which is based on the inverse scattering transform. A comprehensive discussion and comparison has been done to explain the benefits of using the Taha scheme [74].

The other methods are based upon the finite Fourier transform. In this method the unknown function $U(x,t)$ is transformed into Fourier space with respect to x. The resulting equation is combined with one of the finite difference schemes to obtain the recurrence relationship at the knots. There are two important schemes, the split step Fourier method of Tappert [76] and the pseudospectral method of Fornberg and Whitham [20]. In the Fourier expansion method, the unknown function is expanded in terms of a Fourier series and the original partial differential equation is reduced to a set of ordinary differential equations with Fourier coefficients. Abe and Inoue [1] used the Runge-Kutta-Gill method for solving the set of differential equations. There are other Fourier expansion schemes due to Gazdag [37] and a Taylor Fourier expansion method proposed by Canosa and Gazdag [12].

The last method, the finite element method; this method is the subdivision of the given domain into a finite number of subregions. This process is called discretization of the domain, each subregion is called an element, and the collection of elements is called the finite element mesh. First labeling of the elements and the nodes, which is simple but it has a big influence on the computational efficiency of the algorithm. Next step is to decide on the nature of the interpolation polynomials to be use. Evaluate the element equations by constructing a suitable weighted residual formula of the given differential equation. Then assemble the element contributions to obtain the equation for the whole problem, impose the boundary conditions of the problem and solve the overall sysytem of equations. The first use of the finite element method was due to Wahlbin [82], who employed the same trial and test functions in this dissipative Galerkin method. Smoothed splines are used as basis functions. Alexander and Morris [4] implemented the numerical scheme for the above Galerkin method, in which trial and test functions were cubic splines. There are advantages with smaller errors for the same mesh if compared with some previous result. Sanz-Serna and Christie [63] presented the a modified Petrov-Galerkin method with piecewise linear trial and cubic spline test functions.

Also Schoombie [72] repeated the above method using linear functions as trial functions and B-splines of various order as test functions. F.D. and A.Van Niekerk [78] proposed a Hermite rational approximation for the KdV equation. Hermite rational basis functions are constructed as trial functions in a Petrov-Galerkin method. Their scheme compares favourably with the methods considered earlier. It has been emphasised that this method gives a consistent numerical system that has better approximation abilities than most other existing numerical methods due to the influence of the rational function. Later, Gardner and his collaborators [5, 22, 24, 6, 17, 31] have set up five finite elements methods to the KdV and $MKdV$ equations using

i-) cubic Hermite polynomials

ii-) cubic spline,

iii-) quadratic spline,

iv) quintic spline,

v) quartic spline

The first three of them are based on the Galerkin method with the same test and shape functions which are cubic Hermite functions, cubic B-splines and quadratic B-splines, respectively. The last two are the spline collocation method, which used quintic B-splines as shape functions and quartic B-splines as shape function. Except for the scheme of Niekerk, which came out at the same time as Gardner's scheme, comparison is made with the best of earlier schemes, based on accuracy and efficency for a single soliton solution and the interaction of two solitons. One infers from their results that their schemes are easily applicable, faster and more accurate and efficient, L_2- error norms and L_∞-norms are smaller, conserved densities are satisfactorily constant. From their discussion, they further concluded that the collocation method with quintic splines as shape functions and quartic splines as shape functions produces the most efficent and accurate solution of the KdV and $MKdV$ equations. All the classical problems including soliton motion, interaction, dissipation for an arbitrary initial condition are used to validate the method. It has been shown that it is adequate to solve the KdV and $MKdV$ equations using the B-splines finite element method.

3.2 A Short Review of the Spline functions

Many scientists are using the approximation methods in many areas of Mathematics, as well as Physics, Chemistry, etc. These methods are dominant tools for modelling and analysing many physical and social events. They used two types of approximation problem. First, approximate unknown functions based on given data, which is called data fitting problems. The second type of approximation emerges from the mathematical model for various physical problems, which are represented by an operator equation. The solutions of the operator equation are sought numerically. Examples include boundary value problems for ordinary and partial differential equations, eigenvalue-eigenvector problems, integro-differential equations and so on. In both models, two important processes arise to find the best approximation:

i-) choose a reasonable class of functions satisfying the approximation conditions,

ii-) a good selection of the scheme for the approximation method is required to make the approach effective.

In numerical analysis, many scientists have concentrated on using polynomials as approximation functions, which possess attractive features. In order to get a good approximation to problems by polynomials, it may be necessary to use a large number of points (or functions). Unfortunately, high degree polynomials can have large oscillatory behaviour which do not represent smooth and desirable approximation so that computational problems arise in approximation when the number of data (functions) is large. The difficulty of these problems can be overcome by using piecewise polynomials.

Piecewise polynomials are suitable for use as an approximation except for discontinuities within the domain. A special class of piecewise polynomials called "spline", can be mentioned. The terminology of spline-functions was first introduced by Schoenberg [71], in fact, there were a number of papers dealing with splines without using the name. Schoenberg used spline terminology due to the resemblance with a mechanical device called a "spline". A spline consists of a strip or a thin rod of some flexible materials designed to attach some weights so that it can be forced to pass through described points. The device is used by draftsmen to draw a smooth curve by adjusting weights at the requested points. Such a graph of the spline is similar to a shape defined by spline functions.

3.2.1 Definition of the Spline function

Let x_i be a strictly increasing sequence of real numbers,

$$-\infty = x_0 < x_1 < \ldots < x_n = x_{n+1} = \infty.$$

A spline function f(x), degree m with knots $x_i, i = 1, \ldots, n$ is a function described on the real line, having the following two properties [3]:

i-) f(x) is some polynomial of degree m or less in every interval (x_i, x_{i+1}), i=0, ..., n where $x_0 = -\infty, x_{n+1} = \infty$,

ii-) f(x) and its derivative of order $1, 2, \ldots, m-1$ are continuous everywhere.

Thus, piecewise polynomials and their derivatives, which comply with some continuity conditions, are called spline functions. According to the above definitions, when m=0 the second condition is not invoked, so that a spline of degree 0 is a step function. A spline of degree 1 is a polygon.

3.2.2 The Usefulness of Spline Functions

Generally, the useful features of splines are concisely gathered [69, 3] as

i-) they constitute the finite-dimensional linear space with convenient bases,

ii-) they are smooth functions,

iii-) the derivatives and anti derivatives of them are also spline functions,

iv-) they are appropriate for computational calculations in terms of manipulation, evaluation, storage on digital computers,

v-) various matrices arising, with the use of spline functions, form the pattern of easy calculations in the approximation due to convenient sign and determinantal properties,

vi-) low degree splines are remarkably flexible. That is, they do not exhibit sharp oscillations,

vii-) the obtained structure at the end of the process of approximation is related to the structure of the polynomial, such as signs and coefficients,

viii-)it is easy to study the convergence and stability of the approximation method when the splines are used,

ix-) functions and their derivatives are simultaneously approximated.

3.2.3 Special spline fuctions

Let $a = x_0 < x_1 < \ldots < x_n = b$ be a partition of [a, b] and $h = \frac{b-a}{n}, x_i = x_{i-1} + h, i = 1, \ldots, n$. The value of a function at these points are given as $g(x_0), g(x_1), \ldots, g(x_n)$ and a set of m-times continuously differentiable functions are denoted as $C^m[a, b]$.

Quadratic splines

$f(x)$ is a quadratic spline function if the following three conditions are satisfied:

i-) $f(x) \in C^1[a,b]$,

ii-) $f(x_j) = g(x_j), 0 \leq j \leq n$,

iii-) $f(x)$ is a piecewise quadratic polynomial for every $[x_j, x_{j+1}]$.

Cubic splines

$f(x)$ is a cubic spline function if the following three conditions are satisfied

i-) $f(x) \in C^2[a,b]$,

ii-) $f(x_j) = g(x_j), 0 \leq j \leq n$,

iii-) $f(x)$ is a piecewise cubic polynomial for every $[x_j, x_{j+1}]$.

3.3 The B-spline Finite Elements

3.3.1 The Linear B-spline Element

The linear B-spline L_m is given by the equations [57]

$$L_m = \frac{1}{h}\begin{cases} (x_{m+1}-x)-2(x_m-x), & [x_{m-1}-x_m] \\ (x_{m+1}-x), & [x_m-x_{m+1}] \\ 0 & \text{otherwise.} \end{cases} \tag{3.3}$$

where $h = (x_{m+1} - x_m)$ for all m. The spline vanishes outside the interval $[x_{m-1}, x_{m+1}]$. Discussing only the interval elements, we see, from equation (3.3), that each spline L_m covers 2 intervals $x_{m-1} \leq x \leq x_{m+1}$ so that 2 splines L_m, L_{m+1} cover each finite element $[x_m, x_{m+1}]$, all other splines are zero in this region.

Defining a local coordinate system for the finite element $[x_m, x_{m+1}]$ by $h\xi = x - x_m, 0 \leq \xi \leq 1$, we obtain expressions for the splines that are independent of the element's position.

$$\mathbf{L^e} = (L_m, L_{m+1}) = (1-\xi, \xi). \tag{3.4}$$

The variation of a function U over the elément $[x_m, x_{m+1}]$, is

$$U = \mathbf{L^e}.\mathbf{d^e} = (1-\xi,\xi)(\delta_m,\delta_{m+1})^T$$

The quantities $\mathbf{d^e} = (\delta_m, \delta_{m+1})^T$ act as element parameters with the element trial functions $\mathbf{L^e} = (L_m, L_{m+1})$. The nodal value U_i at the knot $x = x_m$, is given in terms of the parameters δ_i by

$$U_m = \delta_m$$

thus for linear B-spline elements the nodal values of the function $U(x,t)$ and the parameters δ_i are identical. The trial functions given by equation (3.4) are the familiar linear shape functions and lead to the familiar finite element description using linear elements [90].

We shall see that for the higher order B-spline finite elements the relationship between the parameters δ_i and the nodal values [22, 23, 24, 33, 26], although simple, leads to a description different from that obtained when the more familiar Hermite and Lagrangian finite elements are used [35, 90].

3.3.2 The Quadratic B-spline Element

Each Quadratic B-spline Q_m [57] covers 3 intervals $x_{m-1} \le x \le x_{m+2}$ so that 3 splines Q_{m-1}, Q_m, Q_{m+1} cover each finite element $[x_m, x_{m+1}]$, all other splines are zero in this region.

$$Q_i(x) = \frac{1}{h^2}\begin{cases} (x_{i+3}-x)^2 - 3(x_{i+2}-x)^2 + 3(x_{i+1}-x)^2 & [x_{i-1}, x_i] \\ (x_{i+3}-x)^2 - 3(x_{i+2}-x)^2 & [x_i, x_{i+1}] \\ (x_{i+3}-x)^2 & [x_{i+1}, x_{i+2}] \\ 0 & \text{otherwise.} \end{cases} \quad (3.5)$$

Using a local coordinate system for the finite element $[x_m, x_{m+1}]$, $h\xi = x - x_m$, $0 \le \xi \le 1$, we obtain for the trial functions expressions that are independent of the elements position [24]

$$Q^e = (Q_{m-1}, Q_m, Q_{m+1})(1-2\xi+\xi^2, 1+2\xi-2\xi^2, \xi^2)$$

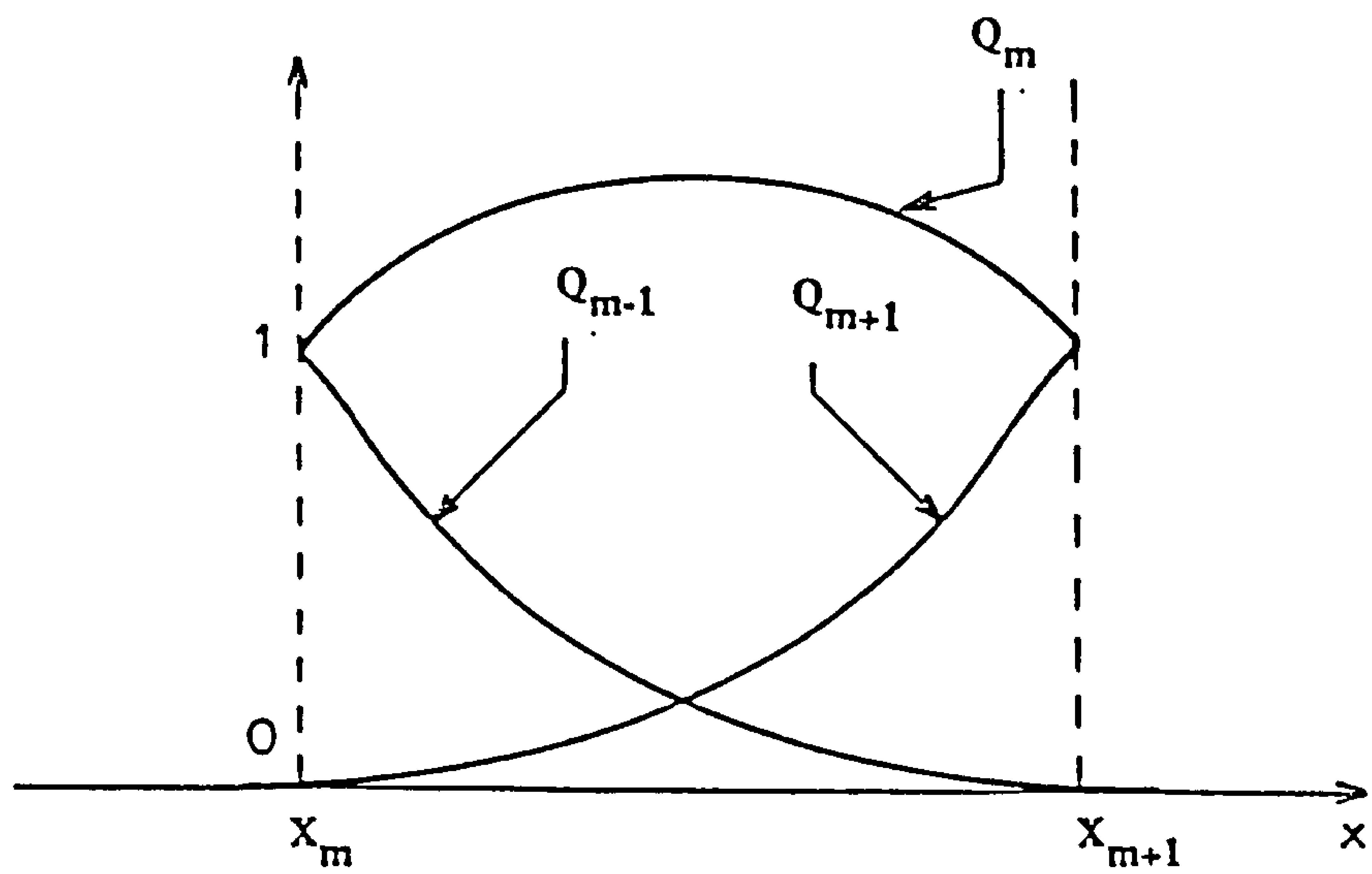

Figure 3.1: The trial functions Q_{m-1}, Q_m, Q_{m+1} for the quadratic B-spline element $[x_m, x_{m+1}]$.

It is the representation of quadratic B-splines that is most appropriate for the finite element approach. These trial functions which are the same for every element are graphed in figure(3.1) [24].

The variation of a function U over the element $[x_m, x_{m+1}]$, is found from[24]

$$
\begin{aligned}
U = Q_{m-1}\delta_{m-1} + Q_m\delta_m + Q_{m+1}\delta_{m+1} &= \mathbf{Q}^{\mathbf{e}}.\mathbf{d}^{\mathbf{e}} \\
&= (1 - 2\xi + \xi^2, 1 + 2\xi - 2\xi^2, \xi^2).\mathbf{d}^{\mathbf{e}}
\end{aligned}
\tag{3.6}
$$

The quantities $\mathbf{d}^{\mathbf{e}} = (\delta_{m-1}, \delta_m, \delta_{m+1})^T$ act as element parameters with the element trial functions $\mathbf{Q}^{\mathbf{e}} = (Q_{m-1}, Q_m, Q_{m+1})$.

The nodal values U_i, U_i', at the knot $x = x_m$, are given in terms of the parameters δ_i by

$$
\begin{aligned}
U_m &= \delta_m + \delta_{m-1} \\
U_m' &= \tfrac{2}{h}(\delta_m - \delta_{m-1})
\end{aligned}
\tag{3.7}
$$

Quadratic B-spline finite elements have the same nodal parameters U_m, U_m', as arise with cubic hermite elements and so have similar continuity properties.

These elements therefore have superior continuity properties to quadratic polynomial elements

The region $[a, b]$ is partitioned into uniformly sized intervals by knots x_i such that $a = x_0 < x_1 < \ldots < x_N = b$ so that from (3.6) the splines $(Q_{-1}, Q_0, Q_1, \ldots, Q_N)$ from a basis for functions defined over $[a, b]$. The global approximation $U_N(x,t)$, to the function $U(x,t)$, which uses these splines as trial functions, is [57]

$$U_N(x,t) = \sum_{j=-1}^{N} Q_j(x)\delta_j(t), \tag{3.8}$$

where the δ_j are time dependent parameters.

To express a function $U(x)$in the form (3.8) the appropriate vector $\mathbf{d}$ representing that function is determined by requiring $U_N(x)$ to satisfy the conditions:

(a) it should agree with the function $U(x)$ at the knots $x_0, \ldots, x_N$; leading to N+1 conditions.

(b) the first derivatives should agree at x_0 $U_N'(x_0) = U'(x_0)$: a further condition. This leads to the matrix equation

$$\mathbf{Md} = \mathbf{b} \tag{3.9}$$

where $\mathbf{M}$ is a matrix

$$\mathbf{d} = (\delta_{-1},\ \delta_0,\ \ldots,\ \delta_N)^T,$$

and

$$\mathbf{b} = (hU'(x_0), U(x_0), U(x_1), \ldots, U(x_N))^T.$$

These equations are easily solved recursively and if we write $U_j = U(x_j)$ then

$$\begin{aligned} \delta_{-1} &= \tfrac{2U_0 + hU_0'}{4}, \\ \delta_0 &= \tfrac{2U_0 - hU_0'}{4}, \end{aligned}$$

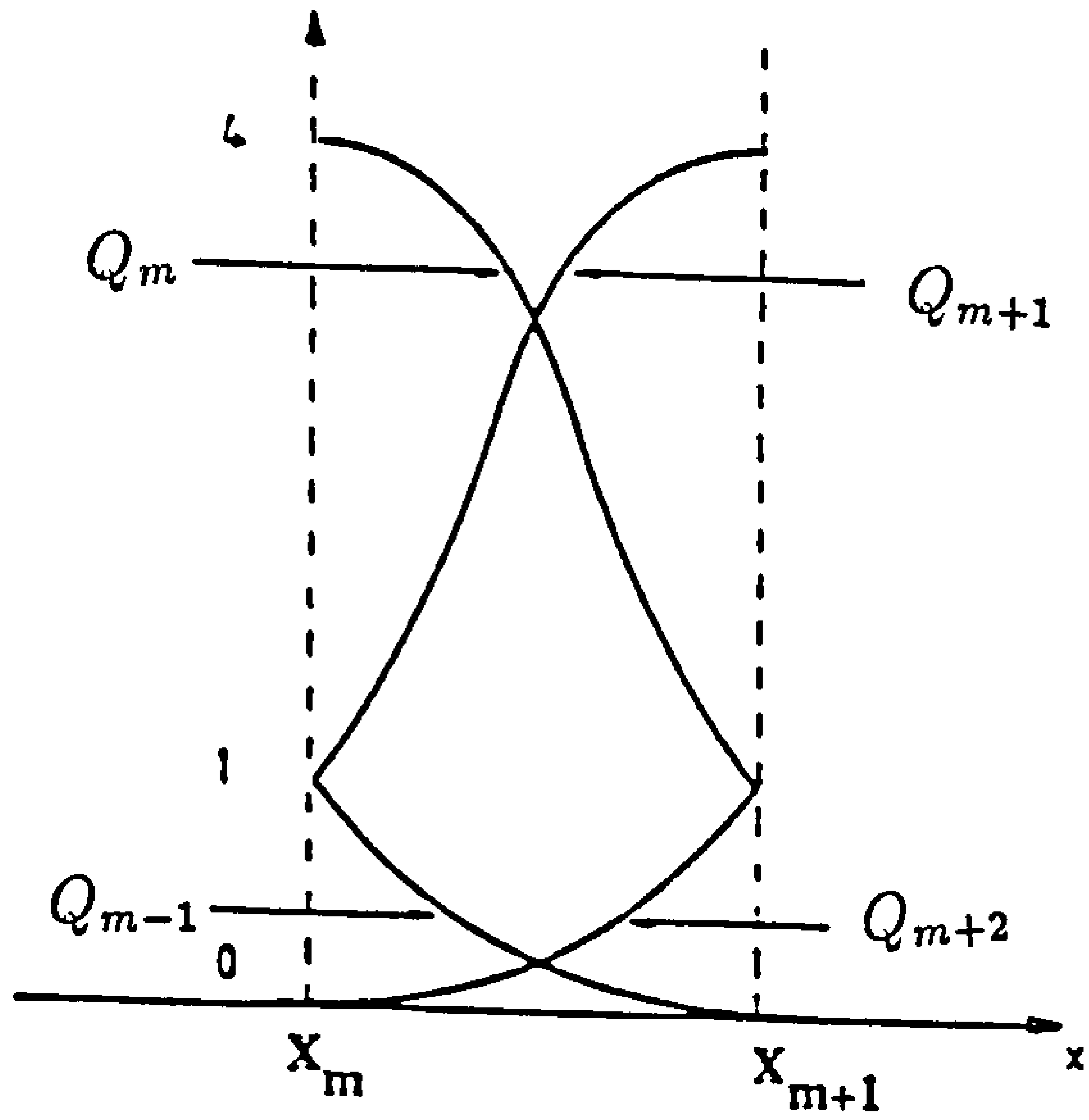

Figure 3.2: The trial functions $Q_{m-1}, Q_m, Q_{m+1}, Q_{m+2}$ for the cubic B-spline element $[x_m, x_{m+1}]$.

and $\delta_j = U_j - \delta_{j-1}$ for $j = 1, \ldots, N$.

The vector $\mathbf{d}$ is thus determined and we have expressed $U(x)$ in the form (3.8).

3.3.3 The Cubic B-spline Element

Each cubic B-spline [57] is non-zero over 4 adjacent elements so that 4 cubic B-splines $Q_{m-1}, Q_m, Q_{m+1}, Q_{m+2}$ cover each finite elements .

$$Q_m(x) = \frac{1}{h^3}\begin{cases} (x_{m+4}-x)^3 - 4(x_{m+3}-x)^3 + 6(x_{m+2}-x)^3 - 4(x_{m+1}-x)^3 & [x_{m-2}, x_{m-1}] \\ (x_{m+4}-x)^3 - 4(x_{m+3}-x)^3 + 6(x_{m+2}-x)^3 & [x_{m-1}, x_m] \\ (x_{m+4}-x)^2 - 4(x_{m+3}-x)^2 & [x_m, x_{m+1}] \\ (x_{m+4}-x)^2 & [x_{m+1}, x_{m+2}] \\ 0 & \text{otherwise.} \end{cases}$$

In terms of a local coordinate system ξ given by $h\xi = x - x_m$, where $0 \leq \xi \leq 1$, expressions for variation of the cubic B-splines $Q_{m-1}, Q_m, Q_{m+1}, Q_{m+2}$ covering the element $[x_m, x_{m+1}]$ and graphed in figure (3.2) [33] can be expressed independently of the actual element coordinates as [33, 36]

$$\mathbf{Q^e} = (1 - 3\xi + 3\xi^2 - \xi^3, 4 - 6\xi^2 + 3\xi^3, 1 + 3\xi + 3\xi^2 - 3\xi^3, \xi^3)^T$$

over the element $[x_m, x_{m+1}]$ the expression for a function U is

$$U^e = \sum_{j=m-1}^{m+2} Q_j \delta_j = \mathbf{Q^e}.\mathbf{d^e},$$

where the δ_j are element free parameters and only the cubic B-splines $\mathbf{Q^e} = (Q_{m-1}, Q_m, Q_{m+1}, Q_{m+2})^T$ are non-zero over this finite element. The splines act as basis functions for the element.

The values of U_m, U'_m, U''_m, at the knot $x = x_m$, are given in terms of the δ_m by [22]

$$\begin{aligned} U_m &= \delta_{m+1} + 4\delta + \delta_{m-1}, \\ hU'_m &= 3(\delta_{m+1} - \delta_{m-1}), \\ h^2 U''_m &= 6(\delta_{m+1} - 2\delta_m + \delta_{m-1}). \end{aligned} \tag{3.10}$$

The region $a = x_0 < x_1 < \ldots < x_N = b$ has been partitioned by equally spaced knots x_i and $Q_i(x)$ are those cubic B-splines with knots at the points x_i. Then the set of functions $Q_{-1}, Q_0, \ldots, Q_N, Q_{N+1}$ forms a basis for functions defined over $[a, b]$. The global approximation $U_N(x,t)$ to the function $U(x,t)$ which uses these splines as trial functions is [57]

$$U_N(x,t) = \sum_{m=-1}^{N+1} Q_m(x)\delta_m(t), \tag{3.11}$$

where the δ_m are time dependent quantities to be determined from the boundary and interpolation conditions.

The vector $\mathbf{d}$ representing the function $U(x)$ can be found from (3.11) by requiring the approximation $U_N(x)$ to satisfy the following constraints;

(a) it shall agree with the function $U(x)$ at the knots $x_0, \ldots, x_N$; leading to $N + 1$ conditions.

(b) derivative boundary conditions are applied at each end. This leads to the matrix equation of the form

$$\mathbf{Md} = \mathbf{b}$$

where $\mathbf{M}$ is a matrix

$$\mathbf{d} = (\delta_{-1}, \delta_0, \delta_1, \ldots, \delta_{N+1})^T,$$

and

$$\mathbf{b} = (hU'(x_0), U(x_0), U(x_1), \ldots, U(x_N), hU'(x_N))^T.$$

This matrix equation can be solved efficently by the Thomas algorithm to give the vector $\mathbf{d}$. When using the method of Collocation, with the collocation points identified with the element nodes, the cubic B-spline interpolation functions can be used with partial differential equations containing derivatives up to order 2 and the values at the collocation points are given by Equation (3.10)-(3.11).

3.3.4 The Quartic B-spline Element

Each quartic B-spline covers 5 elements thus each element $[x_m, x_{m+1}]$ is covered by 5 splines. Using a local coordinate system ξ given by $h\xi = x - x_m$, where $0 \leq \xi \leq 1$, enables the expressions for the element splines to be expressed independently of the actual element coordinates as and graphed in figure (3.3). Over the element $[x_m, x_{m+1}]$ the variation of the function $U(x,t)$ is given by

$$\begin{aligned}
Q_{m-2} &= 1 - 4\xi + 6\xi^2 - 4\xi^3 + \xi^4 \\
Q_{m-1} &= 11 - 12\xi - 6\xi^2 + 12\xi^3 - \xi^4 \\
Q_m &= 11 + 12\xi - 6\xi^2 - 12\xi^3 + \xi^4 \\
Q_{m+1} &= 1 + 4\xi + 6\xi^2 + 4\xi^3 - \xi^4 \\
Q_{m+2} &= \xi^4
\end{aligned} \tag{3.12}$$

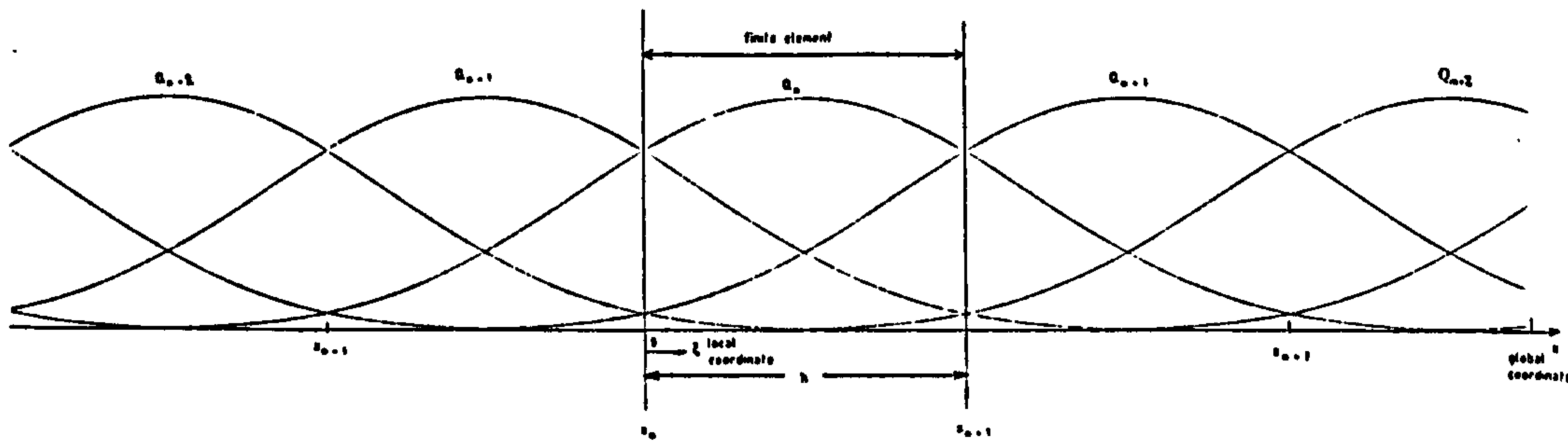

Figure 3.3: The trial functions $Q_{m-2}, Q_{m-1}, Q_m, Q_{m+1}, Q_{m+2}$ for the quartic B-spline element $[x_m, x_{m+1}]$.

$$U(x,t) = \mathrm{Q^e.d^e} = (Q_{m-2}, Q_{m-1}, Q_m, Q_{m+1}, Q_{m+2}).(\delta_{m-2}, \delta_{m-1}, \delta_m, \delta_{m+1}, \delta_{m+2})^T$$

At the knot x_i the numerical solution $U_N(x,t)$ is given by [26, 31]

$$\begin{aligned}
U_m &= \delta_{m+1} + 11\delta_m + 11\delta_{m-1} + \delta_{m-2}, \\
hU'_m &= 4(\delta_{m+1} + 3\delta_m - 3\delta_{m-1} - \delta_{m-2}), \\
h^2U''_m &= 12(\delta_{m+1} - \delta_m - \delta_{m-1} + \delta_{m-2}) \\
h^3U'''_m &= 24(\delta_{m+1} - 3\delta_m + 3\delta_{m-1} - \delta_{m-2}).
\end{aligned} \tag{3.13}$$

When using the method of collocation, with the collocation points identified with the element nodes, the quartic B-spline interpolation functions can be used with partial differential equations containing derivatives up to order 3 and the values at the collocation points are given above.

3.3.5 The Quintic B-spline Element

Each quintic B-spline Q_m covers 6 intervals $x_{m-3} \leq x \leq x_{m+3}$ so that 6 splines $Q_{m-2}, Q_{m-1}, Q_m, Q_{m+1}, Q_{m+2}, Q_{m+3}$ cover each finite element $[x_m, x_{m+1}]$, all other splines are zero in this region.

Using a local coordinate system ξ given by $h\xi = x - x_m$, where $0 \le \xi \le 1$ enables the expressions for the element splines to be expressed independently of the actual element coordinates as [23]

$$\begin{aligned}
Q_{m-2} &= 1 - 5\xi + 10\xi^2 - 10\xi^3 + 5\xi^4 - \xi^5 \\
Q_{m-1} &= 26 - 50\xi + 20\xi^2 + 20\xi^3 - 20\xi^4 + 5\xi^5 \\
Q_m &= 66 - 60\xi^2 + 30\xi^4 - 10\xi^5 \\
Q_{m+1} &= 26 + 50\xi + 20\xi^2 - 20\xi^3 - 20\xi^4 + 10\xi^5 \\
Q_{m+2} &= 1 + 5\xi + 10\xi^2 + 10\xi^3 + 5\xi^4 - 5\xi^5 \\
Q_{m+3} &= \xi^5
\end{aligned} \tag{3.14}$$

Over the element $[x_m, x_{m+1}]$ the variation of the function $U(x,t)$ is given by

$$U(x,t) = \mathbf{Q}^e.\mathbf{d}^e = (Q_{m-2}, Q_{m-1}, Q_m, Q_{m+1}, Q_{m+2}, Q_{m+3}).(\delta_{m-2}, \delta_{m-1}, \delta_m, \delta_{m+1}, \delta_{m+2}, \delta_{m+3})^T$$

At the knot x_i the numerical solution $U_N(x,t)$ is given by [23]

$$\begin{aligned}
U_i &= \delta_{i+2} + 26\delta_{i+1} + 66\delta_i + 26\delta_{i-1} + \delta_{i-2}, \\
hU_i' &= 5(\delta_{i+2} + 10\delta_{i+1} - 10\delta_{i-1} - \delta_{i-2}), \\
h^2U_i'' &= 20(\delta_{i+2} + 2\delta_{i+1} - 6\delta_i + 2\delta_{i-1} + \delta_{i-2}), \\
h^3U_i''' &= 60(\delta_{i+2} - 2\delta_{i+1} + 2\delta_{i-1} - \delta_{i-2}), \\
h^4U_i^{IV} &= 120(\delta_{i+2} - 4\delta_{i+1} + 6\delta_i - 4\delta_{i-1} + \delta_{i-2}).
\end{aligned} \tag{3.15}$$

The function and its first 4 derivatives are continuous across element boundaries. Quintic B-spline finite elements thus have trial functions with continuity of type C^4.

When using the method of collocation, with the collocation points identified with the element nodes, the quintic B-spline interpolation functions can be used with partial differential equations containing derivatives up to order 4. The values at the collocation points are given by Equation (3.15). The use quintic B-splines to approximate the function $U(x,t)$ and $a = x_0 < x_1 < \ldots < x_N = b$ be a partition of $[a,b]$ by the points x_i, and let $Q_i(x)$ be those quintic B-splines with knots at the points x_i. The splines $\{Q_{-2}, Q_{-1}, Q_0, \ldots, Q_N, Q_{N+1}, Q_{N+2}\}$ form a basis for functions defined over $[a, b]$. A global approximation $U_N(x,t)$ to the solution $U(x,t)$ is given by

$$U_N(x,t) = \sum_{i=-2}^{N+2} Q_i(x)\delta_i(t), \tag{3.16}$$

where the δ_i are unknown time dependent parameters.

The vector $\mathbf{d}$ describing the function $U(x)$ can be determined in the following way. The approximation $U_N(x)$ [57] must satisfy the following conditions.

(a) it shall agree with the function $U(x)$ at the knots $x_0, \ldots, x_N$; leading to $N+1$ conditions

(b) the first and second derivatives of the approximation shall agree with those of the exact function at both ends of the range: 4 further conditions.

This leads to the matrix equation of the form

$$\mathbf{Md} = \mathbf{b}$$

where $\mathbf{M}$ is a matrix

$$\mathbf{d} = (\delta_{-2}, \delta_{-1}, \delta_0, \ldots, \delta_{N+2})^T,$$

and

$$\mathbf{b} = (hU'(x_0), h^2U''(x_0), U(x_0), U(x_1), \ldots, U(x_N), hU'(x_N), h^2U''(x_N))^T.$$

The vector $\mathbf{d}$ is determined as the solution of this matrix equation.

3.3.6 The Sextic B-spline Element

Each sextic B-spline covers 7 elements thus each element $[x_m, x_{m+1}]$ is covered by 7 splines. Using a local coordinate system ξ defined by

$h\xi = x - x_m$, where $0 \leq \xi \leq 1$, enables the expressions for the element splines to be expressed independently of the actual element coordinates as

$$\begin{aligned}
Q_{m-3} &= 1 - 6\xi + 15\xi^2 - 20\xi^3 + 15\xi^4 - 6\xi^5 + \xi^6 \\
Q_{m-2} &= 57 - 150\xi + 135\xi^2 - 20\xi^3 - 45\xi^4 + 30\xi^5 - 6\xi^6 \\
Q_{m-1} &= 302 - 240\xi - 150\xi^2 + 160\xi^3 + 30\xi^4 - 60\xi^5 + 15\xi^6 \\
Q_m &= 302 + 240\xi - 150\xi^2 - 160\xi^3 + 30\xi^4 + 60\xi^5 - 20\xi^6 \\
Q_{m+1} &= 57 + 150\xi + 135\xi^2 + 20\xi^3 - 45\xi^4 - 30\xi^5 + 15\xi^6 \\
Q_{m+2} &= 1 + 6\xi + 15\xi^2 + 20\xi^3 + 15\xi^4 + 6\xi^5 - 6\xi^6 \\
Q_{m+3} &= \xi^6
\end{aligned} \tag{3.17}$$

Over the element $[x_m, x_{m+1}]$ the variation of the function $U(x,t)$ is given by

$$U(x,t) = \mathbf{Q}^e.\mathrm{d}^e = (Q_{m-2}, Q_{m-1}, Q_m, Q_{m+1}, Q_{m+2}, Q_{m+3}).(\delta_{m-2}, \delta_{m-1}, \delta_m, \delta_{m+1}, \delta_{m+2}, \delta_{m+3})^T$$

At the knot x_i the numerical solution $U_N(x,t)$ is given by

$$\begin{aligned}
U_i &= \delta_{i+2} + 57\delta_{i+1} + 302\delta_i + 302\delta_{i-1} + 57\delta_{i-2} + \delta_{i-3}, \\
hU_i' &= 6(\delta_{i+2} + 25\delta_{i+1} + 40\delta_i - 40\delta_{i-1} - 25\delta_{i-2} - \delta_{i-3}), \\
h^2U_i'' &= 30(\delta_{i+2} + 9\delta_{i+1} - 10\delta_i - 10\delta_{i-1} + 9\delta_{i-2} + \delta_{i-3}), \\
h^3U_i''' &= 120(\delta_{i+2} + \delta_{i+1} - 8\delta_i + 8\delta_{i-1} - \delta_{i-2} - \delta_{i-3}), \\
h^4U_i^{IV} &= 360(\delta_{i+2} - 3\delta_{i+1} + 2\delta_i + 2\delta_{i-1} - 3\delta_{i-2} + \delta_{i-3}), \\
h^5U_i^{V} &= 720(\delta_{i+2} - 5\delta_{i+1} + 10\delta_i - 10\delta_{i-1} + 5\delta_{i-2} - \delta_{i-3}).
\end{aligned} \tag{3.18}$$

The function and its first 5 derivatives are continuous across element boundaries. Sextic B-spline finite elements thus have trial functions with continuity of type C^5.

Chapter 4

A New B-spline Finite Element Solution for the KdV Equation

4.1 Introduction

In this present chapter we will study two problems on the KdV equation. A new numerical solution to the Korteweg-de Vries equation is obtained using the Galerkin method with quadratic B-spline finite elements over which the non-linear term is locally linearised.

A-) Section 4.1: In this section we will study a new quadratic B-spline finite element algorithm, in which the non-linear term UU_x is linearised by replacing the function U by its mean value over each element, formulated for the Korteweg-de Vries (KdV) equation. Values of the L_2 error norm and KdV invariants for soliton simulations using this method are compared with those obtained using the (consistent) fully non-linear algorithm [24], a product approximation approach and other published work [85]-[74].

B-) Section 4.3: In this section we studied again the Kortweg-de Vries equation.

There are many investigations into the numerical solution of the Korteweg-de Vries (KdV) equation [85]-[26], including a Petrov-Galerkin approach in which the weight functions are cubic splines and shape functions linear [72, 64].

We have set up several numerical solutions for the KdV equation using Bubnov-Galerkin methods in which the same B-splines are used for both weight and shape functions [22, 24]. However, there are distinct advantages to be obtained if Petrov-Galerkin methods are considered since the bandwidth of the resulting matrix equation may be lowered if the weight functions are of lower order than the shape functions.

In this present study we develop a numerical solution algorithm based on a Petrov-Galerkin approach in which the element shape functions are quadratic B-splines and the weight functions linear polynomials and compare its performance with earlier work.

4.1.1 The governing equation

The KdV equation has the form

$$U_t + \epsilon U U_x + \mu U_{xxx} = 0, \qquad a \le x \le b, \tag{4.1}$$

where ϵ, μ are positive parameters and the subscripts x and t denote differentiation. The boundary conditions will be chosen from

$$\begin{array}{ll} U(a,t) = 0, & U(b,t) = 0 \\ U_x(a,t) = 0, & U_x(b,t) = 0 \end{array} \tag{4.2}$$

Let us apply the Galerkin method to equation (4.1) with weight function $V(x)$ and integrating by parts, and using equation (4.2), leads to the equation

$$\int_a^b V(U_t + \epsilon U U_x)dx - \int_a^b \mu V_x U_{xx} dx = -[\mu V U_{xx}]_a^b \tag{4.3}$$

and using the boundary conditions (4.2), equation (4.3) reduces to:

$$\int_a^b V(U_t + \epsilon U U_x) - \int_a^b \mu V_x U_{xx} dx = 0. \tag{4.4}$$

The presence of the second spatial derivative within the integrand means that the interpolation functions and their first derivatives must be continuous throughout the region. Quadratic B-spline finite elements satisfy this requirement.

4.1.2 The Finite Element Solution

In this section we approximate the solution $U(x,t)$ using quadratic B-spline interpolation functions.

Set up a uniform linear array of quadratic B-spline finite elements. Partition the region [a,b] into N finite elements of equal length h by knots x_i such that $a = x_0 < x_1 \ldots < x_N = b$ and let $Q_i(x)$ be those quadratic B-splines with knots at the x_i. Then the splines $(Q_{-1}, Q_0, Q_1, \ldots, Q_N)$ form a basis for functions defined over [a,b]. We look for the approximation solution $U_N(x,t)$ to the solution $U(x,t)$ which uses these splines as trial functions. We look for the approximation $U_N(x,t)$ to the solution $U(x,t)$ which uses these splines as trial functions

$$U_N(x,t) = \delta_{-1}(t)Q_{-1}(x) + \delta_0(t)Q_0(x) + \ldots + \delta_N(t)Q_N(x)$$
$$U_N(x,t) = \textstyle\sum_{j=-1}^{N} \delta_j(t)Q_j(x)$$

Where the δ_j are time dependent parameters which are determined from conditions based on equation (4.4) and the boundary conditions (4.2).

An element contributes to equation (4.4) through the integral

$$\int_{x_m}^{x_{m+1}} [V\{U_t + \lambda U_x\} - \mu V_x U_{xx}] dx, \tag{4.5}$$

where $\lambda = \epsilon U$. Identifying the weight function V with a spline Q_i and using

(3,5) and (3.6) we obtain the element contributions

$$\begin{aligned}&\textstyle\sum_{j=m-1}^{m+1}\{\int_0^h Q_iQ_jdx\}\dot{\delta}_j^e+\lambda\sum_{j=m-1}^{m+1}\{\int_0^h Q_iQ_j'dx\}\delta_j^e\\&-\mu\textstyle\sum_{j=m-1}^{m+1}\{\int_0^h Q_i'Q_j''dx\}\delta_j^e,\end{aligned} \tag{4.6}$$

where

$$\mathbf{d^e} = \{\delta_{m-1}\ ,\ \delta_m\ ,\ \delta_{m+1}\}^T, \tag{4.7}$$

are the relevant element parameters. In matrix notation this expression becomes

$$A^e\dot{\mathbf{d}}^\mathbf{e}+\lambda B^e\mathbf{d^e}-\mu C^e\mathbf{d^e}, \tag{4.8}$$

where

$$\begin{aligned}A_{ij}^e &= \textstyle\int_0^h Q_iQ_jdx,\\ \lambda B_{ij}^e &= \lambda\textstyle\int_0^h Q_iQ_j'dx,\\ C_{ij}^e &= \textstyle\int_0^h Q_i'Q_j''dx,\end{aligned} \tag{4.9}$$

and where the element average value for λ is found from $\frac{1}{2}(U_m+U_{m+1})$ as

$$\lambda=\frac{\epsilon}{2}(\delta_{m-1}+2\delta_m+\delta_{m+1}). \tag{4.10}$$

The sufficies i,j take only the values $m-1,m,m+1$ for the element $[x_m,x_{m+1}]$. The matrices A^e, B^e and C^e have the form [24]

$$A^e=\frac{h}{30}\begin{pmatrix}6&13&1\\13&54&13\\1&13&6\end{pmatrix}, \tag{4.11}$$

$$\lambda B^e=\frac{\lambda}{6}\begin{pmatrix}-3&2&1\\-8&0&8\\-1&-2&3\end{pmatrix}, \tag{4.12}$$

and

$$C^e = \frac{2}{h^2}\begin{pmatrix} -1 & 2 & -1 \\ 0 & 0 & 0 \\ 1 & -2 & 1 \end{pmatrix}, \tag{4.13}$$

where λ given by (4.10) depends on the element considered.

Combining together the N trial functions for each element produces the global trial function for the region $[x_0, x_N]$

$$U_N(x,t) = \sum_{i=-1}^{N} \delta_i Q_i = Qd, \tag{4.14}$$

where

$$\mathrm{d} \;=\; \{\delta_{-1},\ \delta_0, \ldots,\ \delta_N\}^T, \tag{4.15}$$

contains all the element parameters.

Assembling contributions from all elements leads to the matrix equation for the time evolution of d,

$$A\dot{\mathrm{d}} + B(\lambda)\mathrm{d} - \mu C\mathrm{d} = 0. \tag{4.16}$$

The matrices A, B, C are pentadiagonal and row m of each has the following form:

$$\begin{aligned} &A : \tfrac{h}{30}(1, 26, 66, 26, 1) \\ &C : \tfrac{2}{h^2}(1, -2, 0, 2, -1) \\ &B(\lambda) : \tfrac{1}{6}(-\lambda_1, -2\lambda_1 - 8\lambda_2, 3\lambda_1 - 3\lambda_3, 8\lambda_2 + 2\lambda_3, \lambda_3) \end{aligned} \tag{4.17}$$

where

$$\begin{aligned} \lambda_1 &= \tfrac{\epsilon}{2}(\delta_{m-2} + 2\delta_{m-1} + \delta_m), \\ \lambda_2 &= \tfrac{\epsilon}{2}(\delta_{m-1} + 2\delta_m + \delta_{m+1}), \\ \lambda_3 &= \tfrac{\epsilon}{2}(\delta_m + 2\delta_{m+1} + \delta_{m+2}). \end{aligned} \tag{4.18}$$

$$m = 1, 2, 3, \ldots, N$$

The basic difference between the present algorithm and that used in ref [24] lies in the form of matrix B. The consistent B used in [85] has row m of the form

$$\tfrac{\epsilon}{12}[-(0.4, 2.8, 0.8, 0, 0)\mathbf{d_m}\ ,\ -(0, 12.4, 24.8, 2.8, 0)\mathbf{d_m}\ ,$$
$$(0.4, 12.4, 0, -12.4, -0.4)\mathbf{d_m}\ ,\ (0, 2.8, 24.8, 12.4, 0)\mathbf{d_m}\ ,$$
$$(0, 0, 0.8, 2.8, 0.4)\mathbf{d_m}],$$

where in the present element average approximation row m of B is

$$\tfrac{\epsilon}{12}[-(1, 2, 1, 0, 0)\mathbf{d_m}\ ,\ -(2, 12, 18, 8, 0)\mathbf{d_m}\ ,$$
$$(3, 6, 0, -6, -3)\mathbf{d_m}\ ,\ (0, 8, 18, 12, 2)\mathbf{d_m}\ ,\ (0, 0, 1, 2, 1)\mathbf{d_m}],$$

where

$$\mathbf{d_m} = (\delta_{m-2}, \delta_{m-1}, \delta_m, \delta_{m+1}, \delta_{m+2})^T.$$

Thus in [85] the central (non-zero) δ value has more influence whereas in the proposed element average method there is less emphasis on the central value and more on the neighbourhood values. The averaged algorithm is easily generalised to cope with higher order non-linearities so that, in particular, numerical simulations for the Modified KdV equation can be set up using this approach.

A popular alternative approximation for the non-linear term is through a product approximation. The analogous form appropriate to the present prescription has U^2 given by

$$U^2 = Q_{m-1}\delta_{m-1}^2 + Q_m\delta_m^2 + Q_{m+1}\delta_{m+1}^2.$$

In this case B^e is of the form

$$\lambda B^e = \frac{1}{6}\begin{pmatrix} -3\delta_1 & 2\delta_2 & 1\delta_3 \\ -8\delta_1 & 0 & 8\delta_3 \\ -1\delta_1 & -2\delta_2 & 3\delta_3 \end{pmatrix},$$

which leads to a matrix B with row m

$$\frac{\epsilon}{12}[-\delta_{m-2}, -10\delta_{m-1}, 0, 10\delta_{m+1}, \delta_{m+2}].$$

Hence using a Crank-Nicolson approach in time, in which d is linearly interpolated between two levels n and $n+1$.

$$d = (1-\theta)d^n + \theta d^{n+1},$$

where $t = (n+\theta)\Delta t$ and $0 \leq \theta \leq 1$. Then the time derivative of d is:

$$\dot{d} = \frac{1}{\Delta t}(d^{n+1} - d^n),$$

using the definitions d and $\dot{d}$, equation (4.16) becomes:

$$[A + \theta \Delta t(B(d) - \mu C)]d^{n+1} = [A - (1-\theta)\Delta t(B(d) + \mu C)]d^n \quad (4.19)$$

giving the parameters θ the values 0, $\frac{1}{2}$ and 1 produces forward, Crank-Nicolson and backward difference schemes respectively. If we let $\theta = \frac{1}{2}$ so that d and its time derivative $\dot{d}$ become:

$$\begin{aligned} d &= \tfrac{1}{2}(d^n + d^{n+1}), \\ \dot{d} &= \tfrac{1}{\Delta t}(d^{n+1} - d^n), \end{aligned} \quad (4.20)$$

we obtain from equation(4.19)

$$[A + \tfrac{\Delta t}{2}B(d) - \tfrac{\mu\Delta t}{2}C]d^{n+1} = [A - \tfrac{\Delta t}{2}B(d) + \tfrac{\mu\Delta t}{2}C]d^n \quad (4.21)$$

a recurrence relationship for d^n, where Δt is the time step.

Applying the boundary conditions which are chosen to be

$$U(a,t) = 0, \qquad U(b,t) = 0$$
$$U_x(a,t) = 0, \qquad U_x(b,t) = 0$$

and these conditions become:

$$\begin{aligned} \delta_{-1} + \delta_0 &= 0 \\ \delta_{-1} - \delta_0 &= 0 \\ \delta_{N-1} + \delta_N &= 0 \\ \delta_{N-1} - \delta_N &= 0 \end{aligned}$$

by eliminating $\delta_{-1}, \delta_0, \delta_{N-1}, \delta_N$ from equation (4.21) we obtain a recurrence relationship for $d^n = (\delta_{-1}, \delta_0, \delta_1, \ldots, \delta_{N-1})^T$.

A Fourier stability analysis of the growth of errors shows that the difference scheme is unconditionally stable.

This matrix equation is pentadiagonal and so is easily and efficiently solved with a variant of the Thomas Algorithm, with an inner iteration also needed at each time step to cope with the non-linear term. The time evolution of d^n and hence $U_N(x,t)$ can be started once the initial vector of parameters d^0 is obtained.

4.1.3 Stability Analysis

The growth factor g for the error in a typical Fourier mode of amplitude $\hat{\delta}^n$,

$$\delta_j^n = \hat{\delta}^n e^{ijkh} ,$$

where k is the mode number and h the element size, is determined for a linearisation of the numerical scheme.

In the linearisation it is assumed that the quantity U in the non-linear term is locally constant. Under these conditions we find that a typical member of equation (4.19) has the form

$$\begin{aligned} &\alpha_1\delta_{j-2}^{n+1} + \alpha_2\delta_{j-1}^{n+1} + \alpha_3\delta_j^{n+1} + \alpha_4\delta_{j+1}^{n+1} + \alpha_5\delta_{j+2}^{n+1} \\ &= \alpha_5\delta_{j-2}^{n} + \alpha_4\delta_{j-1}^{n} + \alpha_3\delta_j^{n} + \alpha_2\delta_{j+1}^{n} + \alpha_1\delta_{j+2}^{n} \end{aligned} \tag{4.22}$$

where

$$\begin{aligned} \alpha_1 &= \alpha - \beta - \gamma, \\ \alpha_2 &= 26\alpha - 10\beta + 2\gamma, \\ \alpha_3 &= 66\alpha, \\ \alpha_4 &= 26\alpha + 10\beta - 2\gamma, \\ \alpha_5 &= \alpha + \beta + \gamma \end{aligned} \tag{4.23}$$

and

$$
\begin{aligned}
\alpha &= \tfrac{h}{30}, \\
\beta &= \tfrac{\lambda \Delta t}{6}, \\
\gamma &= \tfrac{\mu \Delta t}{h^2}.
\end{aligned}
\tag{4.24}
$$

substituting the above Fourier mode gives

$$(a+ib)\hat{\delta}^{n+1} = (a-ib)\hat{\delta}^{n} \tag{4.25}$$

where

$$a = \alpha(33 + \cos 2kh + 26\cos kh) \tag{4.26}$$

and

$$b = (\beta+\gamma)\sin 2kh + (10\beta - 2\gamma)\sin kh. \tag{4.27}$$

Writing $\hat{\delta}^{n+1} = g\hat{\delta}^{n}$, it is observed that $g = \frac{a-ib}{a+ib}$ and so has unit modulus. The linearised recurrence relationship based on the present numerical method is therefore unconditionally stable.

4.1.4 The Initial state

Combine together the local trial functions over each element to give the global trial function

$$U_N(x,0) = \sum_{j=-1}^{N} \delta_j^0 Q_j(x),$$

and require $U_N(x,t)$ to satisfy two conditions.

a-) It should agree with the initial condition $U(x,0)$ at the knots $x_0, \ldots, x_N$; leading to $N+1$ conditions.

b-) Its first derivative should agree with that of the exact condition at x_0 i.e. $U(x_0) = 0$: a further condition.

This leads to the matrix equation [24]

$$Ad^0 = b,$$

where

$$A = \begin{bmatrix} 1 & -1 & & & & & \\ 1 & 1 & & & & & \\ & 1 & 1 & & & & \\ & & & \ddots & & & \\ & & & & 1 & 1 & \\ & & & & & 1 & 1 \end{bmatrix}, \tag{4.28}$$

$$d^0 = (\delta^0_{-1},\ \delta^0_0,\ \ldots,\ \delta^0_N)^T,$$

and

$$b = (0,\ U(x_0),\ U(x_1),\ \ldots,\ U(x_N))^T.$$

These equations are easily solved recursively and if we write $U_j = U(x_j)$

$$\begin{aligned} \delta^0_{-1} &= \tfrac{U_0}{2}, \\ \delta^0_0 &= \tfrac{U_0}{2}, \\ \delta^0_j &= U_j - \delta^0_{j-1} \end{aligned} \tag{4.29}$$

$$\text{for } j = 1, \ldots, N.$$

Thus the initial vector d^0 is determined [85].

4.2 Test problems

The KdV equation has stable soliton solutions which obey an infinity of conservation laws. A numerical scheme for calculating the solitons of the KdV equation should determine accurately the position and shape of a wave

Table 4.1: Single soliton: $h = 0.01, \Delta t = 0.005$ averaged algorithm

time	I_1	I_2	I_3	$L_2 \times 10^3$
0.0	0.144598	0.086759	0.046733	0.000
0.5	0.144633	0.086759	0.046734	0.630
1.0	0.144574	0.086759	0.046734	1.165
1.5	0.144535	0.086758	0.046733	1.744
2.0	0.144541	0.086757	0.046733	2.345
2.5	0.144529	0.086757	0.046732	2.972
3.0	0.144553	0.086756	0.046732	3.557

and should exhibit, at least, the lower order conservation properties of the analytic solutions [85]. The L_2 error norm

$$\|U^{exact} - U^n\|_2 = [h \sum_j^N \mid U_j^{exact} - U_j^N \mid^2]^{\frac{1}{2}} \tag{4.30}$$

is used to measure the difference between the numerical and analytical solutions and hence to show how well the scheme predicts the position and amplitude of the solution as the simulation proceeds. The conservation properties of the solution are examined by calculating the invariants [20],

$$\begin{aligned} I_1 &= \textstyle\int_a^b U dx \\ I_2 &= \textstyle\int_a^b U^2 dx \\ I_3 &= \textstyle\int_a^b [U^3 - \frac{3\mu}{\epsilon}(U_x)^2] dx \end{aligned} \tag{4.31}$$

Numerical solutions to the KdV equation for the following two problems are obtained and discussed.

a-) The KdV equation has an analytic solution of a form given in [4]. The motion of a single soliton with initial condition given by

$$U(x, 0) = 3c\mathrm{sech}^2(Ax + D),$$

can be derived from the analytic solution of the KdV equation which has the form:

$$U(x,t) = 3c\,\mathrm{sech}^2(Ax - Bt + D) \tag{4.32}$$

where

$$A = \frac{1}{2}\left[\frac{\epsilon c}{\mu}\right]^{\frac{1}{2}}, \text{ and } B = \epsilon c A, \tag{4.33}$$

representing a single soliton moving to the right with velocity ϵc. We take as initial condition (4.32) at $t = 0$ and use as boundary conditions:

$$\left.\begin{array}{l} U(0,t) = U(2,t) = 0 \\ U_x(0,t) = U_x(2,t) = 0 \end{array}\right\} \text{ for all time.} \tag{4.34}$$

To allow comparison with earlier work [64] set $\epsilon = 1$, $\mu = 4.84 \times 10^{-4}, c = 0.3, D = -6, h = 0.01, \Delta t = 0.005$. Figure (4.1) shows the behaviour of the computed solution for times from $t = 0.0$ to $t = 3.0$. The exact solution is plotted on the same figure all curves are indistinguishable.

The soliton is observed to move to the right at constant speed with unchanged amplitude. The agreement between numerical and analytic solutions is excellent. To make this observation quantitative the L_2 error norm and invariants C_1, C_2 and C_3 have been determined and given in Table (4.1) for times up to $t = 3.0$. It is found that C_1 changes by about $\sim 0.07\%, C_2$ by about $\sim 0.003\%$ and C_3 changes by about $\sim 0.004\%$, so all are reasonably constant. The L_2 error norm reaches a maximum of 3.554×10^{-3} at the end of the run, and has a value of 1.165×10^{-3} at $t = 1.0$ which compares favourably with many other algorithms: see Table (4.2) [64]. If the space step is reduced to $h = 0.005$, while retaining the same timestep, the magnitude of the L_2 error norm at $t = 3.0$ is reduced to 1.29×10^{-3} and the percentage changes in C_1, C_2 and C_3 are also reduced in proportion. In Table (4.3) the invariants and I_2 error norm for the fully consistent algorithm [24] are

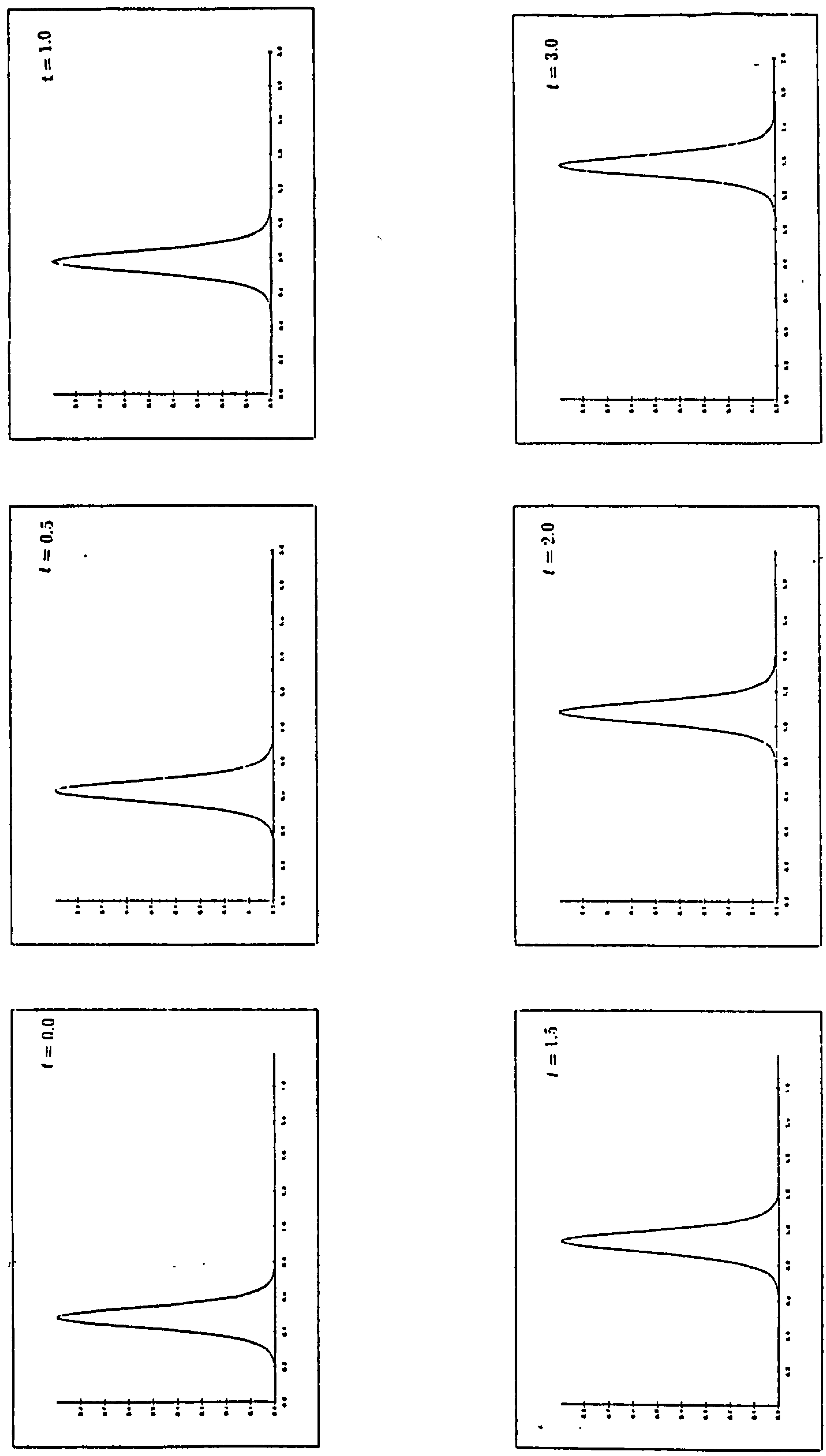

Figure 4.1: The motion of a single soliton with $h = 0.01, \Delta t = 0.005$. Time 0.0-3.0

Table 4.2: Single soliton simulations

Time	Zabusky-Kruskal [85]	Hopscotch [4]	Petrov-Galerkin [64]	Modified P-G [64]
$L_2 - error \times 10^3$ $\Delta x = 0.01, \Delta t = 0.0005$			$h = 0.01$ $\Delta t = 0.005$	
0.25	5.94	3.79	4.46	0.21
0.50	13.17	9.28	7.01	0.38
0.75	21.08	14.14	10.08	0.57
1.00	28.66	18.72	13.26	0.74

Table 4.3: Single soliton: $h = 0.01, \Delta t = 0.005$ consistent algorithm [24]

time	I_1	I_2	I_3	$L_2 \times 10^3$
0.0	0.144598	0.086759	0.046850	0.000
0.5	0.144598	0.086761	0.046735	0.037
1.0	0.144602	0.086763	0.046736	0.060
1.5	0.144604	0.086765	0.046739	0.077
2.0	0.144606	0.086767	0.046740	0.086
2.5	0.144607	0.086769	0.046742	0.101
3.0	0.144610	0.086771	0.046744	0.107

Table 4.4: Single soliton: $h = 0.01, \Delta t = 0.005$ product approximation

time	I_1	I_2	I_3	$L_2 \times 10^3$
0.0	0.144598	0.086759	0.046733	0.000
0.5	0.144654	0.086761	0.046736	0.977
1.0	0.144566	0.086761	0.046736	1.832
1.5	0.144510	0.086761	0.046736	2.755
2.0	0.144522	0.086761	0.046736	3.711
2.5	0.144507	0.086762	0.046736	4.721
3.0	0.144543	0.086762	0.046737	5.664

Table 4.5: Single soliton: $h = 0.005, \Delta t = 0.0025$ averaged algorithm

time	I_1	I_2	I_3	$L_2 \times 10^3$
0.0	0.144598	0.086759	0.046821	0.000
0.5	0.144594	0.086760	0.046822	0.105
1.0	0.144608	0.086762	0.046823	0.162
1.5	0.144604	0.086763	0.046824	0.231
2.0	0.144597	0.086764	0.046825	0.312
2.5	0.144592	0.086765	0.046826	0.390
3.0	0.144591	0.086766	0.046827	0.470

Table 4.6: Single soliton: $h = 0.005, \Delta t = 0.0025$ product approximation

time	I_1	I_2	I_3	$L_2 \times 10^3$
0.0	0.144598	0.086759	0.046821	0.000
0.5	0.144593	0.086762	0.046824	0.159
1.0	0.144615	0.086765	0.046826	0.251
1.5	0.144609	0.086768	0.046829	0.365
2.0	0.144601	0.086771	0.046831	0.500
2.5	0.144594	0.086774	0.046834	0.630
3.0	0.144592	0.086776	0.046836	0.769

given. All 3 invariants are satisfactorily constant changing by less than 0.02% during the simulation and the L_2 norm is less then or equal to 10^{-4} and so is satisfactorily small. As expected the performance of the consistent algorithm is superior, even though the invariant C_2 for the averaged algorithm undergoes the smaller change during the experiments.

When a product approximation is used we obtain the results given in Table (4.4). The L_2 error norm is less satisfactory rising as it does to over 5.6×10^{-3}, by time $t = 3.0$, a value even larger than for the averaged algorithm. However C_1 changes by about $\sim 0.1\%$, C_2 by about $\sim 0.0035\%$ and C_3 changes by about $\sim 0.12\%$ so all are reasonably constant.

If the space and and time steps for both the averaged algorithm and the product approximation are reduced by half down to $h = 0.005$ and $\Delta t = 0.0025$ we obtain the results given in Table (4.5) and (4.6). The values of the L_2 error norm are reduced to less than 10^{-3} and so become much more acceptable.

b-) A second problem concerns the interaction of two well separated solitons. As in case (a) we take $\epsilon = 1.0$ and $\mu = 4.84 \times 10^{-4}$. The initial condition used is derived from the analytic solution [74].

$$U(x,t) = 12(\frac{\mu}{\epsilon})(\log F)_{xx}, \tag{4.35}$$

where

$$\begin{aligned} F &= 1 + e^{\eta_1} + e^{\eta_2} + \beta e^{(\eta_1+\eta_2)}, \\ \eta_i &= \alpha_i x - \alpha_i^3 \mu t + b_i, \\ \beta &= [\tfrac{\alpha_1-\alpha_2}{\alpha_1+\alpha_2}]^2 \end{aligned} \tag{4.36}$$

with

$$\begin{aligned} \alpha_1 &= \sqrt{\tfrac{0.3}{\mu}}, \\ \alpha_2 &= \sqrt{\tfrac{0.1}{\mu}}, \end{aligned} \tag{4.37}$$

and

$$\begin{aligned} b_1 &= -0.48\alpha_1 \\ b_2 &= -1.07\alpha_2, \end{aligned} \tag{4.38}$$

by taking $t = 0$. Together with the boundary conditions which are given by:

$$\left.\begin{aligned} U(0,t) = U(4,t) = 0 \\ U_x(0,t) = U_x(4,t) = 0 \end{aligned}\right\} \text{for all time.} \tag{4.39}$$

Figure(4.2) shows that two separated solitons, the large and small, two solitons of magnitudes 0.3 and 0.9 with the larger placed to the left of the smaller so that as time proceeds an interaction occurs. We use a space step $h = 0.01$, a time step $\Delta t = 0.005$, and the region $0 \leq x \leq 4$.

From figure (4.2) we see that the larger soliton is placed behind and separated from the smaller one. As the time increases, the larger soliton catches up with the smaller when the time $t = 3.0$. The overlapping process continues and the larger soliton overtakes the smaller one at time $t = 4$. About time $t = 6$ the interaction process is complete and the larger soliton has separated completely from the smaller one. Data for the present averaged algorithm are given in Table (4.7) and those for the consistent algorithm,

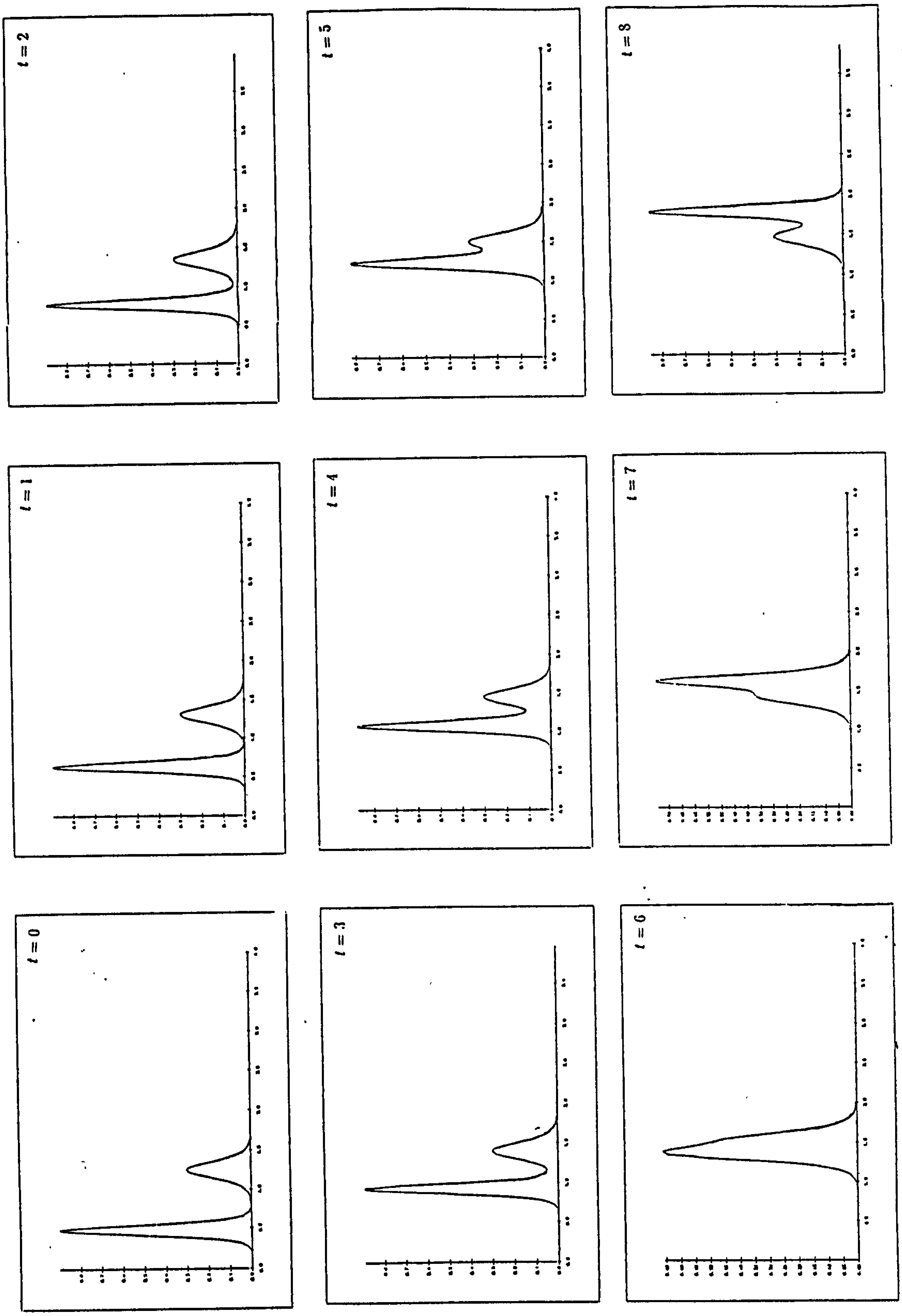

Figure 4.2: The motion of double solitons with $h = 0.01, \Delta t = 0.005$. Time 1.0-8.0.

Table 4.7: Double soliton: $h = 0.01, \Delta t = 0.005$ averaged algorithm

time	I_1	I_2	I_3	$L_2 \times 10^3$
1.00	0.228119	0.103458	0.049739	0.63
2.00	0.228059	0.103460	0.049741	1.18
3.00	0.228023	0.103465	0.049748	1.73
4.00	0.228023	0.103483	0.049772	2.25
5.00	0.228030	0.103533	0.049851	2.49
6.00	0.228047	0.103602	0.049969	2.04
7.00	0.228055	0.103577	0.049924	2.48
8.00	0.228083	0.103508	0.049809	3.92

in Table (4.8). For the averaged algorithm the L_2 error norm, although somewhat larger than that obtained in reference[24], is still quite respectable, and all the invariants C_1, C_2 and C_3 are conserved reasonably well, changing by less than 0.5% over the simulation. However, as can be seen from Table (4.8), these three invariants change by less than 0.05% when the consistent algorithm [24] is used.

If the space step is reduced to $h = 0.005$ and the time step to $\Delta t = 0.0025$ we obtain the results given in Table (4.9). The maximum value taken by the L_2 error norm for the averaged algorithm is reduced to 0.66×10^{-3} and the changes in the 3 invariants are less than 0.04% over the simulation.

Table 4.8: Double soliton: $h = 0.01, \Delta t = 0.005$ consistent algorithm [24]

time	I_1	I_2	I_3	$L_2 \times 10^3$
1.00	0.228088	0.103461	0.049741	0.063
2.00	0.228093	0.103466	0.049757	0.084
3.00	0.228099	0.103472	0.049755	0.075
4.00	0.228107	0.103477	0.049780	0.078
5.00	0.228112	0.103482	0.049758	0.075
6.00	0.228119	0.103487	0.049760	0.116
7.00	0.228123	0.103491	0.049764	0.209
8.00	0.228129	0.103496	0.049768	0.338

Table 4.9: Double soliton: $h = 0.005, \Delta t = 0.0025$ averaged algorithm

time	I_1	I_2	I_3	$L_2 \times 10^3$
1.00	0.228073	0.103458	0.049827	0.11
2.00	0.228085	0.103459	0.049829	0.16
3.00	0.228076	0.103461	0.049830	0.24
4.00	0.228061	0.103463	0.049832	0.32
5.00	0.228048	0.103465	0.049834	0.40
6.00	0.228031	0.103468	0.049836	0.49
7.00	0.228015	0.103471	0.049839	0.57
8.00	0.228987	0.103475	0.049844	0.66

4.3 A Modified Petrov-Galerkin Algorithm for the KdV Equation

4.3.1 The governing equation

Numerical solutions for the KdV equation

$$U_t + \epsilon U U_x + \mu U_{xxx} = 0, \qquad a \le x \le b, \tag{4.40}$$

where ϵ, μ are positive parameters and the subscripts x and t denote differentiation, are obtained. The boundary conditions are chosen from

$$\begin{array}{ll} U(a,t) = 0, & U(b,t) = 0 \\ U_x(a,t) = 0, & U_x(b,t) = 0 \end{array} \tag{4.41}$$

to approximate the physical condition that $U \to 0$ as $x \to \pm\infty$.

Using the Galerkin's method with weight function $V(x)$, and integrating by parts and using equation (4.41) leads to the equation we obtain the weak form of (4.40)

$$\int_a^b V(U_t + \epsilon U U_x)dx - \int_a^b \mu V_x U_{xx} dx = -[\mu V U_{xx}]_a^b \tag{4.42}$$

and using the boundary conditions (4.41) equation (4.42) is reduced to:

$$\int_a^b V(U_t + \epsilon U U_x)dx - \int_a^b \mu V_x U_{xx} dx = 0. \tag{4.43}$$

The presence of the second spatial derivative within the integrand means that the interpolation functions and their first derivatives must be continuous throughout the region. Quadratic B-spline finite elements satisfy this requirement.

4.3.2 The Finite Element Solution

Now we approximate the solution $U(x,t)$ using quadratic B-spline interpolation functions.

Set up a uniform linear array of quadratic B-spline finite elements. Partition the region [a , b] by knots x_i such that $a = x_0 < x_1 \ldots < x_N = b$ and let $Q_i(x)$ be those quadratic B-splines with knots at the x_i. Then the splines $(Q_{-1},\ Q_0,\ Q_1,\ \ldots,\ Q_N)$ form a basis for functions defined over [a , b].

We look for the approximation $U_N(x,t)$ to the solution $U(x,t)$ which uses these splines as trial functions

$$\begin{aligned} U_N(x,t) &= \delta_{-1}(t)Q_{-1}(x) + \delta_0(t)Q_0(x) + \ldots + \delta_N(t)Q_N(x) \\ U_N(x,t) &= \textstyle\sum_{j=-1}^{N} \delta_j(t)Q_j(x) \end{aligned} \tag{4.44}$$

Where the δ_j are time dependent parameters which are determined from conditions based on equation (4.42) and the boundary conditions (4.41).

An element contributes to Equation(4.43) through the integral

$$\int_{x_m}^{x_{m+1}} [V\{U_t + \lambda U_x\} - \mu V_x U_{xx}]dx, \tag{4.45}$$

where $\lambda = \epsilon U$. The weight function V is taken as a linear B-spline L_i. Using (3.5) and (3.6) we obtain the element contributions in the form.

$$\begin{aligned} &\textstyle\sum_{j=m-1}^{m+1}[\int_0^h L_iQ_jdx]\dot{\delta}_j^e + \lambda \sum_{j=m-1}^{m+1}[\int_0^h L_iQ'_jdx]\delta_j^e \\ &-\mu \textstyle\sum_{j=m-1}^{m+1}[\int_0^h L'_iQ''_jdx]\delta_j^e, \end{aligned} \tag{4.46}$$

i=1, 2

where

$$\mathbf{d}^e = \{\delta_{m-1}\ ,\ \delta_m\ ,\ \delta_{m+1}\}^T, \tag{4.47}$$

are the relevant element parameters. Expressions for the linear splines for the finite element $[x_m, x_{m+1}]$ in terms of the local coordinate system ξ defined by $\xi = x - x_m$, $0 \le \xi \le h$, are

$$L = (L_1, L_2) = [1 - \frac{\xi}{h}, \frac{\xi}{h}]. \tag{4.48}$$

In matrix notation equation (4.46) becomes

$$A^e\dot{\mathbf{d}}^e + \lambda B^e\mathbf{d}^e - \mu C^e\mathbf{d}^e, \tag{4.49}$$

where

$$\begin{aligned} A^e_{ij} &= \textstyle\int_0^h L_i Q_j dx, \\ \lambda B^e_{ij} &= \lambda \textstyle\int_0^h L_i Q'_j dx, \\ C^e_{ij} &= \textstyle\int_0^h L'_i Q''_j dx, \end{aligned} \tag{4.50}$$

and where the element average value for λ is found from $\frac{1}{2}(U_m + U_{m+1})$ as

$$\lambda = \frac{\epsilon}{2}(\delta_{m-1} + 2\delta_m + \delta_{m+1}). \tag{4.51}$$

In (4.50) the suffix i takes only the values 1 and 2 and sufficies j and k only the values $m-1, m, m+1$ for the element $[x_m, x_{m+1}]$. The matrices A^e, B^e and C^e are rectangular 2×3, and given by

$$A^e = \frac{h}{12}\begin{pmatrix} 3 & 8 & 1 \\ 1 & 8 & 3 \end{pmatrix}, \tag{4.52}$$

$$\lambda B^e = \frac{\lambda}{3}\begin{pmatrix} -2 & 1 & 1 \\ -1 & -1 & 2 \end{pmatrix}, \tag{4.53}$$

and

$$C^e = \frac{2}{h^2}\begin{pmatrix} -1 & 2 & -1 \\ 1 & -2 & 1 \end{pmatrix}, \tag{4.54}$$

where λ given by (4.51) depends on the element considered.

Assembling contributions from all elements leads to the matrix equation

$$A\dot{d} + B(\lambda)d - \mu C d = 0. \tag{4.55}$$

where

$$d = \{\delta_{-1}, \delta_0, \ldots, \delta_N\}^T, \tag{4.56}$$

contains all the element parameters. The matrices A, B, C are rectangular $(N+1) \times (N+2)$ and row m of each has the following form in which the centre value lies on the main diagonal.

The matrices A, B, C are pentadiagonal and row m of each has the following form:

$$\begin{array}{l} A : \frac{h}{12}(1, 11, 11, 1, 0) \\ C : \frac{2}{h^2}(1, -3, 3, -1, 0) \\ B(\lambda) : \frac{1}{3}(-\lambda_1, -\lambda_1 - 2\lambda_2, 2\lambda_1 + \lambda_2, \lambda_2, 0) \end{array} \quad (4.57)$$

where

$$\begin{aligned} \lambda_1 &= \tfrac{\epsilon}{2}(\delta_{m-2} + 2\delta_{m-1} + \delta_m), \\ \lambda_2 &= \tfrac{\epsilon}{2}(\delta_{m-1} + 2\delta_m + \delta_{m+1}), \\ \lambda_3 &= \tfrac{\epsilon}{2}(\delta_m + 2\delta_{m+1} + \delta_{m+2}). \end{aligned} \quad (4.58)$$

$$m = 1, 2, 3, \ldots, N.$$

Hence using a Crank-Nicolson approach in time the vector d is linearly interpolated between two levels n and $n+1$.

$$d = (1-\theta)d^n + \theta d^{n+1},$$

where $t = (n+\theta)\Delta t$ and $0 \leq \theta \leq 1$. Then the time derivative of d is:

$$\dot{d} = \tfrac{1}{\Delta t}(d^{n+1} - d^n),$$

using the definitions d and $\dot{d}$, equation(4.55) becomes:

$$[A + \theta \Delta t(B(d) - \mu C)]d^{n+1} = [A - (1-\theta)\Delta t(B(d) + \mu C]d^n \quad (4.59)$$

giving the parameters θ the values 0, $\frac{1}{2}$ and 1 produces forward, Crank-Nicolson and backward difference schemes respectively. If we let $\theta = \frac{1}{2}$ so that d and its time derivative $\dot{d}$ become:

$$\begin{aligned} d &= \tfrac{1}{2}(d^n + d^{n+1}), \\ \dot{d} &= \tfrac{1}{\Delta t}(d^{n+1} - d^n), \end{aligned} \quad (4.60)$$

where the superscript n is a time label. We obtain from equation (4.59)

$$[A + \tfrac{\Delta t}{2}B(d) - \tfrac{\mu\Delta t}{2}C]d^{n+1} = [A - \tfrac{\Delta t}{2}B(d) + \tfrac{\mu\Delta t}{2}C]d^n \quad (4.61)$$

which is a recurrence relationship for d^n, where Δt is the time step. Now apply the boundary conditions.

$$\begin{aligned} U(a,t) &= 0, \qquad & U(b,t) &= 0 \\ U_x(a,t) &= 0, \qquad & U_x(b,t) &= 0 \end{aligned} \tag{4.62}$$

so that these conditions become:

$$\begin{aligned} \delta_{-1} + \delta_0 &= 0 \\ \delta_{-1} - \delta_0 &= 0 \\ \delta_{N-1} + \delta_N &= 0 \\ \delta_{N-1} - \delta_N &= 0 \end{aligned}$$

so that

$$\delta_{-1} = \delta_0 = \delta_N = \delta_{N-1} = 0. \tag{4.63}$$

Using the boundary conditions we make the matrix equation square; the resulting matrices are asymmetrically banded but may be considered depleted pentadiagonal and so are easily and efficiently solved with an appropriate variant of the Thomas Algorithm together with an inner iteration at each time step to cope with the non-linear term. The time evolution of d^n and hence $U_N(x,t)$ can be started once the initial vector of parameters d^0 is obtained. The nodal values of the function $U(x,t)$ can be recovered from d^n using equation (3.7) when required.

4.4 Test problems

The KdV equation has stable soliton solutions which obey an infinity of conservation laws. A numerical scheme for calculating the solitons of the KdV equation should determine accurately the position and shape of a wave and should exhibit, at least, the lower order conservation properties of the analytic solutions [4]. The L_2 error norm is used to measure the

Table 4.10: Single soliton: $h = 0.01, \Delta t = 0.005$ Present Petrov-Galerkin algorithm

time	I_1	I_2	I_3	$L_2 \times 10^3$
0.0	0.144598	0.086759	0.046733	0.000
0.5	0.144667	0.086761	0.046737	1.648
1.0	0.144590	0.086761	0.046737	1.794
1.5	0.144494	0.086761	0.046737	1.922
2.0	0.144459	0.086761	0.046737	2.074
2.5	0.144454	0.086761	0.046737	2.242
3.0	0.144463	0.086761	0.046737	2.417

difference between the numerical and analytical solutions and hence to show how well the scheme predicts the position and amplitude of the solution as the simulation proceeds. Numerical solutions to the KdV equation for the following two problems are obtained and discussed.

a-) The KdV equation has an analytic solution of a form given in [4]. The motion of the single soliton with initial condition given by

$$U(x,0) = 3c\mathrm{sech}^2(Ax + D), \tag{4.64}$$

can be derived from the analytic solution of the KdV equation which has the form:

$$U(x,t) = 3c\mathrm{sech}^2(Ax - Bt + D), \tag{4.65}$$

where

$$A = \frac{1}{2}[\frac{\epsilon c}{\mu}]^{\frac{1}{2}}, \text{ and } B = \epsilon c A, \tag{4.66}$$

representing a single soliton moving to the right with velocity ϵc. We take as initial condition (4.65) at $t = 0$ and use as boundary conditions:

$$\left.\begin{aligned} U(0,t) = U(2,t) = 0 \\ U_x(0,t) = U_x(2,t) = 0 \end{aligned}\right\} \text{for all time.} \tag{4.67}$$

To allow comparison with earlier work [85, 4, 64, 24] set $\epsilon = 1$, $\mu = 4.84 \times 10^{-4}, c = 0.3, D = -6, h = 0.01, \Delta t = 0.005$. Figure (4.3) shows the behaviour of the computed solution for times from $t = 0.0$ to $t = 3.0$. The soliton is observed to move to the right at constant speed with unchanged amplitude.

When the exact solution (4.65) is plotted on the same figures, the curves are indistinguishable. To make this observation quantitative the numerical solution is compared with the analytic solution using the L_2 error norm. The 3 invariants C_1, C_2 and C_3 together with the L_2 error norm for problem (a) are given in Table (4.10) for times up to $t = 3.0$.

All 3 invariants are satisfactorily constant; C_1 changes by less than $\sim 0.02\%$, and C_2 and C_3 by less than $\sim 0.003\%$ during the simulation. The L_2 error norm is less than or equal to 2.5×10^{-3} and so is reasonably small.

We have also compared the present results with simulations reported and collected together by Sanz Serna and Christie [64]. These are reproduced in Table(4.11) for various space and time steps. It is seen that the present method compares favourably with the other methods listed. However Table(4.12) shows clearly that Galerkin method [24] with quadratic B-splines as both weight and shape functions produces much better results, particlarly for the L_2 error norm which has a maximum of 0.107. Results for the present Petrov-Galerkin method improve considerably if the time and space steps used are halved; see Table (4.13)

b-) The second problem studied concerns the interaction of two well separated solitons. As in case (a) we take $\epsilon = 1.0$ and $\mu = 4.84 \times 10^{-4}$. The

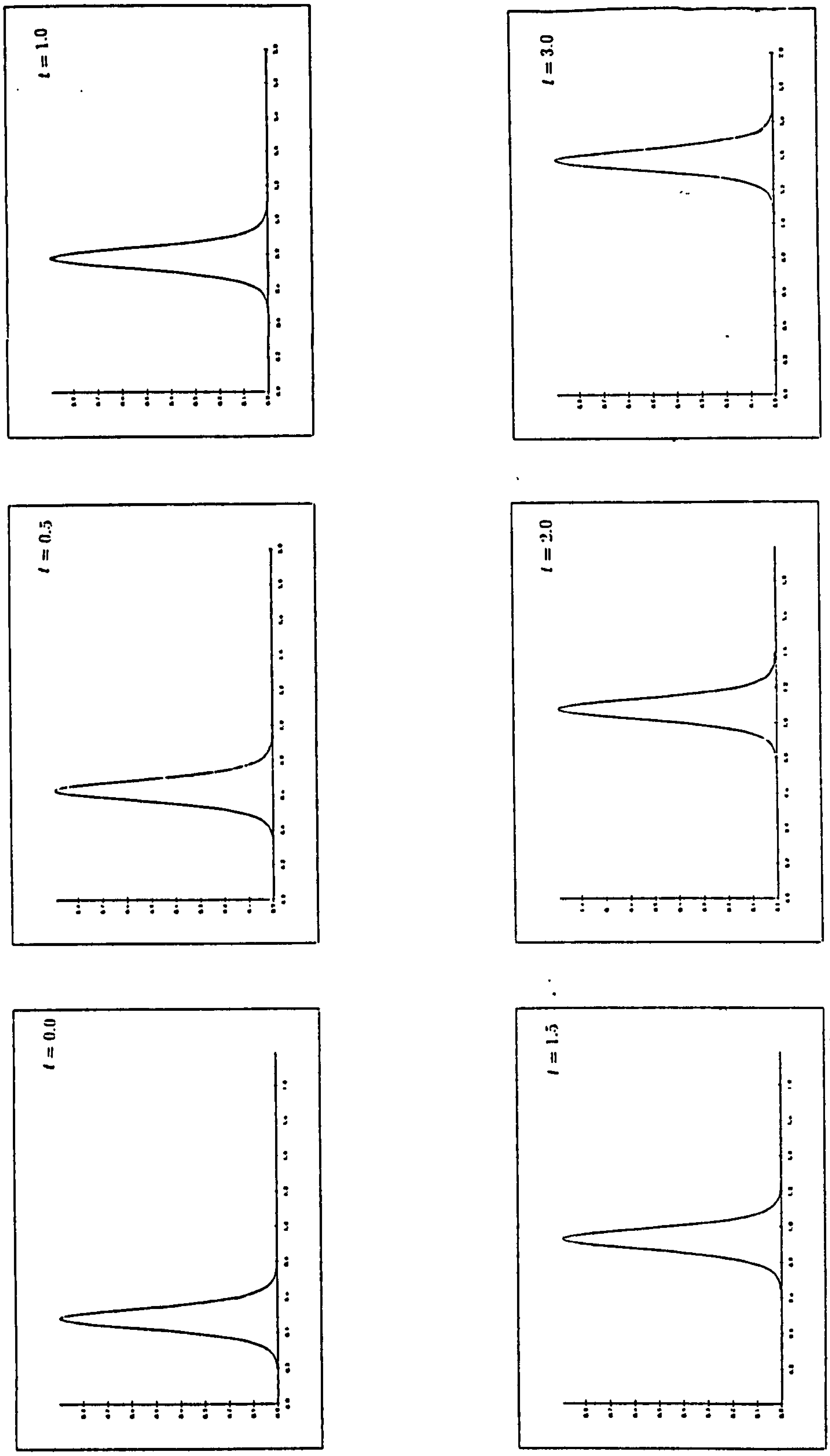

Figure 4.3: The motion of a single soliton with $h = 0.01, \Delta t = 0.005$. Time 0.0-3.0.

Table 4.11: Single soliton simulations

time	Zabusky-Kruskal [85]	Hopscotch [4]	Present Petrov-Galerkin method	Petrov-Galerkin [64]	Modified P-G [64]
$L_2 - error \times 10^3$ $\Delta x = 0.05, \Delta t = 0.025$			$h = 0.05, \Delta t = 0.025$		
0.25	34.64	61.21		81.39	52.15
0.50	122.68	122.41		102.54	64.90
0.75	210.44	181.35		125.84	89.01
1.00	298.19	228.10		150.57	107.20
$L_2 - error \times 10^3$			$h = 0.33, \Delta t = 0.01$		
0.25				31.18	5.94
0.50				43.35	7.56
0.75				56.21	8.70
1.00				74.08	9.49
$L_2 - error \times 10^3$ $\Delta x = 0.01, \Delta t = 0.0005$			$h = 0.01, \Delta t = 0.025$		
0.25	5.94	3.79		4.46	0.21
0.50	13.17	9.28	1.65	7.01	0.38
0.75	21.08	14.14		10.08	0.57
1.00	28.66	18.72	1.79	13.26	0.74

Table 4.12: Single soliton: $h = 0.01, \Delta t = 0.005$ results from ref. [24]

time	I_1	I_2	I_3	$L_2 \times 10^3$
0.0	0.144598	0.086759	0.046850	0.000
0.5	0.144598	0.086761	0.046735	0.037
1.0	0.144602	0.086763	0.046736	0.060
1.5	0.144604	0.086765	0.046739	0.077
2.0	0.144606	0.086767	0.046740	0.086
2.5	0.144607	0.086769	0.046742	0.101
3.0	0.144610	0.086771	0.046744	0.107

Table 4.13: Single soliton: $h = 0.005, \Delta t = 0.0025$ present Petrov-Galerkin algorithm

time	I_1	I_2	I_3	$L_2 \times 10^3$
0.0	0.144598	0.086759	0.046821	0.000
0.5	0.144590	0.086760	0.046821	0.359
1.0	0.144616	0.086761	0.046822	0.411
1.5	0.144617	0.086761	0.046823	0.434
2.0	0.144601	0.086762	0.046823	0.441
2.5	0.144588	0.086763	0.046824	0.454
3.0	0.144579	0.086764	0.046825	0.469

initial condition used is derived from the analytic solution.

$$U(x,t) = 12(\frac{\mu}{\epsilon})(\log F)_{xx}, \tag{4.68}$$

where

$$\begin{aligned} F &= 1 + e^{\eta_1} + e^{\eta_2} + \beta e^{(\eta_1+\eta_2)}, \\ \eta_i &= \alpha_i x - \alpha_i^3 \mu t + b_i, \\ \beta &= [\tfrac{\alpha_1-\alpha_2}{\alpha_1+\alpha_2}]^2 \end{aligned} \tag{4.69}$$

with

$$\begin{aligned} \alpha_1 &= \sqrt{\tfrac{0.3}{\mu}}, \\ \alpha_2 &= \sqrt{\tfrac{0.1}{\mu}}, \end{aligned} \tag{4.70}$$

and

$$\begin{aligned} b_1 &= 0.48\alpha_1, \\ b_2 &= -1.07\alpha_2, \end{aligned} \tag{4.71}$$

by taking $t = 0$. Together with the boundary conditions which are given by:

$$\left.\begin{aligned} U(0,t) &= U(4,t) = 0 \\ U_x(0,t) &= U_x(4,t) = 0 \end{aligned}\right\} \text{for all time.} \tag{4.72}$$

Figure (4.4) shows that after the initialisation gives rise to two separated solitons the large and small, two solitons of magnitudes 0.3 and 0.9 with the larger placed to the left of the smaller so that as time proceeds an interaction occurs. In the simulations a space step $h = 0.01$, a time step $\Delta t = 0.005$, and the region $0 \leq x \leq 4$ are used.

From figure (4.4) we see that the larger soliton is placed on and seperated from the smaller one. As the time increases, the larger soliton catches up with the smaller when the time $t = 3.0$. The overlapping process continues and the larger soliton overtakes the smaller one at time $t = 4.0$. About time $t = 6.0$ the interraction process is complete and the larger soliton has separated completely from the smaller one.

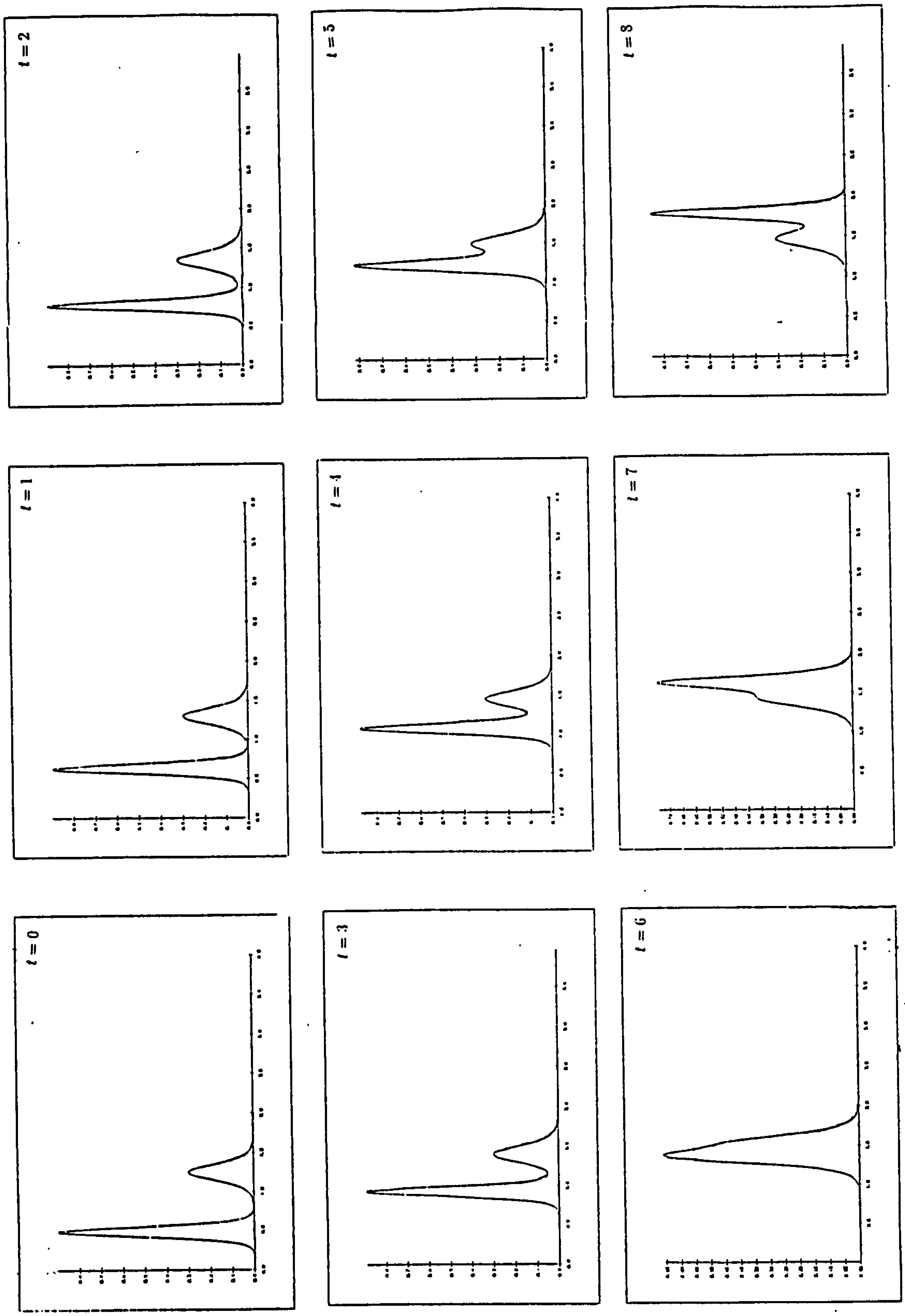

Figure 4.4: The motion of double solitons with $h = 0.01, \Delta t = 0.005$. Time 1.0-8.0.

Table 4.14: Double soliton: $h = 0.01, \Delta t = 0.005$ present Petrov-Galerkin algorithm

time	I_1	I_2	I_3	$L_2 \times 10^3$
1.00	0.228153	0.103458	0.049740	1.645
2.00	0.228073	0.103460	0.049741	1.791
3.00	0.228974	0.103464	0.049746	1.874
4.00	0.228951	0.103481	0.049765	2.077
5.00	0.228944	0.103531	0.049825	1.991
6.00	0.228945	0.103600	0.049914	1.411
7.00	0.228958	0.103577	0.049882	1.366
8.00	0.228978	0.103509	0.049796	1.934

The invariants C_1 to C_3 and L_2 error norm are listed in Table (4.14). The L_2 error norm is less than 2×10^{-3} and so is reasonably small implying that the position and magnitude of the solitons are well represented during the interaction. The conservation of all 3 quantities is good; C_1 and C_2 change by about 0.01% while C_3 changes by less than 0.5% during the run up to $t = 8.0$. If the space and time steps are halved Table (4.15) the L_2 error norm does not exceed 6×10^{-4} during the simulation and the invariants change by less than 0.02%. This compares well with the results deduced in [24] and Table (4.16) for the Bubnov-Galerkin method where the L_2 error norm does not exceed 4×10^{-4} and the invariants change by less than 0.06% during a corresponding simulation.

Table 4.15: Double soliton: $h = 0.005, \Delta t = 0.0025$ present Petrov-Galerkin algorithm

time	I_1	I_2	I_3	$L_2 \times 10^3$
1.00	0.228069	0.103457	0.049826	0.360
2.00	0.228092	0.103458	0.049827	0.411
3.00	0.228087	0.103459	0.049828	0.443
4.00	0.228065	0.103460	0.049828	0.444
5.00	0.228041	0.103461	0.049830	0.442
6.00	0.228017	0.103463	0.049831	0.469
7.00	0.227994	0.103465	0.049833	0.504
8.00	0.227963	0.103469	0.049837	0.536

Table 4.16: Double soliton: $h = 0.01, \Delta t = 0.005$ Quadratic B-spline Galerkin algorithm [24]

time	I_1	I_2	I_3	$L_2 \times 10^3$
1.00	0.228088	0.103461	0.049741	0.063
2.00	0.228093	0.103466	0.049757	0.084
3.00	0.228099	0.103472	0.049755	0.075
4.00	0.228107	0.103477	0.049780	0.078
5.00	0.228112	0.103482	0.049758	0.075
6.00	0.228119	0.103487	0.049760	0.116
7.00	0.227123	0.103491	0.049764	0.209
8.00	0.227129	0.103496	0.049768	0.338

4.5 Discussion

A-) Section 4.1: The simulations have shown that solving the KdV equation by the element averaged algorithm, leads to less accurate results than those found with the consistent scheme, using similar space and time steps, but better results than are obtained with a product approximation. The errors can be reduced substantially by using smaller space and time steps. Results of simulations presented in Section 3 indicate that to obtain very acceptable L_2 error norms and invariants we should use space and time steps of about half the size of those required for the consistent algorithm. An important advantage of the averaged algoritm is that, unlike the consistent approach, it is easily generalised to cope with higher order non-linearities. Thus, in particular, the Modified KdV equation can be studied through numerical simulation using the averaged approach.

B-) Section 4.3: The simulations have shown that a Petrov-Galerkin method involving linear weight functions and quadratic B-spline finite elements can be used to produce reasonably accurate numerical solutions of the KdV equation. However, to obtain error norms of similar order to those obtained in [24] using quadratic B-splines as both weight and interpolation functions requires space and time steps of smaller size than those used here.

Chapter 5

Simulations of solitons of the Modified KdV equation

5.1 Introduction

In this chapter we will study the Modified Korteweg-de Vries equation using a new numerical solution. The Modified Korteweg-de Vries equation is obtained using a "lumped " Galerkin method with quadratic B-spline finite elements. A linear stability analysis of the scheme shows the method to be unconditionally stable. Classical problems concerning the development, motion and interaction of solitons are used to validate the method.
Theoretical and numerical studies of the Modified Kortewg-de Vries ($MKdV$) equation from various groups have appeared in the literature [85] - [75]. We have previously solved the $MKdV$ equation using the method of collocation with quintic B-spline finite elements [23]. In the present study we set up a new numerical algorithm based on a "lumped" Galerkin method with quadratic B-spline finite elements [24]. The two methods are used to study the motion, interaction and generation of solitons and their performances compared.

5.1.1 The governing equation

The $MKdV$ equation has the form

$$U_t + \epsilon U^2 U_x + \mu U_{xxx} = 0, \qquad a \leq x \leq b, \tag{5.1}$$

where ϵ, μ are positive parameters and the subscripts x and t denote differentiation. The boundary conditions will be taken from

$$\begin{aligned} U(a,t) &= 0, & U(b,t) &= 0 \\ U_x(a,t) &= 0, & U_x(b,t) &= 0 \end{aligned} \tag{5.2}$$

Applying the Galerkin method to Equation(5.1) with weight function $V(x)$, integrating by parts and using Equation(5.2) leads to the equation

$$\int_a^b V(U_t + \epsilon U^2 U_x)dx - \int_a^b \mu V_x U_{xx} dx = -[\mu V U_{xx}]_a^b \tag{5.3}$$

and using the boundary conditions (5.2) equation(5.3) reduced to:

$$\int_a^b V(U_t + \epsilon U^2 U_x)dx - \int_a^b \mu V_x U_{xx} dx = 0. \tag{5.4}$$

The presence of the second spatial derivative within the integrand means that the interpolation functions and their first derivatives must be continuous throughout the region. Quadratic B-spline finite elements satisfy this requirement.

5.1.2 The Finite Element Solution

In this section we approximate the solution $U(x,t)$ using quadratic B-spline interpolation functions.

An element contributes to Equation(5.4) through the integral

$$\int_{x_m}^{x_{m+1}} [V\{U_t + \lambda U_x\} - \mu V_x U_{xx}]dx, \tag{5.5}$$

where $\lambda = \epsilon U^2$. Identifying the weight function V with a spline Q_i and using (3,5) and (3.6) we obtain the element contributions

$$\begin{aligned}&\textstyle\sum_{j=m-1}^{m+1}[\int_0^h Q_iQ_jdx]\dot{\delta}_j^e + \lambda\sum_{j=m-1}^{m+1}[\int_0^h Q_iQ_j'dx]\delta_j^e\\ &-\mu\textstyle\sum_{j=m-1}^{m+1}[\int_0^h Q_i'Q_j''dx]\delta_j^e,\end{aligned} \tag{5.6}$$

where

$$\mathbf{d^e} \;=\; \{\delta_{m-1}\;,\;\delta_m\;,\;\delta_{m+1}\}^T, \tag{5.7}$$

are the relevant element parameters. In matrix notation this equation becomes

$$\mathbf{A^e\dot{d}^e} + \lambda\mathbf{B^e d^e} - \mu\mathbf{C^e d^e}, \tag{5.8}$$

where

$$\begin{aligned} A_{ij}^e &= \textstyle\int_0^h Q_iQ_jdx,\\ \lambda B_{ij}^e &= \lambda\textstyle\int_0^h Q_iQ_j'dx,\\ C_{ij}^e &= \textstyle\int_0^h Q_i'Q_j''dx,\end{aligned} \tag{5.9}$$

and a "lumped" value for λ is found from $\frac{1}{2}(U_m + U_{m+1})$ as

$$\lambda = \frac{\epsilon}{4}(\delta_{m-1} + 2\delta_m + \delta_{m+1})^2. \tag{5.10}$$

For the element $[x_m, x_{m+1}]$ the sufficies i, j, k take only the values $m-1$, $m, m+1$ so that the matrices A^e, B^e and C^e are 3×3,

$$A^e = \frac{h}{30}\begin{pmatrix} 6 & 13 & 1\\ 13 & 54 & 13\\ 1 & 13 & 6\end{pmatrix}, \tag{5.11}$$

$$\lambda B^e = \frac{\lambda}{6}\begin{pmatrix} -3 & 2 & 1\\ -8 & 0 & 8\\ -1 & -2 & 3\end{pmatrix}, \tag{5.12}$$

and

$$C^e = \frac{2}{h^2}\begin{pmatrix} -1 & 2 & -1 \\ 0 & 0 & 0 \\ 1 & -2 & 1 \end{pmatrix}, \tag{5.13}$$

where λ given by (5.10) depends on the element considered.

Combining together the N trial functions for each element (3.5) produces the global trial function for the region $[x_0, x_N]$

$$U_N(x,t) = \sum_{i=-1}^{N} \delta_i Q_i = Qd, \tag{5.14}$$

where

$$d = \{\delta_{-1}, \delta_0, \ldots, \delta_N\}^T, \tag{5.15}$$

contains all the element parameters.

Assembling contributions from all elements leads to the matrix equation for the time evolution of d ,

$$A\dot{d} + B(\lambda)d - \mu Cd = 0. \tag{5.16}$$

The matrices A, B, C are pentadiagonal and row m of each has the following form:

$$\begin{aligned} &A : \tfrac{h}{30}(1, 26, 66, 26, 1) \\ &C : \tfrac{2}{h^2}(1, -2, 0, 2, -1) \\ &B(\lambda) : \tfrac{1}{6}(-\lambda_1, -2\lambda_1 - 8\lambda_2, 3\lambda_1 - 3\lambda_3, 8\lambda_2 + 2\lambda_3, \lambda_3) \end{aligned} \tag{5.17}$$

where

$$\begin{aligned} \lambda_1 &= \tfrac{\epsilon}{4}(\delta_{m-2} + 2\delta_{m-1} + \delta_m)^2, \\ \lambda_2 &= \tfrac{\epsilon}{4}(\delta_{m-1} + 2\delta_m + \delta_{m+1})^2, \\ \lambda_3 &= \tfrac{\epsilon}{4}(\delta_m + 2\delta_{m+1} + \delta_{m+2})^2. \end{aligned} \tag{5.18}$$

Hence using a Crank-Nicolson approach in time, in which d is linearly interpolated between two levels n and $n+1$.

$$d = (1-\theta)d^n + \theta d^{n+1},$$

where $t = (n+\theta)\Delta t$ and $0 \leq \theta \leq 1$. Then the time derivative of d is:

$$\dot{d} = \frac{1}{\Delta t}(d^{n+1} - d^n),$$

using the definitions d and $\dot{d}$, equation(5.16) becomes:

$$[A + \theta \Delta t(B(d) - \mu C)]d^{n+1} = [A - \theta \Delta t(B(d) + \mu C)]d^n \tag{5.19}$$

giving the parameters θ the values 0, $\frac{1}{2}$ and 1 produces forward, Crank-Nicolson and bacward difference Schemes respectively. If we let $\theta = \frac{1}{2}$,so that d and its time derivative $\dot{d}$ become:

$$\begin{aligned} d &= \tfrac{1}{2}(d^n + d^{n+1}), \\ \dot{d} &= \tfrac{1}{\Delta t}(d^{n+1} - d^n), \end{aligned} \tag{5.20}$$

we obtain from equation(5.19)

$$\{A + \frac{\Delta t}{2}B(d) - \frac{\mu \Delta t}{2}C\}d^{n+1} = \{A - \frac{\Delta t}{2}B(d) + \frac{\mu \Delta t}{2}C\}d^n \tag{5.21}$$

a recurrence relationship for d^n , where Δt is the time step.

Applying the boundary conditions which are chosen to be

$$U(a,t) = 0, \qquad U(b,t) = 0$$
$$U_x(a,t) = 0, \qquad U_x(b,t) = 0$$

and these conditions becomes:

$$\begin{aligned} \delta_{-1} + \delta_0 &= 0 \\ \delta_{-1} - \delta_0 &= 0 \\ \delta_{N-1} + \delta_N &= 0 \\ \delta_{N-1} - \delta_N &= 0 \end{aligned}$$

by eliminating $\delta_{-1}, \delta_0, \delta_{N-1}, \delta_N$ from equation (5.21) produces a recurrence relationship for $d^n = (\delta_{-1}\ \delta_0\ \delta_1,\ \ldots\ \delta_{N-1})^T$.
A Fourier stability analysis of the growth of errors shows that the difference scheme is unconditionally stable.

The matrices are pentadiagonal and so are easily and efficiently solved with a variant of the Thomas Algorithm, but an inner iteration is also needed at each time step to cope with the non-linear term. The time evolution of d^n and hence $U_N(x,t)$ can be started once the initial vector of parameters d^0 is obtained. The function $U(x,t)$ can be recovered from d^n using Equations(3.6) and (3.7) if required.

5.1.3 Stability Analysis

The growth factor g of the error in a typical Fourier mode of amplitude δ^n,

$$\delta_j^n = \hat{\delta}^n e^{ijkh},$$

where k is the mode number and h the element size, is determined for a linearisation of the numerical scheme.

In the linearisation it is assumed that the quantity U^2 in the non-linear term is locally constant. Under these conditions we find that a typical member of Equation(5.21) has the form

$$\begin{aligned}
&\alpha_1\delta_{j-2}^{n+1} + \alpha_2\delta_{j-1}^{n+1} + \alpha_3\delta_j^{n+1} + \alpha_4\delta_{j+1}^{n+1} + \alpha_5\delta_{j+2}^{n+1} \\
&= \alpha_5\delta_{j-2}^n + \alpha_4\delta_{j-1}^n + \alpha_3\delta_j^n + \alpha_2\delta_{j+1}^n + \alpha_1\delta_{j+2}^n
\end{aligned} \tag{5.22}$$

where

$$\begin{aligned}
\alpha_1 &= \alpha - \beta - \gamma, \\
\alpha_2 &= 26\alpha - 10\beta + 2\gamma, \\
\alpha_3 &= 66\alpha, \\
\alpha_4 &= 26\alpha + 10\beta - 2\gamma, \\
\alpha_5 &= \alpha + \beta + \gamma
\end{aligned} \tag{5.23}$$

and

$$\begin{aligned}
\alpha &= \tfrac{h}{30}, \\
\beta &= \tfrac{\lambda \Delta t}{6}, \\
\gamma &= \tfrac{\mu \Delta t}{h^2}.
\end{aligned} \tag{5.24}$$

substituting the above Fourier mode leads to

$$(a + ib)\hat{\delta}^{n+1} = (a - ib)\hat{\delta}^{n} \tag{5.25}$$

where

$$a = \alpha(33 + \cos 2kh + 26 \cos kh) \tag{5.26}$$

and

$$b = (\beta + \gamma)\sin 2kh + (10\beta - 2\gamma)\sin kh. \tag{5.27}$$

Writing $\hat{\delta}^{n+1} = g\hat{\delta}^{n}$, it is observed that $g = \frac{a-ib}{a+ib}$ and so has unit modulus. The linearised recurrence relationship based on the present numerical method is therefore unconditionally stable.

5.2 Simulations

Like the KdV equation the $MKdV$ equation has stable soliton solutions which obey an infinity of conservation laws. A numerical scheme for calculating the solitons of the $MKdV$ equation should determine accurately the position and shape of a wave and should exhibit, at least, the lower order conservation properties of the analytic solutions [41]. The L_2 error norm is used to measure the difference between the numerical and analytical solutions and hence to show how well the scheme predicts the position and amplitude of the solution as the simulation proceeds. The conservation properties of the solution are examined by calculating the invariants [41],

$$\begin{aligned} I_1 &= \textstyle\int_a^b U dx \\ I_2 &= \textstyle\int_a^b U^2 dx \\ I_3 &= \textstyle\int_a^b [U^4 - \frac{6\mu}{\epsilon}(U_x)^2] dx \end{aligned} \tag{5.28}$$

These expressions are derived by assuming either that boundary conditions are periodic or that $U \rightarrow 0$ as $x \rightarrow \pm\infty$.

Numerical solutions to the $MKdV$ equation for the following problems are obtained and discussed.

a-) The $MKdV$ equation has an analytic solution of the form [41]

$$U(x,t) = kp\text{sech}(kx - kx_0 - k^3\mu t) \tag{5.29}$$

where

$$p = [\frac{6\mu}{\epsilon}]^{\frac{1}{2}}, \tag{5.30}$$

which represents a single soliton originally sited at x_0 moving to the right with velocity $k^2\mu$. Solitons may have positive or negative amplitudes depending on the sign of k but all have positive velocities.

We take as initial condition (5.29) at $t = 0$ and to allow comparison with earlier work [23] we use $\epsilon = 3.0$, $\mu = 1.0$, $kp = c = 1.3$, $x_0 = 15$, $h = 0.2$, $\Delta t = 0.025$ and $0 \leq x \leq 200$. We can see figure (5.1), time up to 10.

The soliton is seen to move to the right at constant speed with unchanged amplitude. To make this observation quantitative we have compared our numerical solution with the analytic solution using the L_2 and L_∞ error norms. For problem (a) these are given in Table (5.1) where they are compared with a similar simulation using the method of collocation and quintic B-splines [23].

The corresponding 3 invariants I_1, I_2 and I_3 for both simulations are given in Table (5.2). We see that in general, the error norms are smaller for

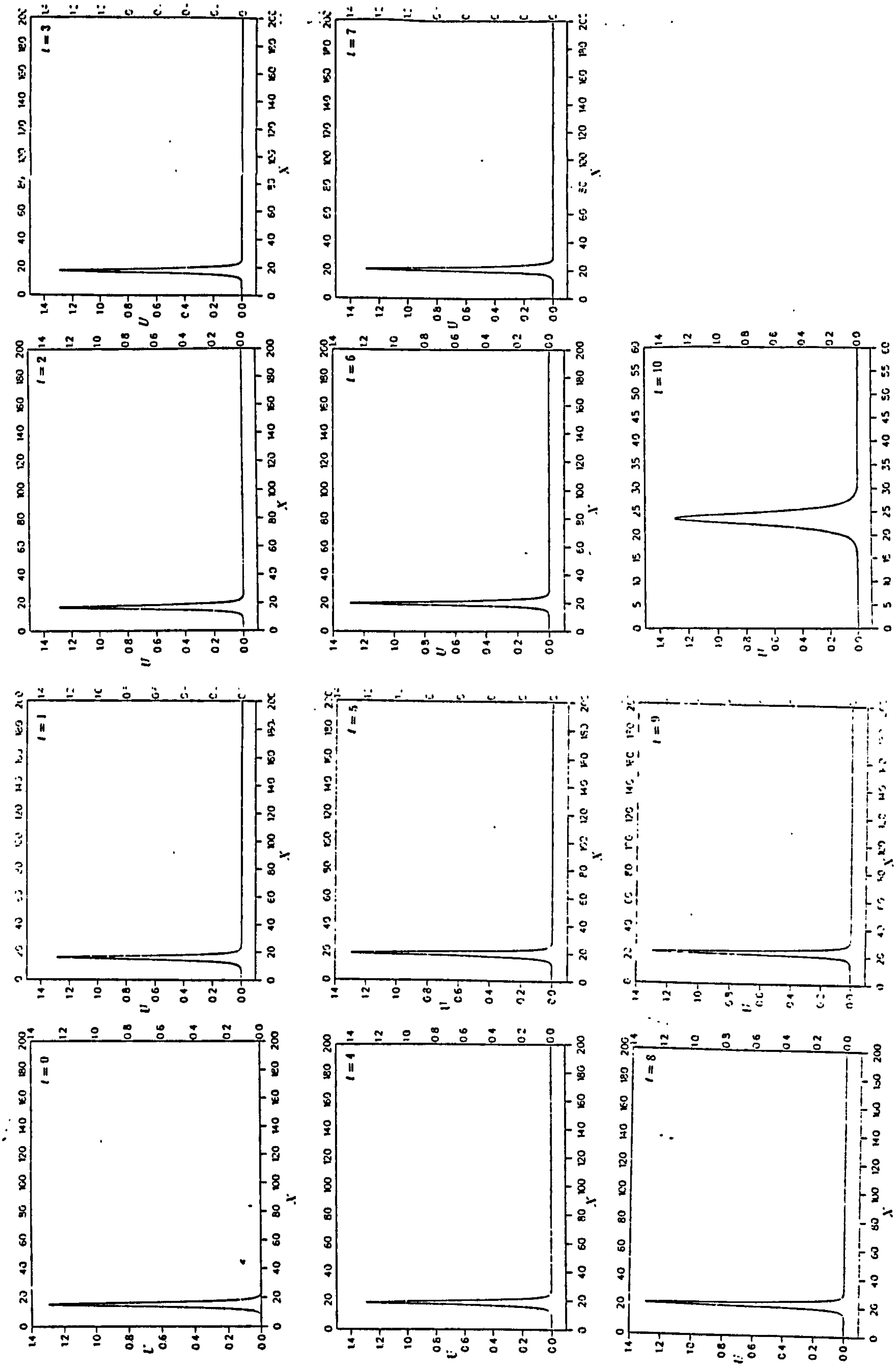

Figure 5.1: Single soliton solution: $\mu = 1.0, \epsilon = 3.0, \Delta t = 0.025$, $h = 0.2$, range $0 \leq x \leq 200$. Time $t = 0.0 - 10.0$.

Table 5.1: Single soliton $h = 0.2, \Delta t = 0.025, 0 \leq x \leq 200$

	lumped quadratic B-spline		quintic B-spline [23]	
time	$L_2 \times 10^3$	$L_\infty \times 10^3$	$L_2 \times 10^3$	$L_\infty \times 10^3$
1.0	3.38	2.03	0.25	0.10
2.0	4.88	3.23	0.35	0.17
3.0	6.32	4.15	0.39	0.25
4.0	7.65	5.00	0.51	0.36
5.0	8.84	5.75	0.75	0.51
6.0	9.83	6.34	1.02	0.67
7.0	10.57	6.71	1.32	0.85
8.0	11.21	7.20	1.66	1.07
9.0	11.34	6.99	2.03	1.03
10.0	11.61	7.33	2.45	1.55

Table 5.2: Invariants: single soliton simulation $h = 0.2, \Delta t = 0.25$

	lumped quadratic B-spline			quintic B-spline [23]		
time	I_1	I_2	I_3	I_1	I_2	I_3
0.0	4.443	3.678	2.055	4.443	3.677	2.071
10.5	4.444	3.677	2.055	4.442	3.676	2.070
20.0	4.443	3.677	2.054	4.442	3.675	2.068
30.0	4.444	3.676	2.054	4.442	3.674	2.067
40.0	4.444	3.676	2.054	4.441	3.674	2.066
50.0	4.443	3.676	2.054	4.441	3.673	2.064
60.0	4.442	3.676	2.053	4.440	3.672	2.063
70.0	4.441	3.676	2.053	4.440	3.671	2.061
80.0	4.441	3.676	2.053	4.440	3.670	2.060
90.0	4.440	3.675	2.052	4.439	3.669	2.058
100.0	4.440	3.675	2.052	4.439	3.668	2.057

the latter simulation while the invariants change least for the former case. For the long run up to $t = 100$, Table (5.2) shows that for the present case both I_1 and I_2 change by less than 0.1% and I_3 changes by less than 0.2%, while for the quintic spline algorithm the changes are somewhat larger but still I_1 changes by less than 0.1%, I_2 by less than 0.25% and I_3 by less than 0.75%.

b-) Our second test will involve soliton interaction, and we take as initial condition

$$U(x,t) = k_1 p \operatorname{sech}(k_1 x - k_1 x_1 - k_1^3 \mu t) + k_2 p \operatorname{sech}(k_2 x - k_2 x_2 - k_2^3 \mu t), \quad (5.31)$$

where

$$p = [\frac{6\mu}{\epsilon}]^{\frac{1}{2}} \tag{5.32}$$

evaluated at $t = 0$.

This condition represents two solitary waves of magnitudes $k_i p$ placed at $x = -\frac{d_i}{k_i}$. The waves move to the right with velocities $k_i^2\mu$ which depend upon their magnitude. To ensure interaction with increasing time we place the larger soliton to the left of the smaller. Thus we place the soliton with magnitude $k_1 p = 1.3$ at $x_1 = 15$ and that with $k_2 p = 0.9$ at $x_2 = 35$, the range is $0 \leq x \leq 200$, $\mu = 0.1$, $\epsilon = 3.0$ so that $p = \sqrt{2}$, $h = 0.2$ and $\Delta t = 0.025$.

Figure (5.2) show the two solitons with large amplitude on the left. As the time increases, the larger soliton catches up with the smaller until, at time $t = 40$, the smaller soliton is being absorbed. The overlapping process continues until, by time $t = 60$, the larger soliton has overtaken the smaller one and is in the process of separating. At time $t = 100$, the interaction is complete and the larger soliton has separated completely from the smaller one.

The solitons are observed to interact and emerge from the collision and resume their former shape and velocity. The values taken by the 3 invariants during this long simulation are given in Table (5.3) from which we see that each is satisfactorily conserved. The change in I_3 is the largest and even that is less than 0.5%. For comparison the invariants for a corresponding simulation using quintic B-spline finite elements [23] are also given. We find that the changes in these invariants are of similar magnitudes.

c-) As a final example we study the temporal development of a Maxwellian initial condition.

$$U(x, 0) = \exp(-x^2). \tag{5.33}$$

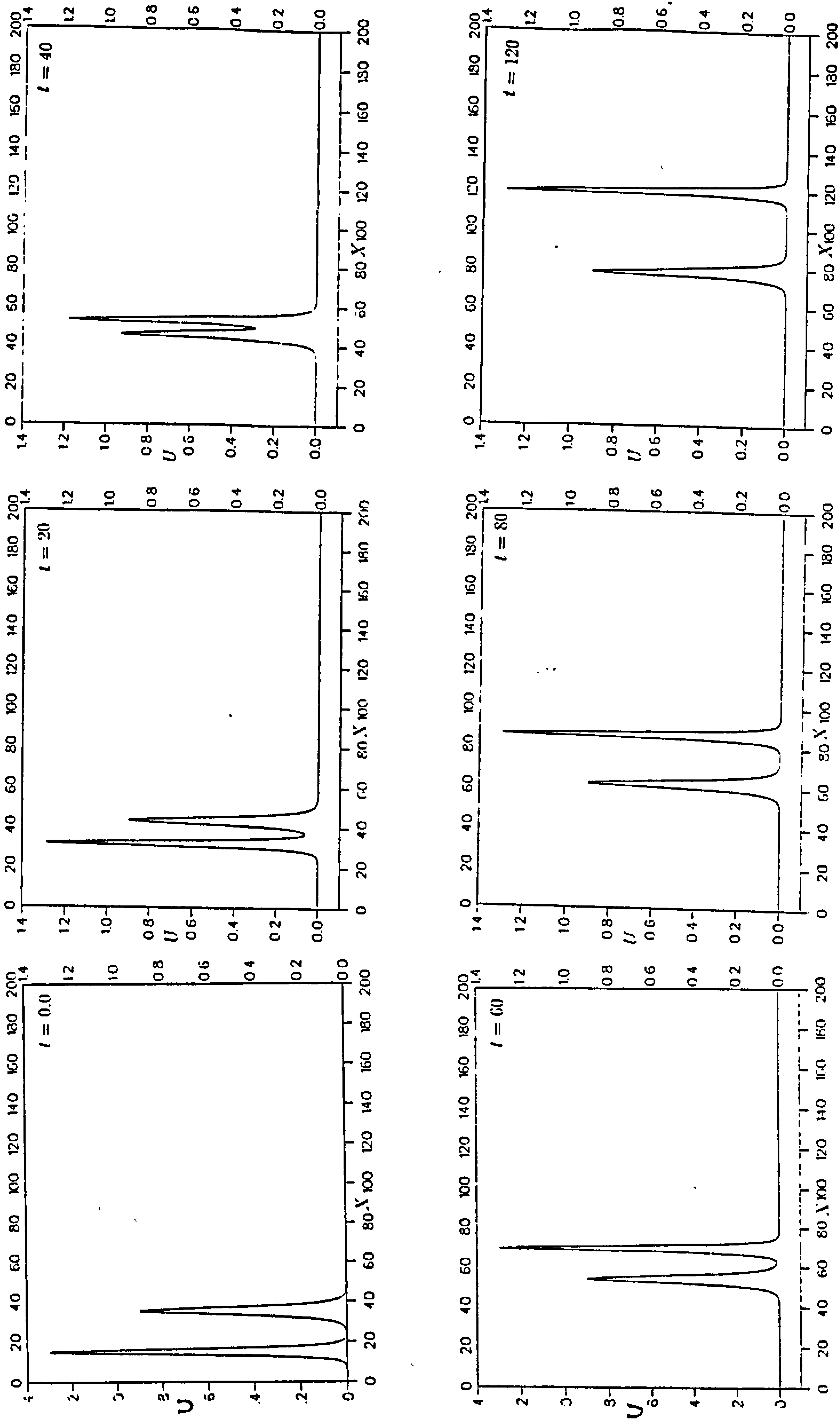

Figure 5.2: Double soliton solution: $\mu = 1.0, \epsilon = 3.0, \Delta t = 0.025$, $h = 0.2$, range $0 \leq x \leq 200$, at time $t = 0.0 - 120$.

Table 5.3: Invariants for two solitons $c_1 = 1.3, c_2 = 0.9, h = 0.2, \Delta t = 0.25$

	lumped quadratic B-spline			quintic B-spline [23]		
time	I_1	I_2	I_3	I_1	I_2	I_3
0.0	8.8857	6.2226	2.7396	8.8858	6.2226	2.7588
20.5	8.8865	6.2222	2.7389	8.8852	6.2212	2.7562
40.0	8.8846	6.2220	2.7388	8.8854	6.2212	2.7559
60.0	8.8845	6.2248	2.7486	8.8851	6.2203	2.7540
80.0	8.8851	6.2253	2.7495	8.8846	6.2188	2.7513
100.0	8.8854	6.2219	2.7383	8.8840	6.2174	2.7487
120.0	8.8846	6.2211	2.7362	8.8834	6.2161	2.7461

We fix the values of ϵ at 1 and examine the evolution of the solution for various values of μ. Integrating (5.28) analytically shows that

$$
\begin{aligned}
I_1 &= \sqrt{(\pi)} = 1.7725, \\
I_2 &= \sqrt{(\tfrac{\pi}{2})} = 1.2533, \\
I_3 &= \tfrac{1}{2}(1 - 6\mu\sqrt{2})\sqrt{(\pi)},
\end{aligned}
$$

so that for $\mu = 0.04$ $I_3 = 0.5854$, $\mu = 0.01$ $I_3 = 0.8110$, $\mu = 0.005$ $I_3 = 0.8486$ and $\mu = 0.0025$ $I_3 = 0.8674$.

First, with $\mu = 0.04$ we use $\Delta t = 0.01$ and $h = 0.1$ over a range $-50 \leq x \leq 50$, and confirm earlier work that the Maxwellian evolves into a single $MKdV$ soliton and an oscillating tail as shown in figure (5.3). The values taken by the lowest invariants up to time of $t = 12.5$ are given in Table (5.4).

second, with $\mu = 0.01$ we use $\Delta t = 0.005$ and $h = 0.05$ over a range $-50 \leq x \leq 50$, two solitons and an oscillating tail as shown in figure (5.4). The values taken by the lowest invariants up to time of $t = 12.5$ are given in

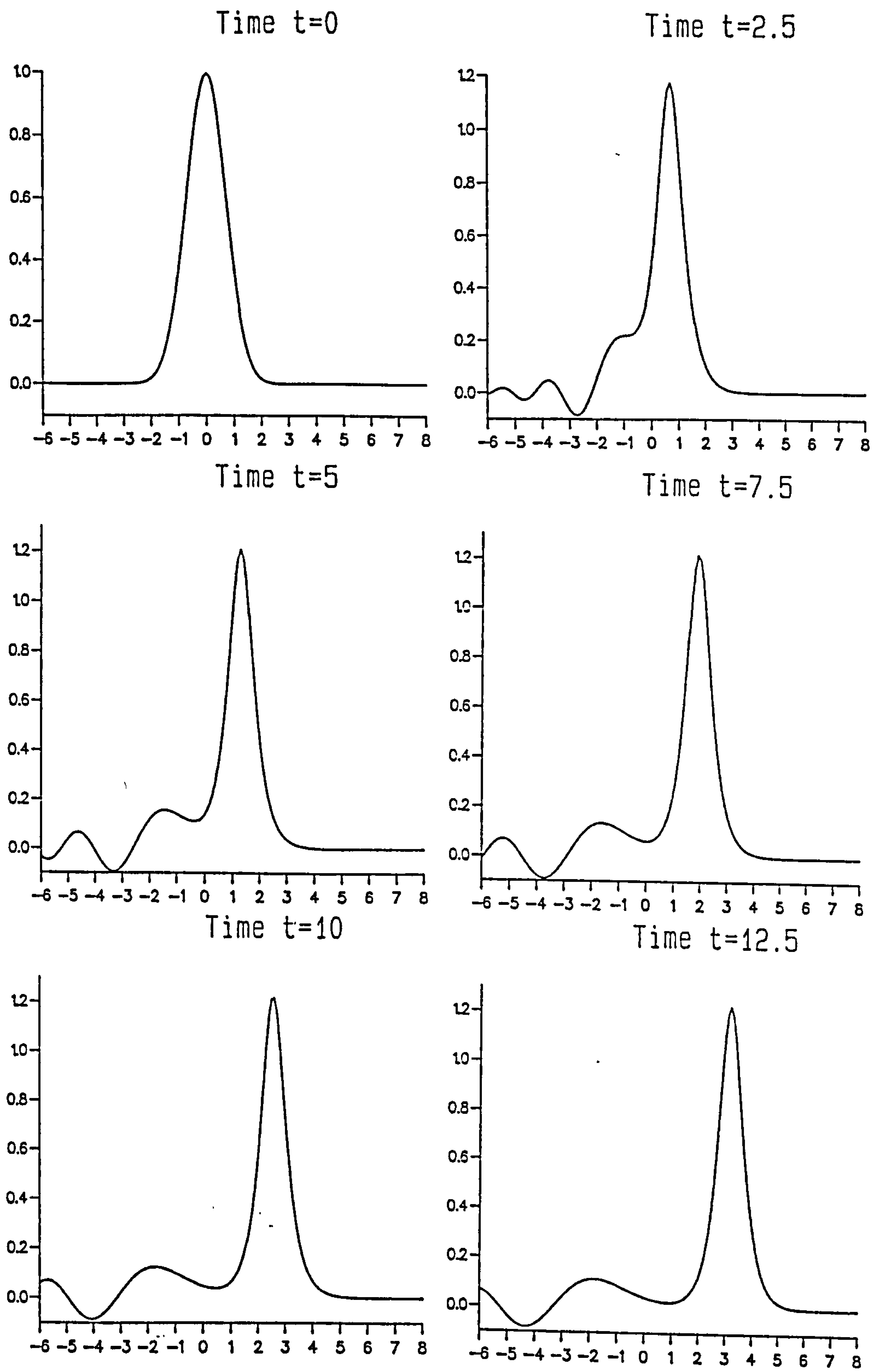

Figure 5.3: Maxwellian initial condition: $\mu = 0.04, \Delta t = 0.01$, $h = 0.1$ range $-50 \leq x \leq 50$, at time $t = 0.0 - 12.5$.

Table 5.4: Invariants for Maxwellian

time	$\mu = 0.04, h = 0.1, \Delta t = 0.01$		
time	I_1	I_2	I_3
0.0	1.7725	1.2533	0.5839
2.5	1.7719	1.2511	0.5756
5.0	1.7716	1.2504	0.5734
7.5	1.7716	1.2501	0.5726
10.0	1.7715	1.2501	0.5723
12.5	1.7716	1.2500	0.5721

Table (5.5).

Third, With $\mu = 0.005$ we use $\Delta t = 0.005$ and $h = 0.01$ over a range $-15 \leq x \leq 15$, and show that the Maxwellian evolves into three $MKdV$ solitons, see Figure (5.5). The values taken by the lowest 3 invariants for simulations are given in Table (5.6). As h decreases the observed value of I_3 at time $t = 0$ moves closer to the analytic value due probably to an improved estimate of U_x.

And last, With $\mu = 0.0025$ we use $\Delta t = 0.005$ and $h = 0.01$ over a range $-15 \leq x \leq 15$, and show that the Maxwellian evolves into five $MKdV$ solitons, see Figure (5.6). The values taken by the lowest 3 invariants for simulations are given in Table (5.7). As h decreases the observed value of I_3 at time $t = 0$ moves closer to the analytic value due probably to an improved estimate of U_x.

d-) The final test problem we shall consider has the initial condition:

$$U(x, 0) = \tfrac{1}{2}[1 - \tanh[\tfrac{|x|-25}{5}]] \quad (5.34)$$

Table 5.5: Invariants for Maxwellian

time	$\mu = 0.01, h = 0.05, \Delta t = 0.005$		
time	I_1	I_2	I_3
0.0	1.7725	1.2533	0.8109
2.5	1.7713	1.2485	0.7889
5.0	1.7708	1.2463	0.7778
7.5	1.7707	1.2460	0.7767
10.0	1.7706	1.2459	0.7764
12.5	1.7706	1.2458	0.7762

Table 5.6: Invariants for Maxwellian

time	$\mu = 0.005, h = 0.01, \Delta t = 0.005$		
time	I_1	I_2	I_3
0.0	1.7725	1.2533	0.8486
2.5	1.7724	1.2529	0.8464
5.0	1.7722	1.2522	0.8438
7.5	1.7720	1.2516	0.8418
10.0	1.7719	1.2510	0.8399
12.5	1.7717	1.2504	0.8380

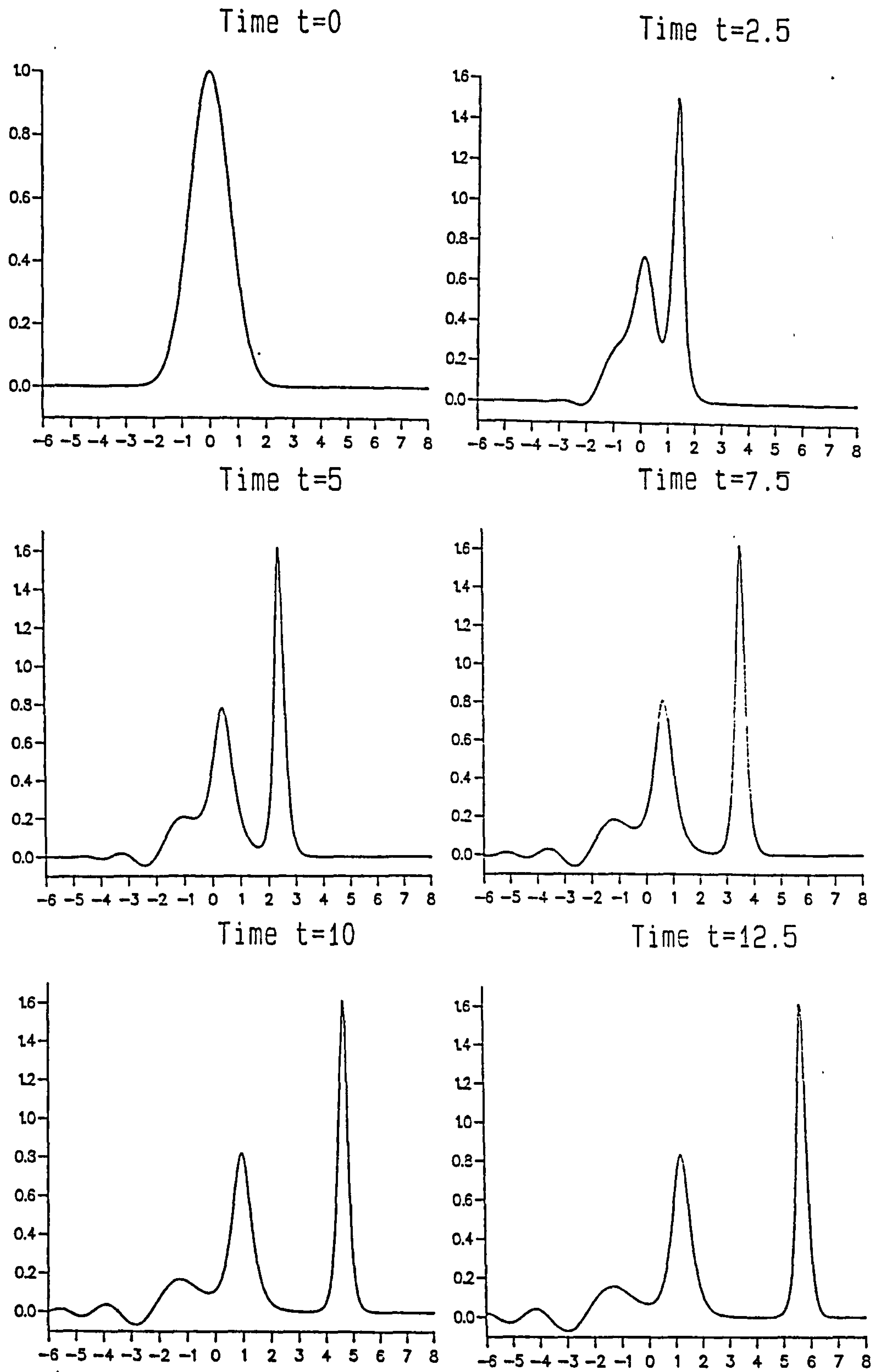

Figure 5.4: Maxwellian initial condition: $\mu = 0.01, \Delta t = 0.005$, $h = 0.05$ range $-50 \leq x \leq 50$, at time $t = 0.0 - 12.5$.

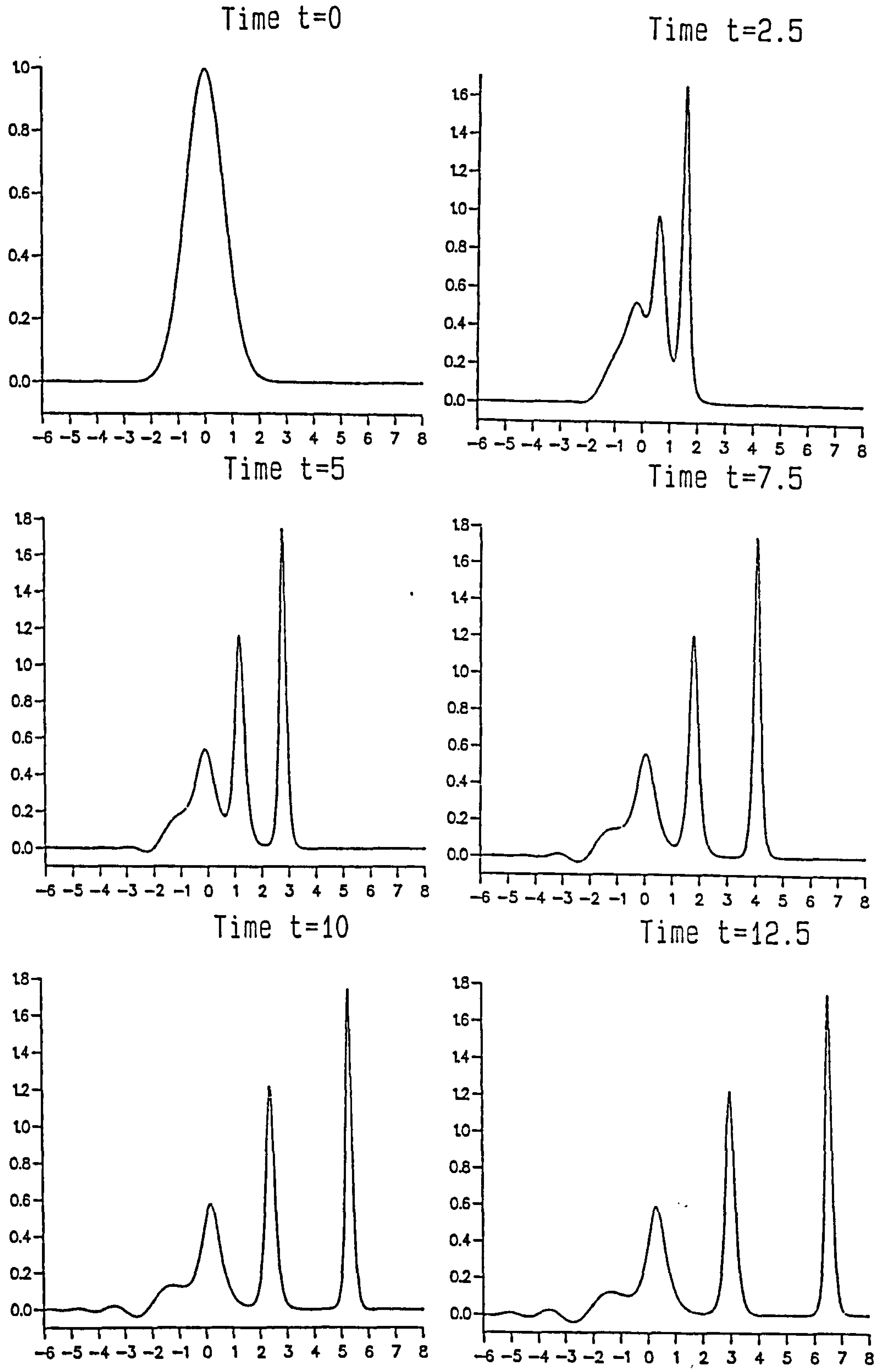

Figure 5.5: Maxwellian initial condition: $\mu = 0.005, \Delta t = 0.005$, $h = 0.01$ range $-15 \leq x \leq 15$, at time $t = 0.0 - 12.5$.

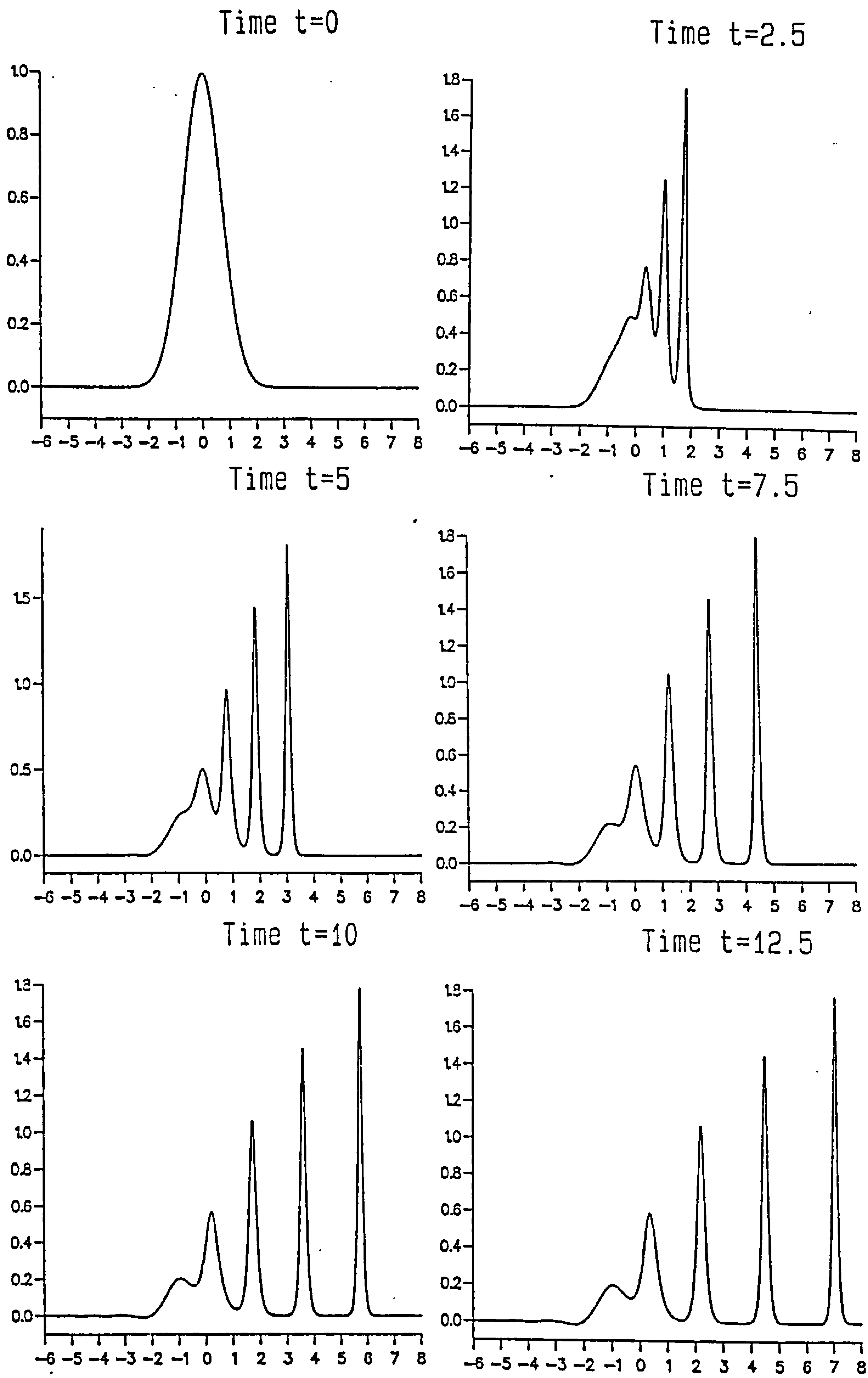

Figure 5.6: Maxwellian initial condition: $\mu = 0.0025, \Delta t = 0.005$, $h = 0.01$ range $-15 \leq x \leq 15$, at time $t = 0.0 - 12.5$.

Table 5.7: Invariants for Maxwellian

time	$\mu = 0.0025, h = 0.01, \Delta t = 0.005$		
time	I_1	I_2	I_3
0.0	1.7725	1.2533	0.8674
2.5	1.7722	1.2520	0.8614
5.0	1.7710	1.2488	0.8504
7.5	1.7699	1.2458	0.8410
10.0	1.7689	1.2431	0.8325
12.5	1.7680	1.2406	0.8247

and the boundary conditions are chosen to be:

$$\left.\begin{array}{l} U(-150,t) = U(150,t) = 0 \\ U_x(-150,t) = U_x(150,t) = 0 \end{array}\right\} \text{for all } t > 0 \qquad (5.35)$$

We have taken $\epsilon = 0.2, \mu = 0.1$ with $\Delta t = 0.05$ and $h = 0.4$. The numerical solution has been determined for the finite range $-150 \leq x \leq 150$ with the boundary conditions, given above applied at $x = \mp 150$.

The behaviour of this solution is given in Figure (5.7). Also we compute the first three conservative quantities up to a time $t = 800$. These are given in Table (5.8).

We have found over the computer runs that the quantities $I_i, (i = 1, \ldots, 3)$ have changed from their original values by less than 0.009%, 0.057% and 0.355% respectively. Therefore we may consider them as relatively constant. The analytic velocity of the soliton in the $MKdV$ equation is defined by $C_a = a^2\epsilon/6$ where a is the amplitude. In this case $a = 1.9884, \epsilon = 0.2$. Hence $C_a \simeq 0.1318$ while the numerical velocity is $C_n = 0.132$. Therefore we find that the analytic and numerical velocities are consistent.

It is observed from Figure (5.7) that the initial perturbation has broken up

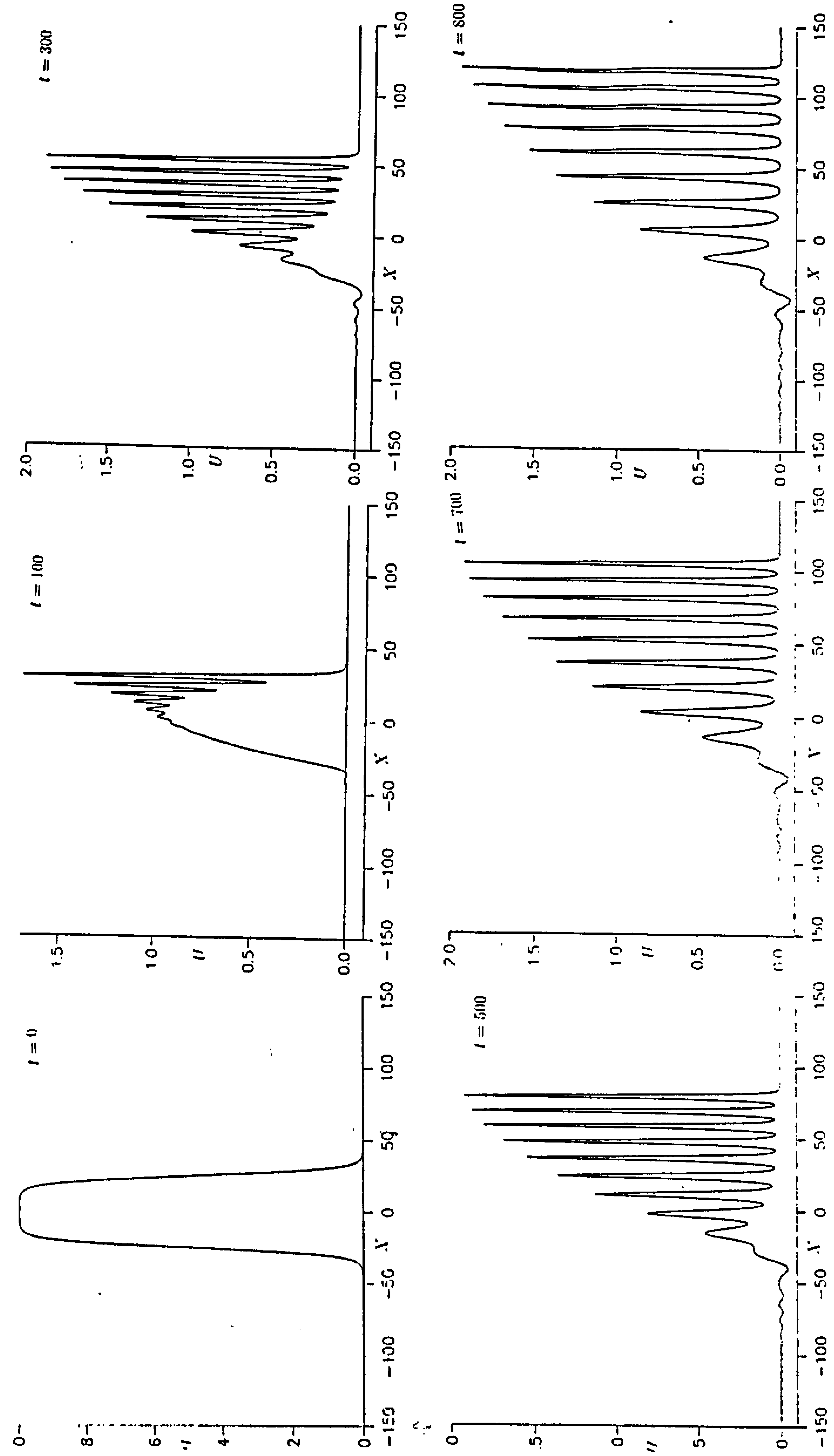

Figure 5.7: Tanh initial condition: $\mu = 0.1, \epsilon = 0.2, \Delta t = 0.05$, $h = 0.4$ range $-150 \leq x \leq 150$, at time $t = 0.0 - 800$.

Table 5.8: Invariants for tanh initial condition.

time	$\epsilon = 0.2, \mu = 0.1, h = 0.4, \Delta t = 0.05$		
time	I_1	I_2	I_3
0.0	50.000244	45.000481	40.433926
100.0	49.983517	44.910309	39.909645
200.0	49.935287	44.674023	38.445984
300.0	49.913094	44.565525	37.815990
400.0	49.905308	44.536327	37.681885
500.0	49.903107	44.530098	37.638954
600.0	49.902920	44.530876	37.612217
700.0	49.908508	44.535641	37.582287
800.0	49.920536	44.540688	37.587090

into a train of solitons, which move steadily to the right with constant speeds whose magnitude depends upon their individual amplitude. It appears, that the amplitudes of the solitons vary approximately linearly. The agreement between the value of the analytic velocity $C_a \approx 0.1318$ for the leading soliton is very satisfactory; especially with these long time and large space steps, we observe that when the time reaches $t = 800$ the initial perturbation has broken up into a train of 9-solitons.

5.3 Discussion

A numerical algorithm for the solution of the $MKdV$ equation based upon a lumped Galerkin method employing quadratic B-spline finite elements has been set up. The scheme is unconditionally stable. It has been used to study the motion, generation and interaction of solitons.

Table 5.9: Single soliton time with accuracy $L_\infty < 0.005$

method	mesh h	mesh Δt	time	$L_2 \times 10^3$	$L_\infty \times 10^3$	$\nu_1 \times 10^4$	$\nu_2 \times 10^4$
quadratic B-spline	0.2	0.025	1.00	3.38	2.03	1.36	2.43
quintic B-spline	0.5	0.025	1.00	6.26	3.30	0.94	4.47
T A [75]	0.1	0.25	1.00		4.48	3.3	55.6
P S [20],[75]	0.625	0.005	1.00		4.57	-14.	-353

In all simulations the 3 invariants I_1, I_2 and I_3 are conserved very well indeed. The error norms observed in simulating the motion of a single soliton are not as small as were obtained with a collocation algorithm and quintic B-spline finite elements using similar space and time steps. However by using smaller steps these errors can easily be reduced.

The present single soliton trials are compared with published work in Table (5.9). The T A scheme due to Taha and Ablowitz [75] is based on the inverse scattering transform and the P S scheme is the pseudospectral method of Forberg and Whitham [20], [75]. The present method performs well.

Chapter 6

Solitary wave solution of the MKdV minus equation

6.1 Introduction

A new numerical solution to the Modified Korteweg-de Vries minus equation is obtained using a "lumped " Galerkin method with quadratic B-spline finite elements. A linear stability analysis of the scheme shows the method to be unconditionally stable. The motion, interaction and generation of solitary waves are studied using the method. The Korteweg-de Vries (KdV) and the Modified Kortewg-de Vries ($MKdV$) equations have been applied to plasma and fluid mechanics problems where perturbations of a small but finite amplitude are considered. In two component models, such as a stratified fluid with 2 layers or a plasma with a 2 temperature electron component, the non-linear term of the KdV equation changes sign for critical values of the physical parameters and the solitons reverse polarity, at least in the case of some slow modes. In the vicinity of the critical parameters higher order non-linearities have to be retained and hence it is thought that the $MKdV$ equation describes the behaviour of the physical system in the transition between a regime with positive KdV solitons to one with negative solitons [16].

Theoretical and numerical studies of both forms of the $MKdV$ equation from various groups have appeared in the literature [85]-[77]. We have previously solved the $MKdV^+$ equation using the method of collocation with quintic B-spline finite elements [23]. In the present studing we set up a new numerical algorithm for the $MKdV^-$ equation based on a "lumped" Galerkin method with quadratic B-spline finite element [24]. The method is used to study the motion, interaction and generation of solitary waves and it performs well. The simulations confirm existing theoretical and numerical work and produce new and interesting results concerning the decay of quasi-soliton initial conditions.

6.1.1 The governing equation

The $MKdV^-$ equation has the form

$$U_t - \epsilon U^2 U_x + U_{xxx} = 0, \qquad \alpha \leq x \leq \beta, \tag{6.1}$$

where the subscripts x and t denote differentiation. The boundary conditions are taken from

$$\begin{aligned} U(\alpha,t) &= a, & U(\beta,t) &= b \\ U_{xx}(\alpha,t) &= 0, & U_{xx}(\beta,t) &= 0 \end{aligned} \tag{6.2}$$

to model the physical boundary conditions that $U(x,t) \rightarrow a$ as $x \rightarrow -\infty$ and $U(x,t) \rightarrow b$ as $x \rightarrow +\infty$. The boundary condition on the second derivative was prefered to one on the first derivative since it let to a very well behaved solution.

The soliton solutions of the $MKdV^-$ equation are distinct from those of the $MKdV^+$ equation and cannot be derived from them. The 1-soliton solution, rising from a background level $U = -a$, is of the form [16]

$$\begin{aligned} U(x,t) = -a[1 - 2\nu^2\{1+ \\ \sqrt{(1-\nu^2)}\cosh 2a\nu[x - x_0 + (6-4\nu^2)a^2t]\}^{-1}], \end{aligned} \tag{6.3}$$

where $0 \leq \nu \leq 1$. This pulse has amplitude $2a[1-\sqrt{(1-\nu^2)}]$ and velocity $-a^2(6-4\nu^2)$. The amplitude and velocity values are limited to the ranges $0 <$ amplitude $< 2a$ and $-6a^2 <$ velocity $< -2a^2$. In contrast to the KdV and $MKdV^+$ equations a smaller $MKdV^-$ soliton moves more rapidly than a larger.
Unlike the $MKdV^+$ equation the $MKdV^-$ equation has also kink travelling wave solutions of the form

$$U(x,t) = \pm a \tanh(ax + 2a^3 t). \tag{6.4}$$

which connects levels $\pm a$ and has velocity $-2a^2$. Only kinks connecting the same two levels can coexist. Similary solitons that coexist with kinks must arise from the same levels and together they form a general solution.

Soliton solutions, for which $U \rightarrow -a$ as $x \rightarrow \pm\infty$, conserve the following integrals

$$\begin{aligned} I_1 &= \int_{-\infty}^{+\infty} U dx \\ I_2 &= \int_{-\infty}^{+\infty} U^2 dx \\ I_3 &= \int_{-\infty}^{+\infty} [U^4 - \tfrac{6\mu}{\epsilon}(U_x)^2] dx \end{aligned} \tag{6.5}$$

6.2 The $MKdV^-$ simulations

6.2.1 Problem 1. Single solitary wave

Firstly, the motion of a single solitary wave is studied using as initial condition (6.3) at $t = 0$.

$$U(x,0) = -a[1 - 2\nu^2\{1 + \sqrt{(1-\nu^2)}\cosh 2a\nu[x - x_0]\}^{-1}], \tag{6.6}$$

In the simulation $x_0 = 0, a = 1, \nu = 0.5, h = 0.1, \Delta t = 0.0005$ and a range $-40 \leq x \leq 20$, superimposed and perspective view graphs of the solitons profile are given in Figures(6.1-6.2), which produces a single soliton

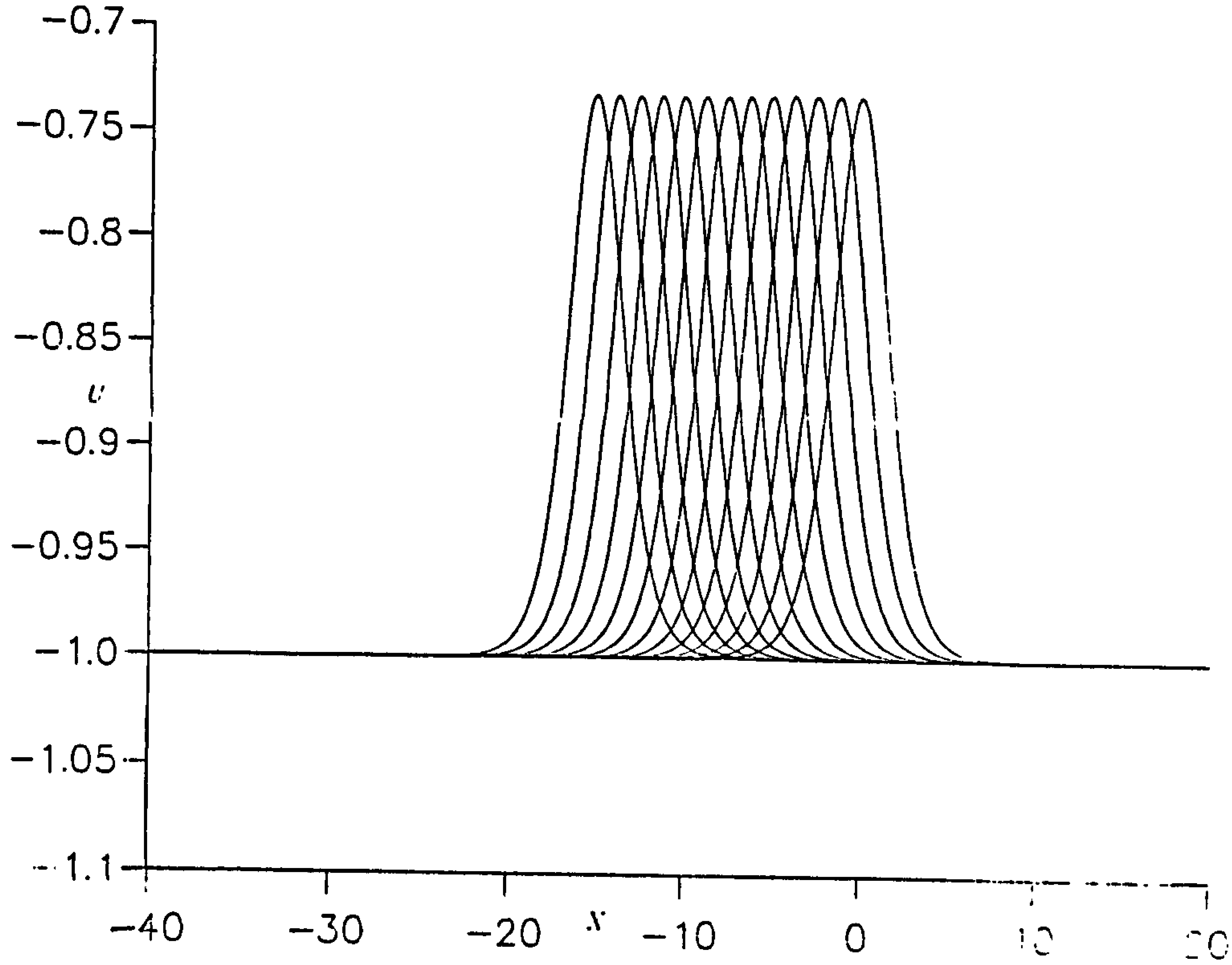

Figure 6.1: The interaction of single soliton, $x_0 = 0, a = 1, \nu = 0.5, h = 0.1, \Delta t = 0.0005$ and a range $-40 \leq x \leq 20$. Superimposed profiles for integer times $t = 0$ to $t = 3.0$.

of amplitude 0.4019 originally sited at $x = 0$ moving to the left with velocity 5.0. The L_2 and L_∞ error norms are computed to estimate the accuracy of the algorithm and the invariants I_1, I_2, I_3 to test its conservation, these are listed in Table (6.1). The error norms are small showing that the position and shape of the soliton are well represented by the numerical solution. The lowest three invariants change by less than 0.05% during the run so that the numerical algorithm has good conservation properties too.

6.2.2 Problem 2. Interaction of 2 solitary waves

Soliton interaction is studied through the 2-soliton solution using as initial condition

$$\begin{aligned} U(x,0) &= -a + 2a\nu_1^2\{1 + \sqrt{(1-\nu_1^2)}\cosh 2a\nu_1[x - x_1]\}^{-1} \\ &+ 2a\nu_2^2\{1 + \sqrt{(1-\nu_2^2)}\cosh 2a\nu_2[x - x_2]\}^{-1} \end{aligned} \tag{6.7}$$

with $\nu_1 = 0.2, \nu_2 = 0.6, x_1 = 10$ and $x_2 = -10$, which leads to a soliton of amplitude 0.0404 originally placed at $x = 10$ moving to the left with

Table 6.1: Error norms and Invariants for a single soliton $a = 1, \nu = 0.5$, $h = 0.1, \Delta t = 0.0005$

time	$L_2 \times 10^3$	$L_\infty \times 10^3$	I_1	I_2	I_3
0.25	0.1212	0.0402	-59.0021	58.1014	56.7696
0.50	0.2261	0.0704	-59.0026	58.1027	56.7717
0.75	0.3288	0.0924	-59.0033	58.1038	56.7737
1.00	0.4260	0.1241	-59.0038	58.1048	56.7757
1.25	0.5367	0.1611	-59.0044	58.1059	56.7778
1.50	0.6537	0.2082	-59.0051	58.1071	56.7801
1.75	0.7748	0.2762	-59.0056	58.1082	56.7821
2.00	0.9071	0.3436	-59.0062	58.1092	56.7841
2.25	1.0520	0.4094	-59.0069	58.1103	56.7863
2.50	1.2001	0.4798	-59.0075	58.1115	56.7886
3.00	1.5045	0.6392	-59.0088	58.1138	56.7930

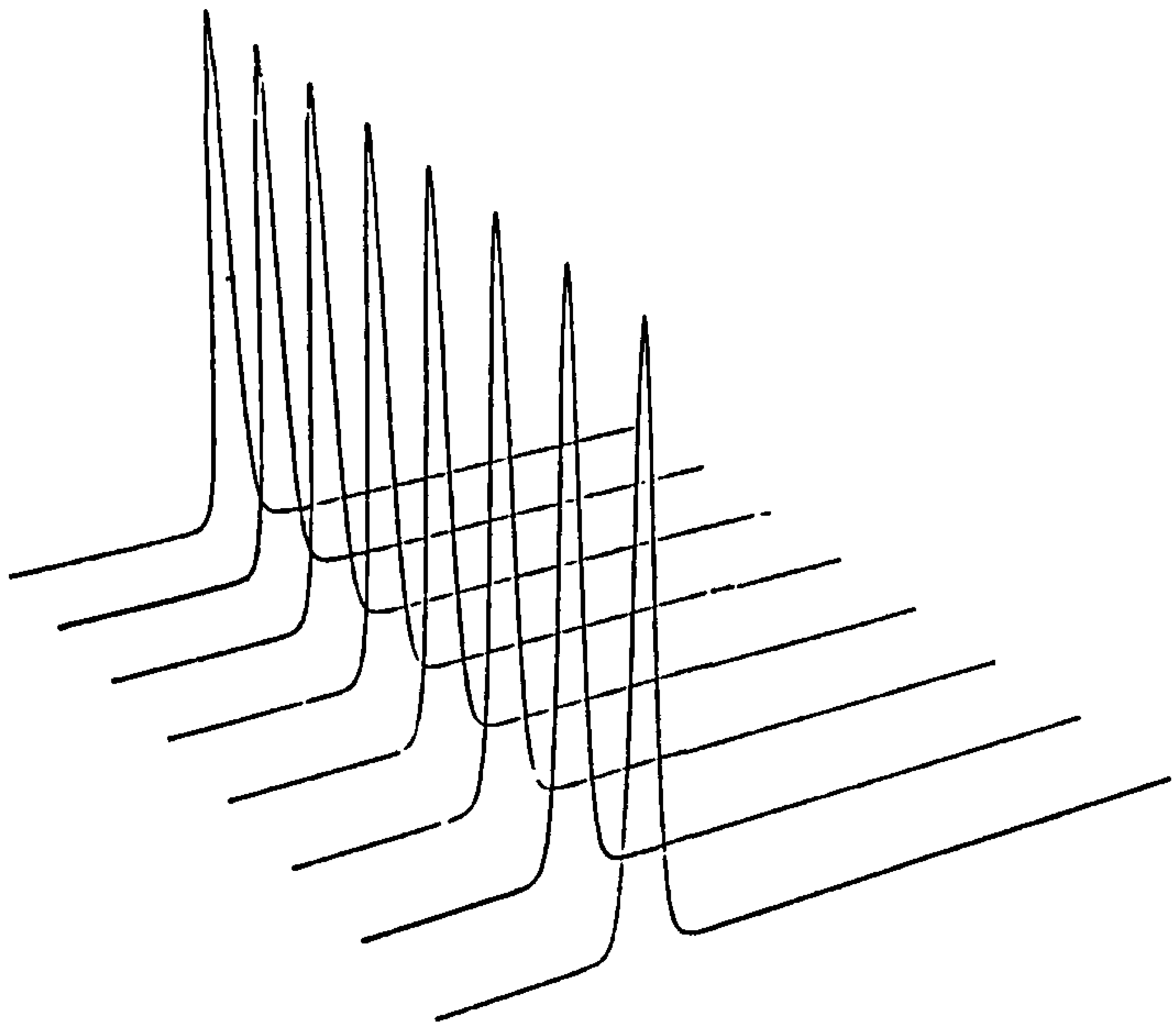

Figure 6.2: The interaction of single soliton. $x_0 = 0, a = 1, \nu = 0.5, h = 0.1, \Delta t = 0.0005$ and a range $-40 \leq x \leq 20$. Perspective view of the simulation.

velocity 5.84 to impact with a soliton of amplitude 0.4 originally at $x = -10$ moving to the left with the lower velocity of 4.56; the interaction is shown in figures(6.3-6.4). In the simulation $a = 1, h = 0.1$, $\Delta t = 0.0005$ and a range $-200 \leq x \leq 20$; superimposed graphs of the solitons' profile are given in figures(6.3-6.4) from which it is seen that when the solitons coalesce the amplitude of the signal is reduced. The conservation properties of this simulation are also examined; the invariants are monitored and changes of less than 0.04% are recorded; see Table (6.2). Perelman et al [56] have shown that the faster ν_1 soliton acquires a positive phase shift Δ while the slower ν_2 soliton acquires a negative shift $-\Delta$ given by

$$\Delta = \ln[\frac{\nu_2 + \nu_1}{\nu_2 - \nu_1}], \tag{6.8}$$

so that after the collision the function profile has equation

$$\begin{aligned} U(x,t) = -a + 2a\nu_1^2\{1 + \sqrt{(1-\nu_1^2)}\cosh 2a\nu_1[x - x_1 + \tfrac{\Delta}{\nu_1} + (6 - 4\nu_1^2)a^2 t]\}^{-1} \\ +2a\nu_2^2\{1 + \sqrt{(1-\nu_2^2)}\cosh 2a\nu_2[x - x_2 - \tfrac{\Delta}{\nu_2} + (6 - 4\nu_2^2)a^2 t]\}^{-1} \end{aligned} \tag{6.9}$$

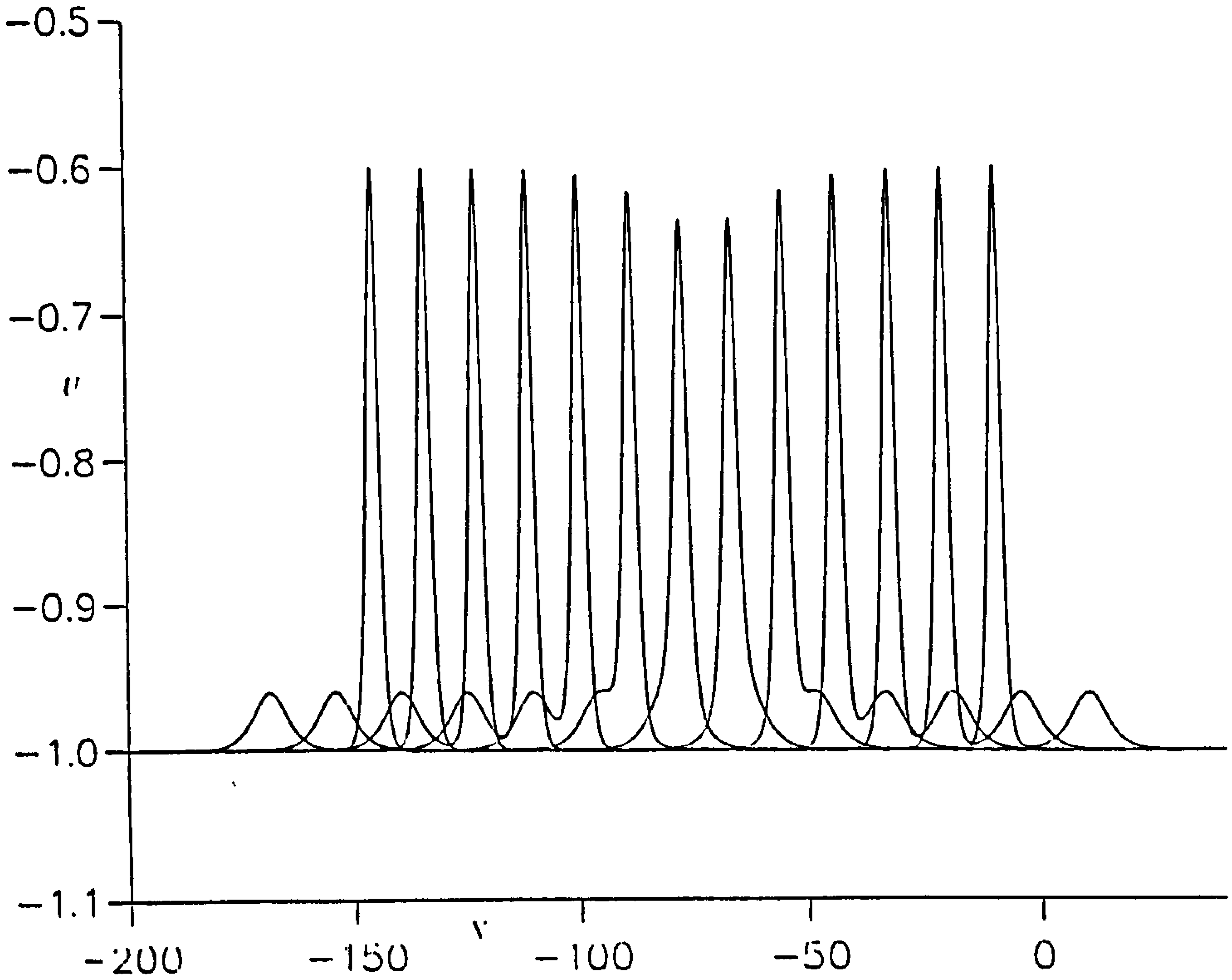

Figure 6.3: The interaction of two solitons, $\nu = 0.2$ and $\nu = 0.6$. Superimposed profiles for integer times $t = 0$ to $t = 12$.

The observed phase shift for soliton 1 is 0.694 and that for soliton 2 is -0.696. The above formula leads to $\Delta = 0.693$ so that the observation are consistent with theory.

6.2.3 Problem 3. A kink pair

To observe the behaviour of two well separated kinks we consider the initial condition

$$U(x,t) = a\{\tanh(ax - ax_0 + 2a^3t) - \tanh(ax - ax_1 + 2a^3t) - 1\}, \quad (6.10)$$

at $t = 0$. Take $a = 1$, so that $U \to -1$ as $x \to \pm\infty, x_0 = -10$ and $x_1 = 10$ and observe the development of the solution with $h = 0.1, \Delta t = 0.0005$ and a range $-60 \leq x \leq 20$; superimposed graphs of the profile of the solution are given in Figures(6.5-6.6).

It is seen that both kinks move to the left with equal velocities $c = 2$ so that the profile of the solution remains constant and is simply rigidly translated through a distance that depends linearly on time. the invariants

Table 6.2: Invariants for two solitons $\nu_1 = 0.2, \nu_2 = 0.6, h = 0.1, \Delta t = 0.0005$

time	I_1	I_2	I_3
0.0	-218.415207	217.014328	215.024094
2.5	-218.420197	217.023972	215.043015
5.0	-218.424408	217.032440	215.060471
7.5	-218.428391	217.040405	215.075607
10.0	-218.431229	217.046021	215.086716
12.5	-218.433426	217.050171	215.095261
15.0	-218.434647	217.052902	215.100830
17.5	-218.435822	217.054413	215.103104
20.0	-218.435455	217.054001	215.101730
22.5	-218.434967	217.052902	215.098953
25.0	-218.433075	217.049362	215.091583
27.5	-218.430588	217.043945	215.080414
30.0	-218.427811	217.038452	215.069611

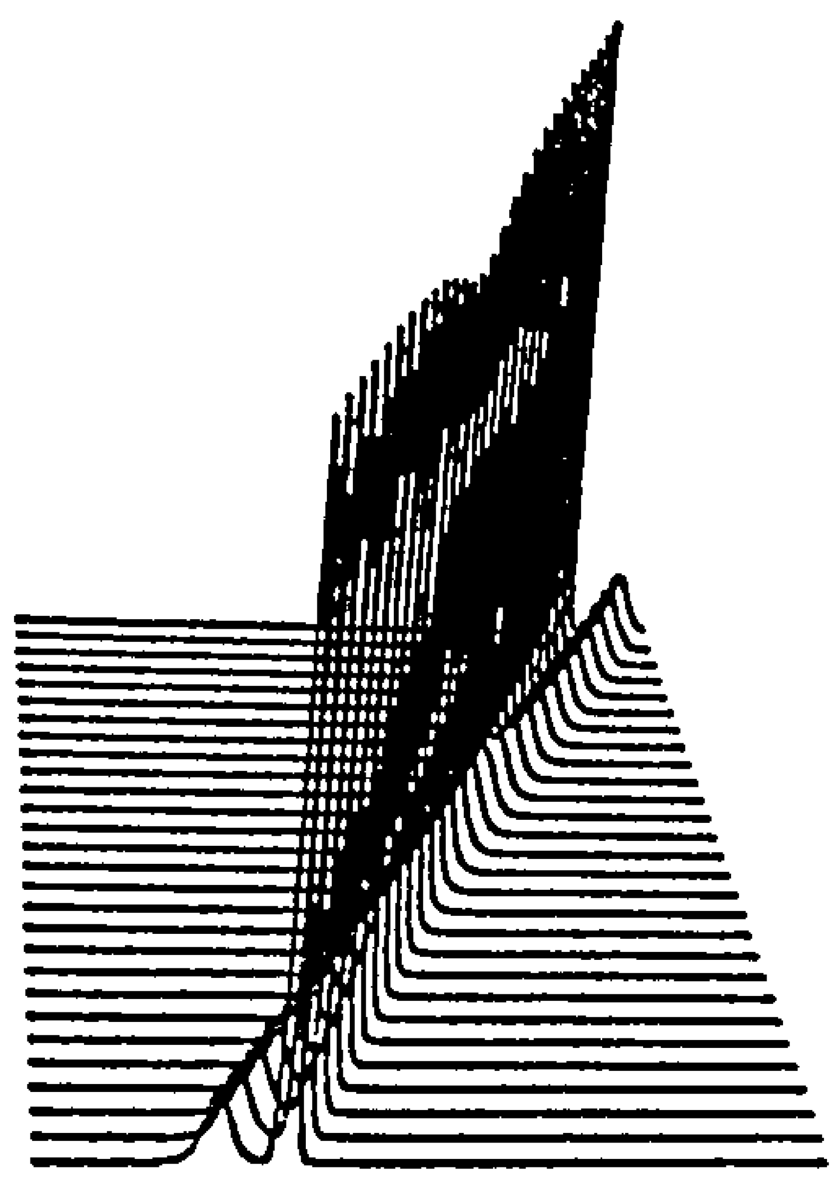

Figure 6.4: The interaction of two solitons, $\nu = 0.2$ and $\nu = 0.6$. Perspective view of the simulation.

for this simulation are given in Table (6.3); they change by less than 0.08% and so are well conserved. Summing the tanh functions together leads to

$$U(x,t) = -1 + 2\nu^2\{1 + \sqrt{(1-\nu^2)}\cosh 2[x + 2t]\}^{-1} \tag{6.11}$$

where $\nu = \tanh(20) \sim 1 - 10^{-17}$ which shows that the kink pair corresponds to an extended soliton [16] with ν differing from 1 by about 10^{-17} so that it has amplitude 2 and speed equal to 2.

6.2.4 Problem 4. Interaction of a soliton with a kink

The interaction of a kink and a soliton is studied via the initial condition

$$U(x,0) = a\tanh(ax) - 2a\nu^2\{1 + \sqrt{(1-\nu^2)}\cosh 2a\nu[x - x_0]\}^{-1}. \tag{6.12}$$

In the simulations $a = 1, h = 0.1, \Delta t = 0.0005$ and a range $-50 \leq x \leq 30$; superimposed graphs of the solution profile are given in figures(6.7-6.15), from which we observe the soliton ($\nu = 0.03$) initially on the right catch up with the kink, pass through it and emerge on the lefthand side inverted but

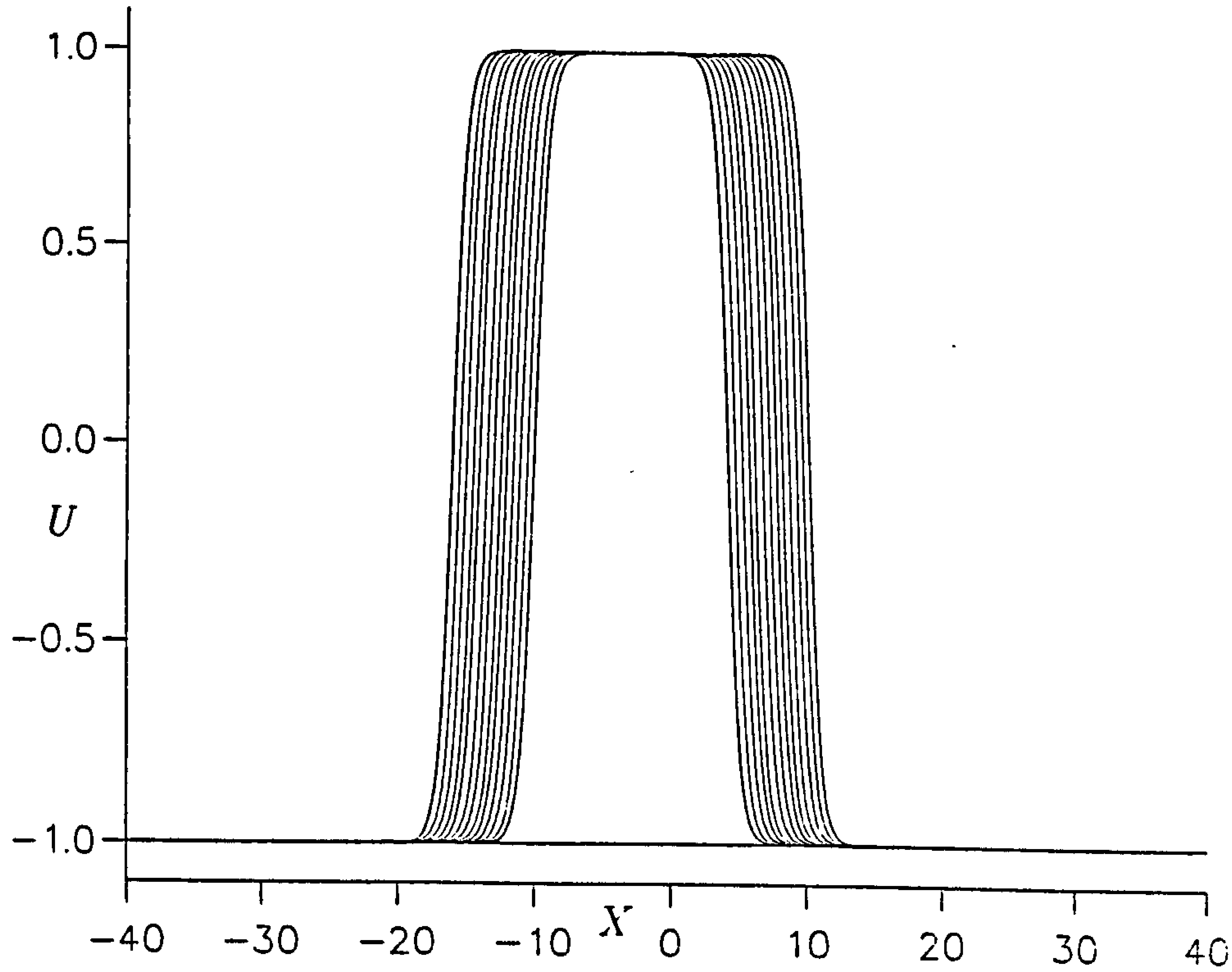

Figure 6.5: Kink pair. $a = 1$. Superimposed profiles.

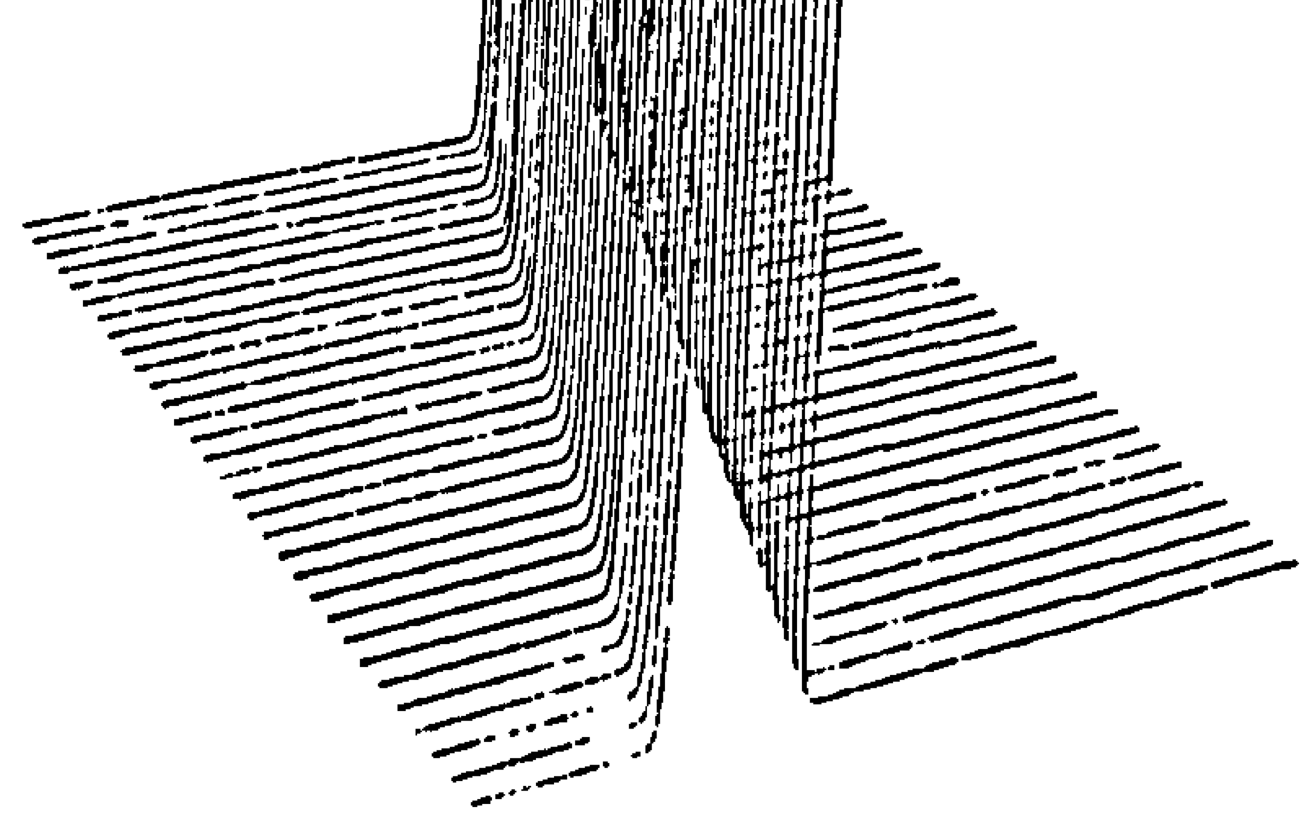

Figure 6.6: Kink pair. $a = 1$. Perspective views of the experiment.

Table 6.3: Invariants for a kink pair $a = 1$

time	I_1	I_2	I_3
0.00	-40.1000	76.1000	77.4370
0.25	-40.1002	76.1019	77.4410
0.50	-40.1004	76.1040	77.4448
0.75	-40.1008	76.1063	77.4494
1.00	-40.1013	76.1090	77.4548
1.25	-40.1019	76.1118	77.4606
1.50	-40.1027	76.1148	77.4666
1.75	-40.1034	76.1180	77.4730
2.00	-40.1040	76.1208	77.4786
2.50	-40.1051	76.1262	77.4894
3.00	-40.1058	76.1310	77.4987

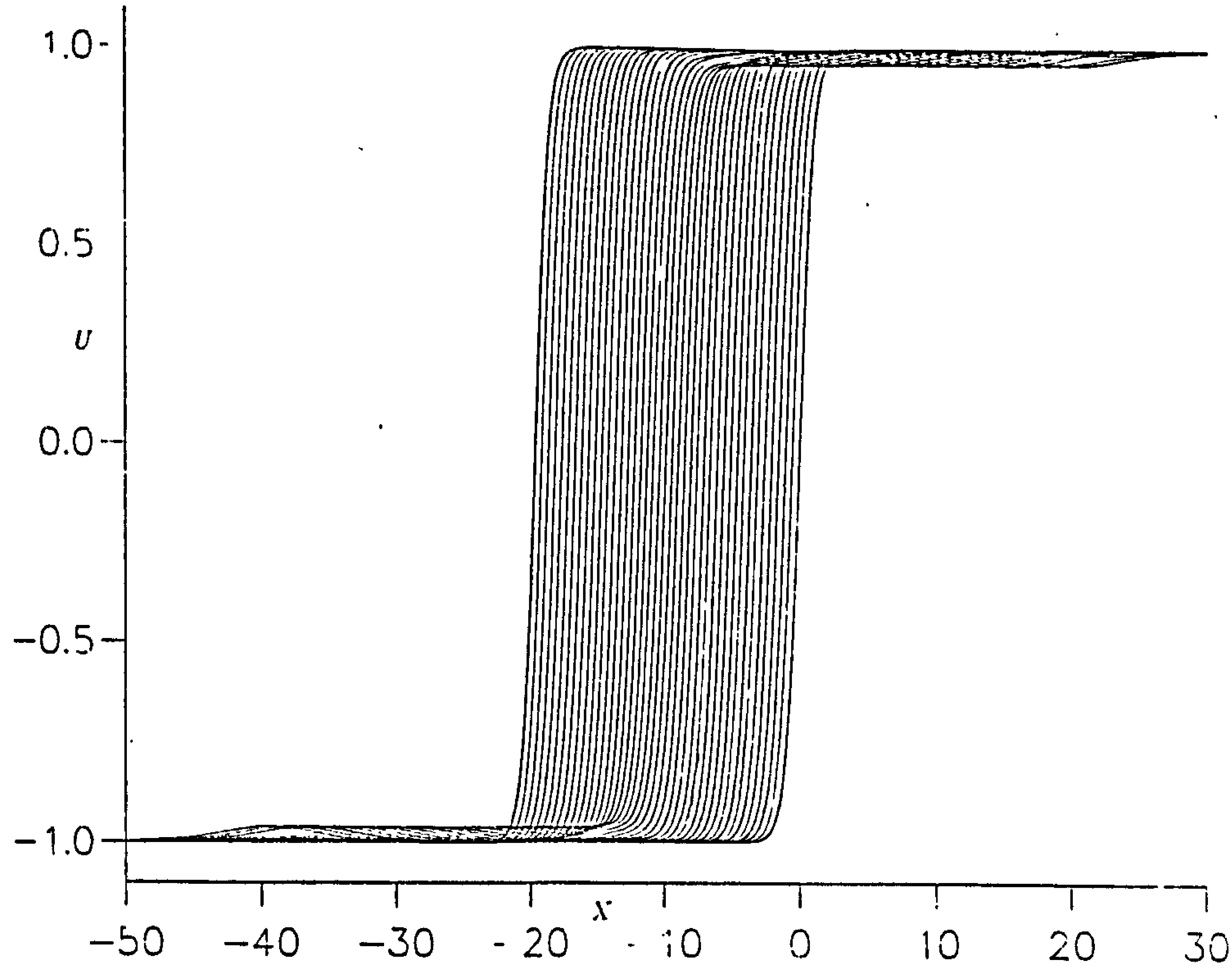

Figure 6.7: The interaction of a soliton, $\nu = 0.2$, with a kink, $a = 1$. Superimposed profiles for integer times.

with unchanged amplitude and velocity and having undergone a phase shift. This interaction has been described theoretically by Perelman et al [56] who show that after the interaction the kink has undergone a negative phase shift

$$\Delta = \ln[\frac{1+\nu}{1-\nu}], \tag{6.13}$$

while the soliton has suffered a positive phase shift of 0.5Δ , so that after the interaction the function profile is given by

$$\begin{aligned} U(x,t) &= a\tanh(ax - \Delta + 2a^3t) \\ &-2a\nu^2\{1+\sqrt{(1-\nu^2)}\cosh 2a\nu[x - x_0 + \tfrac{\Delta}{2\nu} + (6-4\nu^2)a^2t]\}^{-1}. \end{aligned} \tag{6.14}$$

The shifts observed in the simulations for values of ν in the range $0.2 \le \nu \le 0.9$ are compared with theoretical values in Table (6.5) and for $\nu = 0.2$ three invariants shown in Table(6.4). Agreement is excellent.

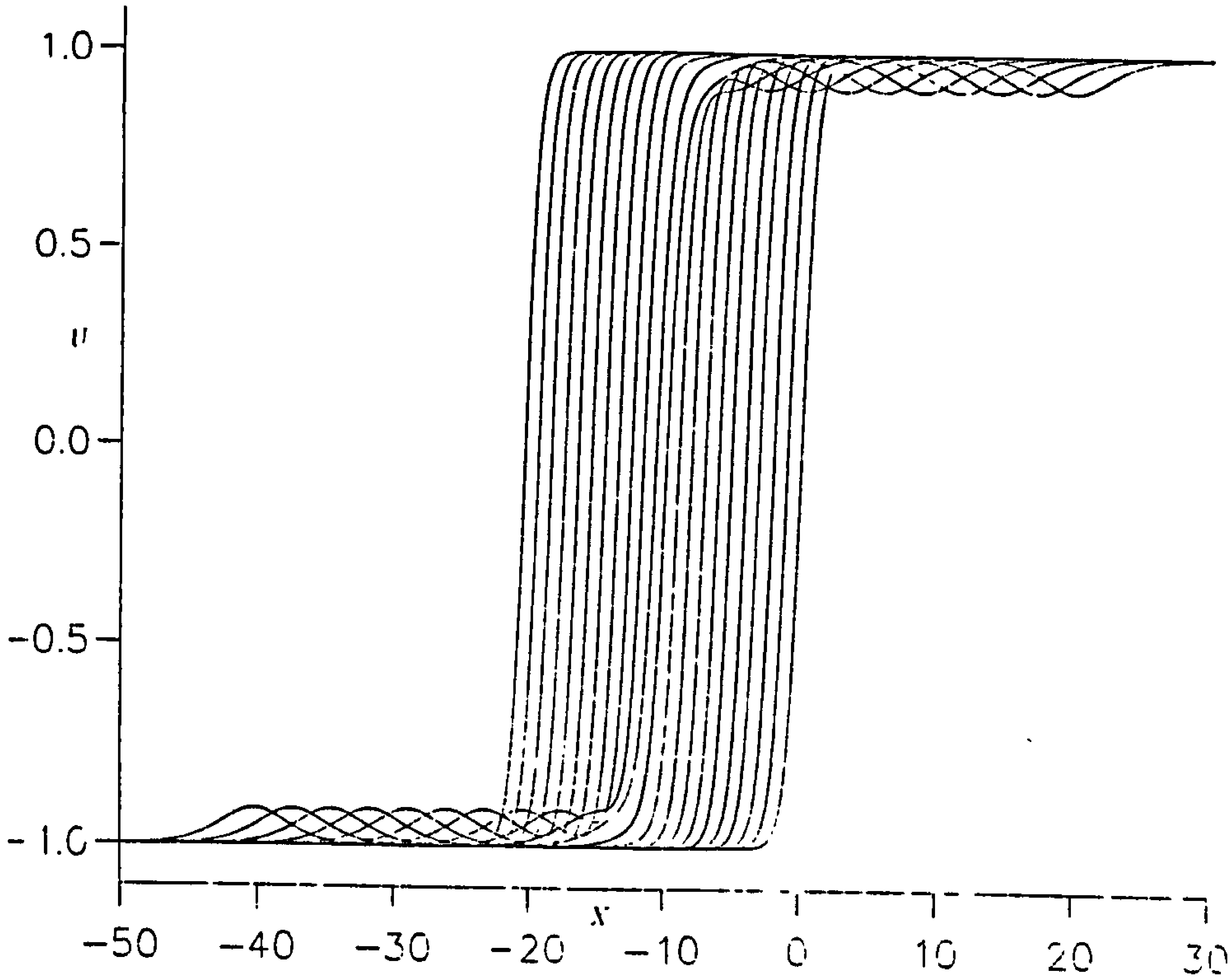

Figure 6.8: The interaction of a soliton, $\nu = 0.3$, with a kink, $a = 1$. Superimposed profilesfor integer times.

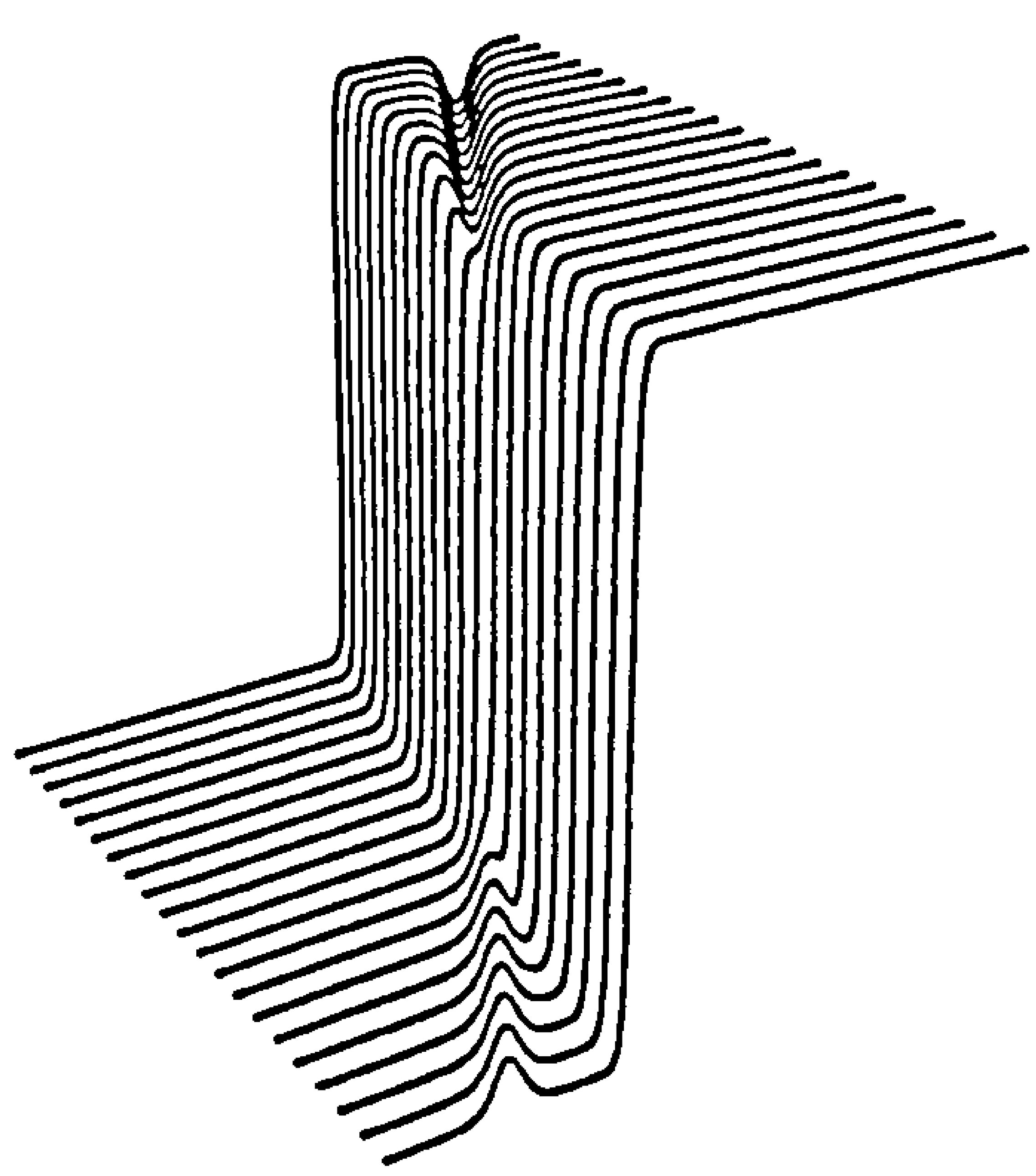

Figure 6.9: The interaction of a soliton, $\nu = 0.4$, with a kink, $a = 1$. Superimposed profilesfor integer times.

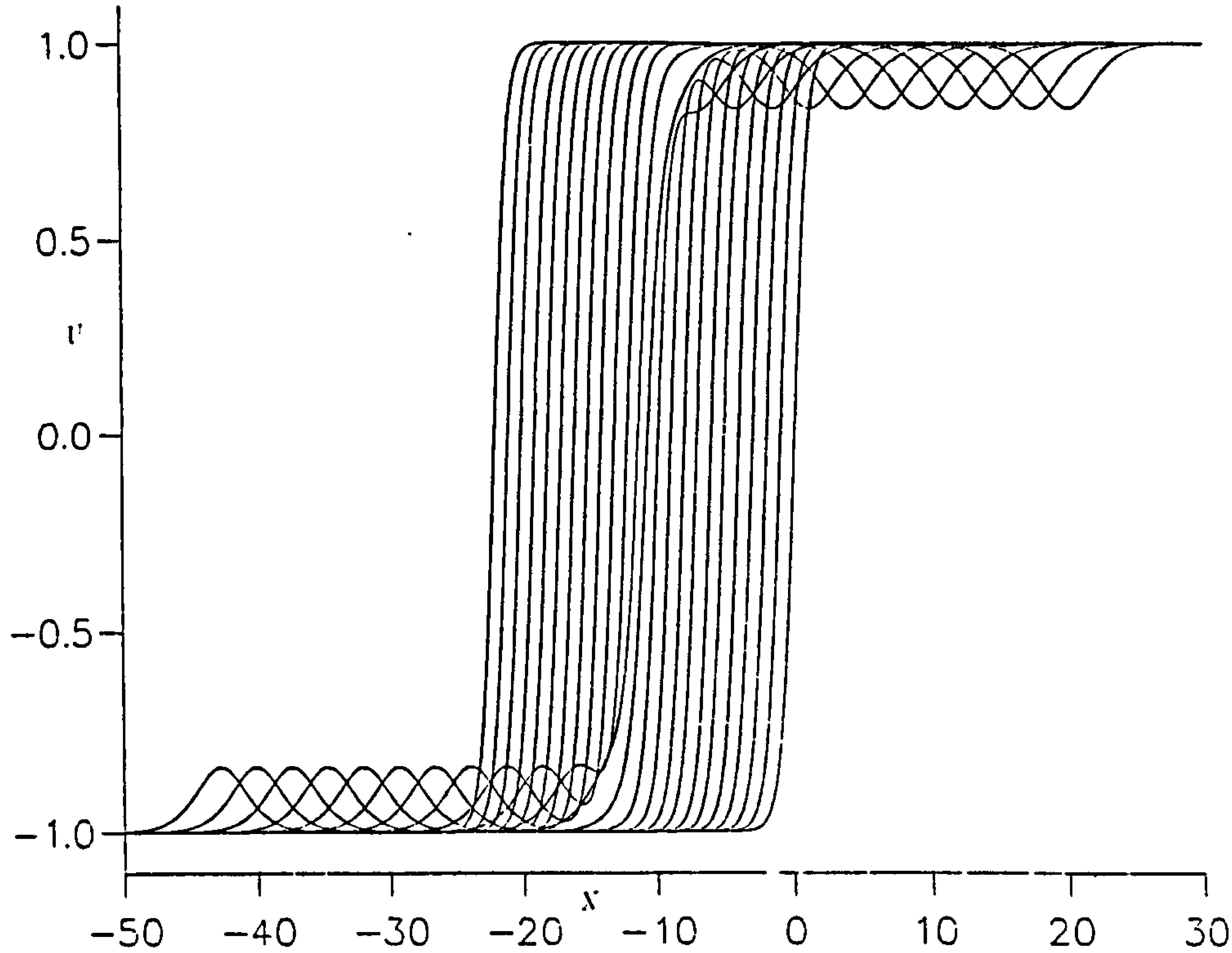

Figure 6.10: The interaction of a soliton, $\nu = 0.4$, with a kink, $a = 1$. perspective view.

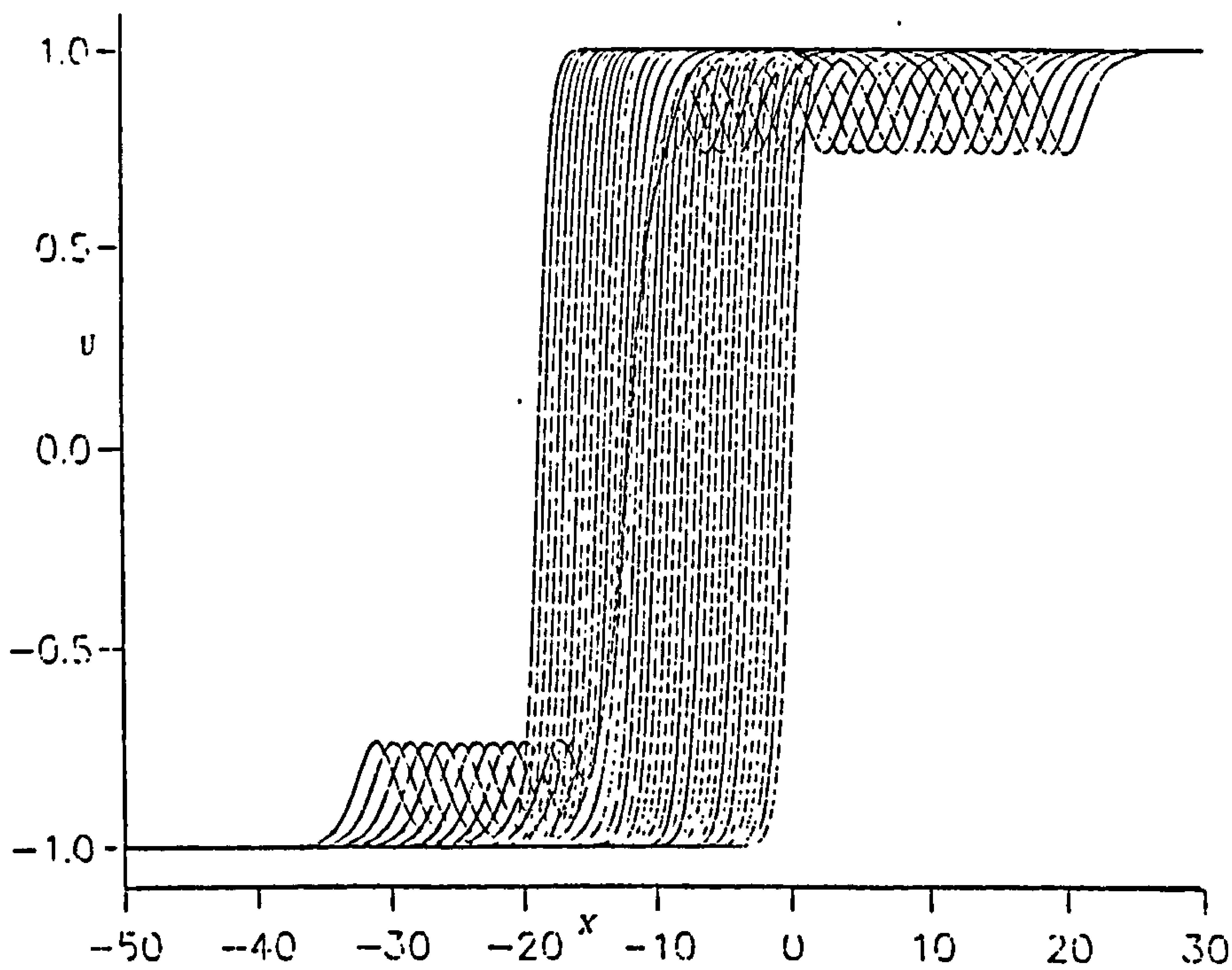

Figure 6.11: The interaction of a soliton, $\nu = 0.5$, with a kink, $a = 1$. Superimposed profilesfor integer times.

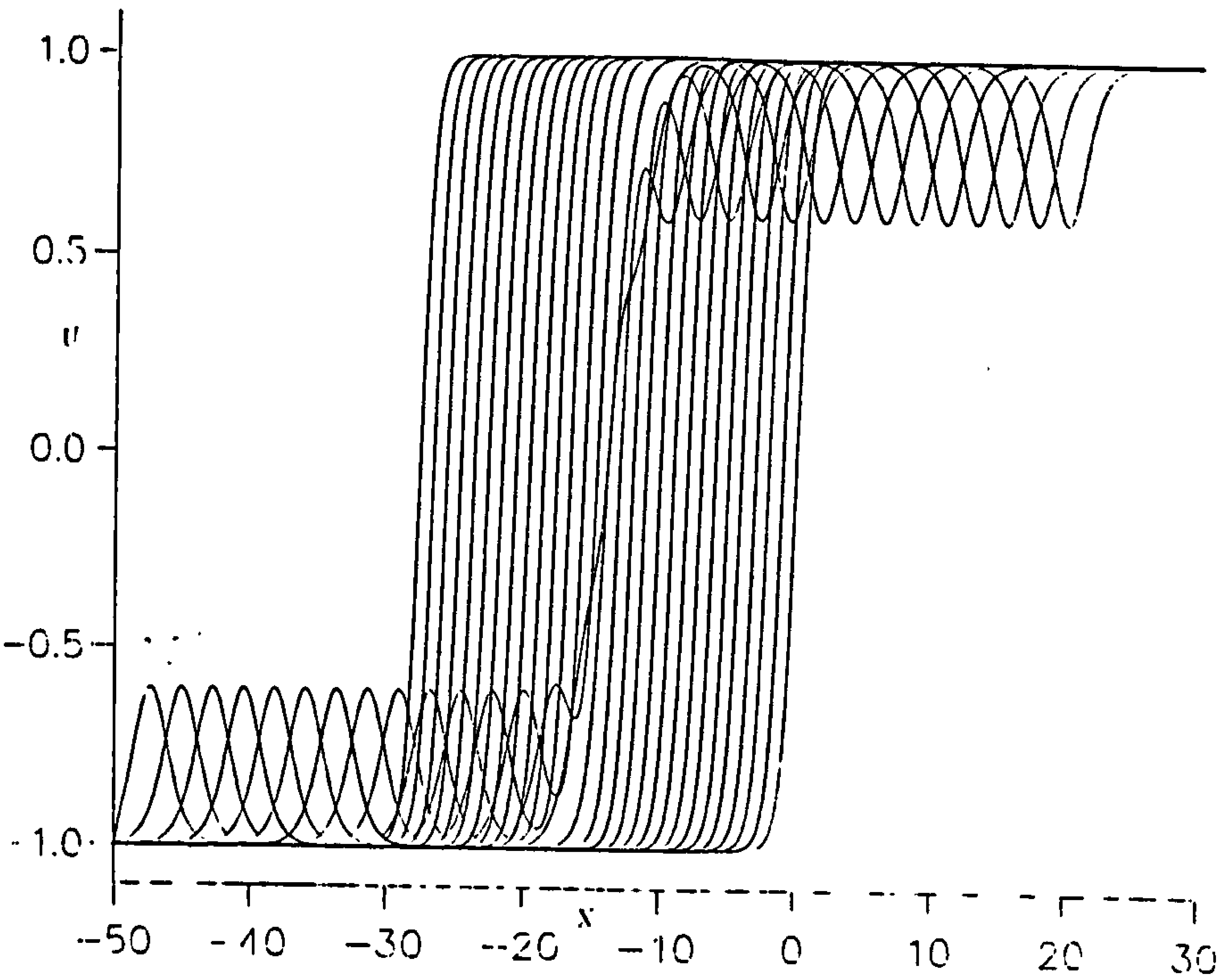

Figure 6.12: The interaction of a soliton, $\nu = 0.6$, with a kink. $a = 1$. Superimposed profilesfor integer times.

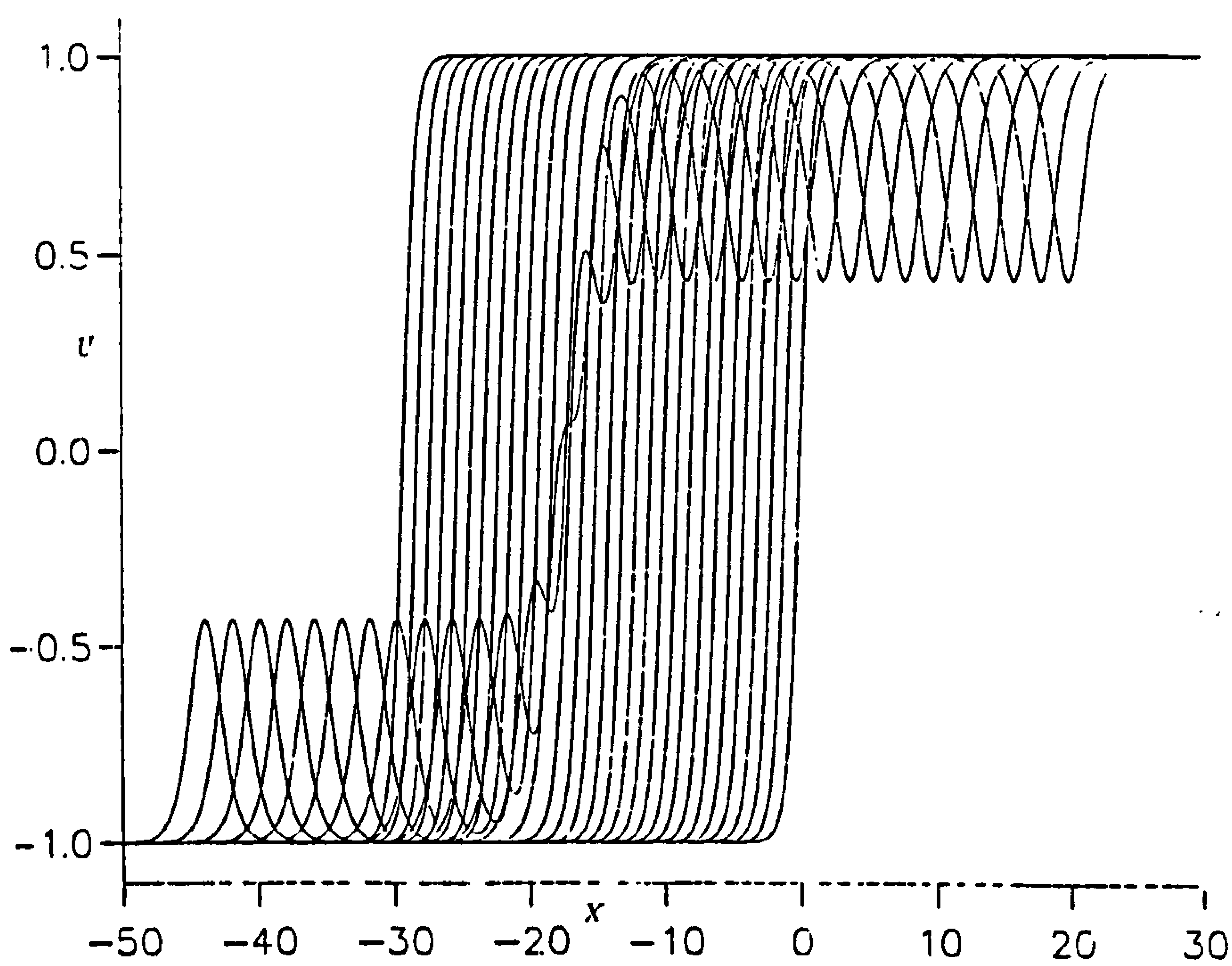

Figure 6.13: The interaction of a soliton, $\nu = 0.7$, with a kink, $a = 1$. Superimposed profilesfor integer times.

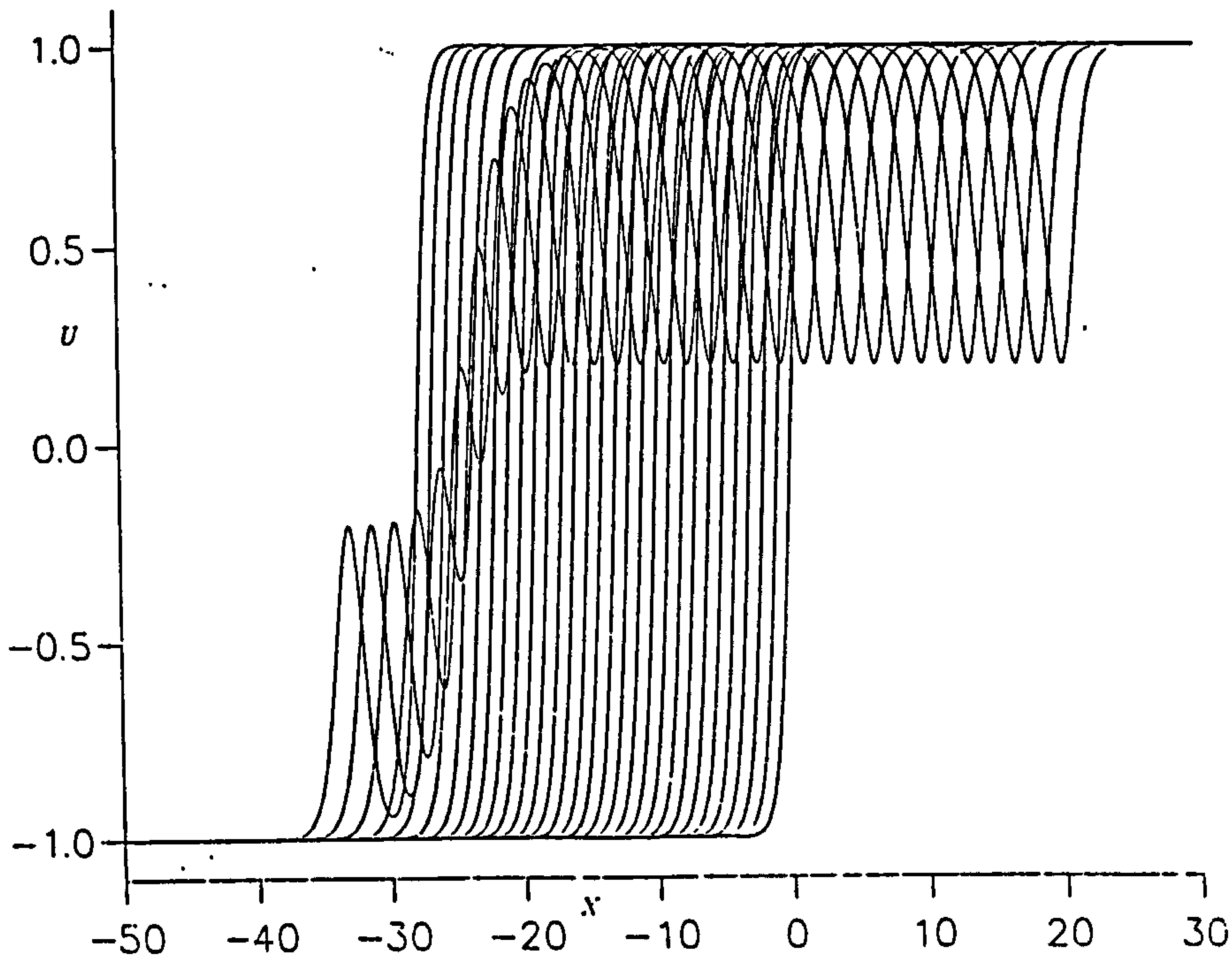

Figure 6.14: The interaction of a soliton, $\nu = 0.8$, with a kink. $a = 1$. Superimposed profilesfor integer times.

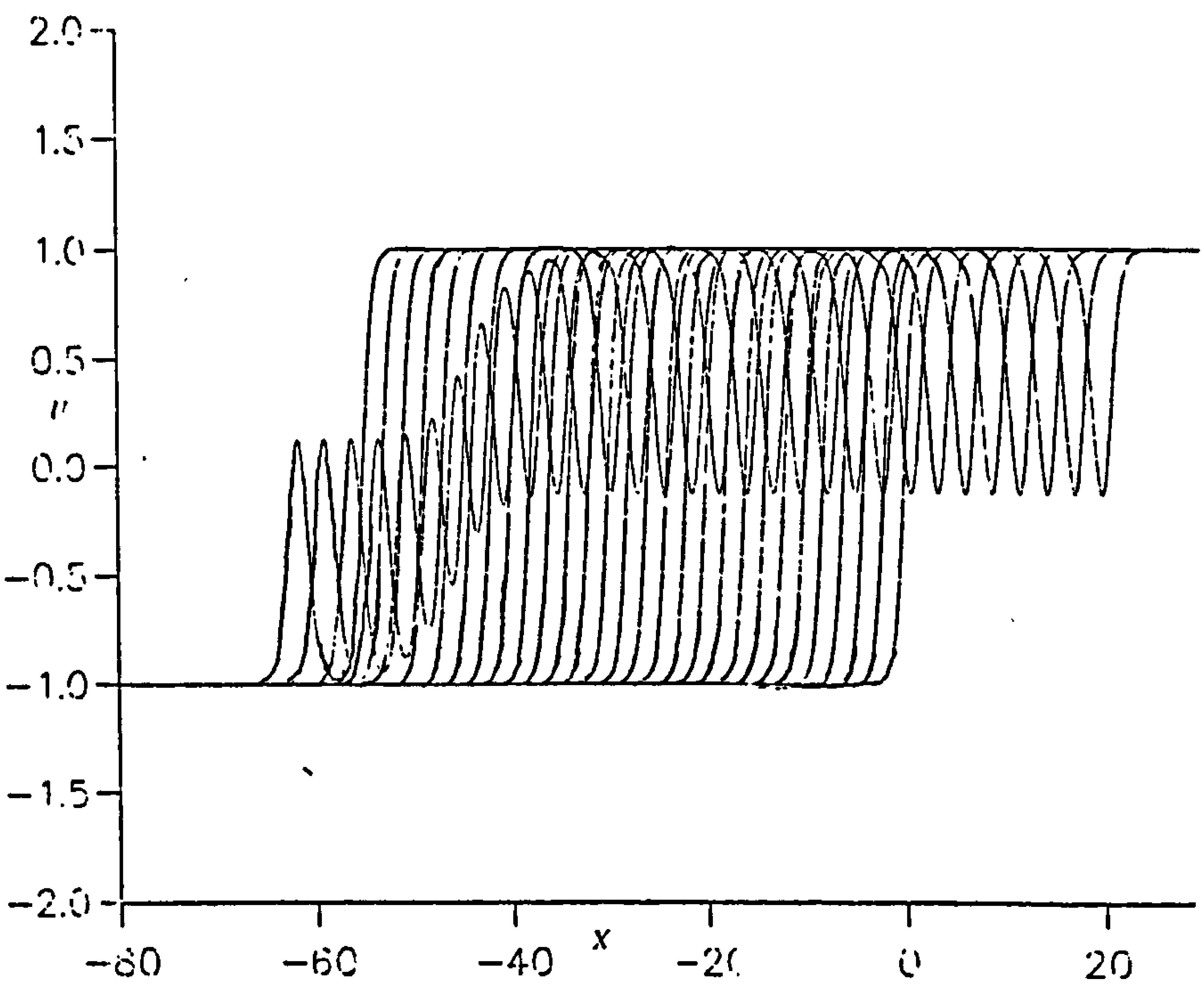

Figure 6.15: The interaction of a soliton, $\nu = 0.9$, with a kink, $a = 1$. Superimposed profilesfor integer times.

Table 6.4: Invariants for soliton-kink interactions: $\nu = 0.2, h = 0.1$, $\Delta t = 0.0005$

time	I_1	I_2	I_3
0.0	77.613525	76.100136	75.435410
1.0	77.618637	76.110428	75.455292
2.0	77.625763	76.123917	75.481735
3.0	77.632744	76.137192	75.507950
4.0	77.639206	76.150940	75.534805
5.0	77.632248	76.164955	75.562202
6.0	77.440979	76.179817	75.590378
7.0	77.581169	76.192924	75.617104
8.0	77.663132	76.205719	75.642456
9.0	77.674553	76.219383	75.669380
10.0	77.681747	76.233078	75.696083

Table 6.5: Observed and theoretical phase shifts for soliton-kink interactions

ν	Δ_k obs	Δ_s obs	Δ_k theor	Δ_s theor
0.2	-0.4	0.2	-0.4	0.2
0.3	-0.62	0.309	-0.619	0.309
0.4	-0.85	0.444	-0.847	0.424
0.5	-1.1	0.55	-1.09	0.545
0.6	-1.4	0.690	-1.39	0.695
0.7	-1.74	0.868	-1.735	0.868
0.8	-2.20	1.10	-2.197	1.10
0.9	-2.88	1.58	-2.94	1.47

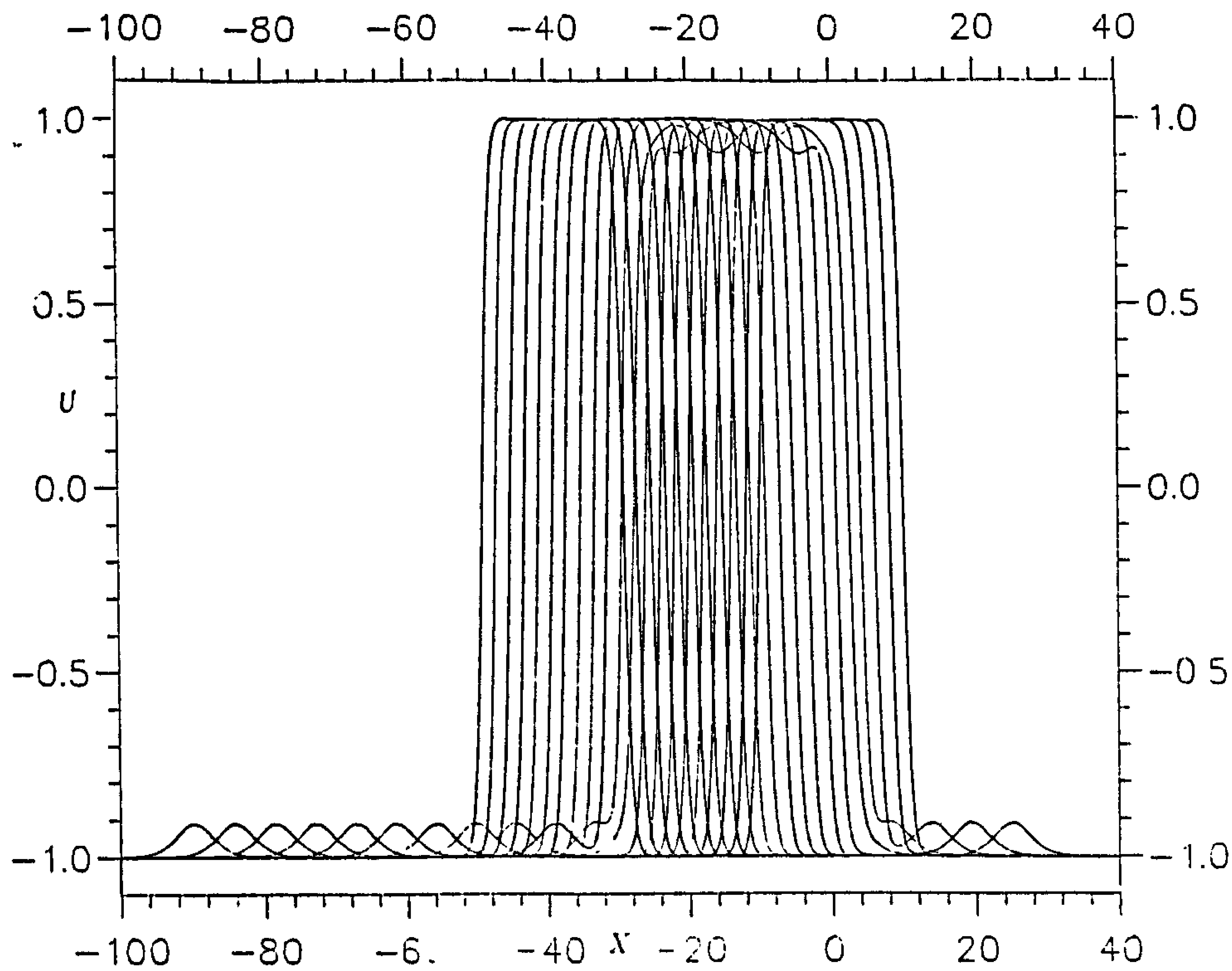

Figure 6.16: The interaction of a soliton, $\nu = 0.3$, with a kink pair, $a = 1$. Superimposed profiles for integer times.

6.2.5 Problem 5. Interaction of a soliton with kink pair

The initial conditions has the form

$$\begin{aligned} U(x,0) &= a[\tanh(ax - ax_0) - \tanh(ax - ax_1) - 1] \\ &-2a\nu^2\{1 + \sqrt{(1-\nu^2)}\cosh 2a\nu[x - x_2]\}^{-1}. \end{aligned} \tag{6.15}$$

In the simulation we use $a = 1, \nu = 0.3, x_0 = -10, x_1 = 10$, $x_2 = 25$ and $h = 0.2, \Delta t = 0.005$ and a range $-100 \leq x \leq 40$.

The soliton passes through each of the kinks as shown in figures(6.16-6.17) and emerges at the left with unchanged size, shape and velocity but having undergone a phase shift of $\Delta_s = -2.07$, while each of the kinks has suffered equal phase shifts of $\Delta_k = 1.25$. As has been seen (Problem 3), a kink pair behaves like a soliton with $\nu = 1$ so one would expect a phase shift of $\Delta_{ks} = 1.238$ which accords with observation. The invariants for this simulation, showing of less than 0.02%, are well conserved; see Table (6.6).

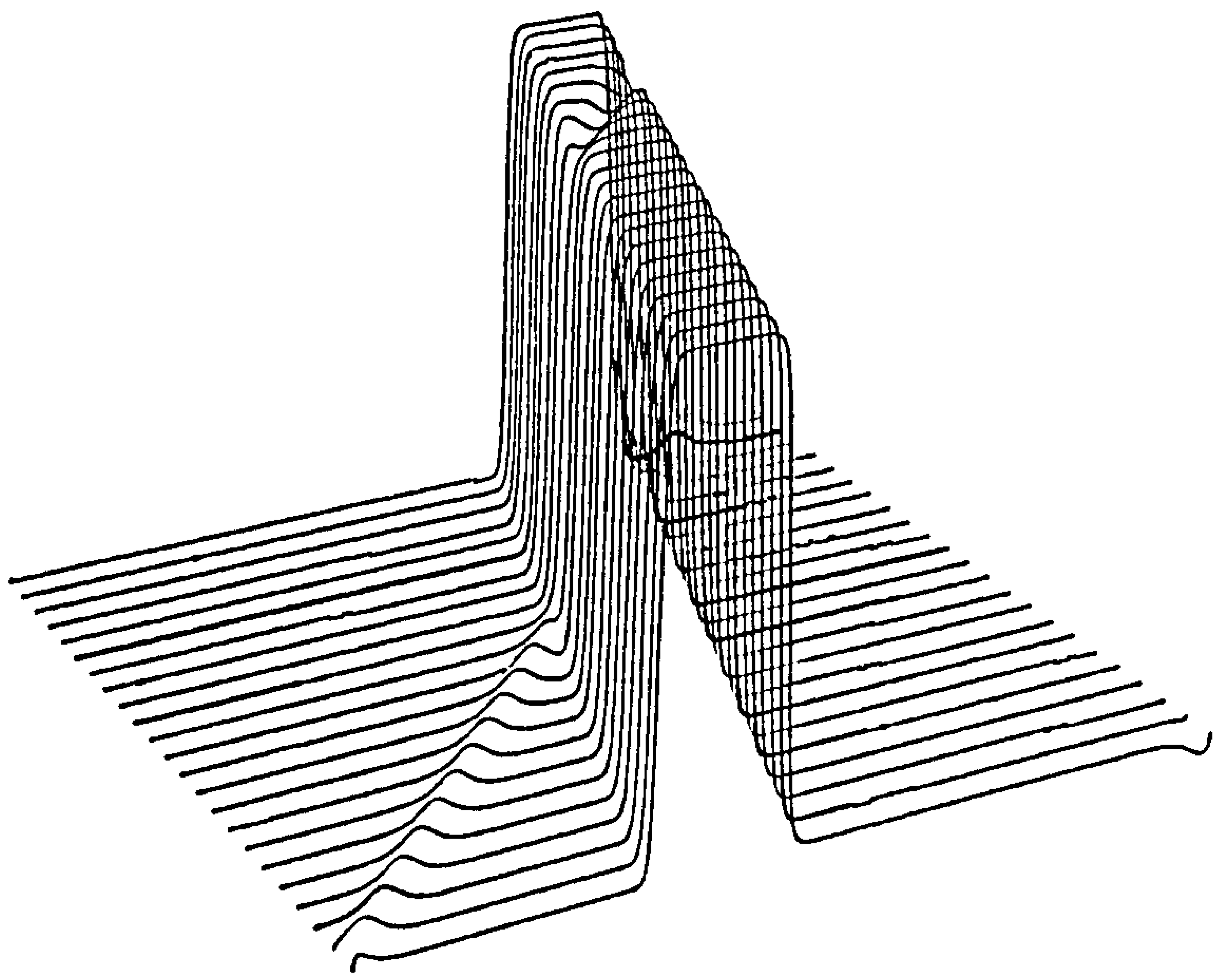

Figure 6.17: The interaction of a soliton, $\nu = 0.3$, with a kink pair, $a = 1$. Perspective view.

Table 6.6: Invariants for a kink pair $a = 1$ and a soliton $\nu = 0.3$

time	I_1	I_2	I_3
0.0	-99.5810	135.001	135.293
1.0	-99.5820	135.003	135.298
2.0	-99.5829	135.006	135.303
4.0	-99.5923	135.012	135.314
6.0	-99.5993	135.012	135.316
8.0	-99.5984	135.015	135.321
10.0	-99.5868	135.017	135.324
12.0	-99.5847	135.016	135.323
14.0	-99.5833	135.015	135.320
15.0	-99.5793	135.007	135.306

6.2.6 Problem 6. The generation of kink and solitons from a tanh initial condition

To study the clean generation of solitons consider initial condition

$$U(x,0) = \tanh(Cx). \tag{6.16}$$

where $C = 1/N$, where N is an integer. When $N = 1$ so that $C = 1$ which is also the amplitude of the tanh function an analytic kink solution is obtained. In what follows the values $N = 2$ to 8 are considered. The case $C = 0.3$ is also studied to determine how it differs from integer cases.

It has been shown that the equilibrium state which develops from this initial condition is completely determined by the governing eigenvalues of the $MKdV^-$ equation. These may be determined analytically from the associated Schrödinger equations [16]

$$\psi_{xx} + [\lambda - (U_0^2 \pm U_{0x})]\psi = 0, \tag{6.17}$$

where U_0 is the initial condition,which have the same discrete spectrum of eigenvalues including the null value. With the given initial condition the Schrödinger potentials are

$$U_0^2 \pm U_{0x} = 1 - (1 \pm C)\text{sech}^2(Cx). \tag{6.18}$$

Since $C(= 1/N)$ is the reciprocal of an integer there is a discrete set of eigenvalues whivh are determined analytically to be given by [16, 24]

$$\begin{aligned} \lambda_r^\pm &= 1 - [1 + (\pm 1 - 1 - 2r)/2N]^2, \\ &\quad \text{for } r = 0, 1, \ldots, N + (\pm 1 - 3)/2. \end{aligned} \tag{6.19}$$

The two sets of eigenvalues obtained by taking either the plus or minus sign are identical apart from the null value. Proceed with the positive set dropping the sign label to obtain

$$\lambda_r = 1 - [1 - r/N]^2, \quad \text{for } r = 0, 1, \ldots, N - 1. \tag{6.20}$$

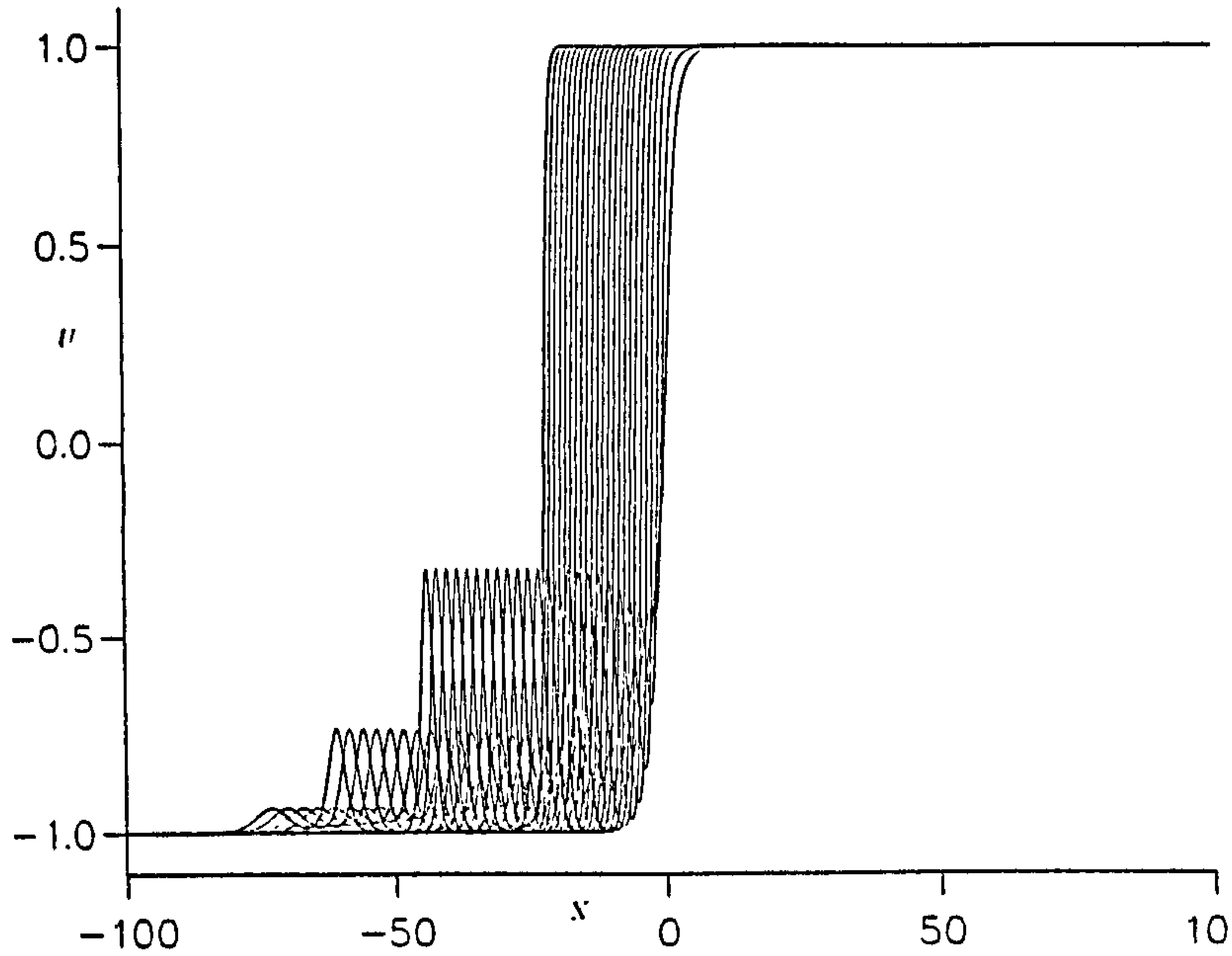

Figure 6.18: $U(x = +\infty) = +1, U(x = -\infty) = -1, c = 0.25, h = 0.2$, $\Delta t = 0.0005$. range $-100 \leq x \leq 100$. The simulation results in the formation of a double layer and three solitary waves. Superimposed profiles.

The eigenvalues are related to the parameters ν appearing in the solitary wave solution (6.3) through [16]

$$\nu_r = \sqrt{(1 - \lambda_r/a^2)}, \tag{6.21}$$

so that the pulse amplitude A_r above the $U = -a$ base level is

$$A_r = 2a[1 - \sqrt{(1 - \nu_r^2)}], \tag{6.22}$$

and the pulse velocity to the left is

$$c_r = (6 - 4\nu_r^2)a^2 = 2a^2 + (2a - A_r)^2. \tag{6.23}$$

Figures(6.19-6.26) show snapshots of the function profile, taken at integer time intervals throughout a simulation with $N = 4$, superimposed upon each other. It is clear that the tanh front steepens so that by the end of the simulation the kink solution has been formed. In so doing it throws off three pulses which have the essential charateristics of $MKdV^-$ solitary waves.

These pulses are formed one in front of the other in decreasing order of magnitude; and since the smaller pulses have the higher velocities they do

Table 6.7: Solitary Wave amplitudes and velocities k=kink, sw=solitary wave, wtf=wave train front

	eigenvalue	amplitude		velocity		
N	computed	computed	measured	computed	measured	remarks
2	0.0000	2.0000	1.992	-2.000	-2.08	k
	0.7500	0.2680	0.267	-5.000	-5.00	sw1
3	0.0000	2.0000	2.000	-2.000	-1.98	k
	0.5556	0.5093	0.510	-4.222	-4.24	sw1
	0.8889	0.1144	0.113	-5.948	-5.60	sw2
4	0.0000	2.0000	1.992	-2.000	-2.08	k
	0.4375	0.6771	0.677	-3.750	-3.80	sw1
	0.7500	0.2686	0.267	-4.998	-4.50	sw2
	0.9375	0.0636	0.065	-5.750	-5.76	sw3
5	0.0000	2.0000	2.003	-2.000	-1.98	k
	0.3600	0.8	0.795	-3.440	-3.46	sw1
	0.0400	0.4	0.397	-4.560	-4.57	sw2
	0.8400	0.1670	0.165	-5.360	-5.37	sw3
	0.9600	0.0404	0.039	-5.840	-5.85	sw4
6	0.0000	2.0000	2.000	-2.000	-2.00	k
	0.3056	0.8945	0.894	-3.222	-3.22	sw1
	0.5556	0.5093	0.509	-4.222	-4.22	sw2
	0.7500	0.2679	0.265	-5.000	-5.02	sw3
	0.8889	0.1144	0.108	-5.555	-5.57	sw4
	0.9722	0.0140	0.023	-5.889	-5.82	sw5
$\frac{10}{3}$	0.0000	2.0000	2.000	-2.000	-1.97	k
	0.51	0.5717	0.570	-4.04	-4.03	sw1
	0.84	0.1670	0.167	-5.36	-5.35	sw2
	0.99	0.0100	0.016	-5.96		?

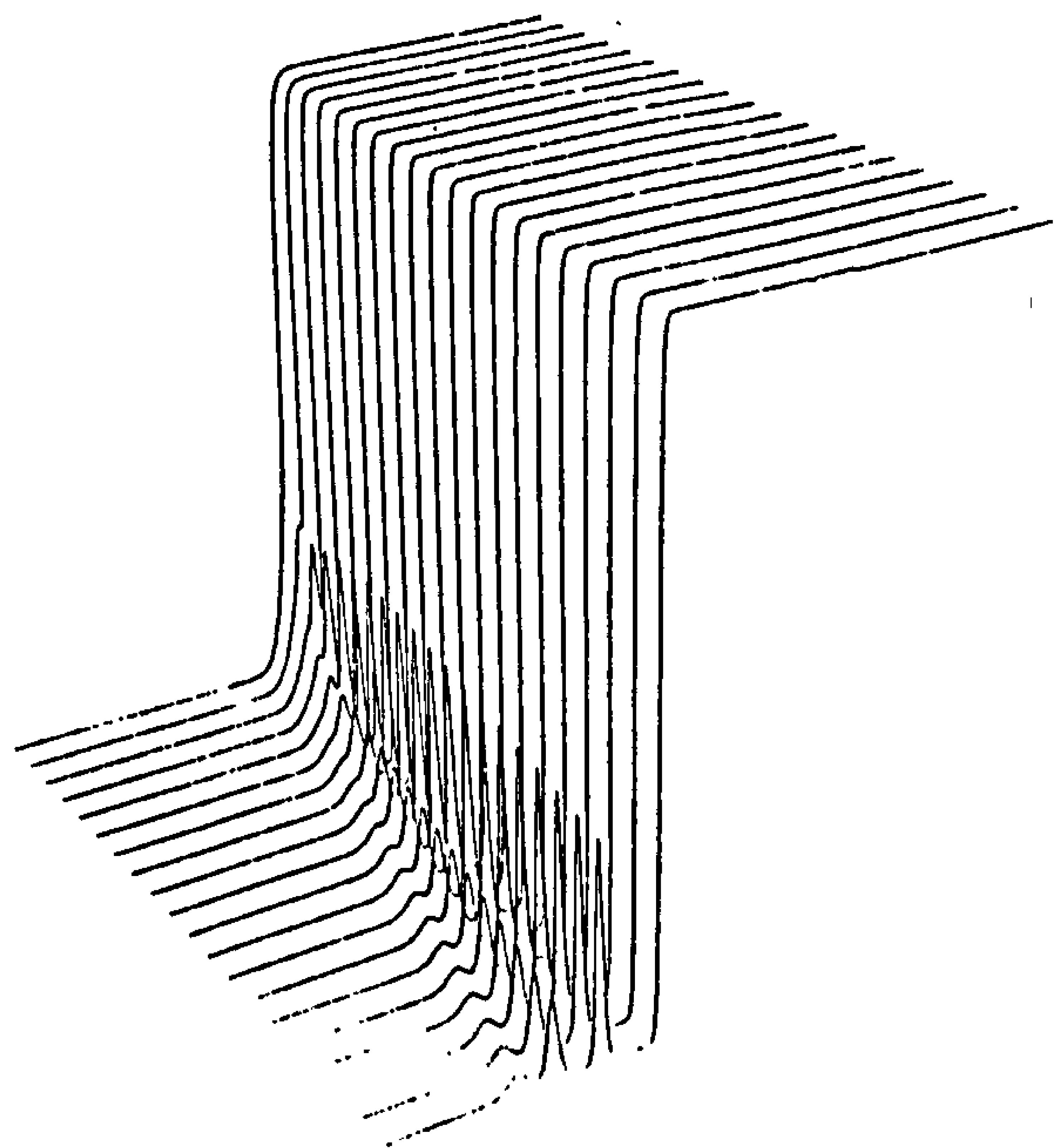

Figure 6.19: $U(x = +\infty) = +1, U(x = -\infty) = -1, c = 0.25, h = 0.2, \Delta t = 0.0005$, range $-100 \leq x \leq 100$. The simulation results in the formation of a double layer and three solitary waves. Perspective view of the development of the profile.

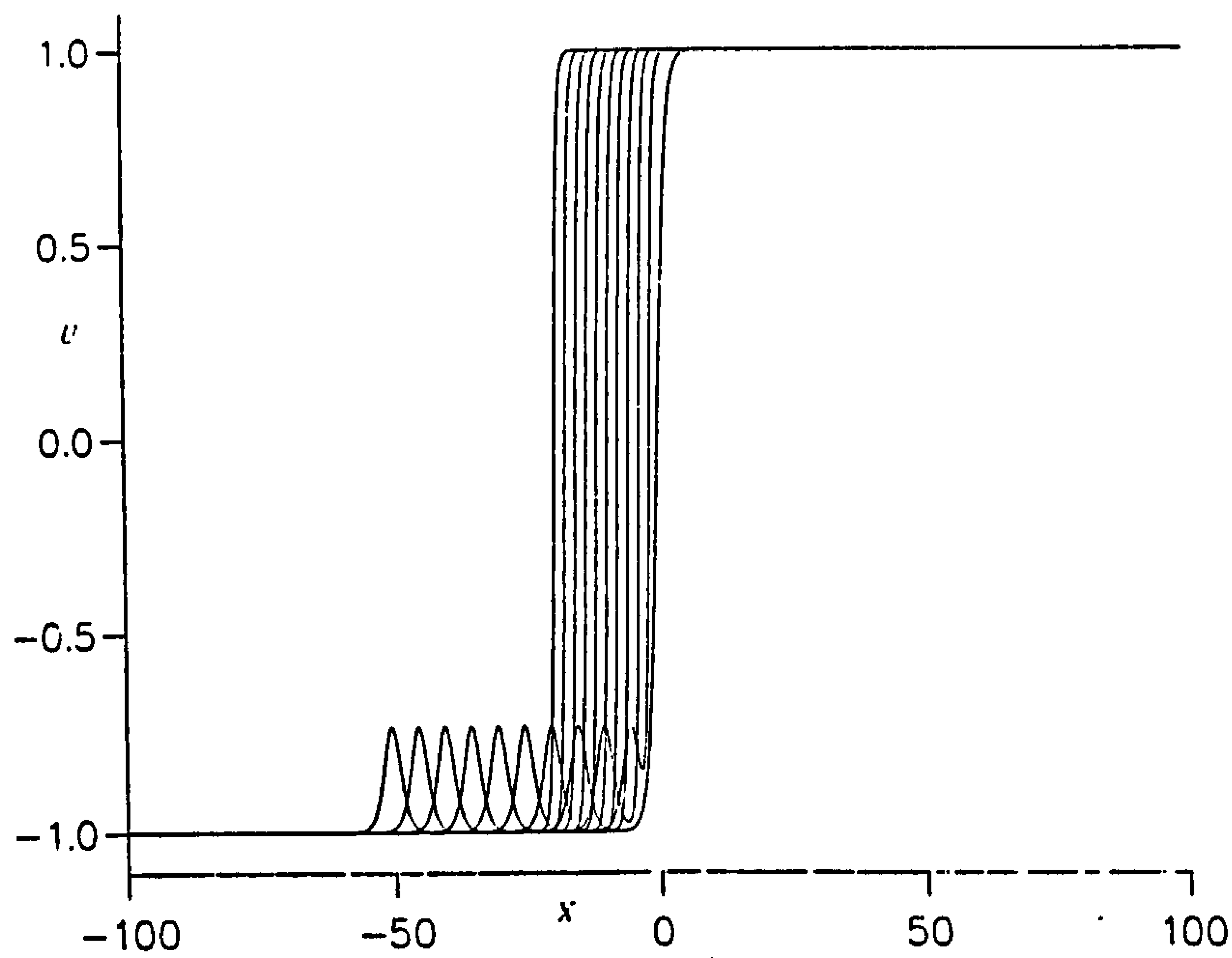

Figure 6.20: $U(x = +\infty) = +1, U(x = -\infty) = -1, c = 0.5, h = 0.2$, $\Delta t = 0.0005$, range $-100 \leq x \leq 100$. The simulation results in the formation of a double layer and one solitary wave. Superimposed profiles.

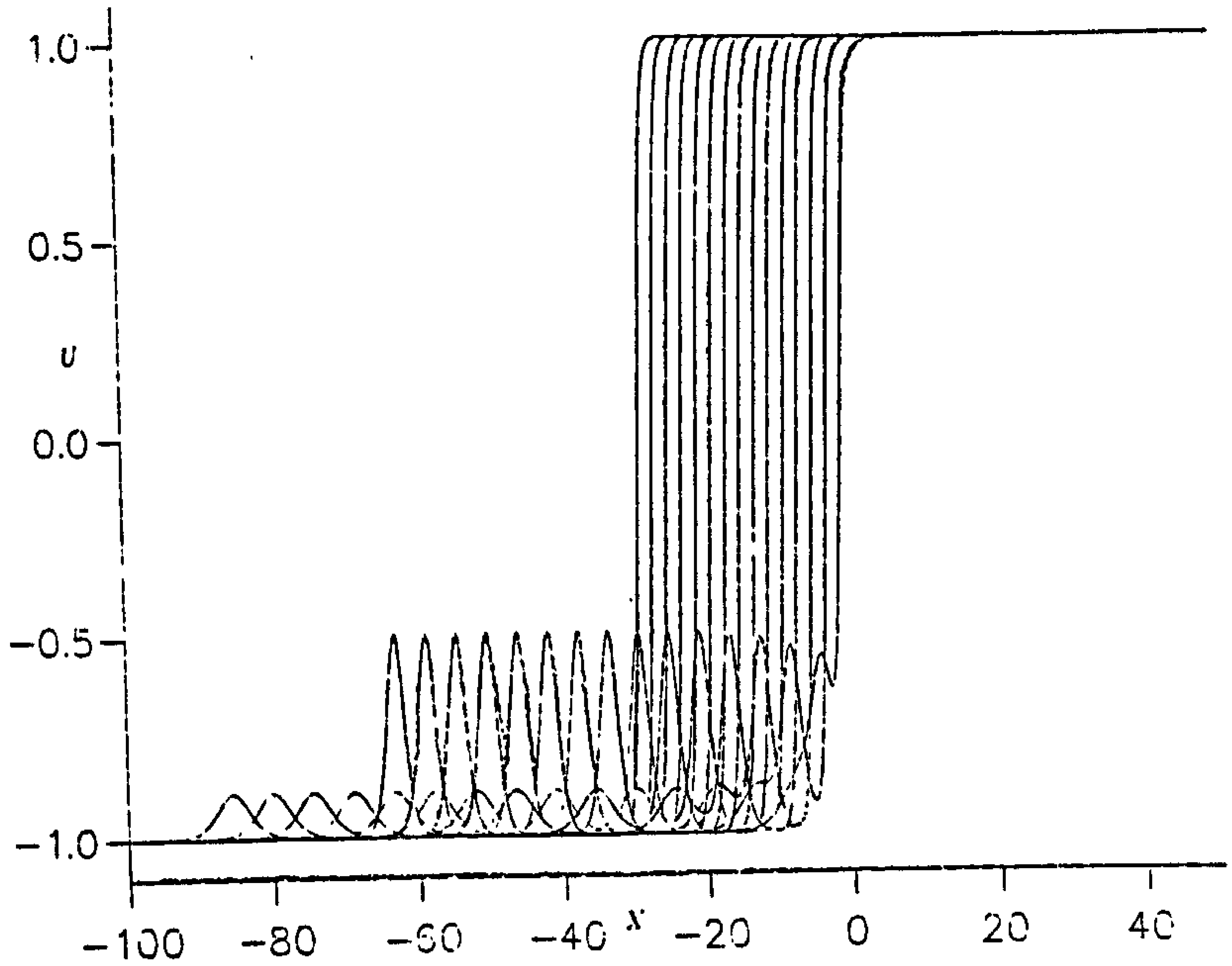

Figure 6.21: $U(x = +\infty) = +1, U(x = -\infty) = -1, n = 3, h = 0.2, \Delta t = 0.0005$, range $-100 \leq x \leq 50$. The simulation results in the formation of a double layer and two solitary waves. Superimposed profiles.

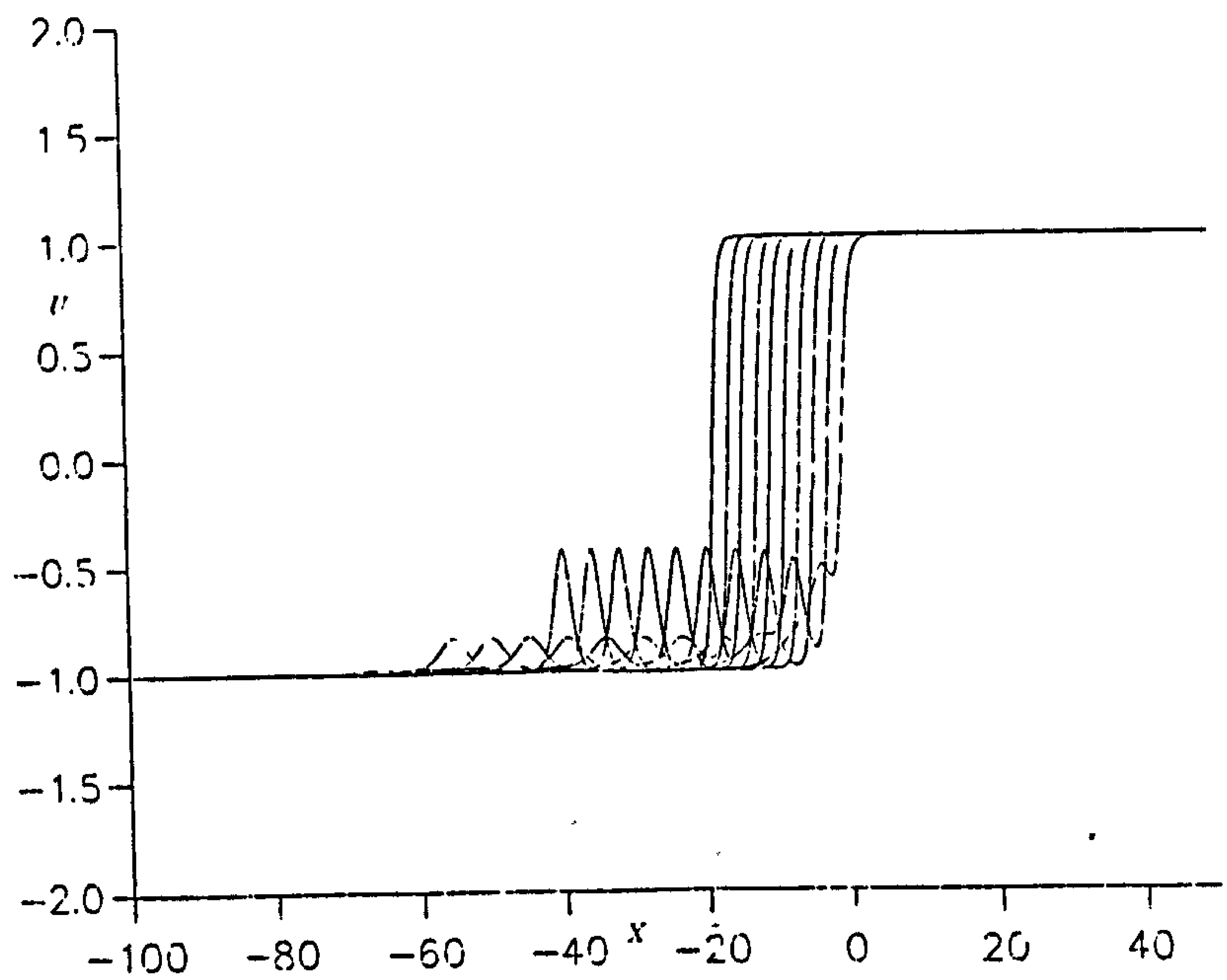

Figure 6.22: $U(x = +\infty) = +1, U(x = -\infty) = -1, n = 0.3, h = 0.2$, $\Delta t = 0.0005$, range $-100 \leq x \leq 50$. The simulation results in the formation of a double layer and two solitary waves. Superimposed profiles.

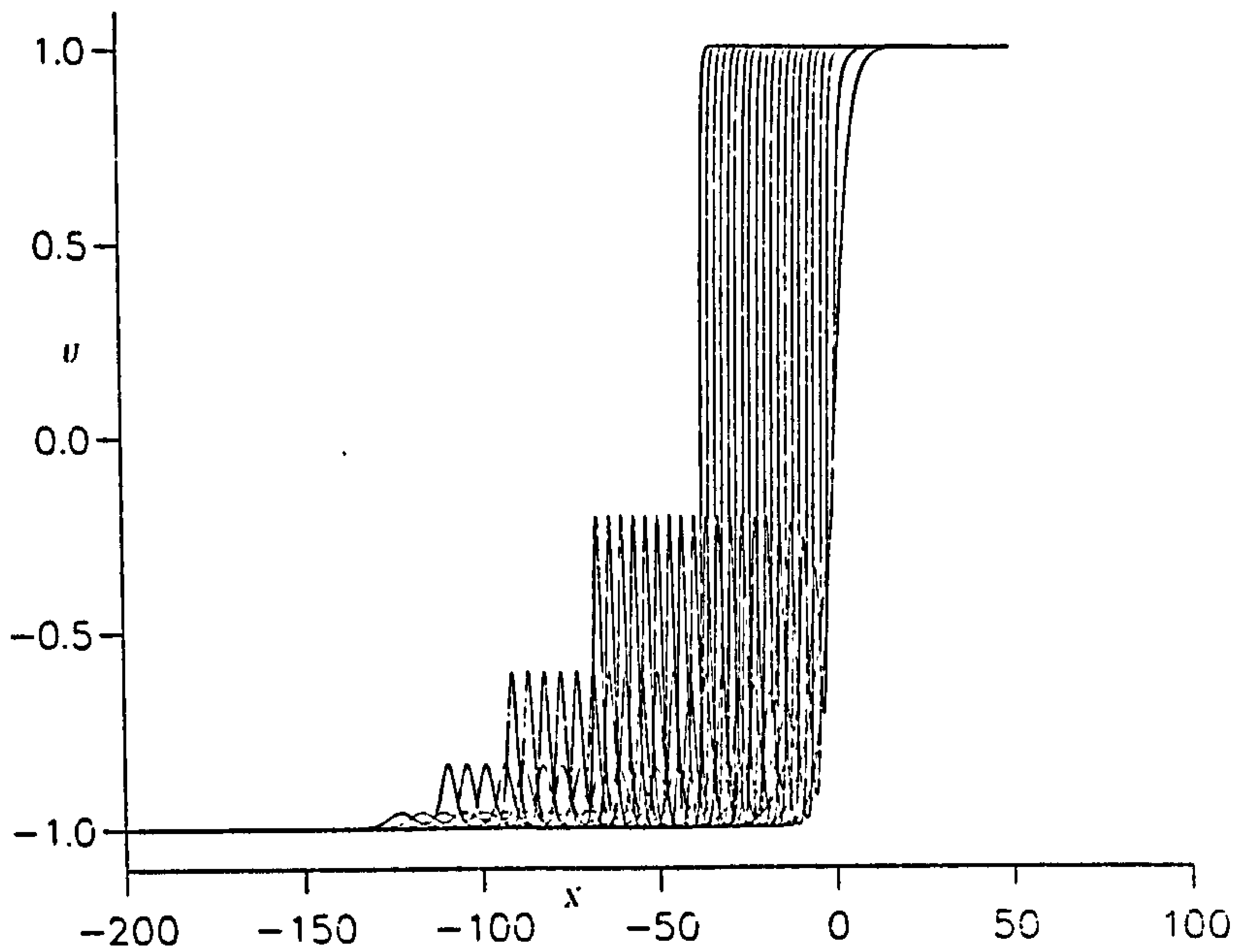

Figure 6.23: $U(x=+\infty)=+1, U(x=-\infty)=-1, n=5, h=0.2, \Delta t=0.0005$, range $-200 \le x \le 50$. The simulation results in the formation of a double layer and four solitary waves. Superimposed profiles.

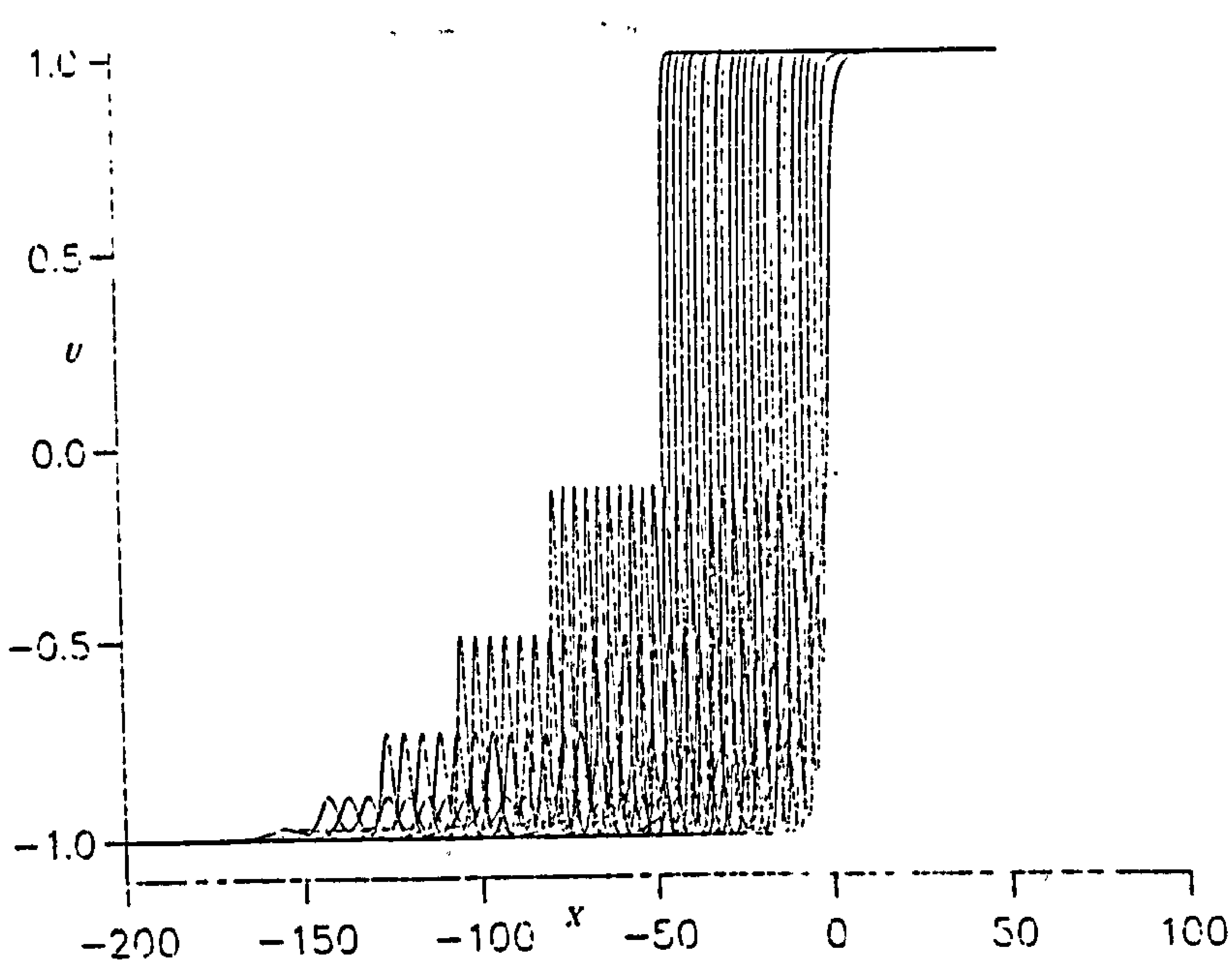

Figure 6.24: $U(x=+\infty)=+1, U(x=-\infty)=-1, n=6, h=0.2, \Delta t=0.0005$, range $-200 \le x \le 50$. The simulation results in the formation of a double layer and five solitary waves. Superimposed profiles.

Table 6.8: $U(x = +\infty) = +1, U(x = -\infty) = -1, n = 5, h = 0.2$, $\Delta t = 0.0005$, range $-200 \leq x \leq 50$.

time	I_1	I_2	I_3
0.0	243.267426	240.200150	237.133453
1.0	243.485840	240.237885	237.209427
2.0	243.911301	240.268524	237.279175
3.0	244.018143	240.317352	237.378224
4.0	244.052887	240.353424	237.446533
5.0	244.071732	240.387161	237.513153
6.0	244.087891	240.413864	237.564774
7.0	244.095184	240.429962	237.597824
8.0	244.112259	240.460205	237.656769
9.0	244.132721	240.500946	237.735992
10.0	244.157227	240.548981	237.831345
11.0	244.180817	240.594604	237.922531
12.0	244.203903	240.641357	238.014191
13.0	244.229370	240.692261	238.114960
14.0	244.250732	240.735352	238.199799
15.0	244.268402	240.768387	238.264526

Table 6.9: $U(x = +\infty) = +1, U(x = -\infty) = -1, n = 8, h = 0.2$, $\Delta t = 0.0005$, range $-250 \leq x \leq 50$.

time	I_1	I_2	I_3
0.0	239.009811	234.100372	228.933182
1.0	239.043503	234.114624	228.966431
2.0	239.414703	234.134613	228.999664
3.0	239.838715	234.155716	229.040039
4.0	239.955902	234.178131	229.083344
5.0	239.994965	234.204712	229.137054
6.0	240.030807	234.245483	229.214310
7.0	240.059402	234.285553	229.293488
8.0	240.081375	234.326736	229.372437
9.0	240.102203	234.366913	229.449951
10.0	240.125946	234.406586	229.527634
11.0	240.142532	234.447311	229.605148
12.0	240.164627	234.487228	229.682129
13.0	240.186722	234.529541	229.764572
14.0	240.208054	234.572586	229.848877
15.0	240.232300	234.615265	229.930908
16.0	240.251190	234.657913	230.013840
17.0	240.276825	234.700394	230.096878
18.0	240.295456	234.743240	230.180145
19.0	240.320114	234.785721	230.262207
20.0	240.341339	234.829315	230.347610

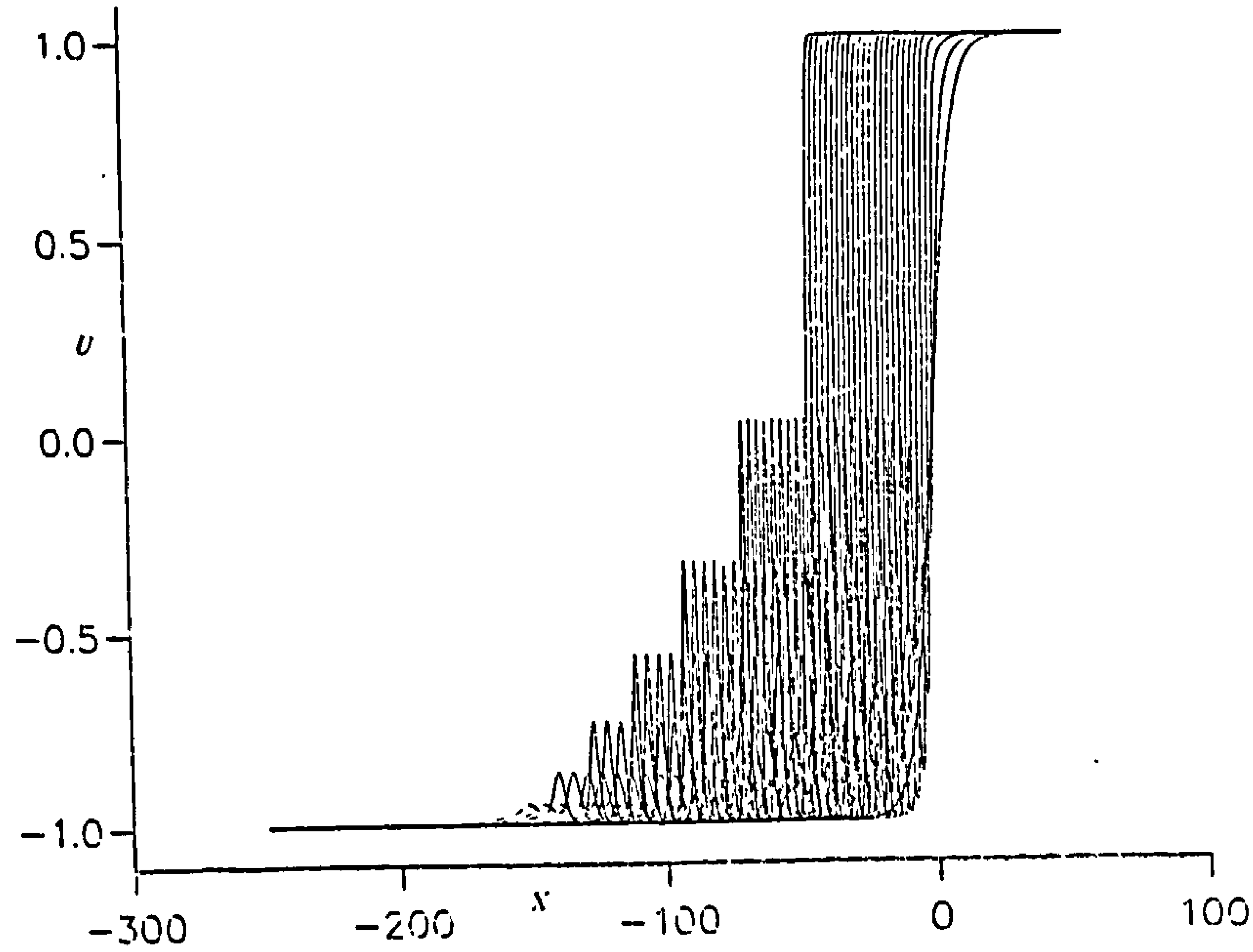

Figure 6.25: $U(x = +\infty) = +1, U(x = -\infty) = -1, n = 8, h = 0.2$. $\Delta t = 0.0005$, range $-250 \leq x \leq 50$. The simulation results in the formation of a double layer and six solitary waves. Superimposed profiles.

not subsequently interact. A perspective view of the solution is also given in figure(6.18-6.25) and also we can see for (n=5,8) three invariants results Table(6.8-6.9). In Table (6.7) the solitary wave amplitudes and velocities predicted from the above theory for various values of N are compared with experimental obsevations; the agreement is good. We have also used the integer theory to predict the eigenvalues and hence the associated amplitudes and velocities of solitary waves for the non integer case $C = 0.3$. The observed values agree well with these predictions.

6.2.7 Problem 7. Non symmetric tanh initial conditions

A study of some initial conditions of the form

$$U(x,0) = \tfrac{1}{2}(U_+ - U_-)\tanh(Cx) + \tfrac{1}{2}(U_+ + U_-) \tag{6.24}$$

which have the asymptotic values

$$U \to U_+ \ \ as \ \ x \to \infty \ \ and \ \ U \to U_- \ \ as \ \ x \to -\infty, \tag{6.25}$$

is also made. The analytic kink solution is obtained if we take

$$C = U_+ = -U_-. \tag{6.26}$$

Simulations with the following parameter values, which do not correspond to analytic solutions, are set up and the development of the function profile is monitored:

a-) $U_+ = 1.2, \quad U_- = -0.8, \quad C = 0.25$

b-) $U_+ = 0.8, \quad U_- = -1.2, \quad C = 0.25$

c-) $U_+ = 1, \quad U_- = 0, \quad C = 0.25$

d-) $U_+ = 0, \quad U_- = -1, \quad C = 0.25$

Examples (a) and (b) are such that $U_+ - U_- = 2$. In all runs take $h = 0.2$ over a range $-100 \leq x \leq 100$ and site the initial condition at $x = 0$, use $\Delta t = 0.001$ and run up to a time $t = 24$.

The results of the simulations are compared with theoretical predictions and the experimental work of Chanteur and Raadu [16]; see Table (6.10).

6.2.8 Problem 7(a): $U_+ = 1.2, U_- = -0.8, C = 0.25$

Snapshots of the function are shown superimposed on each other together with a perspective view in figures(6.26-6.28). For this problem we start with an initial condition which is not antisymmetric in its asymptotic values. As it transforms itself into a kink solution between levels $U = \pm 1.2$ it gives off two solitary waves and then sets up a wave train to return to the prescribed level of $U \to -0.8$ as $x \to \infty$. The end result of this process is shown clearly in figures(6.29-6.30) for time $t = 5.5$. An analtic expression for the eigenvalues

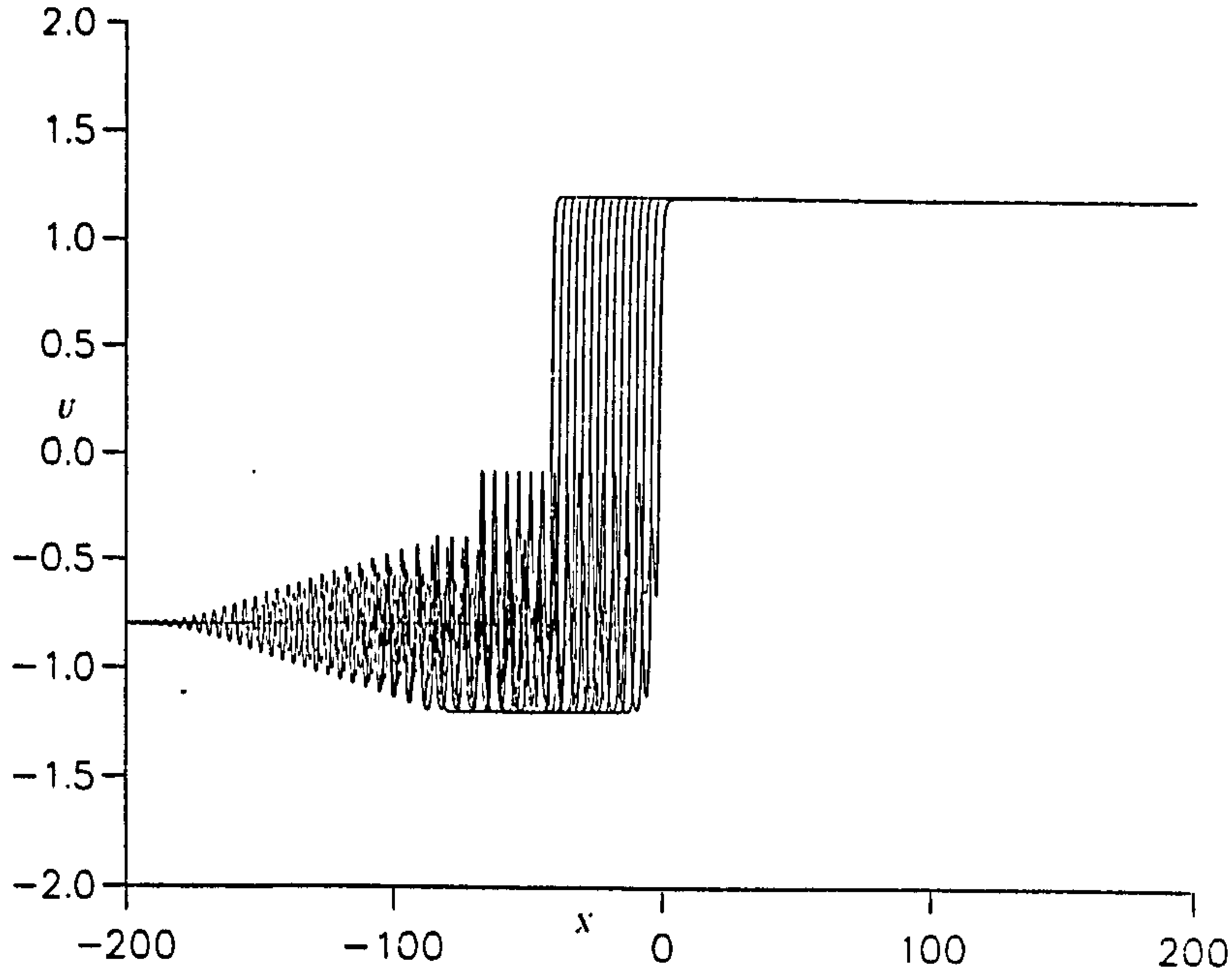

Figure 6.26: $U(x = +\infty) = +1.2, U(x = -\infty) = -0.8, c = 0.25, h = 0.2$, $\Delta t = 0.001$, range $-100 \leq x \leq 100$. The simulation results in the formation of a double layer and two solitary waves and a wave train.

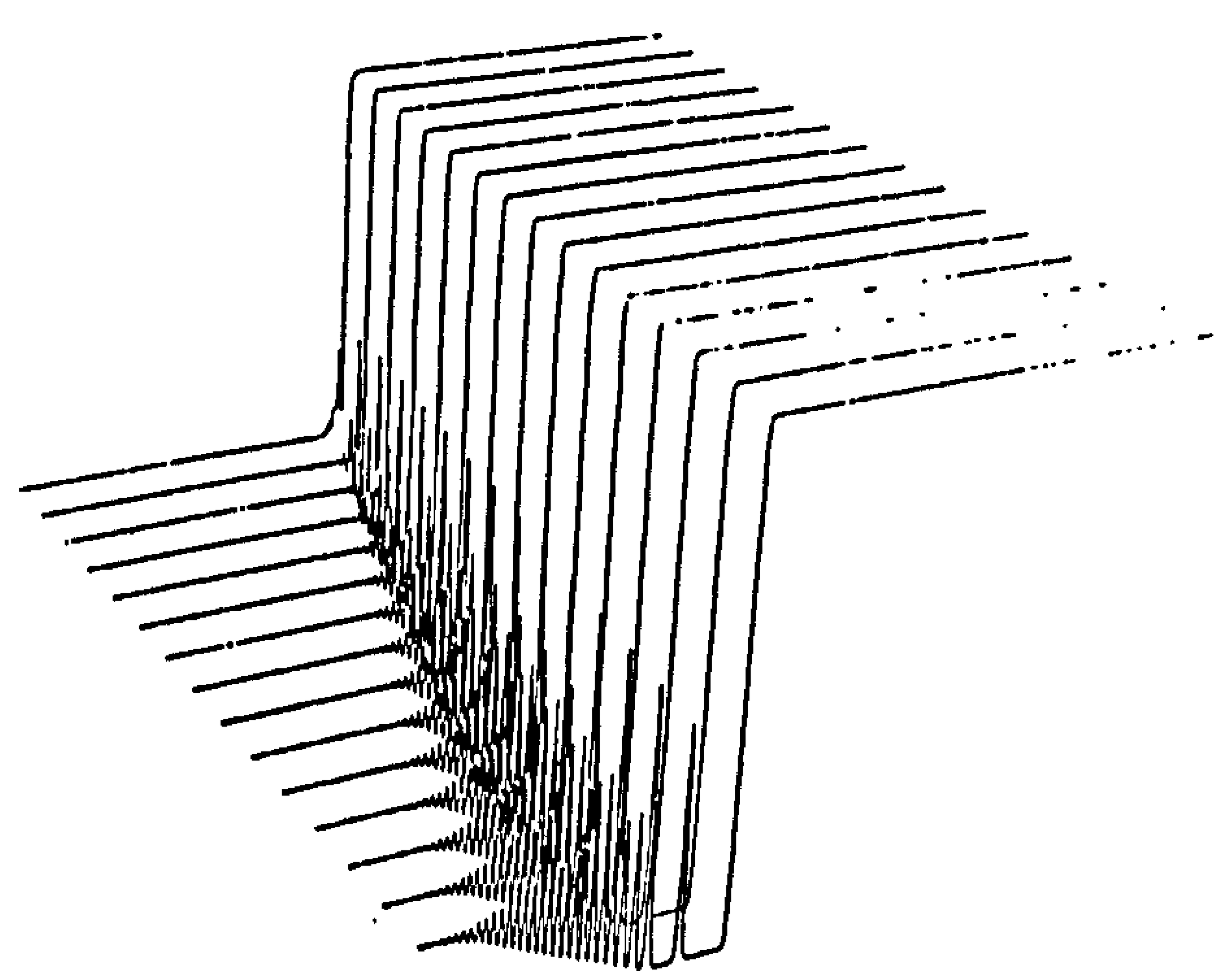

Figure 6.27: $U(x = +\infty) = +1.2, U(x = -\infty) = -0.8, c = 0.25, h = 0.2, \Delta t = 0.001$, range $-100 \leq x \leq 100$. The simulation results in the formation of a double layer and two solitary waves and a wave train.

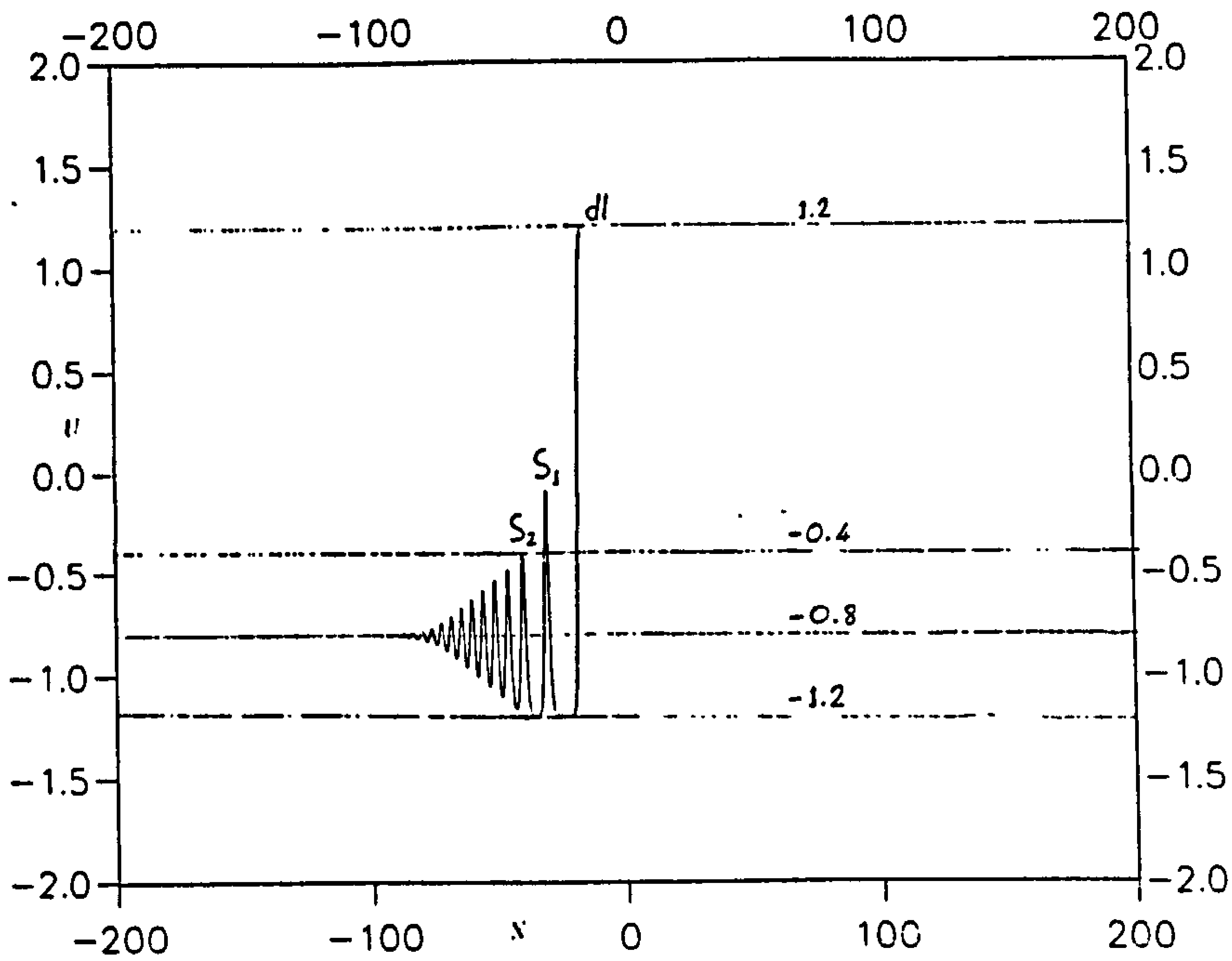

Figure 6.28: $U(x = +\infty) = +1.2, U(x = -\infty) = -0.8, c = 0.25, h = 0.2, \Delta t = 0.001$, range $-100 \leq x \leq 100$. The simulation results in the formation of a double layer and two solitary waves and a wave train.

Table 6.10: Solitary Wave amplitudes and velocities k=kink. sw=solitary wave, wtf=wave train front

	eigenvalue	amplitudes			velocities			
run	computed [16]	computed [16]	measure	measure [16]	computed [16]	measure	measure	mar
a	0.000	2.4000	2.390	2.395	-2.880	-2.92	-2.86	k
	0.4064	1.1250	1.121	1.118	-4.506	-4.50	-4.49	sw1
	0.6300	0.8125	0.807	0.803	-5.400	-5.45	-5.41	sw2
	0.64	0.8	0.755	0.751	-5.44	-5.62	-5.53	wtf
b	0.0000	1.6000	1.599	1.596	-1.280	-1.30	-1.32	k
	0.4064	0.3250	0.325	0.326	-2.906	-2.91	-2.90	sw1
	0.6300	0.0125	0.026	0.020	-3.800	-3.83	-3.88	sw2

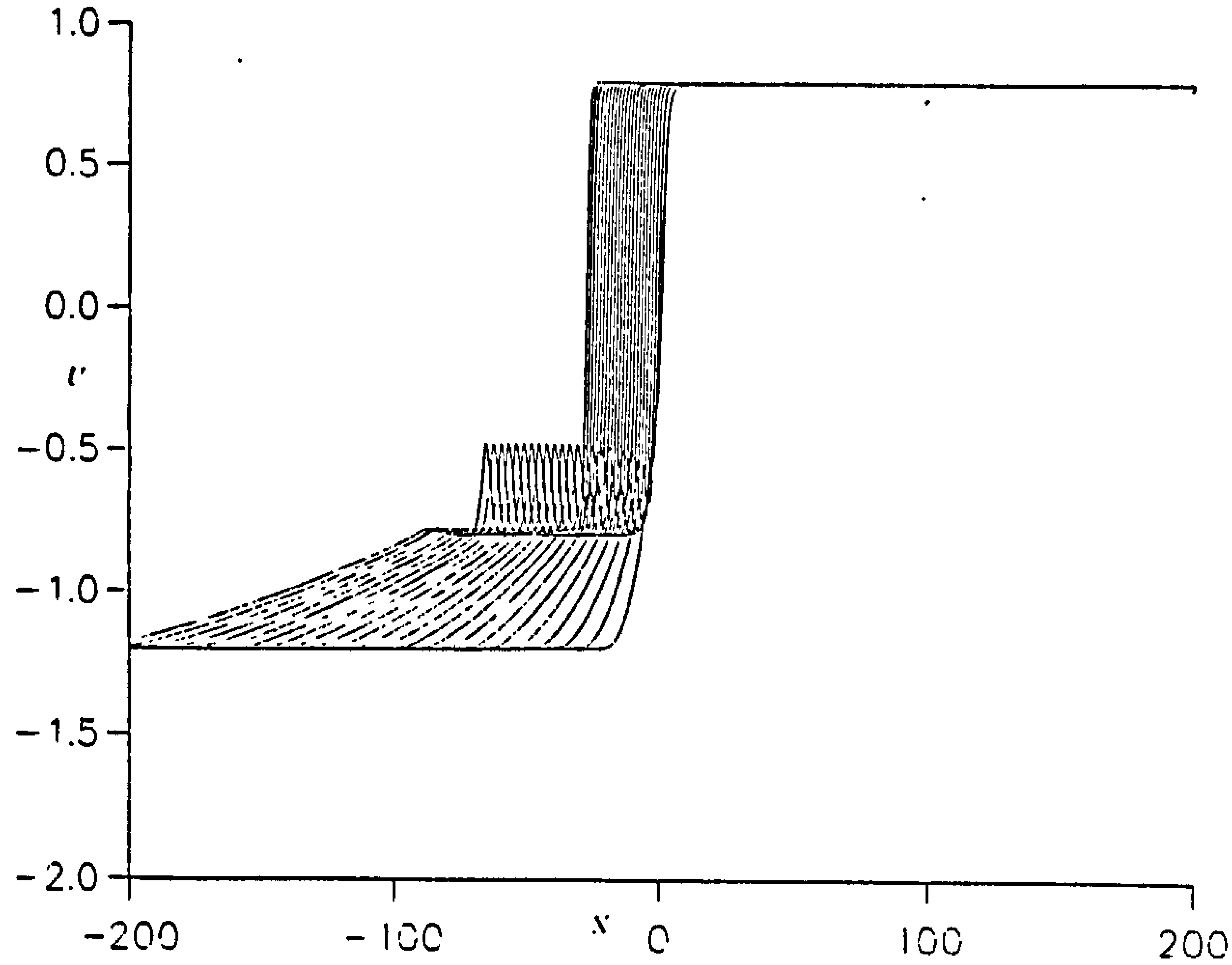

Figure 6.29: $U(x = +\infty) = +0.8, U(x = -\infty) = -1.2, c = 0.25, h = 0.2, \Delta t = 0.001$, range $-100 \leq x \leq 100$. The simulation results in the formation of a double layer and two solitary waves and a wave and a ramp. Superimposed profiles.

of this problem is not available, but values have been obtained by solving the associated Schrödinger equation numerically [16] to give $\lambda_0 = 0.0000, \lambda_1 = 0.4064, \lambda_2 = 0.6300$; these leads to the computed soliton values given in Table (6.10). The limit for eigenvalues is $0.64 = 1/1.2^2$, which implies amplitude and velocity limits of $A_{lim} = 0.8$ and $V_{lim} = -5.44$ that should correspond to the amplitude and velocity of the leading wave in the wave train. We observe the values $A_{front} = 0.751$, and $V_{front} = -5.53$ which compare reasonably with those found earlier [16] $A_{front} = 0.755$, and $V_{front} = -5.62$.

6.2.9 Problem 7(b): $U_+ = 0.8, U_- = -1.2, C = 0.25$

Again for this problem superimposed snapshots and perspective views of the progress of the experiment are given; see (6.29-6.30). As in problem 7(a) the asymptotic values are not equal and opposite, but this time the negative value is larger and consequently the subsequent development is different. As

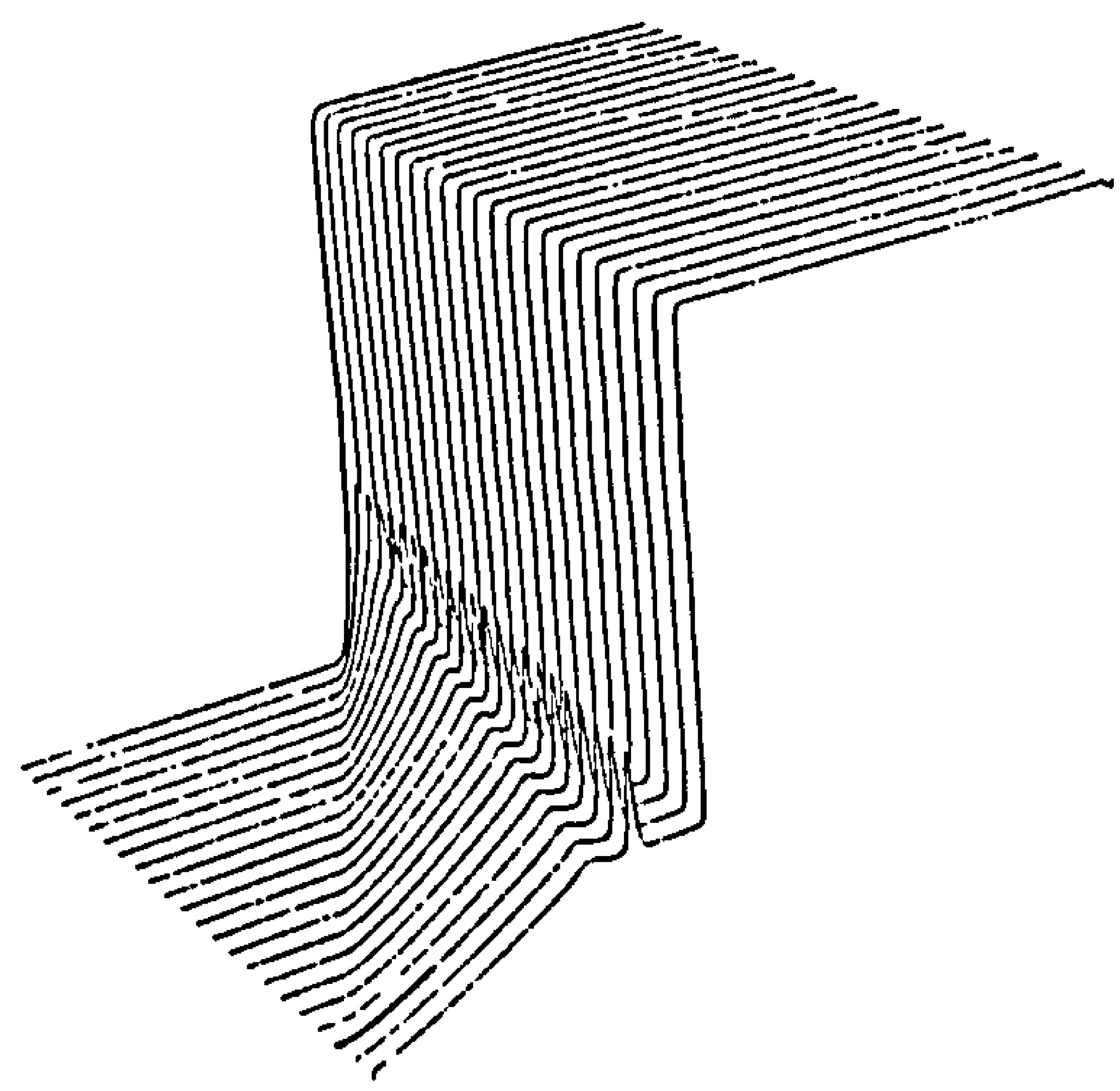

Figure 6.30: $U(x = +\infty) = +0.8, U(x = -\infty) = -1.2, c = 0.25$, $h = 0.2, \Delta t = 0.001$, range $-100 \leq x \leq 100$. The simulation results in the formation of a double layer and two solitary waves and a wave and a ramp. Perspective view.

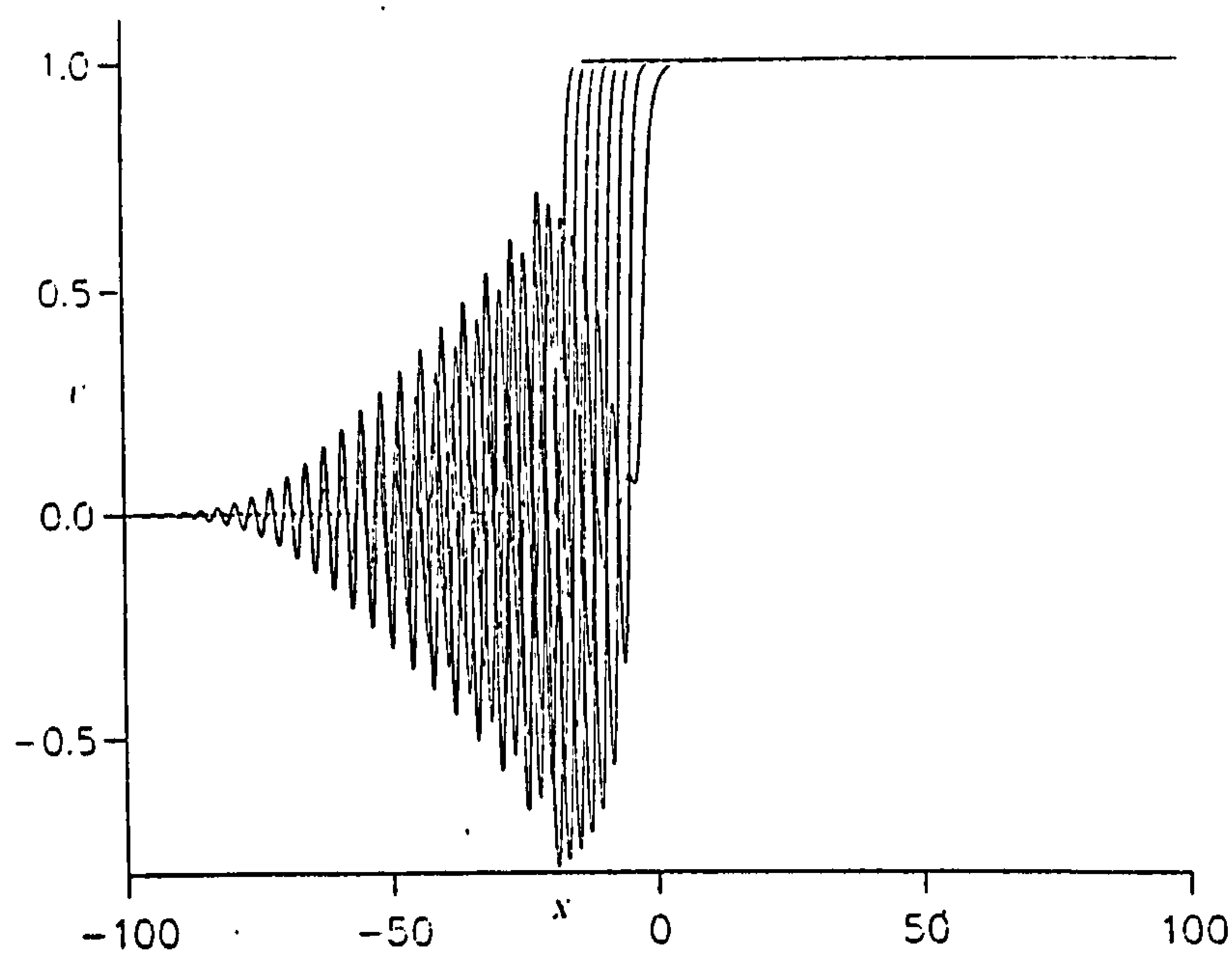

Figure 6.31: $U(x = +\infty) = +1.0, U(x = -\infty) = 0, c = 0.25$, $h = 0.2, \Delta t = 0.001$, range $-100 \leq x \leq 100$. We see that a wave train has formed but no double layer or solitary waves. Superimposed profiles.

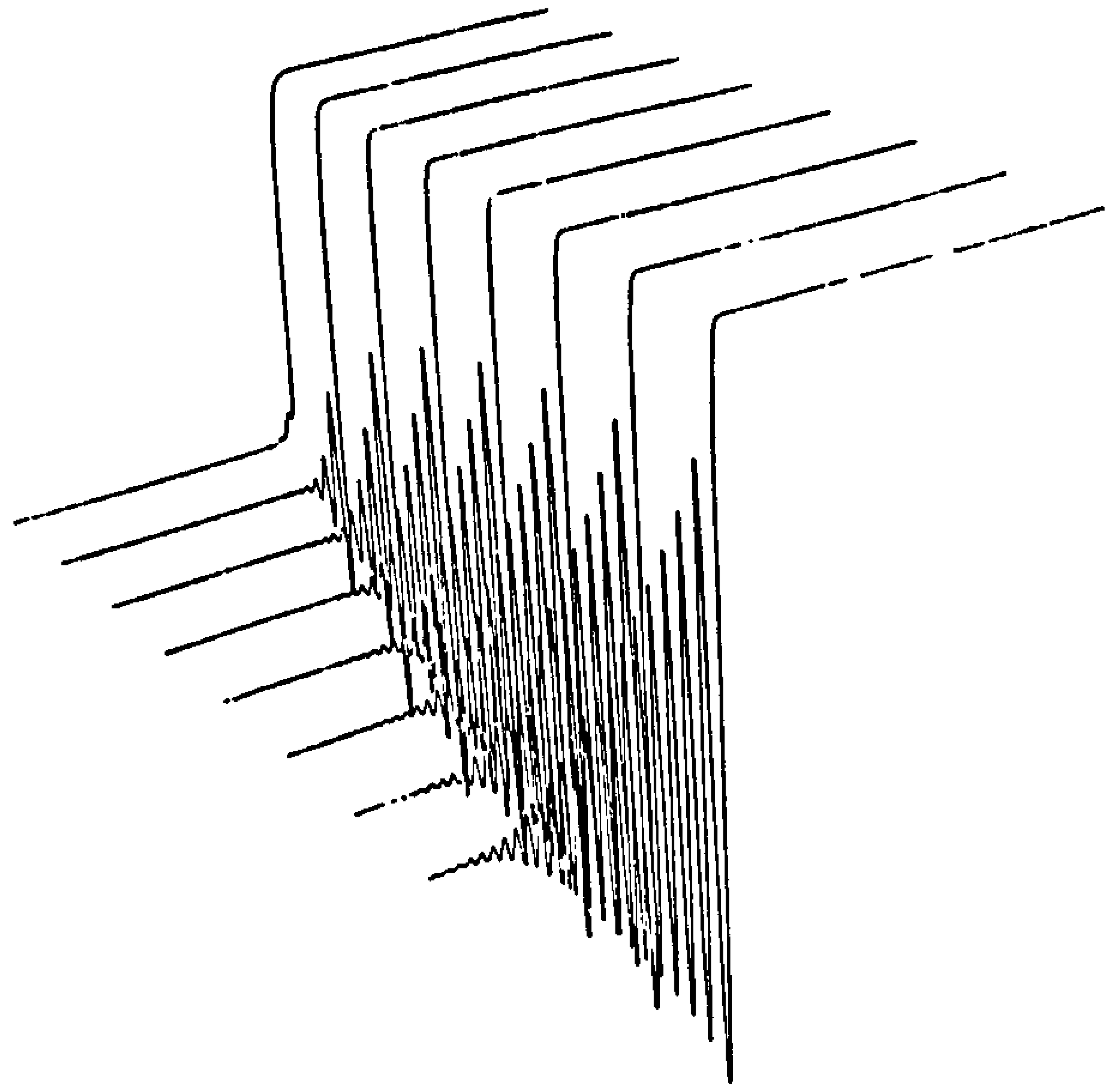

Figure 6.32: $U(x = +\infty) = +1.0, U(x = -\infty) = 0, c = 0.25$, $h = 0.2, \Delta t = 0.001$, range $-100 \leq x \leq 100$. We see that a wave train has formed but no double layer or solitary waves. Perspective view.

the wave front steepens and forms a kink solution between levels $U = \pm 0.8$. it gives off 2 solitary waves and forms a ramp to return to the asymptotic value $U \rightarrow -1.2$ as $x \rightarrow -\infty$. Eigenvalues determined by solving the associated Schrödinger equation numerically [16] are $\lambda_0 = 0.0000, \lambda_1 = 0.4064, \lambda_2 = 0.6300$; these lead to the computed soliton amplitudes and velocities given in Table (6.10).

6.2.10 Problem 7(c): $U_+ = 1, U_- = 0, C = 0.25$ 7(d) : $U_+ = 0, U_- = -1, C = 0.25$

Snapshots and a perspective view of the simulation are given in Figures (6.31-6.32). For this problems 7(c) and 7(d) one of the asymptotic values is zero so that kink solutions are not expected to form. The results of our simulations confirm this. For 7(c) the initial profile evolves into a wave train travelling to the left along the $U = 0$ level, no solitary waves form. For 7(d) only a smooth ramp connecting the two levels is formed confirming earlier observations [16].

6.2.11 Problem 8

The generation of kink and solitons from a quasisoliton initial condition of the form.

$$U(x,0) = -1 + \tanh(2\Delta)\{\tanh[C(x - x_0 + \Delta)] - \tanh[C(x - x_0 - \Delta)]\}. \tag{6.27}$$

where $C = 1/N, N$ an integer. Using the appropriate formulae and identifying $\nu = \tanh(2C\Delta)$ it is easy to show that this initial condition can also be written as

$$U(x,0) = -1 + 2\nu \tanh(2\Delta)/\{1 + \sqrt{(1-\nu^2)} \cosh 2C(x - x_0)\}. \tag{6.28}$$

which is similar in form the equation for a single soliton (6.3).

When Δ is large, the tanh functions well separated and each tanh behaves independently and since $C(= 1/N)$ is the reciprocal of an integer there is a discrete set of eigenvalues which may be determined analytically [16], and corresponding to each a daughter soliton is born; this process has already been described for problem 6.

As Δ takes smaller values the tanh functions become closer together as do the corresponding solitons in each of the wave trains, and when the tanh profiles are sufficiently close the wave trains coincide. When Δ is reduced still further the soliton solution is replaced by a stable pulse preceeded by a wave train.

Simulations are set up with $\Delta = 10, 1, 0.2$ (which have $\nu = 1 - 10^{-17}$, $0.9640, 0.37998$) and $C = 1/N$ where $N = 2, 4$. The case $\Delta = 10$ corresponds to the well separated situation and two trains of solitons are generated, one arising from each tanh function. When $\Delta = 1$, $2C\Delta \sim 1$, a single train of solitons is observed, while with $\Delta = 0.2$ a stable pulse preceeded by a wave train forms .

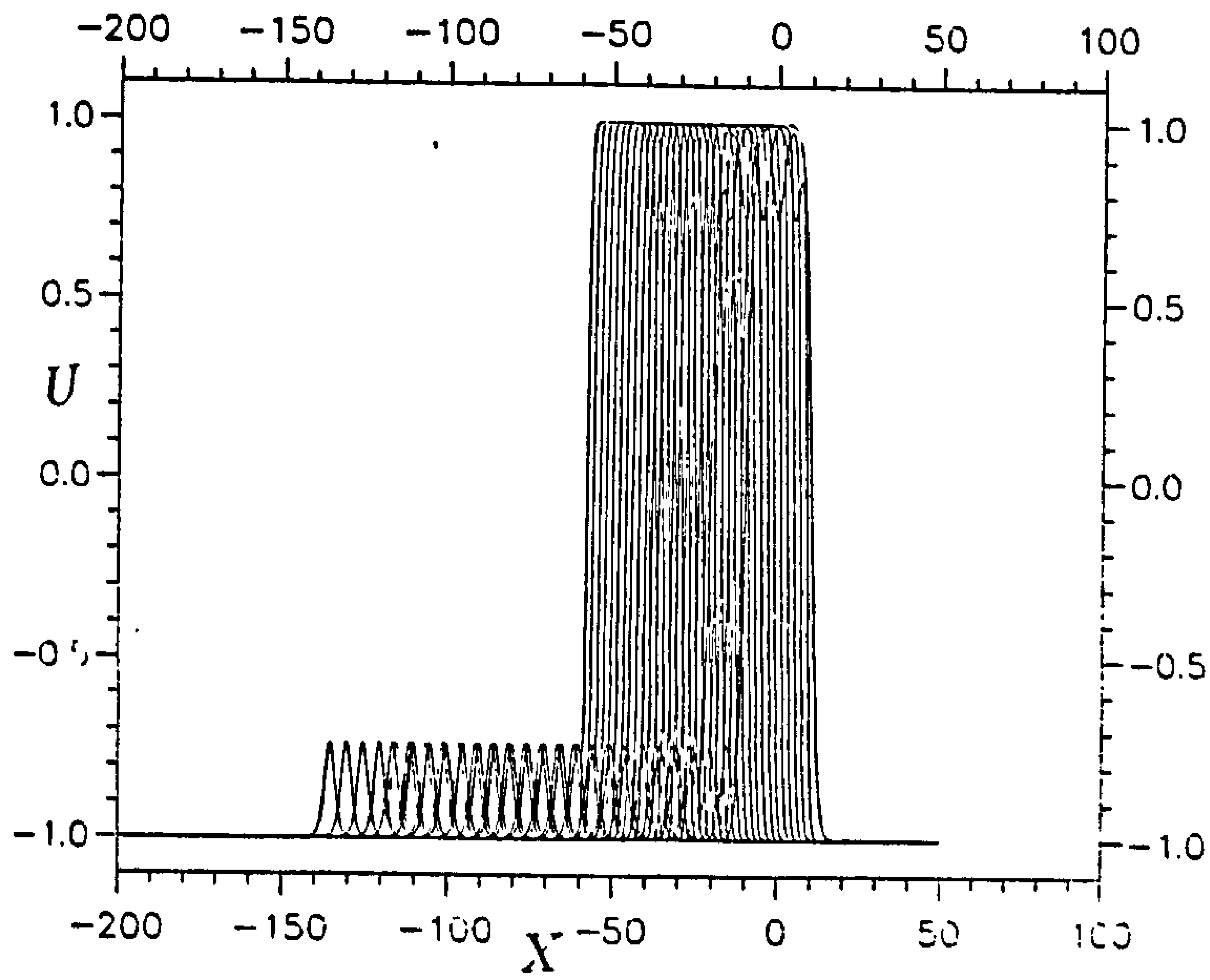

Figure 6.33: Double tanh initial condition (6.27). $N = 2$. $\Delta = 10$. Superimposed profiles.

6.2.12 Numerical experiment series 1. $N = 2$

a-) When $\Delta = 10$ we take a region $-150 \leq x \leq 50$. $h = 0.2$. $\Delta t = 0.005$ and run the simulation up to time $t = 15$. The invariants are listed in Table (6.11). The progress of the run is shown in figures (6.33-6.34). The initial state is an obvious double tanh of equal and opposite slope. The slopes of the tanh functions do not combine with their amplitudes to produce an exact kink configuration. In the simulation the tanh functions retain their original amplitude but steepen into a double kink configuration and in so doing each tanh emits a soliton moving to left as is shown clearly in figures(6.33-6.34). The daughter of the right hand kink has first to climb over the double kink to join the daughter of the other kink. As seen in later stages of the simulation both solitons have identical amplitudes (0.267) and travel across the mesh with identical speeds (5.0).

b-) When $\Delta = 1$ we take a region $-200 \leq x \leq 50$ and $h = 0.2, \Delta t = 0.005$ and run the simulation to time $t = 1.5$. The invariants are listed in

Table 6.11: Invariants for two tanh with $\Delta = 10$.

time	I_1	I_2	I_3
0.0	-160.200119	192.200043	190.868484
1.0	-160.200714	192.192276	190.866180
2.0	-160.201431	192.192047	190.864838
3.0	-160.202866	192.193594	190.868286
4.0	-160.204407	192.197235	190.874344
5.0	-160.203934	192.201385	190.882828
6.0	-160.194275	192.209534	190.893097
7.0	-160.186432	192.206436	190.892395
8.0	-160.186218	192.207291	190.893921
9.0	-160.187149	192.209213	190.897598
10.0	-160.187897	192.211090	190.901062
11.0	-160.188126	192.212708	190.904388
12.0	-160.188568	192.214035	190.907257
13.0	-160.188980	192.215256	190.909592
14.0	-160.189056	192.216354	190.911606
15.0	-160.189080	192.216365	190.911598

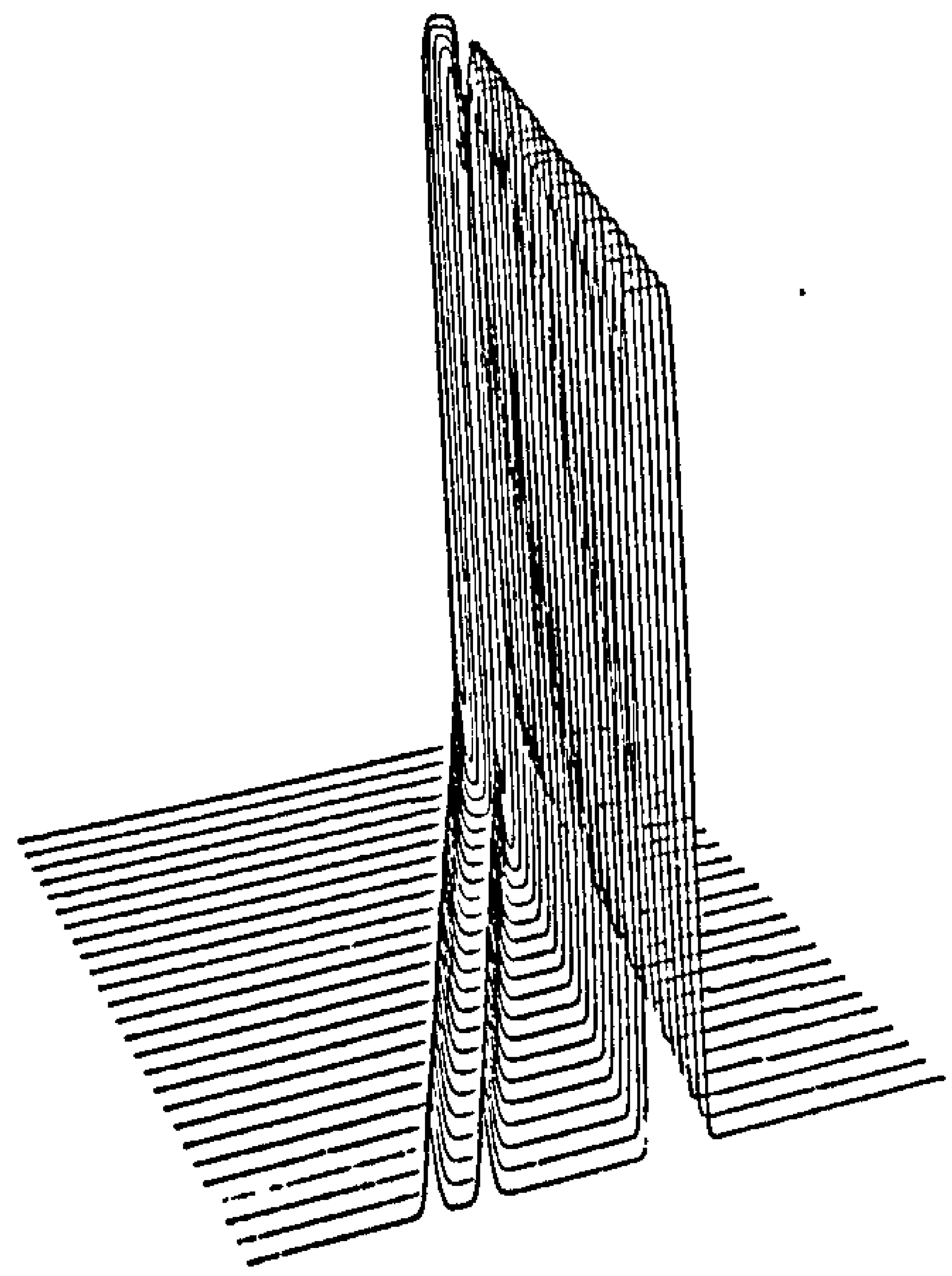

Figure 6.34: Double tanh initial condition (6.27). $N = 2, \Delta = 10$. Perspective view.

Table (6.12). As shown in figures (6.35-6.36) the initial pulse, which is very similar in appearance to a soliton, grows in amplitude and its slope steepens until a soliton configuration of amplitude 1.10 and velocity -2.81 is achieved. In so doing a single smaller soliton of amplitude 0.216 is ejected with velocity -5.18.

c-) When $\Delta = 0.2$ we take a region $-250 \leq x \leq 50$ and $h = 0.2$, $\Delta t = 0.005$ and run the simulation to time $t = 15$. We see in figures (6.37-6.38) the amplitude of the initial pulse decreases until a stable height is reached, at the same time a wave train is created in front of the pulse. The invariants are listed in Table (6.13). Since in this experiment Δ was of the same size as the grid spacing h there was some feeling that this might have influenced the outcome. It was decided to reduced the grid spacing to $h = 0.05$ and rerun the experiment. No significant changes in the results or outcome were observed.

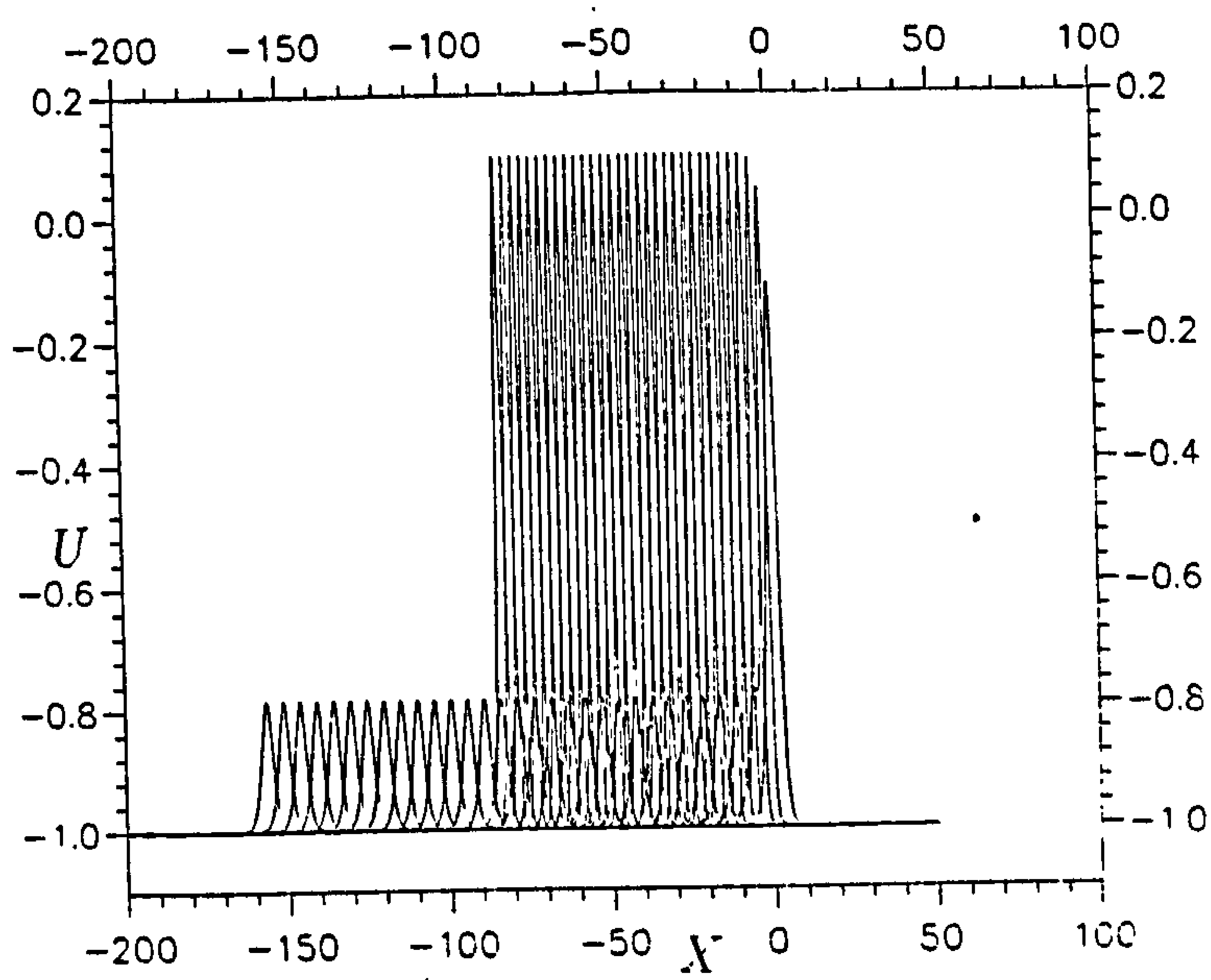

Figure 6.35: Double tanh initial condition (6.27). $N = 2, \Delta = 1$. Superimposed profiles.

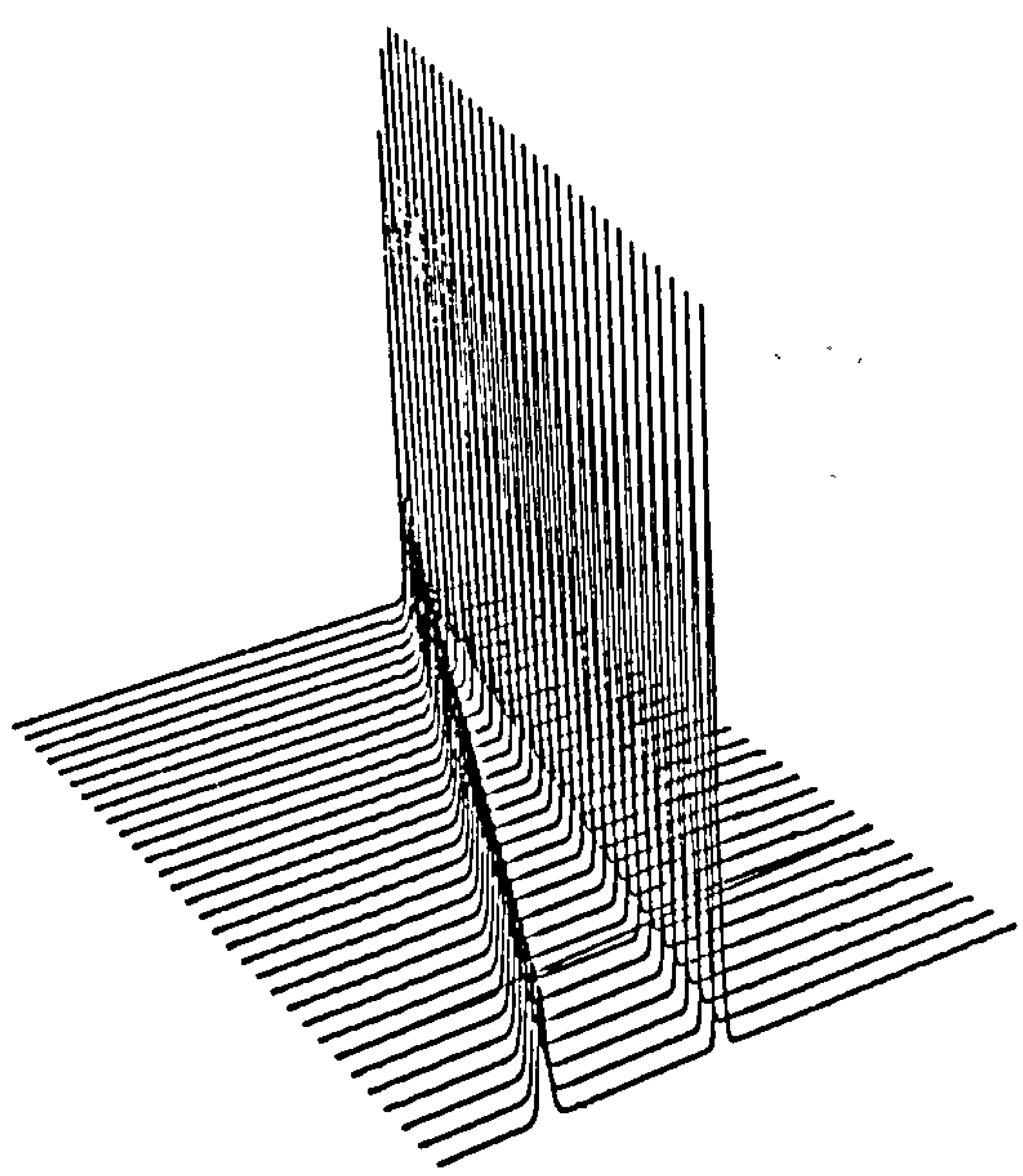

Figure 6.36: Double tanh initial condition (6.27). $N = 2, \Delta = 1$. Perspective view.

Table 6.12: Invariants for two tanh N=2 with $\Delta = 1$.

time	I_1	I_2	I_3
0.0	-246.343964	244.815216	243.736420
1.0	-246.343826	244.815094	243.742630
2.0	-246.344879	244.816040	243.746338
3.0	-246.346512	244.818604	243.751953
4.0	-246.348511	244.824097	243.759354
5.0	-246.351074	244.827927	243.767258
6.0	-246.353226	244.831619	243.774948
7.0	-246.354828	244.834869	243.781494
8.0	-246.356598	244.838303	243.788574
9.0	-246.358444	244.841385	243.794357
10.0	-246.359589	244.843948	243.799515
11.0	-246.361237	244.847610	243.806122
12.0	-246.362762	244.850098	243.811859
13.0	-246.363312	244.851105	243.813889
14.0	-246.364426	244.853592	243.819092
15.0	-246.364914	244.853851	243.819611

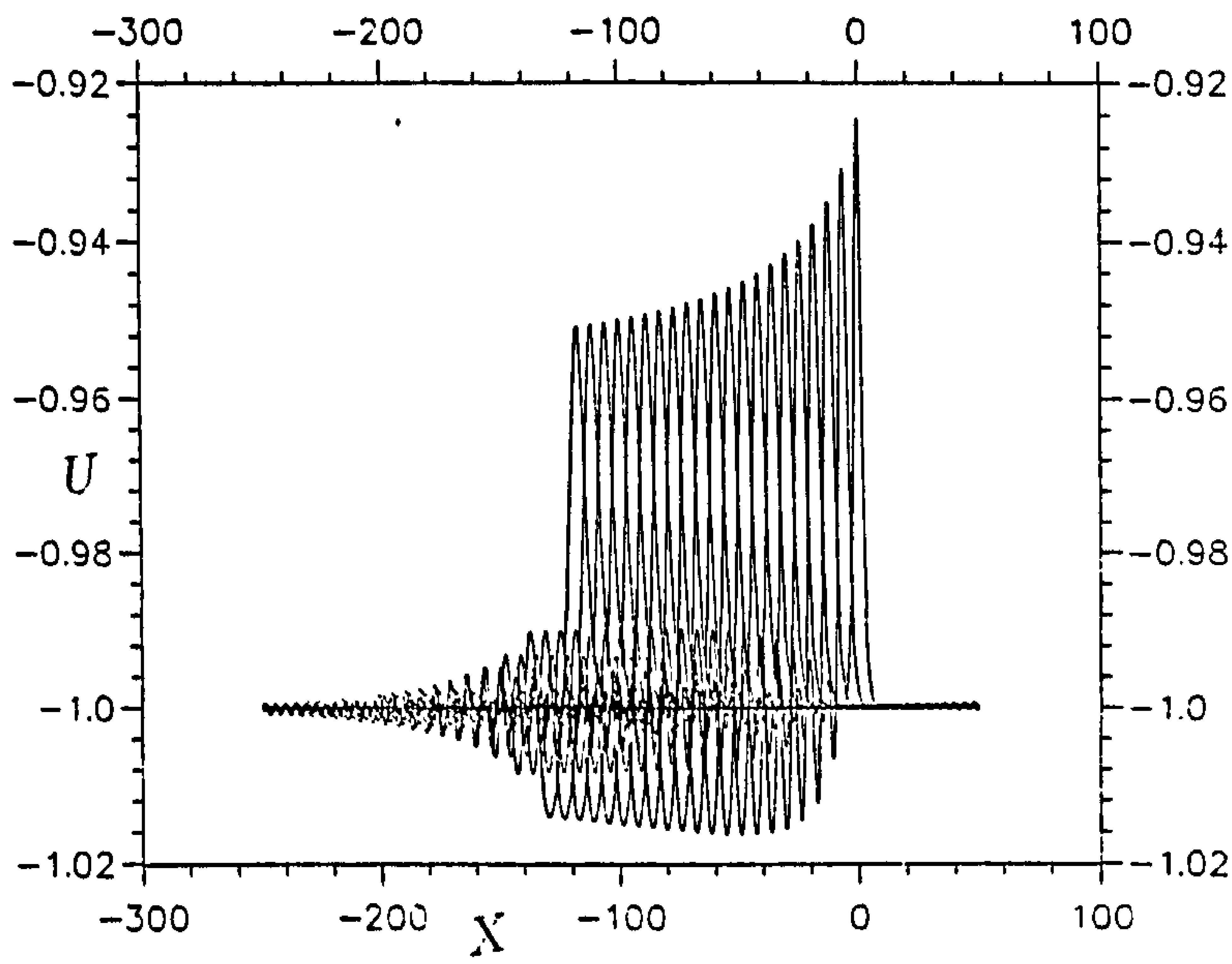

Figure 6.37: Double tanh initial condition (6.27). $N = 2$. $\Delta = 0.2$. Superimposed profiles.

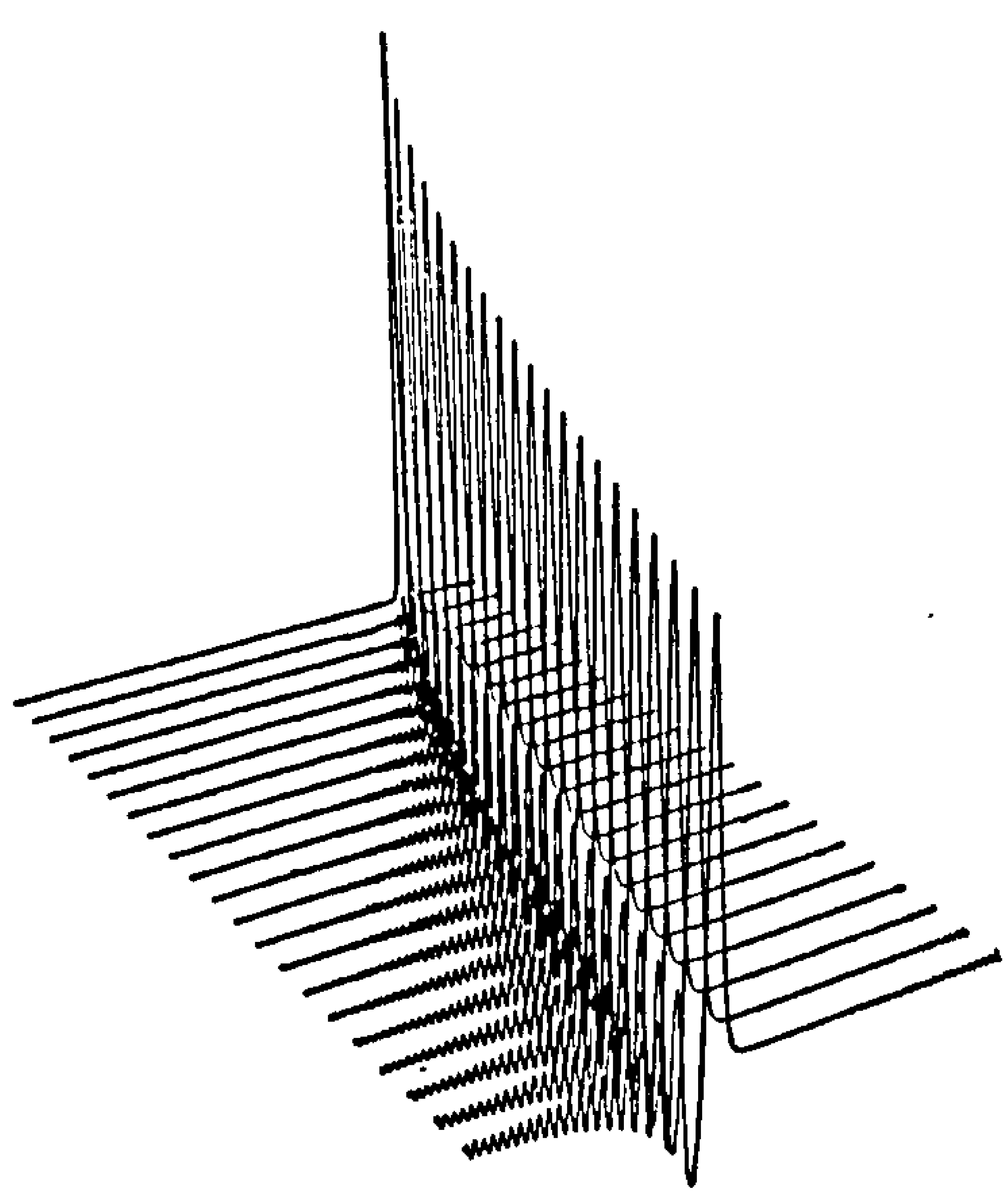

Figure 6.38: Double tanh initial condition (6.27). $N = 2, \Delta = 0.2$. Perspective view.

Table 6.13: Invariants for two tanh N=2 with $\Delta = 0.2$.

time	I_1	I_2	I_3
0.0	-299.896149	299.607544	299.075623
1.0	-299.897156	299.610870	299.087372
2.0	-299.898499	299.614807	299.093689
3.0	-299.900757	299.618103	299.100830
4.0	-299.903717	299.624939	299.110413
5.0	-299.905670	299.631653	299.119415
6.0	-299.907806	299.635681	299.130463
7.0	-299.911316	299.639465	299.139069
8.0	-299.915558	299.642700	299.146545
9.0	-299.917480	299.646423	299.155365
10.0	-299.919189	299.651123	299.163391
11.0	-299.920776	299.655151	299.171112
12.0	-299.922150	299.658539	299.177551
13.0	-299.923157	299.661377	299.183624
14.0	-299.924744	299.664886	299.189484
15.0	-299.926331	299.667664	299.195740

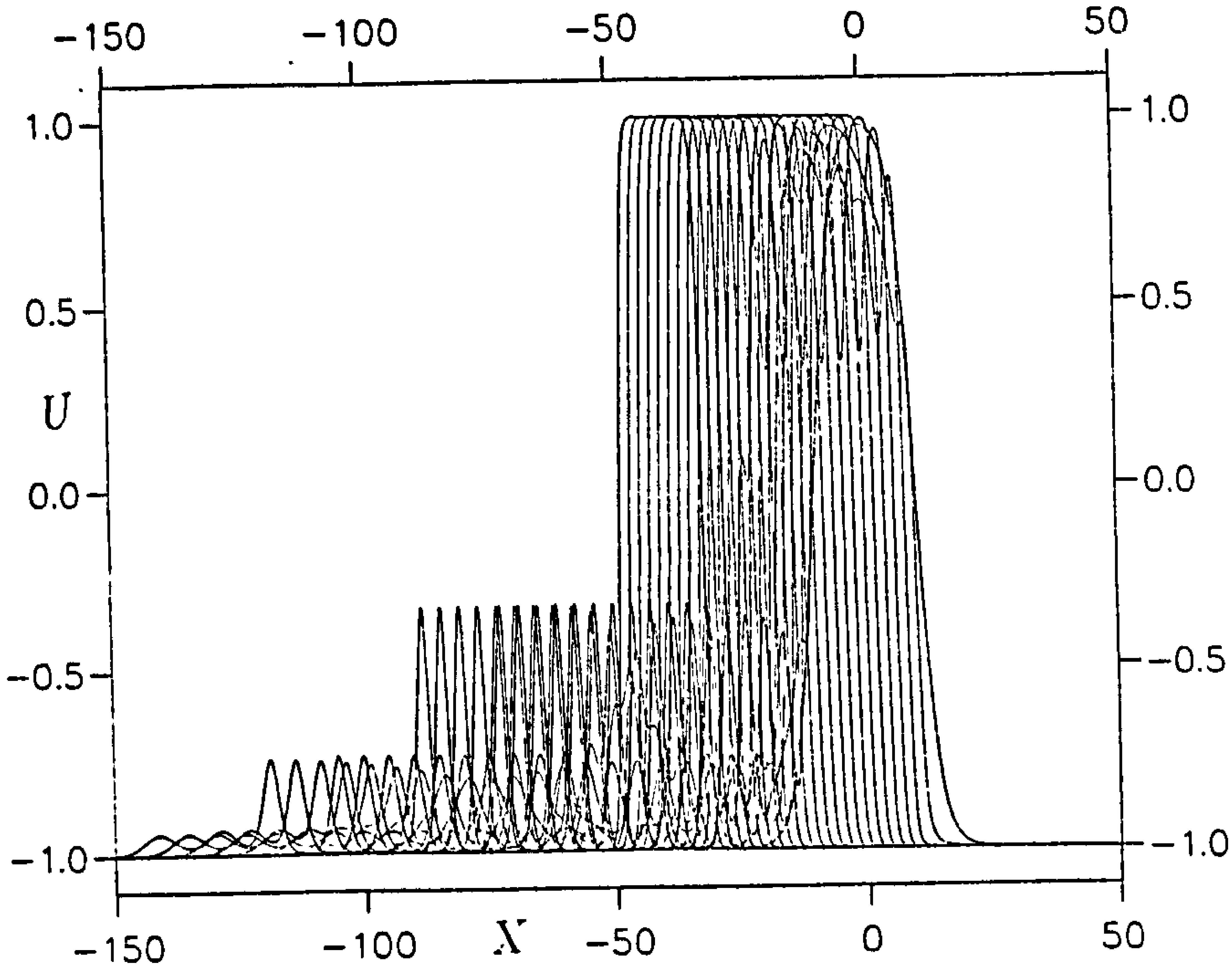

Figure 6.39: Double tanh initial condition (6.27). $N = 4, \Delta = 10$. Superimposed profiles.

6.2.13 Numerical experiments series 2. $N = 4$

In this series of experiments we take a region $-200 \leq x \leq 50$. $h = 0.2, \Delta t = 0.005$ and run the simulation up to time $t = 15$.

a-) For $\Delta = 10$, the invariants are listed in Table (6.14). The progress of the run is shown in figures(6.39-6.40). Like the corresponding experiment in series 1, the slopes of the tanh functions do not combine with their amplitudes to give an exact kink configuration. Once more the tanh functions keep their original amplitude but steepen into a double kink configuration with velocity -2.03 and in so doing each tanh emits 3 solitons as is shown clearly in Figures (6.39-6.40).

The paired daughter solitons have identical amplitudes $(0.675, 0.269, 0.063)$ and travel across the mesh with identical speeds $(-3.88, -5.06, -5.71)$, which compare well with free soliton speeds of $-3.76, -5.00$ and -5.75.

b-) For $\Delta = 1$ the invariants are listed Table (6.15). As shown in figures (6.41-6.42) the initial pulse grows in amplitude and its slope steepens until

Table 6.14: Invariants for two tanh N=4 with $\Delta = 10$.

time	I_1	I_2	I_3
0.0	-210.200195	234.207596	229.564163
1.0	-210.200882	234.204422	229.568604
2.0	-210.201172	234.193726	229.558792
3.0	-210.199677	234.193848	229.555130
4.0	-210.196121	234.198532	229.563019
5.0	-210.188309	234.203781	229.571381
6.0	-210.177826	234.204681	229.574799
7.0	-210.176971	234.205276	229.577789
8.0	-210.175873	234.209183	229.586426
9.0	-210.167450	234.218552	229.597198
10.0	-210.159225	234.216599	229.599167
11.0	-210.158249	234.216629	229.598557
12.0	-210.158539	234.217804	229.600998
13.0	-210.159698	234.219086	229.603851
14.0	-210.160599	234.220703	229.606476
15.0	-210.160934	234.221878	229.609131

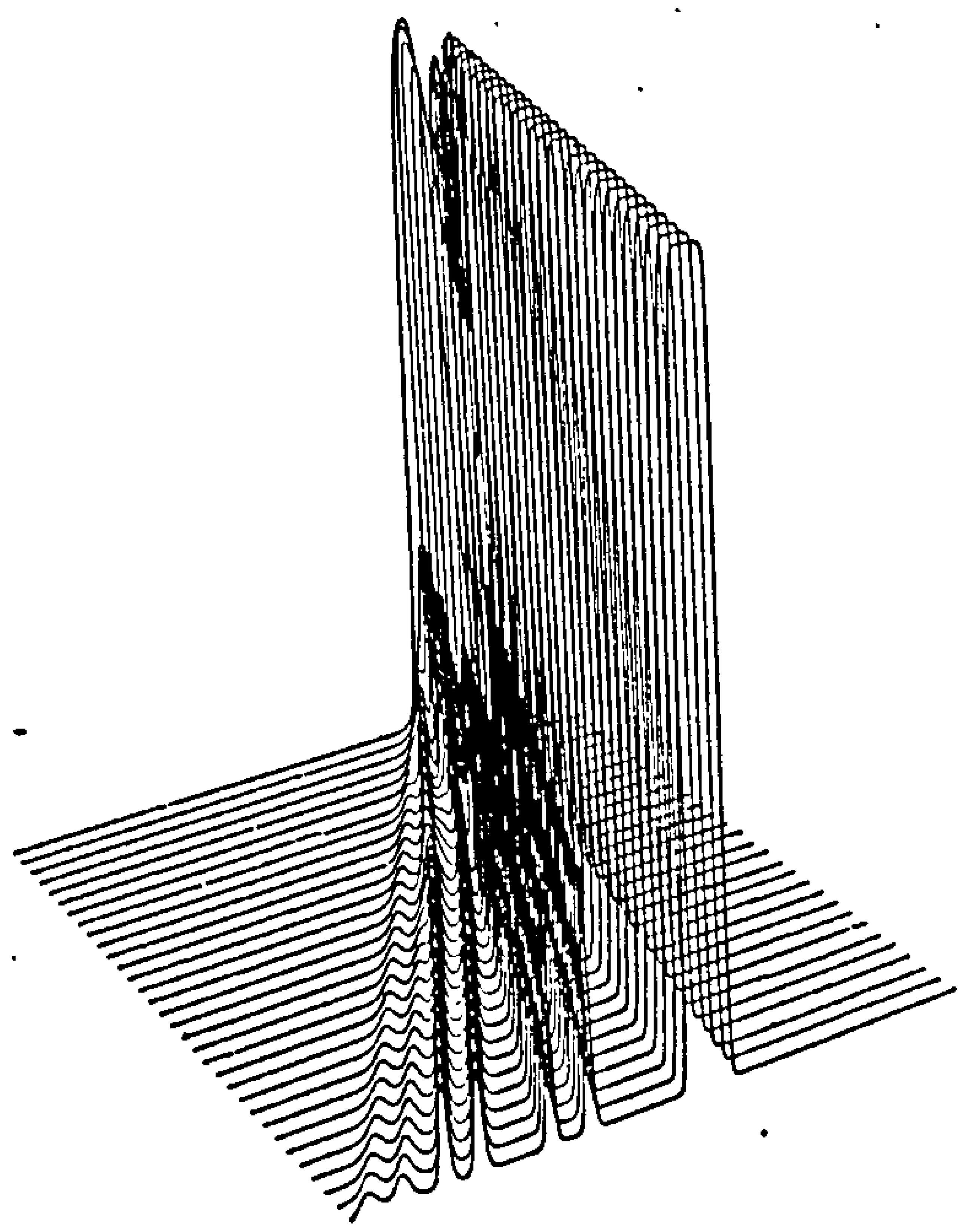

Figure 6.40: Double tanh initial condition (6.27). $N = 4$, $\Delta = 10$. Perspective view.

a soliton configuration of amplitude 0.6975 and velocity -3.693 is observed; a free soliton with similar amplitude has velocity -3.6965. In so doing three smaller solitons of amplitudes 0.3052, 0.0921 and 0.007 are ejected, the larger pair having velocities -4.8723, -5.61; free solitons of equal amplitudes have velocities. We were unable to determine the velocity of the smallest soliton.

c-) For $\Delta = 0.2$ we see in figures(6.43-6.44) the amplitude of the initial pulse decreases in height. By time $t = 15$ the amplitude is 0.1178 and the velocity -5.54, at the same time a wave train has been created in front of the pulse; a soliton of equal height would have velocity -5.844. The invariants for this simulation, which are listed in Table (6.16), show satisfactory conservation.

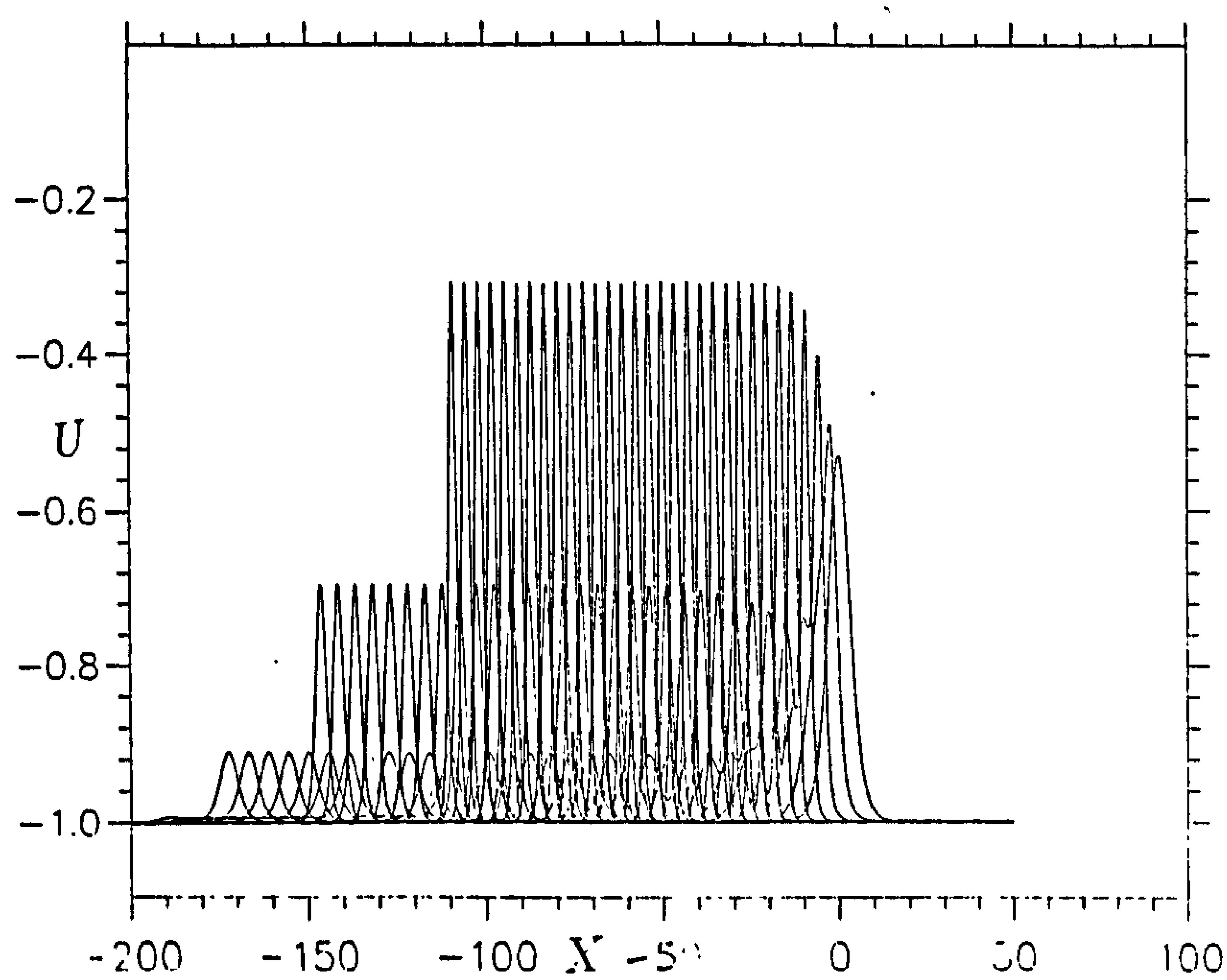

Figure 6.41: Double tanh initial condition (6.27). $N = 4, \Delta = 1$. Superimposed profiles.

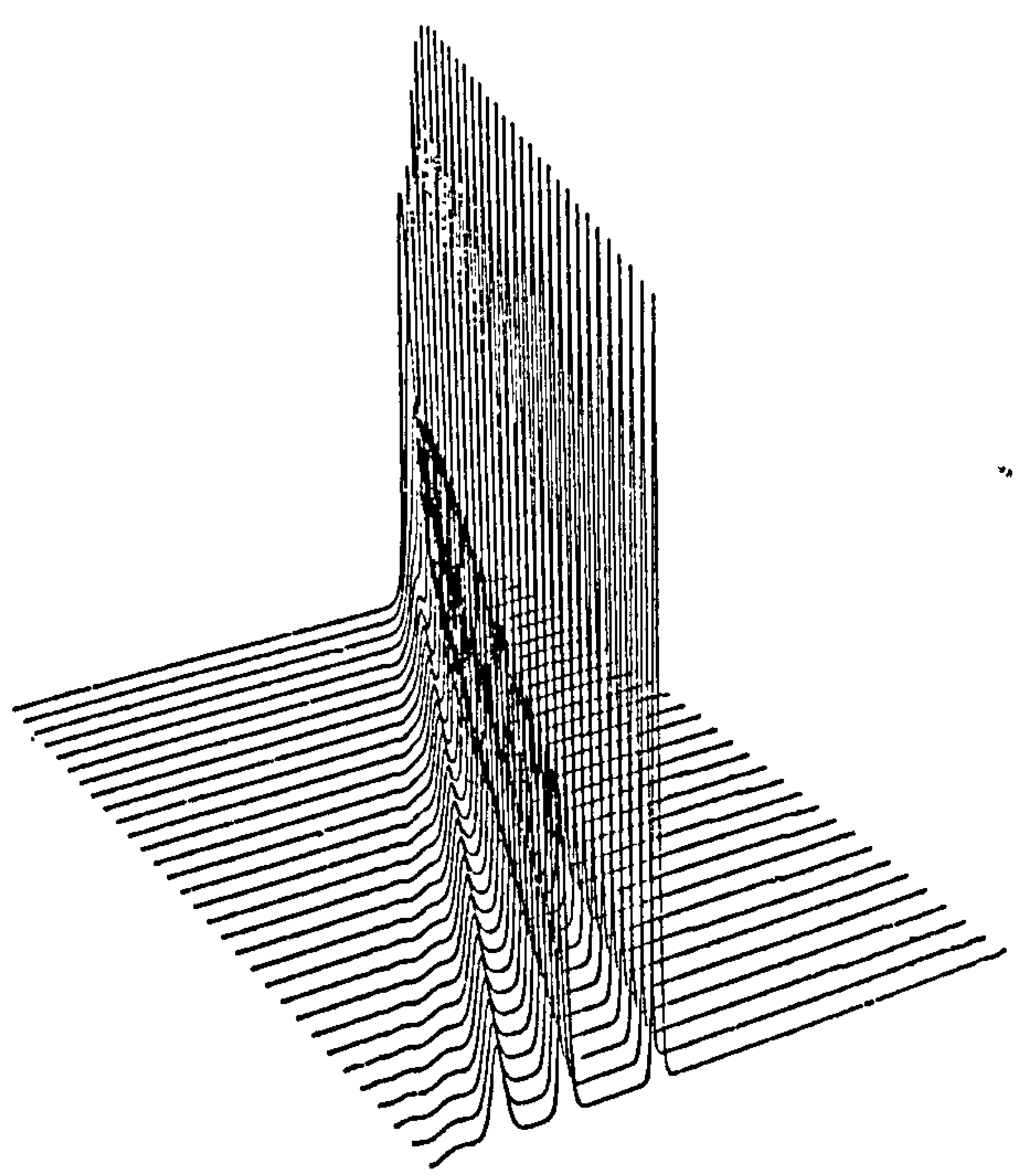

Figure 6.42: Double tanh initial condition (6.27). $N = 4, \Delta = 1$. Perspective view.

Table 6.15: Invariants for two tanh N=4 with $\Delta = 1$.

time	I_1	I_2	I_3
0.0	-246.344070	243.707123	240.489777
1.0	-246.344971	243.710114	240.498505
2.0	-246.345749	243.711639	240.502167
3.0	-246.346802	243.713699	240.504105
4.0	-246.348907	243.718140	240.510986
5.0	-246.351883	243.720413	240.515961
6.0	-246.353760	243.724411	240.523285
7.0	-246.355927	243.727493	240.530365
8.0	-246.356644	243.729538	240.535309
9.0	-246.357880	243.732758	240.540359
10.0	-246.359497	243.735474	240.545609
11.0	-246.361053	243.737793	240.550217
12.0	-246.362396	243.740387	240.554657
13.0	-246.363327	243.743195	240.559418
24.0	-246.364136	243.744797	240.562958
15.0	-246.365076	243.746429	240.566940

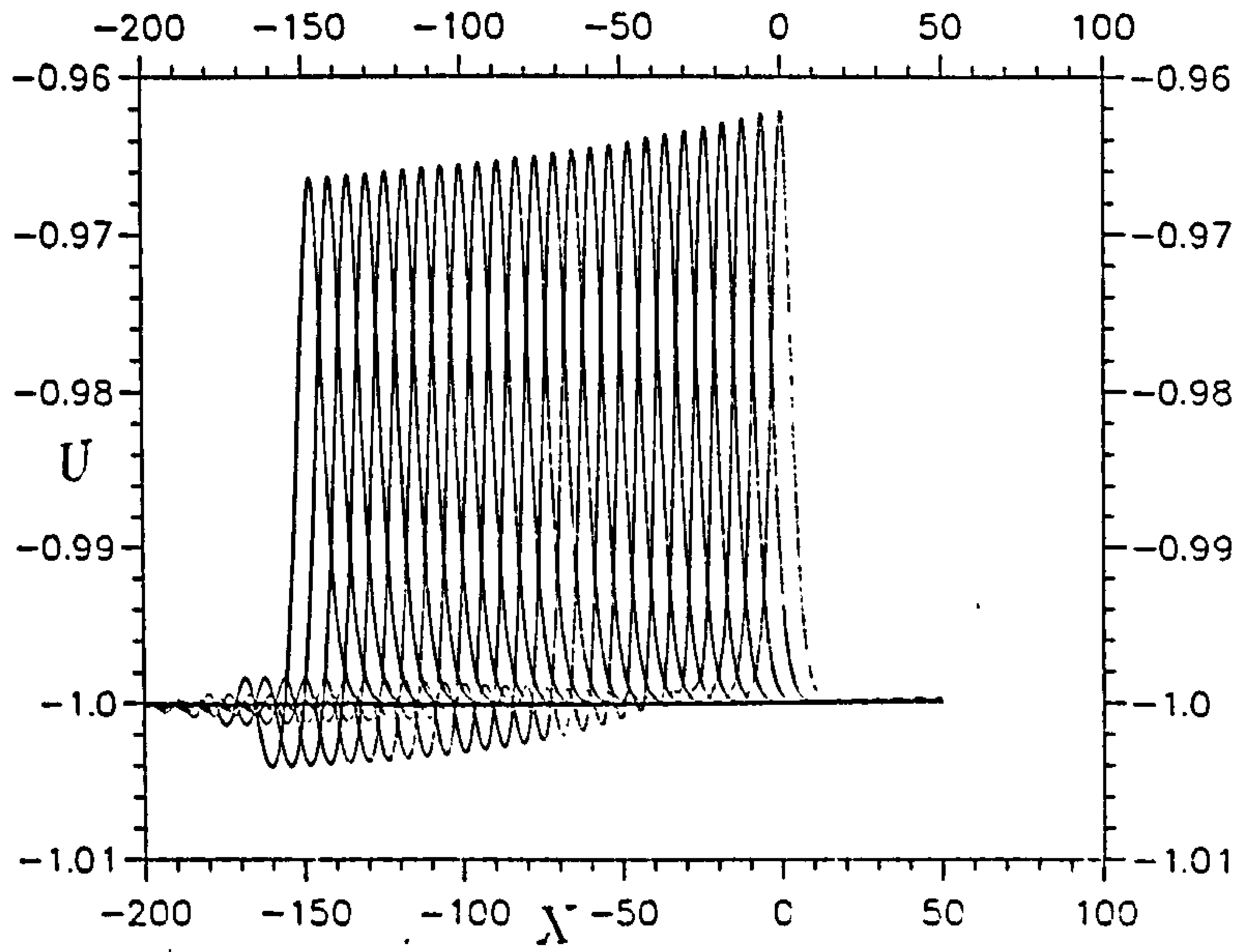

Figure 6.43: Double tanh initial condition (6.27). $N = 4, \Delta = 0.2$. Superimposed profiles.

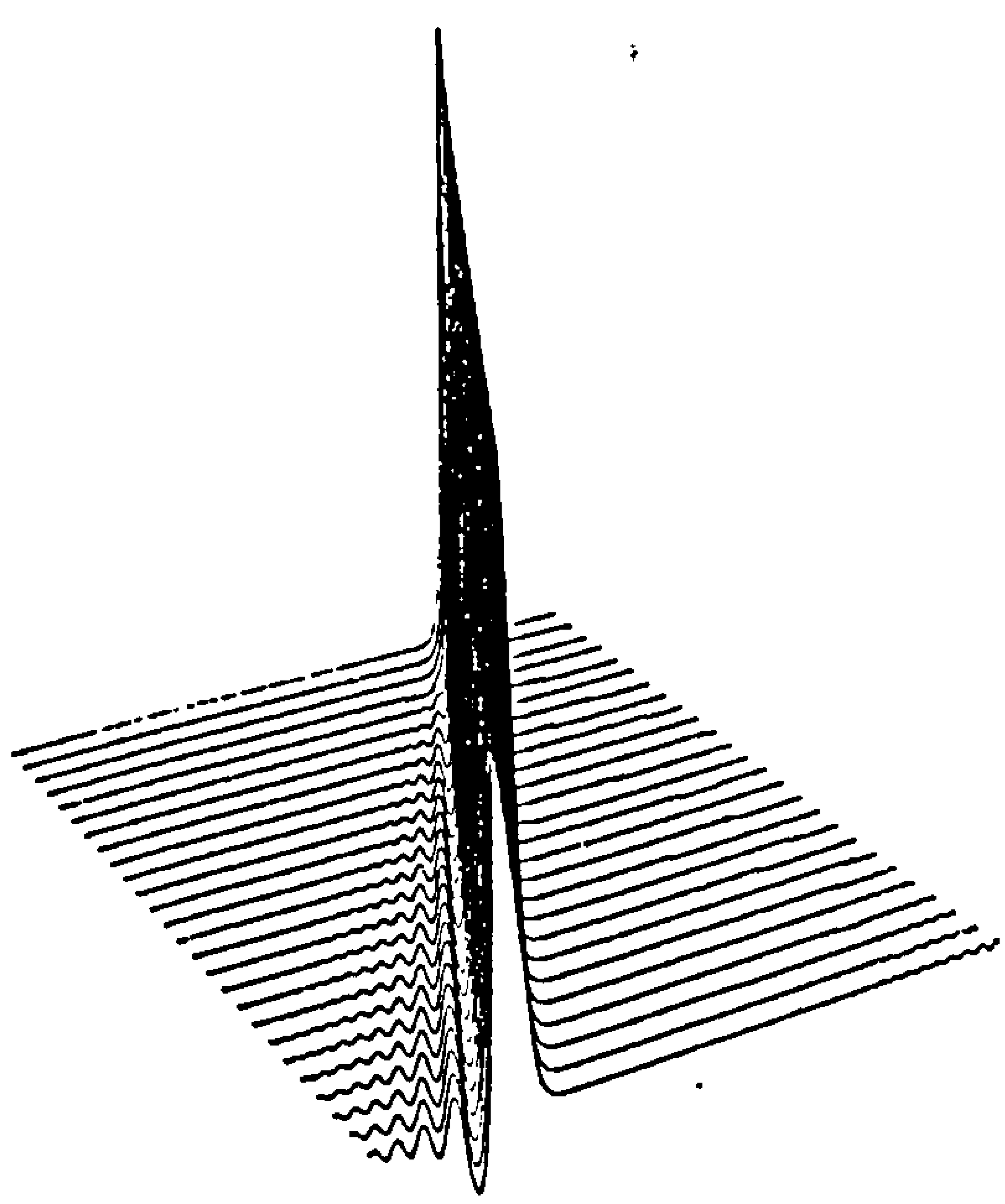

Figure 6.44: Double tanh initial condition (6.27). $N = 4, \Delta = 0.2$. Perspective view.

Table 6.16: Invariants for two tanh N=4 with $\Delta = 0.2$.

time	I_1	I_2	I_3
0.0	-249.896164	249.599930	249.029938
1.0	-249.897095	249.603073	249.039597
2.0	-249.897995	249.605621	249.044510
3.0	-249.899200	249.608856	249.049438
4.0	-249.901947	249.614258	249.057526
5.0	-249.904572	249.617218	249.063599
6.0	-249.905256	249.621536	249.072220
7.0	-249.908859	249.624634	249.079437
8.0	-249.909744	249.627243	249.084885
9.0	-249.910675	249.630295	249.090530
10.0	-249.912140	249.633392	249.095993
11.0	-249.913940	249.635406	249.101395
12.0	-249.915695	249.638229	249.106247
13.0	-249.917603	249.642776	249.111206
14.0	-249.917603	249.642776	249.115997
15.0	-249.918411	249.644455	249.119583

6.2.14 Problem 9

If we get the generation of kink and solitons from a quasisoliton initial condition of the form.

$$U(x,0) = -1 + a\tanh(2C\Delta)[\tanh(C(ax + a\Delta)) - \tanh(C(ax - a\Delta))]. \tag{6.29}$$

where $C = 1/N, N$ an integer.

When Δ is large, the tanh functions well separated and each tanh behaves independently and since $C(= 1/N)$ is the reciprocal of an integer there is a discrete set of eigenvalues which may be determined analytically [16], and corresponding to each a daughter soliton is born; this process has already been described for problem 6.

As Δ takes smaller values the tanh functions become closer together as do the corresponding solitons in each of the wave trains, and when the tanh profiles are sufficiently close the wave trains coincide. When Δ is reduced still further the soliton solution is replaced by a stable pulse preceed by a wave train.

Simulations are set up with $\Delta = 2, 1, 0.2$ and $C = 1/N$ where $N = 2, 4$. The case $\Delta = 2$ corresponds to the well separated situation and two trains of solitons are generated, one arising from each tanh functions. When $\Delta = 1$, $2C\Delta \sim 1$, a single train of solitons is observed, while with $\Delta = 0.2$ a stable pulse preceded by a wave train forms .

6.2.15 Numerical experiment series 1. $N = 2$

a-) When $\Delta = 2$ we take a region $-300 \leq x \leq 20$,$h = 0.2, \Delta t = 0.005$ and run the simulation up to time $t = 15$. The invariants are listed in Table (6.17). The progress of the run is shown in figures (6.45-6.46). The initial pulse, which is very similar in appearance to a soliton, grows in amplitude and its slope steepens until a soliton configuration of amplitude 1.7746 and

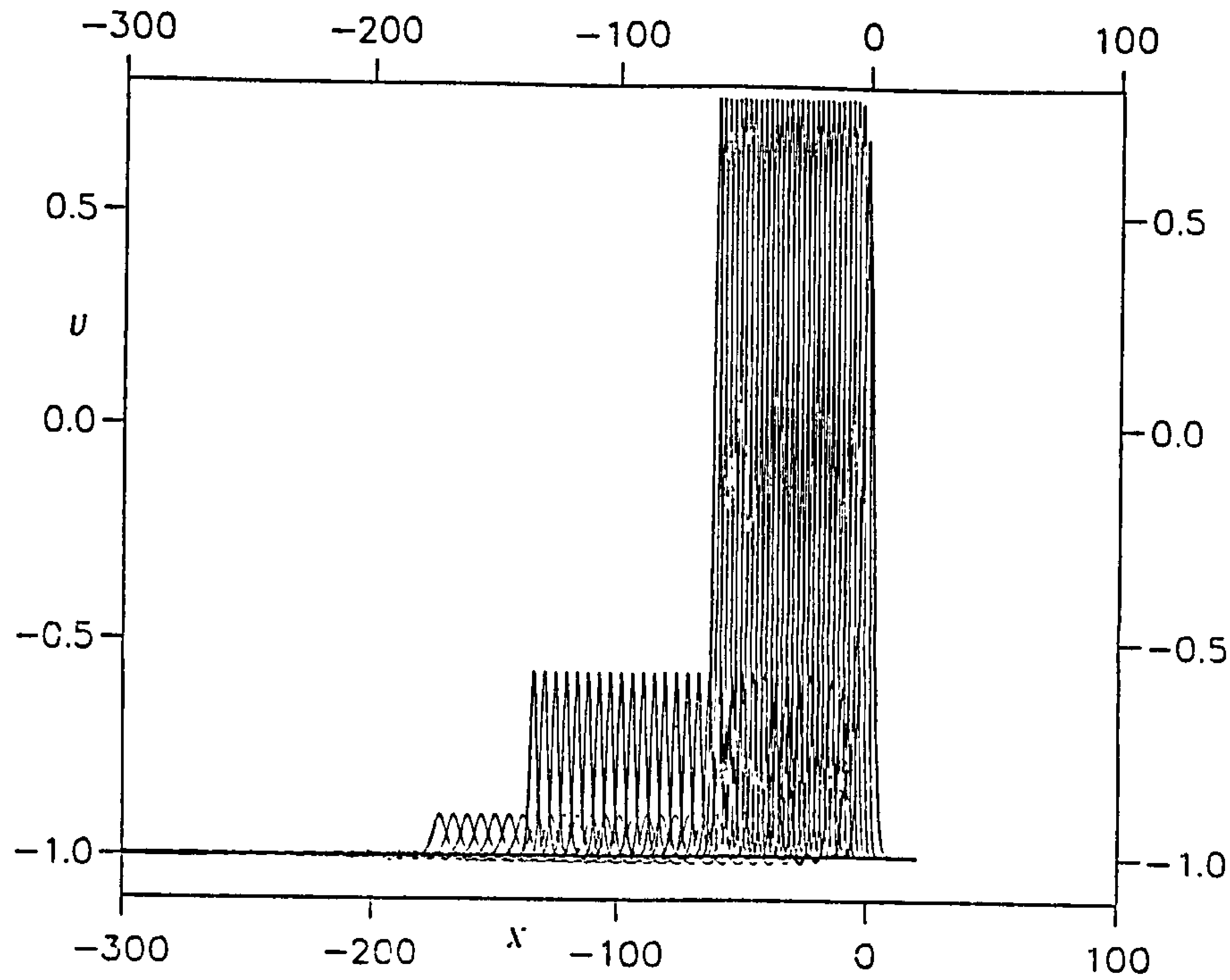

Figure 6.45: Double tanh initial condition (6.29). $N = 2, \Delta = 2$. Superimposed profiles.

velocity -2.0 is achieved. In so doing a single smaller soliton of amplitude (0.4247, 0.1066) is ejected with velocities (-4.40, -6.40).

b-) When $\Delta = 1$ we take a region $-300 \leq x \leq 20$ and $h = 0.2, \Delta t = 0.005$ and run the simulation to time $t = 1.5$. The invariants are listed in Table (6.18). As shown in figures (6.47-6.48) the initial pulse, which is very similar in appearance to a soliton, grows in amplitude and its slope steepens until a soliton configuration of amplitude 0.8599 and velocity -3.20 is achieved. In so doing a single smaller soliton of amplitude 0.1507 is ejected with velocity -6.50.

c-) When $\Delta = 0.2$ we take a region $-300 \leq x \leq 20$ and $h = 0.2, \Delta t = 0.005$ and run the simulation to time $t = 15$. We see in figures (6.49-6.50) the amplitude of the initial pulse decreases until a stable height is reached, at the same time a wave train is created in front of the pulse. The invariants are listed in Table (6.19). Since in this experiment Δ was of the same size as the grid spacing h there was some feeling that this might have influenced the outcome. It was decided to reduced the grid spacing to $h = 0.05$ and

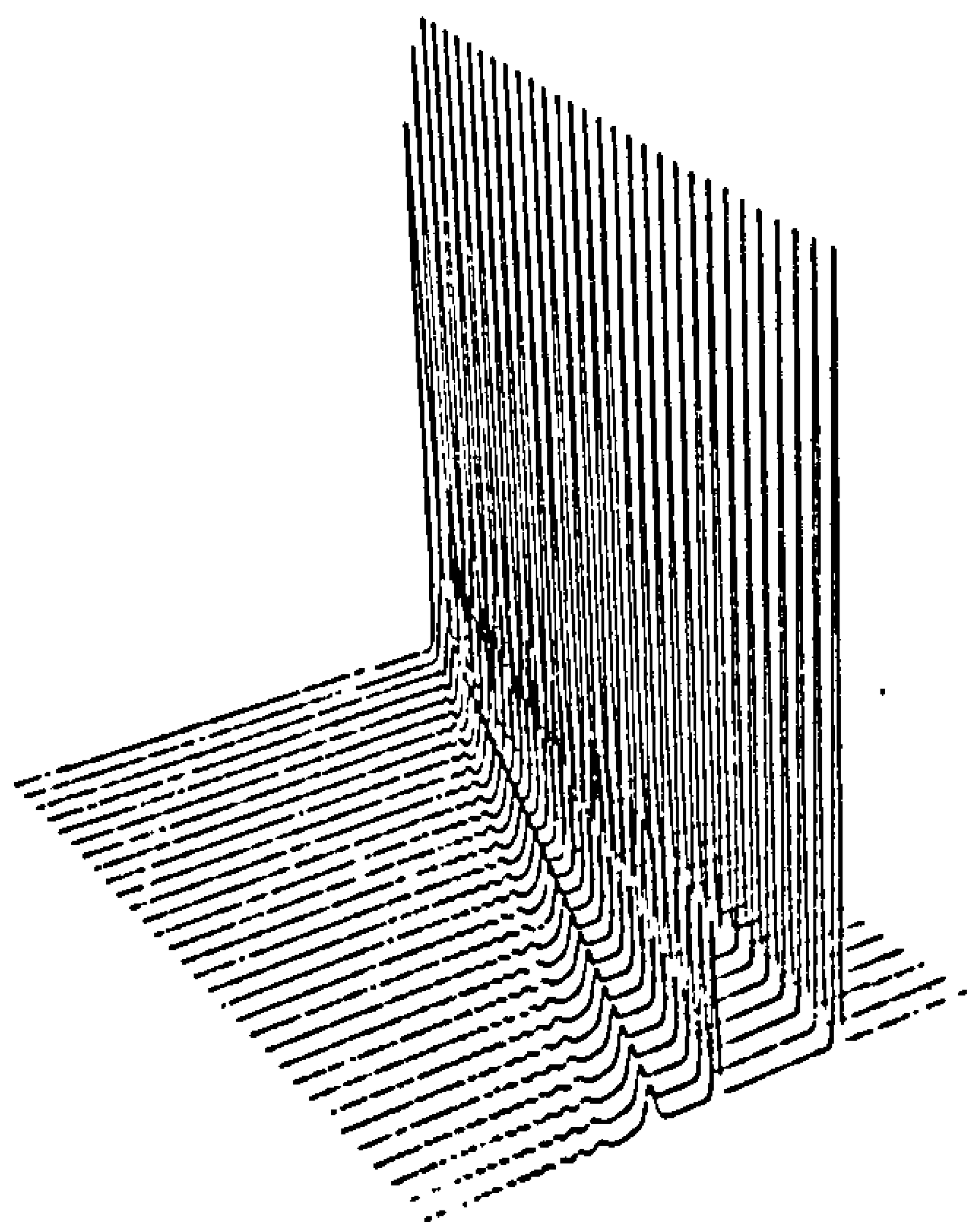

Figure 6.46: Double tanh initial condition (6.29). $N = 2, \Delta = 2$. Perspective view.

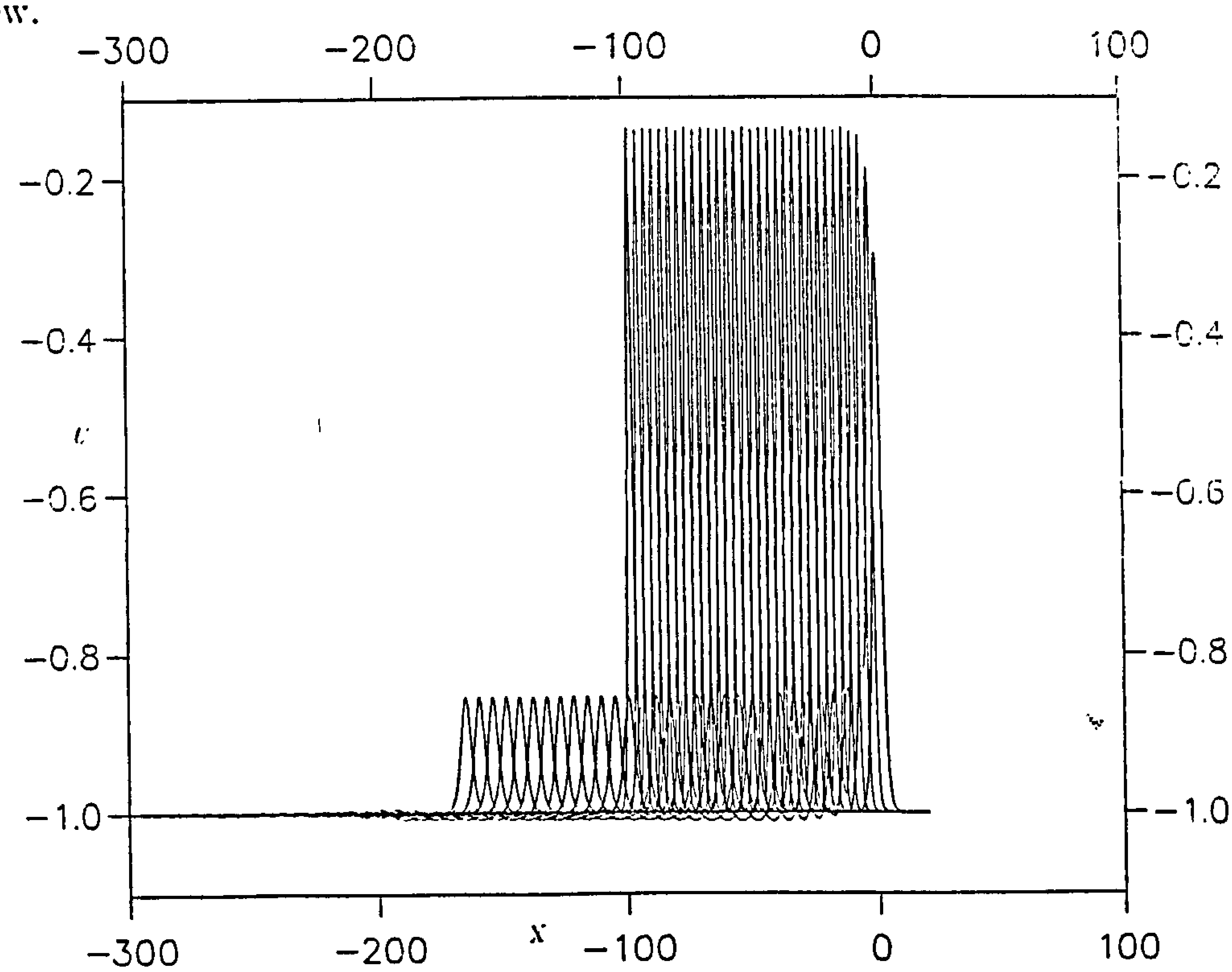

Figure 6.47: Double tanh initial condition (6.29). $N = 2, \Delta = 1$. Superimposed profiles.

Table 6.17: Invariants for two tanh n=2 with $\Delta = 2$.

time	I_1	I_2	I_3
0.0	-312.487823	312.765320	312.003357
1.0	-312.482635	312.761047	312.009125
2.0	-312.478882	312.756653	312.007385
3.0	-312.480103	312.760681	312.009521
4.0	-312.483459	312.767365	312.021301
5.0	-312.488312	312.770355	312.028595
6.0	-312.491028	312.776550	312.039520
7.0	-312.493195	312.781281	312.048645
8.0	-312.494751	312.785461	312.058228
9.0	-312.496429	312.789886	312.065491
10.0	-312.498718	312.794098	312.074036
11.0	-312.500641	312.798279	312.082275
12.0	-312.502380	312.802338	312.089447
13.0	-312.504639	312.805420	312.097015
14.0	-312.506378	312.808685	312.103607
15.0	-312.508514	312.811584	312.109924

Table 6.18: Invariants for two tanh N=2 with $\Delta = 1$.

time	I_1	I_2	I_3
0.0	-317.153778	315.559814	314.183434
1.0	-317.154266	315.561432	314.192383
2.0	-317.155029	315.564117	314.198181
3.0	-317.157318	315.568848	314.201965
4.0	-317.161163	135.574219	314.212311
5.0	-317.163910	315.579254	314.222107
6.0	-317.166382	315.584593	314.232452
7.0	-317.169464	315.593811	314.243225
8.0	-317.171906	315.598206	314.252041
9.0	-317.174225	315.602753	314.261169
10.0	-317.175995	315.607361	314.269562
11.0	-317.177979	315.610962	314.278168
12.0	-317.180237	315.610962	314.285828
13.0	-317.182190	315.614441	314.293274
14.0	-317.183929	315.618347	314.300537
15.0	-317.185547	315.621033	314.306396

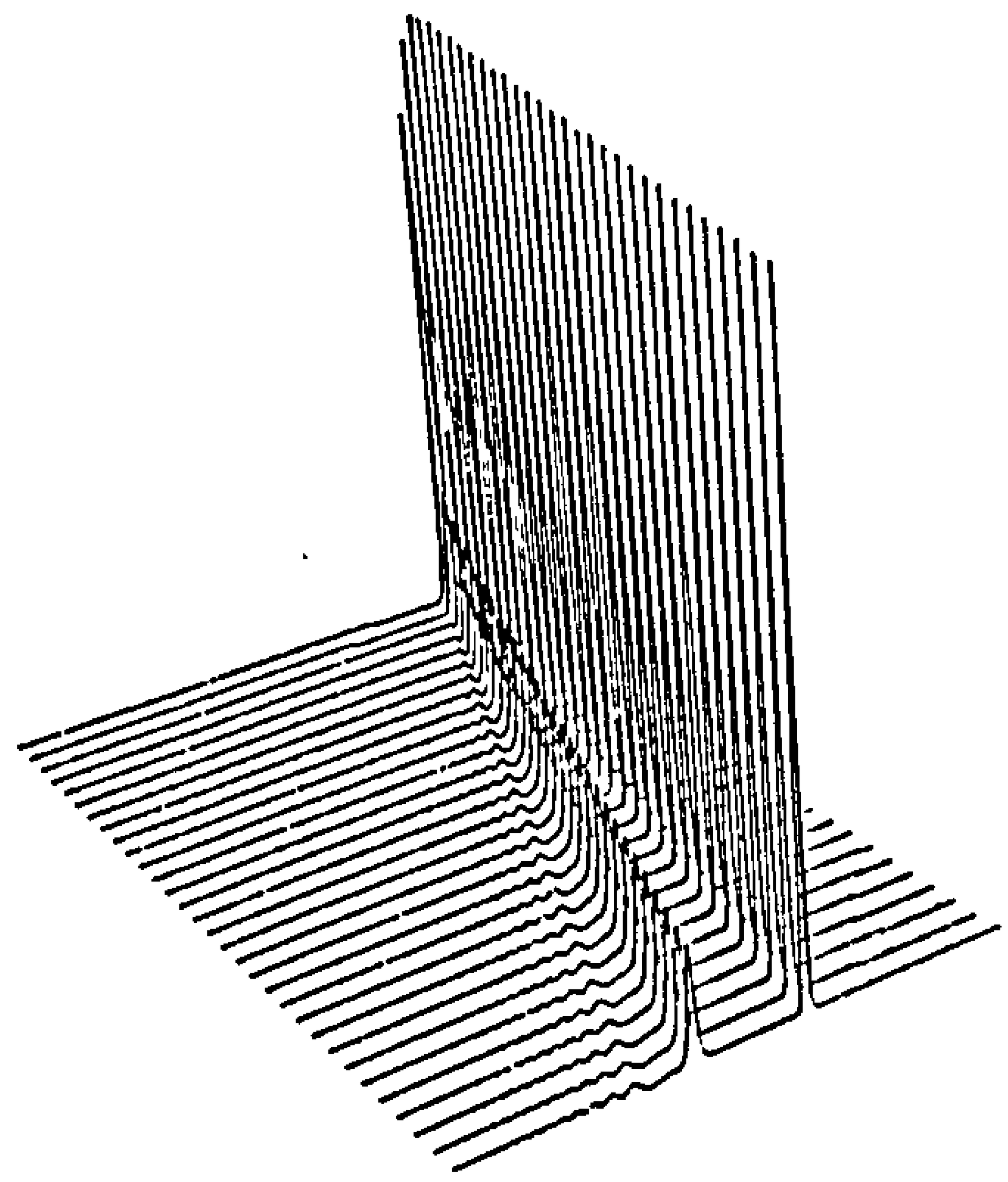

Figure 6.48: Double tanh initial condition (6.29). $N = 2, \Delta = 1$. Perspective view.

rerun the experiment. No significant changes in the results or outcome were observed.

6.2.16 Numerical experiments series 2. $N = 4$

In this series of experiments we take a region $-300 \leq x \leq 20$, $h = 0.2$, $\Delta t = 0.005$ and run the simulation up to time $t = 15$.

a-) For $\Delta = 1$ the invariants are listed Table (6.20). As shown in figures (6.51-6.52) the initial pulse grows in amplitude and its slopes steepen until a soliton configuration of amplitude 0.2849 and velocity -5.0 is observed. In so doing three smaller solitons of amplitudes 0.2849, 0.0853 and 0.0003 are ejekted the larger pair having velocities -5.0, -6.0. We were unable to determine the velocity of the smallest soliton.

b-) For $\Delta = 0.2$ we see in figures (6.53-6.54) the amplitude of the initial pulse decrease in height. By time $t = 15$ the amplitude is 0.99 and the velocity -6.133, at the same time a wave train has been created in front of the pulse; a soliton of equal height would have velocity -6.1333. The invari-

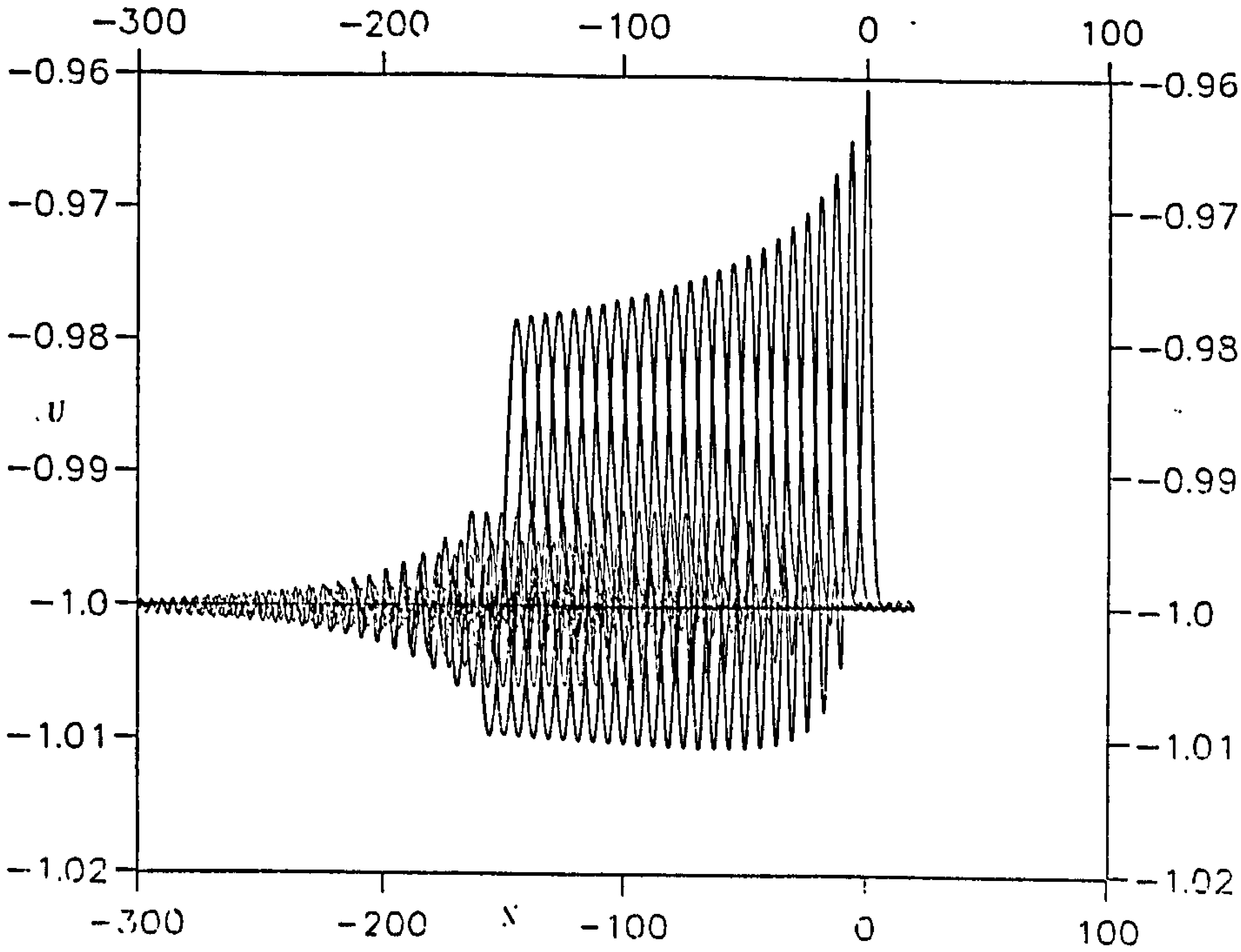

Figure 6.49: Double tanh initial condition (6.29). $N = 2, \Delta = 0.2$. Superimposed profiles.

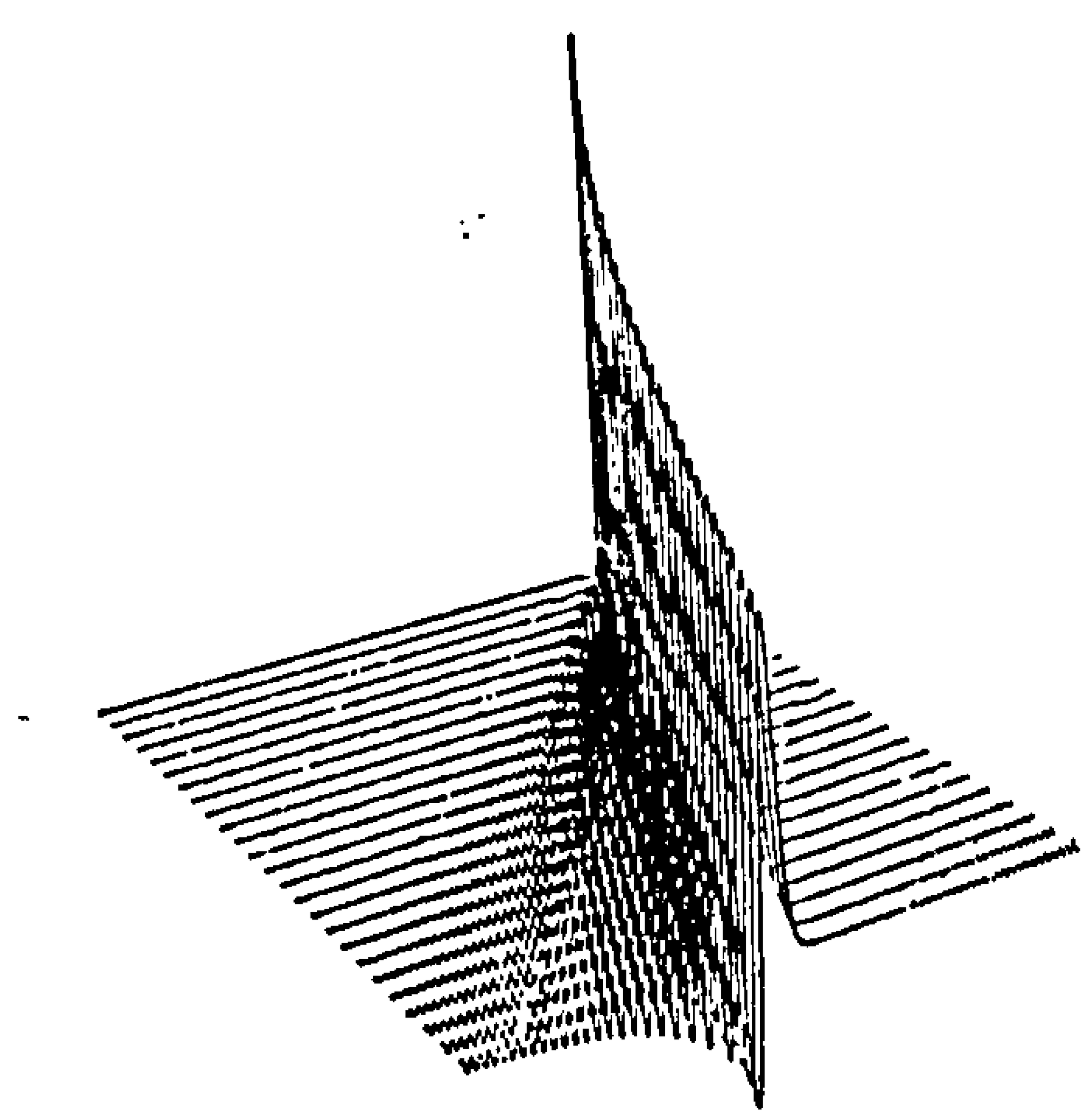

Figure 6.50: Double tanh initial condition (6.29). $N = 2, \Delta = 0.2$. Perspective view.

Table 6.19: Invariants for two tanh N=2 with $\Delta = 0.2$.

time	I_1	I_2	I_3
0.0	-320.042053	319.888397	319.593567
1.0	-320.043030	319.891785	319.605316
2.0	-320.044250	319.895416	319.613220
3.0	-320.046387	319.901093	319.617859
4.0	-320.053406	319.911438	319.638977
5.0	-320.055725	319.917175	319.649902
6.0	-320.058655	319.922272	319.660187
7.0	-320.061523	319.926025	319.669373
8.0	-320.063904	319.930817	319.678345
9.0	-320.065643	319.935333	319.686768
10.0	-320.067566	319.939667	319.694977
11.0	-320.069763	319.943634	319.703186
12.0	-320.069865	319.943735	319.704956
13.0	-320.071838	319.947174	319.710602
14.0	-320.073578	319.951111	319.717834
15.0	-320.074657	319.951121	319.717956

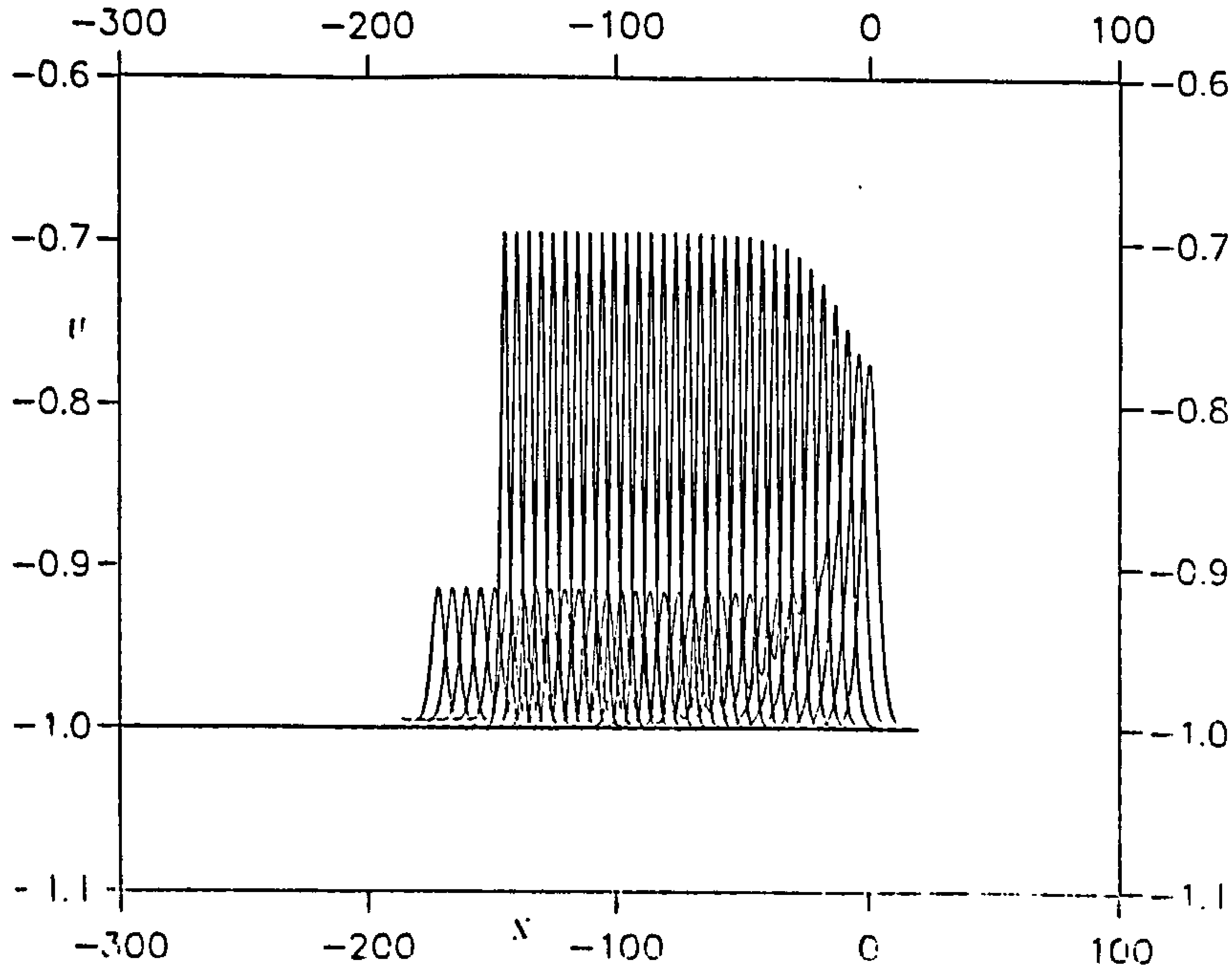

Figure 6.51: Double tanh initial condition (6.29). $N = 4, \Delta = 1$. Superimposed profiles.

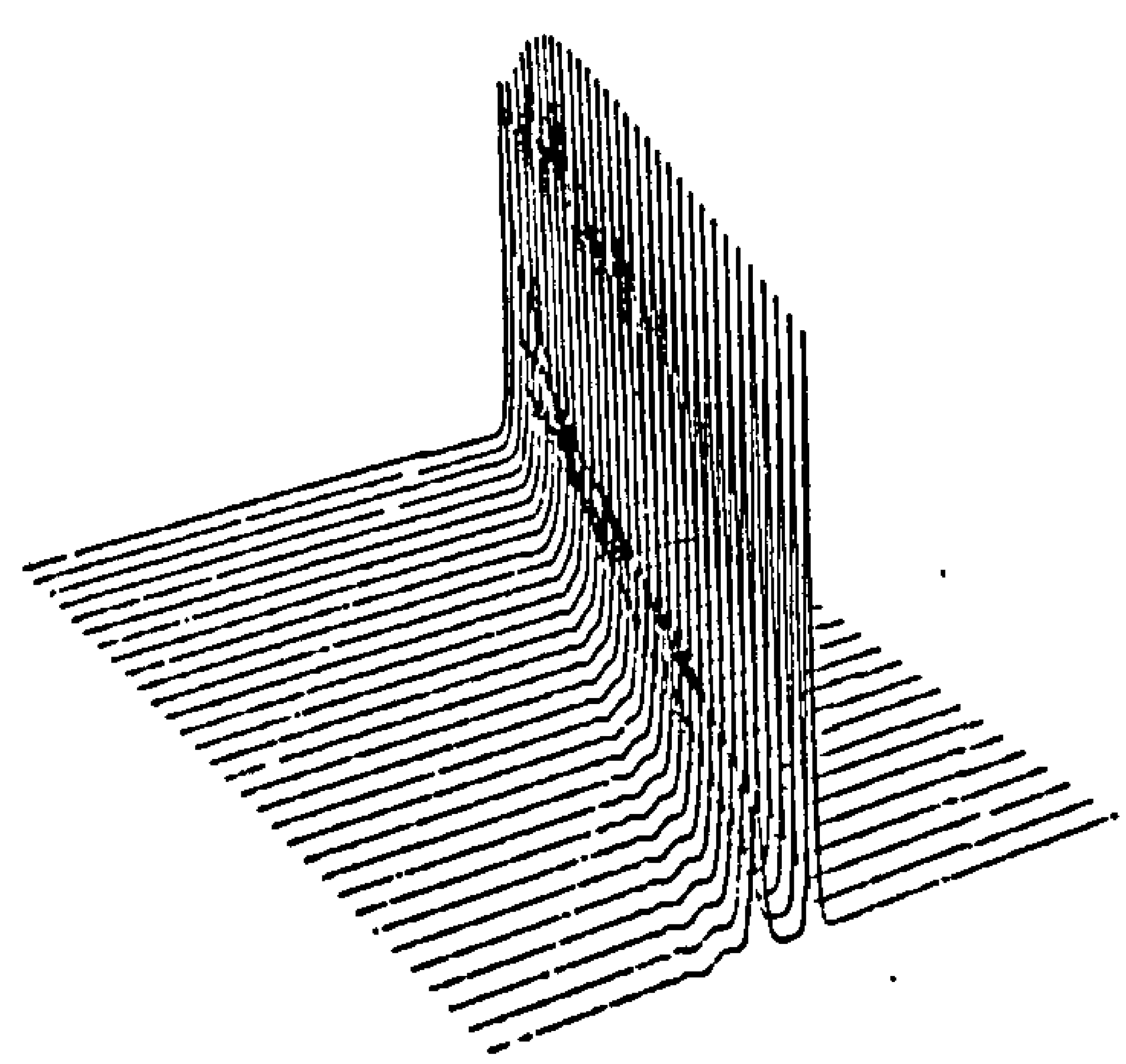

Figure 6.52: Double tanh initial condition (6.29). $N = 4, \Delta = 1$. Perspective view.

Table 6.20: Invariants for two tanh N=4 with $\Delta = 1$.

time	I_1	I_2	I_3
0.0	-318.351746	316.783478	314.307190
1.0	-318.352783	316.786804	314.318787
2.0	-318.353638	316.789856	314.325775
3.0	-318.354950	316.794922	314.332397
4.0	-318.358459	316.802063	314.342560
5.0	-318.363190	316.805481	314.350586
6.0	-318.365997	316.811890	314.361237
7.0	-318.368561	316.816589	314.371185
8.0	-318.369141	316.818970	314.378601
9.0	-318.370087	316.823425	314.387115
10.0	-318.372681	316.828308	314.393463
11.0	-318.376038	316.831482	314.401611
12.0	-318.378784	316.834534	314.409607
13.0	-318.381012	316.839111	314.417206
14.0	-318.382477	316.842926	314.424347
15.0	-318.383270	316.845764	314.430878

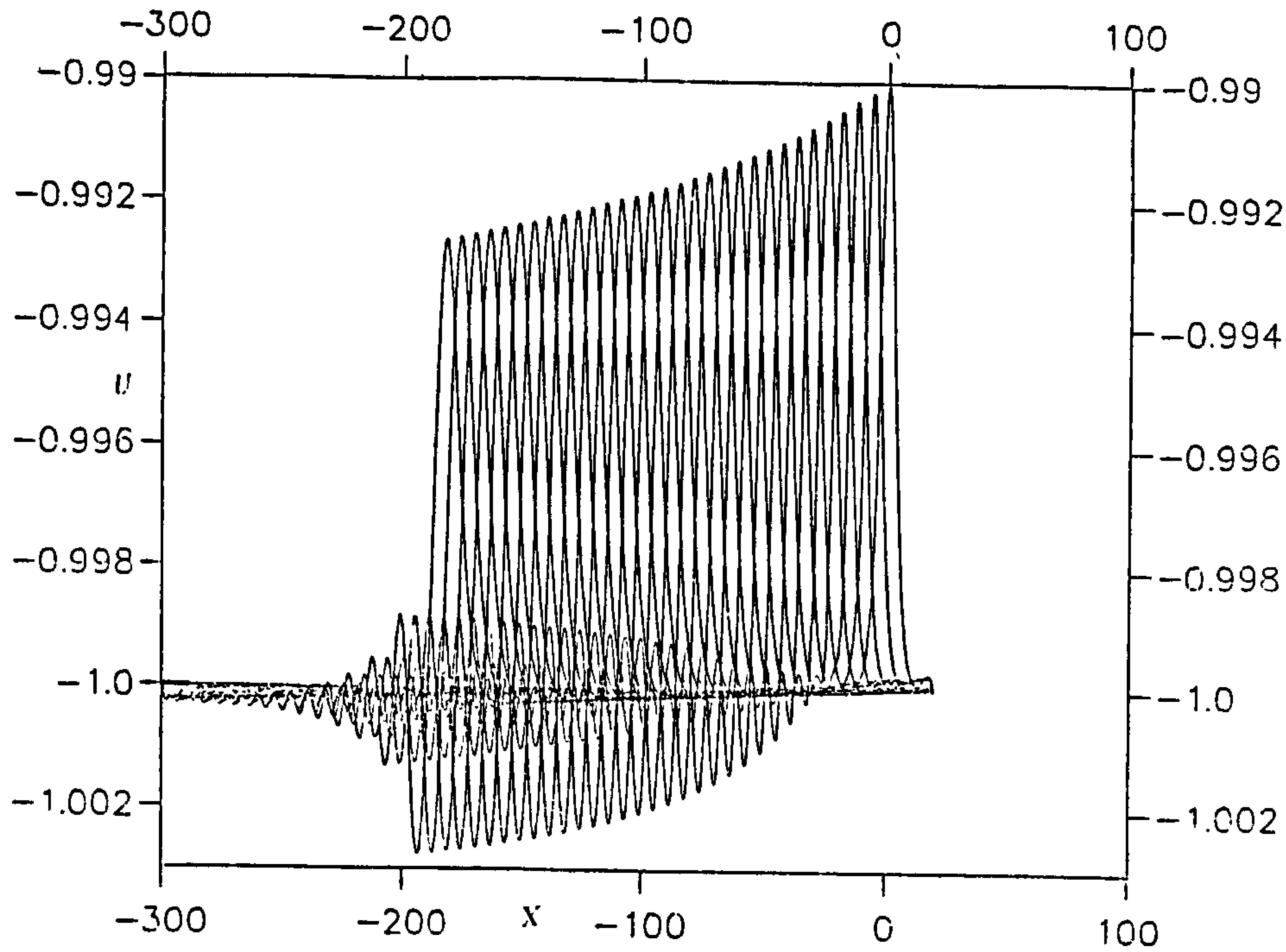

Figure 6.53: Double tanh initial condition (6.29). $N = 4, \Delta = 0.2$. Superimposed profiles.

ants for this simulation, which are listed in Table (6.21), show satisfactory conservation.

6.2.17 Problem 10

When we get the quasisoliton initial condition of the form.

$$U(x,0) = -1 + [\tanh(P(x+\Delta)) - \tanh(P(x-\Delta))]. \qquad (6.30)$$

where $P = 1/2$ and $\Delta = 0.2$. In this series of experiments we take a region $-250 \leq x \leq 20, h = 0.2, \Delta t = 0.005$ and run the simulation up to time $t = 15$.

For $\Delta = 0.2$ we see in figure (6.55) the amplitude of the initial pulse decreases in height. By time $t = 15$ the amplitude is 0.199 and the velocity -5.555, at the same time a wave train has been created in front of the pulse; a soliton of equal height would have velocity -5.555. The invariants for this simulation, which are listed in Table (6.22), show satisfactory conservation.

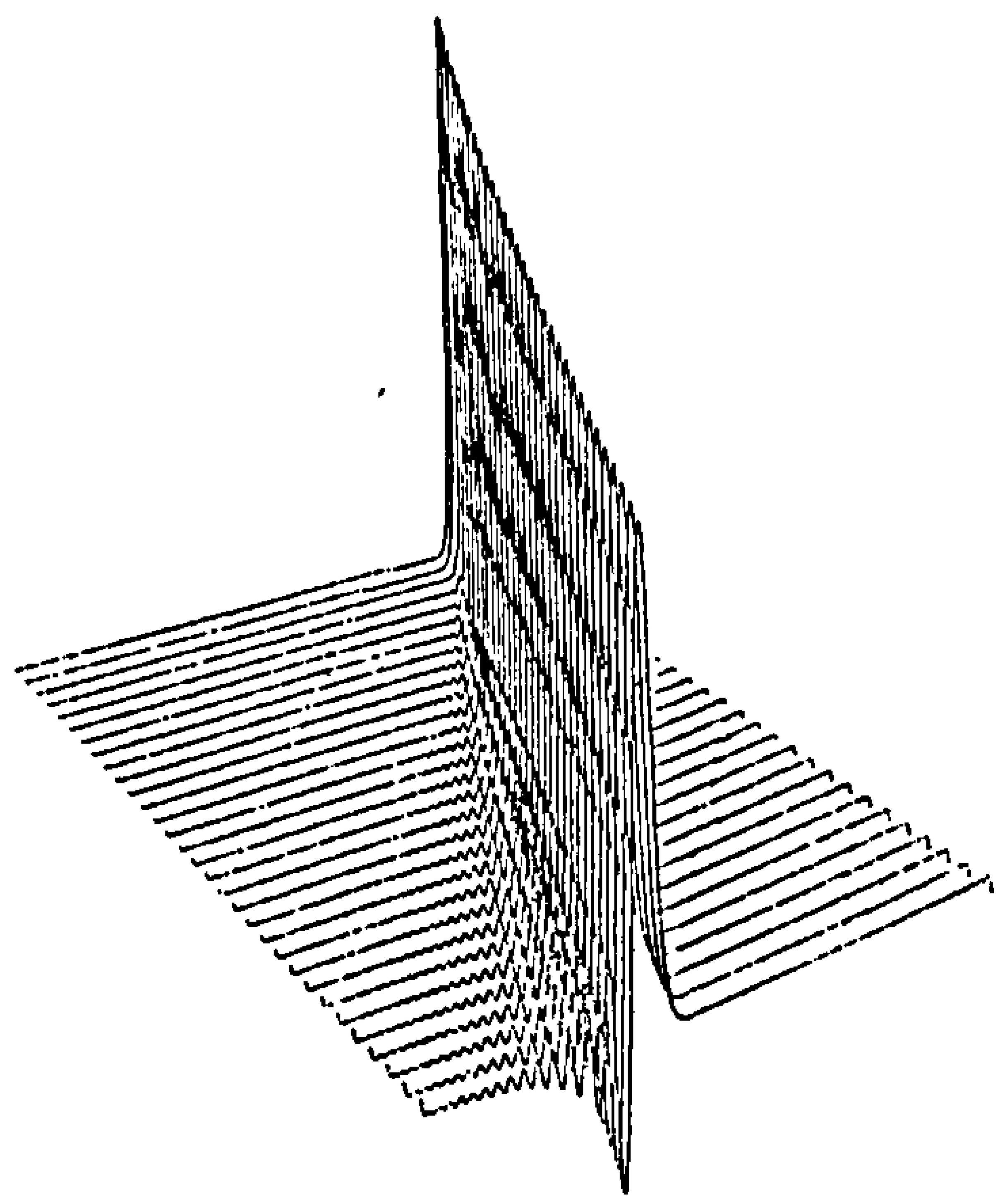

Figure 6.54: Double tanh initial condition (6.29). $N = 4, \Delta = 0.2$. Perspective view.

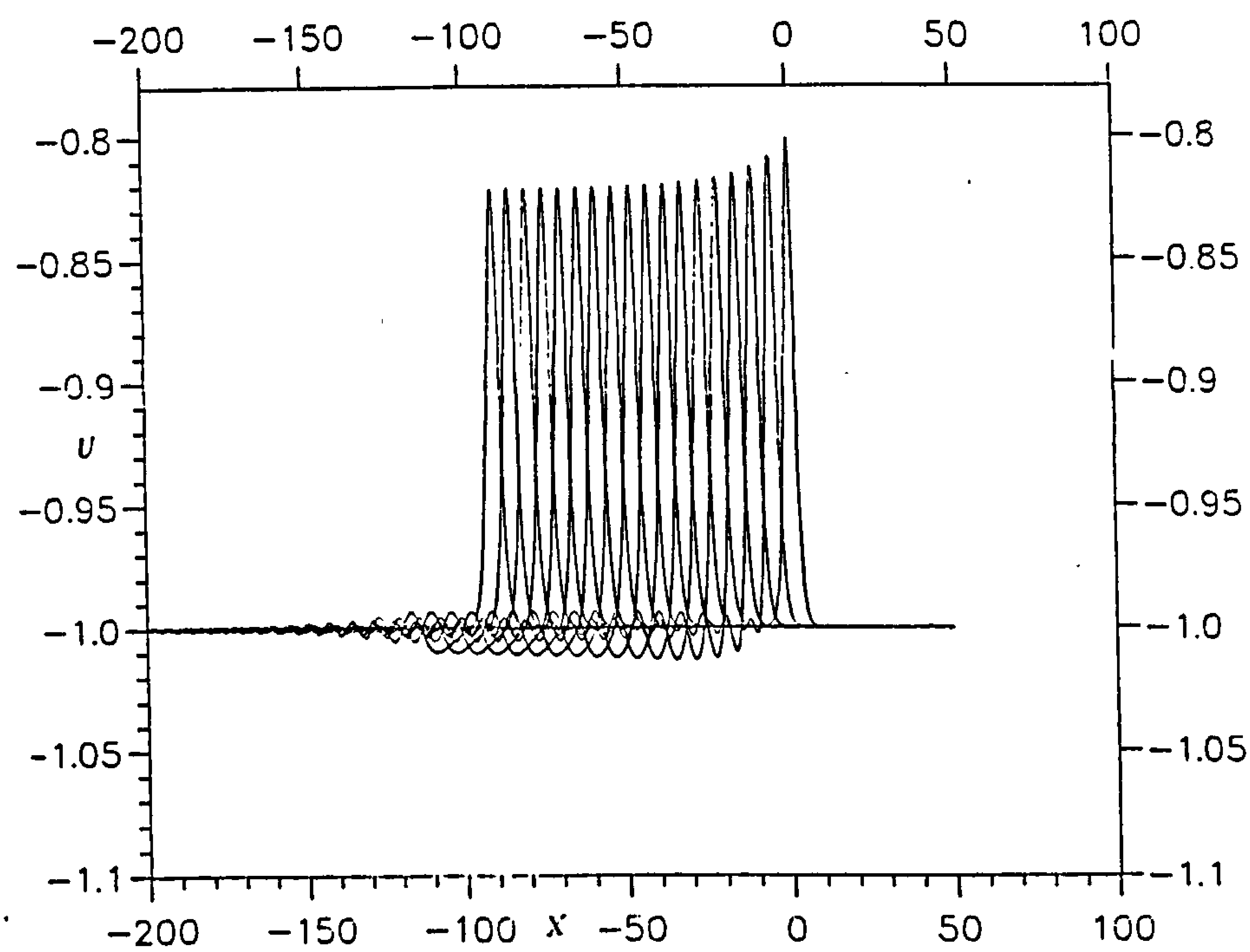

Figure 6.55: Double tanh initial condition (6.30). $P = 1/2, \Delta = 0.2$.

Table 6.21: Invariants for two tanh N=4 with $\Delta = 0.2$.

time	I_1	I_2	I_3
0.0	-320.120514	320.041168	319.884399
1.0	-320.121429	320.044312	319.895691
2.0	-320.122070	320.046814	319.901550
3.0	-320.123077	320.050720	319.908020
4.0	-320.124969	320.058533	319.919495
5.0	-320.130371	320.063416	319.925232
6.0	-320.133850	320.067902	319.938293
7.0	-320.136658	320.073608	319.946838
8.0	-320.138702	320.076263	319.956421
9.0	-320.139221	320.079346	319.962738
10.0	-320.141296	320.084045	319.971558
11.0	-320.143250	320.088806	319.978577
12.0	-320.146179	320.092010	319.986572
13.0	-320.148865	320.095825	319.994202
14.0	-320.150421	320.099518	320.001221
15.0	-320.151428	320.102386	320.008240

Table 6.22: Invariants for two tanh P=1/2 with $\Delta = 0.2$.

time	I_1	I_2	I_3
0.0	-249.400055	248.706451	247.594559
1.0	-249.401031	248.709915	247.603546
2.0	-249.402740	248.713303	247.610138
3.0	-249.404739	248.716156	247.616669
4.0	-249.406418	248.721680	247.624390
5.0	-249.409210	248.725861	247.631744
6.0	-249.411087	248.729401	247.639618
7.0	-249.413284	248.733002	247.646805
8.0	-249.414352	248.736130	247.653366
9.0	-249.415894	248.739136	247.659378
10.0	-249.417694	248.741623	247.664886
11.0	-249.419464	248.744843	247.670746
12.0	-249.420578	248.747070	247.675095
13.0	-249.421878	248.749756	247.680740
14.0	-249.421951	248.750214	247.681396
15.0	-249.422044	248.750345	247.681403

6.2.18 Problem 11

In this simulation we will study single soliton solution using the initial condition

$$U(x,0) = -1 + 2q\nu^2\{1 + \sqrt{(1-\nu^2)}\cosh 2\nu(x - x_0)\}^{-1}. \qquad (6.31)$$

In this series of experiments, when we get $q = 1$ then it is giving a single soliton. We will study $q = 1.01, 1.1, 0.99, 0.9$ and we take a region $-250 \leq x \leq 20, h = 0.2, \Delta t = 0.005, \nu = 0.3$ and run the simulation up to time $t = 15$. we can see four different simulation in figures (6.56-6.59).

First $q = 1.01$ and run up to time $t = 15$. We can see in figure (6.56) the amplitude of the initial pulse increase in height. By time $t = 15$ the amplitude is 0.0925.

Second $q = 1.1$ and run up to time $t = 15$. We can see in figure (6.57) the amplitude of the initial pulse increase in height. By time $t = 15$ the amplitude is 0.105 and at the same time a wave train has been created in front of the pulse.

Third $q = 0.99$ and run up to time $t = 15$. We can see in figure (6.58) the amplitude of the initial pulse increase in height. By time $t = 15$ the amplitude is 0.0911.

Last we get $q = 0.9$ and run up to time $t = 15$. We can see in figure (6.59) the amplitude of the initial pulse decrease in height. By time $t = 15$ the amplitude is 0.0841 and at the same time a wave train has been created in front of the pulse.

6.2.19 Problem 12

In this simulation we will study single soliton solution. Using the initial condition

$$U(x,0) = -1 + 2\nu^2\{1 + \sqrt{(1-\nu^2)}\cosh P(x - x_0)\}^{-1}. \qquad (6.32)$$

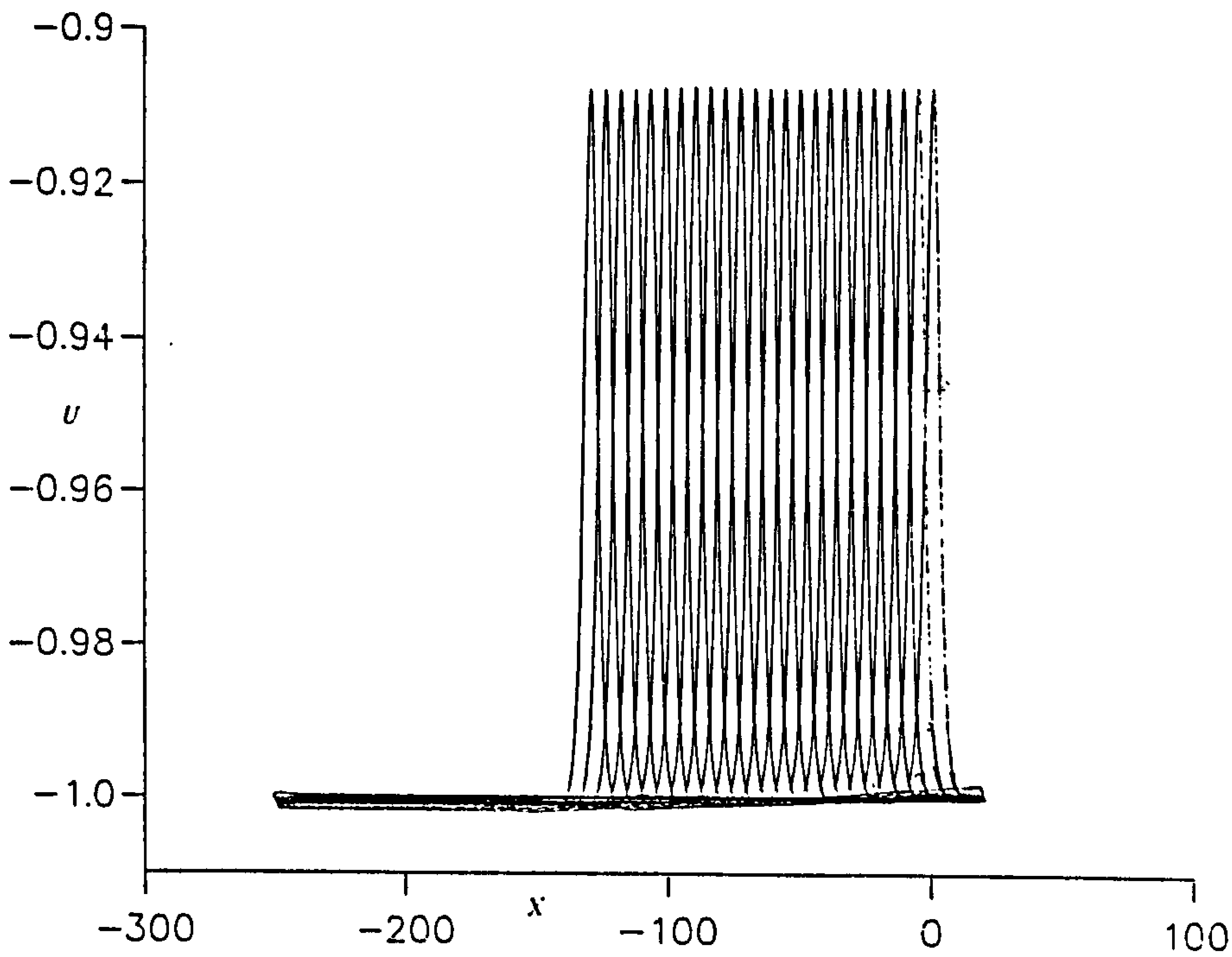

Figure 6.56: Single soliton initial condition (6.31). $q = 1.01$.

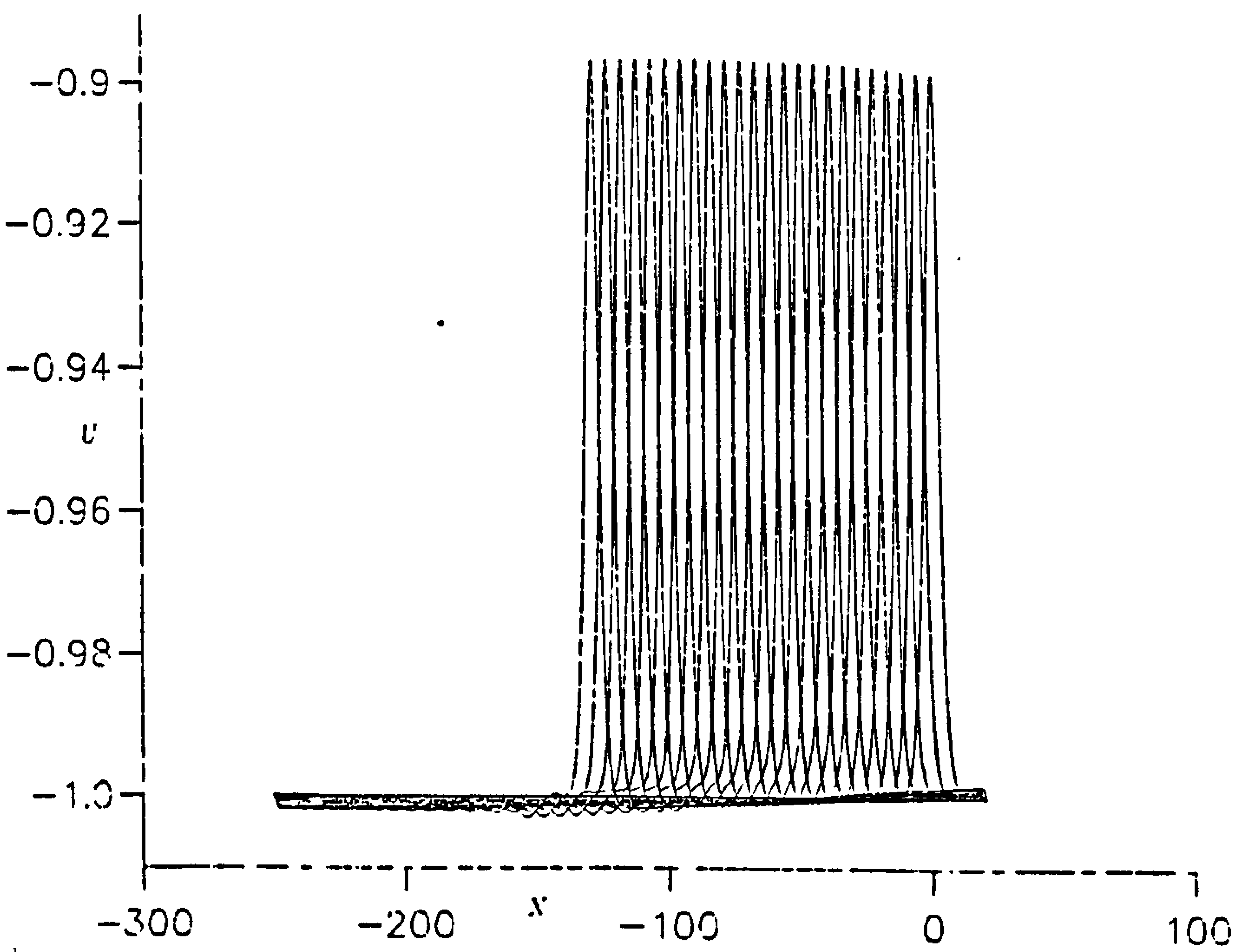

Figure 6.57: Single soliton initial condition (6.31). $q = 1.1$.

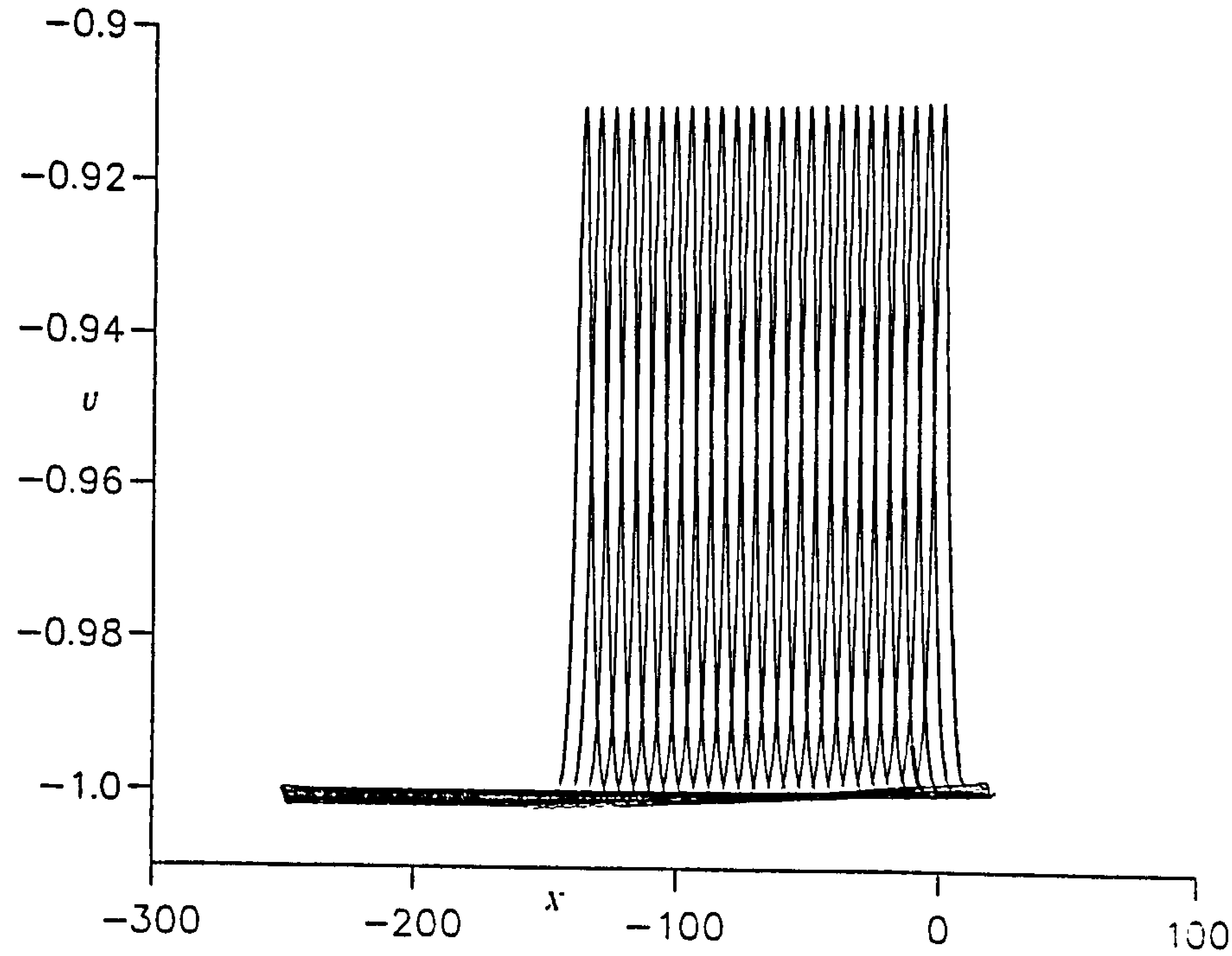

Figure 6.58: Single soliton initial condition (6.31). $q = .99$.

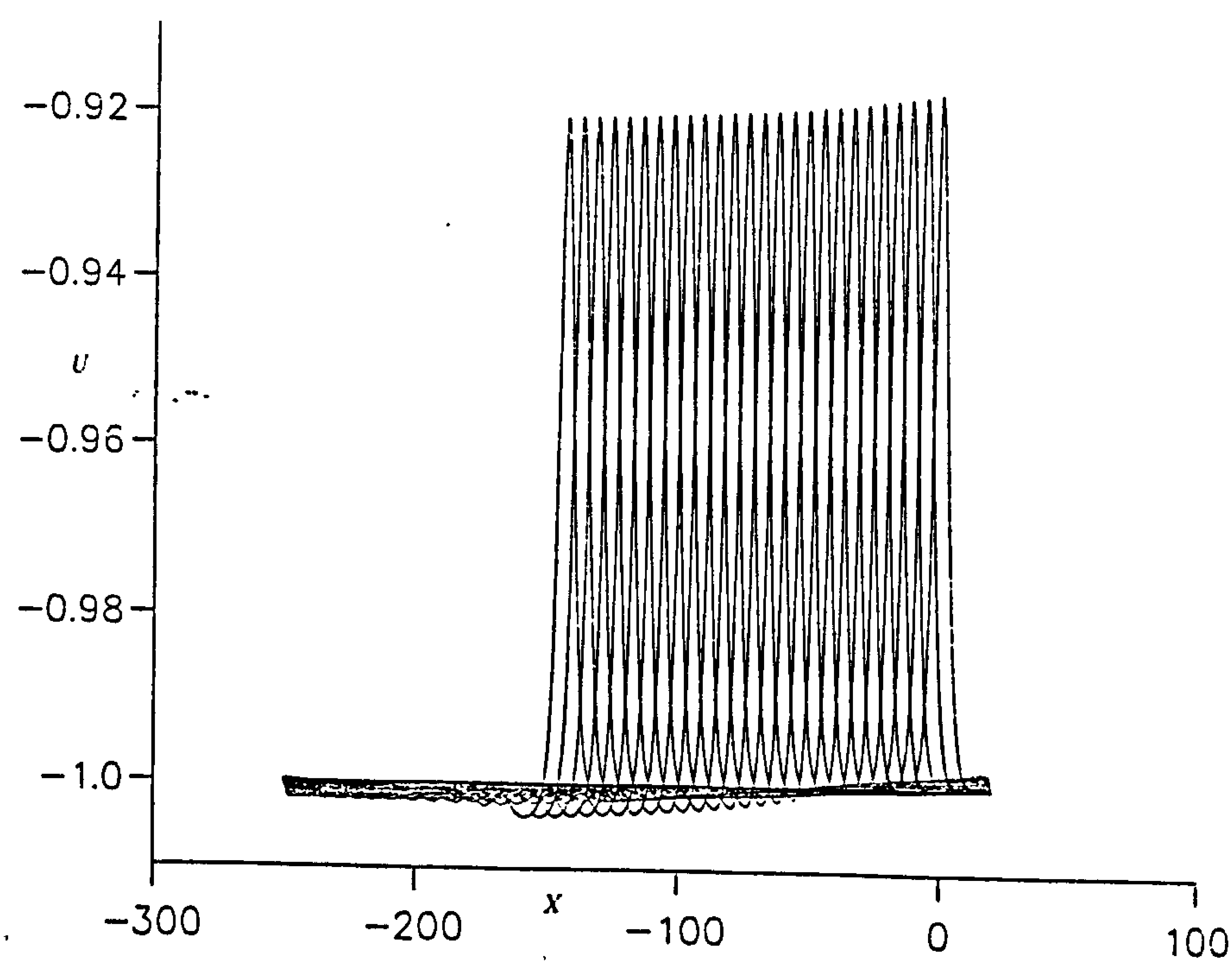

Figure 6.59: Single soliton initial condition (6.31). $q = 0.9$.

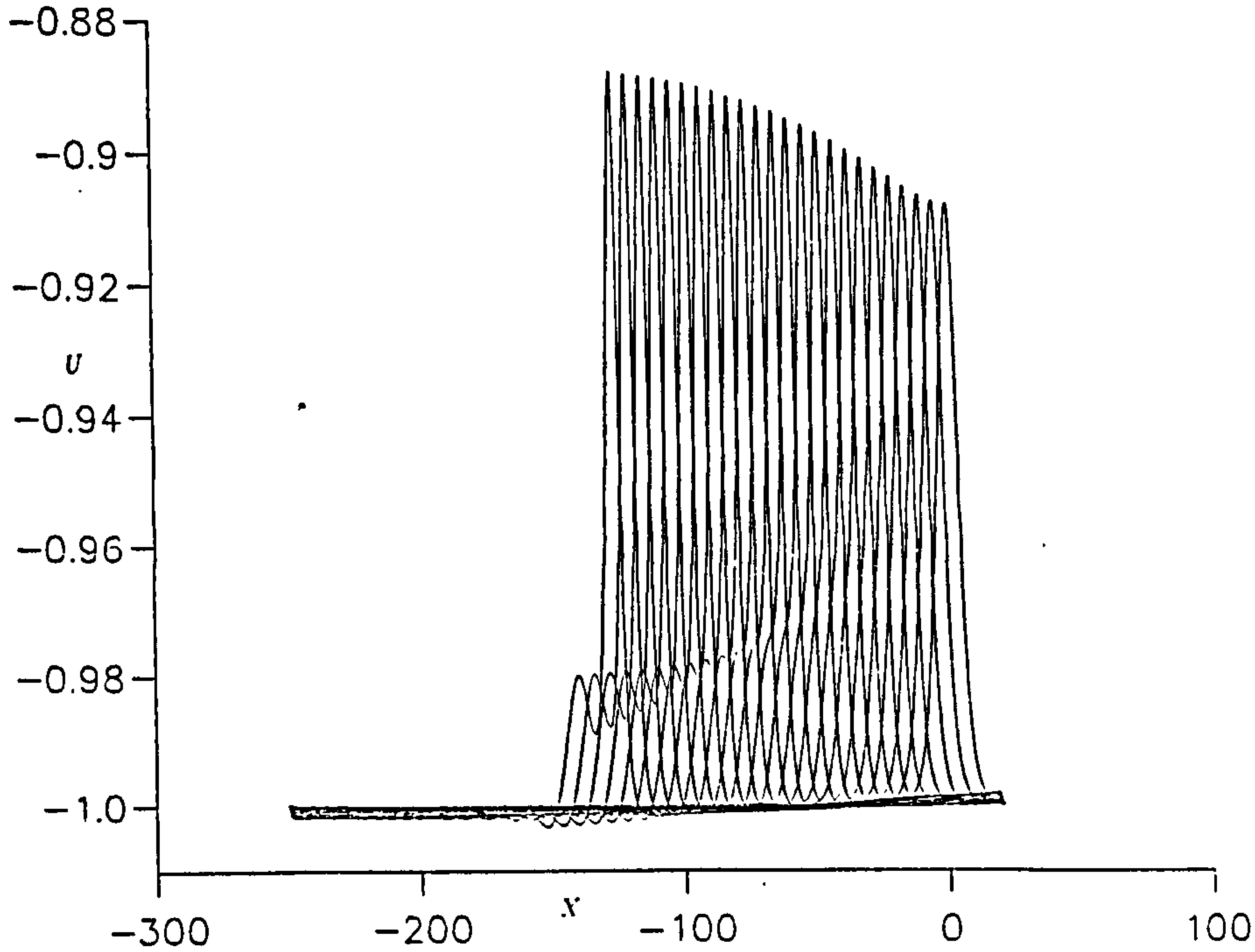

Figure 6.60: Single soliton initial condition (6.32). $P = 0.4$.

In this series of experiments, when we set $P = 0.6$ then gives single soliton. We will study $P = 0.4, 0.8, 0.58, 0.62$ and we take a region $-250 \leq x \leq 20, h = 0.2, \Delta t = 0.005, \nu = 0.3$ and run the simulation up to time $t = 15$. Four different simulations are shown in figures (6.60-6.63).

First $P = 0.4$ and run up to time $t = 15$. We can see in figure (6.60) the amplitude of the initial pulse increase in height. By time $t = 15$ the amplitude is 0.096.

Second $P = 0.8$ and run up to time $t = 15$. We can see in figure (6.61) the amplitude of the initial pulse increase in height. By time $t = 15$ the amplitude is 0.0922 and at the same time a wave train has been created in front of the pulse.

Third $P = 0.58$ and run up to time $t = 15$. We can see in figure (6.62) the amplitude of the initial pulse increases in height. By time $t = 15$ the amplitude is 0.1118.

Last we use $P = 0.62$ and run up to time $t = 15$. We can see in figure (6.63) the amplitude of the initial pulse decrease in height. By time $t = 15$ the amplitude is 0.0911.

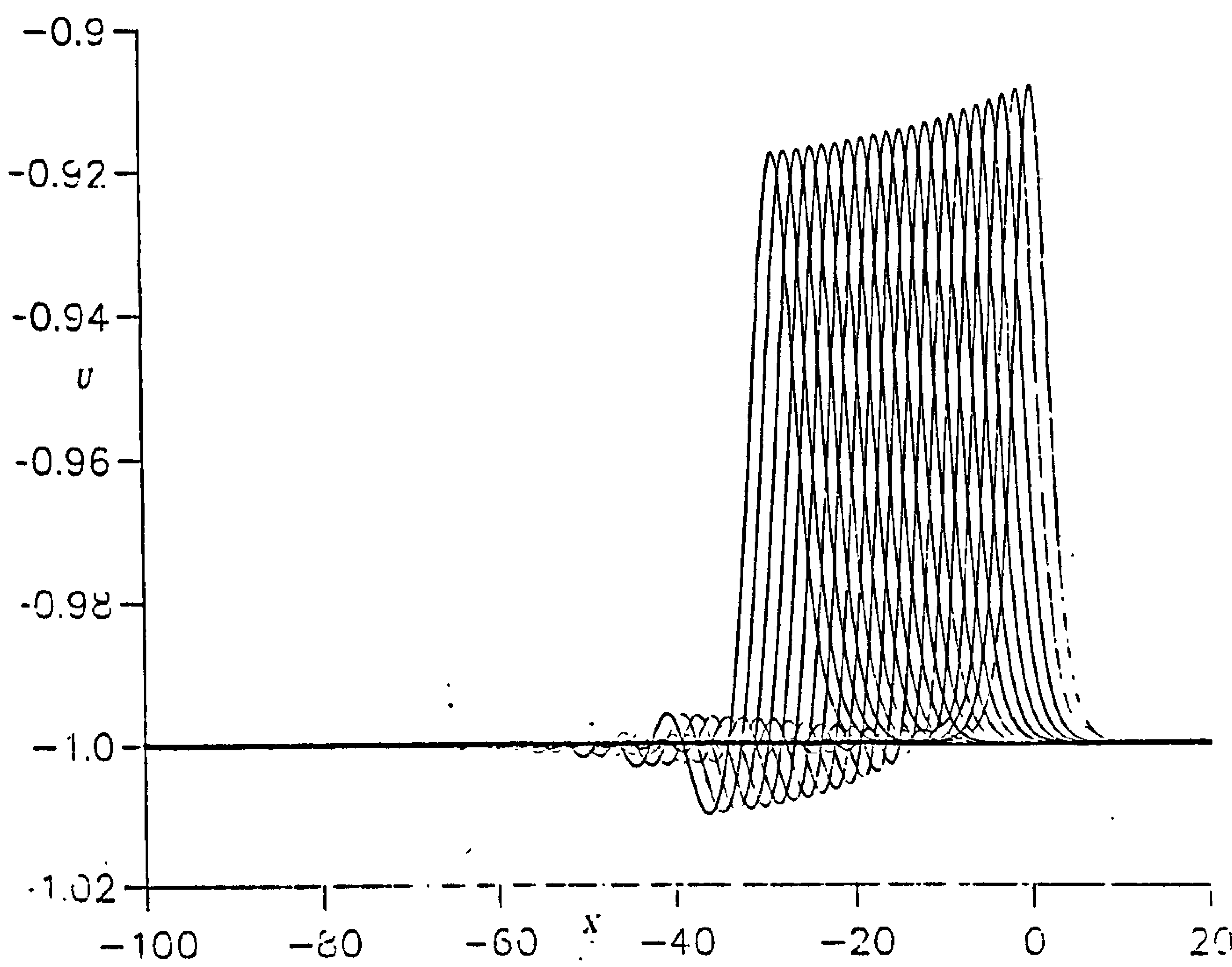

Figure 6.61: Single soliton initial condition (6.32). $P = 0.8$.

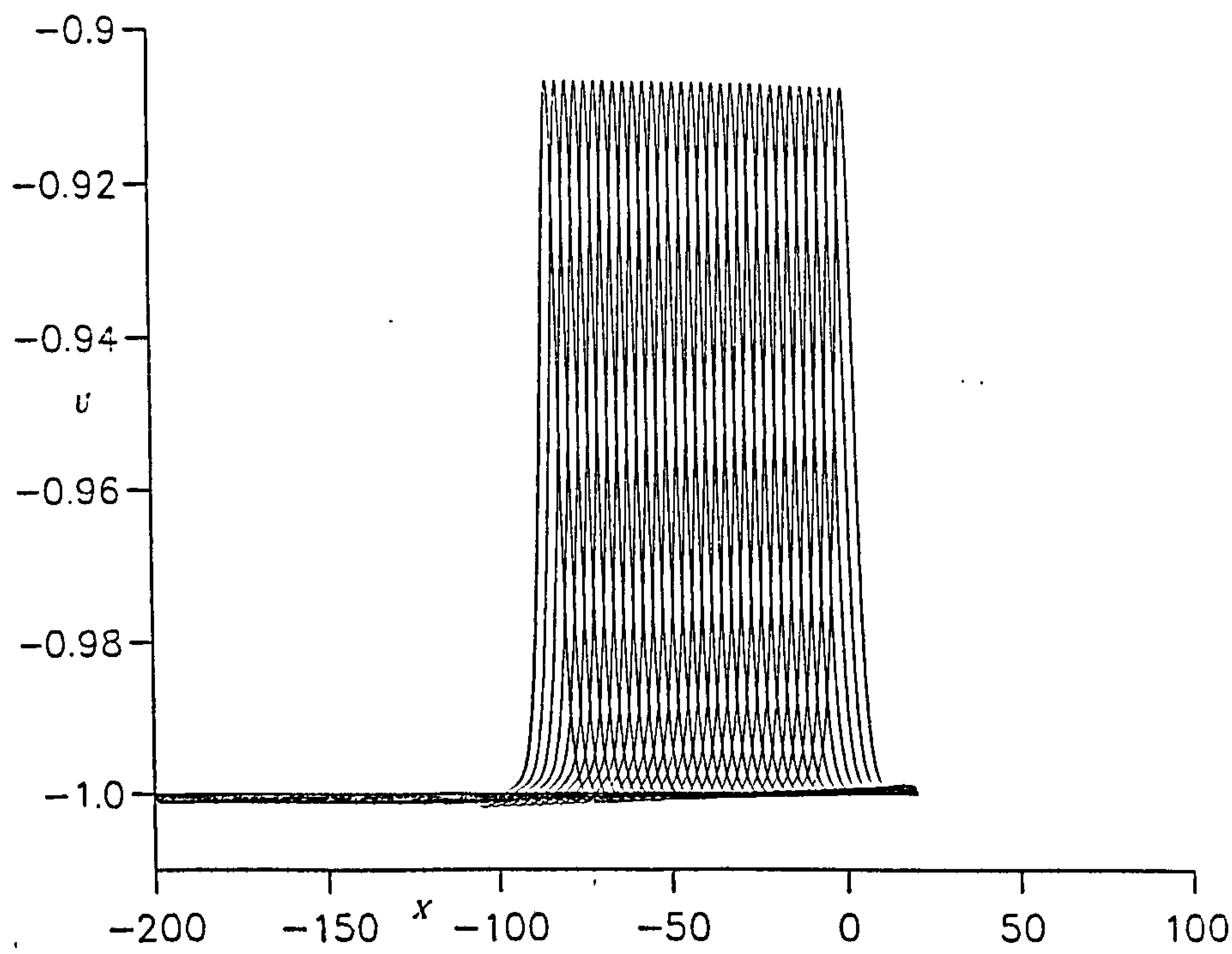

Figure 6.62: Single soliton initial condition (6.32). $P = 0.58$.

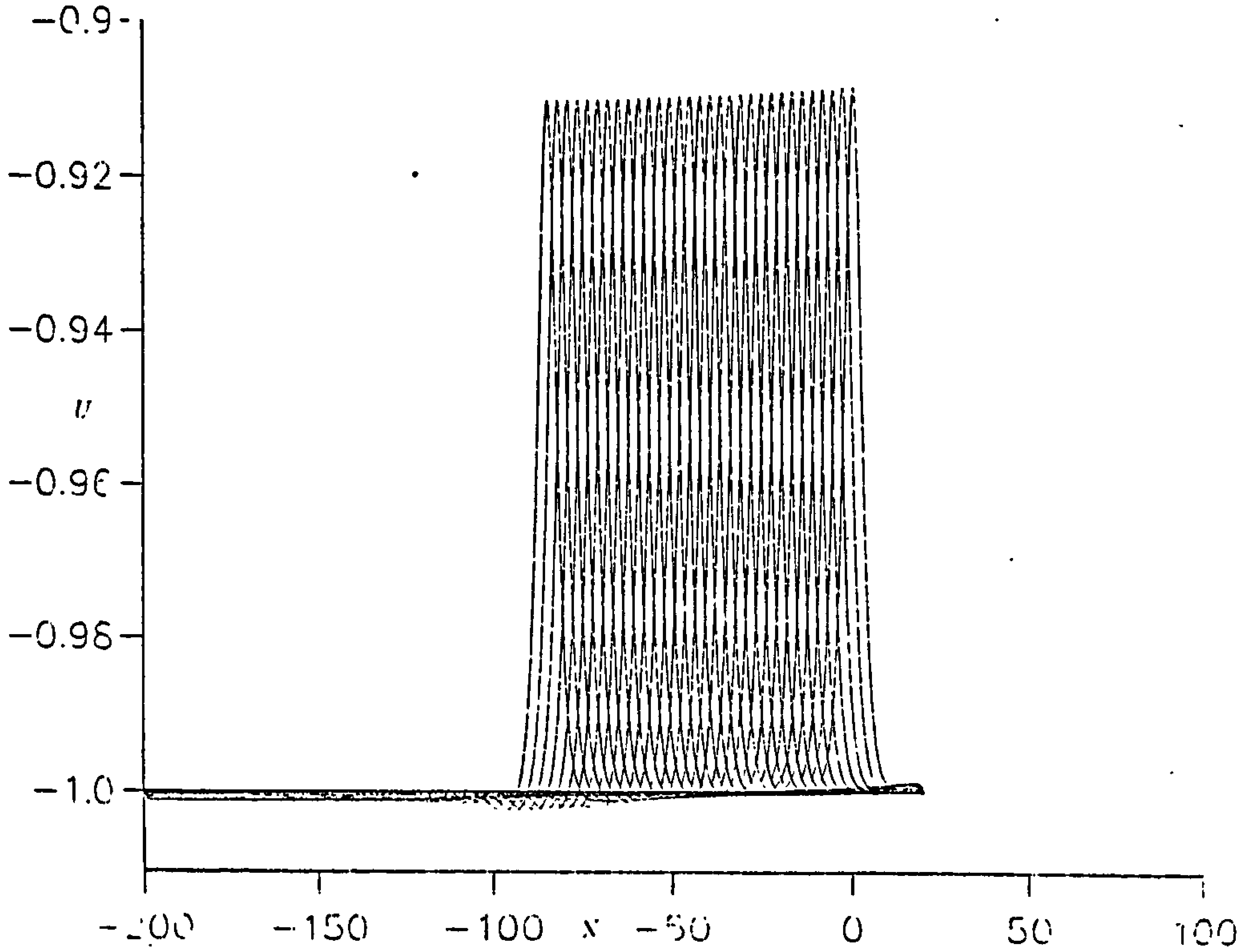

Figure 6.63: Single soliton initial condition (6.32). $P = 0.62$.

6.3 Discussion

In Section 6.2 it is first shown that the proposed numerical algorithm obtained using a "lumped" Galerkin method with quadratic B-spline finite elements provides an adequate representation of a single $MKdV^-$ soliton (problem 1), of soliton interaction (problem 2) and of kink travelling waves and their interactions (problems 3-5).

The decay of a symmetric tanh initial condition into a kink travelling wave plus a number of solitons is then examined and results in good agreement with theory obtained, as shown in Table (6.7).

The decay of a non-symmetric tanh initial condition, with C=0.25, is also studied and observations compared with theory and other numerical experiment [16]; data is collected together in Table(6.23). In run (a) $U_{+\infty} = 1.2, U_{-\infty} = -0.8$, run (b) $U_{+\infty} = 0.8, U_{-\infty} = -1.2$ and, for completeness, run (c) $U_{+\infty} = 1.0, U_{-\infty} = -1.0$. In all cases there is good agreement between theory and the experimental results.

Finally, the decay of a quasi-soliton constructed from 2 tanh initial con-

Table 6.23: Solitary Wave amplitudes and velocities k=kink, sw=solitary wave, wtf=wave train front

	eigenvalue	amplitudes			velocities			
run	computed [16]	computed [16]	observd	observd [16]	computed [16]	observd	observd	
a	0.000	2.4000	2.390	2.395	-2.880	-2.92	-2.86	k
	0.4064	1.1250	1.121	1.118	-4.506	-4.50	-4.49	sw1
	0.6300	0.8125	0.807	0.803	-5.400	-5.45	-5.41	sw2
	0.64	0.8	0.755	0.751	-5.44	-5.62	-5.53	wtf
b	0.0000	1.6000	1.599	1.596	-1.280	-1.30	-1.32	k
	0.4064	0.3250	0.325	0.326	-2.906	-2.91	-2.90	sw1
	0.6300	0.0125	0.026	0.020	-3.800	-3.83	-3.88	sw2
c	0.0000	2.0000	1.999	1.992	-2.000	-2.01	-2.08	k
	0.4375	0.6771	0.677	0.677	-3.750	-3.75	-3.80	sw1
	0.7500	0.2686	0.267	0.267	-4.998	-5.02	-4.50	sw2
	0.9375	0.0636	0.065	0.065	-5.750	-5.76	-5.76	sw3

ditions is examined. It is found that when the tanh functions are initially well separated, $\Delta = 10$, each tanh acts independently, spontaneously transforming into a pair of true kink travelling waves by emitting the appropriate number of pulse soliton pairs in the manner described under problem 6. When the tanh functions are placed closer together, $\Delta = 1$, they form a quasi-soliton pulse which on decay transforms itself into a true soliton as it emits a number of smaller solitons consistent with the process by which a tanh initial condition transforms itself into a true kink travelling wave; see problem 6. When placed even closer, $\Delta = 0.2$, the initial pulse decays into what appears a soliton plus a wave train, a behaviour inconsistent with a symmetric tanh condition and reminiscent of that sometimes obtained with a non-symmetric tanh [16].

Chapter 7

The Boundary Forced MKdV Equation

7.1 Introduction

An unconditionally stable numerical algorithm for the modified Korteweg-de Vries equation based on the B-spline finite element method is described. The algorithm is validated through a single soliton simulation. In further numerical experiments forced boundary conditions $U = U_0$ are applied at the end $x = 0$ and the generated states of solitary waves are studied. By long impulse experiments these are shown to be generated periodically with period (ΔT_B) proportional to U_0^{-3} and to have a limiting amplitude proportional to U_0. This limit is achieved by all waves, after the first, provided the experiment proceeds long enough. The temporal development of the derivatives $U'(0,t), U''(0,t)$ and $U'''(0,t)$ is also periodic, with period $\Delta\ T_B$. This behaviour is similar to that observed for the KdV equation reported in earlier work [15, 11]. The effect of negative forcing is to generate a train of negative waves. The solitary waves states generated by applying a positive impulse followed immediately by an equal negative impulse is dependent on the period of forcing. The solitary functions possesses many of the attributes of free solitons.

The modified Korteweg-de Vries ($MKdV$) equation plays a significant rôle in the study of non-linear dispersive waves. It has been found to describe a wide class of physical phenomena such as acoustic waves in unharmonic lattices [88] and Alfén waves in collisionless plasmas [41].

Analytical studies of the $MKdV$ equation have been given by several authors [88] - [20]. When the normalised $MKdV$ equation

$$U_t + \epsilon U^2 U_x + \mu U_{xxx} = 0, \tag{7.1}$$

where the subscripts t and x denote differentiation and ϵ and μ are positive constants, is solved analytically in an unbounded region with the physical boundary conditions $U \rightarrow 0$ as $x \rightarrow \pm\infty$ it has a solution of the form [88]

$$U(x,t) = kp\text{sech}(kx - kx_0 - k^3\mu t) \tag{7.2}$$

where

$$p = \sqrt{(6\mu/\epsilon)}, \tag{7.3}$$

which represents a single soliton originally sited at x_0 moving to the right with velocity $k^2\mu$. Such solitons may have positive or negative amplitudes depending on the sign of k but all have positive velocities. It is expected that this analytic solution will also be valid for bounded regions which are sufficiently large.

The exact two soliton solution, under the conditions given above, is [75]

$$U(x,t) = ip(\log[f^*/f])_x, \tag{7.4}$$

where $*$ denotes the complex conjugate and

$$\begin{gathered} f = 1 + i\exp(\eta_1) + i\exp(\eta_2) - \beta\exp(\eta_1 + \eta_2), \\ \eta_i = k_i x - k_i{}^3\mu t + \eta_i{}^0, \\ \beta = [\tfrac{k_1 - k_2}{k_1 + k_2}]^2. \end{gathered} \tag{7.5}$$

This represents two solitons of amplitudes $k_i p$ and velocities $k_i{}^2\mu$. When the soliton with the larger amplitude is originally sited on the left a collision eventually occurs during which each wave undergoes a phase shift of magnitude Δ/k_i where $\Delta = log(1/\beta)$; that of the larger being positive and that of the smaller negative. Solitons of the $MKdV$ equation subjected to the above boundary conditions obey an infinity of conservation laws of which the lowest 4 invariants are [20]

$$\begin{aligned} I_1 &= \textstyle\int_{-\infty}^{\infty} U dx, \\ I_2 &= \textstyle\int_{-\infty}^{\infty} U^2 dx, \\ I_3 &= \textstyle\int_{-\infty}^{\infty} (U^4 - 6\frac{\mu}{\epsilon} U_x^2) dx, \\ I_4 &= \textstyle\int_{-\infty}^{\infty} (U^6 - 30\frac{\mu}{\epsilon} U^2 U_x^2 + 18\frac{\mu^2}{\epsilon^2} U_{xx}^2) dx. \end{aligned} \tag{7.6}$$

Studies of boundary forcing applied to the KdV and Regularized Long-Wave (RLW) equations have been given [15] - [13]. Here the effects of boundary forcing on solutions of the $MKdV$ equation are studied through computer simulation. Numerical solutions using pseudospectral methods, split-step Fourier methods and B-spline finite element methods have been given [20] - [23]. We have previously used the B-spline finite element method in the study of solitons and solitary waves of the KdV and other non-linear wave equation [23] - [26]. In this work we set up a collocation method using B-splines [26], [57] over finite elements which is both fast and accurate in performance. In validation runs we use the homogeneous boundary conditions described above, and forced boundary conditions are applied in section 4 [15], [11] at one end of a finite region and the resulting states examined.

7.1.1 The finite element solution

A numerical solution for the $MKdV$ equation in the normalised form (7.1) over the region $0 \le x \le L$, is developed.

Set up $0 = x_0 < x_1 ... < x_N = L$ as a partition of $[0, L]$ by the points x_j into finite elements of equal size $h = (x_{m+1} - x_m)$, and let $\phi_j(x)$ be those quartic B-splines with knots at the points $x = x_j$. Then the set of splines $\{\phi_{-2}, \phi_{-1}, ..., \phi_N, \phi_{N+1}\}$ forms a basis for functions defined over $[0, L]$. We seek the approximation $U_N(x,t)$ to the solution $U(x,t)$ which uses these splines as trial functions [57], i.e.

$$\begin{aligned} U_N(x,t) &= \phi_{-2}(x)\delta_{-2}(t) + \phi_{-1}(x)\delta_{-1}(t) + \ldots + \phi_{N+1}(x)\delta_{N+1}(t) \\ U_N(x,t) &= \textstyle\sum_{j=-2}^{N+1} \phi_j(x)\delta_j(t). \end{aligned} \tag{7.7}$$

where the δ_j are unknown time dependent parameters to be determined. Each quartic B-spline covers 5 elements thus each element $[x_m, x_{m+1}]$ is covered by 5 splines. Using a local coordinate system ξ given by $h\xi = x - x_m$, where $0 \leq \xi \leq 1$, expression for the element splines are [57]

$$\begin{aligned} \phi_{m-2} &= 1 - 4\xi + 6\xi^2 - 4\xi^3 + \xi^4 \\ \phi_{m-1} &= 11 - 12\xi - 6\xi^2 + 12\xi^3 - \xi^4 \\ \phi_m &= 11 + 12\xi - 6\xi^2 - 12\xi^3 + 6\xi^4 \\ \phi_{m+1} &= 1 + 4\xi + 6\xi^2 + 4\xi^3 - 4\xi^4 \\ \phi_{m+2} &= \xi^4 \end{aligned} \tag{7.8}$$

The quartic B-spline $\phi_i(x)$ and its three principle derivatives vanish outside the interval $[x_{i-3}, x_{i+2}]$. In Table 7.1 the values of $\phi_i(x)$ and its principle derivatives at the relevant knots are listed for convenience:

Over the element $[x_m, x_{m+1}]$ the variation of the function $U(x,t)$ is given by

$$\begin{aligned} U(x,t) = \phi^e.d^e &= (\phi_{m-2}, \phi_{m-1}, \phi_m, \phi_{m+1}, \phi_{m+2}). \\ &(\delta_{m-2}, \delta_{m-1}, \delta_m, \delta_{m+1}, \delta_{m+2})^T \end{aligned} \tag{7.9}$$

At the knot x_j the numerical solution $U_N(x,t)$ is given by

Table 7.1:

x	x_{i-3}	x_{i-2}	x_{i-1}	x_i	x_{i+1}	x_{i+2}
$\phi_i(x)$	0	1	11	11	1	0
$\phi_i'(x)$	0	$\frac{-4}{h}$	$\frac{-12}{h}$	$\frac{12}{h}$	$\frac{4}{h}$	0
$\phi_i''(x)$	0	$\frac{12}{h^2}$	$\frac{-12}{h^2}$	$\frac{-12}{h^2}$	$\frac{12}{h^2}$	0
$\phi_i'''(x)$	0	$\frac{-24}{h^3}$	$\frac{72}{h^3}$	$\frac{-72}{h^3}$	$\frac{24}{h^3}$	0

$$\begin{aligned} U_i &= \delta_{i+1} + 11\delta_i + 11\delta_{i-1} + \delta_{i-2} \\ hU'_i &= 4(\delta_{i+1} + 3\delta_i - 3\delta_{i-1} - \delta_{i-2}) \\ h^2U''_i &= 12(\delta_{i+1} - \delta_i - \delta_{i-1} + \delta_{i-2}) \\ h^3U'''_i &= 24(\delta_{i+1} - 3\delta_i + 3\delta_{i-1} - \delta_{i-2}) \end{aligned} \tag{7.10}$$

Where the dashes denote differentation with respect to x. We identify the collocation points with the knots, use Equations (7.10) to evaluate U_i and its space derivatives and substitute into (7.1) to obtain a set of coupled ordinary differential equations, one for each knot. The collocation conditions are given by

$$U_{Nt}(x_j,t) + \epsilon U_N(x_j,t)^2 U_{Nx}(x_j,t) + \mu U_{Nxxx}(x_j,t) = 0, \quad j = 0,1,2,\ldots,N$$

and on substituting from (7.10) we obtain.

$$\begin{aligned} &\dot{\delta}_{i-2} + 11\dot{\delta}_{i-1} + 11\dot{\delta}_i + \dot{\delta}_{i+1} - \\ &\tfrac{4\epsilon}{h}(\delta_{i-2} + 11\delta_{i-1} + 11\delta_i + \delta_{i+1})^2.(\delta_{i-2} + 3\delta_{i-1} - 3\delta_i - \delta_{i+1}) \\ &-\tfrac{24\mu}{h^3}(\delta_{i-2} - 3\delta_{i-1} + 3\delta_i - \delta_{i+1}) = 0 \end{aligned} \tag{7.11}$$

Suppose that δ_i is linearly interpolated between two time levels n and $n+1$ by:

$$\delta_i = (1-\theta)\delta_i^n + \theta\delta_i^{n+1} \tag{7.12}$$

where $0 \le \theta \le 1$ and δ_i^n are the parameters at the time $n \Delta t$. The time derivative is discretised using the standard finite difference formula

$$\frac{d\delta_i}{dt} = \frac{1}{\Delta t}(\delta_i^{n+1} - \delta_i^n). \tag{7.13}$$

Giving the parameter θ the values 0 , $\frac{1}{2}$, 1 produces explicit, Crank-Nicolson and backward difference scheme respectively. Now assume $\theta = \frac{1}{2}$ in which case equation (7.11) becomes

$$\begin{aligned}
&[(\delta_{i-2}^{n+1} - \delta_{i-2}^n) + 11(\delta_{i-1}^{n+1} - \delta_{i-1}^n) + 11(\delta_i^{n+1} - \delta_i^n) + (\delta_{i+1}^{n+1} - \delta_{i+1}^n)] - \\
&\tfrac{4\epsilon\Delta t}{2h}(\delta_{i-2} + 11\delta_{i-1} + 11\delta_i + \delta_{i+1})^2[(\delta_{i-2}^n + \delta_{i-2}^{n+1}) + 3(\delta_{i-1}^n + \delta_{i-1}^{n+1}) - \\
&3(\delta_i^n + \delta_i^{n+1}) - (\delta_{i+1}^n + \delta_{i+1}^{n+1})] - \tfrac{24\mu\Delta t}{2h^3}[(\delta_{i-2}^n + \delta_{i-2}^{n+1}) - 3(\delta_{i-1}^n + \delta_{i-1}^{n+1}) \\
&+3(\delta_i^n + \delta_i^{n+1}) - (\delta_{i+1}^n + \delta_{i+1}^{n+1})] = 0 \\
&i = 0, 1, \ldots, N
\end{aligned} \tag{7.14}$$

Hence with a Crank-Nicolson approximation in time, we have for each knot an equation relating parameters at adjacent time levels, δ_i^{n+1} to δ_i^n

$$\begin{aligned}
&\alpha_{i1}\delta_{i-2}^{n+1} + \alpha_{i2}\delta_{i-1}^{n+1} + \alpha_{i3}\delta_i^{n+1} + \alpha_{i4}\delta_{i+1}^{n+1} \\
&= \alpha_{i4}\delta_{i-2}^n + \alpha_{i3}\delta_{i-1}^n + \alpha_{i2}\delta_i^n + \alpha_{i1}\delta_{i+1}^n
\end{aligned} \tag{7.15}$$

where

$$\begin{aligned}
\alpha_{i1} &= 1 - Z_i - M \\
\alpha_{i2} &= 11 - 3Z_i + 3M \\
\alpha_{i3} &= 11 + 3Z_i - 3M \\
\alpha_{i4} &= 1 + Z_i + M \\
Z_i &= \tfrac{2\epsilon}{h}\Delta t(\delta_{i-2} + 11\delta_{i-1} + 11\delta_i + \delta_{i+1})^2, \\
M &= \tfrac{12\mu}{h^3}\Delta t. \\
i &= 0, 1, 2, \ldots, N-1, N
\end{aligned} \tag{7.16}$$

The system (7.15) consists of N + 1 linear equation in N + 4 unknowns $d = (\delta_{-2}, \delta_{-1}, \delta_0, ..., \delta_N, \delta_{N+1})^T$. To obtain a unique solution to this system the 3 additional constraints needed are obtained from the boundary conditions:

$$
\begin{array}{lll}
U_0 & \delta_{-2} + 11\delta_{-1} + 11\delta_0 + \delta_1 = U_o, & \\
U_N = 0 & \delta_{N-2} + 11\delta_{N-1} + 11\delta_N + \delta_{N+1} = 0, & (7.17) \\
U'_N = 0 & \delta_{N-2} + 3\delta_{N-1} - 3\delta_N - \delta_{N+1} = 0, &
\end{array}
$$

These conditions enable us to eliminate $\delta_{-2}, \delta_N, \delta_{N+1}$ from equation (7.15) which then consists of $N+1$ linear equations in $N+1$ unknowns $d = (\delta_{-1}, \delta_0, ..., \delta_{N-2}, \delta_{N-1})^T$.

By solving the first one equation of (7.17) simultaneously for δ_{-2}, we obtain

$$\delta_{-2} = U_0 - 11\delta_{-2} - 11\delta_0 - \delta_1. \tag{7.18}$$

Similarly, solve the last two equations of (7.17) simultaneously for δ_N, δ_{N+1} , to get

$$
\begin{aligned}
\delta_N &= -\tfrac{1}{4}\delta_{N-2} - \tfrac{7}{4}\delta_{N-1} \\
\delta_{N+1} &= \tfrac{7}{4}\delta_{N-2} + \tfrac{33}{4}\delta_{N-1}.
\end{aligned} \tag{7.19}
$$

Eliminating δ_{-2} from the first equation of the system (7.15) using equation (7.18) to obtain

$$S_1\delta_{-1}^{n+1} + S_2\delta_0^{n+1} + S_3\delta_1^{n+1} = S_4\delta_{-1}^n + S_5\delta_0^n + S_6\delta_1^n + \beta_1, \tag{7.20}$$

where

$$
\begin{aligned}
S_1 &= -2Z_0 + 14M \\
S_2 &= 14Z_0 + 8M \\
S_3 &= 2Z_0 + 2M \\
S_4 &= -8Z_0 - 14M \\
S_5 &= -14Z_0 - 8M \\
S_6 &= -2Z_0 - 2M \\
\beta_1 &= U_0[2Z_0 + 2M] \\
Z_0 &= \tfrac{2\epsilon}{h}\Delta t(\delta_{-2} + 11\delta_{-1} + 11\delta_0 + \delta_1)^2, \\
M &= \tfrac{12\mu}{h^3}\Delta t.
\end{aligned}
\tag{7.21}
$$

Similarly, eliminating δ_N and δ_{N+1} from the last two equations of (7.15) and using equations (7.19) to obtain

$$
\begin{aligned}
&\alpha_{(N-1)1}\delta_{N-3}^{n+1} + Y_1\delta_{N-2}^{n+1} + Y_2\delta_{N-1}^{n+1} \\
&= \alpha_{(N-1)4}\delta_{N-3}^{n} + Y_3\delta_{N-2}^{n} + Y_4\delta_{N-1}^{n},
\end{aligned}
\tag{7.22}
$$

where

$$
\begin{aligned}
\alpha_{(N-1)1} &= 1 - Z_{N-1} - M \\
\alpha_{(N-1)4} &= 1 + Z_{N-1} + M \\
Y_1 &= \tfrac{43}{4} - \tfrac{13}{4}Z_{N-1} + \tfrac{11}{4}M \\
Y_2 &= \tfrac{37}{4} + \tfrac{5}{4}Z_{N-1} - \tfrac{19}{4}M \\
Y_3 &= \tfrac{43}{4} + \tfrac{13}{4}Z_{N-1} - \tfrac{11}{4}M \\
Y_4 &= \tfrac{37}{4} - \tfrac{19}{4}Z_{N-1} + \tfrac{5}{4}M \\
Z_{N-1} &= \tfrac{2\epsilon}{h}\Delta t(\delta_{N-3} + 11\delta_{N-2} + 11\delta_{N-1} + \delta_N)^2 \\
M &= \tfrac{12\mu}{h^3}\Delta t,
\end{aligned}
\tag{7.23}
$$

and

$$
Y_5\delta_{N-2}^{n+1} + Y_6\delta_{N-1}^{n+1} = Y_7\delta_{N-2}^{n} + Y_8\delta_{N-1}^{n}, \tag{7.24}
$$

where

$$
\begin{aligned}
Y_5 &= \tfrac{6}{4}M \\
Y_6 &= \tfrac{66}{4}M \\
Y_7 &= -\tfrac{6}{4}M \\
Y_8 &= \tfrac{66}{4}Z_N \\
Z_N &= \tfrac{2\epsilon}{h}\Delta t(\delta_{N-2} + 11\delta_{N-1} + 11\delta_N + \delta_{N+1})^2 \\
M &= \tfrac{12\mu}{h^3}\Delta t.
\end{aligned}
\tag{7.25}
$$

The time evolution of the approximate solution $U_N(x,t)$ is determined by the time evolution of the vector d^n. This is found by repeatedly solving the recurrence relationship (7.15) once the initial vector d^0 has been computed from the initial conditions. The recurrence relationship is defective pentadiagonal so a direct algorithm for its solution exists; an inner iteration is also needed at each time step to cope with the non-linear term.

7.1.2 Stability Analysis

A Neumann stability analysis is set up in which the growth factor of the error in a typical Fourier mode

$$\delta_j^n = \hat{\delta}^n e^{ijkh}, \tag{7.26}$$

where k is the mode number and h the element size , is determined for the linearised scheme. The linearisation is effected by supposing that U^2 in the non-linear term is locally constant which is equivalent to assuming that in (7.15) all the δ_j^n are equal to a local constant d, so that $Z_j = Z = \frac{2\epsilon\Delta t}{h}(24d)^2$

for all j. Equation (7.15) can now be written

$$\begin{aligned}
&(1-Z-M)\delta_{i-2}^{n+1}+(11-3Z+3M)\delta_{i-1}^{n+1} \\
&+(11+3Z-3M)\delta_{i}^{n+1}+(1+Z+M)\delta_{i+1}^{n+1} \\
&=(1+Z+M)\delta_{i-2}^{n}+(11+3Z-3M)\delta_{i-1}^{n} \qquad (7.27)\\
&+(11-3Z+3M)\delta_{i}^{n}+(1-Z-M)\delta_{i+1}^{n} \\
&i=0,1,...,N
\end{aligned}$$

Substituting the Fourier mode (7.26) into (7.27) leads to

$$g=\frac{a-ib}{a+ib} \qquad (7.28)$$

where

$$\begin{aligned}
a &= 2\cos\tfrac{3}{2}kh+22\cos\tfrac{1}{2}kh \\
b &= 2(Z+M)\sin\tfrac{3}{2}kh+6(Z-M)\sin\tfrac{1}{2}kh
\end{aligned} \qquad (7.29)$$

The modulus of g is therefore 1 and the linearised scheme is unconditionally stable.

7.1.3 Validation Experiment

To test the behaviour of the proposed algorithm a single soliton simulation is used. Take as initial condition equation (7.2) with $\epsilon=3,\mu=1$ and $kp=1.3,x_o=15,t=0$. At time $t=0$ the global trial function (7.7) becomes

$$U_N(x,0)=\sum_{j=-2}^{N+1}\delta_j{}^0\phi_j(x). \qquad (7.30)$$

To determine the $N+4$ unknowns $\delta_j{}^0$ for the validation experiment we require $U_N(x,0)$ to satisfy the following conditions;

a-) it shall agree with the initial condition $U(x,0)$ at the knots $x_0,...,x_N$; leading to $N+1$ conditions.

b-) its first two derivatives shall agree with those of the exact condition at x_0, i.e. $U'(x_0)=0$ and $U''(x_N)=0$ giving a further two conditions, c-) its first derivative shall agree with that of the exact condition at x_N i.e. $U'(x_N) = 0$ a further condition.

These conditions (a-), (b-) and (c-) can be expresed as:

$$\begin{aligned} &U'_N(x_0, 0) = 0 \\ &U''_N(x_0, 0) = 0 \\ &U_N(x_i, 0) = U(x_i, 0), \quad \text{i} = 0,1,\ldots,\text{N} \\ &U'_N(x_N, 0) = 0 \end{aligned} \tag{7.31}$$

from Table 7.1 the system (7.31) can be reduced to:

$$\begin{aligned} -\delta_{-2} - 3\delta_{-1} + 3\delta_0 + \delta_1 &= 0 \\ \delta_{-2} - \delta_{-1} - \delta_0 + \delta_1 &= 0 \\ \delta_{i-2} + 11\delta_{i-1} + 11\delta_i + \delta_{i+1} &= U(x_i, 0), \quad \text{i} = 0,1,\ldots,\text{N} \\ -\delta_{N-2} - 3\delta_{N-1} + 3\delta_N + \delta_{N+1} &= 0 \end{aligned} \tag{7.32}$$

This leads to the matrix equation

$$Md^0 = b \tag{7.33}$$

where

$$M = \begin{pmatrix} -1 & -3 & 3 & 1 & & & & & \\ 1 & -1 & -1 & 1 & & & & & \\ & 1 & 11 & 11 & 1 & & & & \\ & & 1 & 11 & 11 & 1 & & & \\ & & & \cdot & & & & & \\ & & & & \cdot & & & & \\ & & & & & \cdot & & & \\ & & & & 1 & 11 & 11 & 1 & \\ & & & & & 1 & 11 & 11 & 1 \\ & & & & & -1 & -3 & 3 & 1 \end{pmatrix}$$

and

$$d^0 = (\delta_{-2}, \delta_{-1}, \delta_0, \ldots, \delta_N, \delta_{N+1})^T, \tag{7.34}$$

and if we write $U_j = U(x_j)$

$$b = (0, 0, U_0, U_1, ..., U_{N-1}, U_N, 0)^T. \tag{7.35}$$

We convert this system to penta-diagonal form by the following steps:

1-) Solve the first two equations of the system (7.33) simultaneously for δ_{-2} and δ_{-1} to obtain:

$$\begin{aligned} \delta_{-2} &= \tfrac{3}{2}\delta_0 - \tfrac{1}{2}\delta_1 \\ \delta_{-1} &= \tfrac{1}{2}\delta_0 + \tfrac{1}{2}\delta_1 \end{aligned} \tag{7.36}$$

2-) Similarly by solving the last equation of the system (7.33) simultaneously we get:

$$\delta_{N+1} = \delta_{N-2} + 3\delta_{N-1} - 3\delta_N \tag{7.37}$$

eliminating δ_{N+1} from the N^{th} equation of the system (7.41) gives:

$$2\delta_{N-2} + 14\delta_{N-1} + 8\delta_N = U(x_N, 0) \tag{7.38}$$

hence the system (7.33) is penta-diagonal form. The system is now solved by the penta-diagonal algorithm to obtain the computed solution $(\delta_0.\delta_1, \ldots, \delta_N)^T$, and hence compute $\delta_{-2}, \delta_{-1}, \delta_{N+1}$ from equations (7.36) and (7.37) so the initial vector δ^0 is determined.

In this experiment step sizes of $\Delta t = 0.001$ and $h = 0.04$ over a range $0 \leq x \leq 40$ are used . The soliton is observed to move across the region with constant profile and velocity. The error norms obtained for this validatory simulation, given in Table 7.2, are satisfactorily small both rising to less than $2 \times 10^{-3} kp$ at time $t = 10$, where kp is the amplitude of the soliton. The soliton amplitude changes from its initial value of 1.3 to 1.29972 by the end of run at $t = 10$; that is by only $2 \times 10^{-3}\%$.

The invariants, listed in table 7.3, show good conservation; I_2, I_3 and I_4 remain constant to 5 decimal places throughout the run at $I_2 = 3.67694, I_3 =$

Table 7.2: Single Soliton $h = 0.04, \Delta t = 0.001, 0 \leq x \leq 40$

time	$L_2 \times 10^3$	$L_\infty x 10^3$
1.0	0.391967	0.279687
2.0	0.620266	0.431269
3.0	0.759408	0.516996
4.0	0.893806	0.596393
5.0	1.027865	0.676982
6.0	1.162426	0.758738
7.0	1.300361	0.841460
8.0	1.440726	0.924846
9.0	1.979842	1.245591
10.0	2.526911	1.568440

Table 7.3: Invariants for Single Soliton

time	I_1	I_2	I_3	I_4
0.0	4.442856	3.676945	2.071337	1.050161
1.0	4.442858	3.676946	2.071338	1.050162
2.0	4.442866	3.676947	2.071337	1.050162
3.0	4.442869	3.676946	2.071338	1.050163
4.0	4.442782	3.676947	2.071336	1.050163
5.0	4.442802	3.676944	2.071336	1.050162
6.0	4.442868	3.676945	2.071338	1.050162
7.0	4.442928	3.676947	2.071338	1.050162
8.0	4.442964	3.676945	2.071338	1.050162
9.0	4.442979	3.676945	2.071337	1.050162
10.0	4.442978	3.676944	2.071337	1.050163

Table 7.4: Comparison of Single Soliton, amplitude = 1, simulations with results from [75] Table(7.1).

Method	h Δt	time	L_∞	$(I_2 - I_{20})/I_{20}$	$(I_3 - I_{30})/I_{30}$
B-spline	0.1	0.25	0.0012	-0.00002	-0.00007
	0.025	0.5	0.0018	-0.00004	-0.00014
		1.0	0.0022	-0.00009	-.000030
A-L global	0.1	0.25	0.0019	0.00009	0.00486
	0.25	0.5	0.0028	0.00017	0.00508
		1.0	0.0045	0.00033	0.00556
A-L local	0.06	0.25	0.0023	0.00002	0.00168
	0.12	0.5	0.0032	0.00003	0.00171
		1.0	0.0047	0.00006	0.00177
Implicit(C-N)	0.08	0.25	0.0023	0.00002	0.00297
	0.1	0.5	0.0031	0.00003	0.00298
		1.0	0.0045	0.00005	0.00303
Pseudospectral	0.625	0.25	0.0026	-0.00120	-0.02976
	0.0055	0.5	0.0041	0.00218	0.07897
		1.0	0.0046	-0.00143	-0.03534
Tappert	0.3125	0.25	0.0036	0.00000	-0.00010
	0.0041	0.5	0.0041	0.00000	-0.00013
		1.0	0.0047	0.00000	0.00001

2.07133 and $I_4 = 1.05016$, changing only in the sixth decimal place, while I_1 changes from 4.4428 by only ± 1 in the fourth decimal place.

To make comparisons with published work [75] we use as initial condition equation (7.2) at $t = 0$ with $k = 1.0, x_0 = 15$ and $\epsilon = 6, \mu = 1$ so that $p = 1.0$. Space and time steps are chosen so that $L_\infty < 0.005$ at $t = 1.0$.

The results are compared in Table (7.4) with others reported by Taha and Ablowitz [75] using a variety of explicit and implicit schemes, the local and global schemes proposed by Ablowitz and Ladik and pseudospectral scheme of Fornberg and Whitham.

Relative changes in the values of I_2 and I_3 are compared at time $t = 1$; the values of I_2 and I_3 at time $t = 0$ are denoted by I_{20} and I_{30}. The present method performs well.

7.2 Simulations 1

The generation of solitary waves by boundary forcing the $MKdV$ equation at $x = 0$ for the finite region $0 \leq x \leq x_{max}$ is studied. initially the region is undisturbed so that at time $t = 0$ all δ_j are zero. The forced boundary condition applied at $x = 0$ is

$$U(0,t) = \begin{cases} U_0 \frac{t}{\tau} & 0 \leq t \leq \tau \\ U_0 & \tau < t < t_0 - \tau \\ U_0 \frac{t_0 - t}{\tau} & t_0 - \tau \leq t \leq t_0 \end{cases} \tag{7.39}$$

Further homogeneous boundary conditions are imposed at $x = x_{max}$. The effect of the impulse is to generate solitary waves at $x = 0$, which grow until they achieve a terminal amplitude determined by the magnitude of the forced boundary value. Solitary waves are continually generated while the forced conditions prevail, then all growth slows and eventually ceases.

7.2.1 Positive forcing Series A

In these experiments $\epsilon = 6, \mu = 1$ so that $p = 1$.

Long Impulse

i-) Boundary condition (7.39) is used with $x_{max} = 80, t_{max} = 10, U_0 = 1, \tau = 0.01, t_0 = 10$ so that the forcing lasts throughout the experiment. The step lengths are $h = 0.04$ and $\Delta t = 0.001$. In this numerical experiment, see Figure(7.1), five solitary waves are generated before the simulation is terminated at $t = 10$. Figures (7.2) and (7.3) show that four achieve their terminal heights and a constant velocity. The generating conditions for the first wave are rather more protracted than those for all subsequent waves, as can be seen from the graphs of the first three derivatives at $x = 0$ given in Figures (7.4-7.6), so it achieves a slightly larger amplitude and velocity than do the following waves. The observations are collected in Table (7.5). The time interval between births of solitary waves is constant at $\Delta T_B = 1.82$, the measured terminal heights for solitary waves 2-4 vary between 2.147 and 2.148 with measured velocities of 4.62. Free solitons of similar heights would have velocities $4.610 - 4.614$, so that agreement is close. After an initial transient the graph of $U_x(0,t)$, Figure (7.4), shows a rounded saw tooth periodic behaviour with maximum of about 0.4, minimum of about 0.33, mean zero and period 1.82. The graphs of $U_{xx}(0,t)$ and $U_{xxx}(0,t)$, Figures (7.5-7.6), also exhibit periodic behaviour with period 1.82.

Rewrite equation (7.1) as an expression for U_{xxx} and evaluate at $x = 0$ to give

$$U_{xxx}(0,t) = -\frac{1}{\mu}\{U_t(0,t) + \epsilon U^2(0,t)U_x(0,t)\}. \tag{7.40}$$

With the forcing $U_0 = 1$ and $\mu = 1, \epsilon = 6$ this reduces to

$$U_{xxx}(0,t) = -6U_x(0,t) \tag{7.41}$$

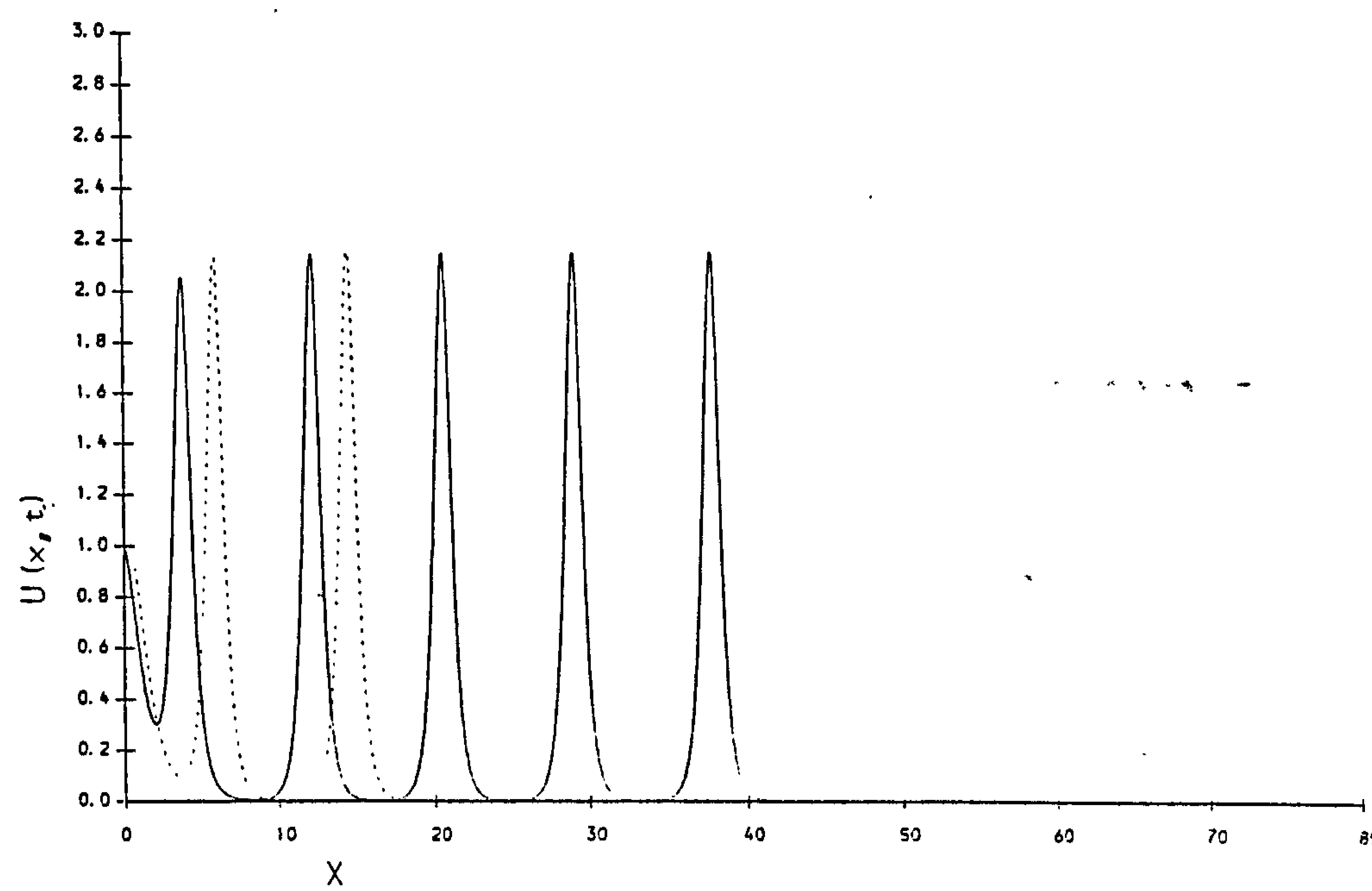

Figure 7.1: Long Impulse. Soliton produced by forced conditions (7.39) with $U_0 = 1, \tau = 0.01, t_0 = \infty, h = 0.01, \Delta t = 0.001$ graphed at $t = 5$ (- - - -) and $t = 10$ (——)

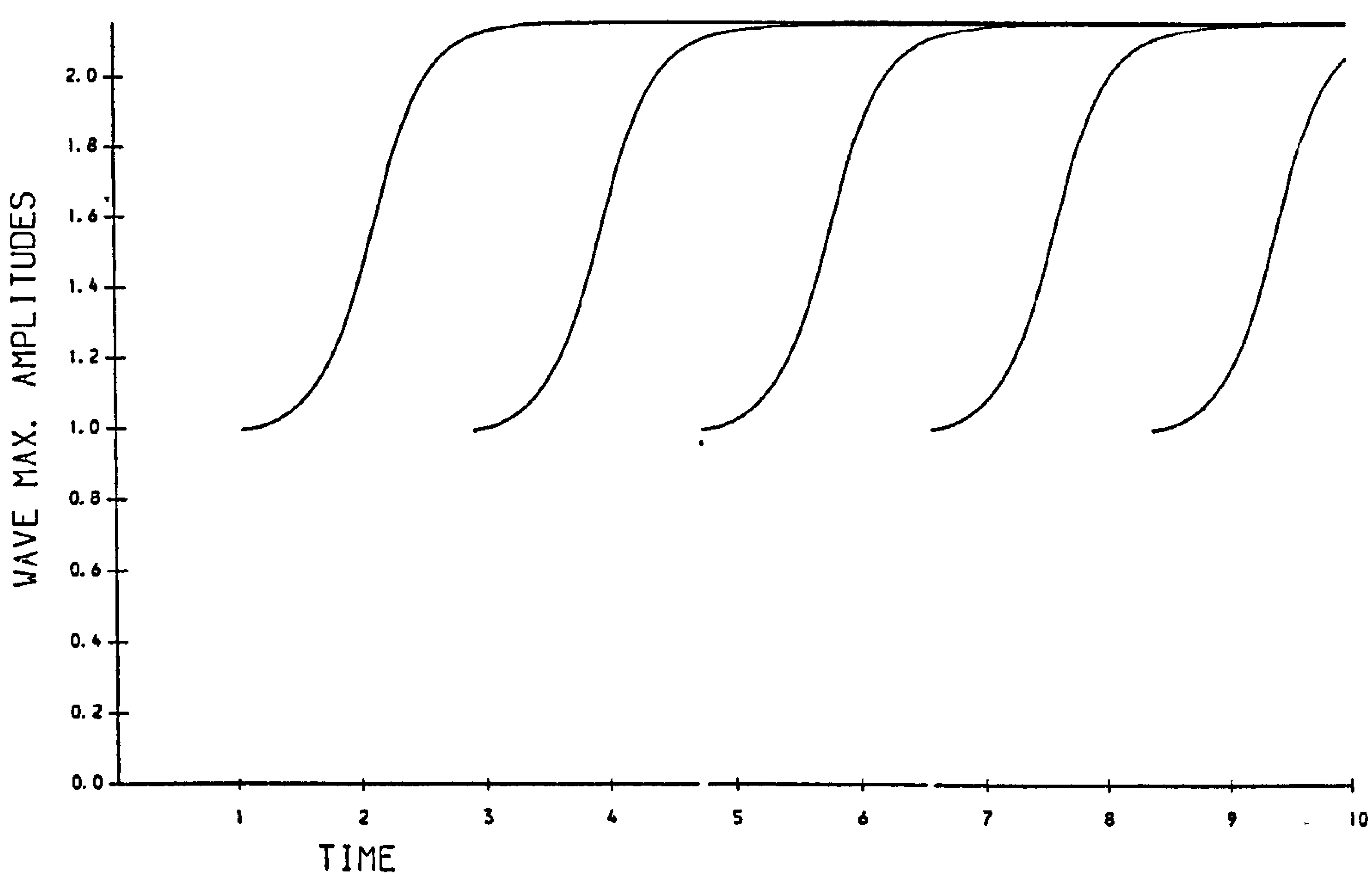

Figure 7.2: Long Impulse. The evolution of the soliton amplitudes. Forced conditions (7.39) with $U_0 = 1, \tau = 0.01, t_0 = \infty, h = 0.04, \Delta t = 0.001$.

Table 7.5: Observations of solitary waves, $U_0 = 1, \epsilon = 6$

wave	birth time	generated waves		free soliton
		amplitude	velocity	velocity
1	1.040	2.155	4.64	4.644
2	2.920	2.148	4.62	4.614
3	4.740	2.147	4.62	4.610
4	6.560	2.147	4.62	4.610
5	8.380	2.058	4.27	4.235

Figure (7.4) and (7.6) show that the simulation produces derivatives which reflect this relationship. By comparing Figures (7.2), (7.4) and (7.5) we observe that the birth of a solitary wave occurs at times when $U_x(0,t) = 0$, and $U_{xx}(0,t)$ is a minimum and negative, while a solitary wave reaches maturity about $1\frac{1}{2}$ periods later when again $U_x(0,t) = 0$, but $U_{xx}(0,t)$ is a maximum and positive.

ii-) An experiment with reduced forcing, $U_0 = 0.5$; boundary condition (7.39) is used with $x_{max} = 80, t_{max} = 80, \tau = 0.01, t_0 = 80$ so that the forcing lasts throughout the experiment. The numerical step lengths are $h = 0.04$ and $\Delta t = 0.001$.

In this numerical experiment, see Figure (7.7) five solitary waves are generated before the simulation is terminated at $t = 80$. Figures (7.8) and (7.9) show that four achieve their terminal heights and a constant velocity.

The generating conditions for the first wave are rather more protracted than those for all subsequent waves, as can be seen from the graphs of the first three derivatives at $x = 0$ given in Figures (7.10-7.12) so it achieves

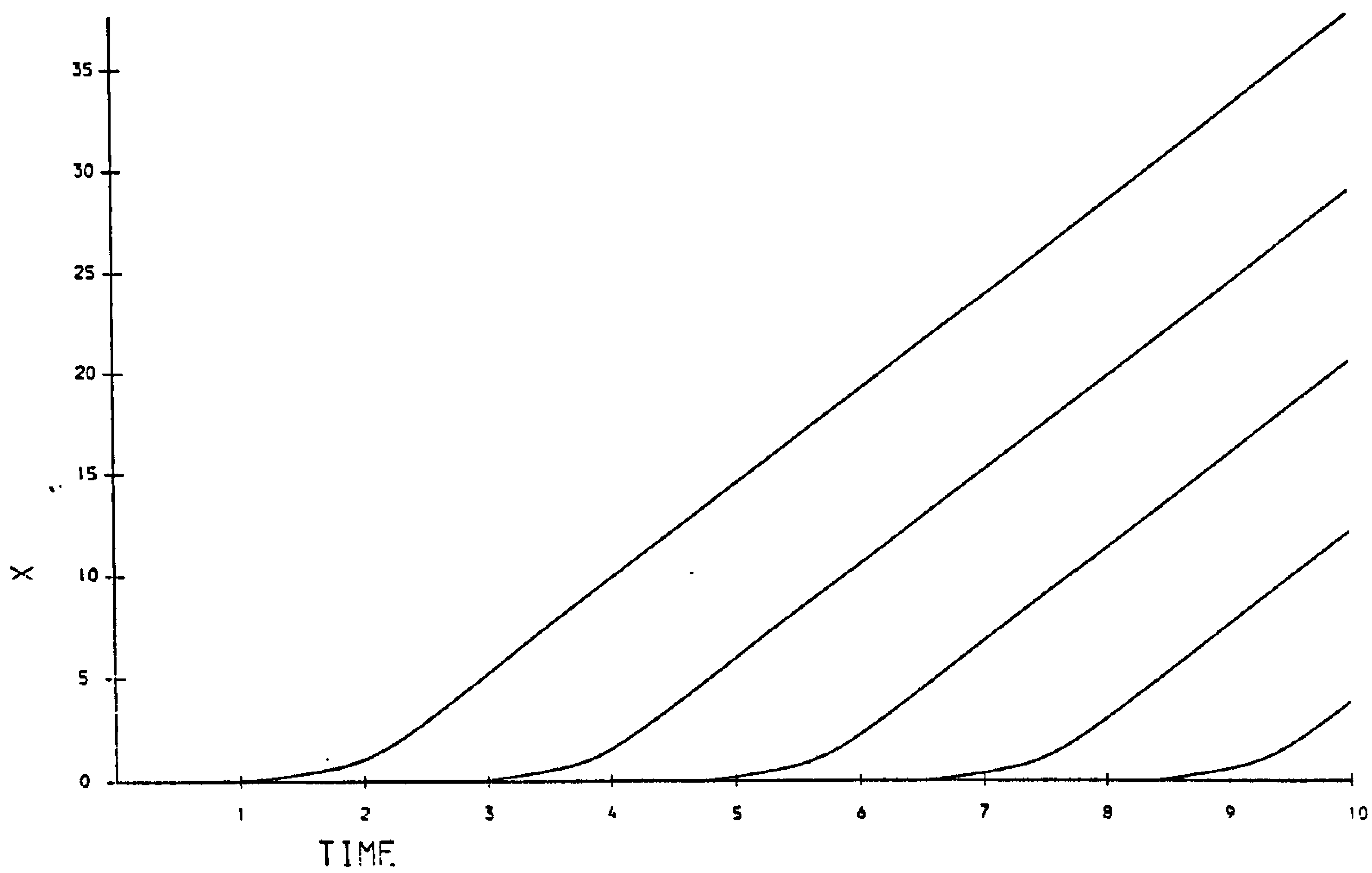

Figure 7.3: Long Impulse. The space-time graphs of the soliton produced by forced conditions (7.39) with $U_0 = 1, \tau = 0.01, t_0 = \infty, h = 0.04, \Delta t = 0.001$.

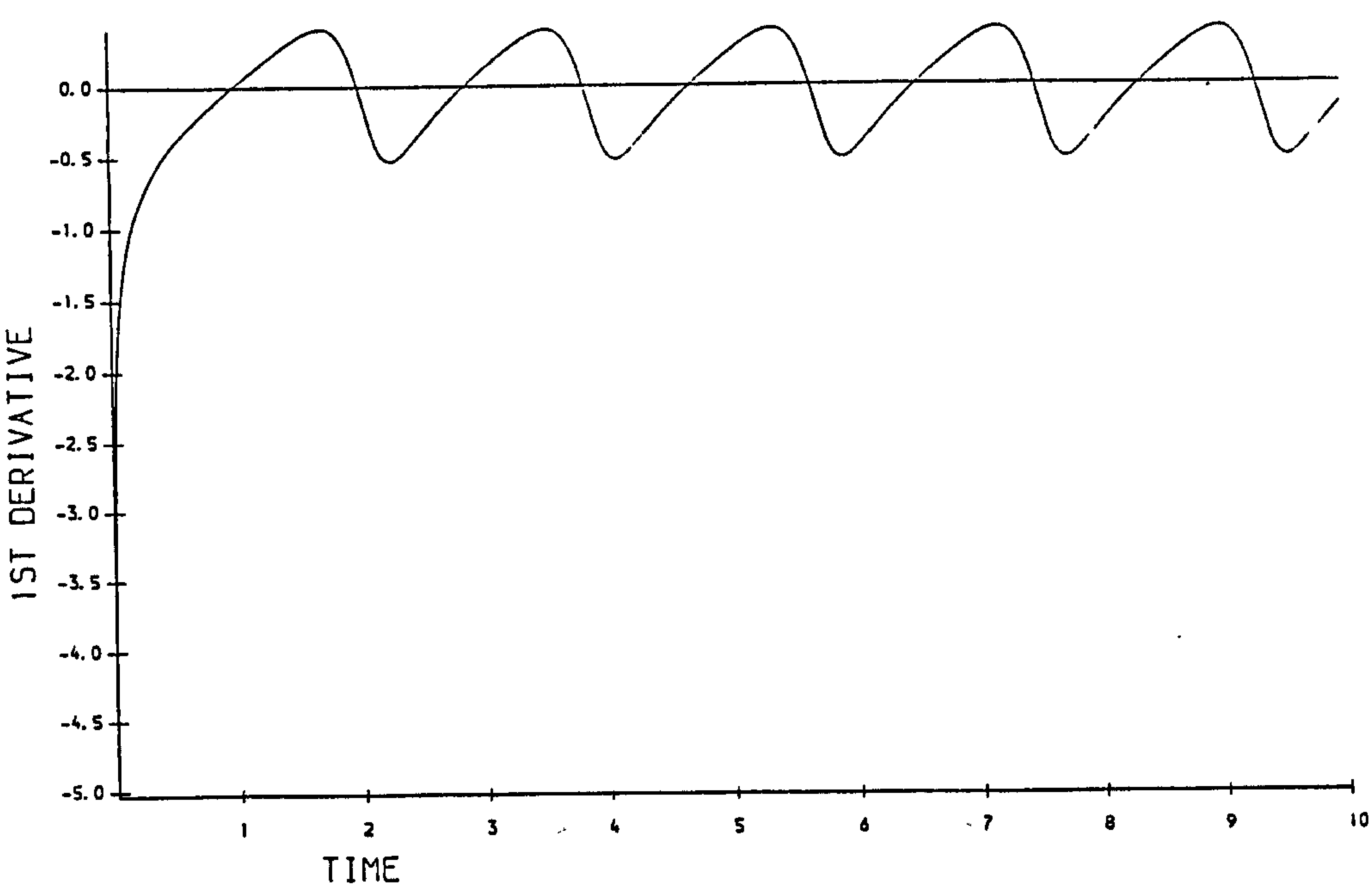

Figure 7.4: Long Impulse. Variation in the first derivative $U_x(0, t)$ at the origin. Forced conditions (7.39) with $U_0 = 1, \tau = 0.01, t_0 = \infty, h = 0.04, \Delta t = 0.001$.

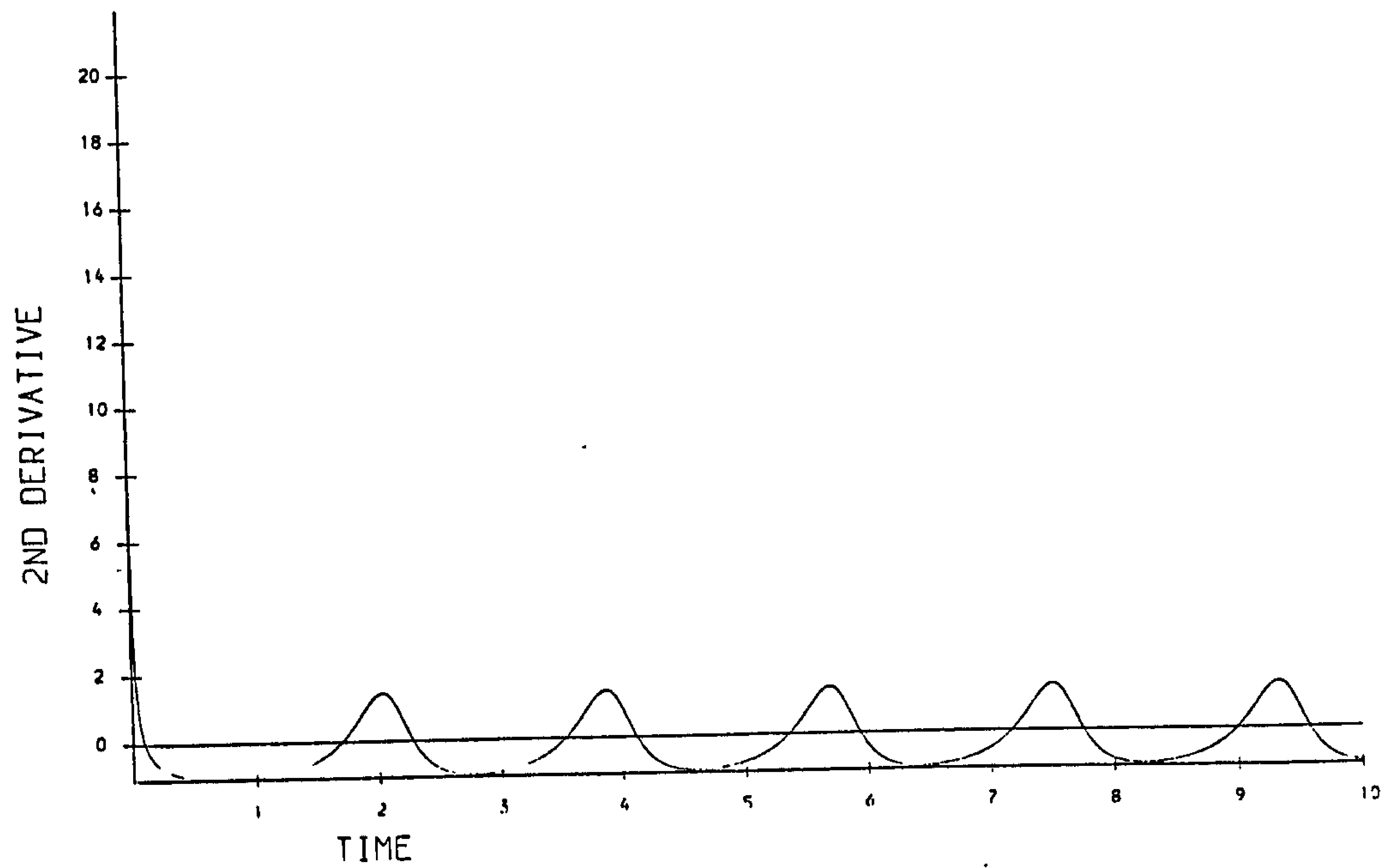

Figure 7.5: Long Impulse. Variation in the second derivative $U_{xx}(0,t)$ at the origin. Forced conditions (7.39) with $U_0 = 1, \tau = 0.01, t_0 = \infty, h = 0.04$, $\Delta t = 0.001$.

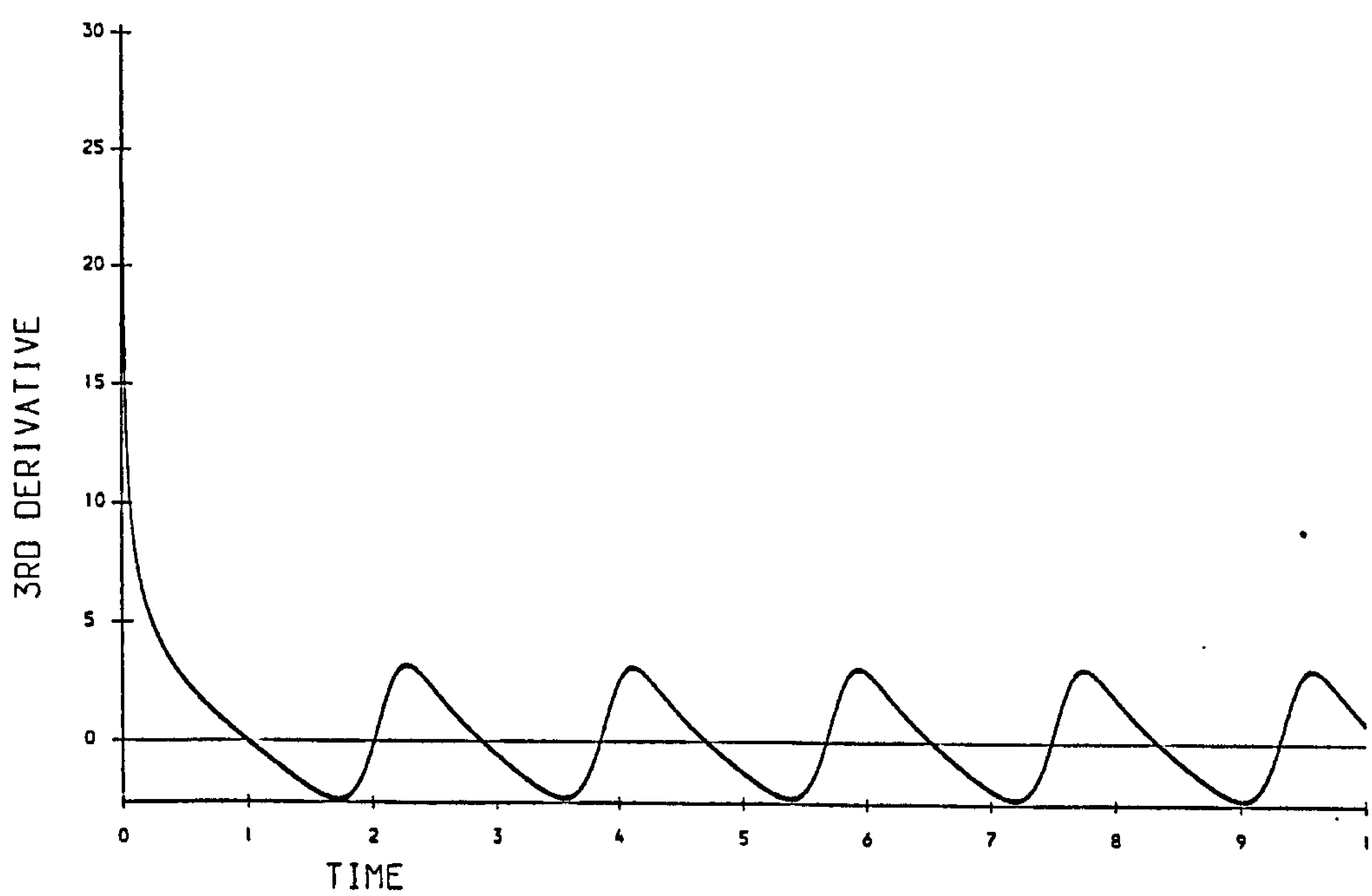

Figure 7.6: Long Impulse. Variation in the third derivative $U_{xxx}(0,t)$ at the origin. Forced conditions (7.39) with $U_0 = 1, \tau = 0.01, t_0 = \infty, h = 0.04$, $\Delta t = 0.001$.

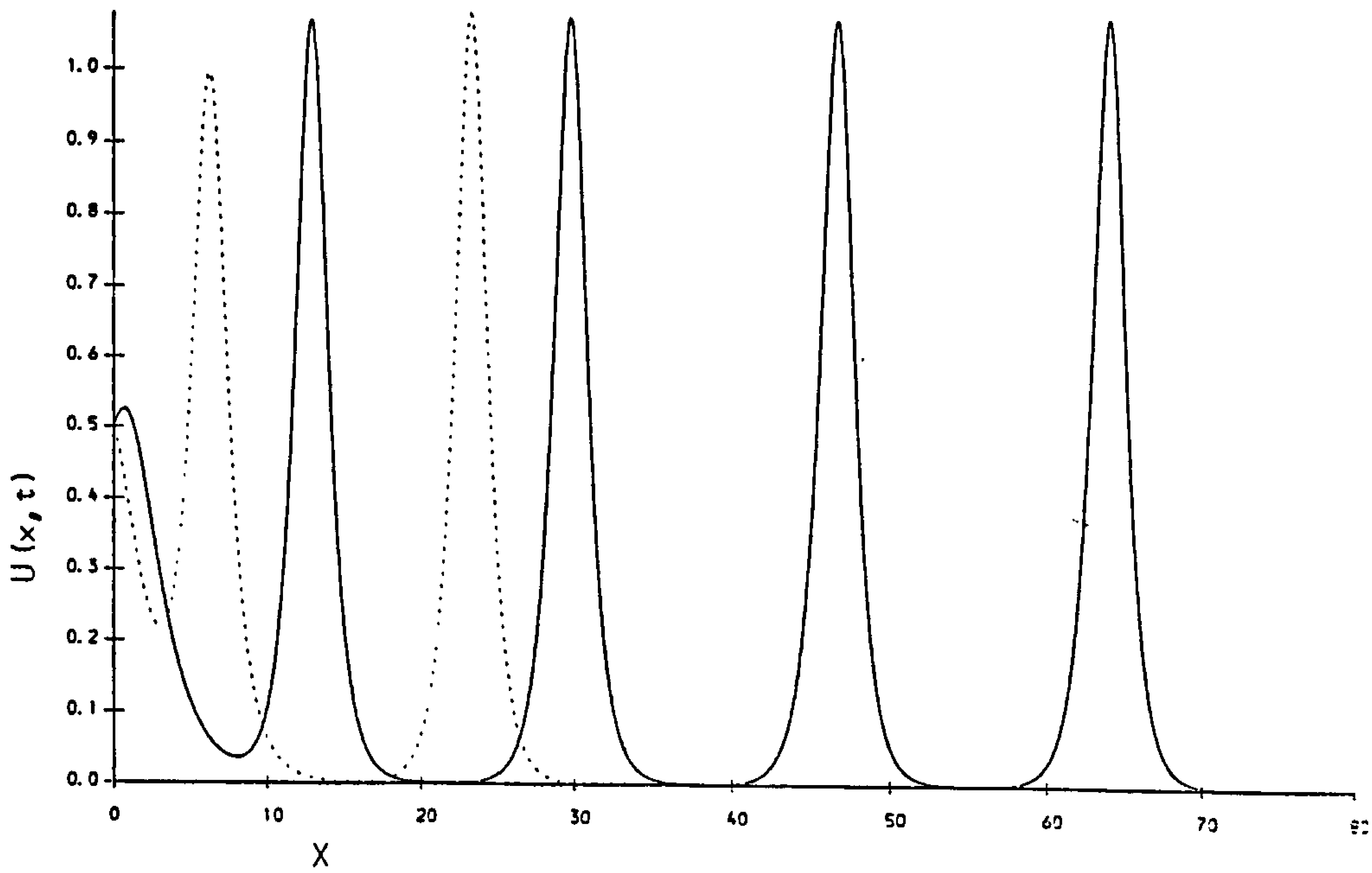

Figure 7.7: Long Impulse. Soliton produced by forced conditions (7.39) with $U_0 = 0.5, \tau = 0.01, t_0 = \infty, h = 0.04, \Delta t = 0.001$ graphed at $t = 35$ (- - - -) and $t = 70$ (——)

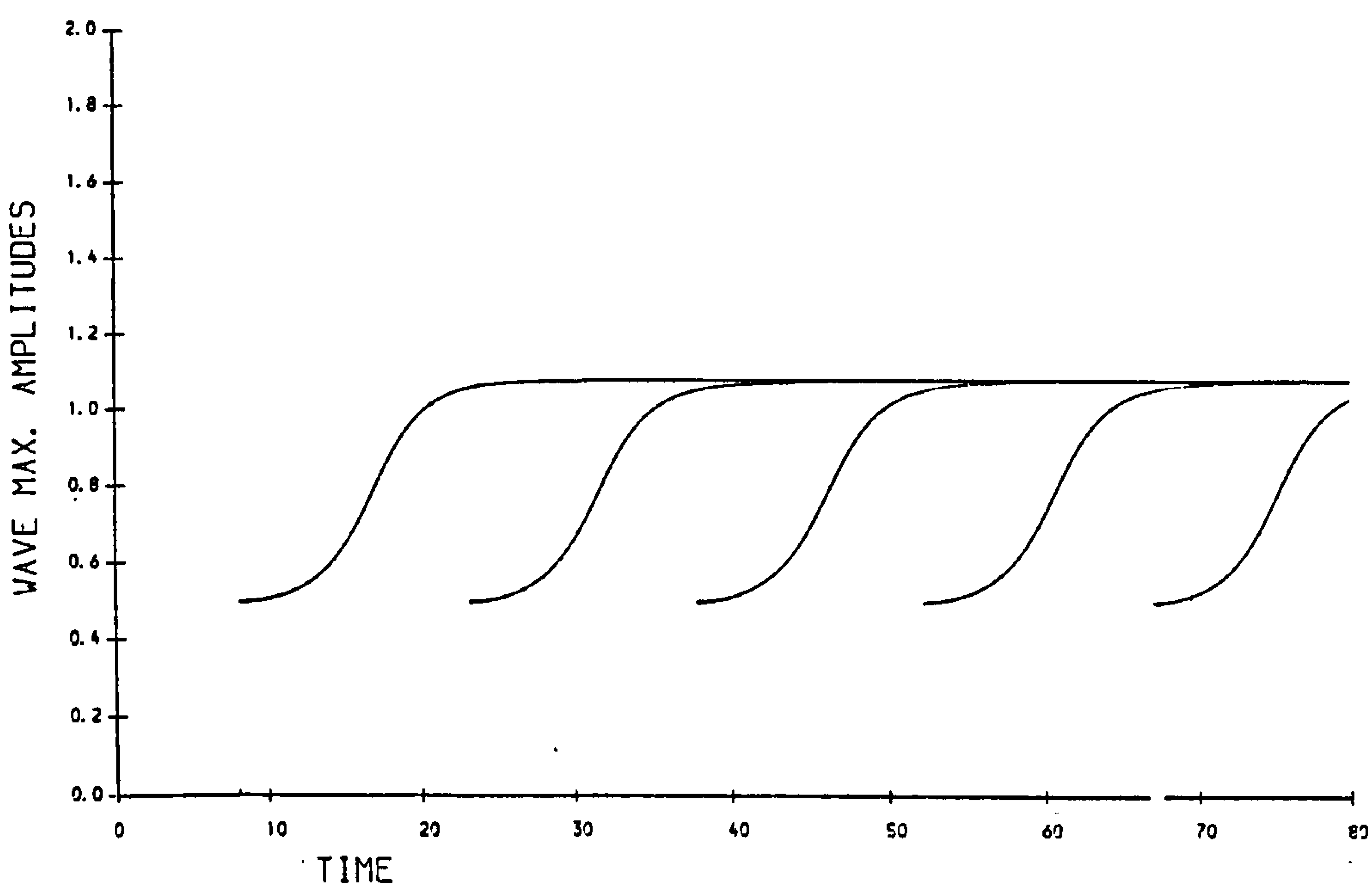

Figure 7.8: Long Impulse. The evolution of the soliton amplitudes. Forced conditions (7.39) with $U_0 = 0.5, \tau = 0.01, t_0 = \infty, h = 0.04, \Delta t = 0.001$.

Table 7.6: Observation of solitary waves, $U_0 = 0.5, \epsilon = 6$

wave	birth time	generated waves		free soliton
		amplitude	velocity	velocity
1	8.08	1.0783	1.164	1.163
2	23.119	1.0749	1.155	1.155
3	37.751	1.0743	1.152	1.154
4	52.303	1.0745	1.152	1.155
5	66.815	0.5014		0.251

Table 7.7: Bounded Forced conditions with $t_0 = \infty, U_0 = 0.5, \epsilon = 6$

time	I_1	I_2	I_3	I_4
0.0	0.000000	0.000000	0.000000	0.000000
0.7	1.349207	0.429793	0.023549	3.624015
14.0	2.456156	1.070081	0.213774	5.733160
21.0	4.421793	2.538082	0.847647	53.388555
28.0	5.444862	3.102128	1.004915	69.229849
35.0	7.493863	4.652092	1.666489	112.170195
42.0	8.465063	5.167089	1.805539	132.777979
49.0	10.560558	6.762980	2.482968	171.353730
56.0	11.500583	7.247047	2.611615	196.384512
63.0	13.617128	8.865708	3.296167	230.192266
70.0	14.546917	9.337076	3.421494	259.999766

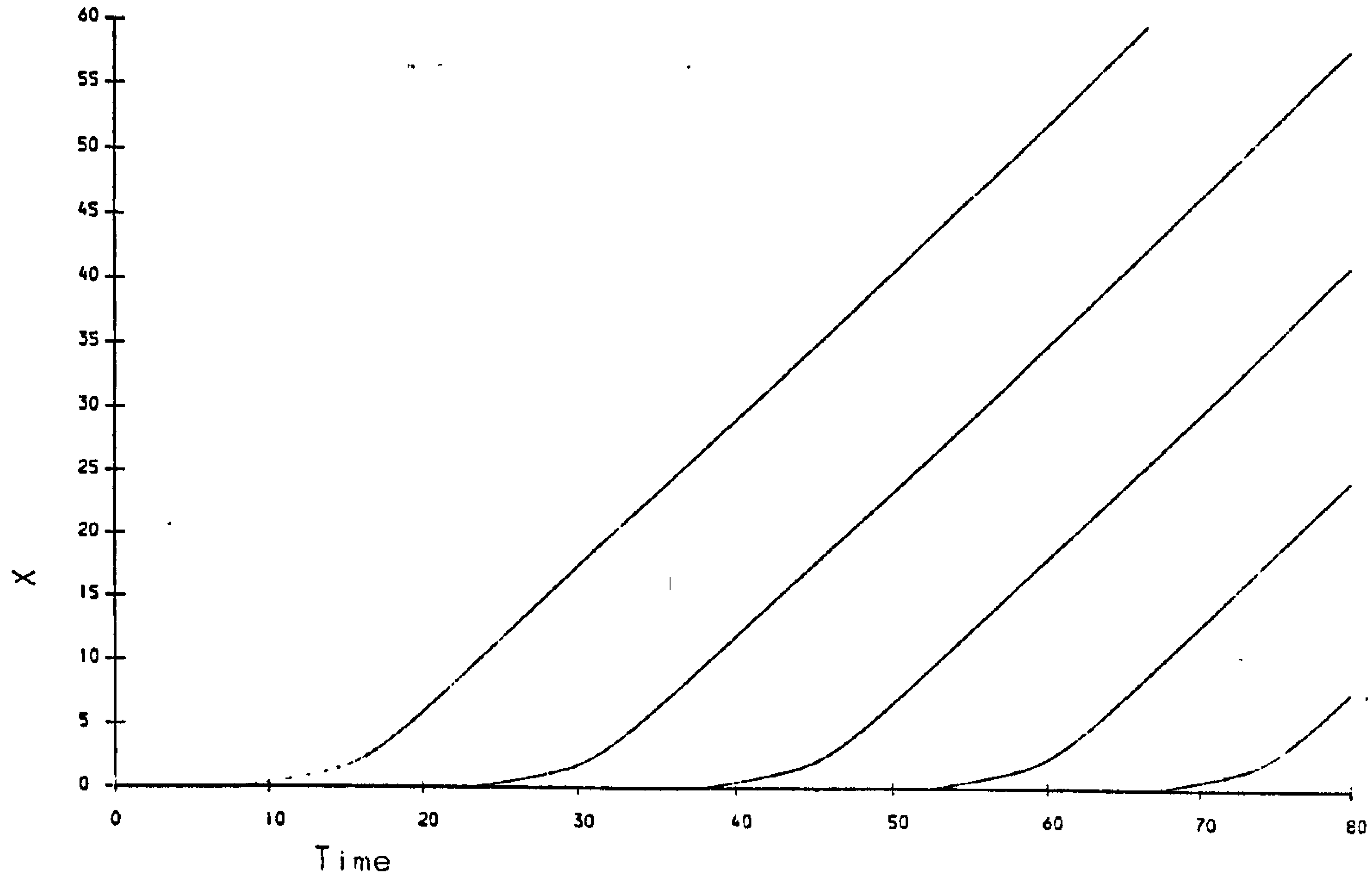

Figure 7.9: Long Impulse. The space-time graphs of the soliton produced by forced conditions (7.39) with $U_0 = 0.5, \tau = 0.01, t_0 = \infty, h = 0.04. \Delta t = 0.001$.

a slightly larger amplitude and velocity than do the following waves. The observation on the solitary waves generated are collected in Table (7.6). The time interval between births of solitary waves is constant at $\Delta T_B = 14.632$, the measured terminal heights for solitary waves 2-4 vary between 1.0749 and 1.0745 with measured velocities of 1.55. Free solitons of similar heights would have velocities 1.154-1.155, so that agreement is close. After an initial transient the graph of $U_x(0,t)$, Figure(7.10), shows a rounded saw tooth periodic behaviour with maximum of about 0.1, minimum of about 0.1 mean zero and period 14.632. The graphs of $U_{xx}(0,t)$ and $U_{xxx}(0,t)$, Figures(7.11-7.12), also exhibit periodic behavior with period 14.632. All the above conclusions are illustrated by the measured values of the quantities given in Table (7.7).

iii-) An experiment with increased forcing, $U_0 = 2.0$; boundary condition (7.39) is used with $x_{max} = 24, t_{max} = 1.2, \tau = 0.01, t_0 = \infty$ so that the forcing again lasts throughout the experiment. The numerical step lengths

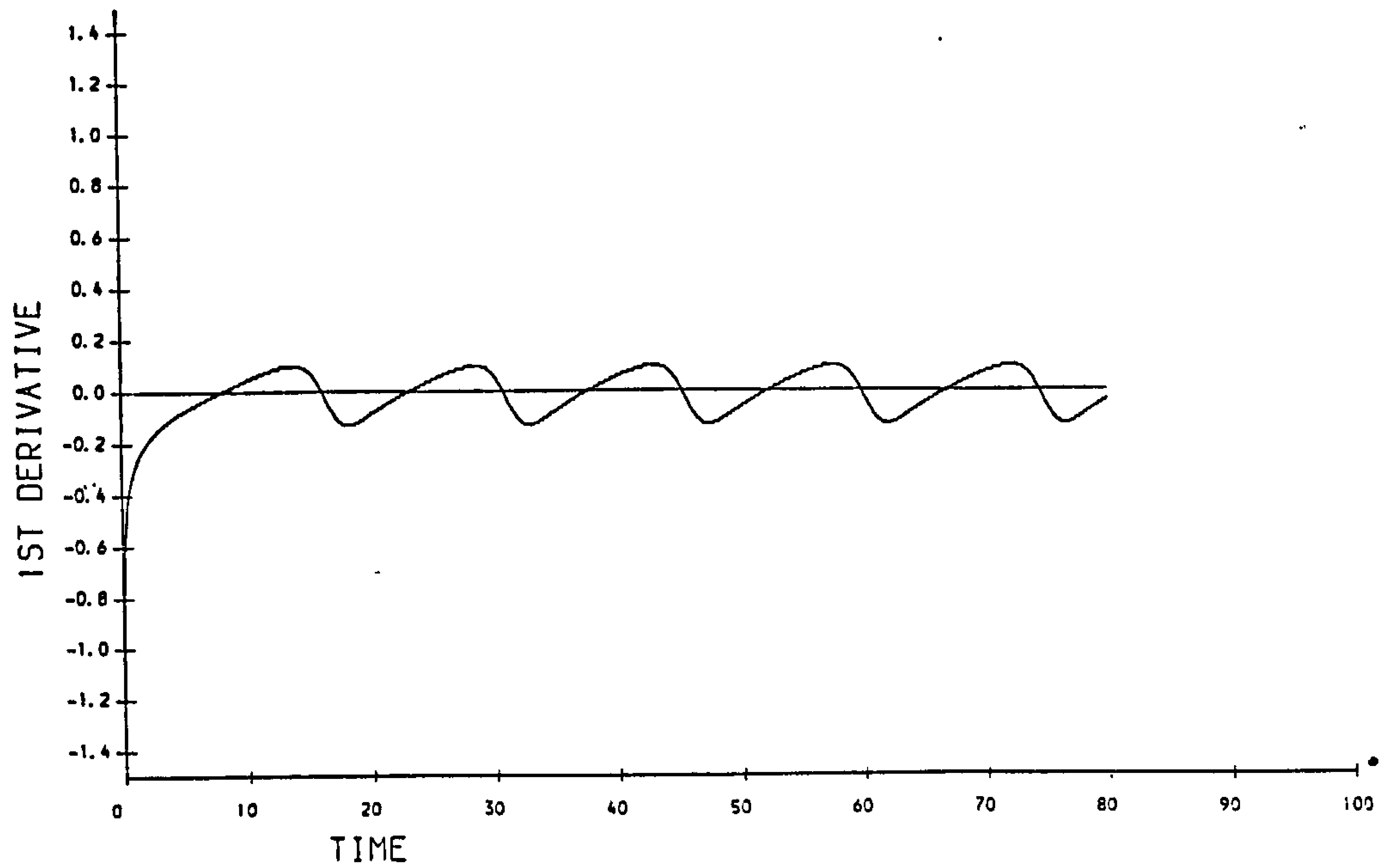

Figure 7.10: Long Impulse. Variation in the first derivative $U_x(0,t)$ at the origin. Forced conditions (7.39) with $U_0 = 0.5, \tau = 0.01, t_0 = \infty, h = 0.04, \Delta t = 0.001$.

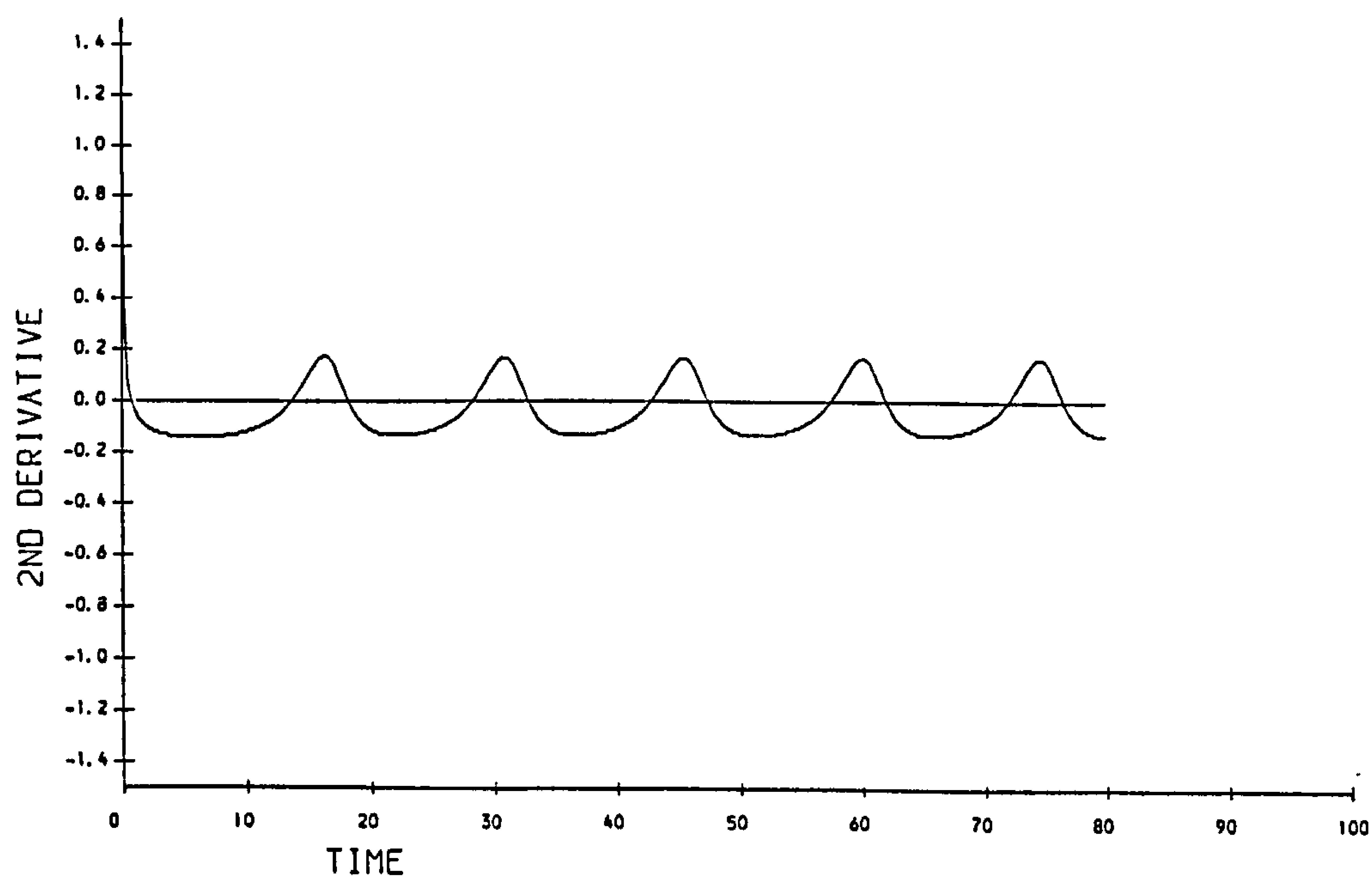

Figure 7.11: Long Impulse. Variation in the second derivative $U_{xx}(0,t)$ at the origin. Forced conditions (7.39) with $U_0 = 0.5, \tau = 0.01, t_0 = \infty, h = 0.04$, $\Delta t = 0.001$.

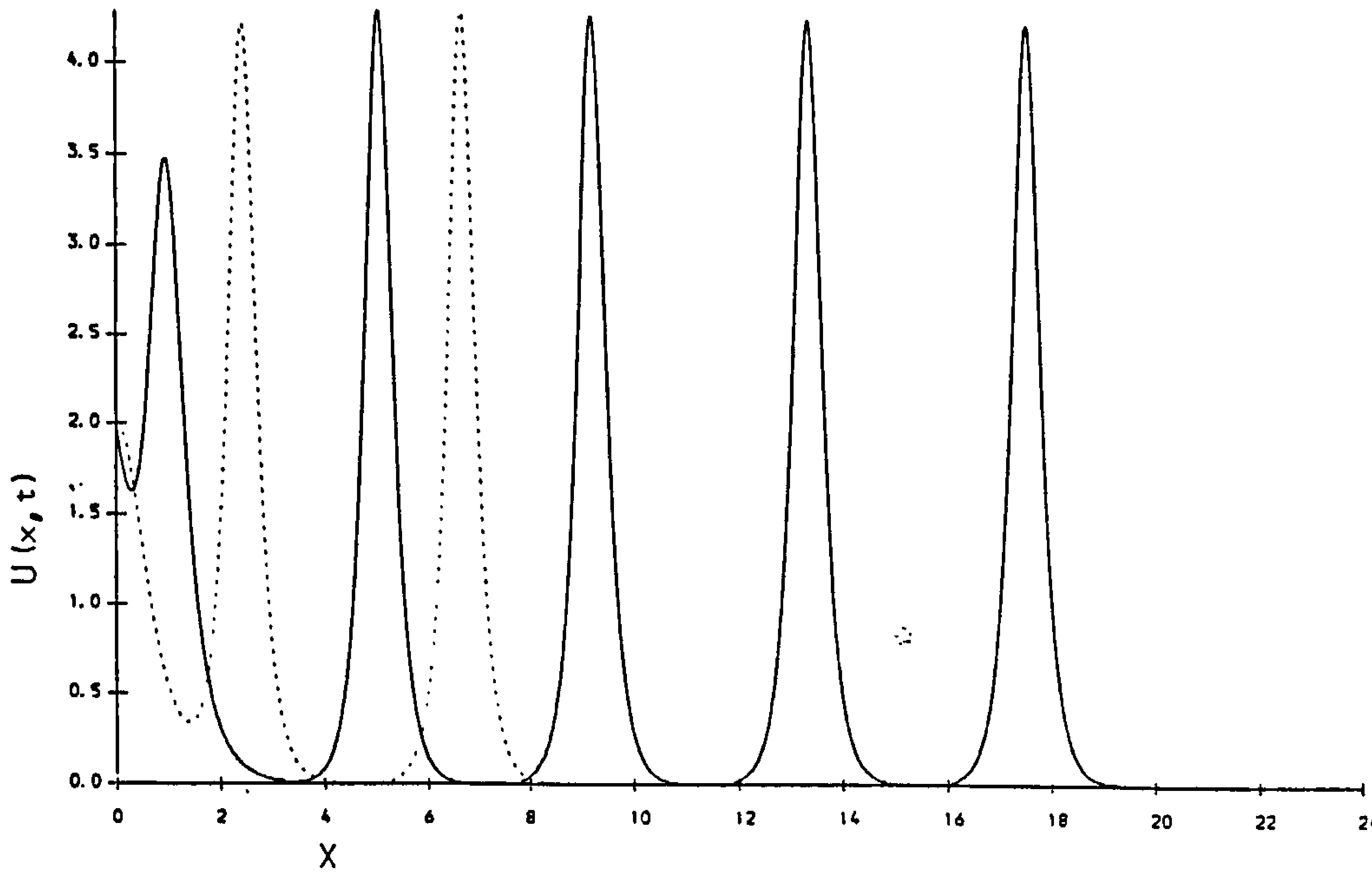

Figure 7.12: Long Impulse. Soliton produced by forced conditions (7.39) with $U_0 = 2, \tau = 0.01, t_0 = \infty, h = 0.02, \Delta t = 0.0005$ graphed at $t = 0.6$ (- - - -) and $t = 1.2$ (——)

are $h = 0.02$ and $\Delta t = 0.0005$. In this numerical experiment, see Figure (7.12), five solitary waves are generated before the simulation is terminated at t = 1.2. Figures (7.13) and (7.14) show that four achieve their terminal heights and a constant velocity.

The generating conditions for the first wave are rather more protracted than those for all subsequent waves, as can be seen from the graphs of the first three derivatives at $x = 0$ given in Figures (7.15-7.17) so it achieves a slightly larger amplitude and velocity than do the following waves. The observation on the solitary waves generated are collected in Table (7.8). The time interval between births of solitary waves is constant at $\Delta T_B = 0.229$, the measured terminal heights for solitary waves 2 - 4 vary between 4.2725 and 4.2843 with measured velocities of 18.125. Free solitons of similar heights would have velocities 18.2542 - 18.3552, so that agreement is close. After an initial transient the graph of $U_x(0,t)$, Figure(7.15), shows a rounded saw tooth periodic behaviour with maximum of about 1.6, minimum of about

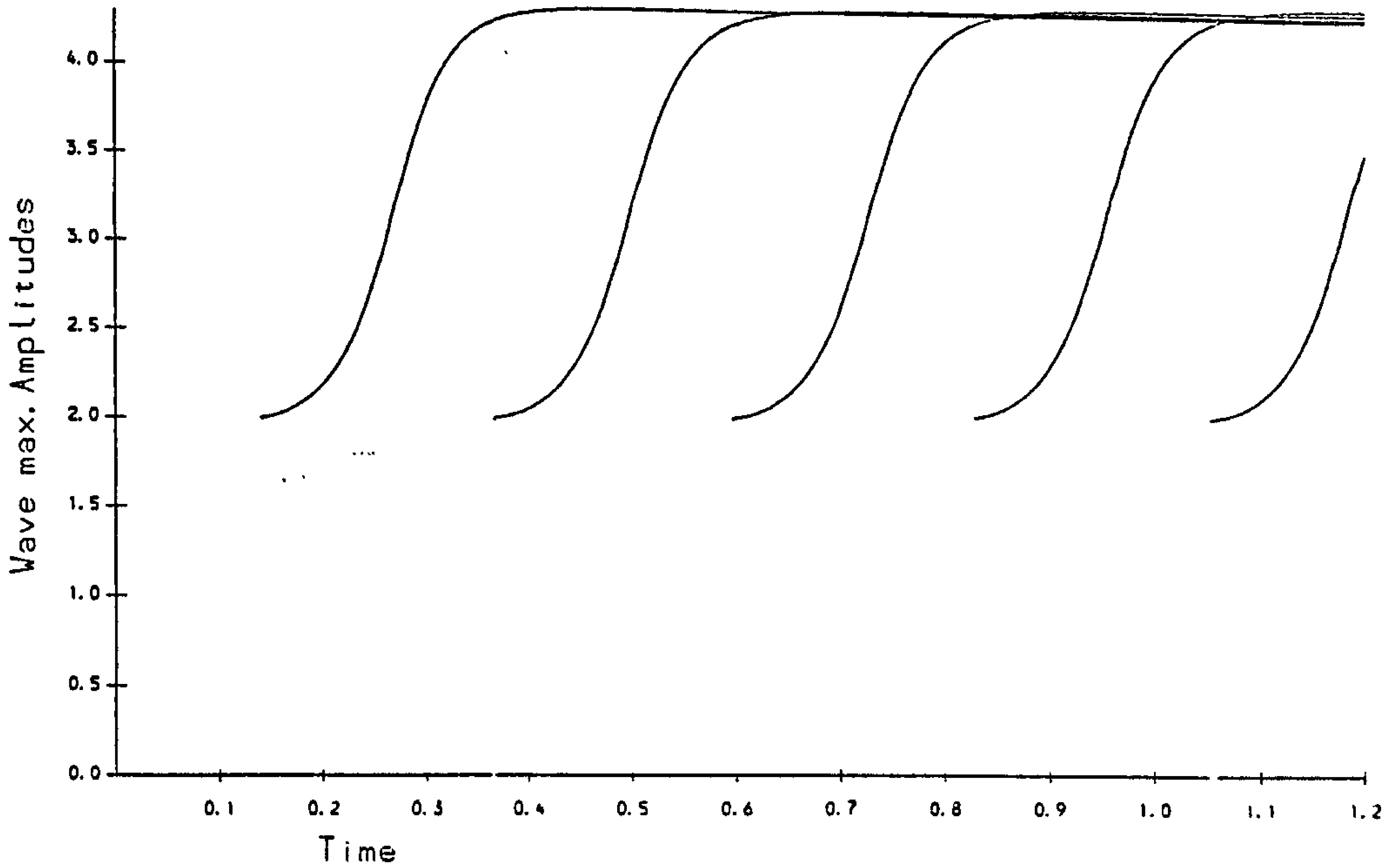

Figure 7.13: Long Impulse. The evolution of the soliton amplitudes. Forced conditions (7.39) with $U_0 = 2, \tau = 0.01, t_0 = \infty, h = 0.02, \Delta t = 0.0005$.

Table 7.8: Observation of solitary waves, $U_0 = 2, \epsilon = 6$

wave	birth time	generated waves		free soliton
		amplitude	velocity	velocity
1	0.133	4.2587	17.8125	18.1365
2	0.419	4.2725	18.1250	18.2542
3	0.648	4.2734	18.1250	18.2619
4	0.876	4.2843	18.4375	18.3552
5	1.105	3.4817		12.1222

Table 7.9: Bounded forced conditions with $t_0 = \infty, U_0 = 2, \epsilon = 6$

time	I_1	I_2	I_3	I_4
0.00	0.000000	0.000000	0.000000	0.000000
0.12	1.398292	1.805501	1.860354	910.825078
0.24	2.797519	5.330557	20.574360	1963.240625
0.36	4.631759	10.531853	55.764072	15445.856250
0.48	6.211320	14.772141	79.774028	18530.415000
0.60	7.862549	19.247795	108.466523	31732.185000
0.72	9.664879	24.370183	139.797295	35129.875000
0.84	11.089539	27.930840	160.266982	47791.040000
0.96	13.096483	33.848005	198.129375	51968.055000
1.08	14.315227	36.587783	211.312969	63539.540000
1.20	16.459493	43.007183	252.903789	69072.985000

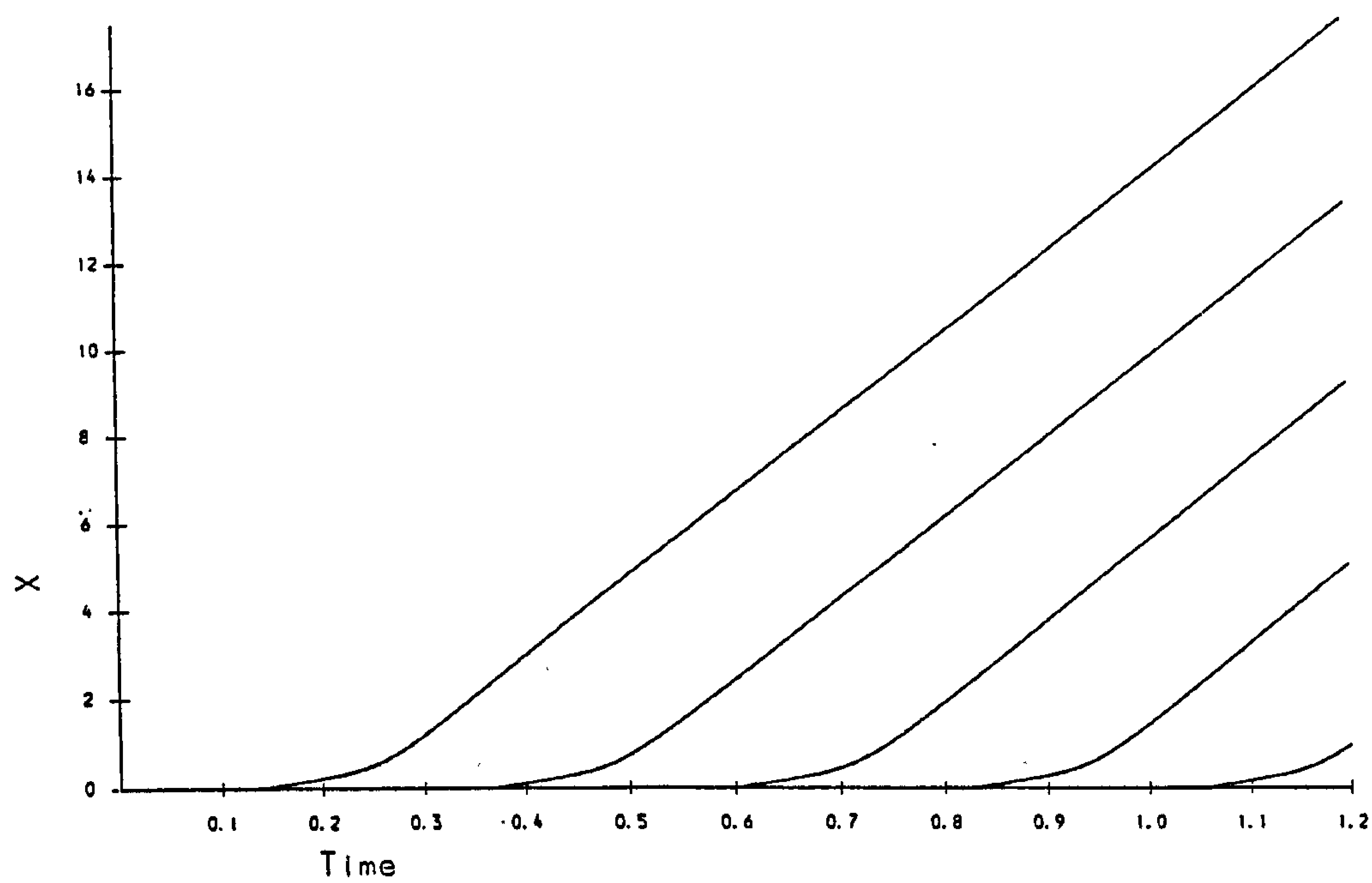

Figure 7.14: Long Impulse. The space-time graphs of the soliton produced by forced conditions (7.39) with $U_0 = 2, \tau = 0.01, t_0 = \infty, h = 0.02, \Delta t = 0.0005$.

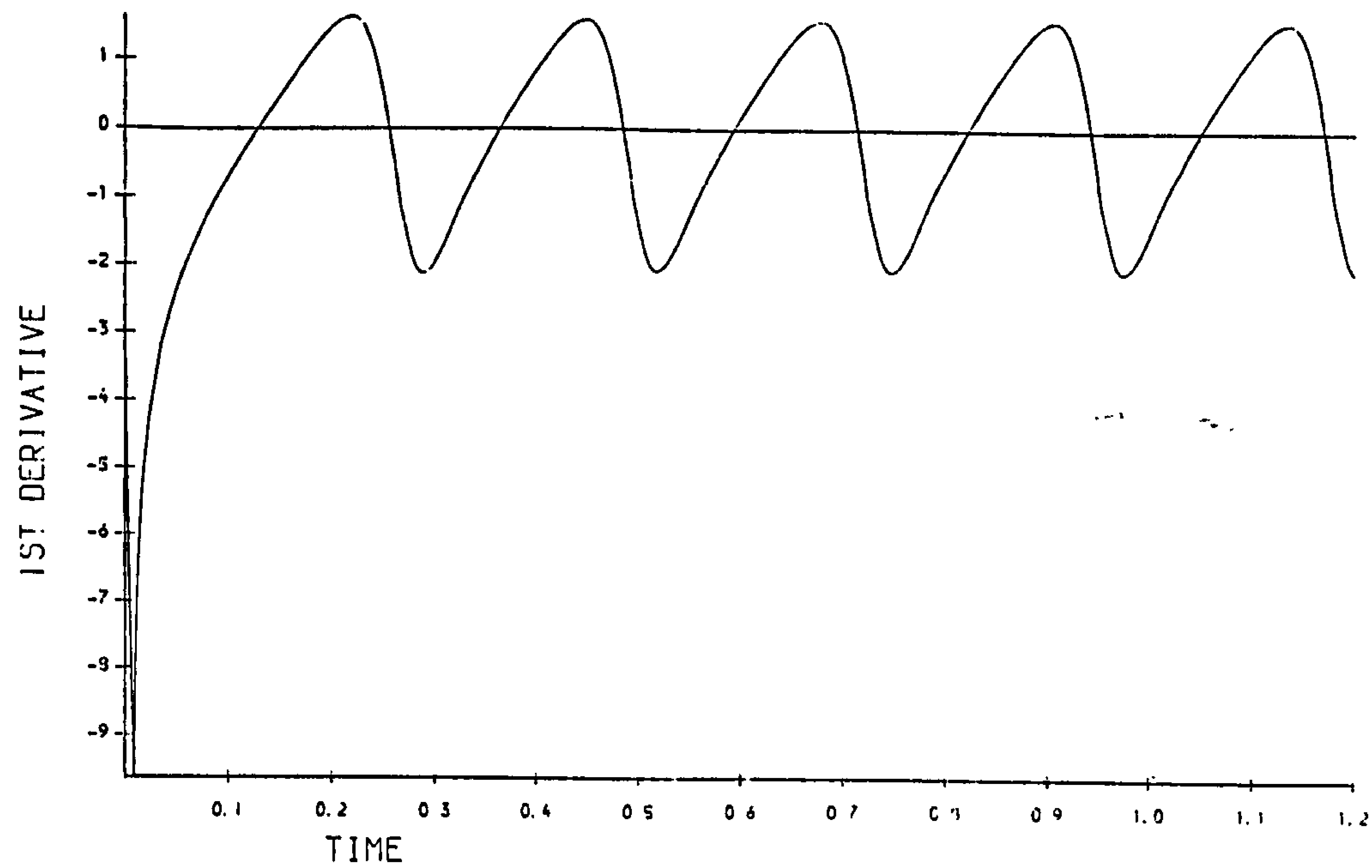

Figure 7.15: Long Impulse. Variation in the first derivative $U_x(0,t)$ at the origin. Forced conditions (7.39) with $U_0 = 2, \tau = 0.01, t_0 = \infty, h = 0.02, \Delta t = 0.0005$.

-2.1 mean zero and period 0.229. The graphs of $U_{xx}(0,t)$ and $U_{xxx}(0,t)$, Figures(7.16-7.17), also exhibit periodic behavior with period 0.229. All the above conclusions are illustrated by the measured values of the quantities given in Table (7.9).

Short Impulse

i-) In this simulation boundary condition (7.39) is used with $U_0 = 1$, $\tau = 0.01, t_0 = 4, h = 0.004, \Delta t = 0.001$. Two solitary waves are generated in the experiment, of which only the first, born at $t = 1.040$, reaches its mature amplitude 2.154 and velocity 4.648, the second born at $t = 2.920$, grows to an amplitude 1.788 and a velocity 3.196; Figures (7.18) and (7.19).

The quantities I_j, equation (7.6), are only constant when the boundary conditions $U \to 0$ as $x \to \pm\infty$ hold. With the forcing conditions (7.39) it is

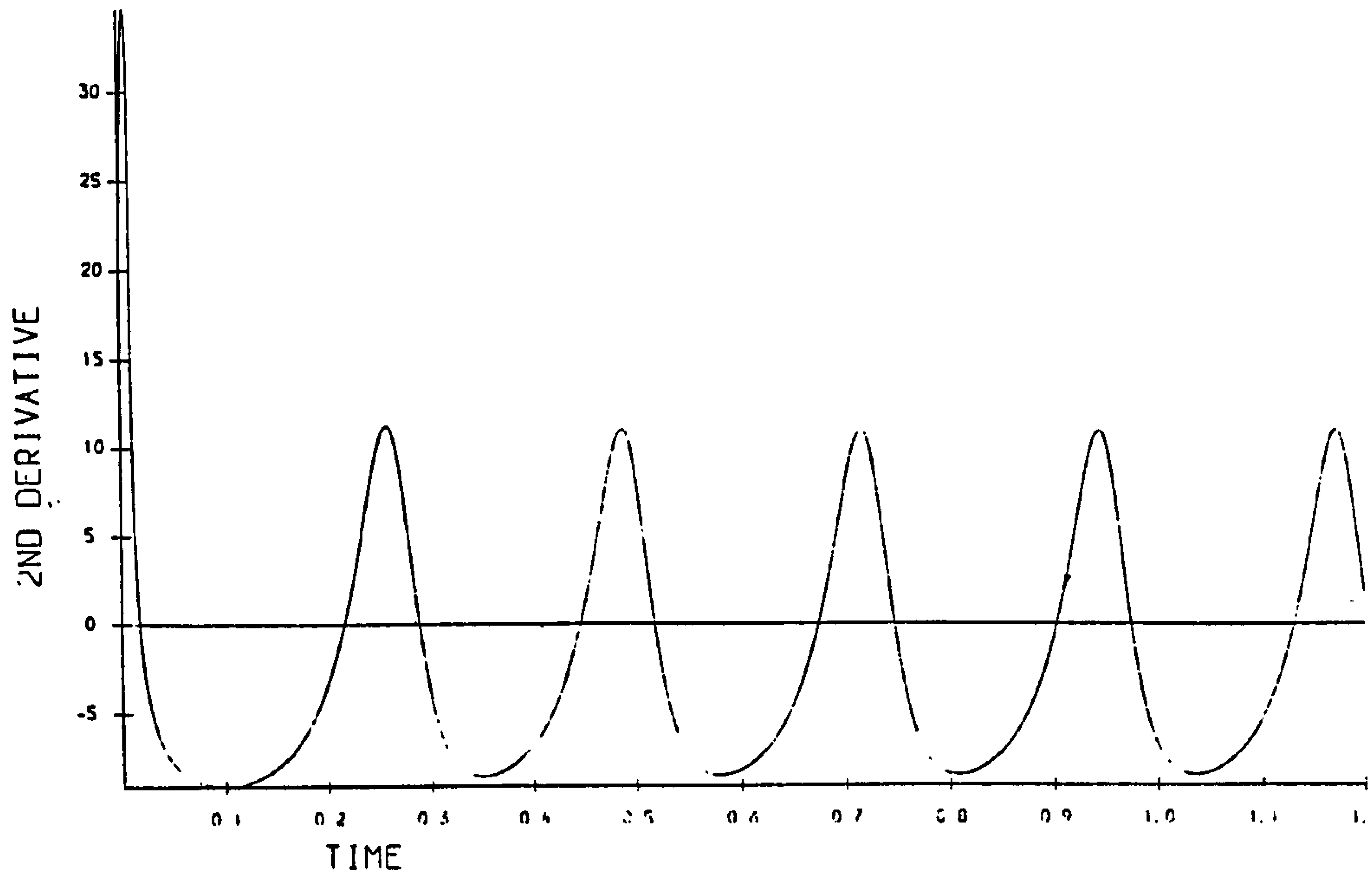

Figure 7.16: Long Impulse. Variation in the second derivative $U_{xx}(0,t)$ at the origin. Forced conditions (7.39) with $U_0 = 2, \tau = 0.01, t_0 = \infty, h = 0.02$, $\Delta t = 0.0005$.

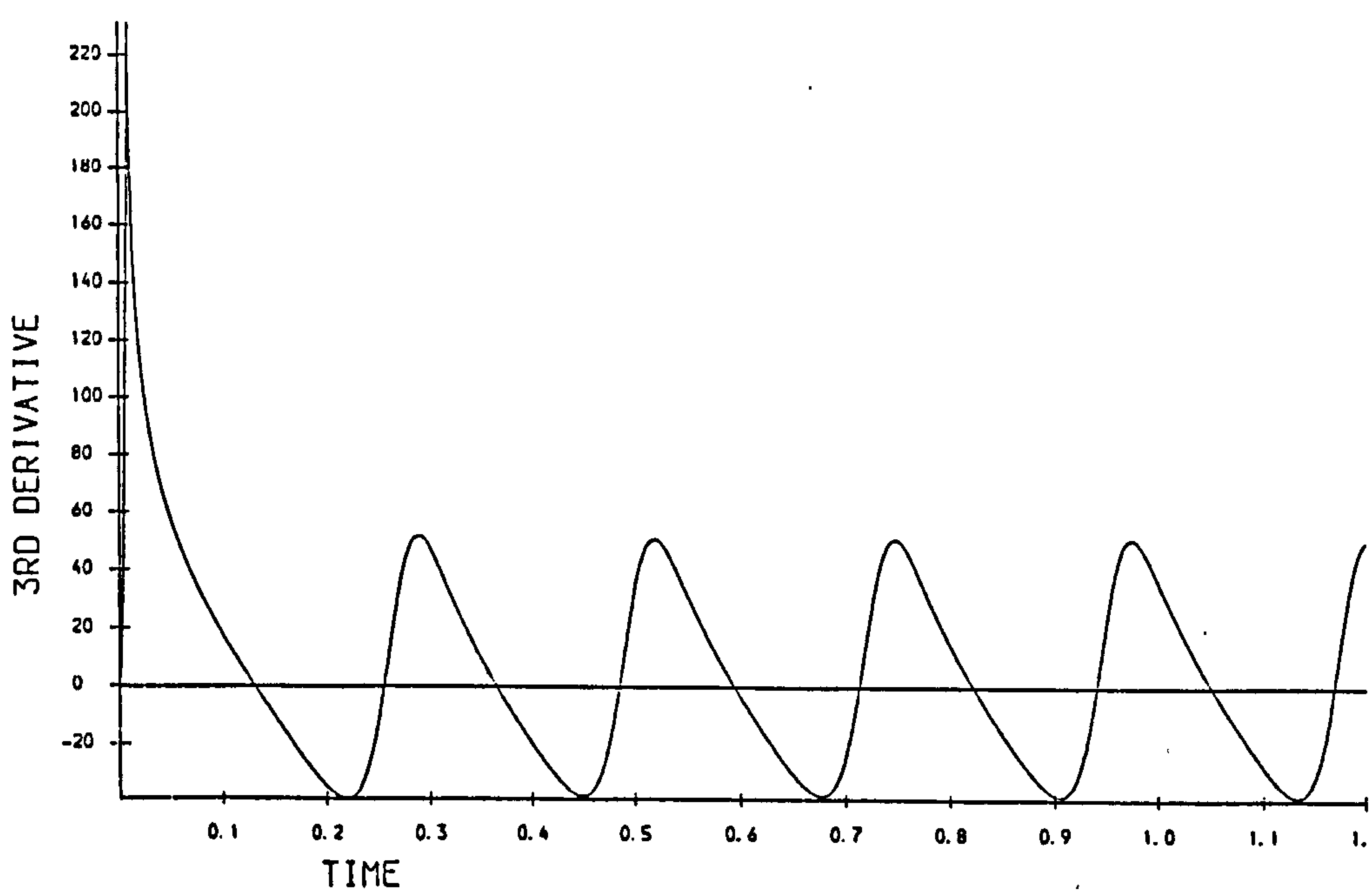

Figure 7.17: Long Impulse. Variation in the third derivative $U_{xxx}(0,t)$ at the origin. Forced conditions (7.39) with $U_0 = 2, \tau = 0.01, t_0 = \infty, h = 0.02$, $\Delta t = 0.0005$.

found that they vary in the following ways:

$$
\begin{aligned}
&I_1(t) = I_1(0) + \textstyle\int_0^t\{\frac{1}{3}\epsilon U^3(0,t) + \mu U_{xx}(0,t)\}dt,\\
&I_2(t) = I_2(0) + \textstyle\int_0^t\{\frac{1}{4}\epsilon U^4(0,t) + \mu U(0,t)U_{xx}(0,t) - \frac{1}{2}\mu U_x^2(0,t)\}dt,\\
&I_3(t) = I_3(0) + \textstyle\int_0^t\{\frac{2}{3}\epsilon U^6(0,t) + 4\mu U^3(0,t)U_{xx}(0,t)\\
&+6\tfrac{\mu^2}{\epsilon}U_{xx}^2(0,t) - 12\tfrac{\mu}{\epsilon}U_x(0,t)U_t(0,t)\}dt,\\
&I_4(t) = I_4(0) + \textstyle\int_0^t\{-\frac{3}{4}\epsilon U^8(0,t) + \mu\{45U^4(0,t)U_x^2(0,t)\\
&-6U^5(0,t)U_{xx}(0,t)\} + 3\tfrac{\mu^2}{\epsilon}\{20U_{xx}^2(0,t)U_x(0,t)U_{xxx}(0,t)\\
&-16U^2(0,t)U_{xx}^2(0,t) - U_x^4(0,t) - 20U(0,t)U_x^2(0,t)U_{xx}(0,t)\}\\
&+36\tfrac{\mu^3}{\epsilon^2}\{\tfrac{1}{2}U_{xxx}^2(0,t) - U_{xx}(0,t)U_{xxxx}(0,t)\}\}dt.
\end{aligned}
\tag{7.42}
$$

Using (7.48) it can be shown that the variation of the I_j depends only on the behaviour of $U(0,t), U_x(0,t)$ and $U_{xx}(0,t)$. Hence over the time period $0 \le t \le 4$, with $\epsilon = 6, \mu = 1$ and $U(0,t) = 1$, the variation in quantities I_j is given by

$$
\begin{aligned}
&I_1(t) = \textstyle\int_0^t\{2 + U_{xx}(0,t)\}dt\\
&I_2(t) = \textstyle\int_0^t\{\frac{3}{2} + U_{xx}(0,t) - \frac{1}{2}U_x^2(0,t)\}dt\\
&I_3(t) = \textstyle\int_0^t\{4 + 4U_{xx}(0,t) + U_{xx}^2(0,t)\}dt\\
&I_4(t) = \textstyle\int_0^t\{-\frac{9}{2} + 3U_x^2(0,t) - 2U_{xx}^2(0,t) - 6U_{xx}(0,t)\\
&-\tfrac{1}{2}U_x^4(0,t) - 4U_x^2(0,t)U_{xx}(0,t) + U_{xx}(0,t)U_{xt}(0,t)\}dt
\end{aligned}
\tag{7.43}
$$

so that all change continuously although the rates will vary since all three integrands vary periodically as can be seen from the graphs of $U_x(0,t)$ and $U_{xx}(0,t)$, given in Figures (7.20) and (7.21).

Figures (7.21) and (7.22) also show that when the forcing is turned off at $t = 4$, for $t > 4$, $U(0,t) = 0$ but as the derivatives $U_x(0,t)$ and $U_{xx}(0,t)$ are not themselves forced to become zero the I_j do not immediately cease to vary. The switching operation causes a spike in the derivative graphs; subsequently $U_x(0,t)$ and $U_{xx}(0,t)$ tend to zero at about the same rate. Thus I_1 continues to change, increasing or decreasing according to the sign of $U_{xx}(0,t)$, through

$$I_1(t) = I_1(4) + \textstyle\int_4^t\{U_{xx}(0,t)\}dt, \tag{7.44}$$

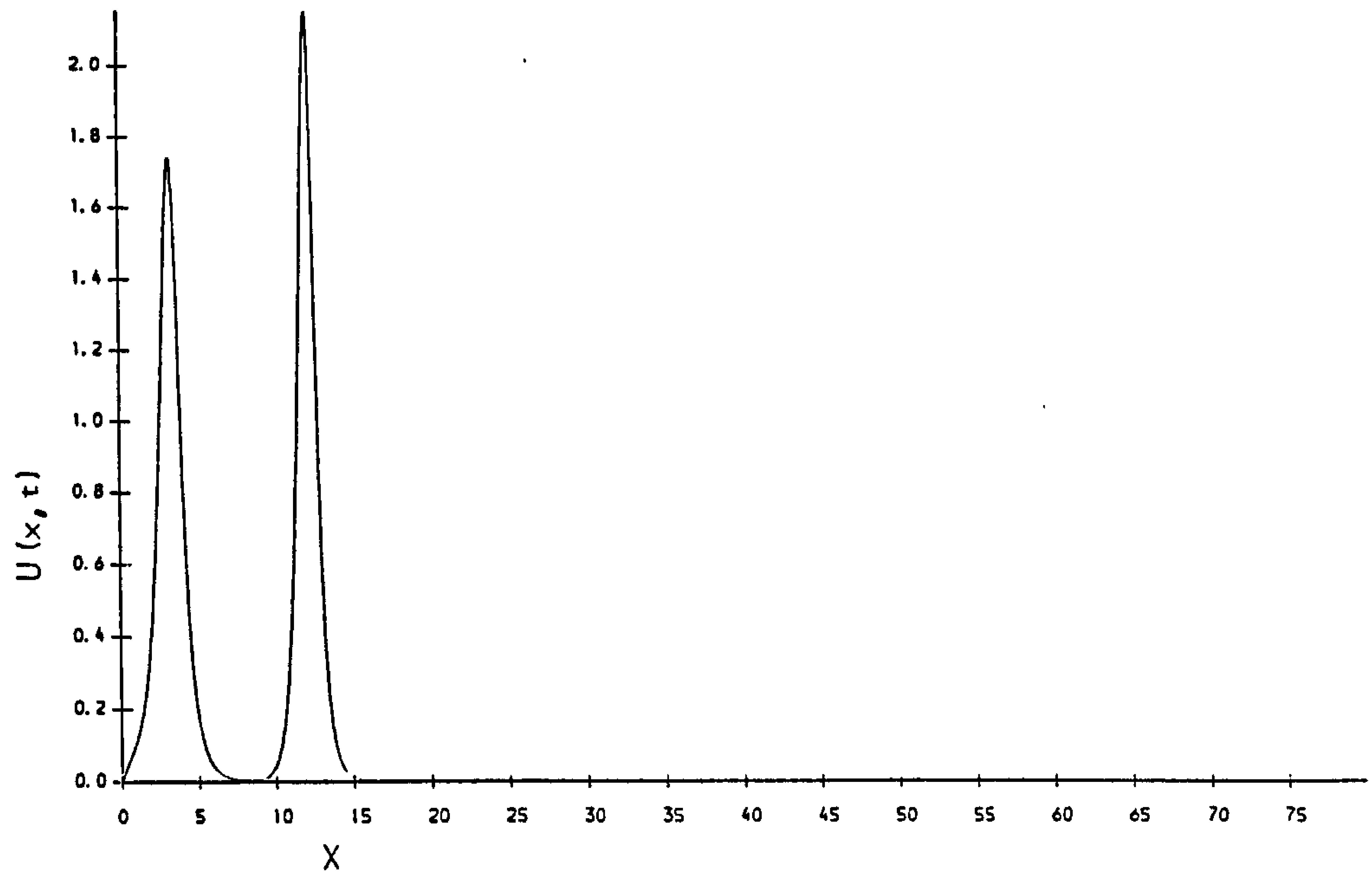

Figure 7.18: Short Impulse. Solitons produced by forced conditions (7.39) with $U_0 = 1, \tau = 0.01, t_0 = 4, h = 0.04, \Delta t = 0.001$ graphed at time $t = 4.5$

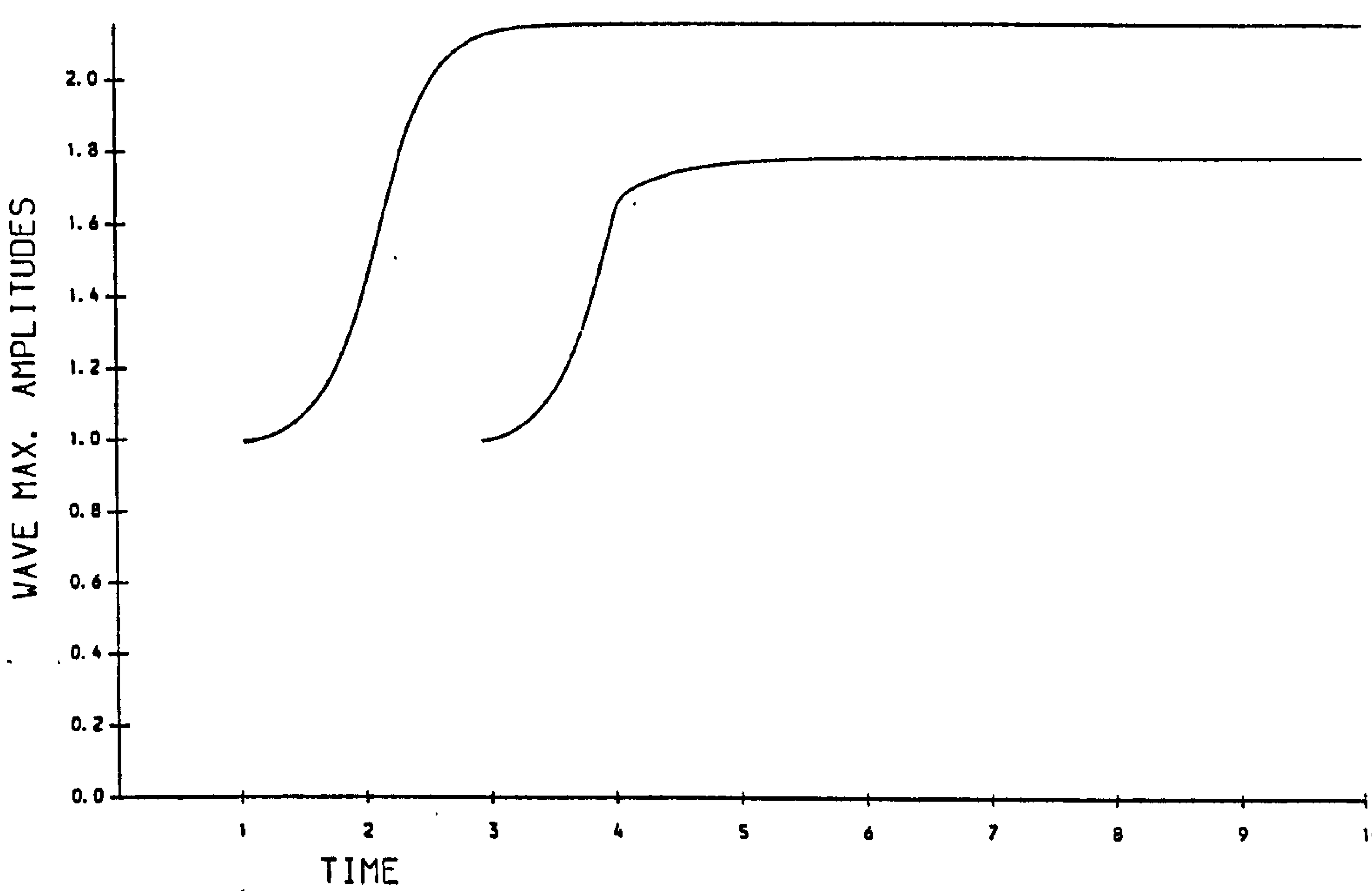

Figure 7.19: Short Impulse. The evolution of the soliton amplitudes. Forced conditions (7.39) with $U_0 = 1, \tau = 0.01, t_0 = 4, h = 0.04, \Delta t = 0.001$.

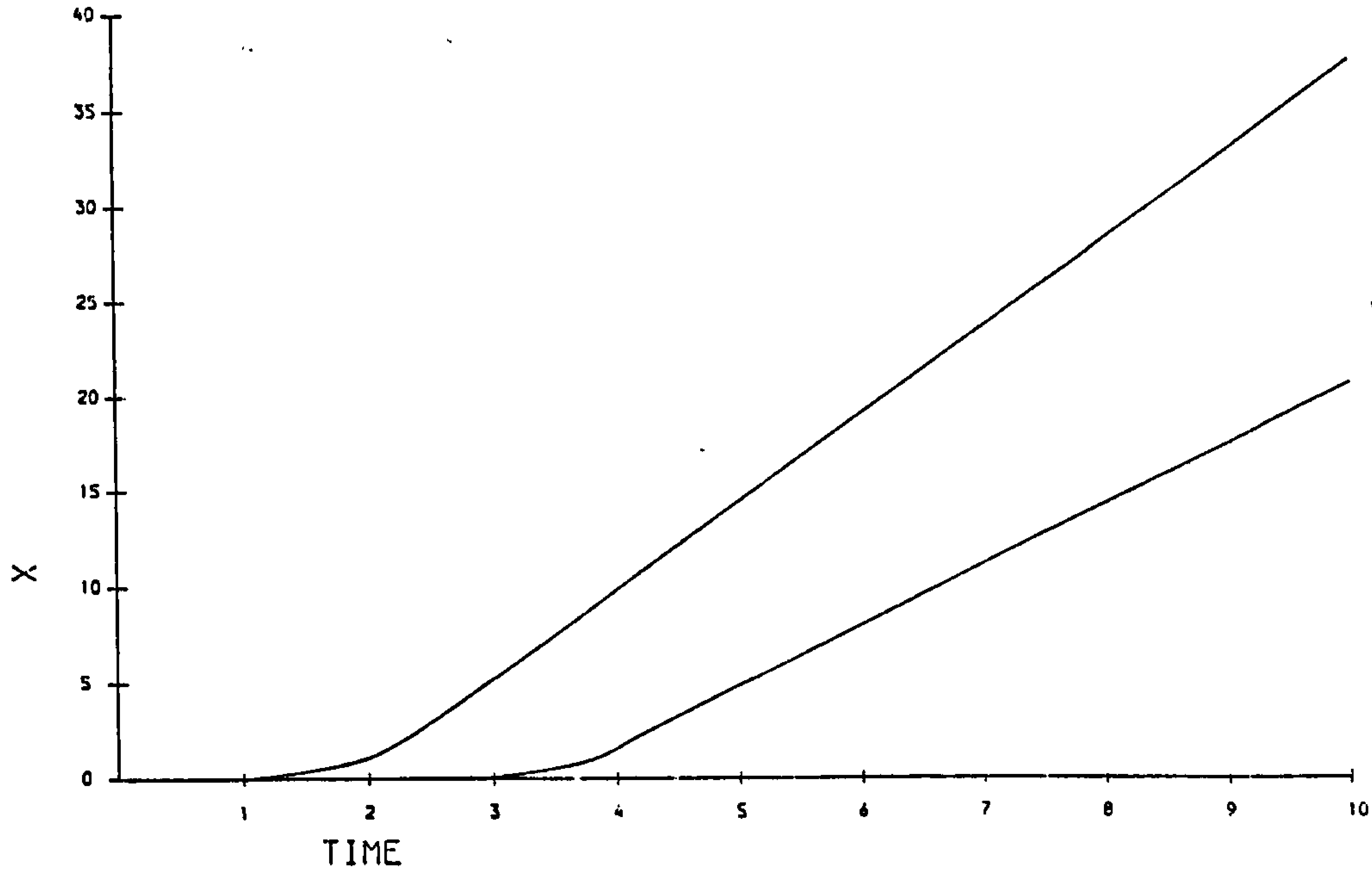

Figure 7.20: Short Impulse. The space-time graphs of the soliton produced by Forced conditions (7.39) with $U_0 = 1, \tau = 0.01, t_0 = 4, h = 0.01. \Delta t = 0.001$.

I_2 start to decrease through

$$I_2(t) = I_2(4) - \textstyle\int_4^t \{\frac{1}{2}U_x^2(0,t)\}dt, \tag{7.45}$$

and I_3 to increase through

$$I_3(t) = I_3(4) + \textstyle\int_4^t \{U_{xx}^2(0,t)\}dt, \tag{7.46}$$

and I_4 changes through

$$I_4(t) = I_4(4) - \textstyle\int_4^t \{\frac{1}{2}U_x^4(0,t) - U_{xx}(0,t)U_{xt}(0,t)\}dt. \tag{7.47}$$

These equations also imply that the development of the last formed solitary wave does not stop abruptly when the forcing is switched off, but continues until $U_x(0,t)$ and $U_{xx}(0,t)$ have decayed to zero. After a time of about $t = 7$, when the influences of forcing have died away, the quantities I_j should remain constant. The above conclusions are illustrated by the measured values of the quantities given in Table (7.10). To inhibit the development of the second solitary wave this experiment is repeated with the forcing cut off at

Table 7.10: Bounded forced conditions with $t_0 = 4, U_0 = 1$

time	I_1	I_2	I_3	I_4
0.0	0.000000	0.000000	0.000000	0.000000
1.0	1.466032	0.962159	0.292959	28.076592
2.0	3.165284	3.280013	3.741442	84.165498
3.0	4.783839	5.414862	7.130536	507.581094
4.0	6.649882	8.192728	9.191598	787.933125
5.0	6.396080	7.888404	10.487765	792.267422
6.0	6.365624	7.886580	10.487621	801.191719
7.0	6.350016	7.885804	10.486644	802.136094
8.0	6.340328	7.885294	10.485490	802.151719
9.0	6.333610	7.884893	10.484285	802.067500
10.0	6.328617	7.884540	10.483065	801.973750

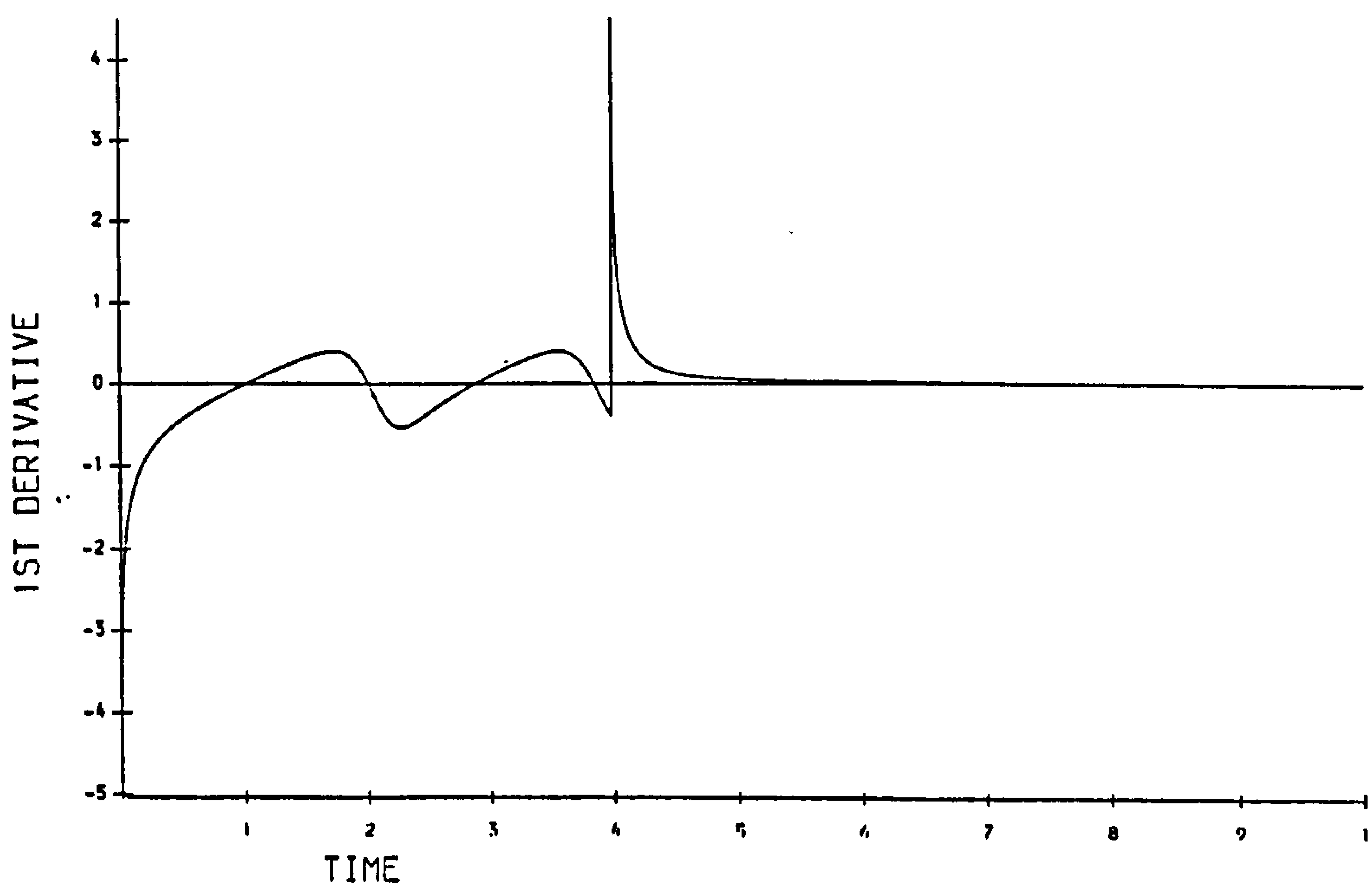

Figure 7.21: Short Impulse. Variation in the first derivative $U_x(0, t)$ at the origin. Forced conditions (7.39) with $U_0 = 1, \tau = 0.01, t_0 = 4, h = 0.04, \Delta t = 0.001$.

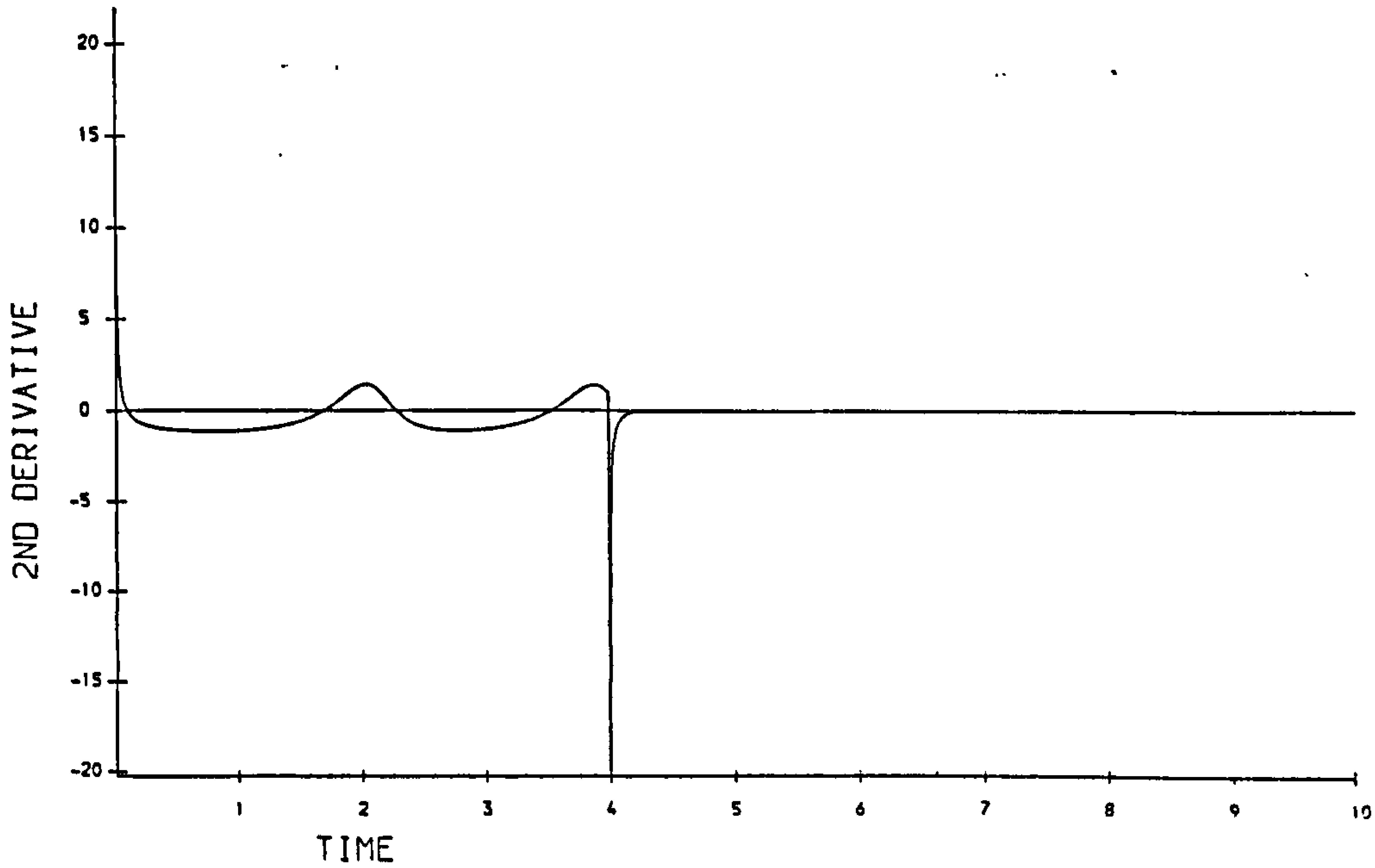

Figure 7.22: Short Impulse. Variation in the second derivative $U_{xx}(0,t)$ at the origin. Forced conditions (7.39) with $U_0 = 1, \tau = 0.01, t_0 = 4, h = 0.04, \Delta t = 0.001$.

$t = 2.9$ just as a second solitary wave is about to be generated see Figure (7.19) and when the initial solitary wave has grown to an amplitude of 2.1157. The single wave continues to develop, as expected from the above analysis, reaching an amplitude of 2.150 at $t = 3.4$ and eventually achieving, at about $t \sim 6$, an amplitude of 2.155 with velocity 4.64. These latter values are identical with those obtained for the initial solitary wave when forcing is continued throughout the experiment Table (7.4).

ii-) An experiment with increased forcing, $U_0 = 2.0$; boundary condition (7.39) is used with $x_{max} = 24, t_{max} = 1.5, \tau = 0.1, t_0 = 1.5$ so that the forcing again lasts throughout the experiment. The numerical step lengths are $h = 0.02$ and $\Delta t = 0.0005$.

In this numerical experiment, see Figure (7.23) five solitary waves are generated before the simulation is terminated at $t = 80$. Figures (7.24) and (7.25) show that four achieve their terminal heights and a constant velocity.

The generating conditions for the first wave are rather more protracted

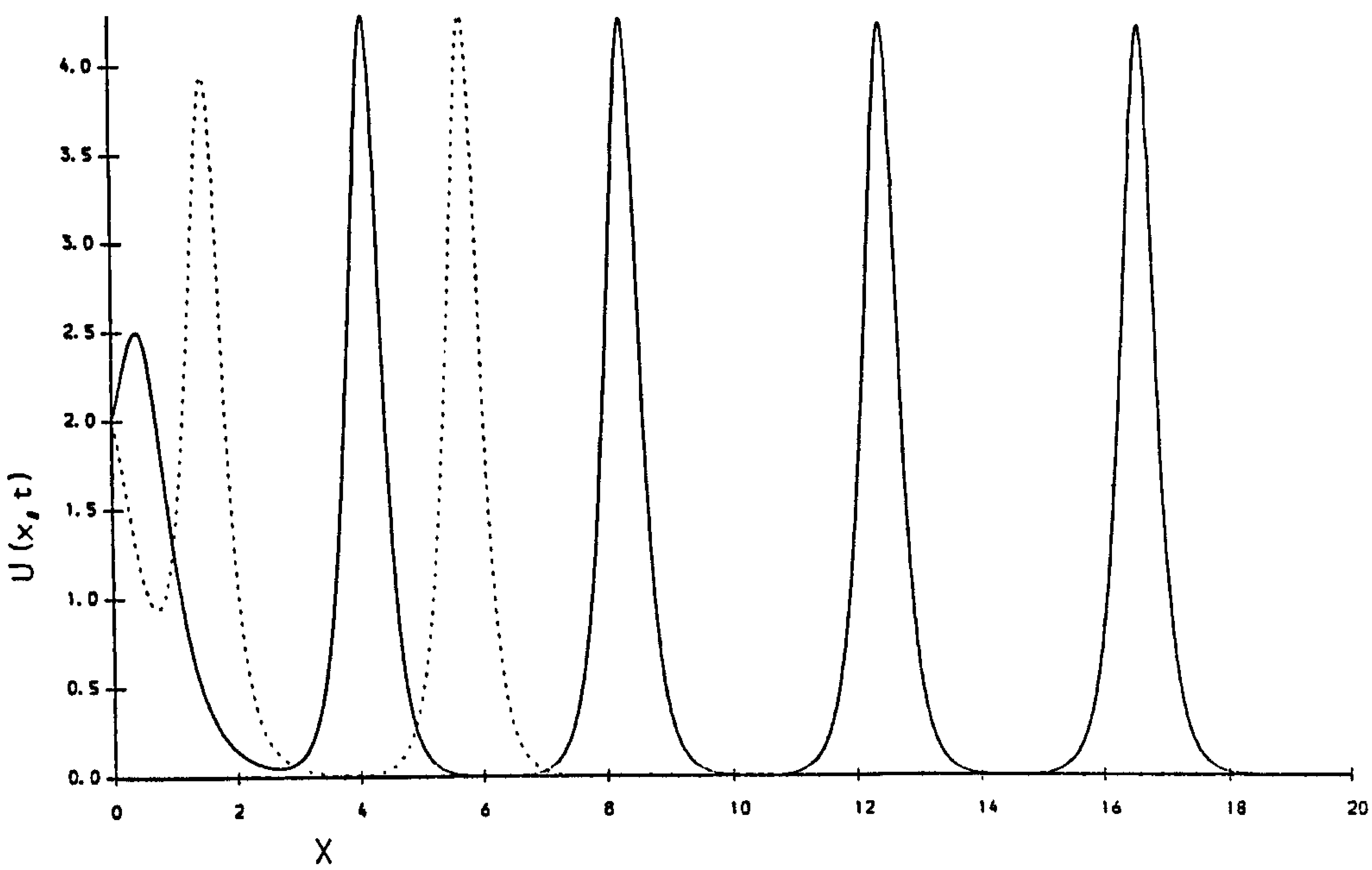

Figure 7.23: Long Impulse. Soliton produced by forced conditions (7.39) with $U_0 = 2, \tau = 0.1, t_0 = 1.5, h = 0.02, \Delta t = 0.0005$ graphed at $t = 0.6$ (- - - -) and $t = 1.2$ (———)

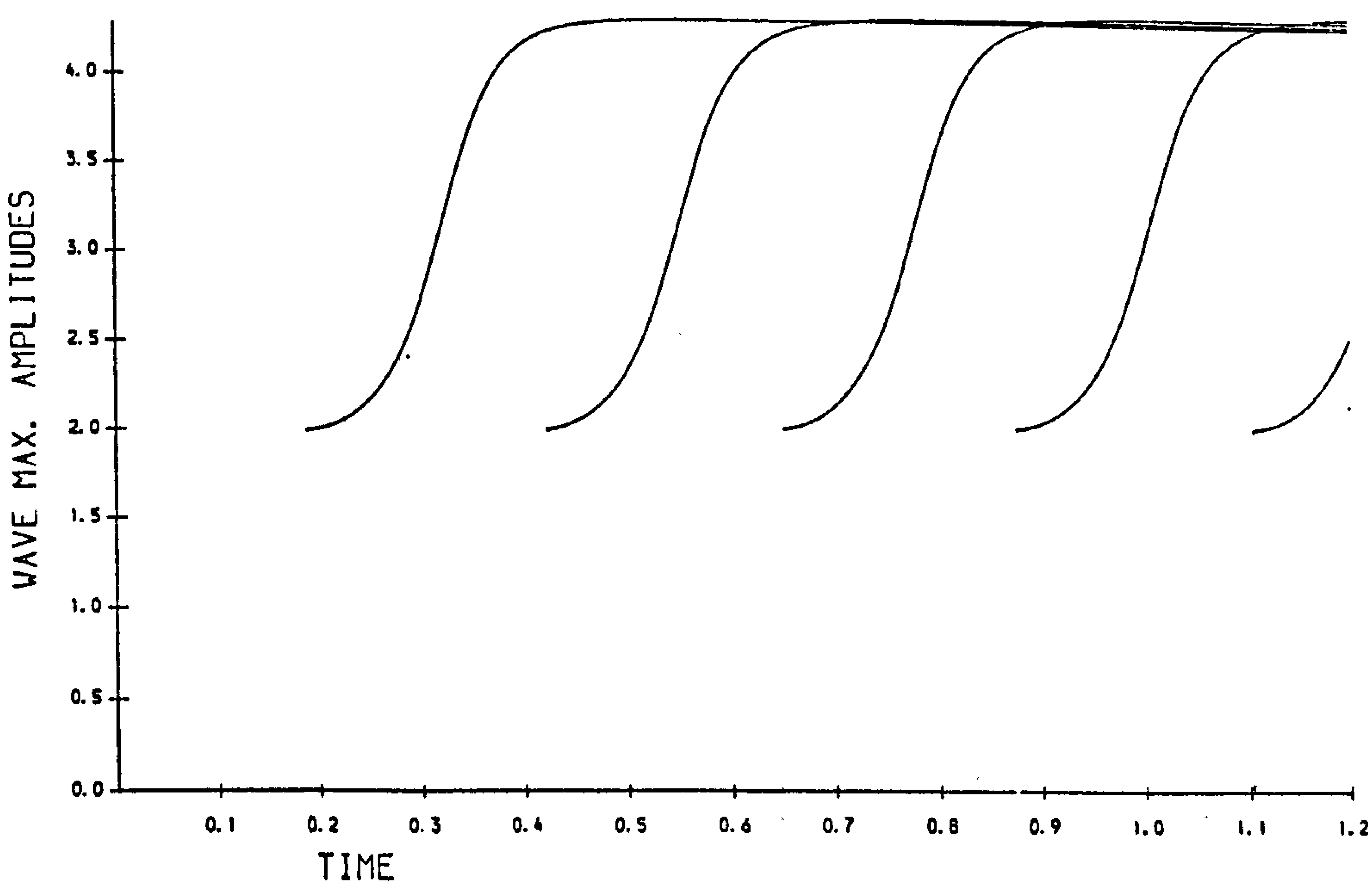

Figure 7.24: Long Impulse. The evolution of the soliton amplitudes. Forced conditions (7.39) with $U_0 = 2, \tau = 0.1, t_0 = 1.5, h = 0.02, \Delta t = 0.0005$.

Table 7.11: Observation of solitary waves, $U_0 = 2, \epsilon = 6$

wave	birth time	generated waves		free soliton
		amplitude	velocity	velocity
1	0.186	4.2901	17.9591	18.4049
2	0.419	4.2833	18.3673	18.3466
3	0.648	4.2837	18.3673	18.3500
4	0.876	4.2850	18.3673	18.3612
5	1.105	2.5035		6.2675

Table 7.12: Bounded forced conditions with $t_0 = 0.1, U_0 = 2, \epsilon = 6$

time	I_1	I_2	I_3	I_4
0.00	0.000000	0.000000	0.000000	0.000000
0.12	1.033281	1.217271	-0.803679	1112.995469
0.24	1.975694	2.974708	6.746223	1016.074297
0.36	4.219995	9.754190	52.380298	10195.346250
0.48	5.259604	11.887833	61.315830	17081.016250
0.60	7.468723	18.520735	105.596367	27605.300000
0.72	8.557607	20.842419	115.209727	33107.910000
0.84	10.699584	27.209331	157.655732	44739.350000
0.96	11.877983	29.865403	169.068867	48956.595000
1.08	13.919520	35.830264	208.728691	61352.285000
1.20	15.228695	38.994795	223.457422	64666.175000

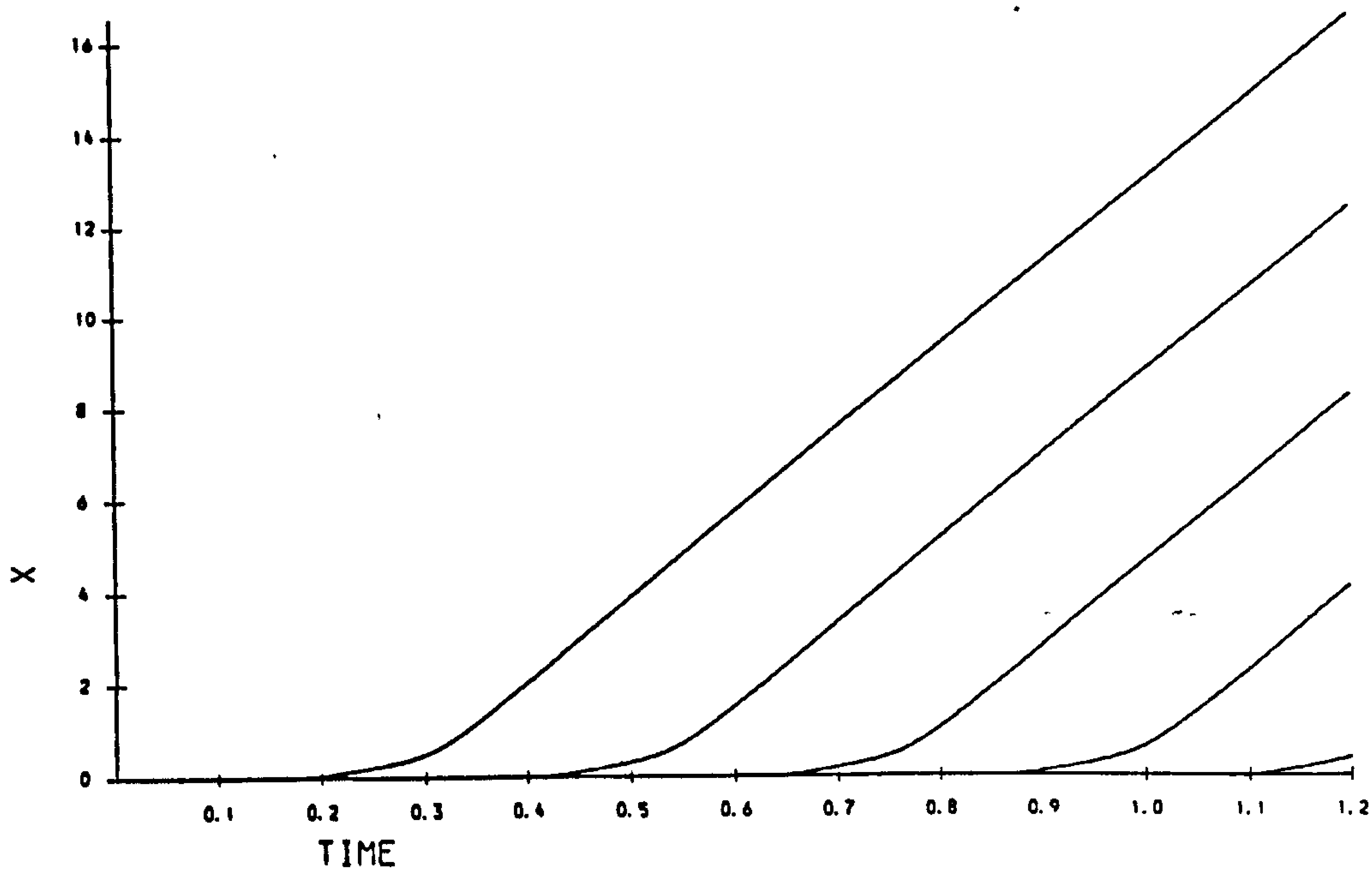

Figure 7.25: Long Impulse. The space-time graphs of the soliton produced by forced conditions (7.39) with $U_0 = 2, \tau = 0.1, t_0 = 1.5, h = 0.02, \Delta t = 0.0005$.

than those for all subsequent waves, as can be seen from the graphs of the first three derivatives at $x = 0$ given in Figures (7.26-7.28) so it achieves a slightly larger amplitude and velocity than do the following waves. The observation on the solitary waves generated are collected in Table (7.11). The time interval between births of solitary waves is constant at $\Delta T_B = 0.228$. the measured terminal heights for solitary waves 2-4 vary between 4.2833 and 4.2850 with measured velocities of 18.3673. Free solitons of similar heights would have velocities 18.3466 - 18.3612, so that agreement is close. After an initial transient the graph of $U_x(0,t)$, Figure(7.26), shows a rounded saw tooth periodic behaviour with maximum of about 0.1, minimum of about -0.1 mean zero and period 0.228. The graphs of $U_{xx}(0,t)$ and $U_{xxx}(0,t)$, Figures(7.27-7.28), also exhibit periodic behavior with period 0.228. All the above conclusions are illustrated by measured values of the quantities given in Table (7.12)

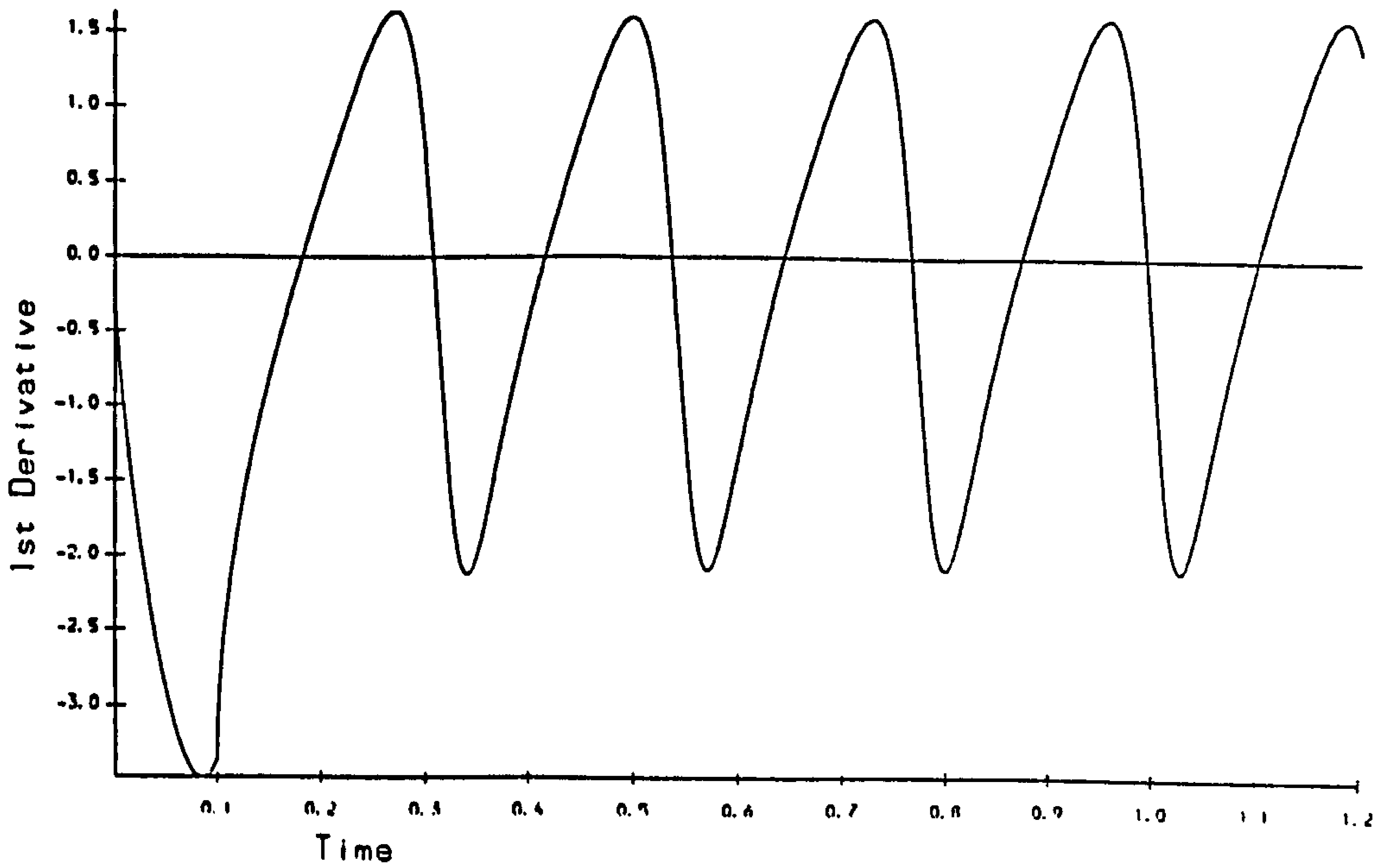

Figure 7.26: Long Impulse. Variation in the first derivative $U_x(0, t)$ at the origin. Forced conditions (7.39) with $U_0 = 2, \tau = 0.1, t_0 = 1.5, h = 0.02, \Delta t = 0.0005$.

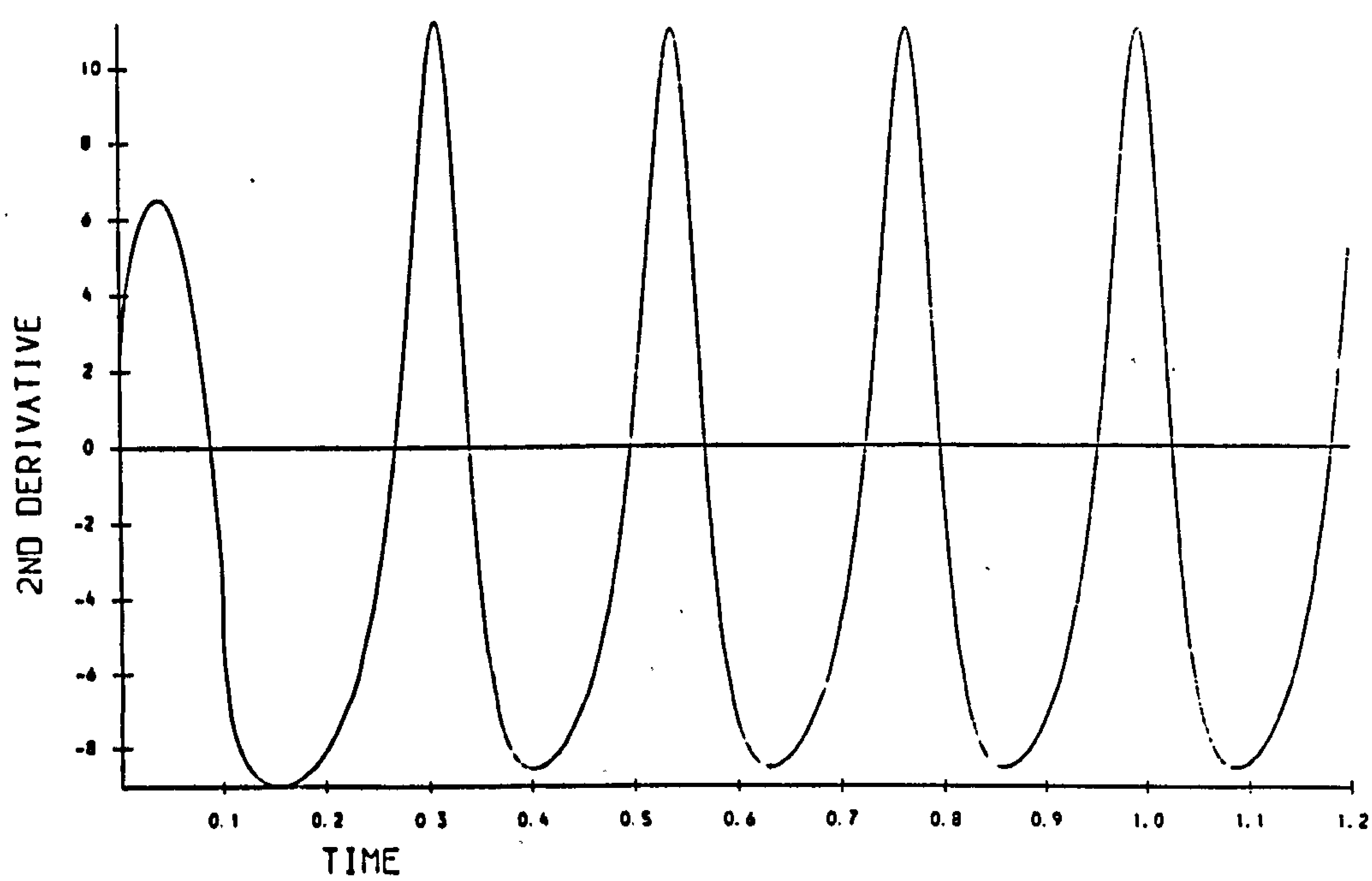

Figure 7.27: Long Impulse. Variation in the second derivative $U_{xx}(0,t)$ at the origin. Forced conditions (7.39) with $U_0 = 2, \tau = 0.1, t_0 = 1.5, h = 0.02$, $\Delta t = 0.0005$.

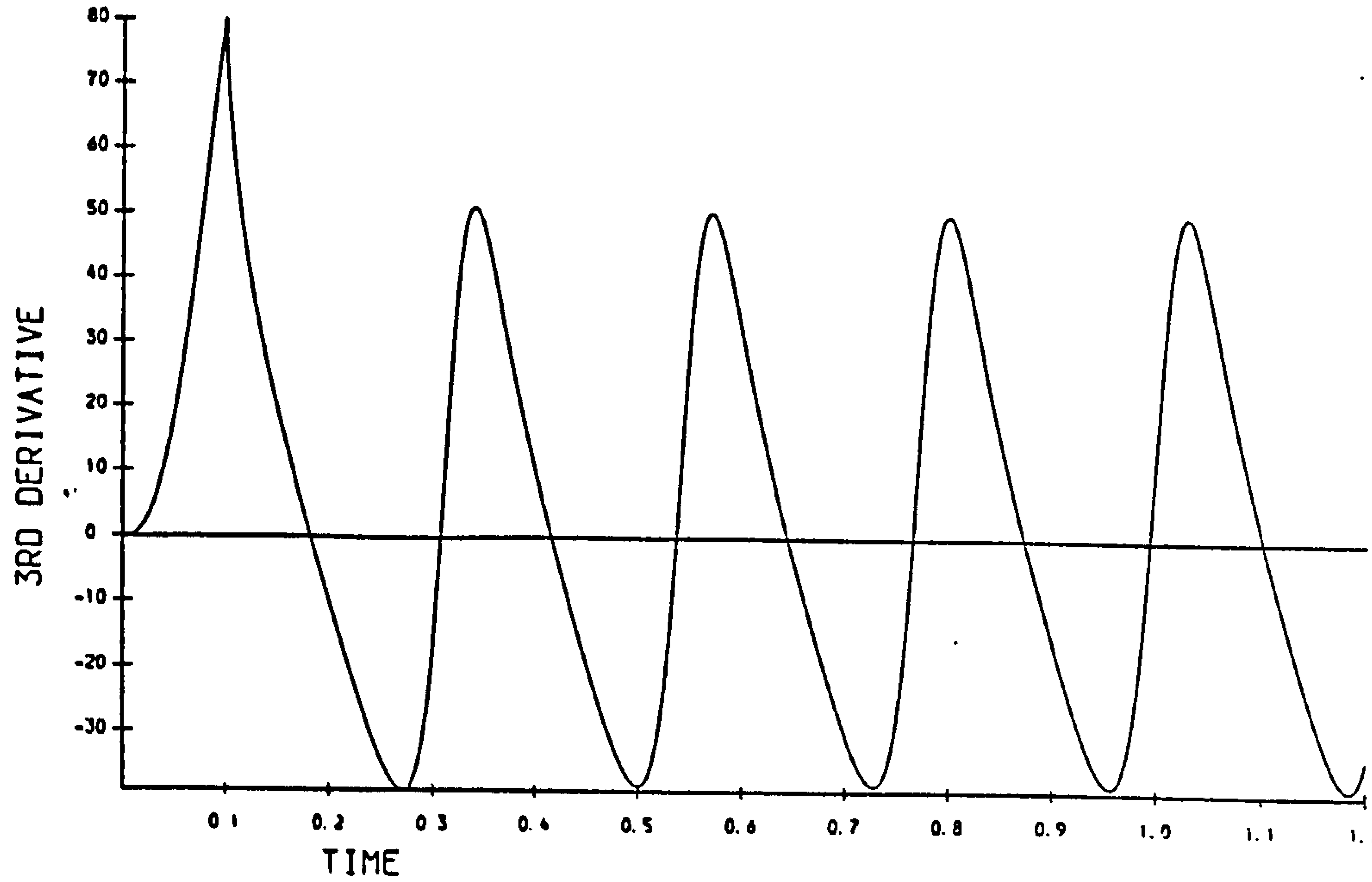

Figure 7.28: Long Impulse. Variation in the third derivative $U_{xxx}(0,t)$ at the origin. Forced conditions (7.39) with $U_0 = 2, \tau = 0.1, t_0 = 1.5, h = 0.02$, $\Delta t = 0.0005$.

7.2.2 Positive forcing Series B

In a second series of experiments $\epsilon = 3, \mu = 1$ so that $p = 1.4142$

Long Impulse

i-) Firstly boundary condition (7.39) is used with $x_{max} = 80$, $t_{max} = 30, U_0 = 1, \tau = 0.01, t_0 = 30$ that the forcing lasts throughout the experiment. The step lengths are $h = 0.04$ and $\Delta t = 0.001$. In this numerical experiment, see Figure (7.29), six solitary waves are generated before the simulation is terminated at $t = 30$. Figures (7.30) and (7.31) show that four achieve their terminal heights and a constant velocity. The generating conditions for the first wave are again slightly different so it attains a slightly larger amplitude and velocity than do subsequent waves. The observations are collected in Table (7.13). The time interval between births of solitary waves is constant at $\Delta T_B = 5.15$. The measured terminal heights for solitary

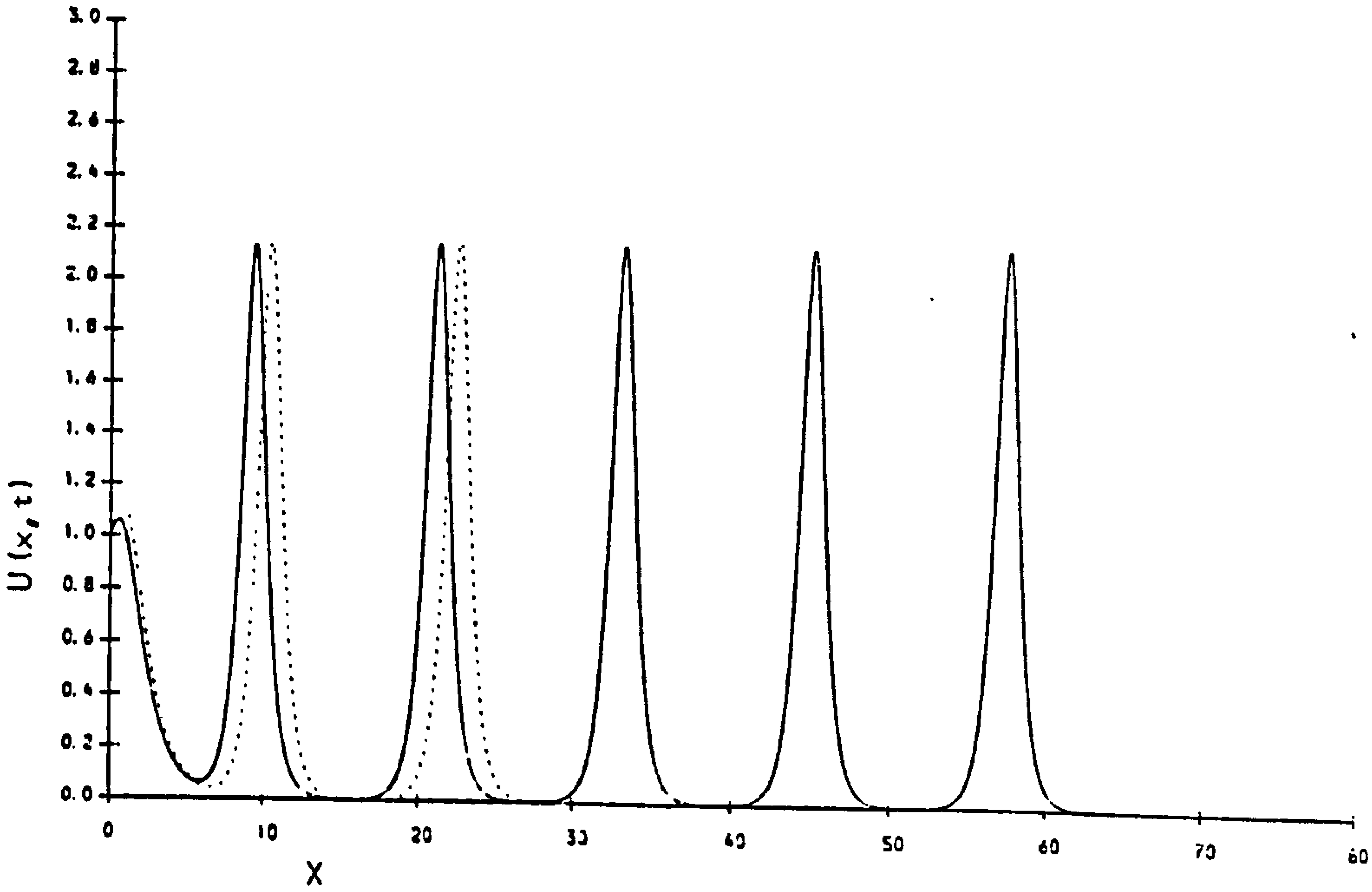

Figure 7.29: Long Impulse. Soliton produced by forced conditions (7.39) with $U_0 = 1, \tau = 0.01, t_0 = \infty, h = 0.04, \Delta t = 0.01$. graphed at $t = 15$ (- - - -) and $t = 30$ (——-). $\epsilon = 3$.

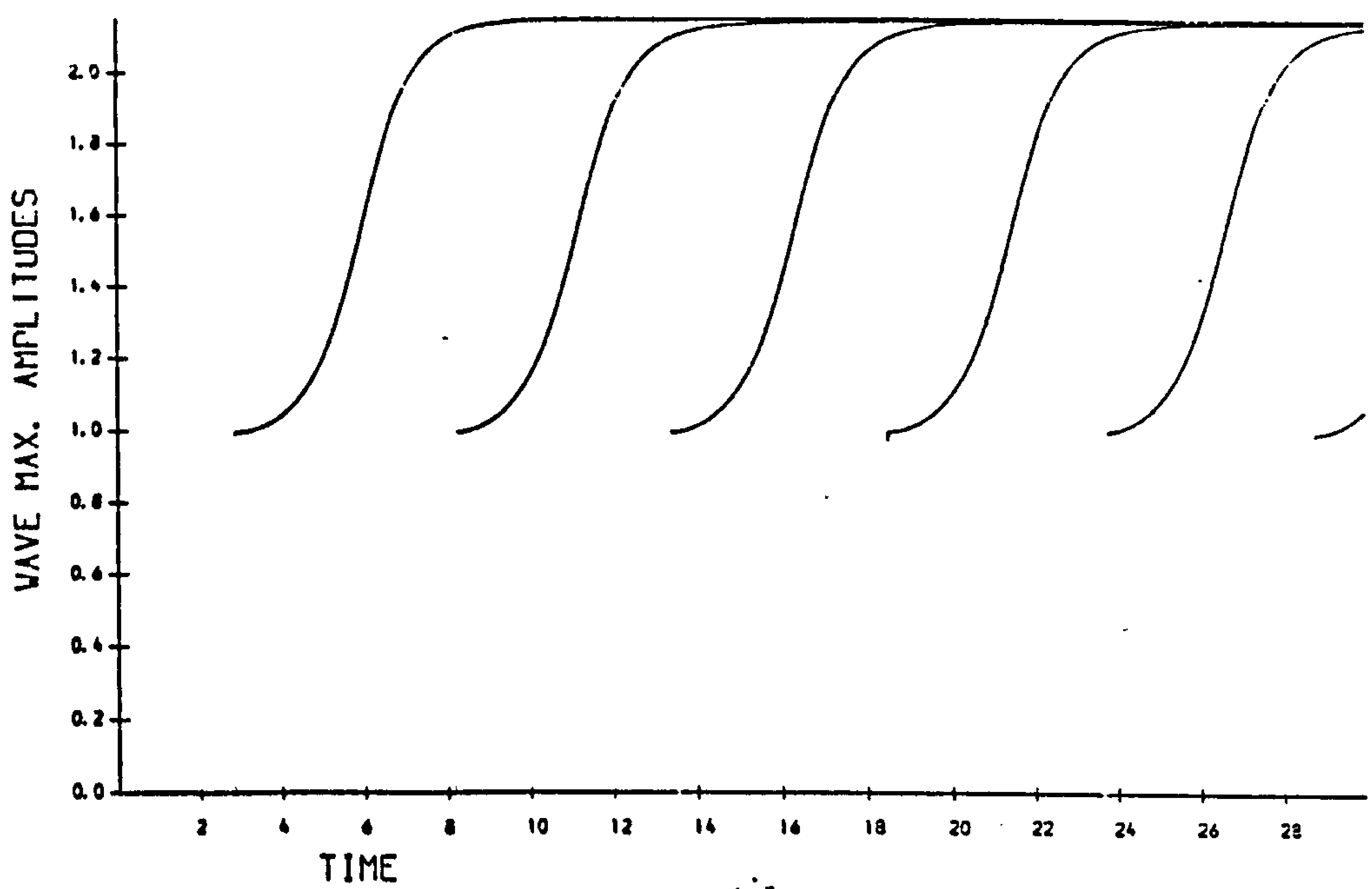

Figure 7.30: Long Impulse. The evolution of the soliton amplitudes. Forced conditions (7.39) with $U_0 = 1, \tau = 0.01, t_0 = \infty$, $h = 0.04, \Delta t = 0.001$. $\epsilon = 3$.

Table 7.13: Observation of solitary waves, $U_0 = 1, \epsilon = 3$

wave	birth time	generated waves		free soliton
		amplitude	velocity	velocity
1	2.84	2.55	2.32	2.322
2	8.14	2.147	2.31	2.305
3	13.30	2.147	2.30	2.305
4	18.49	2.147	2.30	2.305
5	23.60	2.137	2.28	2.283

waves 2-4 vary between 2.147 and 2.148 with measured velocities of 2.31. Free solitons of similar heights would also have velocities 2.31.

After an initial transient the graph of $U_x(0,t)$, Figure (7.32) , shows a rounded saw tooth periodic behaviour with maximum of about 0.5, minimum of about -0.5, mean zero and period 5.15. The graphs of $U_{xx}(0,t)$ and $U_{xxx}(0,t)$, Figures (7.33-7.34) , also exhibit periodic behaviour with period 5.15. By comparing Figures (7.30), (7.32) and (7.33) we observe that the birth of a solitary wave occurs at times when $U_x(0,t) = 0$ and $U_{xx}(0,t)$ is a minimum and negative while a solitary wave reaches maturity about $1\frac{1}{2}$ periods later when again $U_x(0,t) = 0$, but $U_{xx}(0,t)$ is a maximum and positive in agreement with Series A simulations.

ii-) In a second experiment with reduced forcing, $U_o = 0.5$, boundary condition (7.39) is used with $x_{max} = 80, t_{max} = 170, \tau = 0.01, t_o = 170$. The forcing lasts throughout the experiment. The numerical step lengths are $h =$ 0.01 and $\Delta t = 0.001$. In this numerical experiment, see Figure (7.35), four solitary waves are generated before the simulation is terminated at $t = 170$. Figures (7.36) and (7.37) show that three achieve their terminal heights and

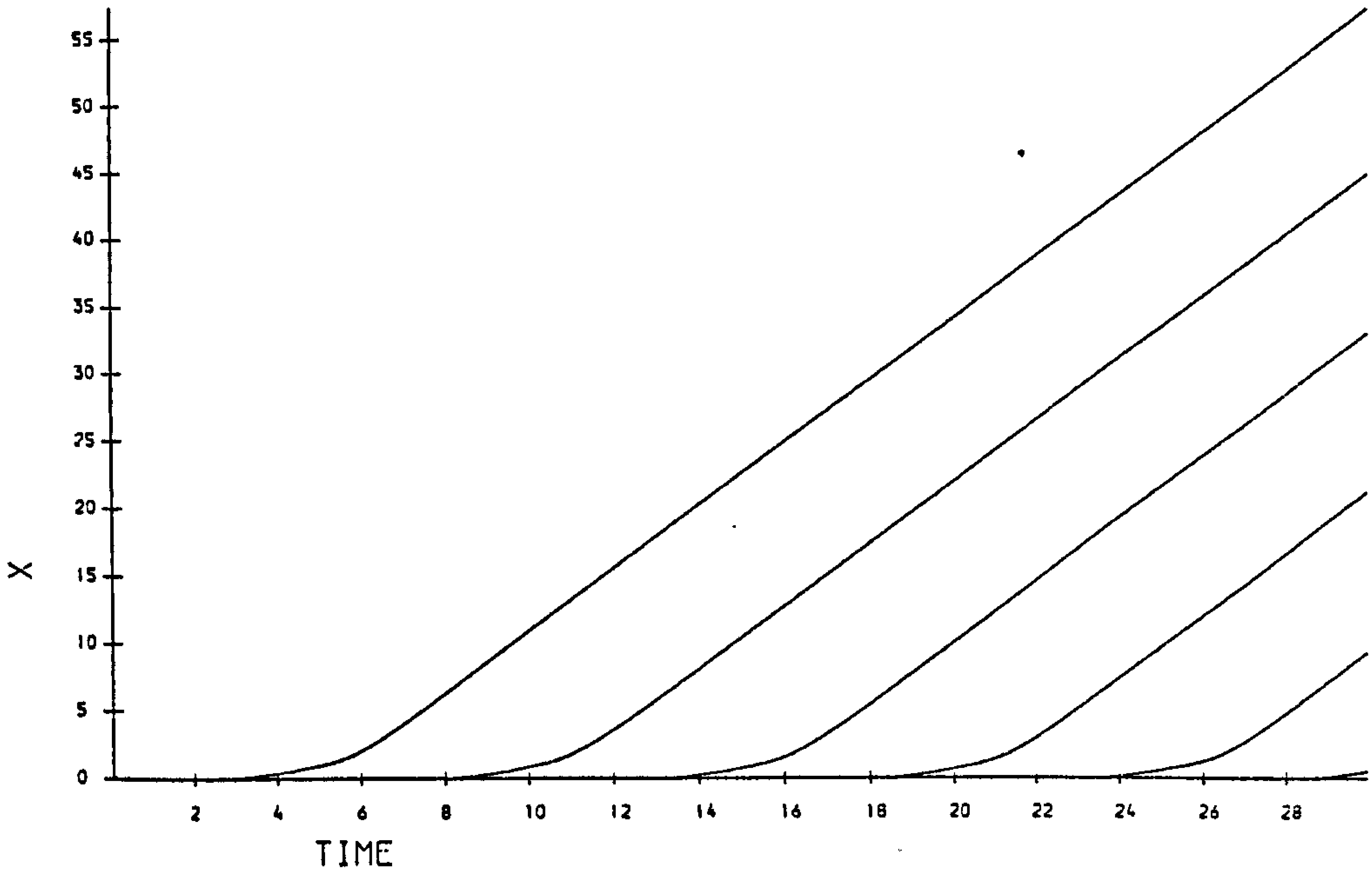

Figure 7.31: Long Impulse. The space-time graphs of the solitons produced by (7.39) with $U_0 = 1, \tau = 0.01, t_0 = \infty, h = 0.04, \Delta t = 0.001$. $\epsilon = 3$.

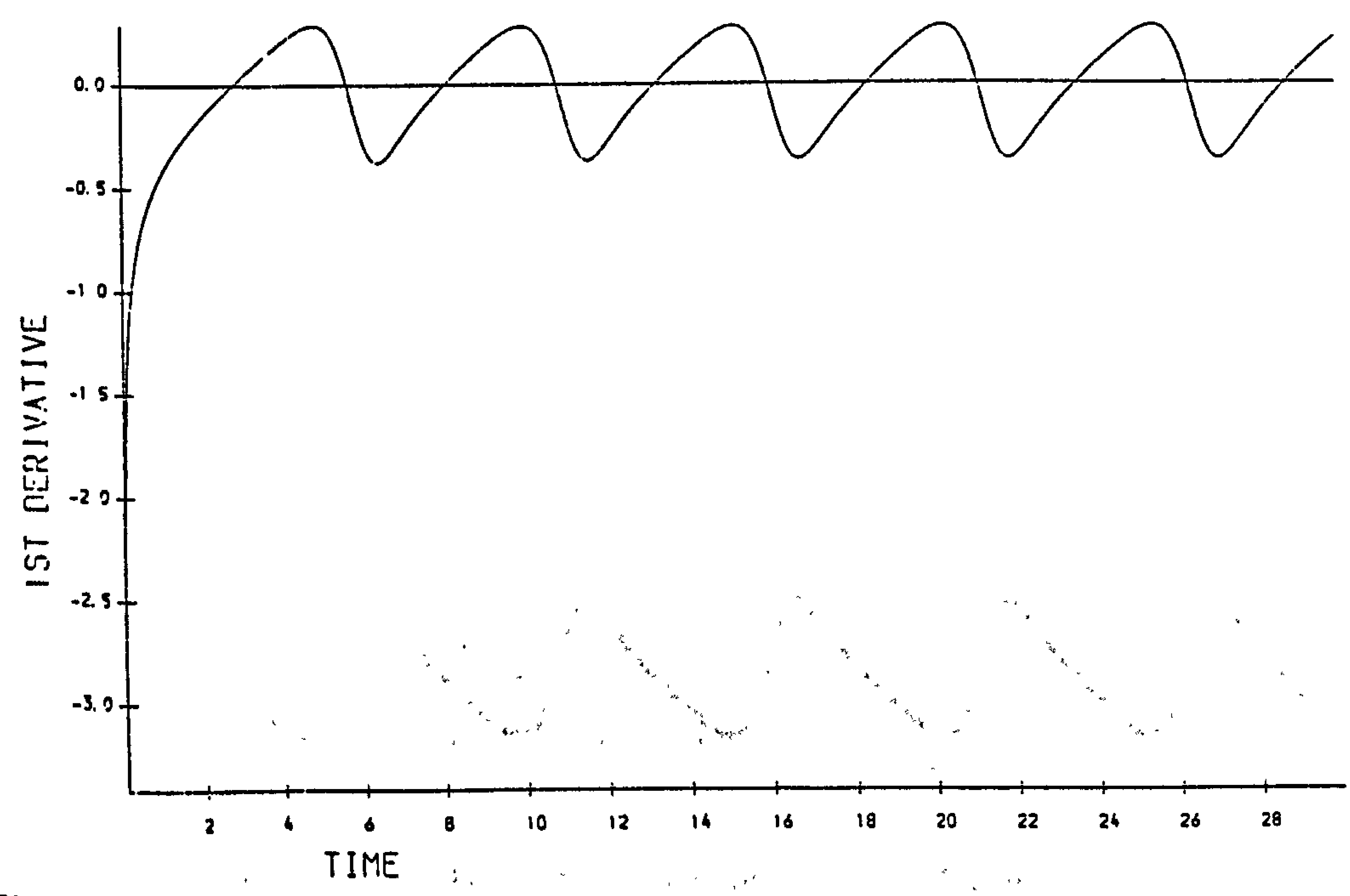

Figure 7.32: Long Impulse. Variation in the first derivative $U_x(0,t)$ at the origin. Forced conditions (7.39) with $U_0 = 1, \tau = 0.01, t_0 = \infty, h = 0.04, \Delta t = 0.001$. $\epsilon = 3$.

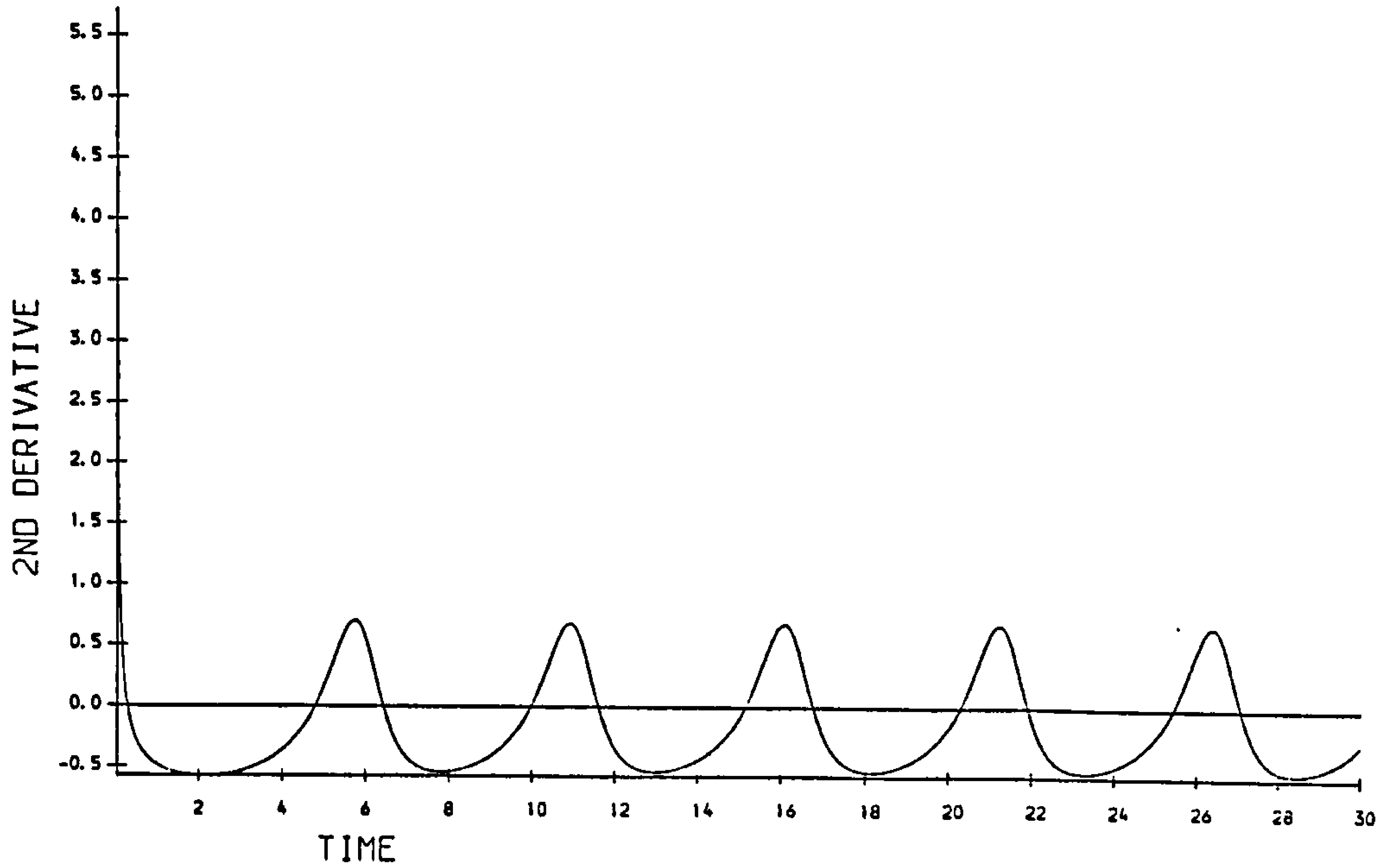

Figure 7.33: Long Impulse. Variation in the second derivative $U_{xx}(0,t)$ at the origin. Forced conditions (7.39) with $U_0 = 1, \tau = 0.01, t_0 = \infty, h = 0.04, \Delta t = 0.001$. $\epsilon = 3$.

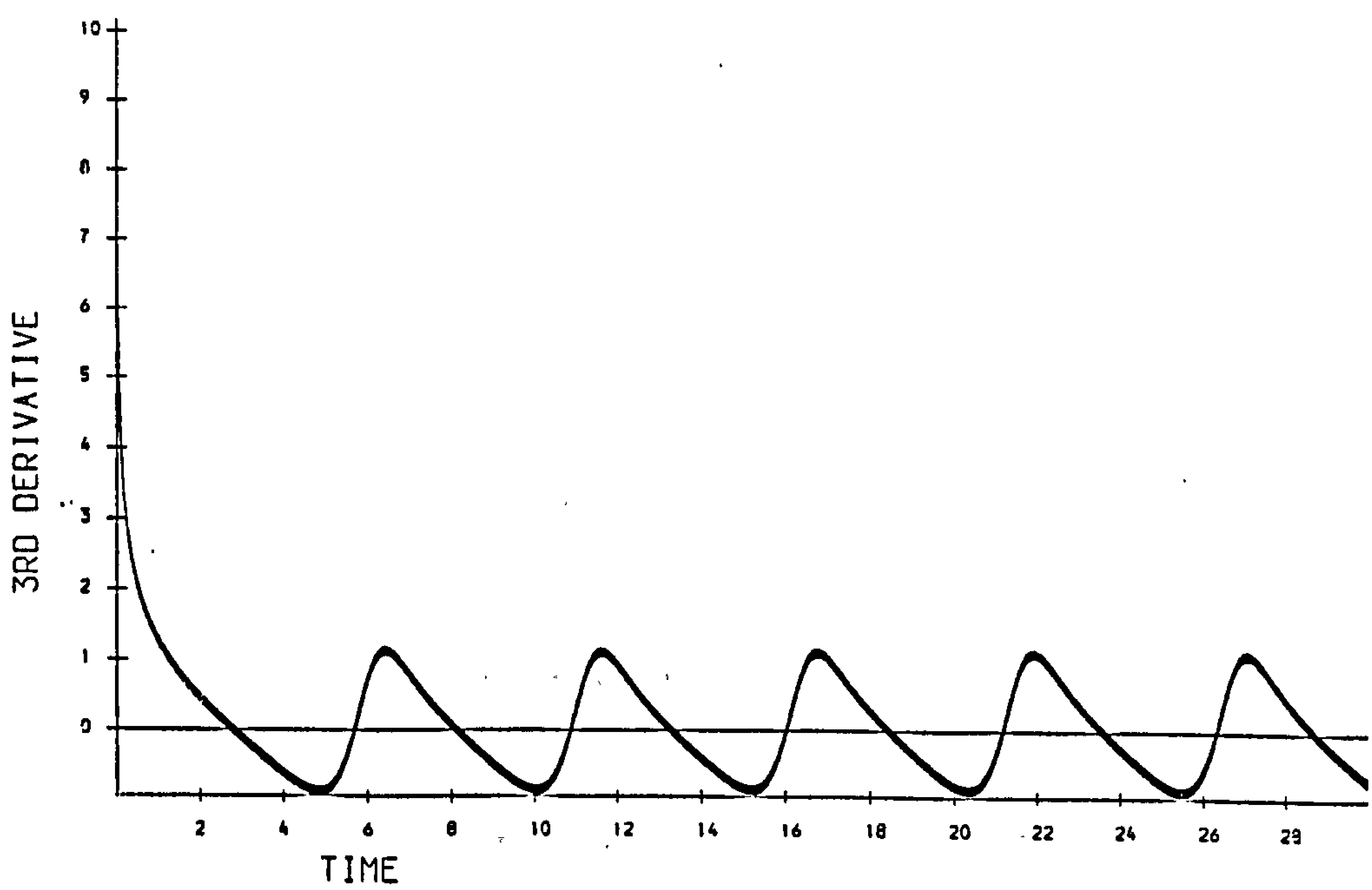

Figure 7.34: Long Impulse. Variation in the third derivative $U_{xxx}(0,t)$ at the origin. Forced conditions (7.39) with $U_0 = 1, \tau = 0.01, t_0 = \infty, h = 0.04, \Delta t = 0.001$. $\epsilon = 3$.

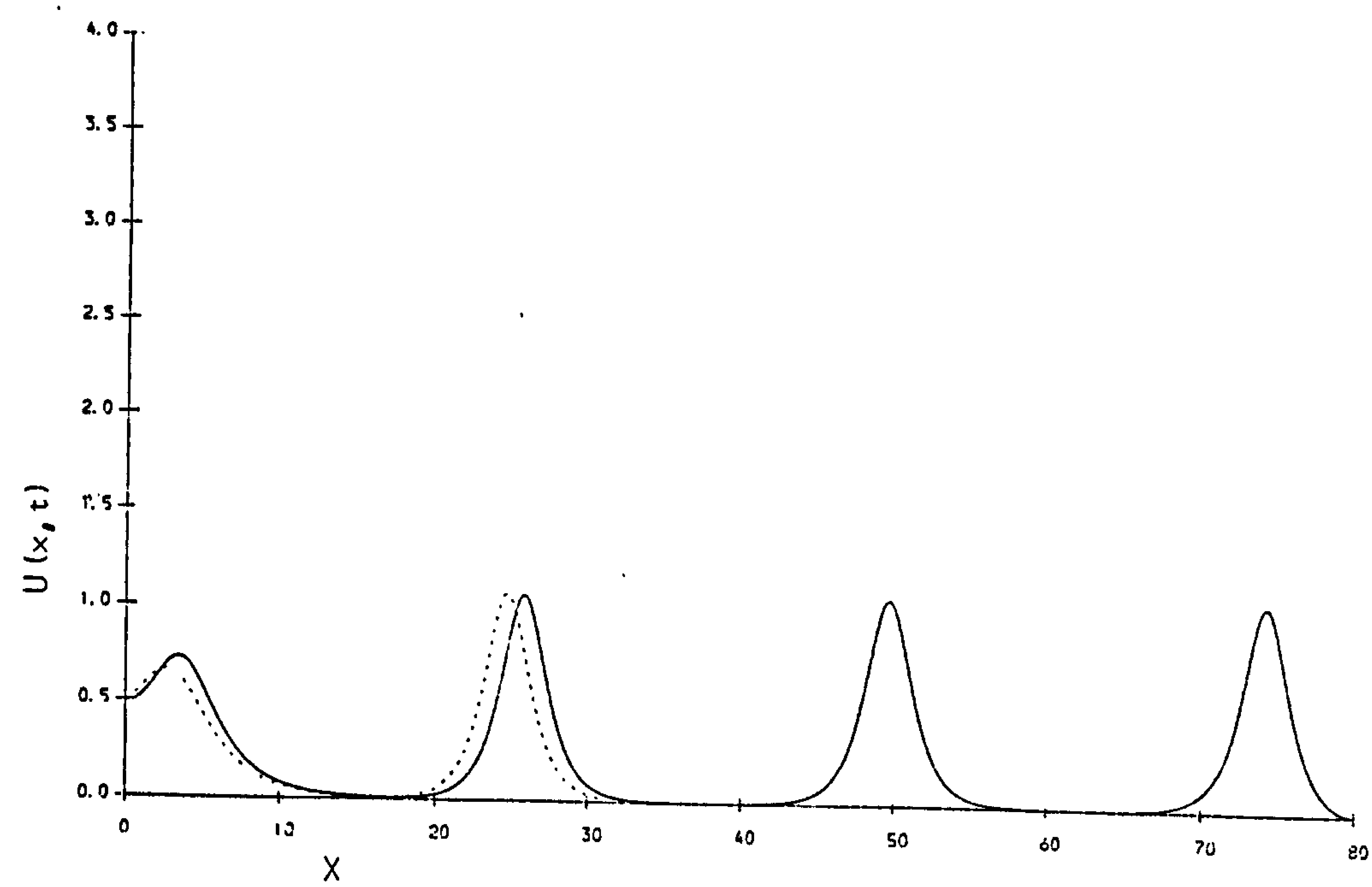

Figure 7.35: Long Impulse. Soliton produced by forced conditions (7.39) with $U_0 = 0.5, \tau = 0.01, t_0 = \infty, h = 0.04. \Delta t = 0.01$. graphed at $t = 85$ (- - - -) and $t = 170$ (——). $\epsilon = 3$.

a constant velocity. The generating conditions for the first wave are again slightly different so it attains a slightly larger amplitude and velocity than do subsequent waves. The observations are collected in Table (7.14). The time interval between births of solitary waves is constant at $\Delta T_B = 41.25$. The measured terminal heights for solitary waves 1-3 vary between 1.0784 and 1.0737 with measured velocities of 0.584. Free solitons of similar heights would also have velocities 0.5814-0.5764, so that agreement is close.

After an initial transient the graph of $U_x(0,t)$, Figure (7.38), shows a rounded saw tooth periodic behaviour with maximum of about 0.09, minimum of about -0.09, mean zero and period 41.25. The graphs of $U_{xx}(0,t)$ and $U_{xxx}(0,t)$, Figures (7.39-7.40), also exhibit periodic behaviour with period 41.25. By comparing Figures (7.36), (7.38) and (7.39) also exhibit periodic behaviour with period 41.25.

iii-) In a third experiment with increased forcing, $U_0 = 2$, boundary condition (7.39) is used with $x_{max} = 80, t_{max} = 4.5, \tau = 0.01, t_o = 4.5$. The

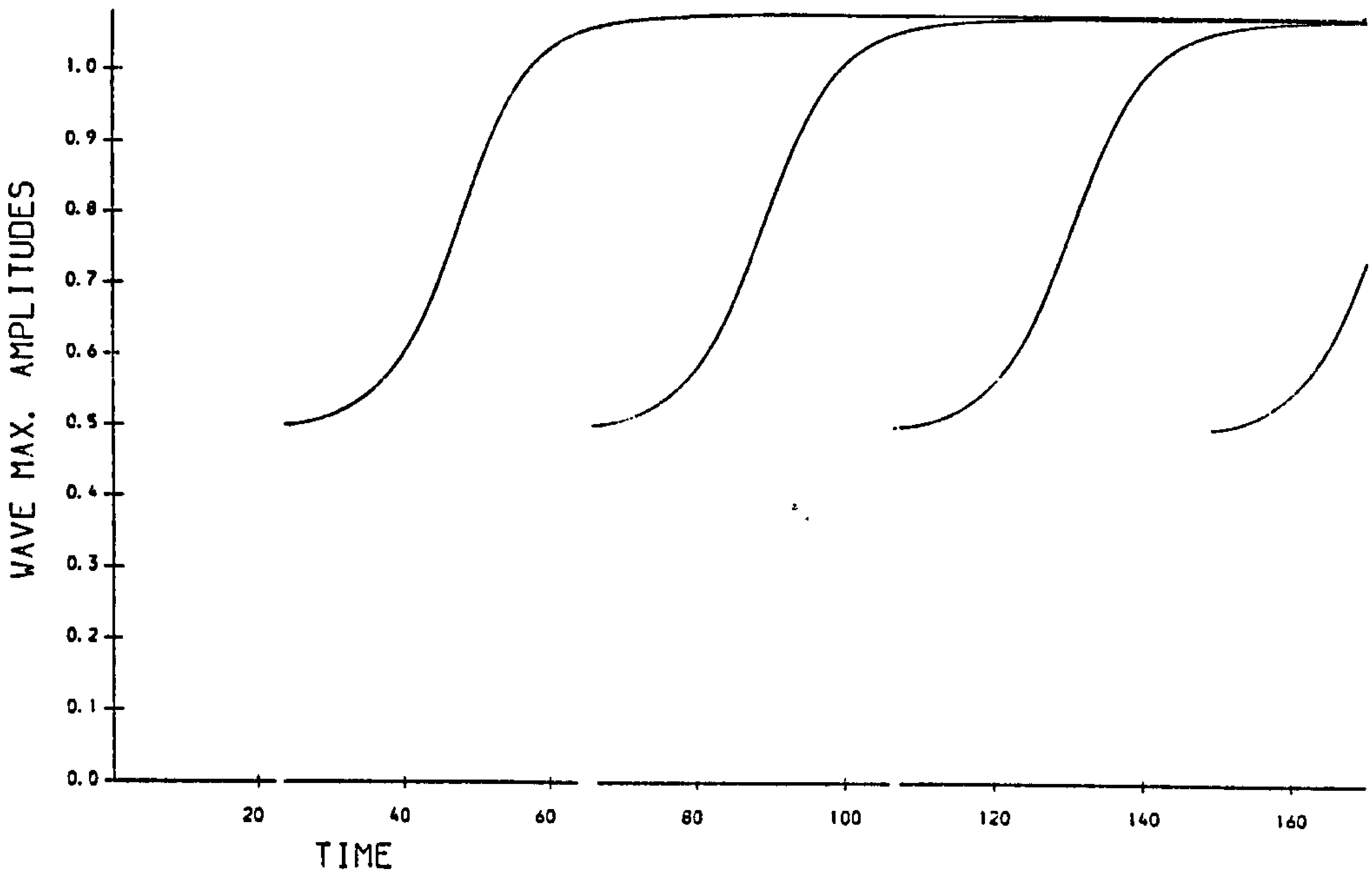

Figure 7.36: Long Impulse. The evolution of the soliton amplitudes. Forced conditions (7.39) with $U_0 = 0.5, \tau = 0.01, t_0 = \infty$, $h = 0.04, \Delta t = 0.001$. $\epsilon = 3$.

Table 7.14: Observation of solitary waves, $U_0 = 0.5, \epsilon = 3$

wave	birth time	generated waves		free soliton
		amplitude	velocity	velocity
1	22.779	1.0811	0.584	0.5814
2	65.256	1.0750	0.580	0.5778
3	106.713	1.0737	0.576	0.5764
4	147.982	0.7337	0.212	0.2691

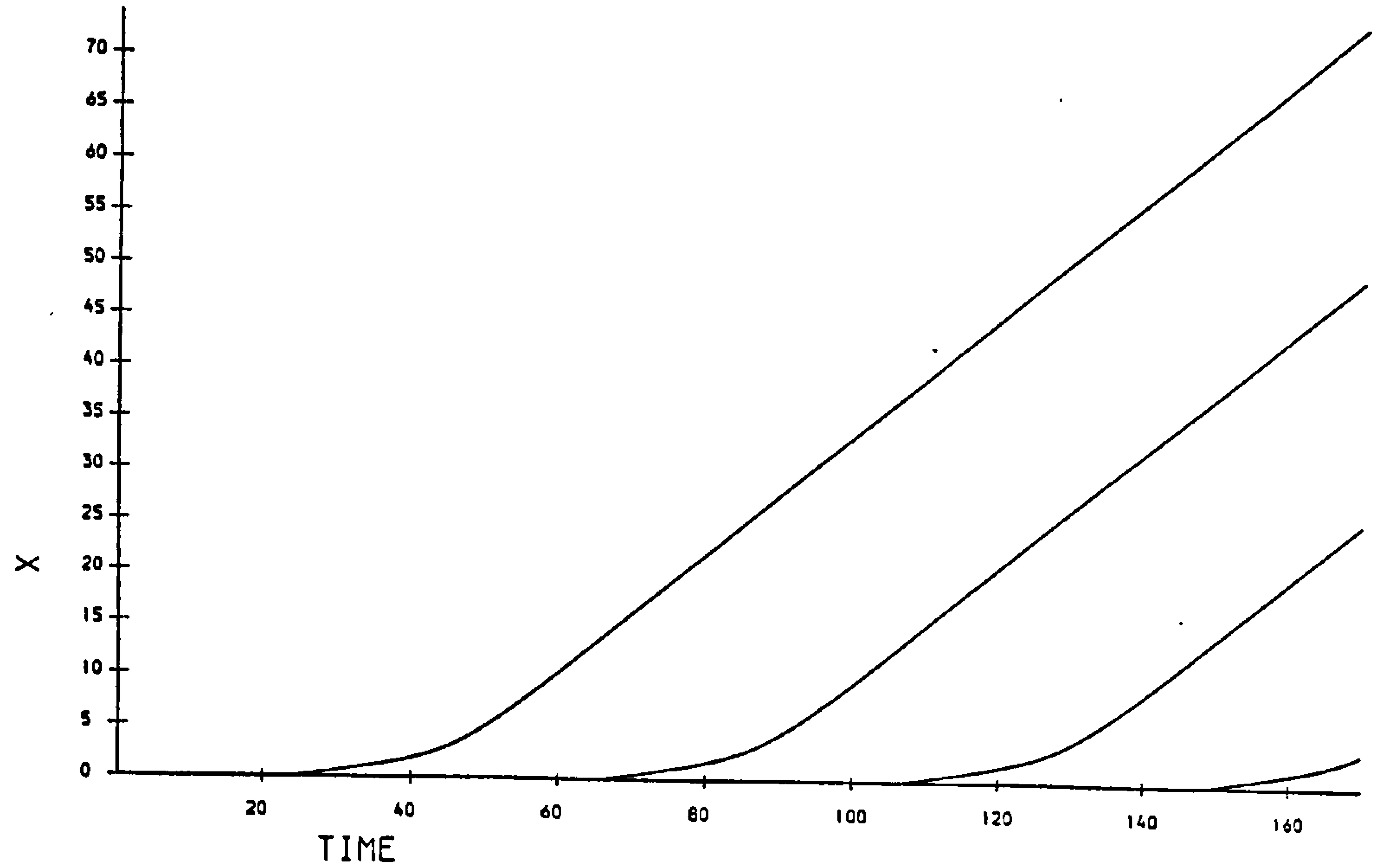

Figure 7.37: Long Impulse. The space-time graphs of the solitons produced by (7.39) with $U_0 = 0.5, \tau = 0.01, t_0 = \infty, h = 0.04, \Delta t = 0.001$. $\epsilon = 3$.

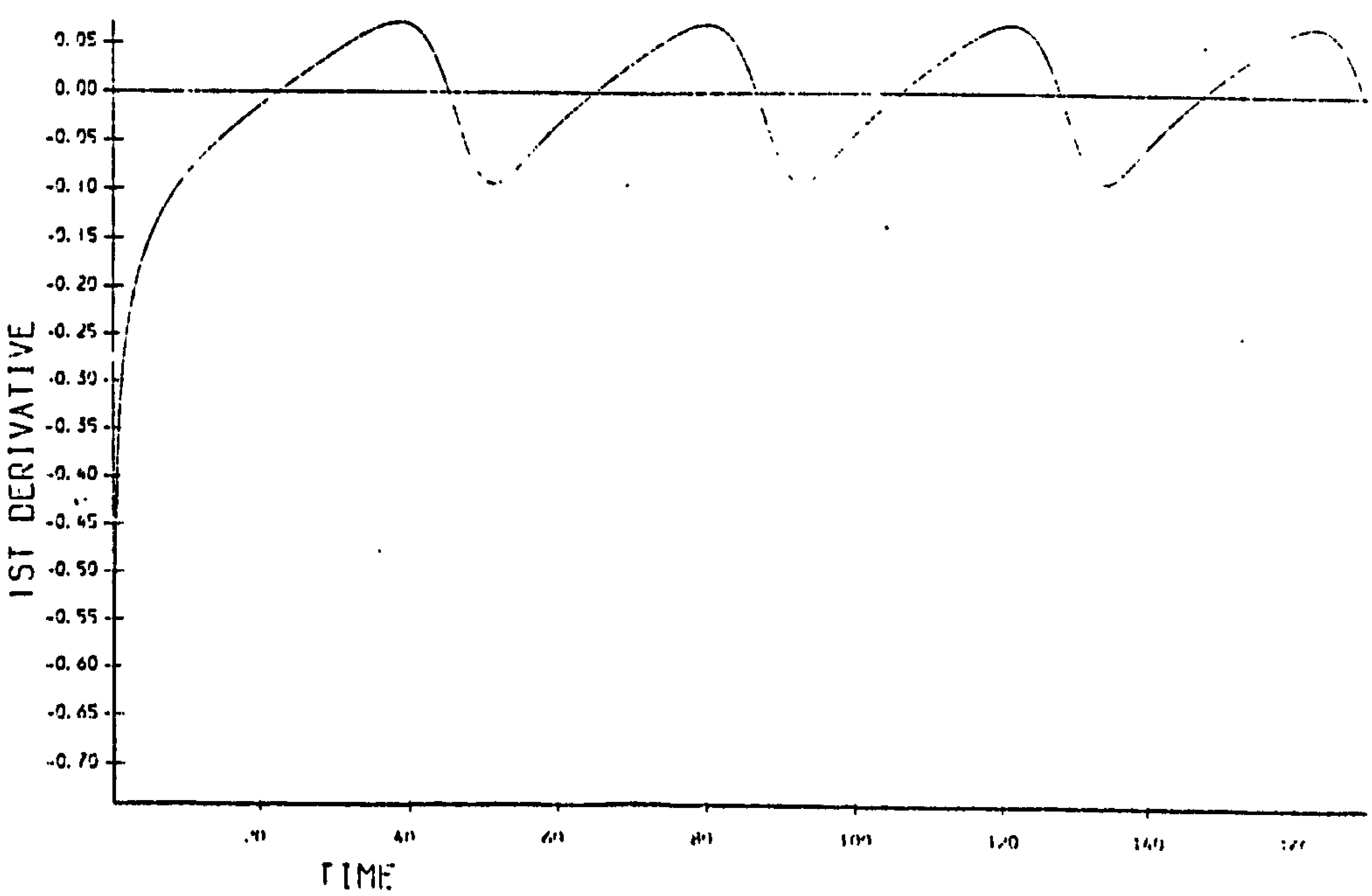

Figure 7.38: Long Impulse. Variation in the first derivative $U_x(0,t)$ at the origin. Forced conditions (7.39) with $U_0 = 0.5, \tau = 0.01, t_0 = \infty, h = 0.04, \Delta t = 0.001$. $\epsilon = 3$.

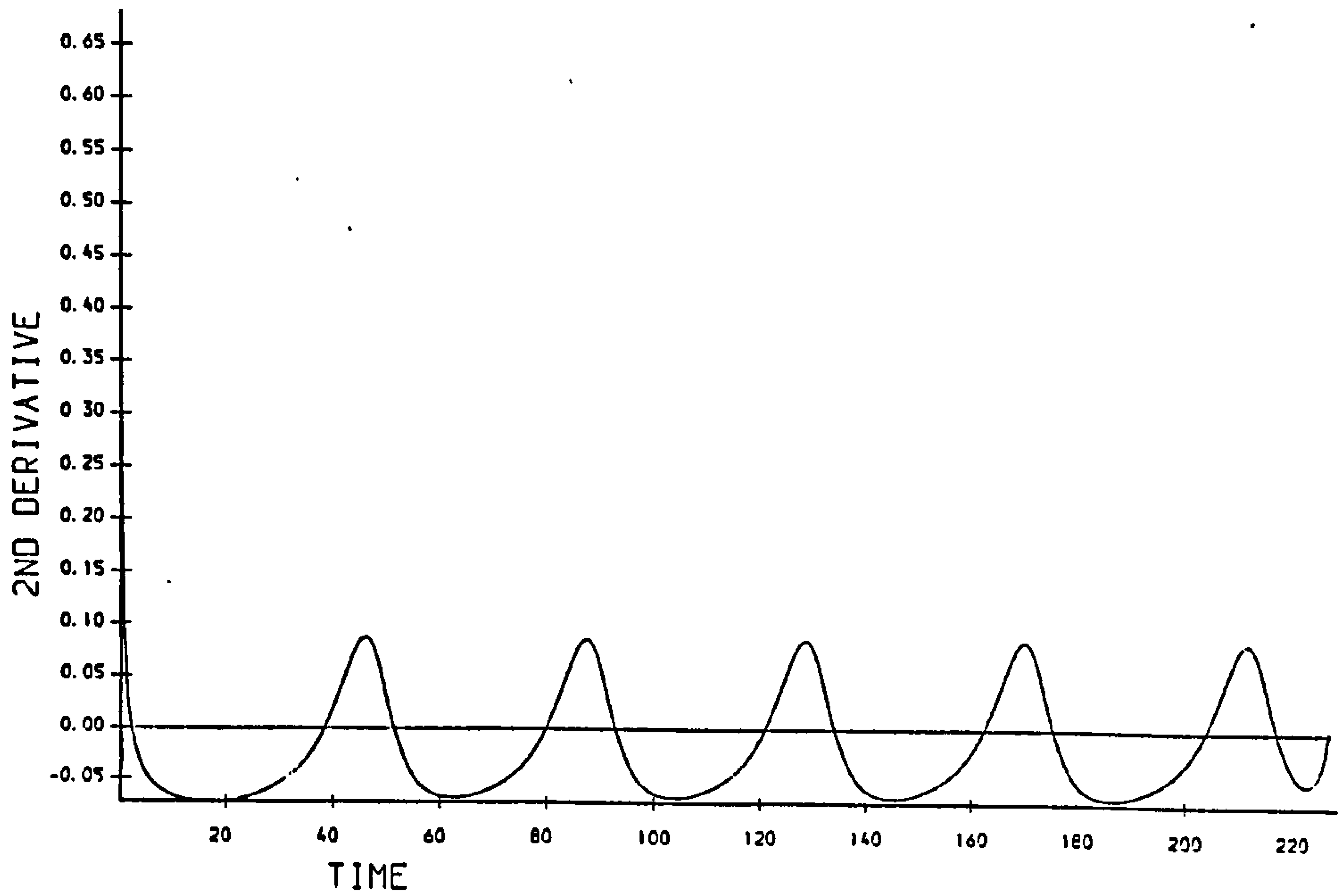

Figure 7.39: Long Impulse. Variation in the second derivative $U_{xx}(0,t)$ at the origin. Forced conditions (7.39) with $U_0 = 0.5, \tau = 0.01,\ t_0 = \infty, h = 0.04, \Delta t = 0.001.\ \epsilon = 3.$

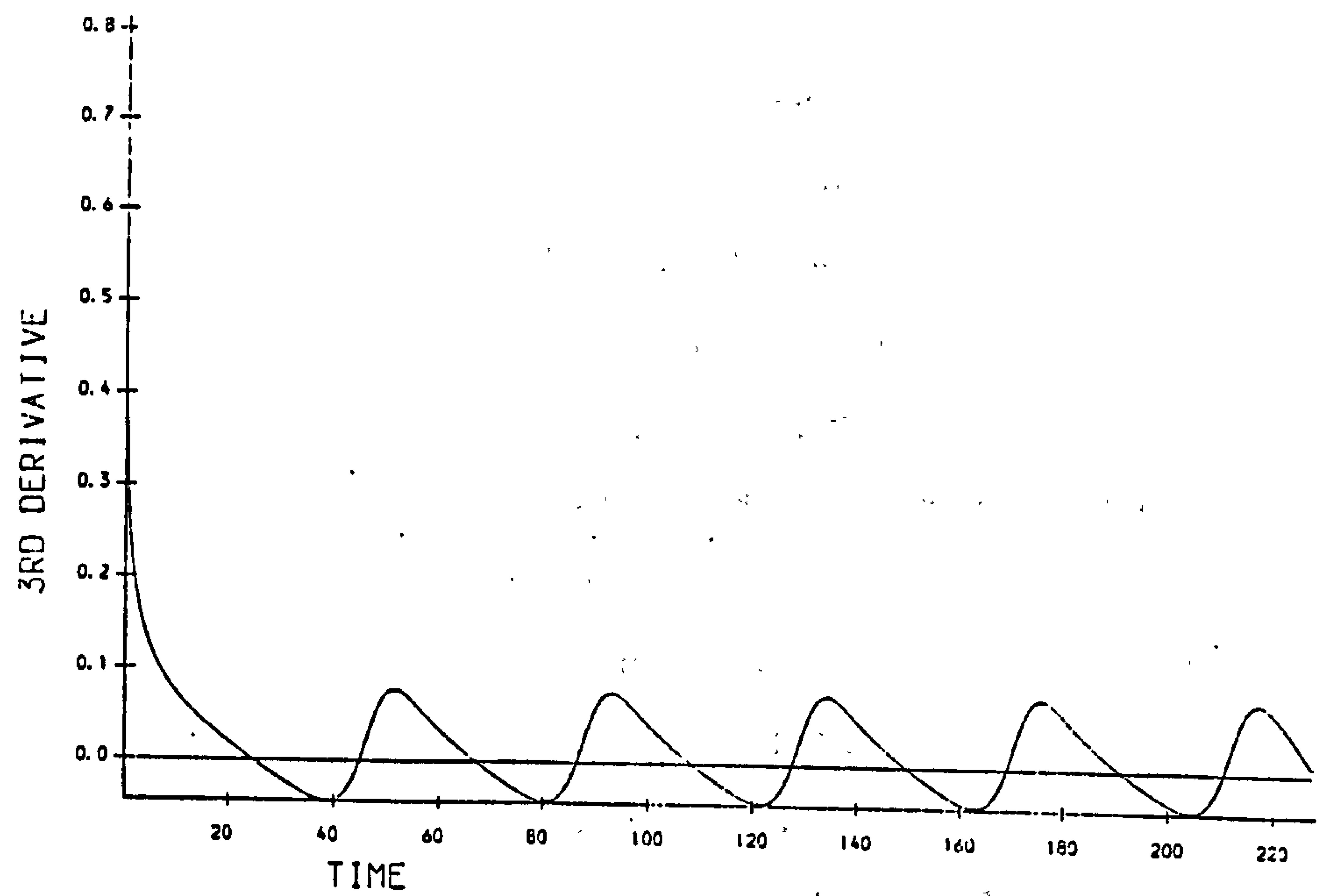

Figure 7.40: Long Impulse. Variation in the third derivative $U_{xxx}(0,t)$ at the origin. Forced conditions (7.39) with $U_0 = 0.5, \tau = 0.01,\ t_0 = \infty, h = 0.04, \Delta t = 0.001.\ \epsilon = 3.$

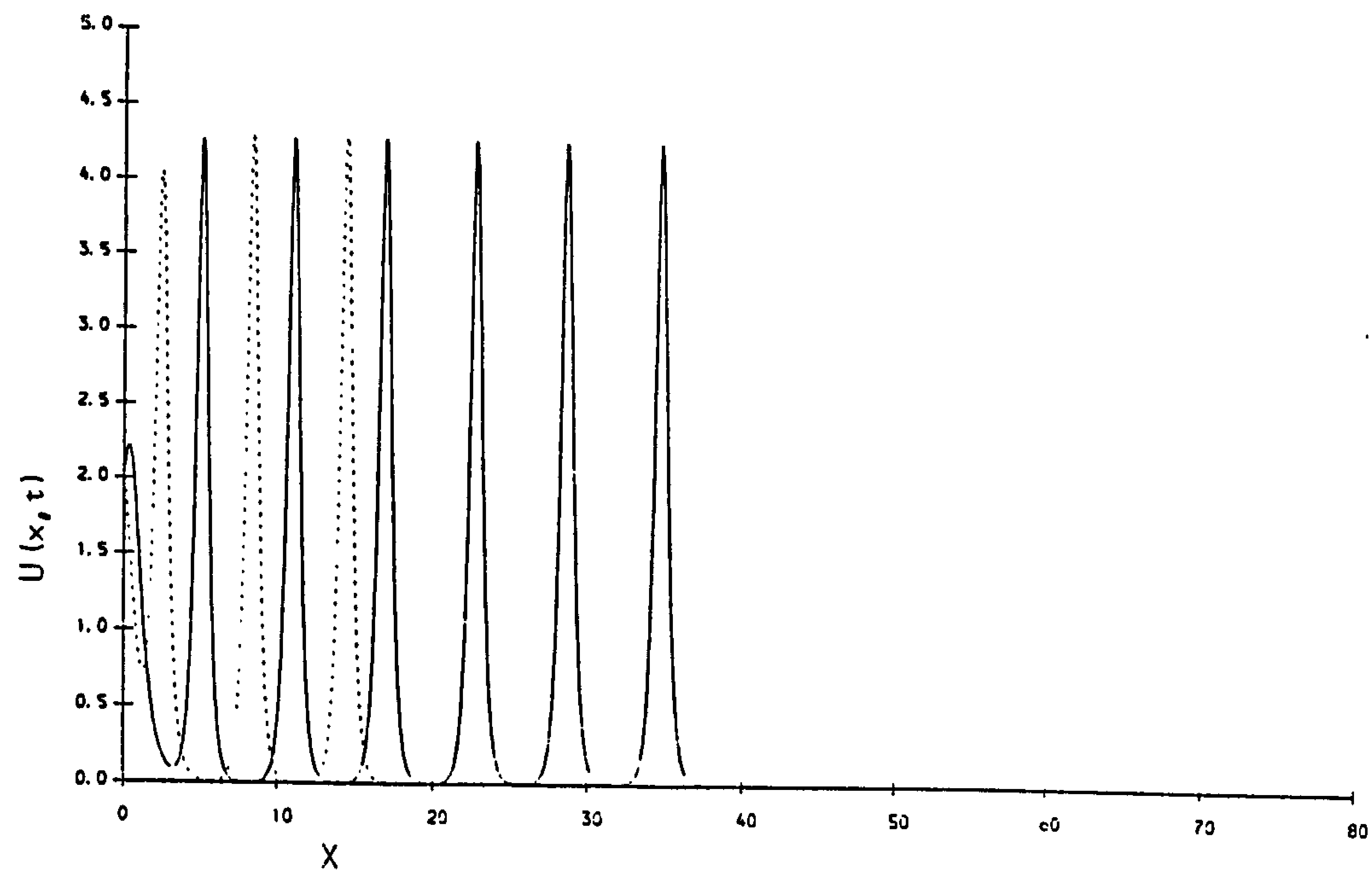

Figure 7.41: Long Impulse. Soliton produced by forced conditions (7.39) with $U_0 = 2, \tau = 0.01, t_0 = \infty, h = 0.04, \Delta t = 0.01$. graphed at $t = 2.25$ (- - - -) and $t = 4.5$ (———). $\epsilon = 3$.

forcing lasts throughout the experiment. The numerical step lengths are $h = 0.04$ and $\Delta t = 0.001$. In this numerical experiment, see Figure (7.41), seven solitary waves are generated before the simulation is terminated at $t = 4.5$. Figures (7.42) and (7.43) show that six achieve their terminal heights and a constant velocity. The generating conditions for the first wave are again slightly different so it attains a slightly larger amplitude and velocity than do subsequent waves. The observations are collected in Table (7.15). The time interval between births of solitary waves is constant at $\Delta T_B = 0.647$. The measured terminal heights for solitary waves 1-6 vary between 4.2984 and 4.2862 with measured velocities of (9.454-8.727). Free solitons of similar heights would also have velocities 9.238-9.185.

After an initial transient the graph of $U_x(0,t)$, Figure (7.44), shows a rounded saw tooth periodic behaviour with maximum of about 1.653, minimum of about -1.615, mean zero and period 0.647. The graph of $U_{xx}(0,t)$, Figure (7.45), also exhibits periodic behaviour with period 0.647.

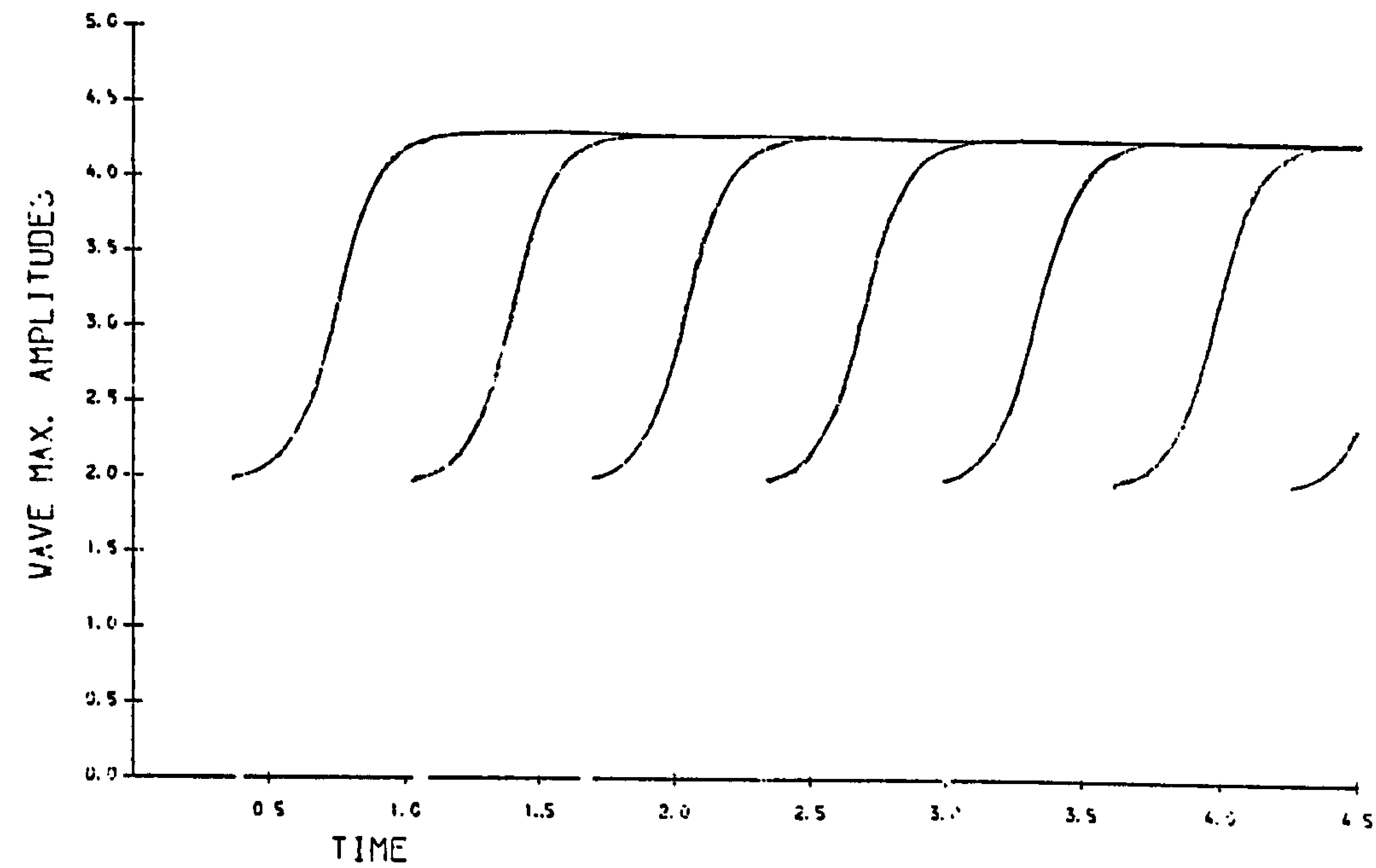

Figure 7.42: Long Impulse. The evolution of the soliton amplitudes. Forced conditions (7.39) with $U_0 = 2, \tau = 0.01, t_0 = \infty, h = 0.04, \Delta t = 0.001.$ $\epsilon = 3.$

Table 7.15: Observation of solitary waves, $U_0 = 2, \epsilon = 3$

wave	birth time	generated waves		free soliton
		amplitude	velocity	velocity
1	0.375	4.2984	9.454	9.238
2	1.036	4.2862	9.454	9.185
3	1.683	4.2852	9.454	9.181
4	2.328	4.2856	9.454	9.183
5	2.971	4.2859	8.727	9.184
6	3.618	4.2862	8.727	9.185
7	4.260	2.3850	2.181	2.844

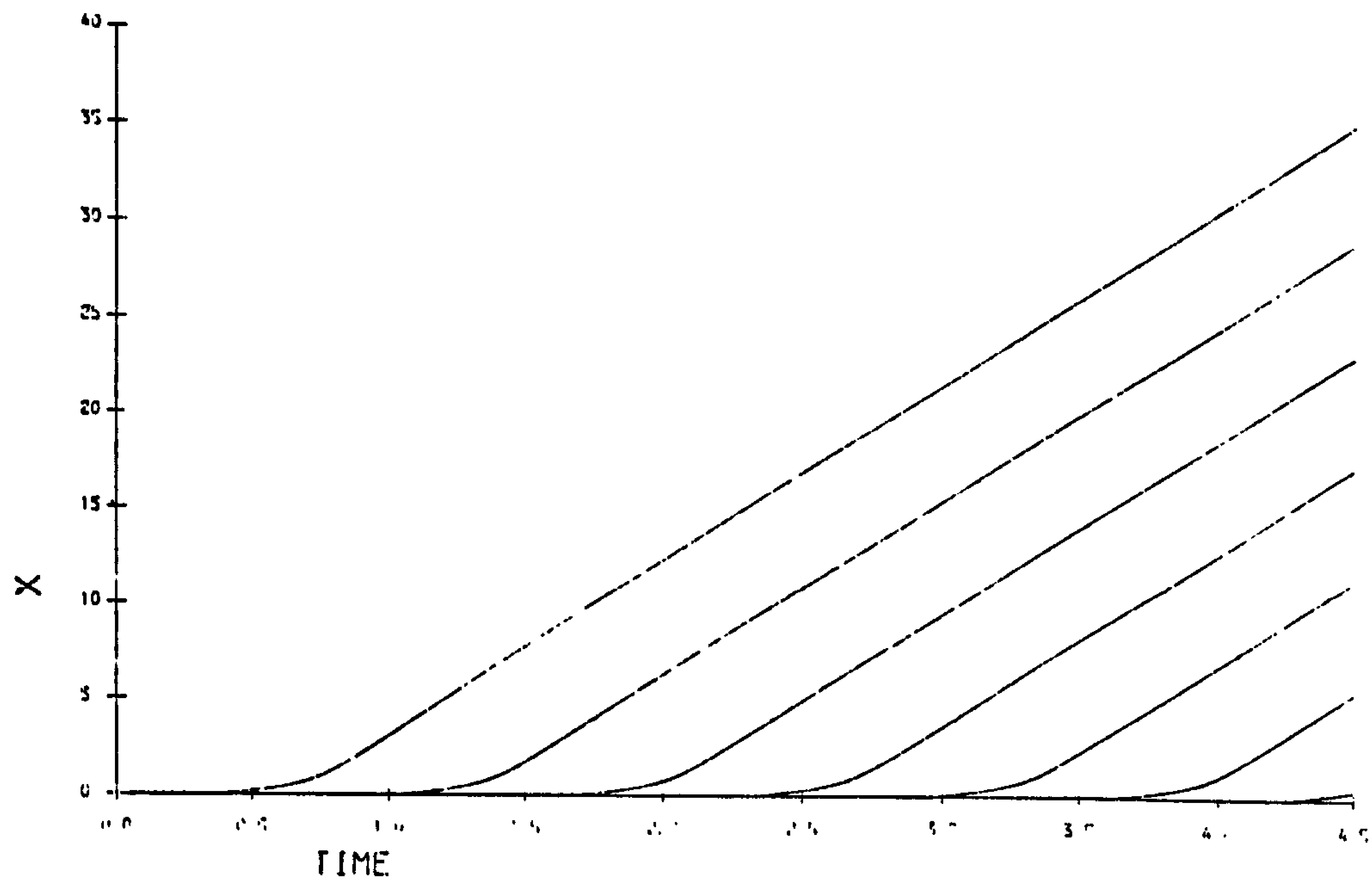

Figure 7.43: Long Impulse. The space-time graphs of the solitons produced by (7.39) with $U_0 = 2, \tau = 0.01. t_0 = \infty, h = 0.04, \Delta t = 0.001.$ $\epsilon = 3$.

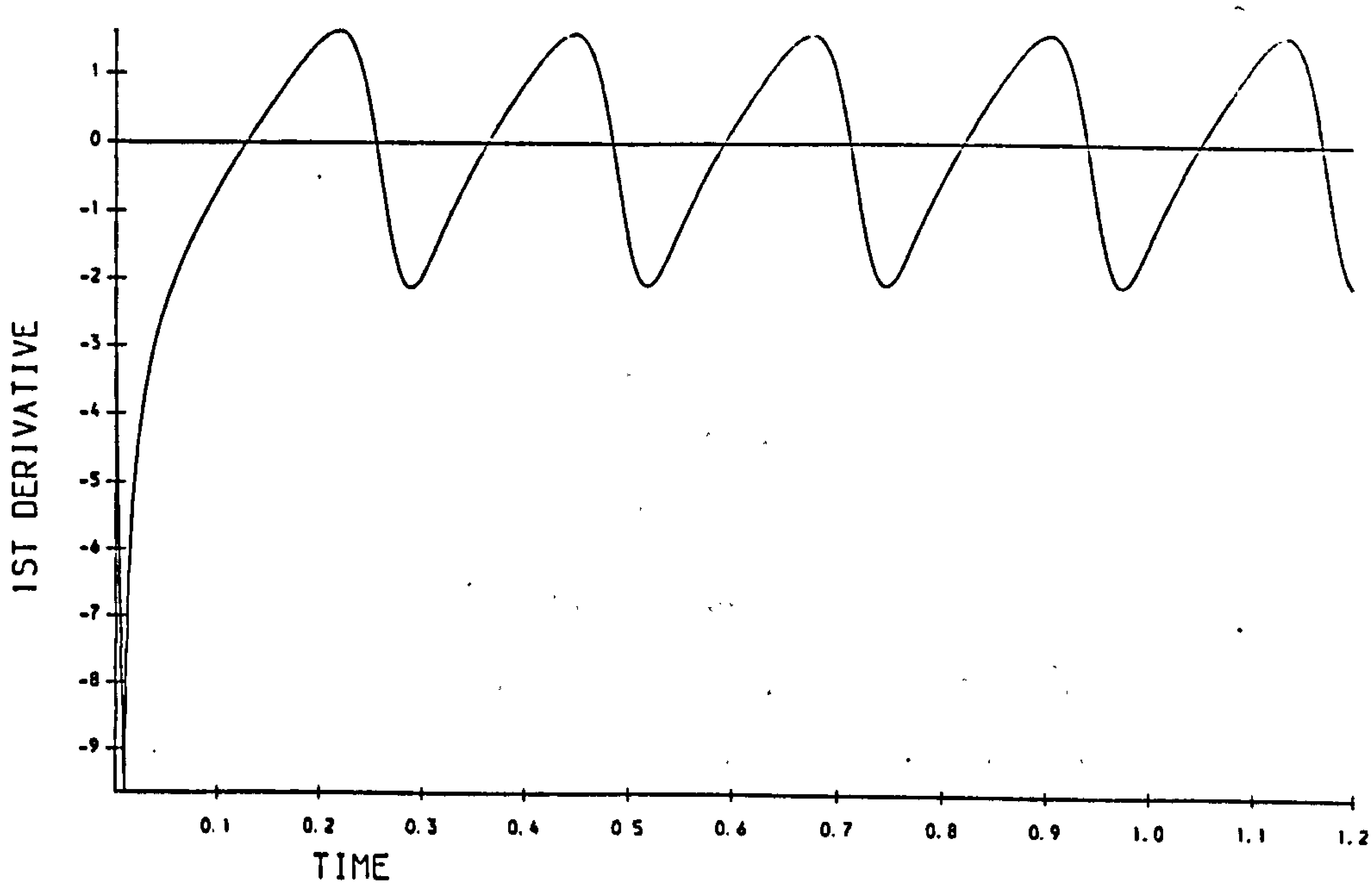

Figure 7.44: Long Impulse. Variation in the first derivative $U_x(0, t)$ at the origin. Forced conditions (7.39) with $U_0 = 2, \tau = 0.01, t_0 = \infty, h = 0.04, \Delta t = 0.001.$ $\epsilon = 3$.

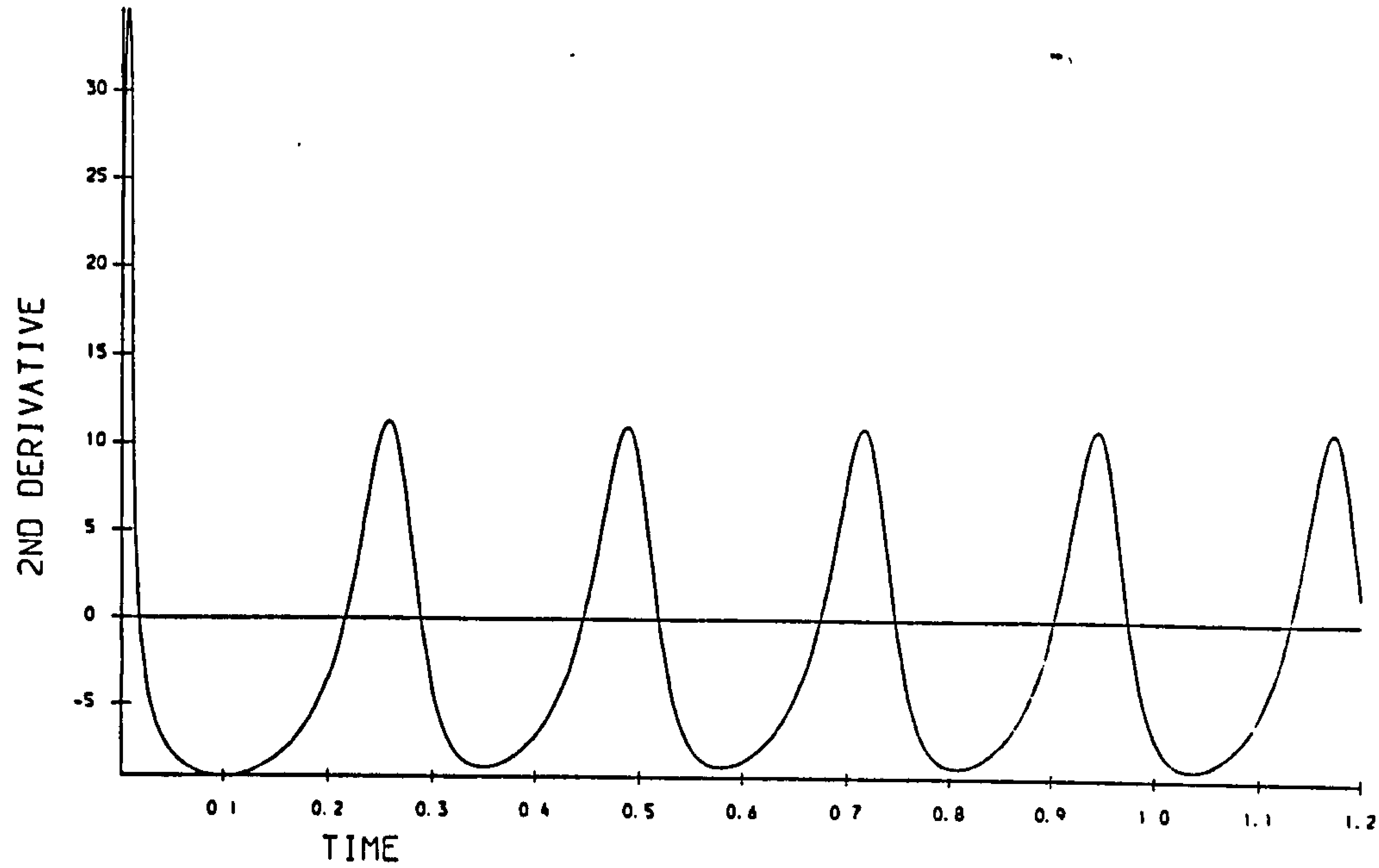

Figure 7.45: Long Impulse. Variation in the second derivative $U_{xx}(0,t)$ at the origin. Forced conditions (7.39) with $U_0 = 2, \tau = 0.01, t_0 = \infty, h = 0.04, \Delta t = 0.001$. $\epsilon = 3$.

Short Impulse

i-) In this simulation boundary condition (7.39) is used with $U_0 = 1$, $\tau = 0.01, t_0 = 11, h = 0.04$, and $\Delta t = 0.001$. In this numerical experiment, see Figure(7.46), two solitary waves are generated in the experiment, of which only the first reaches its mature amplitude 2.14 and velocity 2.21, the second has amplitude 1.43 and a velocity 1.02: see Figures (7.39) and (7.48).

Figures (7.49) and (7.50) also show that when the forcing is turned off at $t = 11$, for $t > 11, U(0,t) = 0$ but as the derivatives $U_x(0,t)$ and $U_{xx}(0,t)$ are not themselves forced to become zero the I_j do not immediately cease to vary. The switching operation causes a spike in the derivative graphs; subsequently $U_x(0,t)$ and $U_{xx}(0,t)$ tend to zero at about the same rate. Thus, as is shown earlier, I_1 continues to change, increasing or decreasing according to the sign of $U_{xx}(0,t)$, through

$$I_1(t) = I_1(11) + \textstyle\int_{11}^{t}\{U_{xx}(0,t)\}dt, \tag{7.48}$$

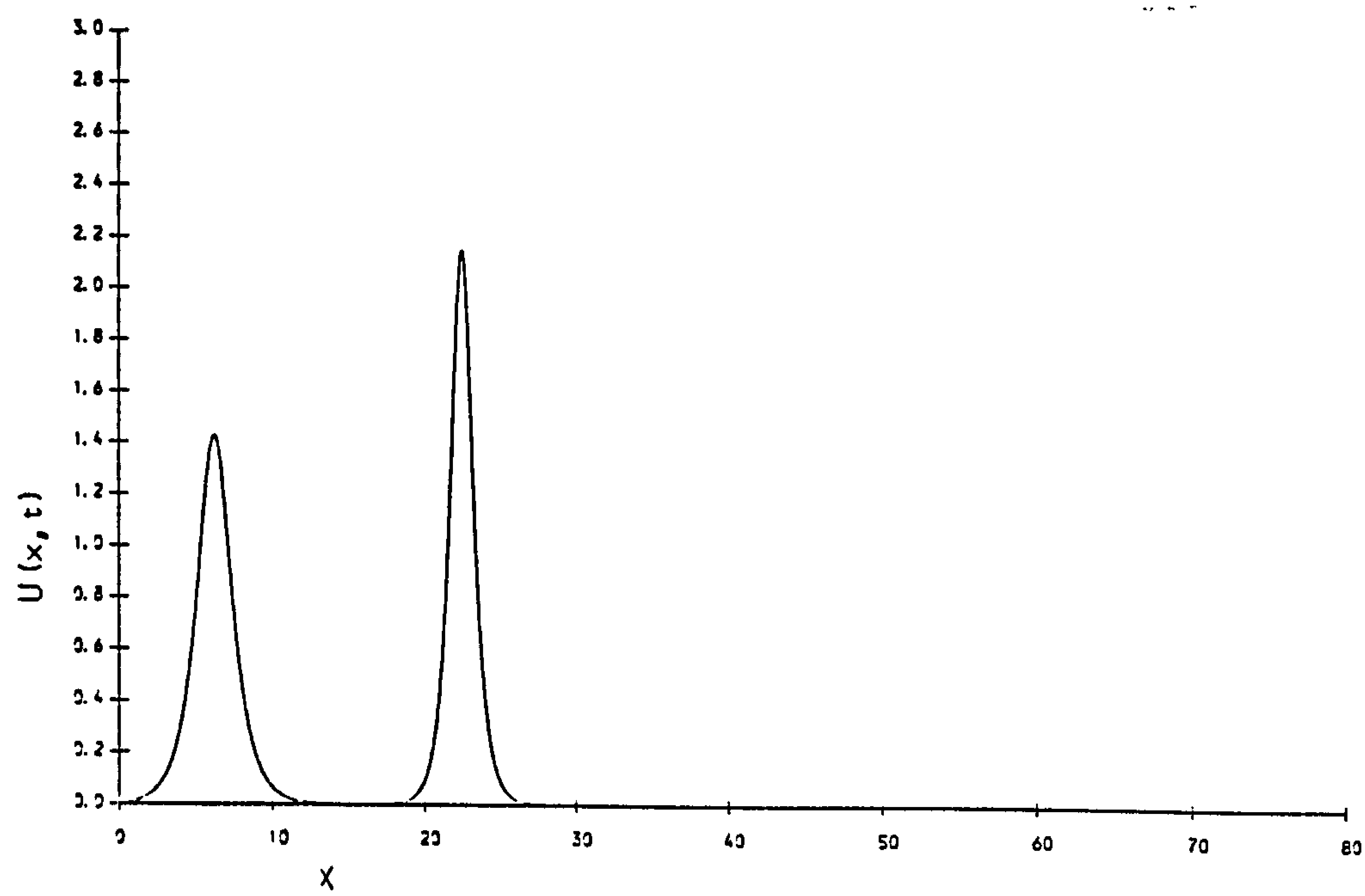

Figure 7.46: Long Impulse. Soliton produced by forced conditions (7.39) with $U_0 = 1, \tau = 0.01, t_0 = 11, h = 0.04, \Delta t = 0.01$. graphed at $t = 15$ (- - -) and $t = 30$ (——-). $\epsilon = 3$.

I_2 start to decrease through

$$I_2(t) = I_2(11) - \int_{11}^{t}\{\tfrac{1}{2}U_x^2(0,t)\}dt, \tag{7.49}$$

and I_3 to increase through

$$I_3(t) = I_3(11) + \int_{11}^{t}\{U_{xx}^2(0,t)\}dt, \tag{7.50}$$

and I_4 changes through

$$I_4(t) = I_4(11) - \int_{11}^{t}\{\tfrac{1}{2}U_x^4(0,t) - U_{xx}(0,t)U_{xt}(0,t)\}dt. \tag{7.51}$$

These equations also imply that the development of the last formed solitary wave does not stop abruptly when the forcing is switched off, but continues until $U_x(0,t)$ and $U_{xx}(0,t)$ have decayed to zero. After a time of about $t = 15$ when the influences of forcing have died away the quantities $I_1 - I_4$ should remain constant. All the above conclusions are illustrated by the measured values of the quantities given Table (7.16-7.17).

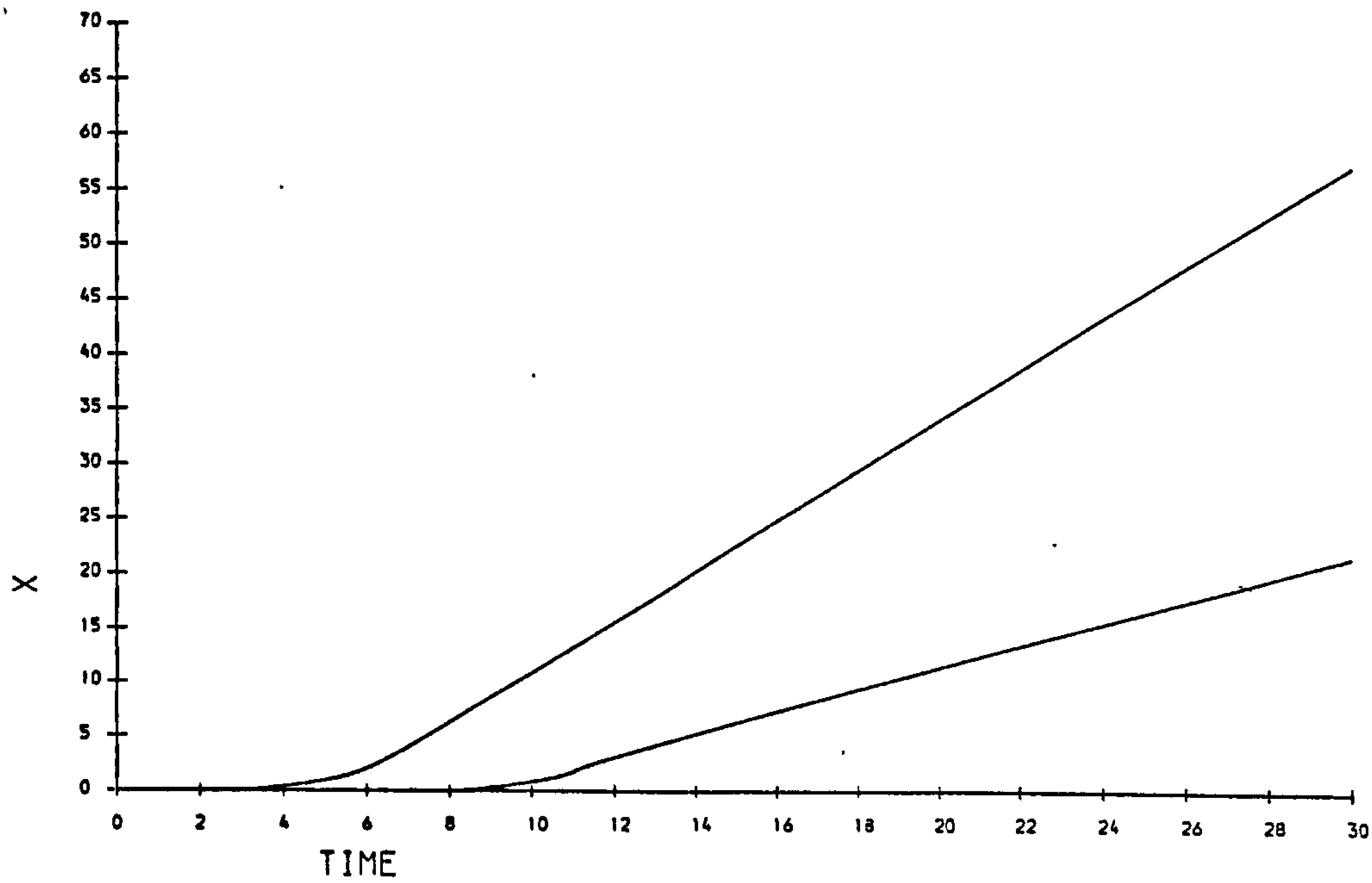

Figure 7.47: Short Impulse. Space-time graphs of the solitons produced by forced condition (7.39) with $U_0 = 1, \tau = 0.01, t_0 = 11, h = 0.04$, $\Delta t = 0.001$. $\epsilon = 3$.

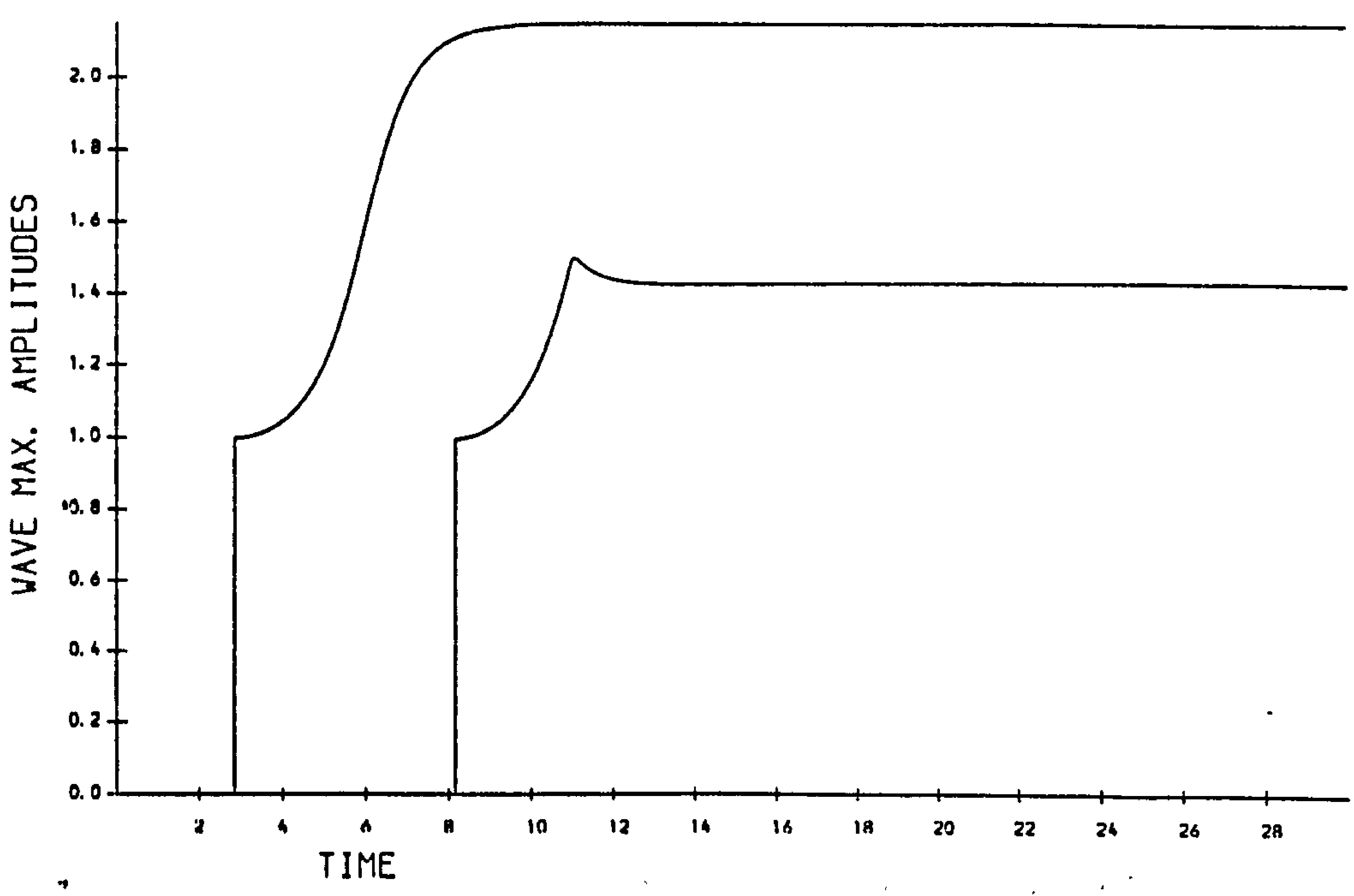

Figure 7.48: Short Impulse. The evolution of the soliton amplitudes. Forced conditions (7.39) with $U_0 = 1, \tau = 0.01, t_0 = 11, h = 0.04$, $\Delta t = 0.001$. $\epsilon = 3$.

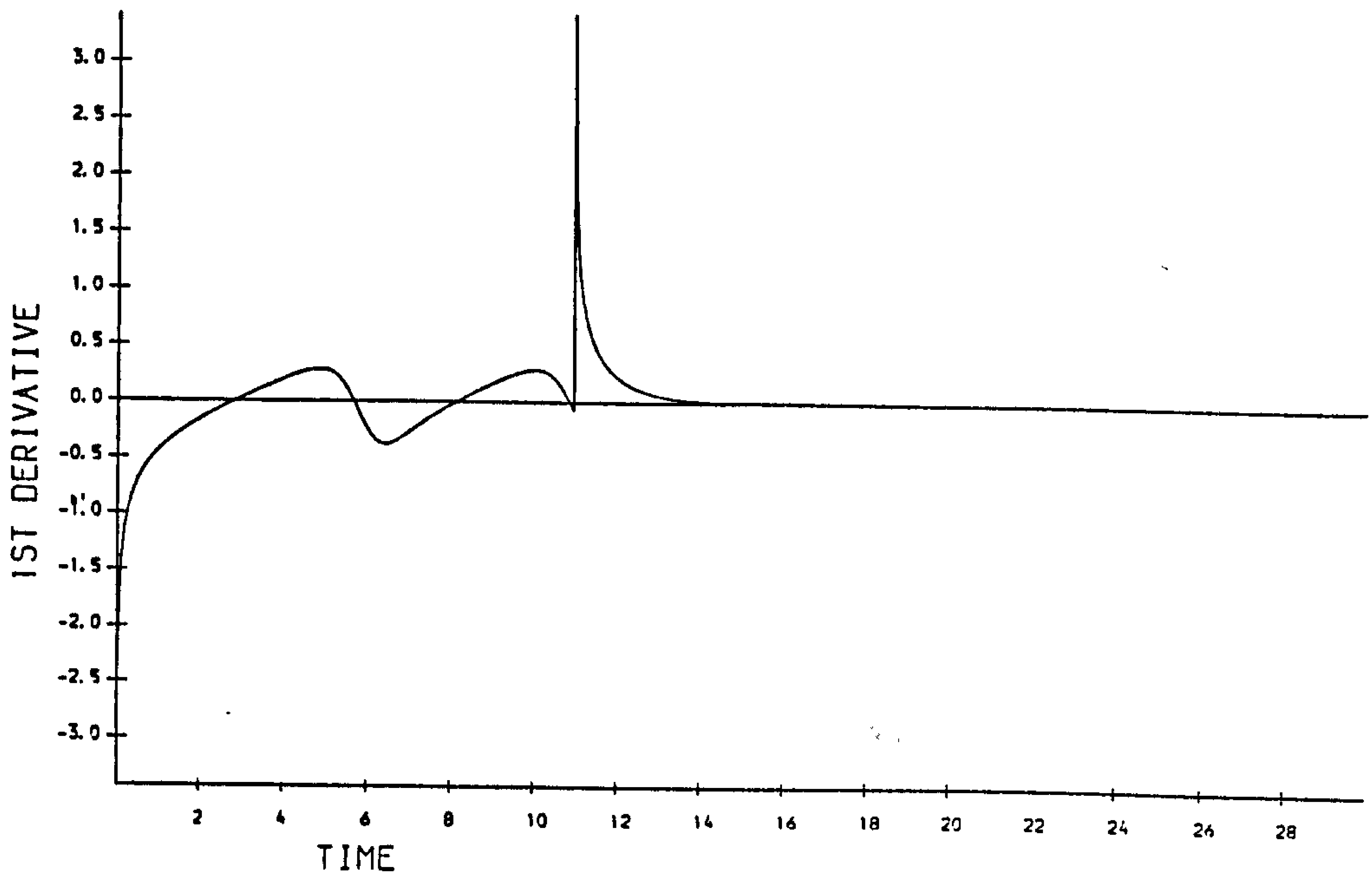

Figure 7.49: Short Impulse. Variation in the first derivative $U_x(0,t)$ at the origin. Forced conditions (7.39) with $U_0 = 1, \tau = 0.01$, $t_0 = 11, h = 0.04, \Delta t = 0.001$. $\epsilon = 3$.

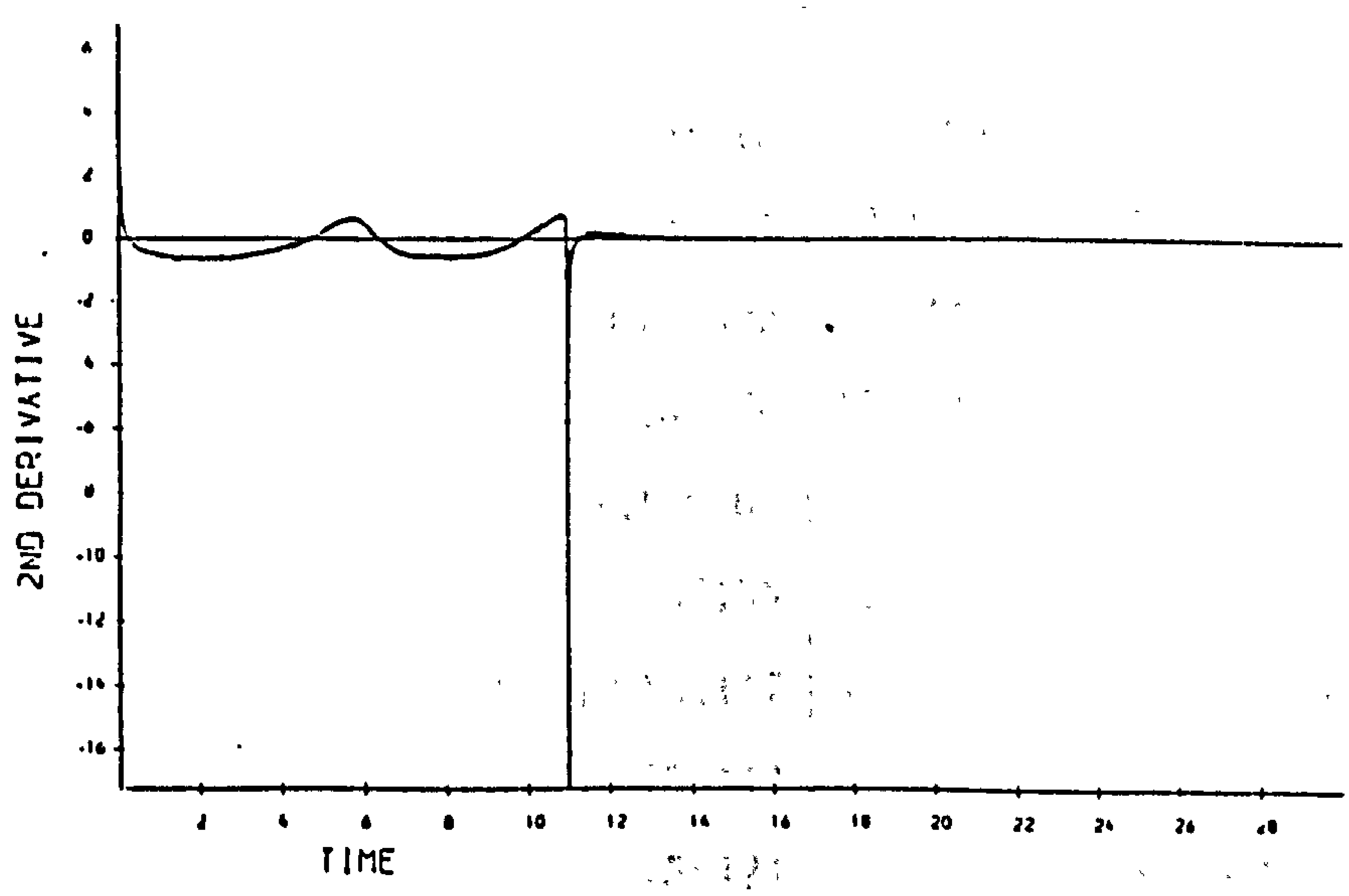

Figure 7.50: Short Impulse. Variation in the second derivative $U_{xx}(0,t)$ at the origin. Forced conditions (7.39) with $U_0 = 1, \tau = 0.01$, $t_0 = 11, h = 0.04, \Delta t = 0.001$. $\epsilon = 3$.

Table 7.16: Bounded forced conditions with $t_0 = 11, U_0 = 1$

time	I_1	I_2	I_3	I_4
0.0	0.000000	0.000000	0.000000	0.000000
1.0	1.254076	0.732673	-0.325532	113.967861
2.0	1.708771	1.056245	0.095382	87.467773
3.0	2.147801	1.427711	0.481942	79.109966
4.0	2.683397	1.982236	1.058721	86.743525
5.0	3.532885	3.112043	2.545068	134.346211
6.0	5.056927	5.625942	7.250250	357.438047
7.0	6.038749	6.976983	9.367068	993.822109
8.0	6.526666	7.427795	9.848875	1373.272969
9.0	7.040863	7.948524	10.379535	1498.814687
10.0	7.800678	8.912701	11.560300	1566.390156
11.0	8.986216	10.865128	9.435049	2393.563906
12.0	8.748550	10.175486	12.221875	1918.638594
13.0	8.837001	10.158010	12.239825	1892.385938
14.0	8.878764	10.156631	12.243621	1888.266719
15.0	8.896052	10.156502	12.244248	1888.608750
16.0	8.902739	10.156476	12.244318	1889.728438
17.0	8.905027	10.156466	12.244297	1890.770938
18.0	8.905532	10.156455	12.244282	1891.576250
19.0	8.905319	10.156447	12.244268	1892.154531
20.0	8.904831	10.156442	12.244226	1892.555625
21.0	8.904262	10.156424	12.244207	1892.829688
22.0	8.903669	10.156423	12.244181	1893.012656
23.0	8.903099	10.156414	12.244156	1893.135000

Table 7.17: Bounded forced conditions with $t_0 = 11, U_0 = 1$

time	I_1	I_2	I_3	I_4
24.0	8.902562	10.156406	12.244117	1893.214687
25.0	8.902054	10.156398	12.244099	1893.266250
26.0	8.901586	10.156387	12.244081	1893.299531
27.0	8.901149	10.156382	12.244054	1893.321406
28.0	8.900743	10.156370	12.244025	1893.333281
29.0	8.900355	10.156363	12.244005	1893.339844
30.0	8.899996	10.156363	12.243967	1893.342969

ii-) In this simulation boundary condition (7.39) is used with $U_0 = 1, \tau = 0.01, t_0 = 12, h = 0.04$, and $\Delta t = 0.001$. In this numerical experiment, see Figure (7.50), two solitary waves are generated in the experiment, of which only the first reaches its mature amplitude 2.1563 and velocity 2.3344, the second has amplitude 2.1046 and a velocity 2.2232: see Figures (7.52) and (7.53). The observations are collected in Table(7.18). The time interval between births of solitary waves is constant at $\Delta T_B = 5.31$. Figures (7.54) and (7.55) also show that when the forcing is turned off at $t = 12$, for $t > 12, U(0,t) = 0$ but as the derivatives $U_x(0,t)$ and $U_{xx}(0,t)$ are not themselves forced to become zero the I_j do not immediately cease to vary. The switching operation causes a spike in the derivative graphs; subsequently $U_x(0,t)$ and $U_{xx}(0,t)$ tend to zero at about the same rate. Thus, as is shown earlier, I_1 continues to change, increasing or decreasing according to the sign of $U_{xx}(0,t)$, through

$$I_1(t) = I_1(12) + \int_{12}^{t}\{U_{xx}(0,t)\}dt. \tag{7.52}$$

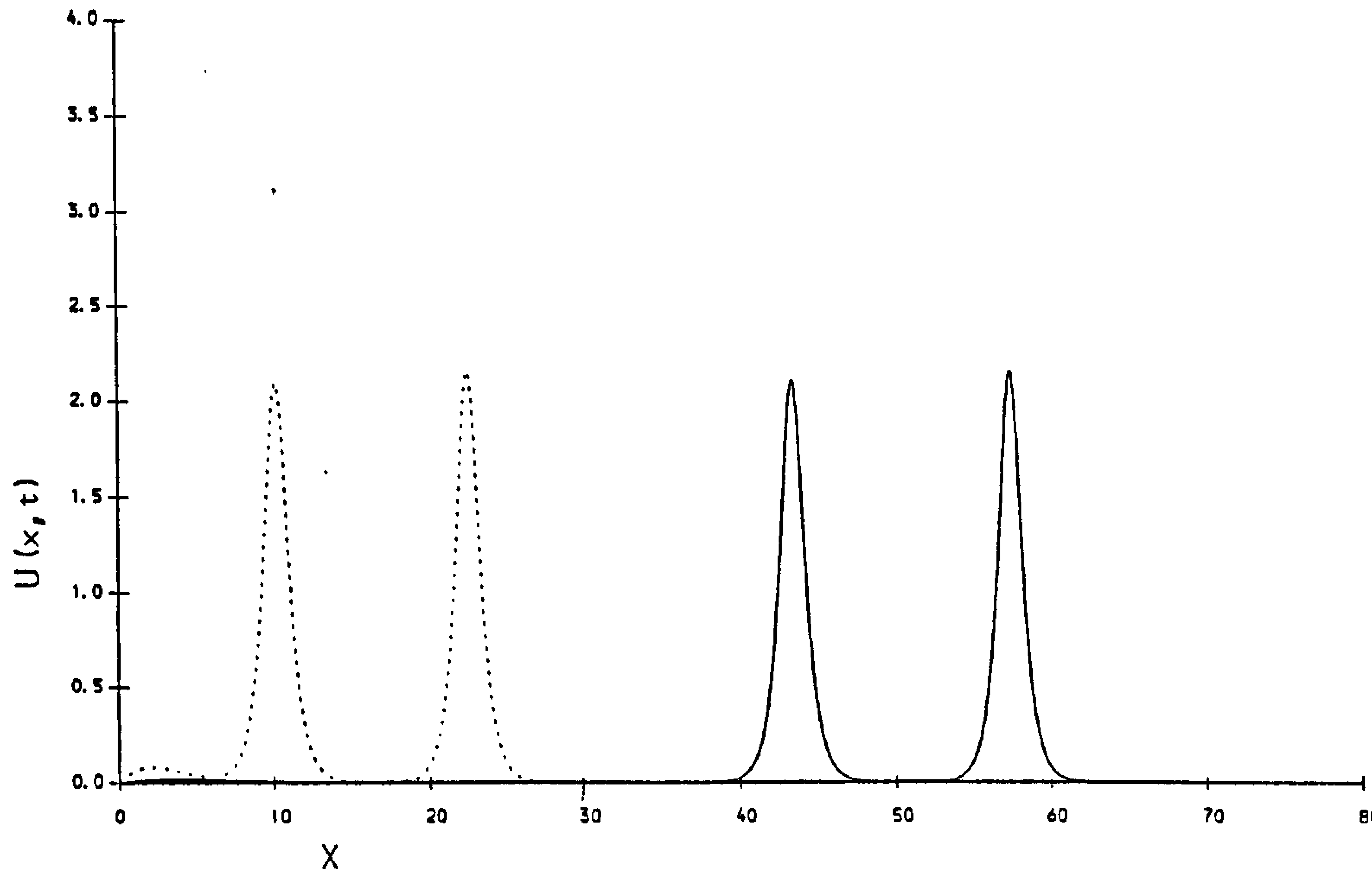

Figure 7.51: Long Impulse. Soliton produced by forced conditions (7.39) with $U_0 = 2, \tau = 0.01, t_0 = 12, h = 0.04, \Delta t = 0.01$. graphed at $t = 15$ (- - - -) and $t = 30$ (——). $\epsilon = 3$.

Table 7.18: Observation of solitary waves, $U_0 = 1, t_0 = 12. \epsilon = 3$

wave	birth time	generated waves		free soliton
		amplitude	velocity	velocity
1	2.880	2.1563	2.3344	2.3248
2	8.190	2.1046	2.2232	2.2146
3	12.000	0.5451		0.1485

I_2 start to decrease through

$$I_2(t) = I_2(12) - \int_{12}^{t}\{\tfrac{1}{2}U_x^2(0,t)\}dt, \tag{7.53}$$

and I_3 to increase through

$$I_3(t) = I_3(12) + \int_{12}^{t}\{U_{xx}^2(0,t)\}dt, \tag{7.54}$$

and I_4 changes through

$$I_4(t) = I_4(12) - \int_{12}^{t}\{\tfrac{1}{2}U_x^4(0,t) - U_{xx}(0,t)U_{xt}(0,t)\}dt. \tag{7.55}$$

These equations also imply that the development of the last formed solitary wave does not stop abruptly when the forcing is switched off, but continues until $U_x(0,t)$ and $U_{xx}(0,t)$ have decayed to zero. After a time of about $t = 15$ when the influences of forcing have died away the quantities $I_1 - I_4$ should remain constant. All the above conclusions are illustrated by the measured values of the quantities given Table (7.20-7.21).

iii-) In a this experiment with increased forcing, $U_0 = 2$, boundary condition (7.39) is used with $x_{max} = 80, t_{max} = 4.5, \tau = 0.1, t_o = 4.5$. The forcing lasts throughout the experiment. The numerical step lengths are $h = 0.04$ and $\Delta t = 0.001$. In this numerical experiment, see Figure (7.56), two solitary waves are generated before the simulation is terminated at
$t = 4.5$. Figures (7.57) and (7.58) show that three achieve their terminal heights and a constant velocity. The generating conditions for the first wave are again slightly different so it attains a slightly larger amplitude and velocity than do subsequent waves. The observations are collected in Table (7.22). The time interval between births of solitary waves is constant at $\Delta T_B = 0.666$. The measured terminal heights for solitary waves 1-2 vary between 4.3009 and 3.1459 with measured velocities of (9.1674-4.9432). Free solitons of similar heights would also have velocities 9.2488-4.9432. After an initial transient the graph of $U_x(0,t)$, Figure (7.59), shows a rounded saw

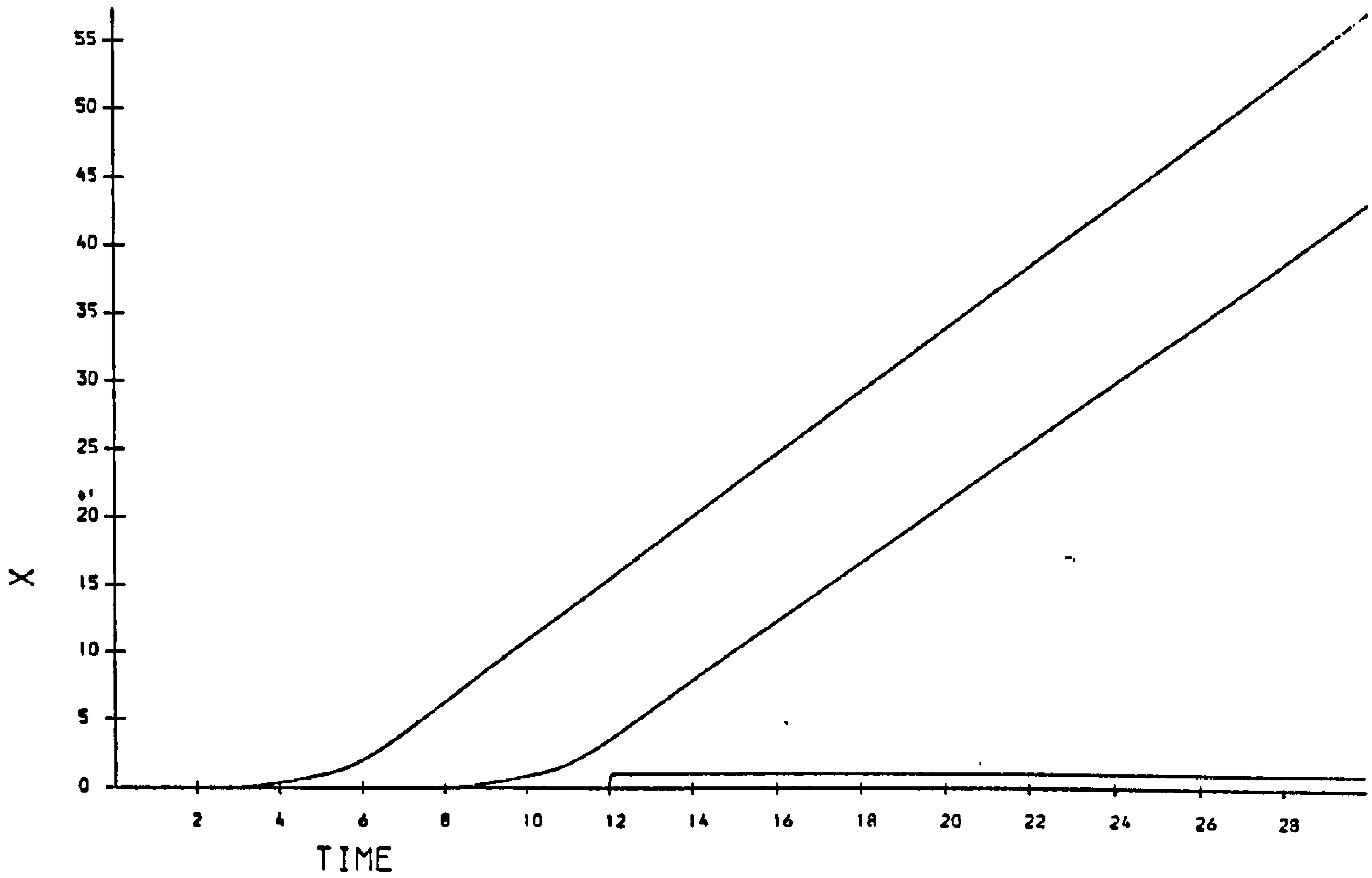

Figure 7.52: Short Impulse. Space-time graphs of the solitons produced by forced condition (7.39) with $U_0 = 1, \tau = 0.01, t_0 = 12, h = 0.04$. $\Delta t = 0.001$. $\epsilon = 3$.

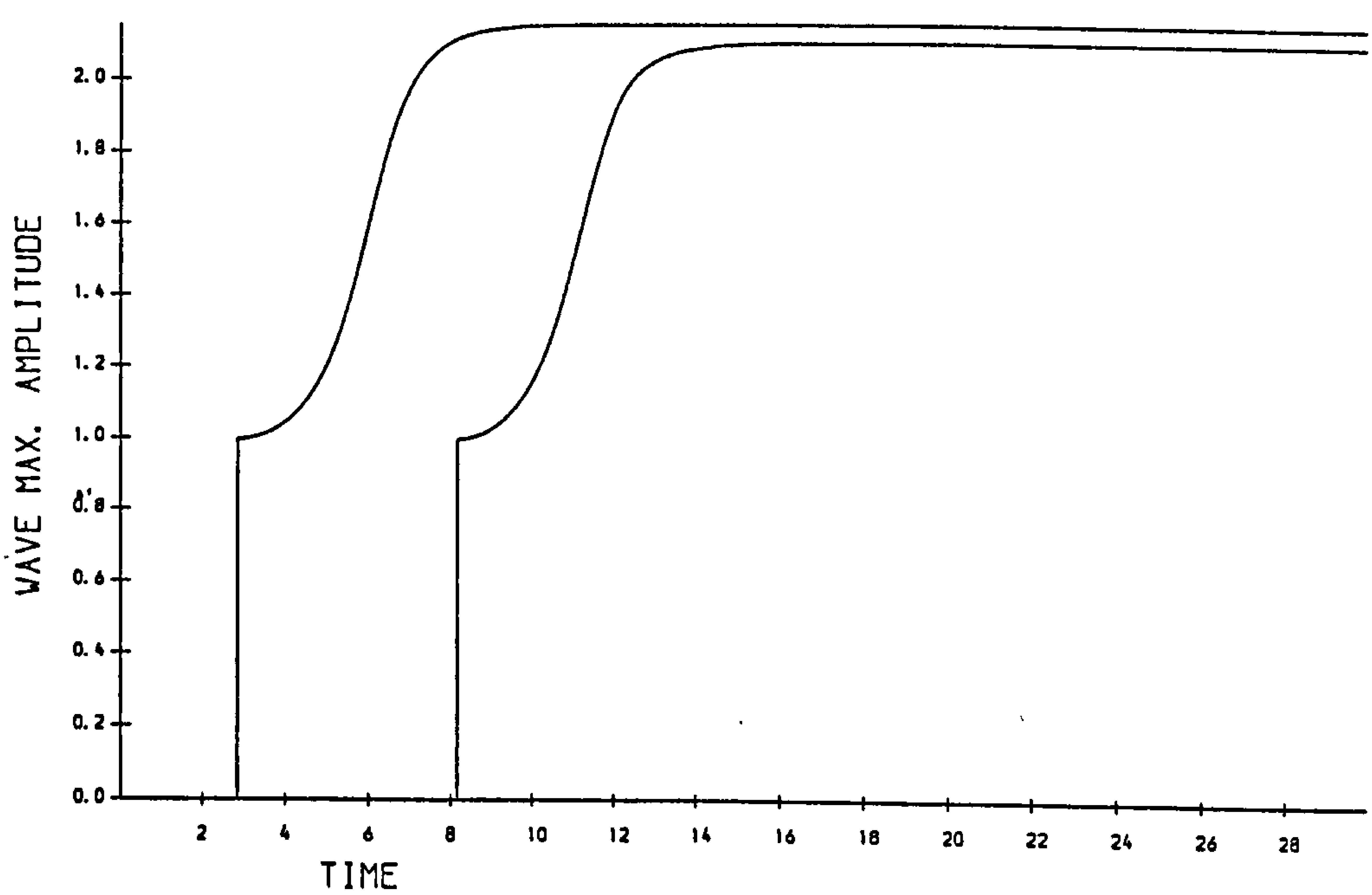

Figure 7.53: Short Impulse. The evolution of the soliton amplitudes. Forced conditions (7.39) with $U_0 = 1, \tau = 0.01, t_0 = 12, h = 0.04$, $\Delta t = 0.001$. $\epsilon = 3$.

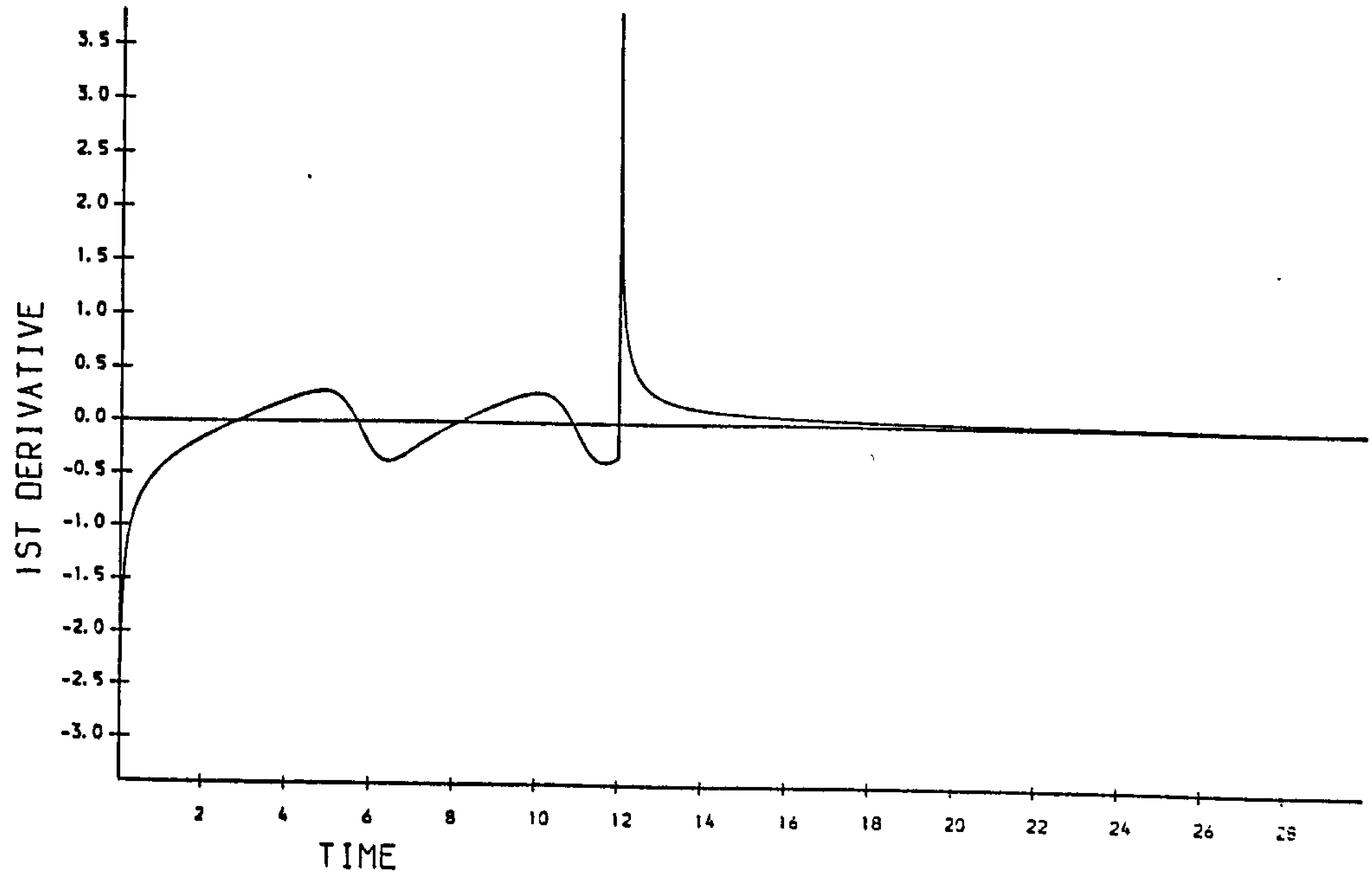

Figure 7.54: Short Impulse. Variation in the first derivative $U_x(0,t)$ at the origin. Forced conditions (7.39) with $U_0 = 1, \tau = 0.01$, $t_0 = 12, h = 0.04, \Delta t = 0.001$. $\epsilon = 3$.

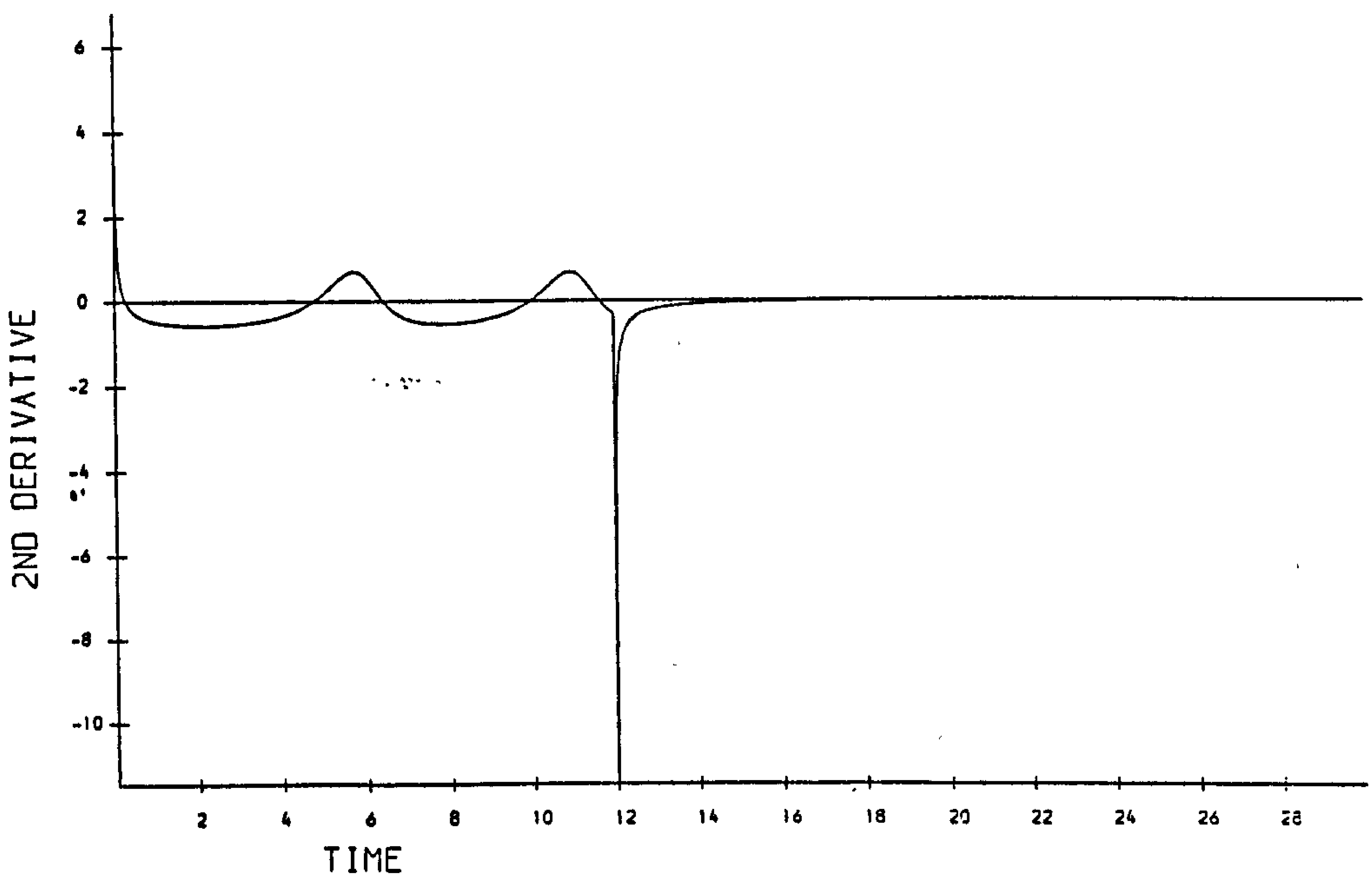

Figure 7.55: Short Impulse. Variation in the second derivative $U_{xx}(0,t)$ at the origin. Forced conditions (7.39) with $U_0 = 1, \tau = 0.01$, $t_0 = 12, h = 0.04, \Delta t = 0.001$. $\epsilon = 3$.

Table 7.19: Bounded forced conditions with $t_0 = 12, U_0 = 1$

time	I_1	I_2	I_3	I_4
0.00	0.000000	0.000000	0.000000	0.000000
1.0	1.254076	0.732673	-0.325532	113.967861
2.0	1.708771	1.056245	0.095382	87.467773
3.0	2.147801	1.427711	0.481942	79.109966
4.0	2.683397	1.982236	1.058721	86.743525
5.0	3.532885	3.112043	2.545068	134.346211
6.0	5.056927	5.625942	7.250250	357.438047
7.0	6.038749	6.976983	9.367068	993.822109
8.0	6.526666	7.427795	9.848875	1373.272969
9.0	7.040863	7.918524	10.379535	1498.814687
10.0	7.800678	8.912701	11.560300	1566.390156
11.0	9.204958	11.179001	15.608090	1730.782500
12.0	10.159774	12.646201	14.408528	2728.620313
13.0	9.451764	12.121727	18.210569	2677.211563
14.0	9.321000	12.090457	18.248320	2780.380625
15.0	9.249912	12.078660	18.259066	2810.517187
16.0	9.203383	12.072618	18.263571	2819.078438
17.0	9.169885	12.069032	18.265853	2821.401875
18.0	9.144307	12.066683	18.267164	2821.968750
19.0	9.123961	12.065046	18.267990	2822.055313
20.0	9.107314	12.063864	18.268510	2822.026563
21.0	9.093373	12.062971	18.268865	2821.979375
22.0	9.081483	12.062271	18.269100	2821.933750
23.0	9.071210	12.061714	18.269283	2821.898438

Table 7.20: Bounded forced conditions with $t_0 = 12, U_0 = 1$

time	I_1	I_2	I_3	I_4
24.0	9.062213	12.061257	18.269390	2821.866562
25.0	9.054254	12.060884	18.269482	2821.839688
26.0	9.047165	12.060570	18.269539	2821.817813
27.0	9.040783	12.060311	18.269576	2821.796562
28.0	9.035013	12.060085	18.269603	2821.782500
29.0	9.029765	12.059889	18.269606	2821.763438
30.0	9.024960	12.059711	18.269607	2821.751250

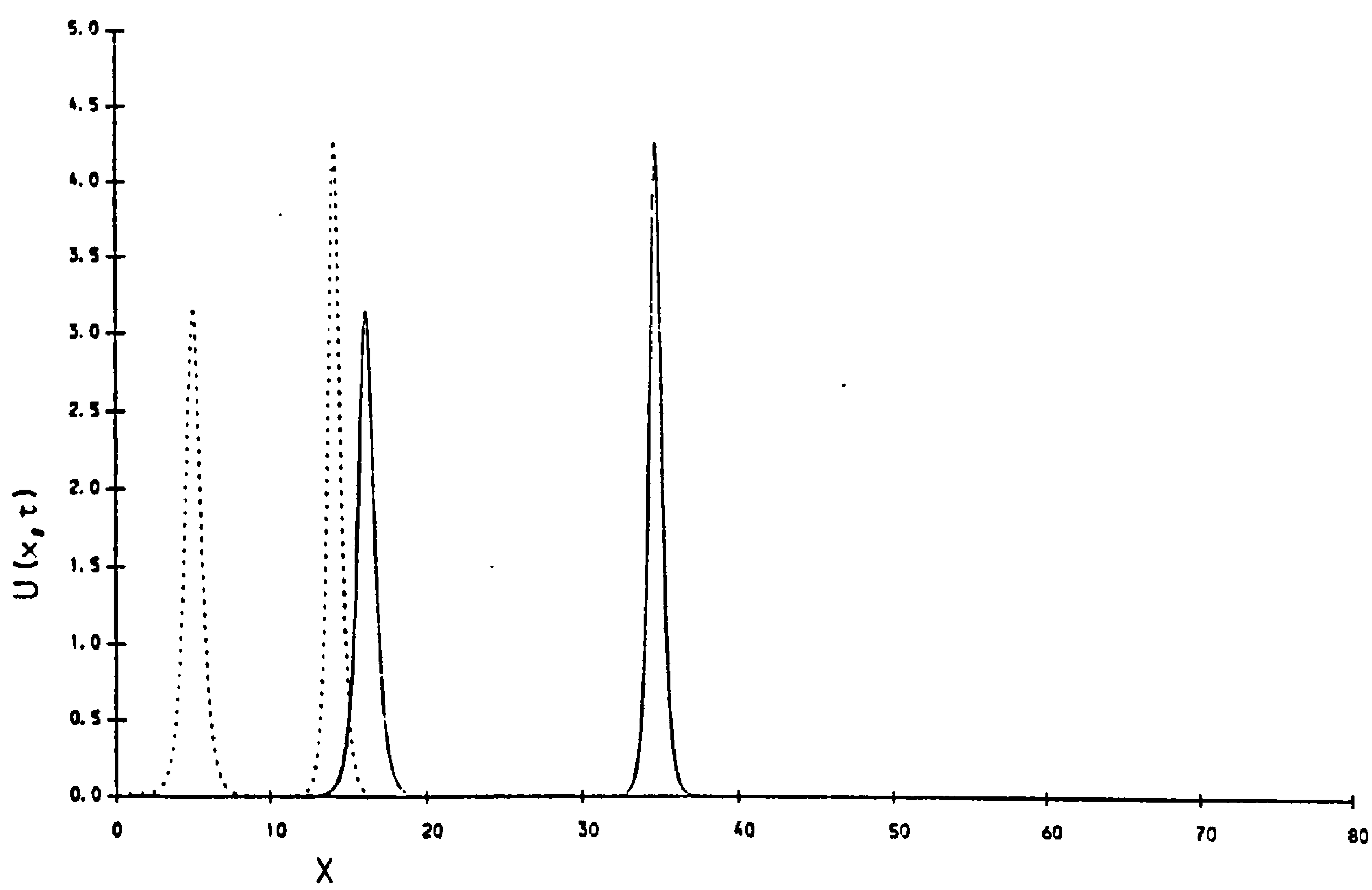

Figure 7.56: Long Impulse. Soliton produced by forced conditions (7.39) with $U_0 = 2, \tau = 0.1, t_0 = 1.5, h = 0.04, \Delta t = 0.01$. graphed at $t = 2.25$ (- - - -) and $t = 4.5$ (——-). $\epsilon = 3$.

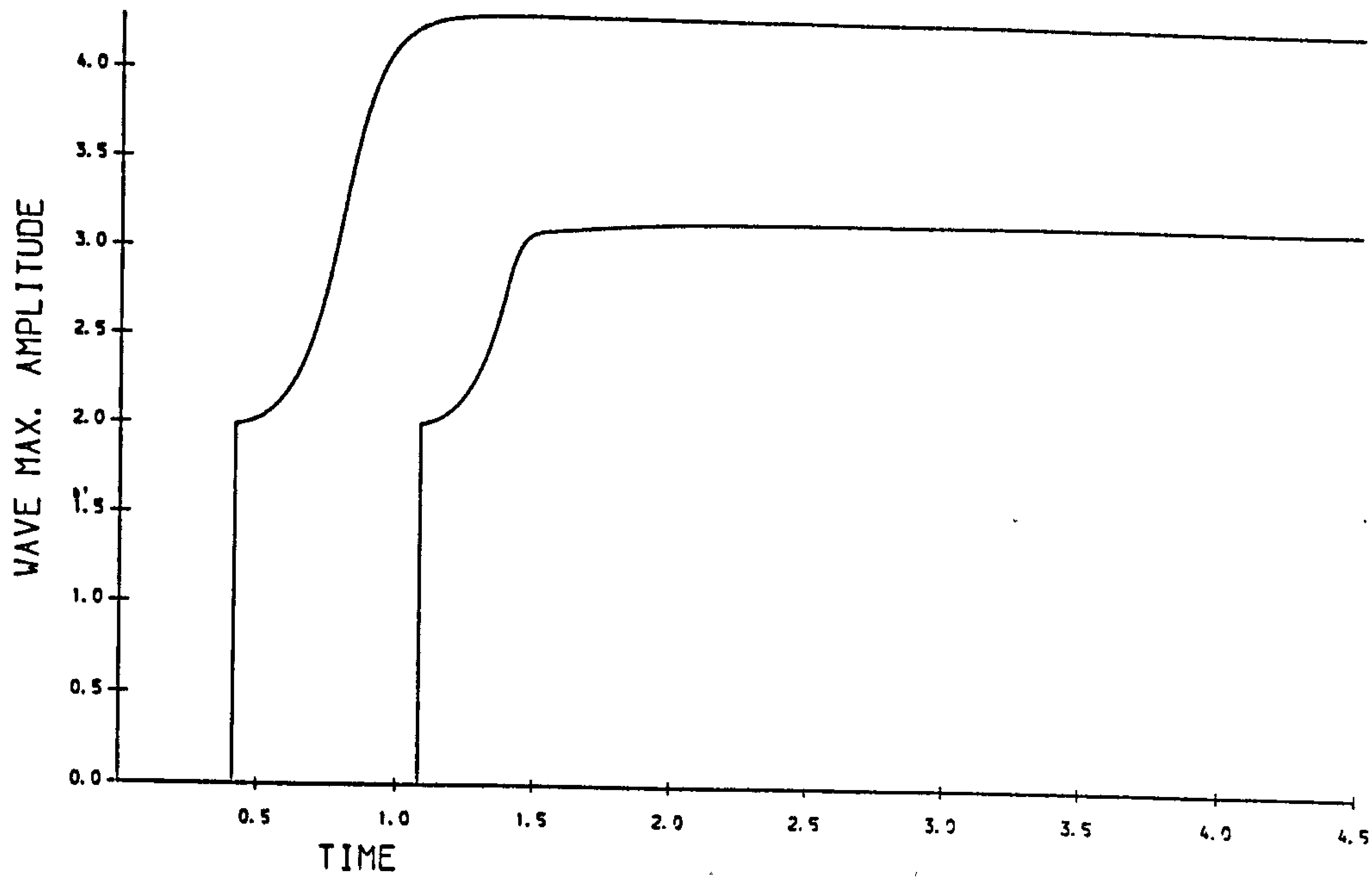

Figure 7.57: Long Impulse. The evolution of the soliton amplitudes. Forced conditions (7.39) with $U_0 = 2, \tau = 0.1, t_0 = 1.5$, $h = 0.04, \Delta t = 0.001$. $\epsilon = 3$.

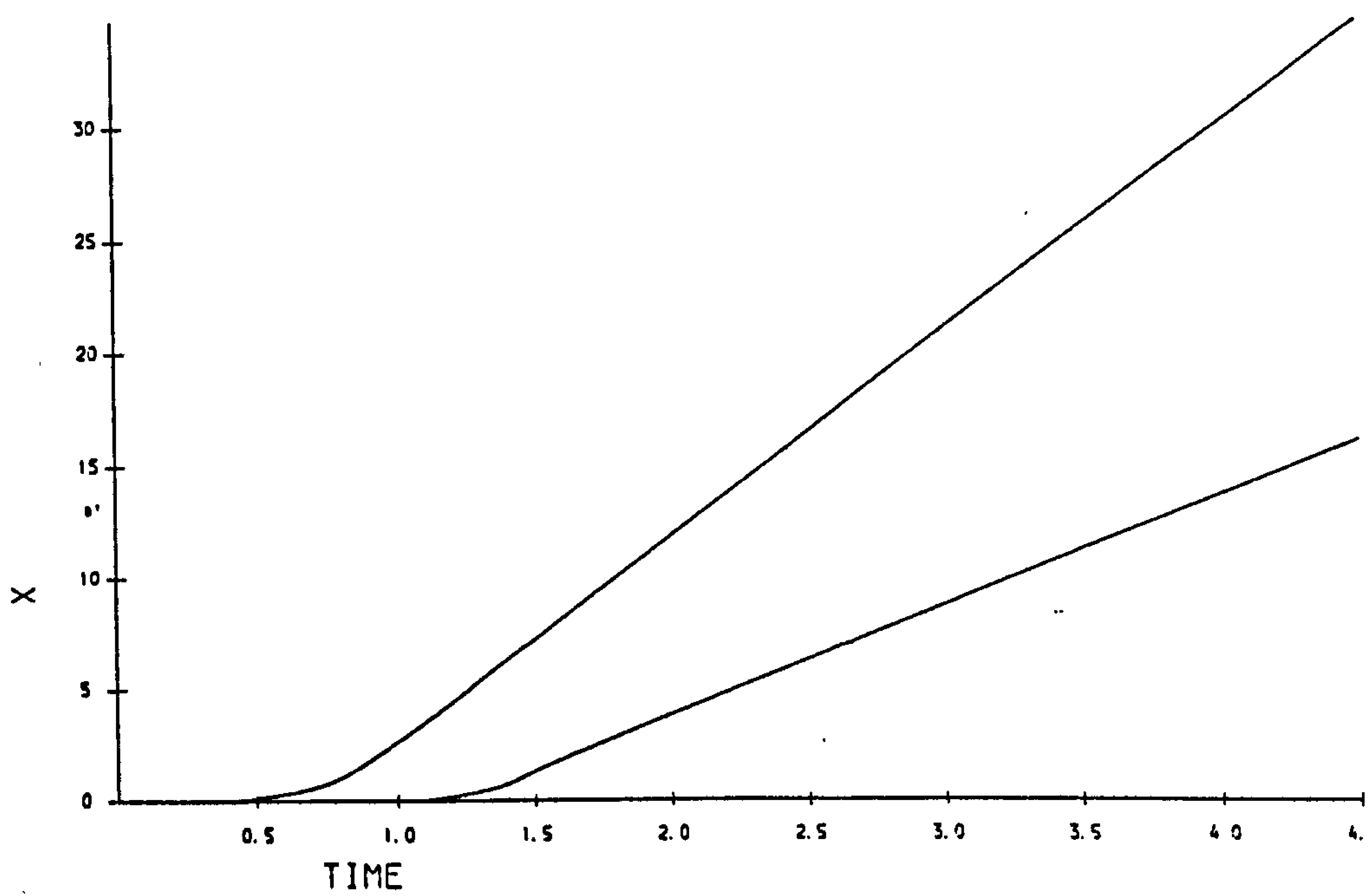

Figure 7.58: Long Impulse. The space-time graphs of the solitons produced by (7.39) with $U_0 = 2, \tau = 0.1, t_0 = 1.5, h = 0.04, \Delta t = 0.001$. $\epsilon = 3$.

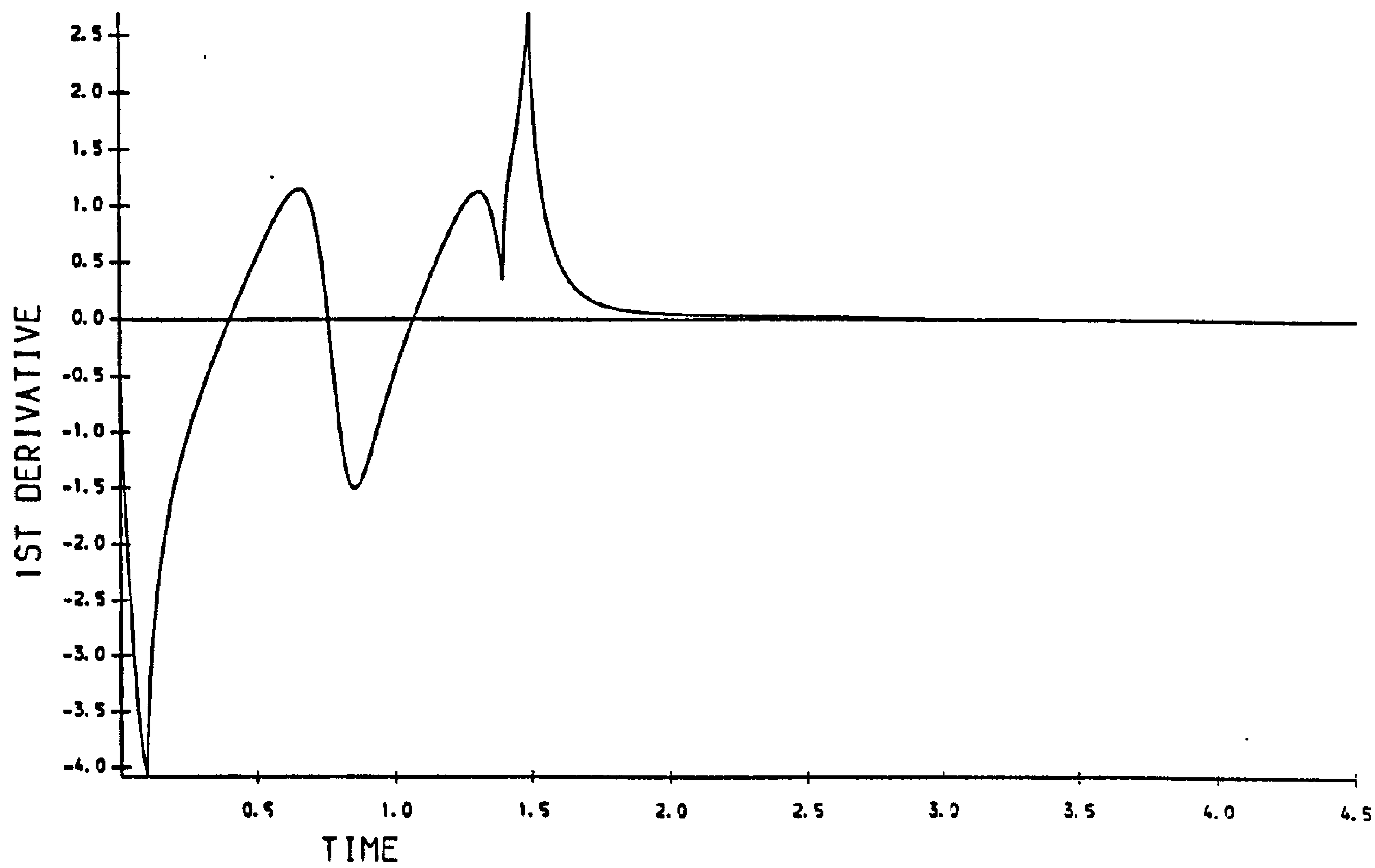

Figure 7.59: Long Impulse. Variation in the first derivative $U_x(0,t)$ at the origin. Forced conditions (7.39) with $U_0 = 2, \tau = 0.1, t_0 = 1.5, h = 0.04, \Delta t = 0.001$. $\epsilon = 3$.

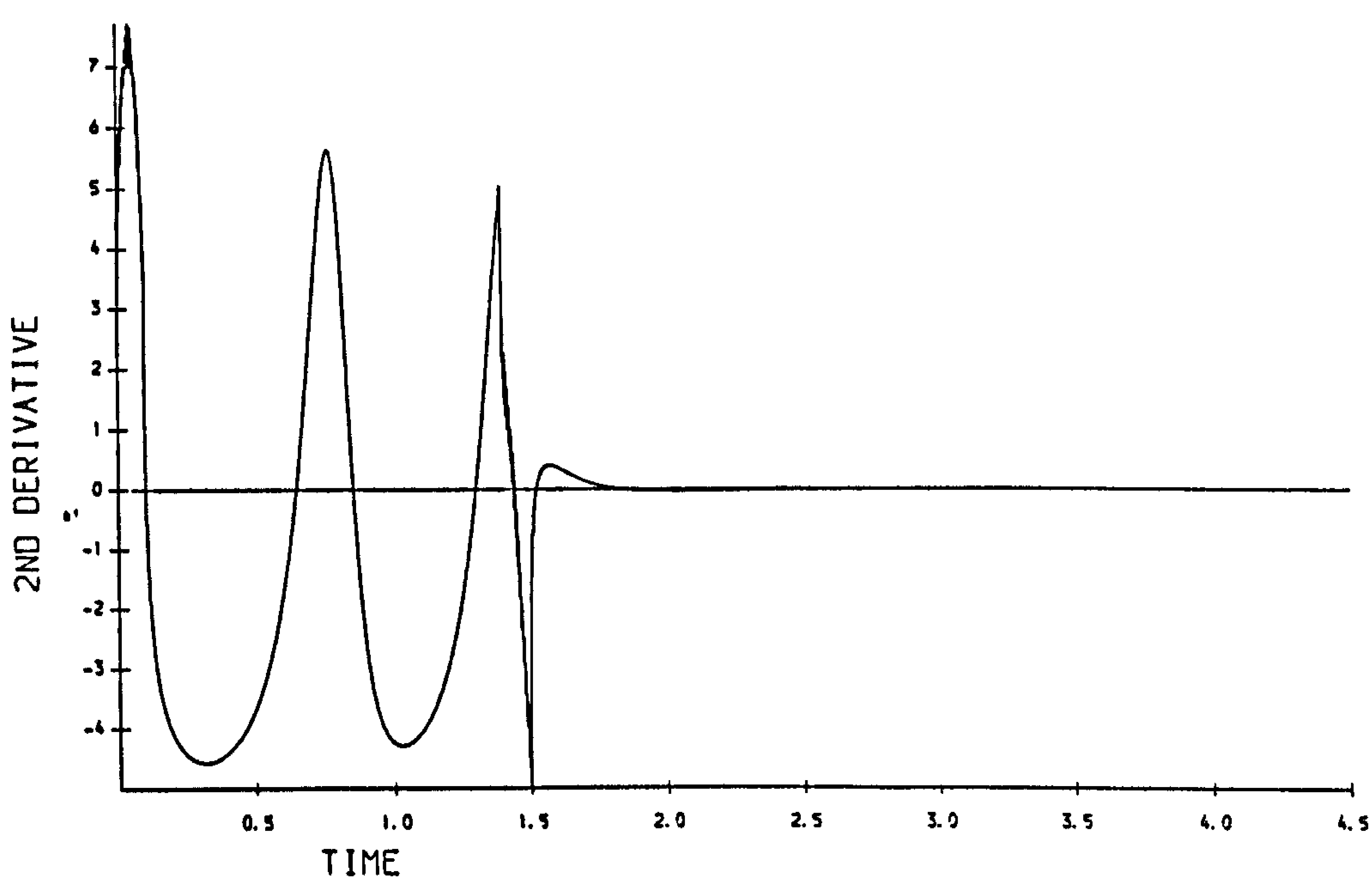

Figure 7.60: Long Impulse. Variation in the second derivative $U_{xx}(0,t)$ at the origin. Forced conditions (7.39) with $U_0 = 2, \tau = 0.1$, $t_0 = 1.5, h = 0.04, \Delta t = 0.001$. $\epsilon = 3$.

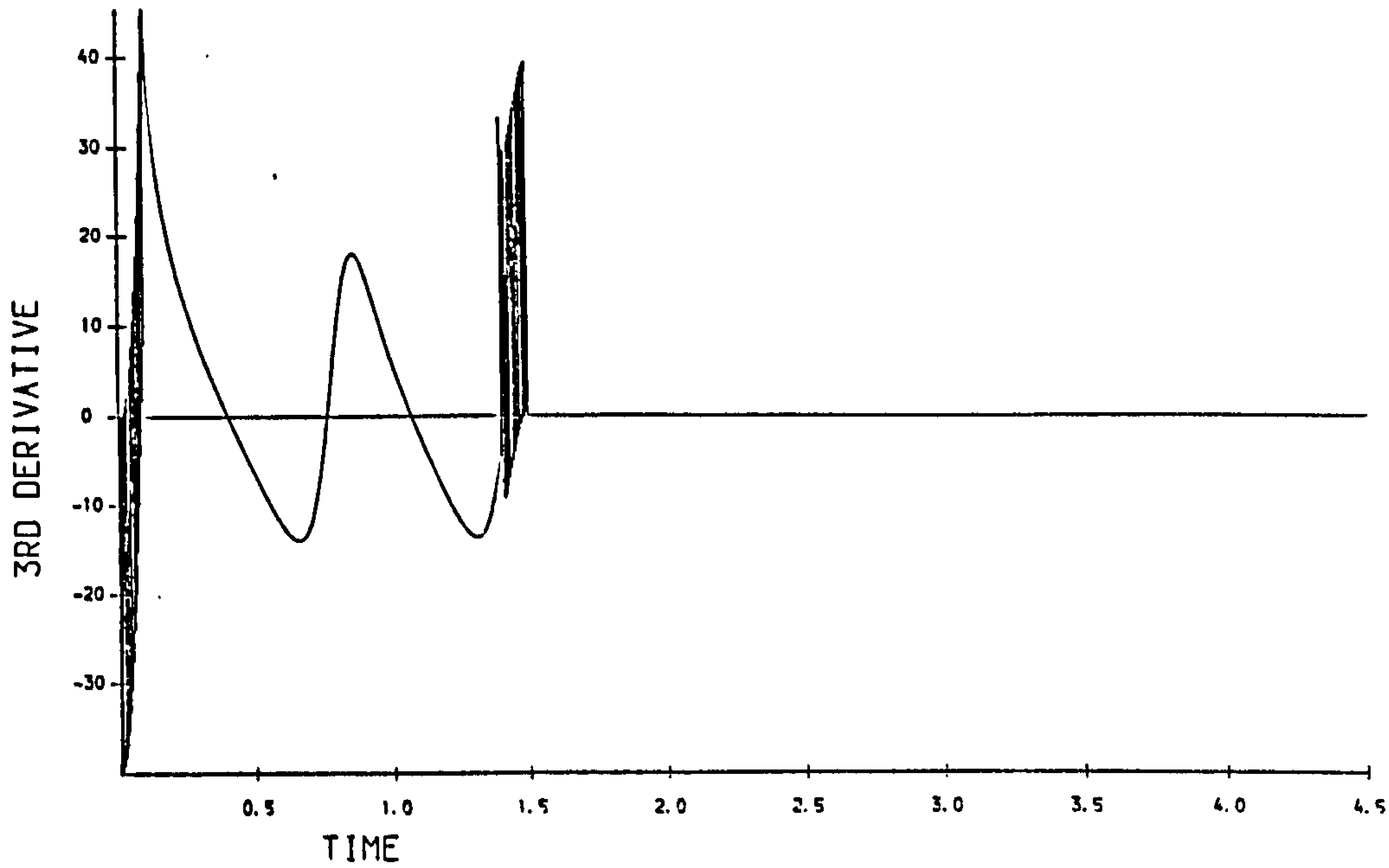

Figure 7.61: Long Impulse. Variation in the third derivative $U_{xxx}(0,t)$ at the origin. Forced conditions (7.39) with $U_0 = 2, \tau = 0.1,\ t_0 = 1.5, h = 0.04, \Delta t = 0.001.\ \epsilon = 3.$

tooth periodic behaviour with maximum of about 1.653, minimum of about -1.615, mean zero and period 0.647. The graphs of $U_{xx}(0,t)$ and $U_{xxx}(0,t)$, Figures (7.60-7.61), also exhibit periodic behaviour with period 5.15.

Table 7.21: Observation of solitary waves, $U_0 = 2, \epsilon = 3$

wave	birth time	generated waves		free soliton
		amplitude	velocity	velocity
1	0.420	4.3009	9.1674	9.2488
2	1.086	3.1459	4.9432	4.9483

7.2.3 Negative forcing

A third series of experiments for which $\epsilon = 3, \mu = 1$ so that $p = 1.4142$. The first experiment involves a negative forcing function. Boundary condition (7.39) is used with $x_{max} = 80, t_{max} = 30, U_0 = -1, \tau = 0.01, t_0 = 30$ so that the forcing lasts throughout the experiment. The result of this experiment is a train of solitary waves with negative amplitudes. The final state is mirror image of the first experiment reported in Series B.

In the two following experiments a short positive impulse is followed by an equal and opposite negative impulse. The forced boundary condition applied at $x = 0$ is

$$U(0,t) = \begin{cases} U_0\frac{t}{\tau} & 0 \le t \le \tau \\ U_0 & \tau < t < t_0 - \tau \\ U_0\frac{t_0-t}{\tau} & t_0 - \tau \le t \le t_0 \end{cases}$$

$$U(0,t) = \begin{cases} -U_0\frac{t-t_0}{\tau} & t_0 \le t \le t_0 + \tau \\ -U_0 & t_0 + \tau < t < 2t_0 - \tau \\ -U_0\frac{2t_0-t}{\tau} & 2t_0 - \tau \le t \le 2t_0 \end{cases} \tag{7.56}$$

i-) First we use $U_0 = 1, \tau = 0.01, t_0 = 11, h = 0.04$, and $\Delta t = 0.001$. The forcing has period $2t_0 = 22$. The progress of the simulation is shown in Figures (7.62). Initially between, $0 \le t \le 11$, the forcing is positive, two solitary waves are born one of which reaches maturity. In the second period, $11 \le t \le 22$, when forcing is negative the smaller of the generated waves is gradually eroded away. At time $t = 30$ the state includes a single solitary wave at about $x = 58$ and a small disturbance located near the origin. As the experiment is run on, the disturbance near the origin dies away and we are left with a single solitary wave of amplitude 2.15.

ii-) The value of t_0 is reduced to 9 so that forcing has the shorter period $2t_0 = 18$. The progress of the simulation is now given in Figures (7.63).

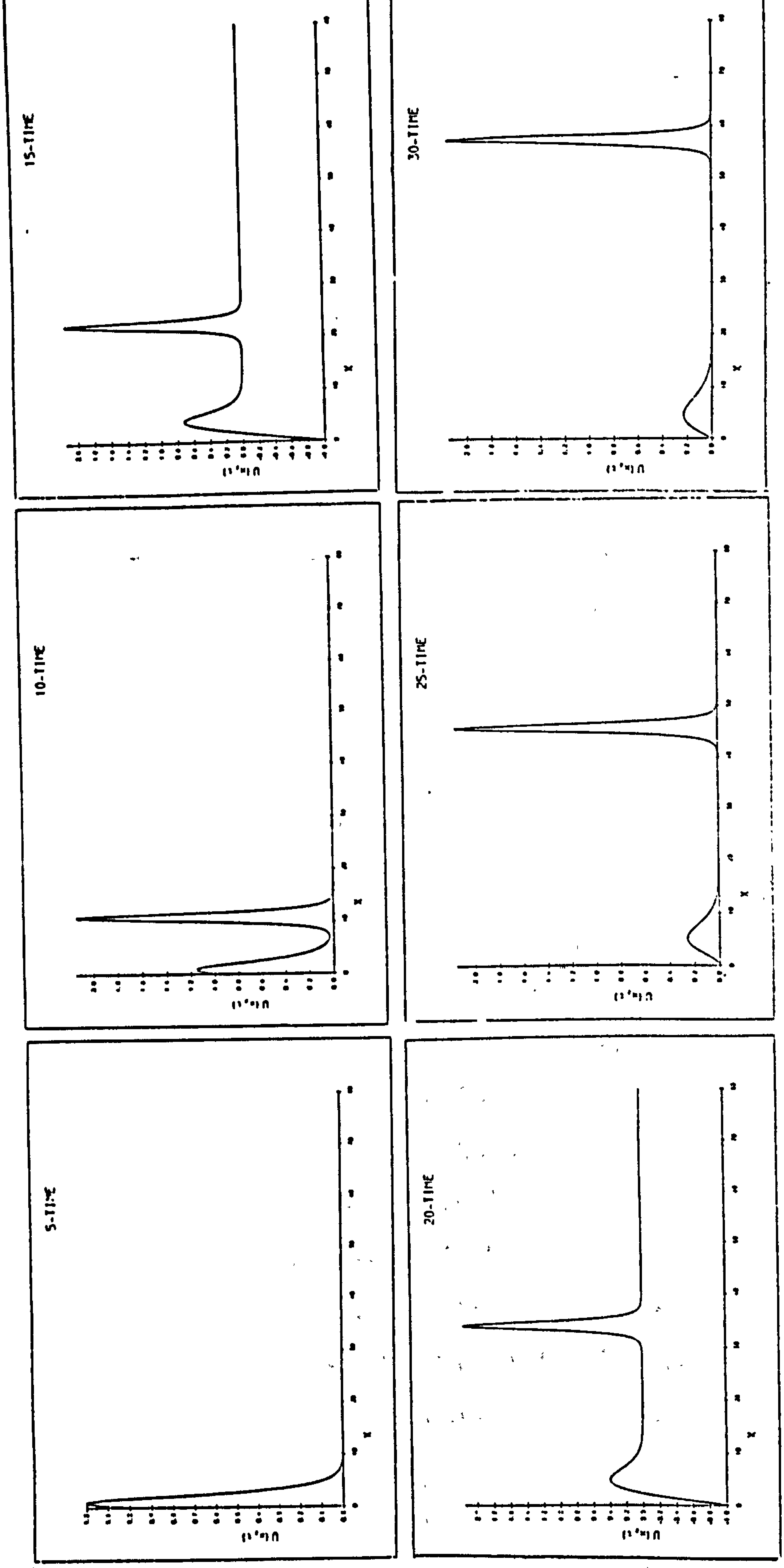

Figure 7.62: Positive/Negative Impulse. Solitons produced by Forced conditions (7.64) with $U_0 = 1, \tau = 0.01, t_0 = 11, h = 0.04, \Delta t = 0.001$ graphed at intervals of $t = 5$. $\epsilon = 3$.

During the positive forcing two solitary waves are generated, the first grows to maturity but the second has barely appeared when the negative forcing comes into operation. The very small positive wave is rapidly eroded away and a negative solitary wave then forms. The final state consists of a positive solitary wave of amplitude 2.15 and a negative solitary wave of amplitude 2.0. The latter is slightly smaller as an incipient positive wave produced near the end of the positive forcing has first to be removed by the negative forcing before a negative wave can start to grow. With t_0 reduced further to 8.1, a positive and a negative solitary wave of approximately equal amplitudes 2.15 are obtained.

7.2.4 Wave interaction

i-) In this experiment two positive solitary waves are generated and allowed to collide. We set $\epsilon = 6, \mu = 1$ so that $p = 1$, and use $x_{max} = 80$, $t_{max} = 10, U_0 = 1, \tau = 0.01, t_0 = 10$ and step lengths $h = 0.04$ and $\Delta t = 0.001$. An initial forcing of magnitude $U_0 = 0.5$ is applied up to time $t = 28$, a wave with amplitude 1.078 is formed. Increased forcing $U_0 = 1.0$ is then applied up to time $t = 30$ and a wave with amplitude 1.940 is generated.

These waves are allowed to interact as shown in Figures (7.64). Details of the interaction are given in Table (7.23). From the observed amplitudes of the two solitary waves we may calculate the theoretically expected velocities of solitons of similar amplitudes as 1.162 and 3.764. Hence, as $p = 1$, we may calculate the expected phase shifts from $\beta = \{\frac{a_1 - a_2}{a_1 + a_2}\}^2$ and $\Delta = \ln(\frac{1}{\beta}) = 2.50$ as $\Delta_1 = -(\frac{\Delta}{a_1}) = -2.319$ and $\Delta_2 = (\frac{\Delta}{a_2}) = 1.289$.

Initial measured velocities are found from $(x_{32.5} - x_{30})/2.5$ as $V_1 = 1.164 \pm 0.02$ and $V_2 = 3.764 \pm 0.02$ and final measured velocities are found from $(x_{40} - x_{37.5})/2.5$ as $V_1 = 1.164 \pm 0.02$ and $V_2 = 3.764 \pm 0.02$. These velocities are consistent with those of solitons of like amplitude. Expected positions,

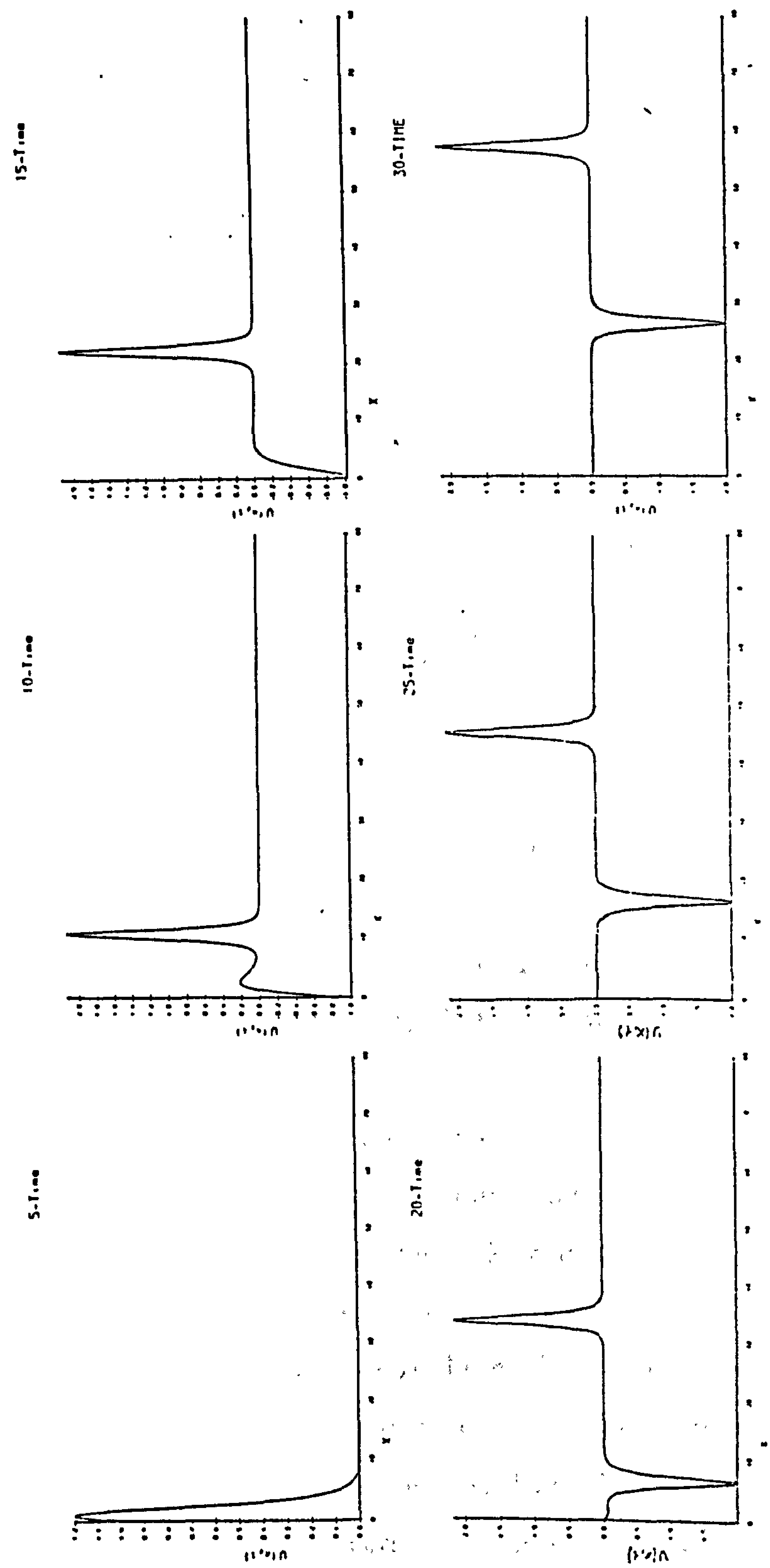

Figure 7.63: Positive/Negative Impulse. Solitons produced by Forced conditions (7.60) with $U_0 = 1, \tau = 0.01, t_0 = 9, h = 0.04, \Delta t = 0.001$ graphed at intervals of $t = 5$. $\epsilon = 3$.

Table 7.22: Positions and amplitudes of the solitary waves throughout the interaction

time	x_1	U_1	x_2	U_2
25.0	11.60	1.070		
27.5	14.48	1.076		
30.0	17.37	1.078	5.42	1.829
32.5	20.28	1.078	14.83	1.920
35.0	20.88	1.080	25.56	1.892
37.5	23.78	1.078	34.94	1.940
40.0	26.69	1.078	44.35	1.940

x^E_{40}, at $T = 40$ are now found and the corresponding phase shift measured. Using $V \times 10 + x_{30} = x^E_{40} - x_{40} = \Delta$, leads to $\Delta_1 = -2.32 \pm 0.02$ and $\Delta_2 = 1.29 \pm 0.02$ values consistent with those expected of solitons. The above measurements indicate clearly that the generated solitary waves are closely identified with free solitons.

ii-) In a second experiment studying the interaction of two positive solitary waves, we interpose after the initial forcing $U_0 = 0.5$ which lasts until $t = 17.5$, a period during which $U_0 = 0$ up to $t = 28$ after which increased forcing $U_0 = 1.0$ is applied up to $t = 30$. These waves are allowed to interact as shown in Figure (7.65). From the growth curves for the wave amplitudes shown in Figure (7.66) we estimate the wave amplitudes both before and after the interaction to be 0.9374 and 1.410 and from the space-time graph in Figure (7.67) the corresponding velocities are 0.880 and 1.988.

Initial measured velocities are found from $(x_{35} - x_{32.5})/2.5$ as $V_1 = 1.988 \pm 0.02$ and $V_2 = 0.880 \pm 0.02$ and final measured velocities from $(x_{50} - x_{47.5})/2.5$

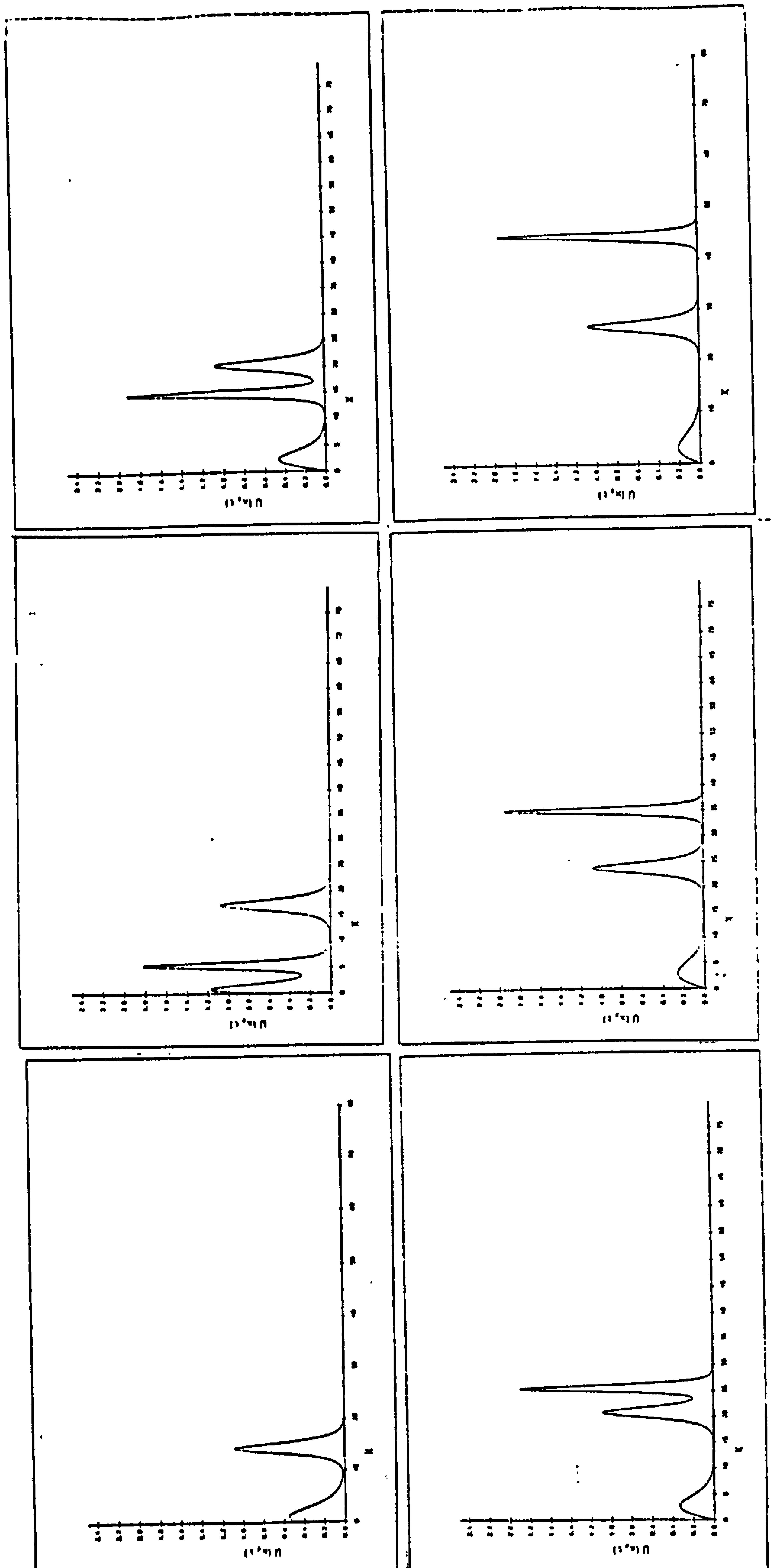

Figure 7.64: Double Impulse. The interaction of two solitons produced by forced conditions with $U_0 = 0.5$ until $t = 28$, and $U_0 = 1.0$ until $t = 30, h = 0.04, \Delta t = 0.001$ graphed at intervals of $t = 2.5. \epsilon = 6$.

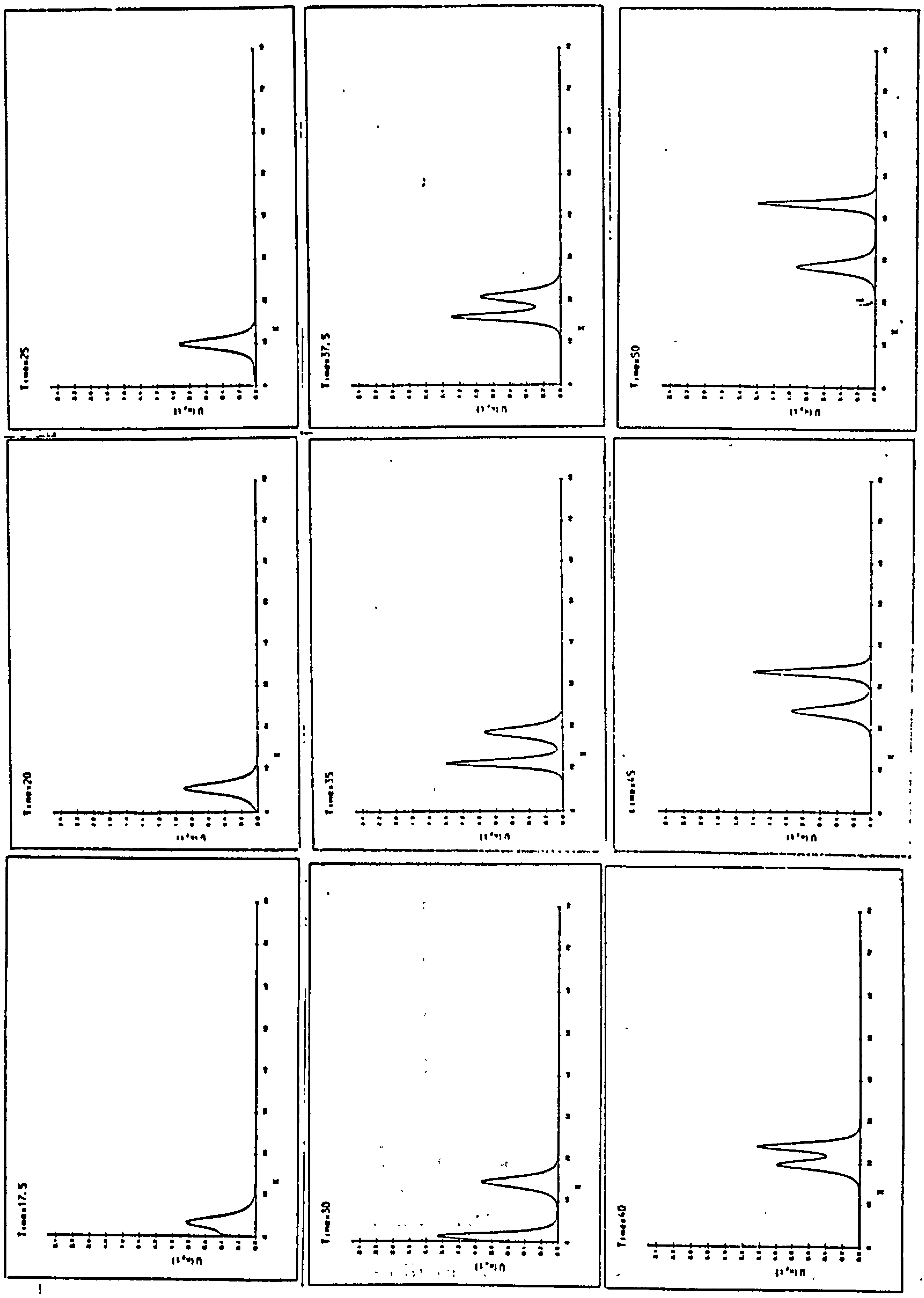

Figure 7.65: Double Impulse. The interaction of two solitons produced by forced conditions with $U_0 = 0.5$ until $t = 17.5$, and $U_0 = 1.0$ until $t = 28$, and $U_0 = 1.0$ until $t = 30, h = 0.04, \Delta t = 0.001$ graphed at various times. $\epsilon = 6$.

Table 7.23: Positions and amplitudes of the solitary waves throughout the interaction.

time	x_1	U_1	x_2	U_2
30.0	1.22	1.475	14.44	0.936
32.5	6.49	1.404	16.64	0.937
35.0	11.46	1.400	18.84	0.938
42.5	28.70	1.392	22.02	0.939
45.0	33.62	1.409	24.22	0.937
47.5	38.60	1.410	26.42	0.937
50.0	43.57	1.411	28.62	0.937

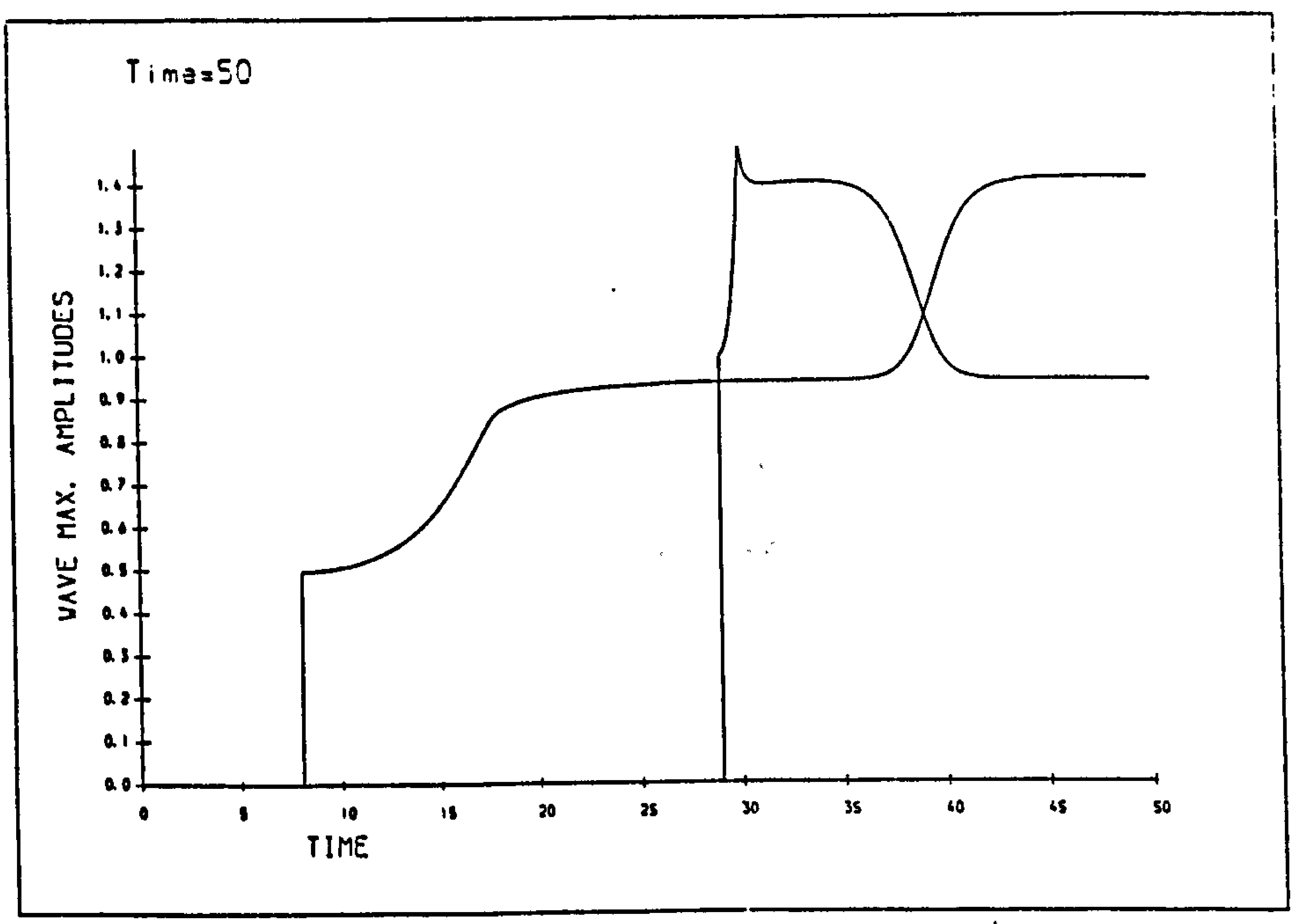

Figure 7.66: Double Impulse. Amplitude growth curves for two solitons produced by forced conditions with $U_0 = 0.5$ until $t = 17.5$, and $U_0 = 1.0$ until $t = 28$, and $U_0 = 1.0$ until $t = 30, h = 0.04, \Delta t = 0.001$ graphed at intervals of $t = 2.5$. $\epsilon = 6$.

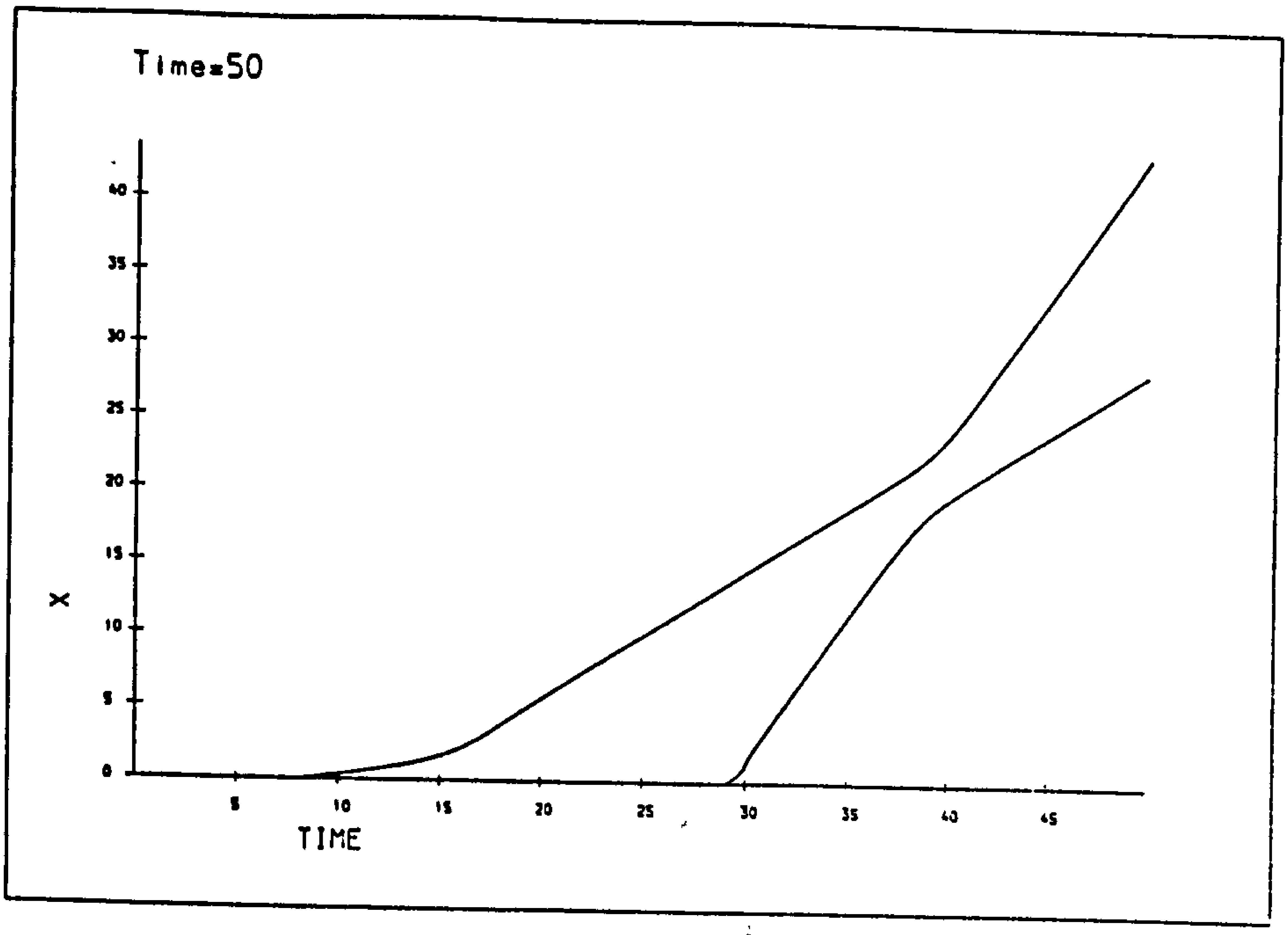

Figure 7.67: Double Impulse. Space-time curves for two solitons produced by forced conditions with $U_0 = 0.5$ until $t = 17.5$, and $U_0 = 1.0$ until $t = 28$. and $U_0 = 1.0$ until $t = 30, h = 0.01, \Delta t = 0.001$ graphed at intervals of $t = 2.5$. $\epsilon = 6$.

as $V_1 = 1.988 \pm 0.02$ and $V_2 = 0.880 \pm 0.02$. These velocities are consistent with those of solitons of like amplitude. Expected positions, x^E_{45}, at $t = 45$ are now found and the corresponding phase shift measured. Using $V \times 10 + x_{35} = x^E_{45} - x_{45} = \Delta_i$, leads to $\Delta_1 = -2.28 \pm 0.02$ and $\Delta_2 = 3.42 \pm 0.02$. From the observed amplitudes of the two solitary waves we may calculate the expected phase shifts as $\Delta_1 = -(\frac{\Delta}{a_1}) = -2.274$ and $\Delta_2 = (\frac{\Delta}{a_2}) = 3.420$. Agreement is close.

7.3 Simulations 2

We also examined the case of a Gaussian boundary function,

$$U(0,t) = U_0 \exp[-\tau(t - t_0)^2] \tag{7.57}$$

where τ and t_0 are now chosen in order to have $U(0,0)$ of the same order as the time step used in the numerical calculations.

Initially the region is undisturbed so that at time $t = 0$ all δ_j are zero. The forced Gaussian boundary condition is applied at $x = 0$ and further homogeneous boundary conditions are imposed at $x = x_{max}$. The effect of the impulse is to generate solitary waves at $x = 0$, which grow until they achieve a terminal amplitude, determined by the magnitude U_0 of the forced boundary value. Solitary waves are continually generated while the forcing conditions prevail, then all growth slows and eventually ceases.

7.3.1 Positive forcing series

In these experiments $\epsilon = 6, \mu = 1$ so that $P = 1$.

i-) Firstly boundary condition (7.65) is used with $U_0 = 2.5, x_{max} = 20, t_{max} = 0.8, \tau = 60, t_0 = 0.4$ so that the forcing lasts throughout the experiment. The numerical step lengths are $h = 0.02$ and $\Delta t = 0.0005$.

In this numerical experiment, see Figure (7.68) two solitary waves are generated before the simulation is terminated at $t = 0.8$. Figures (7.69) and (7.70) show that 2 achieve their terminal heights and a constant velocity.

The generating conditions for the first wave are rather more protracted than those for all subsequent waves, as can be seen from the graphs of the first two derivatives at $x = 0$ given in Figures (7.71-7.72) so it achieves a slightly larger amplitude and velocity than do the following waves. The observation on the solitary waves generated are collected in Table (7.24). The time interval between births of solitary waves is constant at $\Delta T_B = 0.137$, the measured terminal heights for solitary waves 1-2 vary between 4.690 and 0.2928 with measured velocities of 21.6. Free solitons of similar heights would have velocities 21.9961 - 0.0857, so that agreement is close. After an initial transient the graph of $U_x(0,t)$, Figure(7.71), shows a rounded saw tooth periodic behaviour with maximum of about 2.69, minimum of about -3.0 mean zero and period 0.137. The graphs of $U_{xx}(0,t)$, Figure(7.72), also

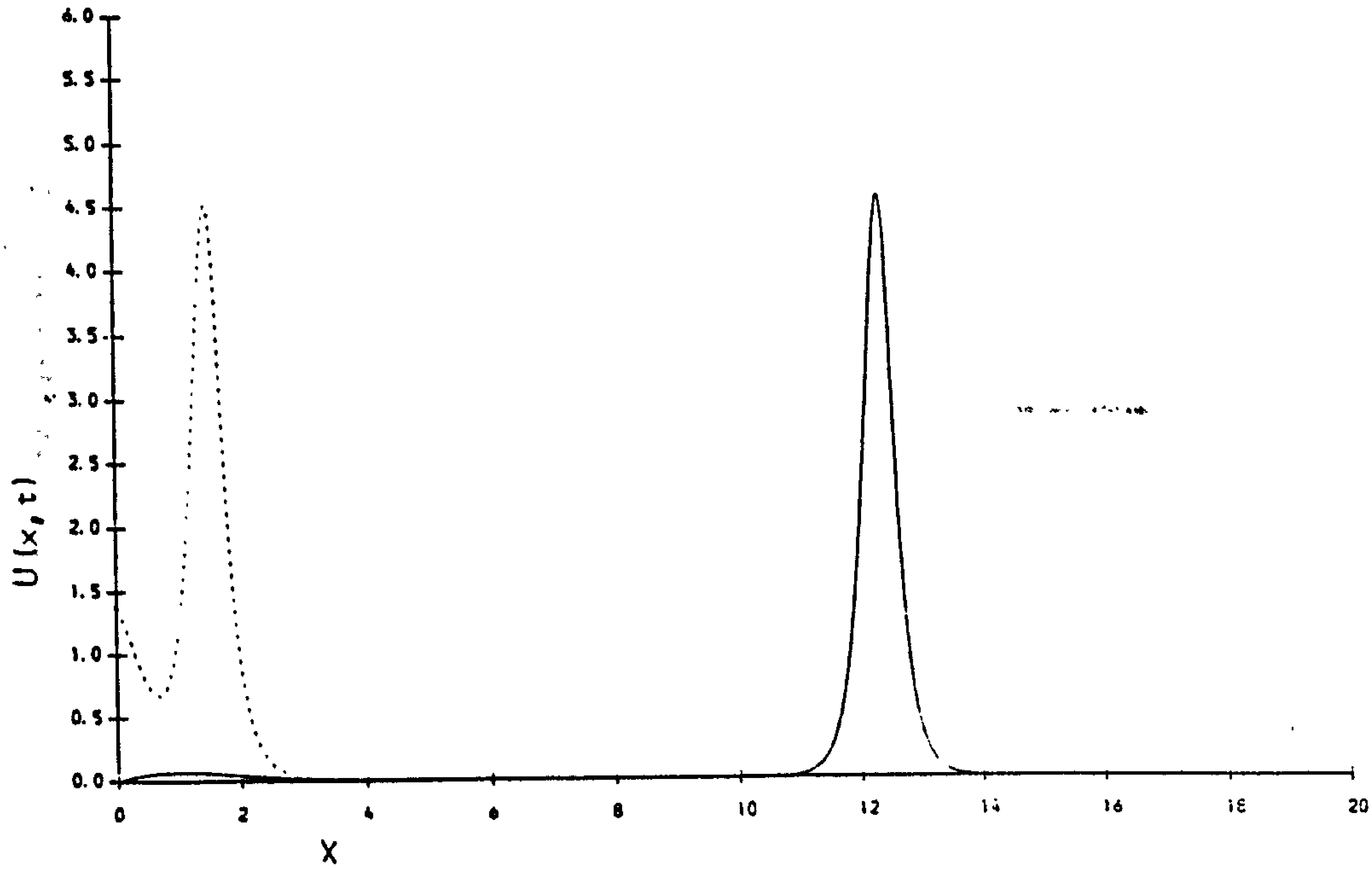

Figure 7.68: Long Impulse. Soliton produced by forced conditions (7.57) with $U_0 = 2.5, \tau = 60, t_0 = 0.4, h = 0.02, \Delta t = 0.0005$ graphed at $t = 0.4$ (- - - -) and $t = 0.8$ (——)

exhibit periodic behavior with period 0.137.

ii-) An experiment with increased forcing, $U_0 = 4$; boundary condition (7.57) is used with $x_{max} = 20, t_{max} = 0.8, \tau = 60, t_0 = 0.40$ so that the forcing lasts throughout the experiment. The numerical step lengths are $h = 0.02$ and $\Delta t = 0.0005$. In this numerical experiment, see Figure (7.73), four solitary waves are generated before the simulation is terminated at t =

Table 7.24: Observation of solitary waves, $U_0 = 2.5, \epsilon = 6$

wave	birth time	generated waves		free soliton
		amplitude	velocity	velocity
1	0.388	4.6900	21.60	21.9961
2	0.525	0.2928		0.0857

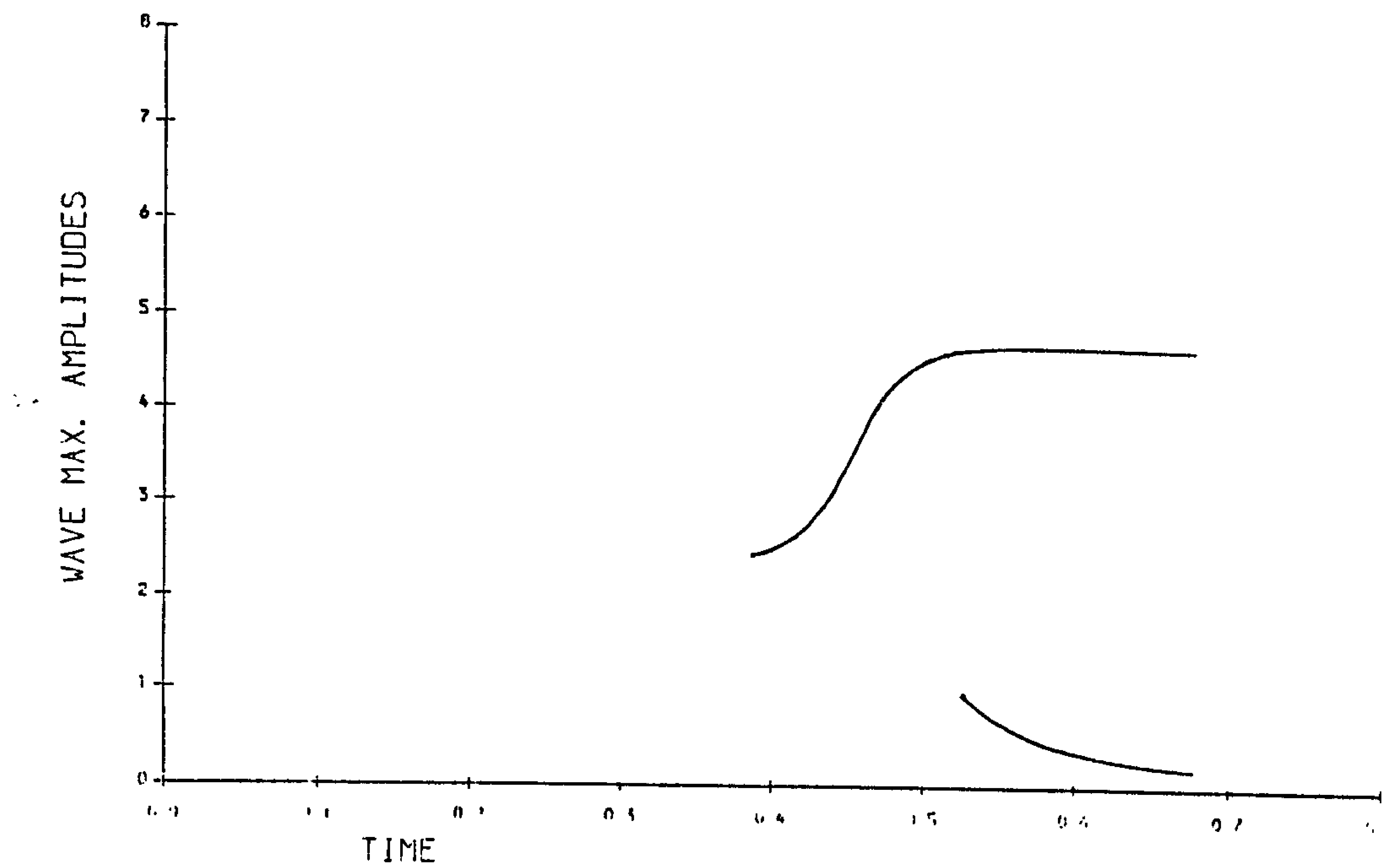

Figure 7.69: Long Impulse. The evolution of the soliton amplitudes. Forced conditions (7.57) with $U_0 = 2.5, \tau = 60, t_0 = 0.4, h = 0.02, \Delta t = 0.0005$.

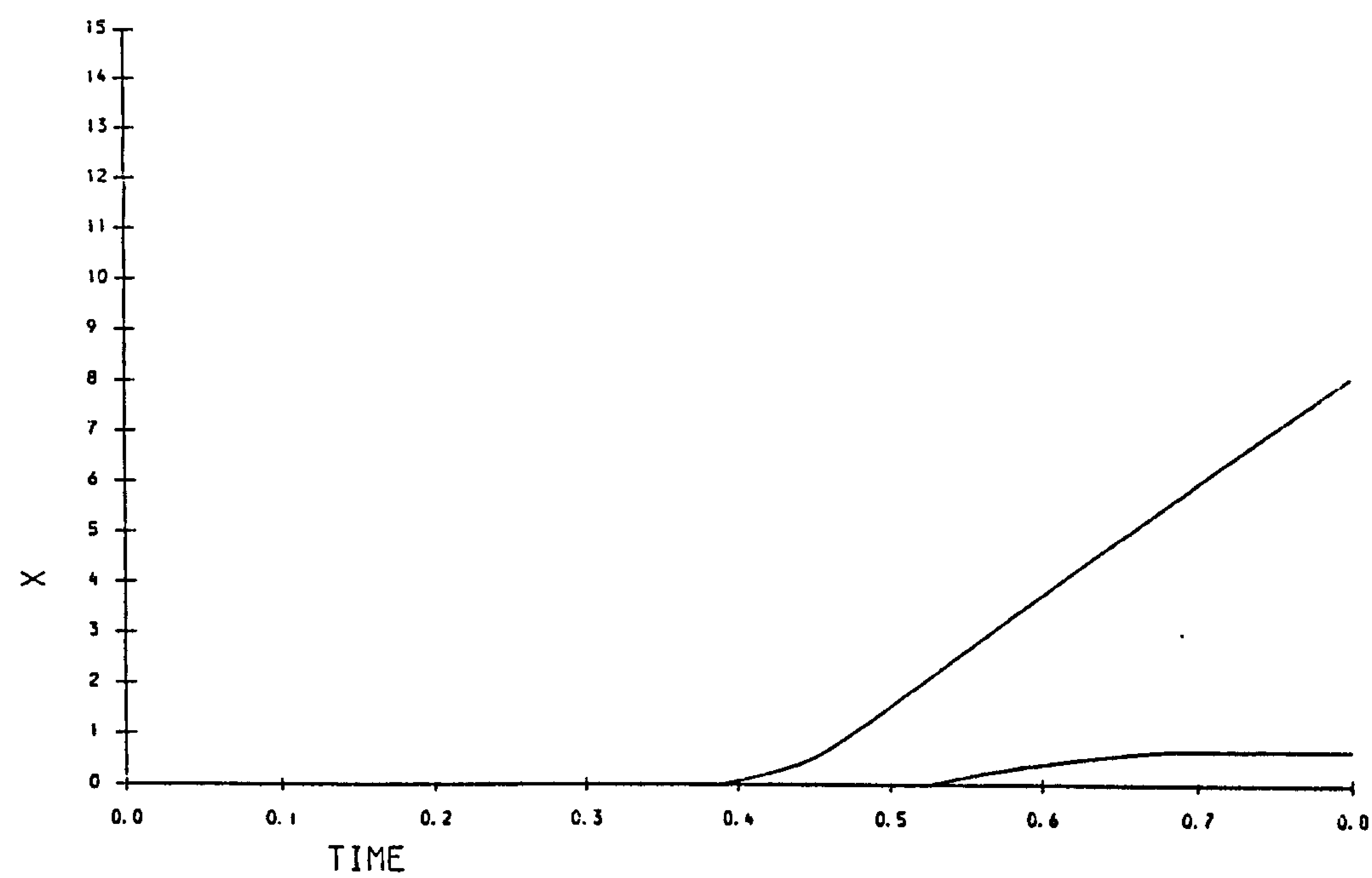

Figure 7.70: Long Impulse. The space-time graphs of the soliton produced by forced conditions (7.57) with $U_0 = 2.5, \tau = 60, t_0 = 0.4, h = 0.02, \Delta t = 0.0005$.

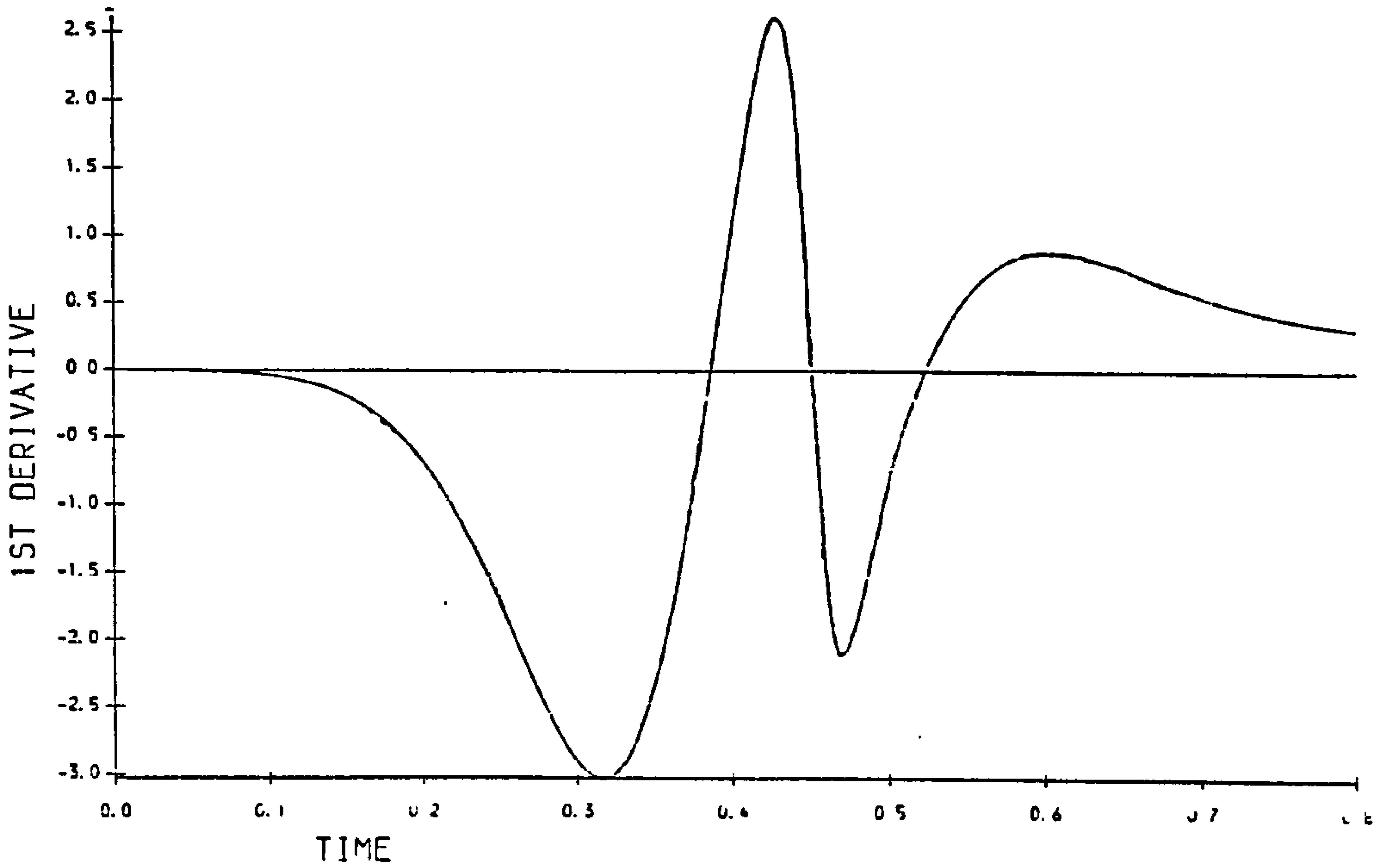

Figure 7.71: Long Impulse. Variation in the first derivative $U_x(0,t)$ at the origin. Forced conditions (7.57) with $U_0 = 2.5, \tau = 60, t_0 = 0.4, h = 0.02$. $\Delta t = 0.0005$.

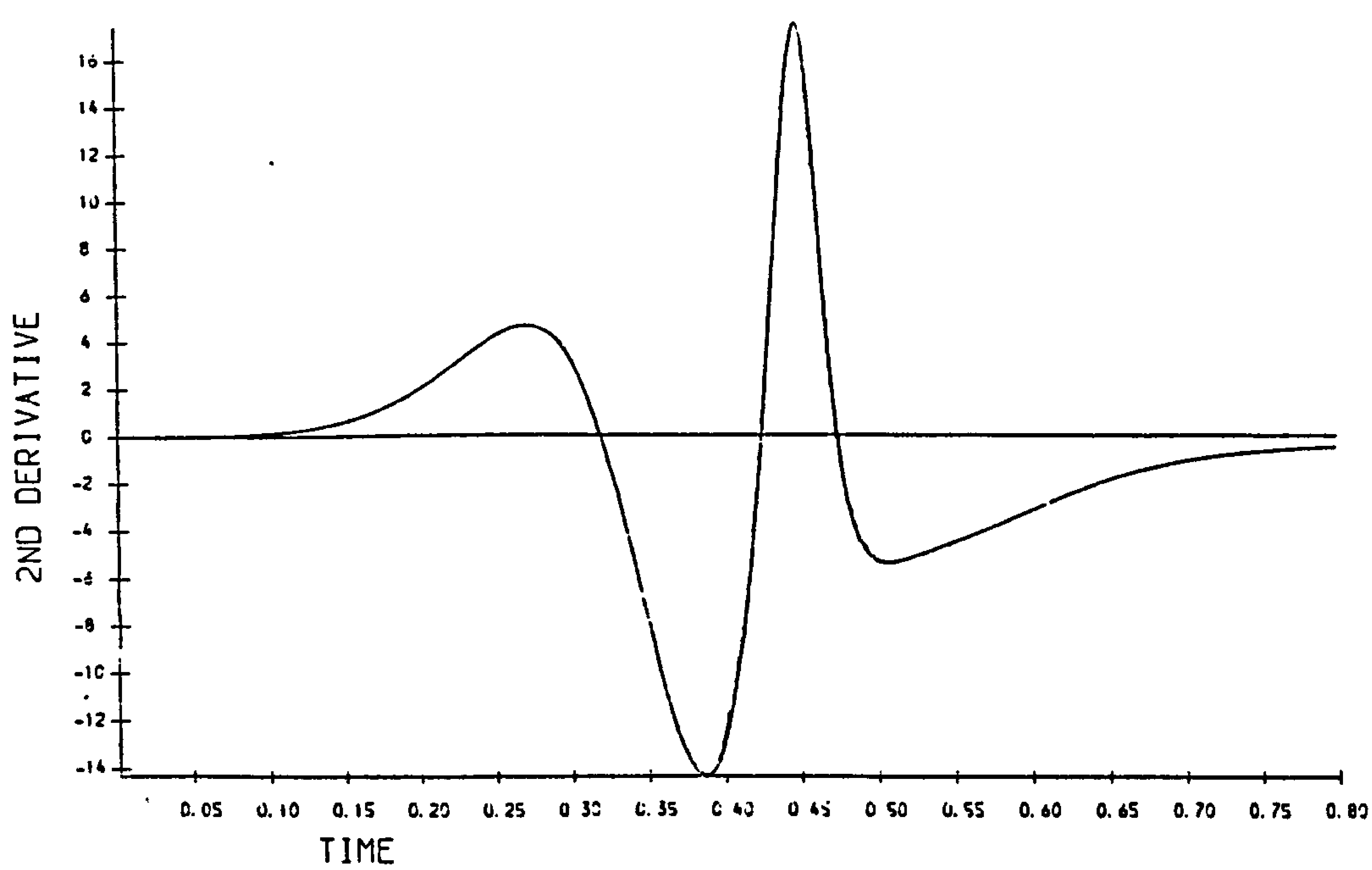

Figure 7.72: Long Impulse. Variation in the second derivative $U_{xx}(0,t)$ at the origin. Forced conditions (7.57) with $U_0 = 2.5, \tau = 60, t_0 = 0.4, h = 0.02$, $\Delta t = 0.0005$.

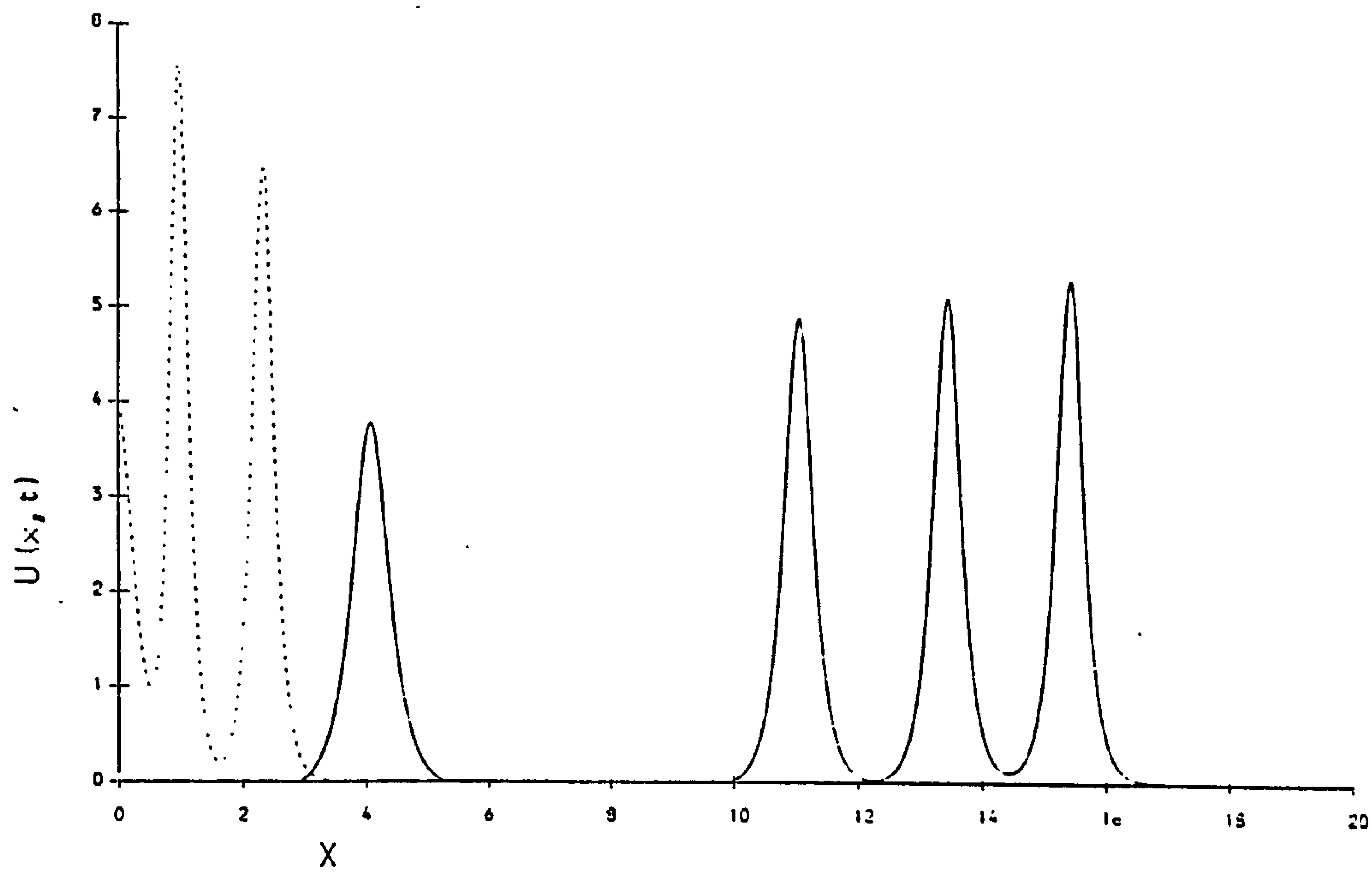

Figure 7.73: Long Impulse. Soliton produced by forced conditions (7.57) with $U_0 = 4, \tau = 60, t_0 = 0.4, h = 0.02, \Delta t = 0.0005$ graphed at $t = 0.4$ (- - - -) and $t = 0.8$ (——)

0.8. Figures (7.74) and (7.75) show that three achieve their terminal heights and a constant velocity.

The generating conditions for the first wave are rather more protracted than those for all subsequent waves, as can be seen from the graphs of the first two derivatives at $x = 0$ given in Figures (7.76-7.77) so it achieves a slightly larger amplitude and velocity than do the following waves. The observation on the solitary waves generated are collected in Table (7.25). The measured terminal heights for solitary waves 2-4 vary between 5.1579 and 3.8013 with measured velocities of 26.6666 - 14.074. Free solitons of similar heights would have velocities 26.6039 - 14.4498, so that agreement is close. After an initial transient the graph of $U_x(0,t)$, Figure(7.76), shows a rounded saw tooth periodic behaviour with maximum of about 7.0, minimum of about -9.0 mean zero, and second derivative graph of $U_{xx}(0,t)$, in Figure (7.77).

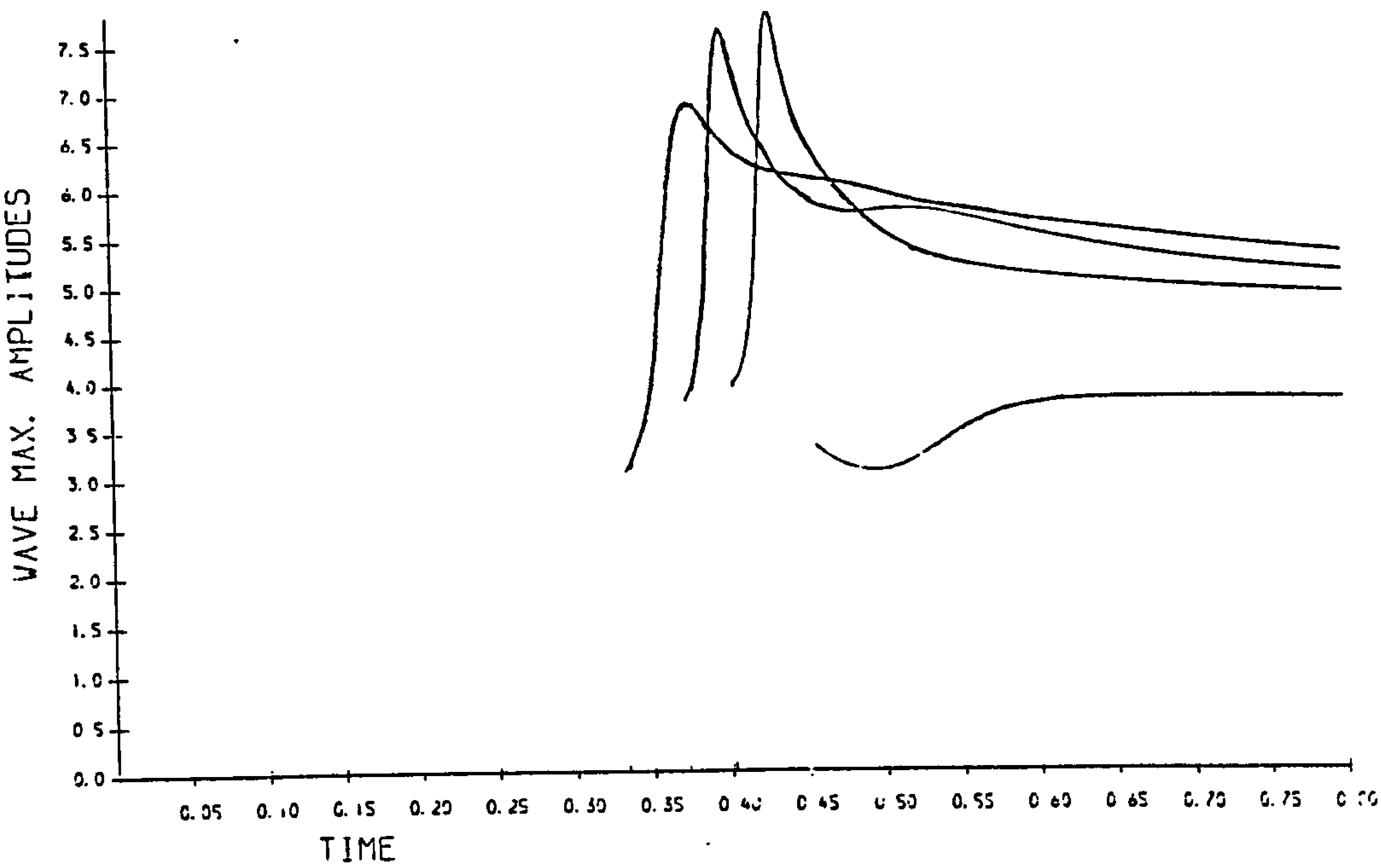

Figure 7.74: Long Impulse. The evolution of the soliton amplitudes. Forced conditions (7.57) with $U_0 = 4, \tau = 60, t_0 = 0.4, h = 0.02, \Delta t = 0.0005$.

Table 7.25: Observation of solitary waves, $U_0 = 4, c = 6$.

wave	birth time	generated waves		free soliton
		amplitude	velocity	velocity
1	0.334	5.3599	28.1481	28.7285
2	0.373	5.1579	26.6666	26.6039
3	0.405	4.9176	23.7037	24.1827
4	0.451	3.8013	14.0740	14.4498

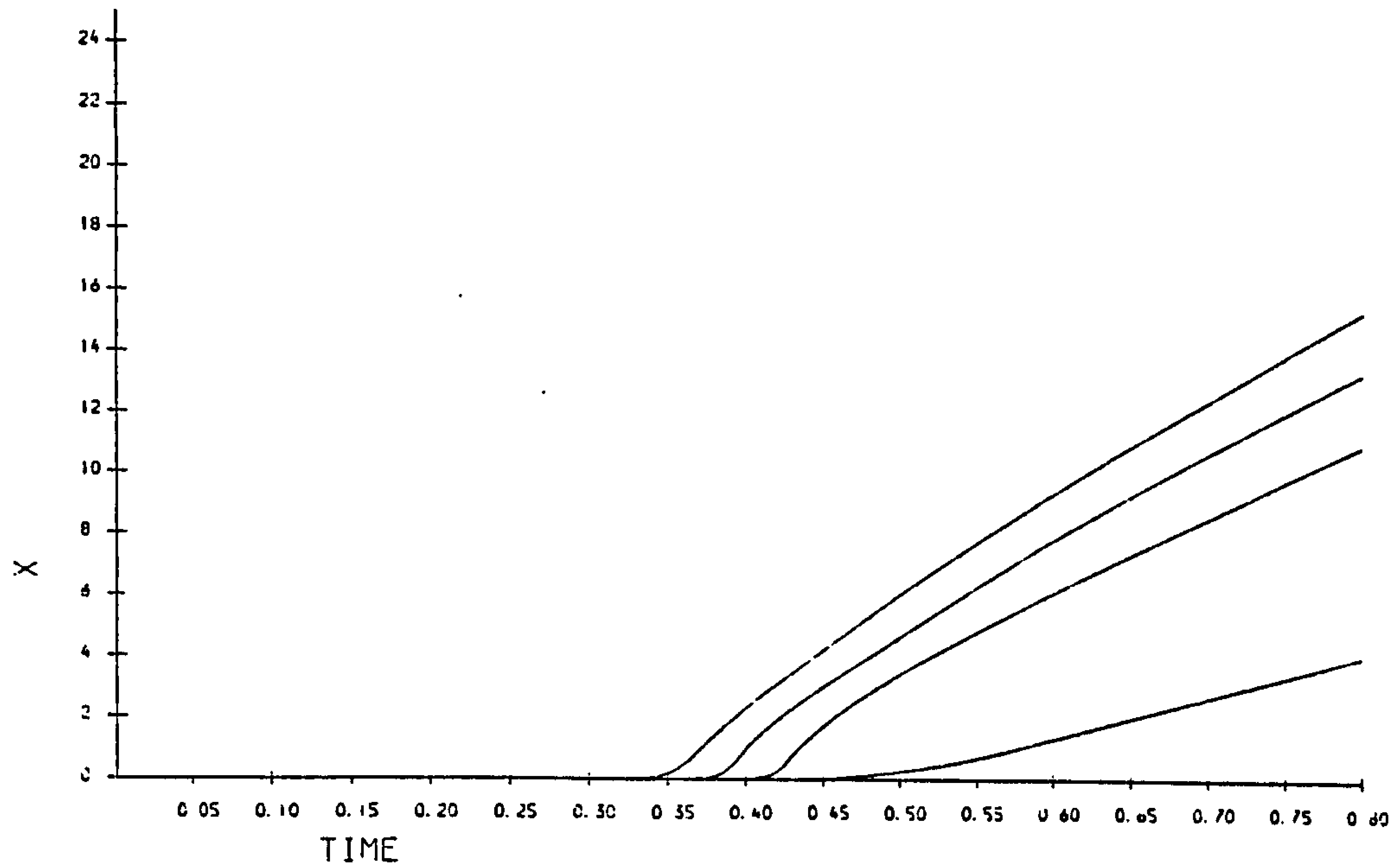

Figure 7.75: Long Impulse. The space-time graphs of the soliton produced by forced conditions (7.57) with $U_0 = 4, \tau = 60, t_0 = 0.4, h = 0.02, \Delta t = 0.0005$.

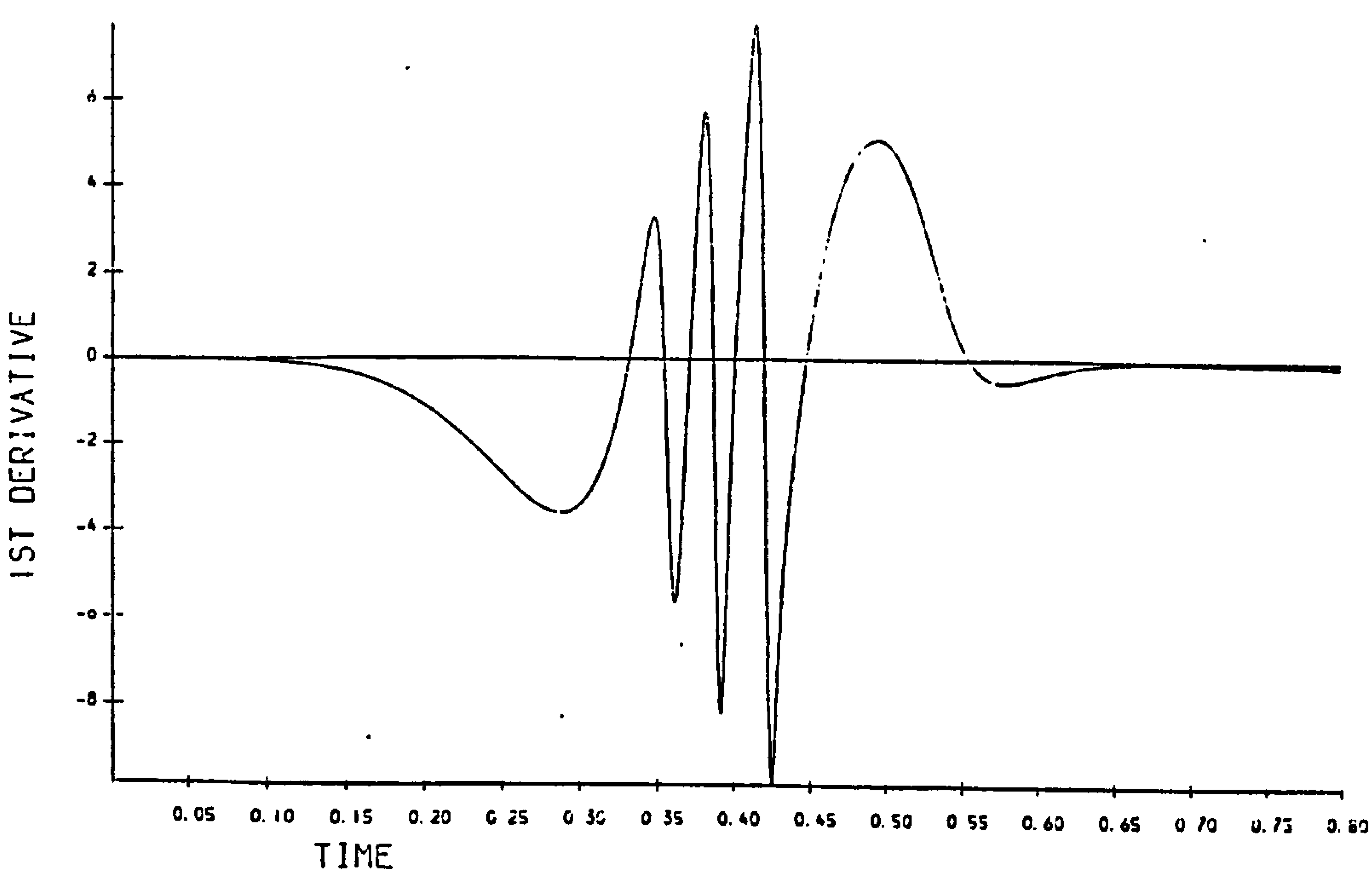

Figure 7.76: Long Im pulse. Variation in the first derivative $U_x(0,t)$ at the origin. Forced conditions (7.57) with $U_0 = 4, \tau = 60, t_0 = 0.4, h = 0.02, \Delta t = 0.0005$.

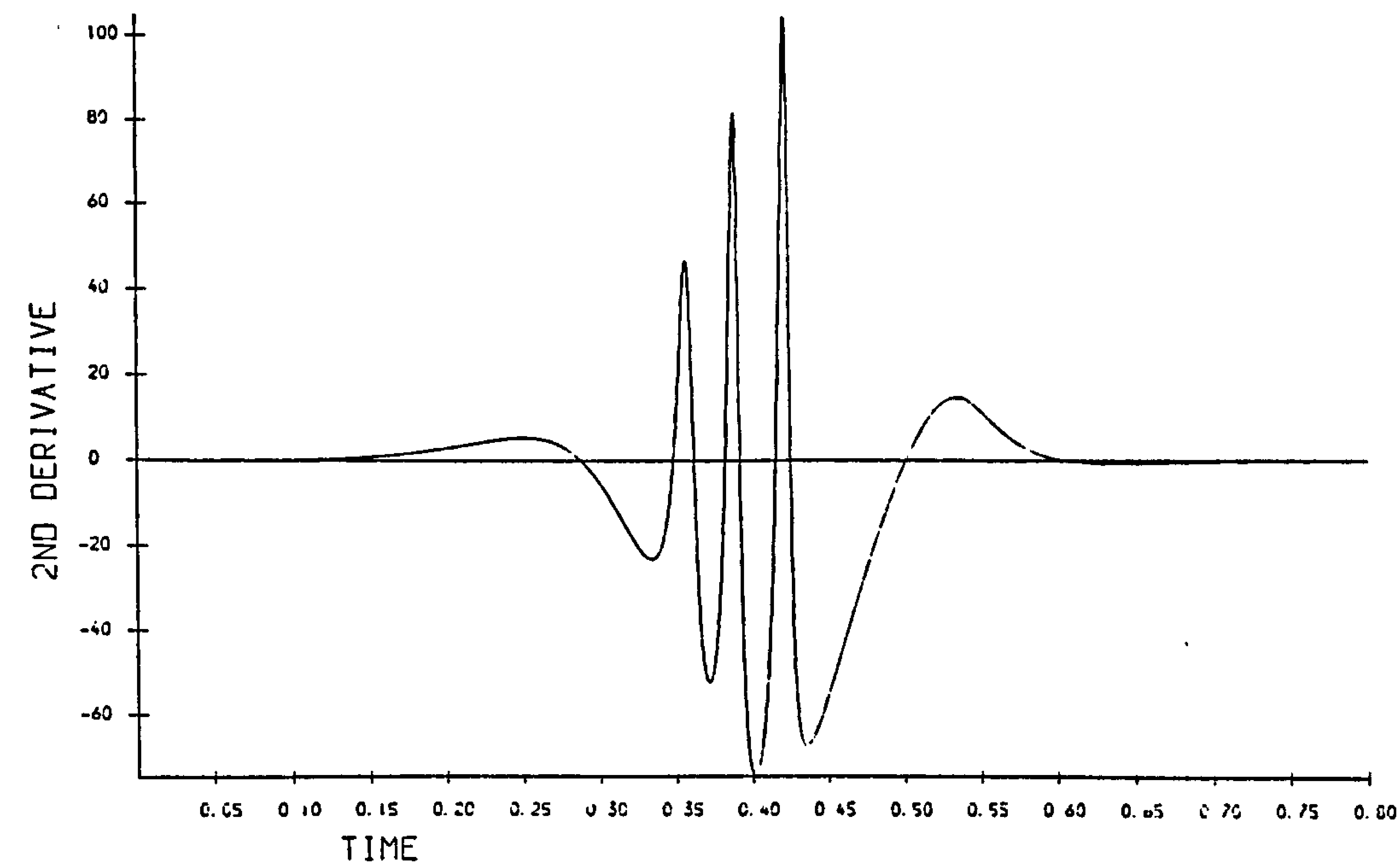

Figure 7.77: Long Impulse. Variation in the second derivative $U_{xx}(0,t)$ at the origin. Forced conditions (7.57) with $U_0 = 4, \tau = 60, t_0 = 0.4, h = 0.02$. $\Delta t = 0.0005$.

7.4 Simulation 3

As a final example we study the temporal development of a Maxwellian initial condition.

$$U(x,0) = \exp(-x^2). \tag{7.58}$$

We fix the value of ϵ at 1 and examine the evolution of the solution for various values of μ. Integrating (7.6) analytically shows that $I_1 = \sqrt{(\pi)} = 1.7725$, $I_2 = \sqrt{(\frac{\pi}{2})} = 1.2533$, $I_3 = \frac{1}{2}(1 - 6\mu\sqrt{2})\sqrt{(\pi)}$ so that for $\mu = 0.04$ $I_3 = 0.5854$, $\mu = 0.01$ $I_3 = 0.8110$, $\mu = 0.005$ $I_3 = 0.8486$ and $\mu = 0.0025$ $I_3 = 0.8674$. With $\mu = 0.04$ we use $\Delta t = 0.01$ and $h = 0.1$ over a range $-50 \leq x \leq 50$, and confirm earlier work that the Maxwellian evolves into a single $MKdV$ soliton and an oscillating tail. The values taken by the lowest invariants up to time of $t = 12.5$ are given in Table (7.26).

With $\mu = 0.01$ we use $\Delta t = 0.005$ and $h = 0.05$ over a range $-50 \leq x \leq 50$, and confirm earlier work that the Maxwellian evolves into $MKdV$

Table 7.26: Invariants for Maxwellian

	$\mu = 0.04, h = 0.1, \Delta t = 0.01$			
time	I_1	I_2	I_3	I_4
0.0	1.772454	1.253314	0.585430	0.300143
2.5	1.772452	1.253307	0.588138	0.301000
5.0	1.772449	1.253304	0.588723	0.301623
7.5	1.772441	1.253301	0.588909	0.301821
10.0	1.772459	1.253298	0.588981	0.301896
12.5	1.772317	1.253295	0.589015	0.301908

Table 7.27: Invariants for Maxwellian

	$\mu = 0.01, h = 0.05, \Delta t = 0.005$			
time	I_1	I_2	I_3	I_4
0.0	1.772454	1.253314	0.811028	0.597435
2.5	1.772447	1.253292	0.816537	0.604749
5.0	1.772415	1.253212	0.819122	0.607861
7.5	1.772376	1.253115	0.819110	0.607780
10.0	1.772335	1.253017	0.818888	0.607455
12.5	1.772295	1.252920	0.818643	0.607111

Table 7.28: Invariants for Maxwellian

	$\mu = 0.005, h = 0.01, \Delta t = 0.005$			
time	I_1	I_2	I_3	I_4
0.0	1.772454	1.253315	0.848628	0.658827
2.5	1.772418	1.253229	0.848988	0.659489
5.0	1.772177	1.252605	0.847364	0.657012
7.5	1.771900	1.251896	0.845243	0.653773
10.0	1.771642	1.251194	0.843128	0.650566
12.5	1.771343	1.250503	0.843128	0.647414

solitons and an oscillating tail. The values taken by the invariants are also given in Table (7.27).

With $\mu = 0.005$ we use $\Delta t = 0.005$ and $h = 0.01$ over a range $-15 \leq x \leq 15$, and show that the Maxwellian evolves into three $MKdV$ solitons respectively. The values taken by the lowest four invariants for both simulations are given in Table (7.28). As h decreases the observed value of I_3 at time $t = 0$ moves closer to the analytic value due probably to an improved estimate of U_x.

With $\mu = 0.0025$ we use $\Delta t = 0.005$ and $h = 0.01$ over a range $-15 \leq x \leq 15$, and show that the Maxwellian evolves into five $MKdV$ solitons respectively. The values taken by the lowest four invariants for both simulations are given in Table (7.29). As h decreases the observed value of I_3 at time $t = 0$ moves closer to the analytic value due probably to an improved estimate of U_x.

Table 7.29: Invariants for Maxwellian

	$\mu = 0.0025, h = 0.01, \Delta t = 0.005$			
time	I_1	I_2	I_3	I_4
0.0	1.772454	1.253315	0.867428	0.690791
2.5	1.772241	1.252774	0.867062	0.690409
5.0	1.771081	1.249709	0.857655	0.674900
7.5	1.769900	1.246613	0.847833	0.659092
10.0	1.768795	1.243732	0.838794	0.644772
12.5	1.767754	1.241044	0.830461	0.631748

7.5 Discussion

The numerical solution algorithm, based on collocation of quartic B-splines over finite elements, described in Section (7.1.1) is validated in Section (7.1.3), by a single soliton simulation, which shows good conservation properties and accuracy.

Constant positive boundary forcing produces a train of solitary waves of like amplitude and velocity generated at a constant rate. The initial wave has a slightly larger amplitude due to a switch-on effect. This behaviour corresponds to that of the KdV equation under similar conditions [15, 11]. Characteristic results for the numerical experiments on positive boundary forcing are listed in Table (7.30). It is deduced that solitary waves are generated with period $\Delta T_B = 1.82(\frac{p}{U_0}{}^3)$, amplitude $2.147 \times U_0$ and velocity $4.62 \times U_0^2$, where U_0 is the magnitude of the forcing; the definition of p is given by equation (7.3).

The birth times recorded in Table-(7.4), (7.5) and (7.6) and referred to in the text are those at which a solitary wave starts to traverse the region. Some small time before this the solitary wave is conceived at the origin as

Table 7.30: Mean observation of solitary waves: long impulse, various forcing

ϵ	p	U_0	ΔT_B	amplitude	velocity
6	1.0	0.5	14.552	1.0746	1.153
6	1.0	1.0	1.82	2.147	4.62
6	1.0	2.0	0.2271	4.295	18.25
3	1.4142	0.5	41.25	1.073	0.572
3	1.4142	1.0	5.15	2.147	2.31

a localised disturbance which begins to develop. If the forcing is removed before separation from the origin (birth) occurs the solitary wave never forms and the small local disturbance which remains located near the origin dies away as the simulation proceeds.

Negative forcing $-U_0$ produces negative solitary waves of equal amplitude to those produced by positive forcing U_0.

A positive impulse followed by an equal negative impulse leads to results that depend on the periodicity of the forcing as well as its magnitude. Two examples are presented. In one a single positive solitary wave is generated, while in another, with a slightly shorter period, a positive and negative solitary wave are generated.

The solitary waves generated by boundary forcing have amplitudes and velocities consistent with those of the free soliton solution of the $MKdV$ equation and behave similarly when they interact. Although these observations are subject to experimental error they tend to support the idea that these solitary waves are indeed identical with free solitons since it does not seem likely that the $MKdV$ equation would support two different solutions with so similar properties.

Conclusion

We have set up a new B-spline finite element algorithm, for the KdV and $MKdV$ equation, which the non-linear terms locally linearised, in the KdV and $MKdV$ equations, UU_x and U^2U_x, are replaced the function U. First, method used is based on the Galerkin method with quadratic B-spline finite elements. A second method used is based on collocation over finite elements using quartic B-spline trial functions.

It has been shown analytically [4, 41] that solutions of the KdV and $MKdV$ equations obey an infinity of conservation laws. It is therefore important that any numerical solution shall satisfy at least the lower order conservation laws. We have shown in earlier chapters that in all the simulations presented here these conservation laws are all satisfactorily obeyed.

Any numerical scheme must be capable of accurately representing the position and amplitude of a soliton as it moves throughout a simulation. The interaction of solitons must also be well described. To evaluate how well our algorithms perform we have used the L_2 and L_∞ error norms. We have shown that throughout the simulations these error norms are satisfactorily small.

A quadratic B-spline finite element algorithm and a Modified Petrov-Galerkin algorithm have been used to study the interaction of soliton solutions for the KdV equation in Chapter 4. Results of simulations presented in this chapter indicate that to obtain very acceptable, L_2-error norms and accurate conservation properties smaller time steps are required. The error can be reduced substantially by using smaller space and time steps. Reasonably accurate numerical solutions of the KdV equation are produced.

We give a quadratic B-spline finite element solution for the Modified Korteweg-de Vries equation in Chapter 5. Results of simulations are very good, L_2 and L_∞ error norms are satisfactorly small and the conservation laws very well indeed. We set up our algorithm for the Modified Korteweg-de Vries minus equation using a 'lumped' Galerkin method with quadratic B-spline finite elements in Chapter 6. The error norms are small showing that the position and shape of a soliton are well represented by the numerical solution. The lowest three invariants change by less than 0.05% during the run so that the numerical algorithm has good conservation properties as well. The interaction of 2 solitary waves, the invariants change by less than 0.04% during the run so that conservation is excellent. Also we applied many different initial conditions. Results are very accurate, invariants are satisfactorily good.

In Chapter 7 an unconditionally stable numerical algorithm for the Modified Korteweg-de Vries equation based on the quartic B-spline finite element method is described. The algorithm is validated through a single soliton simulation. In further numerical experiments forced boundary conditions $u = U_0$ are applied at the end $x = 0$ and the generated states of solitary waves are studied. The solitary wave states generated by applying a positive impulse followed immediately by an equal negative impulse is dependent on the period of forcing. The solitary waves generated by these various forcing functions posses many of the attributes of free solitons

Bibliography

[1] ABE, K., AND INOUE, O., *"Fourier expansion solution of the Korteweg-de-Vries Equation". J. Comp. Phys. 31. 202-210, (1980).*

[2] ABLOWITZ, M.J., AND CLARKSON, P.A., *"Solitons, Nonlinear Evolution Equations and Inverse Scattering " Cambridge University Press (1991).*

[3] AHLBERG, NILSON AND WALSH *"The Theory of Splines and Their Applications", New York, Academic Press, (1969).*

[4] ALEXANDER, M.E., AND MORRIS, J.LL., *"Galerkin Methods for some Model Equations for non-linear dispersive waves", J. Comp. Phys., 30, 428-451, (1979).*

[5] ALI, A.H.A., *"Finite Element Studies of the Korteweg-de Vries Equation, Ph.D Thesis", University College of North Wales, Bangor, Gwynedd (U.K.), (1989).*

[6] ALI, A.H.A., GARDNER, L.R.T. AND GARDNER, G.A., *"A Collocation Solution for Burger's Equation Using Cubic B-spline Finite Element", Com. Met. Appl. Mec. Eng. 100,325-337(1992).*

[7] AIRY, G.B., *"Tides and waves". Encylopedia Metrepolotana, vol.5, 241-396, London, (1845).*

[8] ARAL, M. M., AND GULCAT, U., *"A Finite Element Laplace Transform Solution Technique for The Wave Equation", Int. J. Num. Meth., 11, 1719-1732 (1977).*

[9] BEREZIN, Y.H., AND KARPMAN, V.I., *" Nonlinear Evolution of Disturbances in Plasmas and Other Dispersive Media", Soviet Phys. JETP, Vol. 24, No.5, 1049-1056,(1967).*

[10] BOUSSINESQ, J., *"Theorie des Ondes it des Remous Quise Propagent le Long d'un Canal Rectangulaire Horizontal, en Commoniquant au Liquide Continu dans ce Canal des Vitesses Sensiblement Parlilles de la Surface au Fond", J. Math. Pures. Appl., Ser 2, 17, 55-108, (1872).*

[11] CAMASSA, R., AND WU, T.Y., *" The Korteweg-de Vries model with boundary forcing", Wave Motion, 11, 495-506 (1989).*

[12] CANOSA, J., AND GAZDAG, J., *"The Korteweg-de Vries-Burgers Equation". J. Comp. Phys. 23, 393-403 (1977).*

[13] CHANG, Q., AND GUO, B., *"Conservative scheme for a model of nonlinear dispersive waves and its solitary waves induced by boundary motion", J. Comp. Phys., 93, 360-375 (1991).*

[14] CHEN, F., *"A galerkin Method for Strongly Nonlinear KdV equations and Schrödinger equations", Proc. Bail. II., (1981).*

[15] CHU, C.K., XIANG, L.W., AND BARANSKY, Y., *" Solitary waves induced by boundary motion ", Comm. Pur. Appl. Math., 36, 495-504 (1983).*

[16] CHANTEUR, C., AND RAADU, M., *"Formation of shock like modified Korteweg-de Vries solutions: Applications to double layers", Phys. Fluid, 30, 2708-2719, (1987).*

[17] DAG, I., *Studies of B-spline Finite Elements, Ph.D Thesis, University College of North Wales, Bangor, Gwynedd (U.K.), 1994.*

[18] DODD, R.K., EILBECK, J.C.,GIBBON, J.D., AND MORRIS, H.C., *"Solitons and Nonlinear Waves Equations". Academic Press,(1984).*

[19] DRAZIN, P.G., *"The Solitons". Cambridge University Press (1986).*

[20] FORNBERG, B., AND WHITHAM, G.B., *" A numerical and theoretical study of certain non-linear wave phenomena ", Phil. Trans. Roy. Soc., 289, 373 - 404, (1978).*

[21] GARDNER, C.S., GREENE, J.M., KRUSKAL, M.D. AND MIURA, R.M., *"Method for the Solving the Korteweg-de Vries Equation", Phys. Rev. Lett., Vol.19, 1095-1097, (1967).*

[22] GARDNER, G.A., ALI, A.H.A., AND GARDNER, L.R.T., *"A finite element solution for the Korteweg-de Vries equation using cubic B-spline shape functions", in ISNME-89 ed R Gruber, J Periaux and R P Shaw, 2, 565-570, Springer-Verlag, (1989).*

[23] GARDNER, G.A., GARDNER, L.R.T., AND ALI, A.H.A., *" Solitons of the MKdV equation ", in Num. Meth. in Engng. (Ed. G N Pande and J Middleton), 1, 590-597, Elsevier Applied Science, London, (1990).*

[24] GARDNER, L.R.T., GARDNER, G.A., AND ALI, A.H.A., *"Simulations of solitons using quadratic spline finite elements", Comp. Meth. Appl. Mech. Engng., 92,231-243, (1991).*

[25] GARDNER, L.R.T., GARDNER, G.A., *" Solitary waves of the equal width wave equation ", J. Comp. Phys., 101, 218-223 (1992).*

[26] GARDNER, G.A., GARDNER, L.R.T., AND ALI, A.H.A., *"Modelling non-linear waves with B-spline finite elements ", in Maths & Num*

aspects of Wave Propagastion (Ed. G Cohen et al.) 533-542, SIAM, Philadelphia, (1991).

[27] GARDNER, L.R.T., GARDNER, G.A., AND GEYIKLI, T., *"New B-spline Finite Element Algorithms for the KdV Equation", U.C.N.W. Maths Preprint 91.28.*

[28] GARDNER, L.R.T., GARDNER, G.A., AND GEYIKLI, T., *"A Modified Petrov-Galerkin Algorithm for the KdV Equation", U.C.N.W. Maths Preprint 91.28.*

[29] GARDNER, L.R.T., GARDNER, G.A., AND GEYIKLI, T., *"Solitary Wave Solutions of the MKdV minus Equation", U.C.N.W. Maths Preprint 93.03.*

[30] GARDNER, L.R.T., GARDNER, G.A., AND GEYIKLI, T., *"Simulations of solitons of the MKdV equation". Advances in Modelling & Analysis, A, AM SE Press, Vol. 18, No 2, 31-42, (1994).*

[31] GARDNER, L.R.T., GARDNER, G.A., AND GEYIKLI, T., *"Numerical studies of the Modified Korteweg-de Vries Equation". Proc. Int. Conf. Signals and System, London (1993).*

[32] GARDNER, L.R.T., GARDNER, G.A., AND GEYIKLI, T., *"The Boundary Forced MKdV Equation". J. Comp. Phys., Vol. 113, No. 1, July (1994).*

[33] GARDNER, L.R.T., GARDNER, G.A., *"Solitary waves of the regularised long wave equation", J. Comp. Phys., 91, 441-459, (1990).*

[34] GARDNER, C.S. AND MORIKAWA, G.K. *"Similarity in the Asymptotic Behaviour of collision Free Hydromagnetic Waves and Water Waves". New York, Courant Inst.Math.Sci., Res. Rep. Nyo-9082,(1960).*

[35] GARDNER, L.R.T., AND ALI, A.H.A., *"A numerical solutions for the Korteweg-de Vries equation using Galerkins method with Hermite polynomial shape functions", Proc. Int. Conf. on Modelling and Simulations, Istanbul, 1C, 81-93,(1988).*

[36] GARDNER, L.R.T., GARDNER, G.A., AND ALI, A.H.A., *"A method of lines solution for Burger's equation", in Computational Mechanics, ed J. H. W. Lee et al., Balkema, Rotterdam, (1991).*

[37] GAZDAG, J., *"Numerical Convective Schemes Based on Accurate Computation of Space Derivatives", J. Comp. Phys. 13,103-130 (1973).*

[38] GODA, K., *"On Stability of Some Finite difference schemes for the Korteweg-de Vries Equation", J. Phys. Soc. Japan 39, 229-236, (1975).*

[39] GREIG, I.S., AND MORRIS, J.LL., *"A Hopscotch Method for the Korteweg-de Vries Equation", J. Comp. Phys., 20, 64-80, (1976).*

[40] HEARN, A.C., *"Reduce users manual version 3.2", Nortwest computer Algorithm, (1986).*

[41] JEFFREY, A., AND KAKUTANI, T., *" Weak non-linear dispersive waves ", SIAM Review 14, 582-643, (1972).*

[42] JEFFREY, A., AND KAKUTANI, T., *"Weak Non-linear Dispersive Waves: a discussion centred around the Korteweg-de Vries equation", SIAM Review 14, 522-643, (1972).*

[43] KAKUTANI, T., AND ONO, *H.,J. Phys. Soc. Japan, Vol.34,1073-1082, (1973).*

[44] KORTEWEG, D.J., AND DE VRIES, G., *"On the Change of Form of Long Waves Advancing In a Rectangular Canal, and on a New Type of Long Stationary Waves", Philos. Mag., 39, 422-443, (1895).*

[45] KRUSKAL, M.D., " *A Symptotology in Numerical Computation: Progress and Plans on the Fermi Pasta Ulam Problem", Proc. IBM Scientific Computing Symposium on Large-Scale Problems in Physics, IBM Data Processing Div., White Plains, N. Y., 43-62, (1965).*

[46] KRUSKAL, M.D., AND ZABUSKY, N.J., *"Progress on the Fermi-Pasta-Ulam Nonlinear String Problem", Princeton Plasma Physics Laboratory Annual Rep. MATT-Q-1, Princeton, N.J. 301-308,(1968).*

[47] LAMB, G.L., *"Elements of Soliton Theory". John Wiley and Sons, (1980).*

[48] LAX, P.D., *"Integrals of Nonlinear Equations of Evolution and Solitary Waves". Comm. Pure Appl. Math. , 29, 569-579 (1967).*

[49] JOHNSON, L.W., AND RIESS, R.D., *Numerical Analysis (1982)* .

[50] MEDINA, F., AND TAYLOR, R.I., *"Finite Element Technique for Problems of Unbounded Domains", Int. J. Num. Meth. Engng.19 ,1209-1226 (1983).*

[51] MILES, J.W., *"The Korteweg-de Vries Equation: A Historical essay", J. Fluid Mech., Vol. 106, 131-147, (1981).*

[52] MIURA, M.R., *"The Korteweg-de Vries Equations: A Survey of Results". SIAM Review, V, 18, No. 3, 412-459 (1976).*

[53] MIURA, R.M., *"Korteweg-de Vries Equation and Generalisations I. A Remarkable Explicit Nonlinear Transformations, J. of Math. Phys., Vol.9, No.8, 1202-1204, (1968).*

[54] MIURA, R.M., GARDNER, C.S., AND KRUSKAL, M.D., *"Korteweg-de Vries Equation and Generalisation. II. Existence of Conservation Laws*

and Constants of Motion", J. of Math. Phys., Vol.9, No.8, 1204-1209, (1968).

[55] NICHOLSON, D.R., *"Introduction to Plasma Theory". John Wiley and Sons (1980).*

[56] PERELMAN, T.L., FRIDMAN, A.KH., AND EL'YASHEVICH, M.M., *"On the relationship between the N-soliton solution of the modified Korteweg-de Vries equation and KdV equation solution", Physics Lett, 47A, 321-323, (1974).*

[57] PRENTER, P.M., *" Splines and variational methods ", J Wiley, New York, (1975).*

[58] PU WANG AND RENE KAHAWITA *"Numerical Integration of Partial Differential Equations using Cubic Splines", Intern. J. Computer Math. 13 ,271-286 (1983).*

[59] RAYLEIGH, L., *"On Waves", Phil. Mag. Ser., (5), 1, 257-279, (1876).*

[60] REDDY, J.N., *"An Introduction to the Finite Element Method", Mc. Graw-Hill Book Company (1984).*

[61] RUBIN, S.G., AND KHOSLA, P.K., *"Higher Order Numerical Solutions using Cubic Splines", AIAA Journal 14, 851-859 (1976).*

[62] RUSSELL, J.S., *"Report on waves", Rep. 14th meeting of the British Assoc. for the Advancement of Science, John Murry, London, pp.311-390+11 plates (1844).*

[63] SANZ-SERNA, J.M., *"An explicit finite-difference scheme with exact conservation properties", J. Comp. Phys., 47, 199-210 (1982).*

[64] SANZ-SERNA, J.M., AND CHRISTIE, I., *"Petrov Galerkin Methods for Non-linear Dispersive Waves", J. Comp. Phys., 39, 94-102, (1981).*

[65] SCHAMEL, H., *"Role of Trapped Particles and Waves in Plasma Solitons Theory and Applications", Physica Scripta, 20, 306-316, (1979).*

[66] SCOTT, A.C., CHU, F.Y.F. AND MCLAUGHLIN, D.W., *"The Soliton: A New Concept in Applied Science", Proc. IEEE, 61, 1443-1483, (1973).*

[67] SMITH, G.D., *"Numerical Solution of Partial Differential Equations: Finite Difference Method", Clarendon Press, Oxford.(1978).*

[68] SIMON A. HANNABY *"A Comparision of four Finite and Infinite Element Techniques", NPL report 123/83, (1988).*

[69] SCHUMAKER, L.L., *"Spline Function: Basic Theory", John Wiley and Sons (1981).*

[70] SJOBERG, A., *"On the Korteweg-de Vries Equation: Existence and Uniqueness". J. Math. Anal. Appl, Vol. 29, 467-490,(1970).*

[71] SCHOENBERG, I.J., *"Contrubutions to the Problem of Approximation of Equidistant Data by Analytic Functions", Quart. Appl.. Math.,4,45-99 (1946).*

[72] SCHOOMBIE, S.W., *"Spline Petrov-Galerkin Methods for the Numerical Solution of the Korteweg-de Vries Equation", IMA J. Num. Anal., 2, 95-109, (1982).*

[73] STOKES, G.G., *"On the theory of oscillatory waves", Camb. Trans., 8, 441-473, (1847).*

[74] TAHA, T.R., AND ABLOWITZ, M.J., *"Analytic and numerical aspects of certain non-linear evolution equations III. Numerical KdV Equation", J. Comp. Phys., 55, 231-253, 1984.*

[75] TAHA, T.R., AND ABLOWITZ, M.J., *"Analytical and numerical aspects of certain nonlinear evolution equations, IV. Numerical MKdV Equations", J. Comp. Phys., 77, 540-548, (1988).*

[76] TAPPERT, F., *Lect. Appl. Math. Am. Math. Soc. 15, 215-215 (1974).*

[77] TORVEN, S., *"Modified Korteweg-de Vries Equation for propagating double layers in Plasmas", Phys. Rev. Lett., 47, 1053-1056, (1981).*

[78] VAN NIEKERK, F.D., AND VAN NIEKERK, A., *"A Hermite Rational Approximation Methos for the Korteweg-de Vries equation", Math. Comput Modelling 13, 63-70 (1990).*

[79] VAN WIJNGAARDEN, L., *"On the Equations of Motion for Mixtures of Liquid and Gas Bubles", J. Fluid Mech., 33, 465-474, (1968).*

[80] VLIEGENTHART, A.C., *"On Finite Difference method for the Korteweg-de Vries Equation", J. Engng. Math., Vol.5.No.2, 137-155, (1971).*

[81] WADATI, M., AND TODA, M., *"The Exact N-soliton Solution of the Korteweg-de Vries Equations", J. Phys. Soc. Japan, Vol. 32, No.5, 1403-1411, (1972).*

[82] WAHLBIN, L.B., *"A dissipative Galerkin Method for the Numerical solution of First Order Hyperbolic Equation". In Mathematical Aspect of Finite Elements In Partial Differential Equations (C. D Boor). New York , Academic Press, 147-169 (1974).*

[83] WASHIMI, H., AND TANIUTI, T., *"Propagation of Ion Acoustic Solitary Waves of Small Amplitude", Phys. Rev. Lett., 17, 996-998, (1966).*

[84] WHITHAM, G.B., *"Nonlinear Dispersive Waves". Proc. Roy. Soc., London A, 283, 38-261, (1965).*

[85] ZABUSKY, N.J., *"A Synergetic Approach to Problem of Non-linear Dispersive Wave Propagation and Interaction", Proc Symp Non-linear Partial Diff Equations, ed W Ames Academic Press, 223-258, (1967).*

[86] ZABUSKY, N.J., *"Review Article: Computational Synergetics and Mathematical Innovation", J. Comp. Phys., 43, 195-249, (1981).*

[87] ZABUSKY, N.J., *"Nonlinear Lattice Dynamics and Energy Sharing". J. Phys. Soc. Japan, 26, 196-202, (1969).*

[88] ZABUSKY, N.J., AND KRUSKAL, M.D., *"Interaction of solitons in a collisionless plasma and the recurrence of initial states ", Phys. Rev. Lett., 15, 240 - 243 (1965).*

[89] KRUSKAL, M.D., AND ZABUSKY, N.J., *"Progress on the Fermi-Pasta-Ulam Nonlinear String Problem", Princeton Plasma Physics Laboratory Annual Rep. MATT-Q-1, Princeton, N.J. 301-308,(1968).*

[90] ZIENKIEWICZ, O.C., *"The Finite Element Method", 3rd ed, McGraw Hill, London, (1979).*

[91] ZIENKIEWICZ, O.C., AND MORGAN, K., *"Finite Element and Approximation", John Wiley & Sons, (1983).*

[92] ZHANG CHUHAN AND ZHAO CHONGBIN *"Coupling Method of Finite and Infinite Elements for Strip Foundation Wave Problems", Earthquake Eng. Struct. Dyn., 15, 839-851 (1987).*